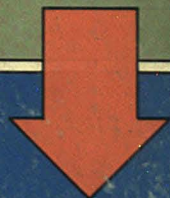
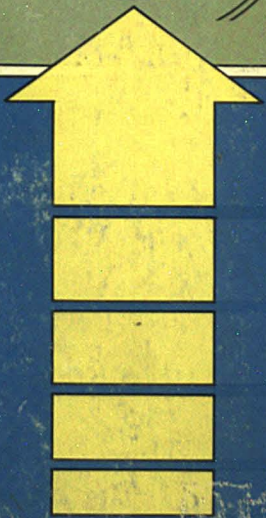
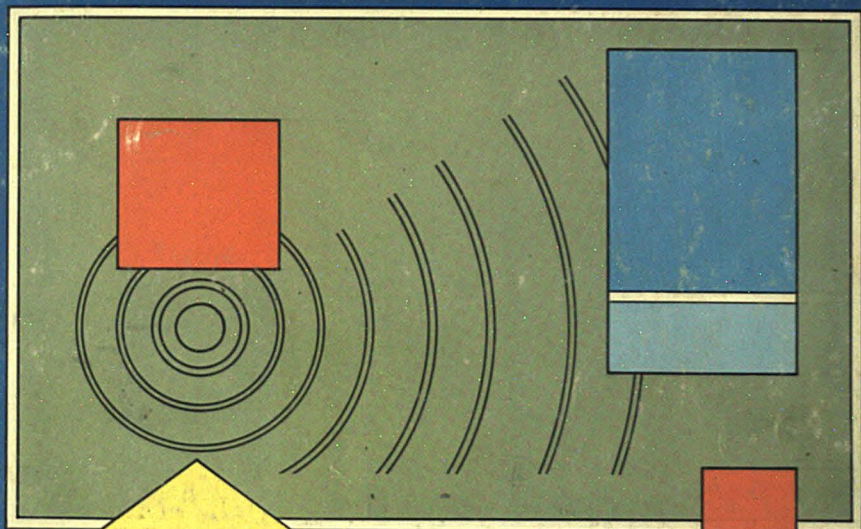


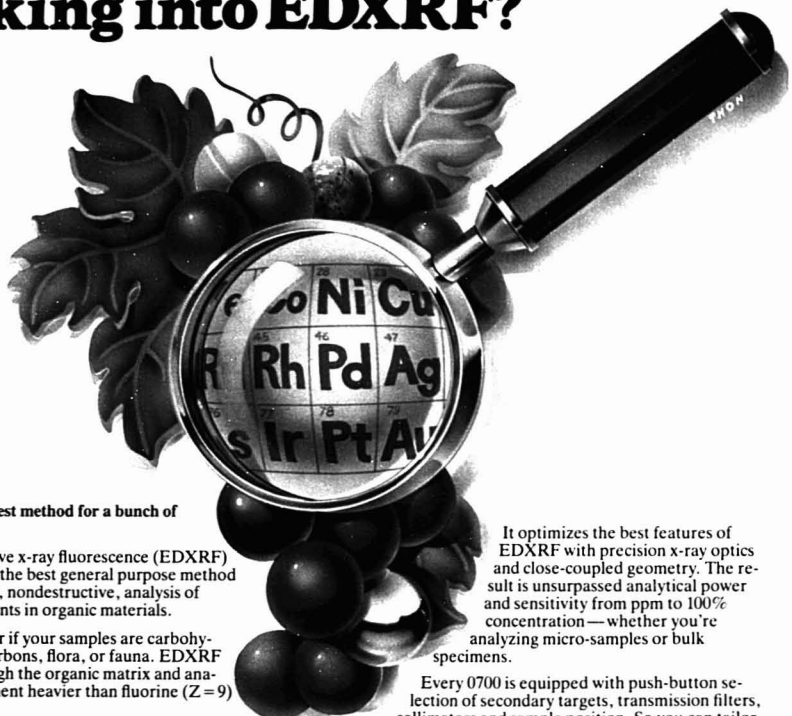
JANUARY 1983

# analytical chemistry



**Photoacoustic  
Spectroscopy**

# If you're analyzing inorganics in organics.....why aren't you looking into EDXRF?



**EDXRF is the best method for a bunch of applications.**

Energy dispersive x-ray fluorescence (EDXRF) spectrometry is the best general purpose method for quantitative, nondestructive, analysis of inorganic elements in organic materials.

It doesn't matter if your samples are carbohydrates, hydrocarbons, flora, or fauna. EDXRF sees right through the organic matrix and analyzes every element heavier than fluorine ( $Z = 9$ ) simultaneously.

That kind of analysis capability makes EDXRF ideal for rapid, multielement analysis of metals in petrochemicals, natural and synthetic polymers, rubber, resins, pharmaceuticals, organometallic complexes and other organic and low-Z materials.

## **Speed without sweat or sacrifice.**

EDXRF is fast. It gives you precise, complete results in minutes—or even seconds.

It's totally nondestructive. There's no wet chemistry—no digesting, no dissolving, no extracting—no sweat.

And during analysis, your samples and standards aren't arced, sparked, consumed or altered in any way. So you can do repetitive testing and still preserve your materials intact. *You don't have to sacrifice your standards or unknowns.*

## **We're telling you all this for a reason.**

We manufacture the world's leading EDXRF system—the KeveX 0700.

DEC and LSI-11 are trademarks of the Digital Equipment Corporation.

It optimizes the best features of EDXRF with precision x-ray optics and close-coupled geometry. The result is unsurpassed analytical power and sensitivity from ppm to 100% concentration—whether you're analyzing micro-samples or bulk specimens.

Every 0700 is equipped with push-button selection of secondary targets, transmission filters, collimators and sample position. So you can tailor analysis strategies to the broadest possible range of applications and still get complete coverage of every element in the periodic table from sodium to uranium.

And the 0700 comes standard with a DEC LSI-11™ series minicomputer with Winchester and/or floppy disk based software to handle all phases of data collection, graphics, storage and automatic operation.

## **We'd like to tell you more...**

If you're analyzing inorganics in organics, and you're not using a KeveX 0700, get in touch with us.

We'll send you a copy of our new applications bulletin, *EDXRF Analysis of Inorganic Elements in Organic Materials*. And we'll give you the details about the 0700 and its capabilities.

Then you'll be able to determine for yourself how the KeveX 0700 can magnify your analytical power.

**KEVEK CORPORATION**  
1101 Chess Drive  
Foster City, CA 94404  
Phone (415) 573-5866





# **G** The GILSON choice is the perfect choice for HPLC.

The flexibility of Gilson HPLC systems lets you choose the system you need. For separations requiring a gradient LC, we offer Systems 41 and 42.

System 41 features two microprocessor-controlled, fast refill pumps capable of microflow rates for precise gradient formation. Other system components include a dual-beam variable wavelength detector, low-volume dynamic mixing chamber, convenient pressure module, 6-port injection valve and an Apple® based Gradient Controller.

The Gradient Controller allows entry and storage of any gradient profile and includes provisions for remote control of devices such as chart recorders and fraction collectors. System 42 is identical to the system described above but is supplied without detector.

If you currently have an Apple II Plus® in your lab, then our easy-to-install Conversion Package will expand your Apple into a Gilson Controller.

Gilson systems are supplied complete for most applications and are easy to set up and maintain. Gilson's modular concept using quality components offers the best price/performance today.

Let our choice be your choice. For more information contact:



**GILSON**  
INTERNATIONAL

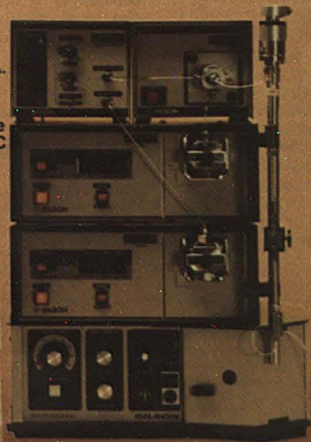
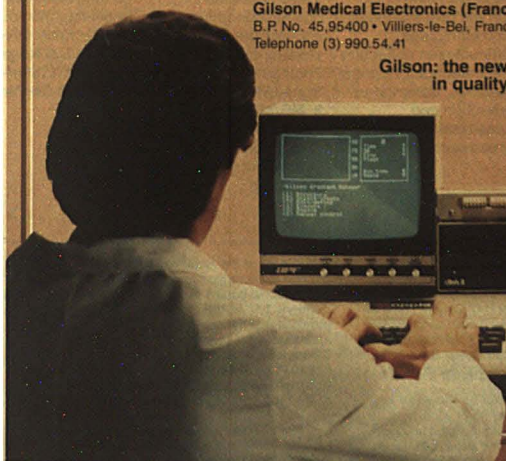
**Gilson Medical Electronics**

Box 27 • Middleton, WI 53562 • USA  
Telephone (608) 836-1551

**Gilson Medical Electronics (France) S.A.**

B. P. No. 45, 95400 • Villiers-le-Bel, France  
Telephone (3) 990.54.41

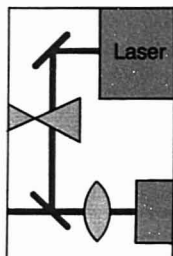
**Gilson: the new name  
in quality HPLC**



Circle 69 for literature.

JANUARY 1983

COVER FEATURE



## REPORT

### **Lasers: practical detectors for chromatography?**

Laser-based detectors are often more sensitive and selective than conventional detectors, but expense and performance problems have delayed their acceptance. Robert Green of the University of Arkansas reports

20 A

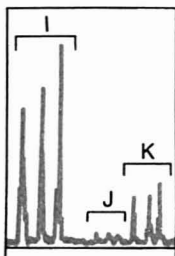


## INSTRUMENTATION

### **Photoacoustic spectroscopy**

can be used to obtain UV, visible, and IR spectra, often with little or no sample preparation. It also eliminates difficulties in collection and detection of optical radiation, common to reflection and transmission spectroscopies

89A



## FOCUS

**Analytical lab managers** met in Madison, Wis., to discuss the instrumentation obsolescence problem and instrumentation funding, according to Thomas Lytle of Iowa State University

► **MS/MS.** Kenneth Busch and R. G. Cooks discuss developments at a recent MS/MS workshop

37 A

## NEWS

**Advisory Board members.** ANALYTICAL CHEMISTRY appoints five new members to serve three-year terms beginning this month.

► John Knox will receive Dal Nogare Award at 1983 Pittsburgh Conference

45 A

Volume 55, No. 1  
January 1983  
ANCHAM  
55(1) 1A-108A  
1-176 (1983)  
ISSN 0003 2700



Registered in U.S.  
Patent and Trademark  
Office; Copyright 1982  
by the American  
Chemical Society

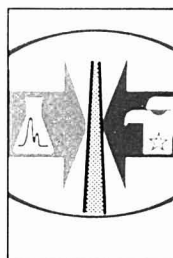
ANALYTICAL CHEMISTRY (ISSN 0003-2700) is published monthly with review issue added in April and Laboratory Guide in August by the American Chemical Society at 1155 16th St., N.W., Washington, D.C. 20036. Editorial offices are located at the same ACS address (202-872-4600). Second-class postage paid at Washington, D.C., and additional mailing offices. Postmaster: Send address changes to Membership & Subscription Services, P.O. Box 3337, Columbus, Ohio 43210.

Claims for missing numbers will not be allowed if loss was due to failure of notice of change of address to be received in the time specified; if claim is dated (a) North America: more than 90 days beyond issue date, (b) all other foreign: more than one year beyond issue date, or if the reason given is "missing from files."

Permission of the American Chemical Society is granted for libraries and other users to make reprographic copies for use beyond that permitted by Sections 107 or 108 of the U.S. Copyright Law, provided that the copying organization pays the appropriate per-copy fee through the Copyright Clearance Center, Inc., 21 Congress St., Salem, Mass. 01970 (617-744-3350). For reprint permission, write to Copyright Administrator, Books and Journals Division, ACS, 1155 16th St., N.W., Washington, D.C. 20036.

Advertising Management: Centcom, Ltd., 25 Sylvan Road South, Westport, Conn. 06881 (203) 226-7131

Technical Contents/Briefs .....	6 A
Call for Papers .....	47 A
Meetings .....	47 A
Short Courses .....	51 A
For Your Information .....	52 A
New Products .....	62 A
Chemicals .....	66 A
Manufacturers' Literature .....	68 A
Advertising Index .....	106 A
Author Index, Future Articles .....	IBC



REGULATIONS

**Acceptable analytical data for trace analysis.** Thomas Cairns and W. Michael Rogers of the FDA propose a standard protocol for quantitative trace analysis in cases where official methods are not available



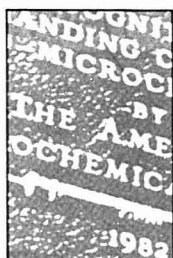
A/C INTERFACE

**Laboratory information management systems** involve some of the most complex software in the analytical laboratory. Contributing Editor Ray Dessy provides a tutorial on the philosophy behind these systems



BOOKS

**Critical reviews.** Books on on-line process analyzers and protein analysis are reviewed by Martin Frant and Nathan Gochman



EDITORS' COLUMN

**EAS.** More than 3400 participants at the 21st Eastern Analytical Symposium in New York City, Nov. 17-19, made this symposium the largest since the EAS group staged a comeback in 1979 with annual full-fledged meetings combining papers and an exhibition



EDITORIAL

**Software and analytical instrumentation.** Many instrument vendors will not share software with purchasers. Some will not even share the algorithm that describes what the software does. Purchasers find this practice alarming because the decision on which instrument to buy may well hinge on the quality of the software

54 A

70 A

83 A

16 A

1

**1983 subscription rates include surface (and air freight) costs**

Members	1 yr	2 yr
Domestic	18	30
Canada	37	68
Foreign	37 (113)	68 (220)
<b>Nonmembers:</b>		
Domestic	24	40
Canada	43	78
Foreign	67 (143)	120 (272)

Three-year and other rates contact: Membership & Subscription Services, ACS, P.O. Box 3337, Columbus, Ohio 43210, (614) 421-3776

**Subscription orders by phone** may be charged to Visa, MasterCard, Barclay card, or Access. Call toll free at (800) 424-6747 from anywhere in the continental U.S.; from Washington, D.C., call 872-8065. Mail orders for new and renewal subscriptions should be sent with payment to the Treasurer's Office at the Washington address.

**Subscription service inquiries and changes of address** (include both old and new addresses with ZIP code and recent mailing label) should be directed to the ACS Columbus address noted above. Please allow six weeks for change of address to become effective.

**ACS membership information:** Ann Donahue, Washington address.

**Single issues,** current year, \$6.00 except review issue and LabGuide, \$7.25; **back issues and volumes and microform editions** available by single volume or back issue collection. For information or to order, call (800) 424-6747 or write the Sales Department at the Washington address.

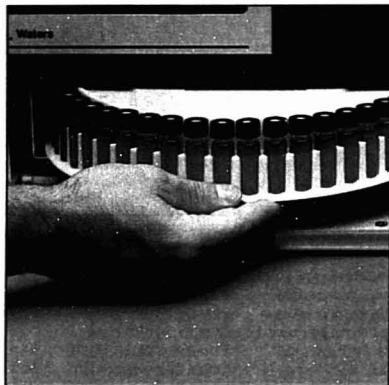
**Nonmember rates in Japan:** Rates at left do not apply to nonmember subscribers in Japan, who must enter subscription orders with Maruzen Company Ltd., 3-10 Nihonbashi 2-chome, Chuo-ku, Tokyo 103, Japan. Tel: (03) 272-7211.

ห้องสมุดเคมีและวิทยาศาสตร์  
11.ม.ค. 2526



# The only HPLC for repetitive

New. Waters QA-1™ Quality Analyzer.



**Just load the samples.**

The new Waters QA-1™ Quality Analyzer creates a totally new concept in liquid chromatography—the first completely automated HPLC system for the special needs of repetitive analysis. This new analyzer reduces an isocratic analysis to two simple steps, and delivers



**Push one button and walk away.**

superior reliability with the reproducibility you need for your analyses.

The Waters QA-1™ Quality Analyzer is totally different.

You don't need special HPLC training to get successful results. *We'll prove it.* Call now for a demonstration of this new compact analyzer, or write for bulletin BH for the latest performance documentation and details.

specifically designed  
analyses.



MILIPORE

# Waters

Waters, the Liquid Chromatography People\*  
34 Maple St./Milford, MA 01757/(617)4/8-2000

CIRCLE 232 ON READER SERVICE CARD

## Separation of Sulfite, Sulfate, and Thiosulfate by Ion Chromatography with Gradient Elution 2

Sulfite, sulfate, and thiosulfate are separated in less than 15 min in a single run. The separation requires a step gradient with 4.8 mM  $\text{NaHCO}_3$ /4.7 mM  $\text{Na}_2\text{CO}_3$  as start eluent and 6.9 mM  $\text{NaHCO}_3$ /8.6 mM  $\text{Na}_2\text{CO}_3$  as final eluent.

Thomas Sundén\*, Mats Lindgren, and Anders Cedergren, Department of Analytical Chemistry, University of Umeå, S-901 87 Umeå, Sweden, and Darryl D. Siemer, Exxon Nuclear Idaho Company, Inc., P.O. Box 2800, Idaho Falls, Idaho 83401  
*Anal. Chem.*, 55 (1983)

## Determination of Cyanide, Sulfide, Iodide, and Bromide by Ion Chromatography with Electrochemical Detection 4

Detection limits for cyanide, sulfide, iodide, and bromide are 2, 30, 10, and 10 ppb, respectively. Cyanide and sulfide can be determined simultaneously.

Roy D. Rocklin\* and Edward L. Johnson, Dionex Corp., 1228 Titan Way, Sunnyvale, Calif. 94086  
*Anal. Chem.*, 55 (1983)

## Dual Electrode Liquid Chromatography Detector for Thiols and Disulfides 8

Thiols separated from disulfides by liquid chromatography are detected only at the downstream electrode. Disulfides are reduced at the upstream electrode and are determined downstream as the electrogenerated thiol.

Laura A. Allison and Ronald E. Shoup\*, Bioanalytical Systems Inc., Research Laboratories, 1205 Kent Avenue, West Lafayette, Ind. 47906  
*Anal. Chem.*, 55 (1983)

## Addition of Complexing Agents in Ion Chromatography for Separation of Polyvalent Metal Ions 12

Metal cations are separated on a cation exchange column of low capacity with an eluent containing ethylenediammonium tartrate and are detected with a conductivity detector.

Gregory J. Sevenich\* and James G. Fritz, Ames Laboratory and Department of Chemistry, Iowa State University, Ames, Iowa 50011  
*Anal. Chem.*, 55 (1983)

## Phenyl-Modified Kel-F as a Column Packing for Liquid Chromatography 17

The phenyl Kel-F column has 8800 plates/m, a reduced plate height of 5.7, and a sample capacity of 100  $\mu\text{g/g}$  packing. The retention mechanism is solvophobic in nature.

Richard W. Siergiej and Neil D. Danielson\*, Department of Chemistry, Miami University, Oxford, Ohio 45056  
*Anal. Chem.*, 55 (1983)

## Liquid Chromatography/Proton Nuclear Magnetic Resonance Spectrometry Average Composition Analysis of Fuels 22

A method is described for obtaining average composition data for alkane, monocyclic aromatic, and bicyclic aromatic fractions of fuels. Average molecular weights for monocyclic and bicyclic aromatic fractions are determined with an accuracy of  $\pm 4$  daltons.

James F. Haw, T. E. Glass, and H. C. Dorn\*, Department of Chemistry, Virginia Polytechnic Institute and State University, Blacksburg, Va. 24061  
*Anal. Chem.*, 55 (1983)

## Determination of Vasodilators and Their Metabolites in Plasma by Liquid Chromatography with a Nitrosyl-Specific Detector 29

Detection limit is 0.1 ng for glycerol trinitrate (GTN) and pentaerythritol tetranitrate (PETN), and 0.2 ng for isosorbide dinitrate (ISDN). At the 5-ng level, RSDs are  $\pm 4.1\%$ ,  $\pm 2.2\%$ , and  $\pm 7.3\%$  for GTN, PETN, and ISDN, respectively.

Wing C. Yu\* and E. Ulku Goff, Thermo Electron Corporation, Analytical Instruments, 101 First Avenue, Waltham, Mass. 02254  
*Anal. Chem.*, 55 (1983)

## Determination of Phencyclidine and Phenobarbital in Complex Mixtures by Fourier-Transformed Infrared Photoacoustic Spectroscopy 32

Controlled substances are determined in substrates such as lactose and parsley. Accuracy to within 1% is demonstrated, although saturation effects may be exhibited in some of the spectra.

M. G. Rockley\*, M. Woodard, H. H. Richardson, D. M. Davis, N. Purdie, and J. M. Bowen, Department of Chemistry, Oklahoma State University, Stillwater, Okla. 74078  
*Anal. Chem.*, 55 (1983)

## Sequential Determination of L-Lactate and Lactate Dehydrogenase with Immobilized Enzyme Electrode 35

Determinations are complete within  $\sim 7$  min. The precision is 1.4% and 2.6% for L-lactate and lactate dehydrogenase, respectively. The electrode can be used for more than 2 weeks and 140 sequential determinations.

Fumio Mizutani\*, Kanji Sasaki, and Yukio Shimura, Research Institute for Polymers and Textiles, 1-1-4 Yatabe-Higashi, Tsukuba, Ibaraki 305, Japan  
*Anal. Chem.*, 55 (1983)

## Determination of Molecular Weight Distribution of Aromatic Components in Petroleum Products by Chemical Ionization Mass Spectrometry with Chlorobenzene as Reagent Gas 38

The mechanism involves selective charge exchange reactions between chlorobenzene and the substituted benzenes and naphthalenes in the sample. Turnaround time is 3 min for screening of successive samples.

L. Wayne Sieck, Chemical Thermodynamics Division, Center for Chemical Physics, National Bureau of Standards, Washington, D.C. 20234  
*Anal. Chem.*, 55 (1983)

\* Corresponding author



# CAPABILITY.

## THE PROBLEM

Low yields of gold-plated lead frames. The manufacturer was dissatisfied with the efficiency of his gold-plating bath and suspected that the ratio of  $\text{Au}^+$  to  $\text{Au(CN)}_2^-$  in the bath was incorrect.

## THE SOLUTION

Analysis of the bath by a Dionex Ion Chromatograph.™ Results were obtained in 12 minutes, following a simple dilution. These showed that the concentration of  $\text{Au(CN)}_2^-$  was too high. The concentration was lowered and Ion Chromatography was used from that point on to monitor and optimize the efficiency of the bath. The manufacturer now also

monitors the concentration of his cobalt brighteners and detects surface contaminants left behind after surface pretreatment.

sensitivity ( $\mu\text{g/L}$  in some cases), little or no sample pretreatment and low operating costs.

Dionex users are offered free training courses and receive regular information on new applications. You also have the assurance of the Dionex service commitment—backed by a complete worldwide service network. And a technical support staff is available to provide individualized assistance in solving all your ion analysis problems.

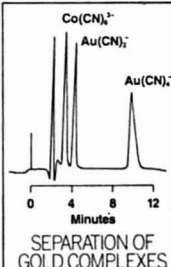
Learn how Dionex Ion Chromatography can provide the solution to your problems by contacting Dr. Art Fitchett at (408) 737-0700, Telex: 348347.

## THE CAPABILITY

The problem-solving capability of Ion Chromatography is becoming increasingly valuable to the plating industry—to every industry in fact, where analysis of complex chemical solutions composed of both inorganic and organic constituents is needed. Dionex Ion Chromatography solves problems involving inorganic anions, amines, organic acids, amino acids, transition and heavy metals, alkali metals and alkaline earths. Ion Chromatography is

also useful for QA screening of incoming materials, detecting ionic contaminants in a wide variety of manufacturing processes, adjusting concentration ratios, analyzing competitors' formulations and monitoring waste materials.

Sophisticated column and detector technologies give Dionex Ion Chromatographs™ the capability to solve your toughest ion analysis problem, regardless of the complexity of the matrix. You get solutions rapidly (often in less than one minute per ion), with high



SERIES 2000i  
**DIONEX**  
ION CHROMATOGRAPHS™

## THE SOLUTION

CIRCLE 60 ON READER SERVICE CARD

DIONEX CORPORATION  
1228 Titan Way  
Sunnyvale, CA 94086  
U.S.A.

**Characterization of the Microstructure and Macrostructure of Coal-Derived Asphaltenes by Nuclear Magnetic Resonance Spectrometry and X-ray Diffraction** 42

Average molecular properties are calculated by NMR, functional group analysis, and elemental and molecular weight methods. Size of the average aromatic structural unit and the number of such units per molecule are estimated by a combined NMR-X-ray procedure.

I. Schwager, P. A. Farmanian, J. T. Kwan, V. A. Weinberg, and T. F. Yen\*, School of Engineering, University of Southern California, University Park, Los Angeles, Calif. 90007  
*Anal. Chem.*, 55 (1983)

**Molar Absorptivities of Ultraviolet and Visible Bands of Ozone in Aqueous Solutions** 46

The absorptivities of the ultraviolet and visible optical absorption bands of aqueous ozone are:  $\epsilon_{260} = 3292 \pm 70 \text{ M}^{-1} \text{ cm}^{-1}$  and  $\epsilon_{590} = 5.1 \pm 0.1 \text{ M}^{-1} \text{ cm}^{-1}$  at the band maxima. The oxidation of  $\text{Fe}^{2+}$  by  $\text{O}_3$  takes place with a stoichiometric ratio of  $\text{Fe}^{3+}/\text{O}_3$  equal to  $1.996 \pm 0.036$ .

Edwin J. Hart\*, Hahn-Meitner-Institut für Kernforschung Berlin GmbH, Bereich Strahlenchemie, D-1000 Berlin 39, Germany, and K. Sehested and J. Holcman, Accelerator Department, Risø National Laboratory, DK 4000 Roskilde, Denmark  
*Anal. Chem.*, 55 (1983)

**Cross-Correlation Analysis of Molecular Fluorescence Spectra** 49

Spectra are obtained with conventional instrumentation and are then transformed to relative time-space by fast Fourier transform procedures. The method is tested on library spectra of polycyclic aromatic hydrocarbons.

Marilyn A. Stadalius and Harvey S. Gold\*, Department of Chemistry, University of Delaware, Newark, Del. 19711  
*Anal. Chem.*, 55 (1983)

**Determination of Salicylic Acid in Aspirin Powder by Second Derivative Ultraviolet Spectrometry** 54

The amount of salicylic acid in a commercial aspirin powder, determined from the height of the second derivative satellite peak, is  $0.0361 \pm 0.0005\%$  at the 95% confidence limit.

Keisuke Kitamura\* and Ryo Majima, Kyoto College of Pharmacy, 5 Nakauchi-cho, Misasagi, Yamashina-ku, Kyoto 607, Japan  
*Anal. Chem.*, 55 (1983)

**Spatial Discrimination in Spark Emission Spectrochemical Analysis** 57

An adjustable waveform spark source and argon flow jet are used to produce a positionally stable spark train. S/N is improved and spectra are simplified by optically masking the center core of the spark train.

John P. Walters\* and William S. Eaton, Department of Chemistry, University of Wisconsin, Madison, Wis. 53706  
*Anal. Chem.*, 55 (1983)

**Analysis of Pharmaceuticals by Fluorine-19 Nuclear Magnetic Resonance Spectrometry of Pentafluoropropionic Anhydride Derivatives** 64

Bulk pharmaceutical materials and drug dosage forms containing hydroxyl and amino groups are analyzed. Most derivatizations are complete in 10 min.

Gary E. Zuber\*, David B. Staiger, Richard J. Warren, Smith Kline & French Laboratories, P.O. Box 7929, Philadelphia, Pa. 19101  
*Anal. Chem.*, 55 (1983)

**Standards for Nanosecond Fluorescence Decay Time Measurements** 68

Literature fluorescence decay parameters for standard compounds are evaluated, and new standards are proposed. Synchronously pumped dye laser excitation and time-correlated single-photon counting detection are used.

Roger A. Lampert, Leslie A. Chewter, and David Phillips\*, Davy Faraday Research Laboratory, The Royal Institution, 21 Albemarle Street, London W1X 4BS, United Kingdom, and Desmond V. O'Connor, Institute for Molecular Sciences, Myodaiji, Okazaki 444, Japan, and Anthony J. Roberts, Unilever Research Laboratories, Port Sunlight, Merseyside, United Kingdom, and Stephen R. Meech, Department of Chemistry, Wayne State University, Detroit, Mich. 48202  
*Anal. Chem.*, 55 (1983)

**Solvent Extraction of Oil-Sand Components for Determination of Trace Elements by Neutron Activation Analysis** 74

Geochemically important and organically associated trace elements in bitumen are determined by subtracting the mineral contributions from the total measured concentrations.

F. S. Jacobs and R. H. Filby\*, Nuclear Radiation Center and Department of Chemistry, Washington State University, Pullman, Wash. 99164-1300  
*Anal. Chem.*, 55 (1983)

**Recovery Factor for Extraction from a Solid, Extractant-Retaining Matrix** 78

Theory and calculation of the recovery factor are presented. The factor consists of two multiplicative factors, one for extraction efficiency and one for extract retention by the sample.

David Emlyn Hughes, Analytical Chemistry Division, Norwich Eaton Pharmaceuticals, Inc., Box 191, Norwich, N.Y. 13815  
*Anal. Chem.*, 55 (1983)

**Interpretation of Sets of Pyrolysis Mass Spectra by Discriminant Analysis and Graphical Rotation** 81

Complex mixture spectra are interpreted in terms of chemical components without knowledge of exact reference spectra. The technique is based on factor analysis, discriminant analysis, and graphical rotation.

Willem Windig, Centraalbureau voor Schimmelmicrocultures, Oosterstraat 1, Baarn, The Netherlands, and FOM-Institute for Atomic and Molecular Physics, Kruislaan 407, 1098 SJ Amsterdam, The Netherlands, and Johan Haverkamp and Piet G. Kistemaker\*, FOM-Institute for Atomic and Molecular Physics, Kruislaan 407, 1098 SJ Amsterdam, The Netherlands  
*Anal. Chem.*, 55 (1983)



## Whatman Membranes. Performance. Reliability.

**Performance:** Improved handling characteristics, consistency of results through narrow pore size distribution and minimal batch-to-batch variation, easy autoclaving due to higher temperature stability, reduction of adverse effects from extractables, and elimination of excessive shrinking problems.

*High performance membranes — Whatman membranes.*

**Reliability:** Assured reproducibility through rigorous quality control for uniformity between lots, physical testing for thickness, wetting time and weight; performance assured by bubble point testing and biological or particle challenges; testing for bacterial retention, optimum recovery and grid line inhibition, and pyrogenicity.

*High reliability membranes — Whatman membranes.*

**Whatman membranes:** Cellulose nitrate and PTFE in a full range of pore sizes and diameters. White, black, green. Plain and gridded. Sterile membranes. Auto-clave packs. Filter holders . . . everything you need.

In performance, reliability and in every quality aspect we think you'll find Whatman membrane filters clearly superior to the membranes you may be using now.

**Whatman membranes:** Readily available from a national network of laboratory supply dealers. Just call your local dealer for ordering information. For technical details contact Whatman Laboratory Products Inc., Whatman Paper Division, 9 Bridewell Place, Clifton, New Jersey 07014. Tel: (201) 773-5800.



**Whatman**

CIRCLE 236 ON READER SERVICE CARD

PAPER DIVISION

ห้องสมุดกรมวิทยาศาสตร์บริการ



**Ionization Spectra of Neodymium and Samarium by Resonance Ionization Mass Spectrometry** 88

Ionization spectra of neodymium and samarium are obtained over the wavelength range of 423 to 463 nm. The observed wavelengths are correlated where possible with allowed transitions between known electronic energy levels. J. P. Young\* and D. L. Donohue, Analytical Chemistry Division, Oak Ridge National Laboratory, Oak Ridge, Tenn. 37830  
*Anal. Chem.*, 55 (1983)

**Determination of Organic-Bound Chlorine and Bromine in Human Body Fluids by Neutron Activation Analysis** 91

Desalted milk and serum fractions are irradiated with neutrons in a nuclear reactor and the resulting  $\gamma$ -rays of  $^{36}\text{Cl}$  and  $^{80}\text{Br}$  are measured. Detection limits are 50 and 5 ppb for organic-bound chlorine and bromine, respectively. James D. McKinney\*, National Institute of Environmental Health Sciences, Research Triangle Park, N.C. 27709, and Adel Abusamra and John H. Reed, Science Applications, Inc., 4030 Sorrento Valley Blvd., San Diego, Calif. 92121  
*Anal. Chem.*, 55 (1983)

**Mathematical Model for Concentric Nebulizer Systems** 94

A model is developed for calculation of the cutoff diameter of the nebulizer system, the normal distribution parameters of the aerosol generated by the nebulizer, the efficiency of the nebulizer system, and the aerosol concentration.

Anders Gustavsson, Department of Analytical Chemistry, The Royal Institute of Technology, Fack, S-100 44 Stockholm, Sweden  
*Anal. Chem.*, 55 (1983)

**Characterization of Two Modified Carbon Rod Atomizers for Atomic Absorption Spectrometry** 99

Unconventional "top-clamped" cup and "tube-cup" carbon rod atomizers give high effective gas-phase temperatures for volatile analyte metals and reduce the observed matrix interferences.

Darryl D. Siemer\* and Leroy C. Lewis, Exxon Nuclear Idaho Co., Inc., Box 2800, Idaho Falls, Idaho 83402  
*Anal. Chem.*, 55 (1983)

**Synthesis of the 38 Tetrachlorodibenzofuran Isomers and Identification by Capillary Column Gas Chromatography/Mass Spectrometry** 104

The positional isomers are synthesized by pyrolysis of specific polychlorinated biphenyl congeners, ultraviolet photolysis of pentachlorodibenzofurans, and chlorination of trichlorodibenzofurans by aromatic substitution.

Thomas Mazer\*, Fred D. Hileman, Roy W. Noble, and Joseph J. Brooks, Monsanto Research Corporation, Dayton Laboratory, 1515 Nicholas Road, Dayton, Ohio 45418  
*Anal. Chem.*, 55 (1983)

**Selective Concentration of Aromatic Bases from Water with a Resin Adsorbent** 111

Concentration factors and selectivities depend on the ratio of the neutral to ionic form capacity factors and on the hydrophobicity of the adsorbent.

Harold A. Stuber and Jerry A. Leenheer\*, U.S. Geological Survey, P.O. Box 25046, Mail Stop 407, Denver Federal Center, Denver, Colo. 80225  
*Anal. Chem.*, 55 (1983)

**Comparison of Priority Pollutant Response Factors for Triple and Single Quadrupole Mass Spectrometers** 116

Seventy-four percent of the electron impact GC/MS response factors determined on a triple quadrupole mass spectrometer for 53 extractable priority pollutants are within  $\pm 15\%$  of values determined in an independent interlaboratory single quadrupole GC/MS study.

A. D. Sauter\* and L. D. Betowski, U.S. Environmental Protection Agency, Environmental Monitoring Systems Laboratory, Las Vegas, Nev. 89114, and J. M. Ballard, Lockheed Engineering and Management Services Company, Inc., P.O. Box 15027, Las Vegas, Nev. 89114  
*Anal. Chem.*, 55 (1983)

**Extension of Potentiometric Stripping Analysis to Electropositive Elements by Solvent Optimization** 120

The sum of sodium and potassium ions is determined in samples such as blood serum and seawater after addition of dimethyl sulfoxide. Some resolution of sodium from potassium occurs in 1-methyl-2-pyrrolidinone and certain other solvents.

J. F. Coetzee\* and Abul Hussam, Department of Chemistry, University of Pittsburgh, Pittsburgh, Pa. 15260, and T. R. Petrick, Department of Chemistry, California State College, California, Pa. 15419  
*Anal. Chem.*, 55 (1983)

**Determination of Petroleum Sterane Distributions by Mass Spectrometry with Selective Metastable Ion Monitoring** 123

The sterane metastable parent ion transitions are separately observed during a single GC/MS run by using a programmable power supply to vary the accelerating voltage while holding the magnetic and electrostatic fields at appropriate constant values.

Geoff A. Warburton, Kratos Limited, Barton Dock Road, Urmston, Manchester M312LD, United Kingdom, and John E. Zumberge\*, Cities Service Research, Box 3908, Tulsa, Okla. 74102  
*Anal. Chem.*, 55 (1983)

**Theoretical and Experimental Determination of Band Broadening in Liquid Chromatography** 127

The axial diffusion term and the mass transfer terms of the band broadening equation are derived from the random walk model. The flow dispersion term is determined experimentally.

Jeng-Chyh Chen and Stephen G. Weber\*, Department of Chemistry, University of Pittsburgh, Pittsburgh, Pa. 15260  
*Anal. Chem.*, 55 (1983)

# Thermolyne's new ovens give you more than just a lot of hot air



## Get a \$100 rebate now and dependable performance for years to come

Introducing Thermolyne's new lab ovens. Sure, they give you a lot of hot air—years and years of it—evenly distributed at accurate temperatures. But these compact ovens are also loaded with great features. They'd cost up to \$200 additional from anyone but us.

You get reliable electronic control, timer, and over-temp alarm. We've also included half-shelving and a reversible left- or right-hand door with a convenient "bump to open" handle. Three chamber sizes, each available with mechanical or convection circulation, do the job for almost every lab application.

With extras like these, our new ovens may be the best value on the market. And our special \$100 rebate makes it even better. Just send in the attached coupon and we'll send you a

certificate good for \$100 off the purchase price of your new Thermolyne oven. That's a lot more than just hot air! (Offer ends June 30, 1983.)

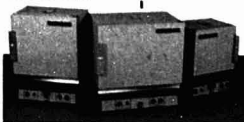
Send in the coupon or see your lab supply dealer now. Thermolyne Corporation, 2555 Kerper Boulevard, Dubuque, Iowa 52001, 1 319 556-2241.

☐ Send my \$100 rebate certificate and include complete information about all the new Thermolyne ovens.

☐ Have a Thermolyne representative call.

NAME/TITLE \_\_\_\_\_  
 COMPANY \_\_\_\_\_  
 ADDRESS \_\_\_\_\_  
 CITY \_\_\_\_\_ STATE \_\_\_\_\_ ZIP \_\_\_\_\_  
 PHONE (\_\_\_\_) \_\_\_\_\_

**Thermolyne**  
 made to last



**Thermolyne**

**SYBRON**

CIRCLE 203 ON READER SERVICE CARD

# MEMO

TO:

**All Quality Gas Mixture Users**

FROM:

**Matheson's Primary Standard Mixture Labs**

SUBJECT:

**Maximum Error**

A recent calculation of the maximum error possible in the preparation of a double dilution Primary Standard Calibration Mixture, namely 50 ppm Carbon Monoxide in Nitrogen, indicates that our stated accuracy of  $\pm 1$  percent of the component value is on the conservative side. All theoretical errors were biased in one direction to maximize the error probability and were based on preparation in a cylinder of 29.5 liter water volume at 2000 psia. Concurrently, an exhaustive round robin test among eleven laboratories indicated that deviations distributed themselves randomly around the stated concentrations of the various components in our Primary Standard Calibration Mixtures using gas chromatographic techniques. Major contributors to error in partial pressure mixtures are temperature and pressure variations and compressibility factors of the gases involved. Because mass measurement is independent of these factors these variables are eliminated.

The accuracy attainable is a function of the weight of the gases being introduced into the cylinder and the accuracy of the analytical balance.

Matheson Primary Standards are prepared down to one part per million on our high load (25 kg to 100 kg capacities) high sensitivity analytical balances strategically located across the U.S., Canada and Europe. The Primary Standards prepared on these balances result in gas calibration standards with accuracies exceeding the capability of gas chromatography and other analytical instruments.

For further information contact your local Matheson branch or circle the reader service number below.

**Matheson**

30 Seaview Drive, Secaucus, NJ 07094

CIRCLE 142 ON READER SERVICE CARD

**Br**

## Correspondence

### Chemiluminescent Detection of Reduced Sulfur Compounds with Ozone

135

Thomas J. Kelly, Jeffrey S. Gaffney\*, Mary F. Phillips, and Roger L. Tanner, Environmental Chemistry Division, Department of Energy and Environment, Brookhaven National Laboratory, Upton, N.Y. 11973  
*Anal. Chem.*, 55 (1983)

### Identification of Triaromatic Azaarenes in Crude Oils by High-Resolution Spectrofluorimetry in Shpol'skii Matrices

138

Philippe Garrigues, Régine De Vazelles, Marc Ewald\*, and Jacques Jousset-Dubien, Laboratoire de Chimie Physique A, Université de Bordeaux I, 33405 Talence Cédex, France, and Jean-Marie Schmitter and Georges Guiochon, Laboratoire de Chimie Analytique Physique, Ecole Polytechnique, 91120 Palaiseau, France  
*Anal. Chem.*, 55 (1983)

### Quantitative Analysis of Coal-Derived Liquids by Thin-Layer Chromatography with Flame Ionization Detection

141

Milan L. Selucky, Coal Research Department, Alberta Research Council, Edmonton, Alberta T6G 2C2, Canada  
*Anal. Chem.*, 55 (1983)

### 1-Methyl-4-acetylpyridinyl Free Radical as an Electron Spin Resonance Spectral Probe of Solvent Polarity

143

Orland W. Kolling, Chemistry Department, Southwestern College, Winfield, Kan. 67156  
*Anal. Chem.*, 55 (1983)

### Quantitative Analysis of Mixed Benzalkonium Chlorides by Laser Mass Spectrometry

145

Kesagapillai Balasamugam and David M. Hercules\*, Department of Chemistry, University of Pittsburgh, Pittsburgh, Pa. 15260  
*Anal. Chem.*, 55 (1983)

### Fiber Optic Probe for Remote Raman Spectrometry

146

Richard L. McCreery\*, Department of Chemistry, The Ohio State University, Columbus, Ohio 43210, and Martin Fleischmann and Patrick Hendra, Department of Chemistry, University of Southampton, Southampton SO9 5NH, England  
*Anal. Chem.*, 55 (1983)

## Aids for Analytical Chemists

### Cadmium Telluride $\gamma$ -Ray Liquid Chromatography Detector for Radiopharmaceuticals

148

Richard E. Needham\* and Michael F. Delaney, Winchester Engineering and Analytical Center, U.S. Food and Drug Administration, Winchester, Mass. 01890, and Department of Chemistry, Boston University, Boston, Mass. 02215  
*Anal. Chem.*, 55 (1983)

### Carbon as a Sample Substrate in Secondary Ion Mass Spectrometry

150

Mark M. Ross and Richard J. Colton\*, Chemistry Division, Naval Research Laboratory, Washington, D.C. 20375  
*Anal. Chem.*, 55 (1983)



# RESEARCH HYDROCARBONS

## Our Label Tells It All

Your work is important. Matheson recognizes this and has taken steps to help you get the most out of the Research Purity Hydrocarbons you buy.

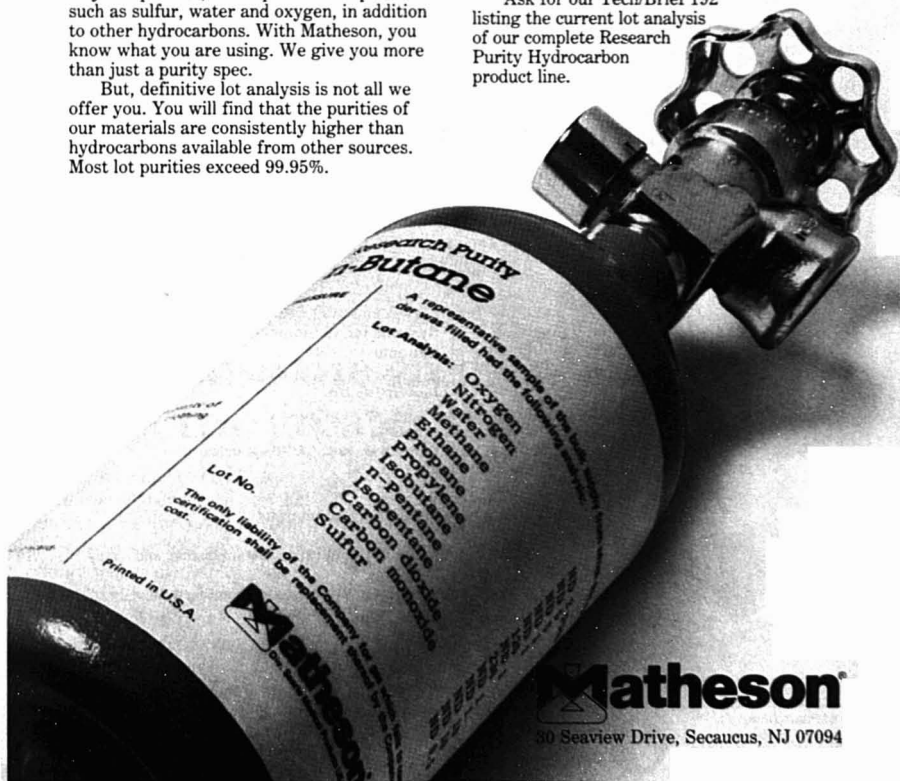
Now, all Research Purity Hydrocarbons supplied by Matheson carry a detailed lot analysis right on the label. Not just a few major impurities, but important components such as sulfur, water and oxygen, in addition to other hydrocarbons. With Matheson, you know what you are using. We give you more than just a purity spec.

But, definitive lot analysis is not all we offer you. You will find that the purities of our materials are consistently higher than hydrocarbons available from other sources. Most lot purities exceed 99.95%.

And, we make available a long list of materials that include:

n-Butane	Ethane	Methane
1,3-Butadiene	Ethylene	3-Methylbutene-
1-Butene	Isobutane	Propane
2,2-Dimethylpropane	Isobutylene	Propylene

Ask for our Tech/Brief 192 listing the current lot analysis of our complete Research Purity Hydrocarbon product line.



**Matheson**

30 Seaview Drive, Secaucus, NJ 07094

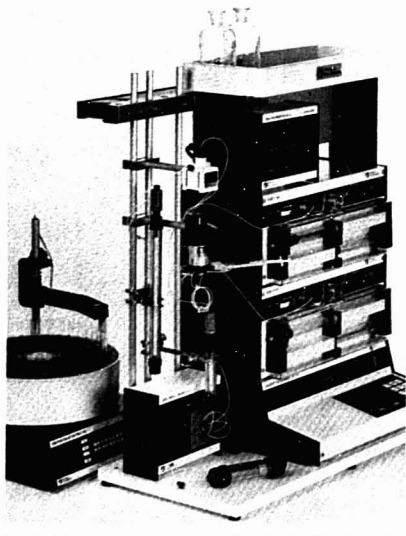
CIRCLE 141 ON READER SERVICE CARD

# High Performance in Biopolymer Separation

When Pharmacia first considered the limitations of traditional HPLC for biopolymers, it was clear that although the speed and resolution could be improved, the major problems concerned the recovery of bio-activity. The discovery of unique, new chromatographic media paved the way for an instrument system designed specifically for biological molecules. This system, The Pharmacia FPLC System, combines high resolution, high recovery of biomolecules, high speed, and enables you to do high performance chromatographic separations of biomolecules as well as traditional chromatography.

For complete information on Fast Protein/Peptide/Polynucleotide Liquid Chromatography, send for the brochure "The Pharmacia FPLC System" today.

Pharmacia products will be on display at the Pittsburgh Conference—Booths #3013, 3015 & 3017 and at the ASM Meeting—Booths #1029, 1030 & 1031.



121

**PHARMACIA FINE CHEMICALS**  
Division of Pharmacia, Inc.  
Piscataway, NJ 08854  
Orders Only: (NJ) 201-457-8150  
800-526-3593  
Information: 201-457-8000



**Pharmacia  
Fine Chemicals**

CIRCLE 163 ON READER SERVICE CARD

## Briefs

### Statistical Evaluation of Calibration Curve Nonlinearity in Isotope Dilution Gas Chromatography/Mass Spectrometry 153

Jozef A. Jonckheere and Andre P. De Leenheer\*,  
Laboratorium voor Medische Biochemie en Klinische Analyse,  
Farmaceutisch Instituut, 9000 Gent, Belgium, and Herman L.  
Steyaert, Seminarie voor Waarschijnlijkheidsrekening en  
Mathematische Statistiek, Rijksuniversiteit Gent, 9000 Gent,  
Belgium *Anal. Chem.*, 55 (1983)

### Desorption of Radon from Activated Carbon into a Liquid Scintillator 155

Howard M. Prichard\* and Koenraad Marien, The University  
of Texas School of Public Health, P.O. Box 20186, Houston, Tex.  
77025 *Anal. Chem.*, 55 (1983)

### Screening Method for Aroclor 1254 in Whole Blood 157

Shane S. Que Hee\*, Jerry A. Ward, M. Wilson Tabor, and  
Raymond R. Suskind, The Kettering Laboratory, University of  
Cincinnati Medical Center, 3223 Eden Avenue, Cincinnati, Ohio  
45267 *Anal. Chem.*, 55 (1983)

### Instrument for Alternating Current Impedance Measurements 161

Sheng-Min Cai, Tadeusz Malinski, Xiang-Qin Lin, Jian-Quan  
Ding, and Karl M. Kadish\*, Department of Chemistry,  
University of Houston, Houston, Tex. 77004  
*Anal. Chem.*, 55 (1983)

### Impedance Measurements for Evaluating the Stability of Aqueous Saturated Calomel Reference Electrodes in Nonaqueous Solvents 163

Karl M. Kadish\*, Sheng-Min Cai, Tadeusz Malinski, Jian-Quan  
Ding, and Xiang-Qin Lin, Department of Chemistry,  
University of Houston, Houston, Tex. 77004  
*Anal. Chem.*, 55 (1983)

### Back-Extraction with Three Aqueous Stripping Systems for 16 Elements from Organometallic-Halide Extracts 166

J. Robert Clark\* and John G. Viets, U.S. Geological Survey,  
Denver, Colo. 80225 *Anal. Chem.*, 55 (1983)

### Correction. 1982 "A"-Page Index 170

### Manuscript Requirements 171

### Analysis, Identification, Determination, and Assay 172

### Guide for Use of Terms in Reporting Data in ANALYTICAL CHEMISTRY 173

### Spectrometry Nomenclature 173

### SI Units 174

### Copyright Transfer Form 175

# Why select a column from Analytichem?



## Because the greater the selection the greater the selectivity.

The new line of HPLC columns from Analytichem provides selectivity unequalled by anyone. The reason is simple. Analytichem offers a wider selection of phases than anyone\*. Now you can choose the phase that is precisely suited to your particular application. These new columns, packed with our unique Sepralyte™ 5µm

spherical media, set an unprecedented standard of chromatographic efficiency... regardless of the phase you select.

The performance of each new Analytichem column is fully guaranteed and backed by the industry's strongest customer service and technical support teams. Our technical advisors have the training and hands-on

experience to assist you in solving virtually any separation problem. Next time you're considering HPLC columns, be selective. Call Analytichem. You'll find the columns you need and the service you deserve.



**Analytichem International**  
24201 Frampton Ave., Harbor City,  
CA 90710, USA, (800) 421-2825.  
In California (213) 539-6490  
TELEX 664832 ANACHEM HRBO

\*C18, C8, C2, Phenyl, Cyano, Amino, Diol, Silica, Quaternary Amine, Carboxylic Acid, Sulfonic Acid.

CIRCLE 3 ON READER SERVICE CARD

### EAS: Soup to Nuts

More than 3400 participants at the 21st Eastern Analytical Symposium (EAS) in New York City, Nov. 17-19, made this symposium the largest since the EAS group staged a comeback in 1979 with annual full-fledged meetings combining papers and an exhibition. This symposium is organized by three separate organizations: the analytical groups of the New York and New Jersey sections of the American Chemical Society; the Delaware Valley, New England, and New York sections of the Society for Applied Spectroscopy; and the American Microchemical Society.

The technical program with 34 invited sessions and two sessions with submitted papers ran the gamut from precious metal analysis to genetic engineering. Most presentations were 30 minutes to an hour long so speakers were able to discuss their topics in depth. The exhibition included about 100 different companies.

There was an undercurrent of concern among participants at this meeting. Many attendees came from industrial locations in New Jersey, New York, Pennsylvania, or Connecticut

where chemists have lost jobs. Checking with the employment service office operating at EAS elicited the information that there were about 100 candidates and about 28 employers. Some of the latter had more than one position open. Nevertheless, the economy has affected employment opportunities for chemists and as a corollary has instilled fear in some working chemists, especially those in their forties or fifties.

#### Some Highlights of the Technical Program

Nobel Prize winner Rosalyn S. Yalow discussed radioimmunoassay methods, in particular how these methods have been applied to certain diabetic patients. The case history approach of Dr. Yalow's talk, which described failures and successes with individual patients, held everyone's interest. Yalow predicted that for many applications radioimmunoassay methods would in large part be replaced by other methods, such as ELISA and fluorescence detection methods. How-

ever, she maintained that for certain studies, radioimmunoassay will continue to be the method of choice because of its specificity and sensitivity.

In a session chaired by R.P.W. Scott of Perkin-Elmer, John Knox from the United Kingdom described in detail the efforts that have been made to find an ideal nonpolar reversed-phase material. He discussed the characteristics of an ideal carbon for chromatography and the steps taken to prepare porous glassy carbon. Professor Knox claims that carbon is still "promising" as a nonpolar reversed-phase material. Chromatography sessions at EAS attracted large numbers of attendees as might be expected given the large numbers of people working in separation areas.

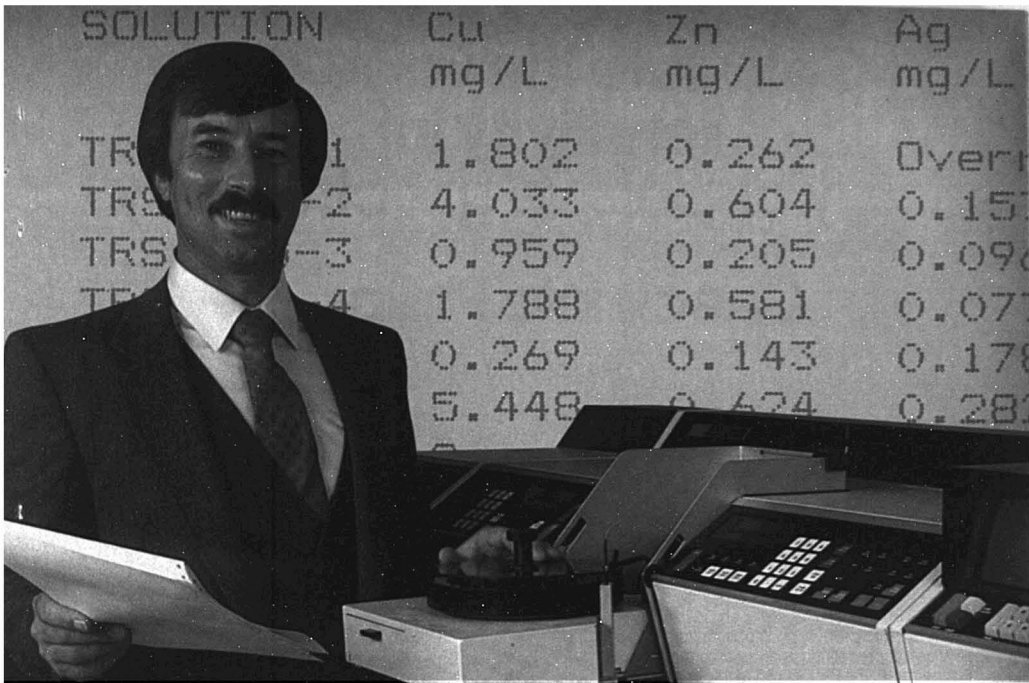
Velmer Fassel led off a session on "Inductively Coupled Plasma Spectroscopy: Quality Assurance" by reminding the audience that it was the 20th anniversary of the first experimentation with ICP. Professor Fassel focused on hyphenated ICP methods, giving examples of interfaces with mass spectrometry and the use of ICP as a detector in gas or liquid chroma-



Linda Cline Love, Seton Hall University, congratulates C.K.N. Patel, Bell Laboratories, after presenting him with the New York Section Award of the Society for Applied Spectroscopy



Jane Perkins, Merck, presents the A.A. Benedetti-Pichler Award to Peter F. Lott, University of Missouri—Kansas City. The award is sponsored by the American Microchemical Society



## Automated Atomic Absorption? Elementary...

Now, automatic atomic absorption is easy and precise. Our microprocessor-controlled accessories give you a quantum jump toward error-free results. And you can choose from twenty-nine Varian AA spectrophotometers — each can make you the master of the elements.

### Just look at our features:

- Turrets for 1, 2, 4 or 12 lamps
- Automatic flame setup to optimized conditions
- Disc storage of operating conditions for all methods
- Programmable samplers — operators are freed for meaningful tasks
- Unattended sample and standard preparation — saves high-priced work hours and avoids errors
- Video graphics for methods development
- Report generation integrated into the system
- Unmatched flame and furnace performance

Among our automation accessories and our 29 spectrophotometers, there's one

configuration that will give you the most cost-effective answers to your metals analysis problems. Varian's AA professionals are ready to help you select the system that will offer you better answers — and more of them. Guaranteed.

For more information, circle Reader Service Number 450. To have a representative contact you, circle Reader Service Number 451.

For immediate assistance contact  
 Florham Park NJ (201) 822-3700  
 Park Ridge IL (312) 825-7772  
 Sugar Land TX (713) 491-7330  
 Los Altos CA (415) 968-8141  
 Georgetown, Ontario (416) 452-4130  
 Or write 611 Hansen Way  
 Palo Alto CA 94303  
 In Europe  
 Steinhäuserstrasse  
 CH-6300 Zug, Switzerland



GTA-95 furnace and sampler



**Intelligent automation...  
from Varian**

CIRCLE 218 ON READER SERVICE CARD



# Calculate the value of sensitivity in energy dispersive spectrometry.

## Check into Philips.

Not only does the Philips PV9500/80 automated energy dispersive system provide more precision and sensitivity for a majority of applications, it also offers a range of capabilities previously found in only the highest priced spectrometers.

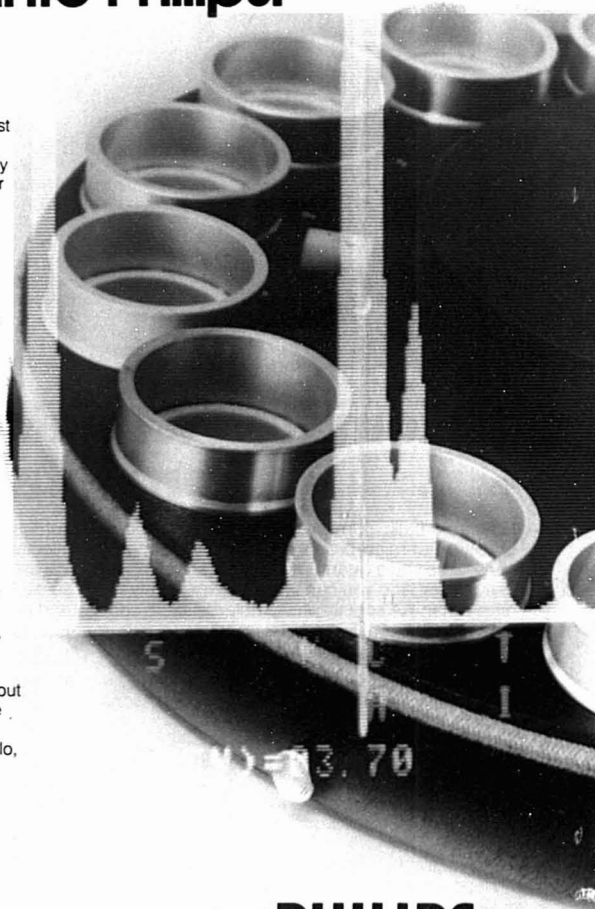
Dollar for feature, the value of this system is virtually unparalleled. It utilizes an advanced automatic changer mechanism giving the user the ability to perform fully automated sequential analysis of up to 15 samples without operator assistance.

A powerful computer-based analyzer carefully controls the assistance-free capabilities. This analyzer can easily guide the user through a series of analytical conditions, whereby simply pushing a button conducts a sophisticated, predefined analysis automatically.

Furthermore, the PV9500/80 employs newly advanced levels of energy dispersive x-ray spectrometry (EDS) and provides simultaneous multi-element analysis of samples in solid, powdered or liquid form. All elements, from sodium to uranium, can be identified and quantified at major constituent levels and down to a few parts per million.

Software packages offer increased flexibility by providing results as a quantitative percent concentration with or without reference standards, or simply as a material classification for go/no-go operation. Special compound computations and film thickness measurements can also be provided through various applications.

By maintaining acute sensitivity to the marketplace, we are able to respond to our customers' needs with innovative product developments like the PV9500/80 automated energy dispersive system. To learn more about this superior analytical value and the nearly incalculable advantages it can offer you, check with Philips today. Write or call: N.V. Philips Analytical X-ray, 7602 EA Almelo, The Netherlands. Tel. (31) 5490-18291. Telex 36591. (In U.S.A.) Philips Electronic Instruments, Inc., Analytical X-ray Group, 85 McKee Drive, Mahwah, NJ 07430. Telephone (201) 529-3800.



**Scientific &  
Analytical Equipment**

**PHILIPS**

CIRCLE 165 ON READER SERVICE CARD

tography and as a source for atomic fluorescence. He predicted its impact would transcend conventional atomic emission spectroscopy because it performs sample transformations with exceptional efficiency and low degrees of interelement interactions. The sessions dealing with ICP were organized by Ramon Barnes.

Sessions on mass spectrometry focused on the analysis of nonvolatile or high molecular weight substances. In one session, chaired by Michael Gross, R. G. Cooks, Frank Field, M. Gross, and F.W. McLafferty presented talks dealing with the latest work in MS/MS and fission fragment ionization mass spectrometry. Fast atom bombardment was the subject of four papers in another session. A final paper "Fast Atom Bombardment—Where Are We Now?" by Catherine Fenselau summed up the topic.

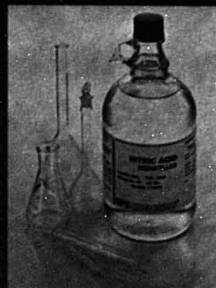
Award winners at EAS included C. Kumar N. Patel of Bell Laboratories, who won the Society for Applied Spectroscopy New York Section Award. In his award address Dr. Patel traced the history of the development of modern optoacoustic spectroscopy all the way back to work by Alexander Graham Bell in 1880. Major developments over the past 15 years have been made possible by the availability of a variety of tunable lasers. Patel reviewed the development of techniques that permit the measurement of ultrasmall absorption coefficients in gaseous samples at a level of  $\sim 10^{-10} \text{ cm}^{-1}$ . In liquids and solids, the ability extends down to  $\sim 10^{-7} \text{ cm}^{-1}$ . According to Patel there are many applications of these capabilities to scientific problems including pollution measurements both in the atmosphere and the stratosphere.

The Benedetti-Pichler Award, sponsored by the American Microchemical Society, was presented to Peter F. Lott of the University of Missouri—Kansas City. His award address, "Serendipity in Analytical Chemistry," dealt with the accidental nature of much analytical problem solving. Dr. Lott suggested that Murphy's law as applied to analytical chemistry says that the problem can be solved if we have just one more instrument or perhaps if we have the instrument that will be developed next year. We liked his statement that "the supreme excellency in analysis is SIMPLICITY." Lott's award address will appear in an early 1983 issue of the JOURNAL.

The 22nd Eastern Analytical Symposium will be held Nov. 16-18, 1983, at the Statler Hotel, New York City.

*Josephine M. Petrucci*

# HIGH PURITY ACIDS



- ACS REAGENT ACIDS
- REDISTILLED ACIDS

Produced by taking ACS Reagent Grade acids and redistilling them in glass. This distillation yields high purity acids with very low or absent trace elements.

- DOUBLE-DISTILLED ACIDS

Manufactured by taking the already very pure redistilled acids and passing them through Vycor / Quartz stills twice. This process removes virtually all volatile and non-volatile impurities.

For details on the full line of GFS Chemicals High Purity Acids, circle the reader service number below.

## GFS CHEMICALS

P.O. Box 23214 • Columbus, Ohio 43223 • (614) 881-5501

CIRCLE 68 ON READER SERVICE CARD

## 1983 Capillary GC Courses

by Prof. K. Grob, et al (EWAG/Switzerland)

Co-sponsored by EPA and the University of Cincinnati, Erba Instruments organizes again a series of practical HRGC courses:

1. March 14-18 (Cinn.)	5 days	\$575	Full
2. March 21-25 (Cinn.)	5 days	\$575	Open
3. March 28-April 1 (Cinn.)	4 days	\$500	Open
4. April (Arizona)	5 days	\$575	Open

Strong emphasis will be placed on injectors, columns, detector design and applications. Please bring your most "difficult" sample for analysis. For more details or registration write now or

### call (617) 535-5986

Erba Instruments, Inc.  
4 Doulton Place  
Peabody, MA 01960

CIRCLE 65 ON READER SERVICE CARD

## Lasers: Practical Detectors for Chromatography?

When will lasers be integrated into routine laboratory practice? This is a reasonable question, since over 20 years have elapsed since the laser's invention. The development of laser-based detectors for chromatography is one example of a new technology's progression from esoteric laboratory experiments to routine application.

In many cases, spectroscopic monitoring of chromatographic eluents using laser-based detectors offers better sensitivity and selectivity than conventional detectors. But the superior properties of laser-based detectors are often outweighed by the need for expensive and complex instrumentation. This, along with their reputation for unreliable performance, has delayed the acceptance of laser-based chromatographic detectors in the laboratory.

Just as the acronym "laser" is a generic term that includes many different devices, laser-based detectors are also characterized by great diversity. This REPORT will survey some of the most promising approaches for coupling laser spectrometry with the separation process. First, the laser properties relevant for chromatographic detection will be briefly reviewed.

### Relevant Laser Properties

The laser does not simply replace an incoherent light source in a conventional spectrometric detector. Almost without exception, the chromatographic detectors that have been devised using lasers have exploited their unique properties.

The most obvious difference between conventional light sources and lasers is the high photon flux provided by the latter. Higher powers provide

minimal benefits for absorption spectrometry. On the other hand, signal-to-noise (S/N) ratios are usually considerably improved for laser-excited fluorometry. The direct proportionality of fluorescence and source intensity is well-known. Unfortunately, scattered light from optical components and "blank" luminescence often limits the sensitivity of laser-excited fluorescence measurements (1). High incident powers may also result in thermal distortions (2). In some cases, this problem may be mitigated with pulsed lasers where the average power is low. The high power provided by the laser greatly enhances nonlinear phenomena. In fact, without the laser, two-photon processes would be of little interest to the analytical chemist.

The monochromaticity of the laser provides obvious advantages in terms of selectivity. This feature is valuable for the detection of eluents in the gas phase. In general, molecular absorption in solution is broad and featureless, and the benefits of a monochromatic source are not as apparent. Spectral rejection of background is improved for normal Raman (NRS) and resonance Raman spectrometry (RRS) when a monochromatic source is used (3). Both resonance Raman and coherent anti-Stokes Raman spectrometry (CARS) require the tunability of dye lasers for wide applicability, and benefit from a relatively narrow band of excitation frequencies. Lasers are capable of much higher resolution than is generally required for liquid chromatographic (LC) detection, even in cases where monochromaticity is desirable.

The excellent spatial coherence of laser radiation permits accurate and

precise positioning of the laser beam. Laser beams that are already highly collimated may be focused to a diffraction-limited spot. In most cases, the detector volume is limited by solution flow characteristics, and not by the laser source (3). The ability to focus the laser beam is also useful for efficiently generating nonlinear processes.

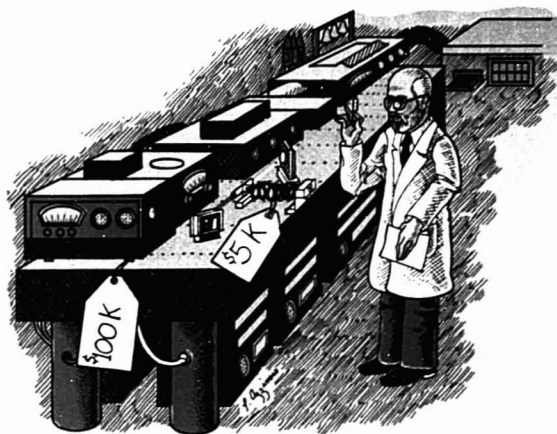
The temporal coherence of the laser emission permits the generation of short-duration pulses. Depending on the type of laser, pulse widths are available from microseconds to picoseconds (4). Time resolution may provide additional useful information about a sample or allow discrimination against unwanted signals.

Finally, the output of most lasers is polarized due to the optical cavity elements. It is possible to take advantage of this property when detecting Raman scattering, discriminating against Rayleigh scattering, or probing molecular energy levels via two-photon processes.

### Laser-Based Detectors for LC

The results of a compilation of literature citations for laser-based detectors for LC are illustrated in Figure 1. The citations have been grouped into general categories according to the property measured. (A complete bibliography may be obtained from the author.) The large number of citations found for LC compared with a similar compilation for gas chromatography (GC) is undoubtedly a response to the need for more sensitive and selective detectors to compensate for the lower resolution provided by LC.

**Laser Light Scattering.** In terms of acceptance for routine applications,



Concept by Robert B. Green

the detection of laser-induced Rayleigh scattering from eluent molecules is the most mature of the laser-based techniques. Rayleigh scattering occurs at the same wavelength as the source when the scattering centers are approximately 10% smaller than the excitation wavelength. Almost all of the detection techniques using Rayleigh scattering employ a low-angle laser light scattering (LALLS) photometer (5) coupled to a gel permeation chromatograph (GPC). Gel permeation chromatography, more generally known as exclusion chromatography, separates molecules based on their size in solution, with larger molecules eluting first. When a GPC is equipped with a concentration-sensitive detector, a molecular weight distribution may be obtained from the interpretation of the chromatogram through the use of a calibration curve relating molecular weight and elution volume (6). Unfortunately, this calibration technique does not always yield the correct molecular weight distribution because the molecular size of a dissolved polymer depends not only on its molecular weight but also on chemical composition, molecular structure, and experimental parameters such as solvent, temperature, and pressure.

Light-scattering detectors provide the necessary information for molecular weight determination and, in addition, respond rapidly with the high sensitivity needed for small sample volumes in a flowing system. Lasers are preferred sources for several reasons. Figure 2 shows a simplified optical diagram for a LALLS photometer (7). Any laser with a Gaussian beam profile (TEM<sub>00</sub>) is usable. A low-power helium-neon (He-Ne) laser is

generally chosen because inexpensive, long-life He-Ne lasers are readily available. Although scattering intensity varies inversely with the fourth power of the wavelength, sample absorption and fluorescence are largely eliminated by using the 633-nm line. A S/N ratio of better than 100 has been reported for pure water, the weakest scattering liquid, using a 3-mW He-Ne laser (7).

In the LALLS photometer shown in Figure 2, the laser beam is focused on the sample, which resides between two relatively thick quartz windows separated by a black Teflon spacer. The background is reduced by these windows and several apertures. The Rayleigh factor, which is related to the weight average molecular weight of the scattering molecule, is calculated from the following expression:  $R_s = P_s / (P_0 \sigma l)$ , where  $P_s$  and  $P_0$  are the radiant powers of the scattered and incident beams, respectively;  $\sigma$  is the solid angle of the detected scattered beam, and  $l$  is the length of the scattering volume, measured parallel to the incident beam.  $P_s$  and  $P_0$  are measured in sequence by replacing the annulus, H3, which defines the scattering angle, with an aperture. Attenuators (A1-A3) are necessary in the optical path of the laser beam because the incident laser beam power is  $10^3$  times greater than the scattered light.

Accurate molecular weight determination requires extrapolation of the results of light-scattering measurements to zero angle and zero concentration. Incoherent light-scattering photometers have minimum scattering angles of 20–30°, which contributes to large extrapolation errors, especially when particles contaminate

the sample. Scattering from foreign particles often makes tedious, time-consuming preparation necessary when conventional light sources are used. The LALLS photometer permits measurements to 2°. Although particle light scattering increases as the scattering angle decreases, this problem is minimized because the focused laser beam reduces the scattering volume tremendously. The probability of foreign particles crossing the beam path is extremely small. A GPC combined with a differential refractometer and a LALLS photometer in series, interfaced to a computer, will yield real-

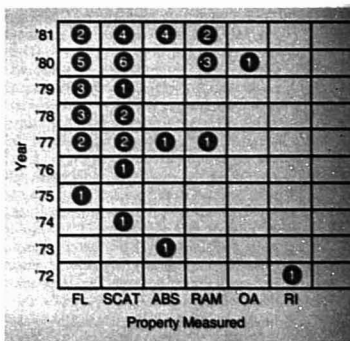
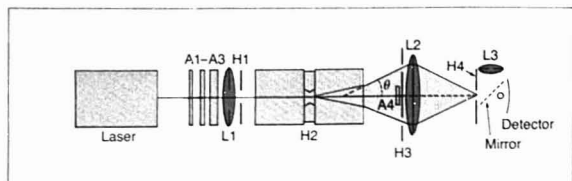
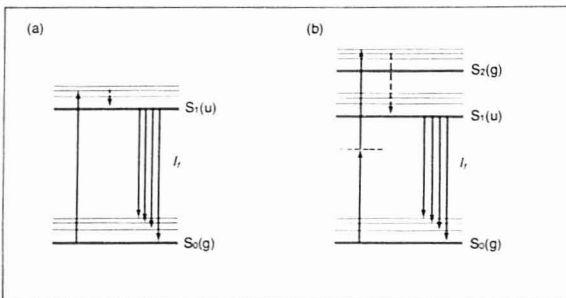


Figure 1. Number of literature citations for laser-based detectors for liquid chromatography as a function of year and property measured

FL, fluorescence; SCAT, Rayleigh scattering; ABS, absorption; RAM, Raman scattering; OA, optical activity; RI, refractive index



**Figure 2.** Diagram of low-angle laser light scattering photometer  
A1-A4, attenuators; H2, Teflon spacer separating the sample cell windows; H3, annulus; H1 and H4, apertures; L1, L2, lenses (7)



**Figure 3.** Transitions in (a) one-photon and (b) two-photon excited fluorescence  
Solid arrows pointed upward indicate absorption. Dashed arrows indicate relaxation.  $I_1$  is fluorescence intensity; g and u are symmetry types. The horizontal dashed line in (b) is a virtual state

time on-line molecular weight distributions without reference to external standards (8). GPC/LALLS is becoming the method of choice for polymer characterization. Although a GPC/LALLS photometer is not being offered as a single unit, a single detector design now manufactured by Chromatix, Inc. has been used almost exclusively in recent work. A GPC interface for the LALLS photometer is offered as an option by the manufacturer.

#### Laser-Induced Fluorescence.

Laser-induced fluorescence (LIF) detection is attractive for high-performance liquid chromatography (HPLC) because of the remarkable sensitivities that have been reported for laser-excited fluorescence measurements (see Figure 3a). The foremost problem with LIF detection has been Rayleigh scattering from eluents and optical components (9). This accounts for the preoccupation with detector cells for LIF.

Several different types of LIF detector cells have been developed for HPLC. The HPLC separation and LIF detection of several aflatoxins have been accomplished using a "flowing droplet" cell (10). The eluent is suspended between the exit of the HPLC column and a solid rod, provid-

ing a 4- $\mu$ L "windowless" cell (see Figure 4a). The laser beam and the collection optics are positioned at 90° to the flowing stream, and the fluorescence is detected by a photomultiplier, which is sampled by a lock-in amplifier. Scattering of the source radiation is largely avoided using this approach. Bubbles in the irradiated volume are minimized by notching the capillary tube.

A submicroliter flow-through cuvette has been demonstrated for LIF monitoring of HPLC effluents (11). The HPLC effluent containing the sample is injected into the solvent stream (sheath) and confined by laminar flow conditions (see Figure 4b). The refractive index difference between the sample and the solvent is much lower than for the quartz and solvent or air interface. The placement of the cuvette's optical windows 5 mm from the sample stream minimizes the amount of scattered light that is imaged by microscope optics, which are orthogonal with the laser beam and the sample stream.

An LIF detector has been developed in which a capillary tube cell is coupled to an optical fiber (12). Optical fibers conduct light by total internal reflectance along their length. A criti-

cal collection volume exists so that light rays entering the fiber at angles less than  $i_c$  will not be transmitted (see Figure 4c). Light rays originating near the center of the detector flow cell generally have larger values for  $i_c$  so that specular scattering from the cell walls is rejected. This detector cell does not depend on droplet shape; nor do bubbles interfere with LIF detection, because they flow around the outside of the optical fiber. A free-falling jet stream produced by a small-bore capillary connected to the exit of an HPLC incorporates some of the properties of other LIF detector cells in a simpler design (13). Scattering background is effectively suppressed by positioning the fluorescence collection optics at a 30° angle with the capillary rather than the typical 90°. The exciting laser beam remains perpendicular to the jet stream. Although all of the LIF detectors have produced picogram or femtogram detection limits, the optical fiber cell (12) and the jet stream cell (13) are more amenable to general applications because they are independent of the solvent and its properties. Both detectors are compatible with gradient elution; the jet stream design is more suited to micro-column HPLC because of its much smaller cell volume.

In addition to Rayleigh scattering, Raman scattering from the solvent and fluorescence from contaminants and optics reduce the sensitivity of LIF detection. Rayleigh and most Raman scattering can be rejected by filtering, but often a solvent Raman band overlaps the fluorescent analyte's emission. In general, Raman scattering may be the ultimate limit to LIF sensitivity. Fluorescence from sample contaminants may be minimized by prepurification of solvents. Even high-purity commercial solvents may contain contaminants that will contribute to the fluorescence background under high-intensity laser excitation. In addition, columns may become saturated with contaminants after prolonged use.

The ability to focus the laser beam has contributed to high specific sensitivities for LIF detectors and has permitted miniaturization. Various gas lasers (e.g., Ar<sup>+</sup>), which provide many different emission lines, are excellent excitation sources for LIF detection of HPLC eluents. These lasers are compatible with routine operation because of their relative simplicity and low maintenance requirements.

A two-photon transition results from the simultaneous absorption of two photons to populate a discrete molecular energy level (see Figure 3b) (14). Two-photon excited fluorescence (TPEF) detection may be applied to most fluorescent molecules because



# ULTIMATE TESTING FLEXIBILITY!



## DYNATECH'S MR 600 MICROPLATE READER

Our new **MR 600** Microplate Reader is a revolutionary instrument that allows the user to change test parameters from well to well through computer programming. The test format may be designed any way you choose within the confines of a 96 well Microtiter® plate.

The **MR 600** reads MIC and bacterial ID's, hemagglutination inhibition, complement fixation, ELISA, monoclonal antibody assays by ELISA, microplate blood grouping methodologies, and cytotoxic effect on cell monolayers.

### AUTOMATIC OR MANUAL TO SUIT THE NEED!

The **MR 600** measures absorbance by dual or single wavelength. It features manual or automatic X-Y axis movement, and manual or automatic single well blanking. Filter selection, calibration, and threshold are set one time, eliminating the need for programming test parameters prior to reading each plate.

An alphanumeric LED displays well position and optical density which are recorded by the **MR 600**'s printer. The printout documents all test

CIRCLE 62 ON READER SERVICE CARD

parameters, mode of operation, and filter position for both sample and reference filters and the calibration settings.

Computer software for ELISA and MIC/ID assays is available. Dynatech also offers custom software support for Hewlett Packard and Apple.

For more information, or a test demonstration, mail the coupon below or phone our *Technical Services Department* TOLL FREE at 800-336-4543.



**DYNATECH  
LABORATORIES, INC.**

AC-183

900 Slaters Lane, Alexandria, Virginia 22314  
TOLL FREE 800-336-4543 • IN VA (703) 548-3889

- ☐ Send me more technical information on the **MR 600**.  
☐ Please contact me and arrange a demonstration.

NAME \_\_\_\_\_ PHONE \_\_\_\_\_

TITLE \_\_\_\_\_ AFFILIATION \_\_\_\_\_

ADDRESS \_\_\_\_\_

CITY \_\_\_\_\_ STATE \_\_\_\_\_ ZIP \_\_\_\_\_

Dynatech is the World's Only Manufacturer of Microtiter® Products

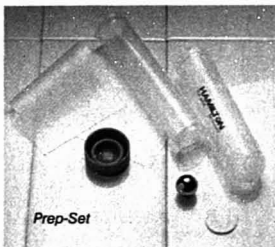


# Improve the efficiency and economy of industrial control analysis.

Now you can streamline your analyses...and reduce costs considerably.

Introducing new AMICA—Automated Modules for Industrial Control Analysis. The effective alternative to manual and continuous flow methods in quality control.

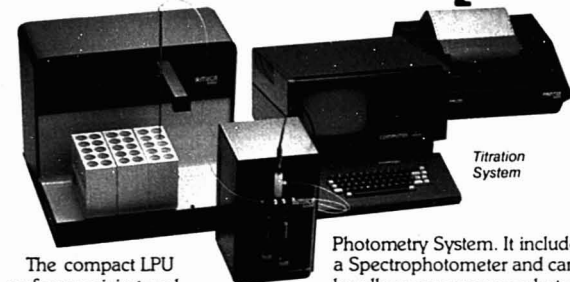
Start with Prep-Set. A durable, time-saving sample preparation kit that simplifies liquid-liquid and liquid-solid extractions.



Prep-Set

Then comes the AMICA LPU—Liquid Processing Unit. The next step in mechanizing homogeneous liquid transfer requirements in an analytical system. Use it as a sampling device for your AA, UV-VIS, or any other spectrophotometer.

CIRCLE 100 ON READER SERVICE CARD



Titration System

The compact LPU performs mixing and other functions automatically.

Titration in Quality Control? You need the AMICA Titration System. Add the Autosampler, LPU, Prep-Set, Microcomputer and Printer for control. The AMICA Titration System provides you with unparalleled QC automation including real-time data display and an automatic results summary.

Or automate all your industrial control analyses. Get the AMICA



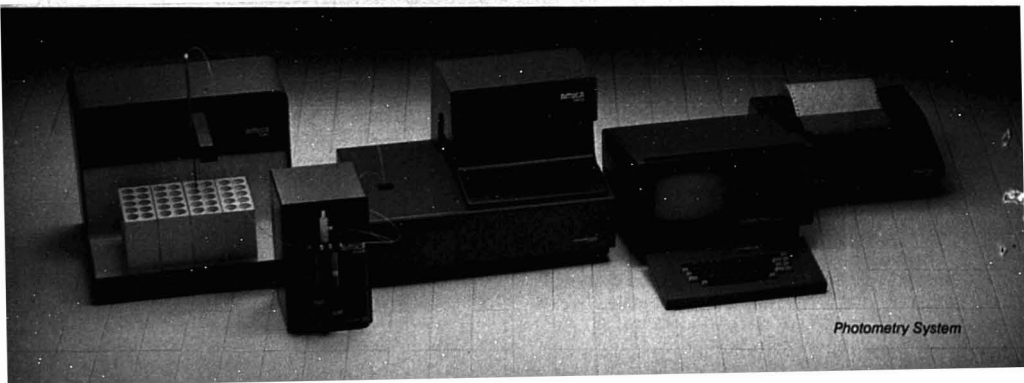
Liquid Processing Unit

Photometry System. It includes a Spectrophotometer and can handle every common photometric procedure—including photometric titrations.

AMICA is completely modular. You can build your system component by component. Buy an entire AMICA system. Or add AMICA to your existing operation. Each component interfaces easily with your equipment via a standard RS-232C interface.

Check out AMICA, today. Call toll-free 800-648-5950. Or write Hamilton Company, P.O. Box 10030, Reno, NV 89510. Put automated efficiency and economy into your quality control laboratory. And take the manual out.

**HAMILTON**  
The measure of excellence.



Photometry System

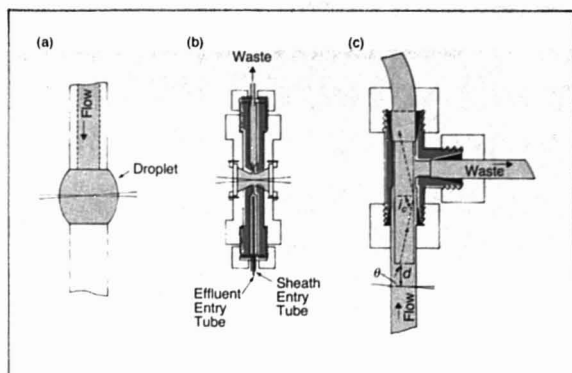


Figure 4. Diagram of LIF detector cells for HPLC

(a) Flowing-droplet cell (10); (b) laminar-flow cell (11); (c) optical-fiber cell (12)

two-photon transitions are as numerous as one-photon transitions. One-photon and two-photon transitions are complementary since they access different excited levels. In spite of their inefficiency, processes involving the absorption of two photons are very attractive for HPLC detection because the availability of high-powered lasers and the absence of background experienced with one-photon excitation permits the detection of analytically useful signals. TPEF usually occurs at shorter wavelengths than the excitation wavelength, simplifying the rejection of Rayleigh or Raman scattering with an appropriate filter and making readily available visible lasers useful excitation sources for most solutes.

Laser TPEF detection for HPLC of several oxadiazoles has been accomplished using 514.5-nm radiation from an argon ion laser (15). Chromatograms of these oxadiazoles in the presence of several polyaromatic hydrocarbons (PAHs) using incoherent ultraviolet (UV) and TPEF detection are easy to distinguish because of the more restrictive selection rules for TPEF (see Figure 5). Detection limits, linearity of response, and precision are comparable for UV and TPEF detection of the oxadiazoles.

Since the fluorescence signal generated by a two-photon process depends inversely on the laser beam's cross-sectional area, reduction in absorption path length may be compensated for by decreasing the focal length of the focusing lens (16). As a result, two-photon processes may find their most important application in low-volume detectors for microscale HPLC.

**Laser-Induced Absorption.** Absorption spectrometry is more general

than fluorescence measurement. Unfortunately, measurements based on transmitted light are limited at trace analyte concentrations because it is difficult to measure the difference in two large signals. The sensitivity of absorption measurements may be improved by detecting associated processes. Laser-induced absorption detection methods owe their diversity to the variety of approaches available for sensing molecular absorption.

**Laser-induced photoacoustic (PA)**

detection has been demonstrated for HPLC (17). A PA detector senses the pressure fluctuations in a medium due to absorption of radiation. Figure 6 shows the PA flow cell design. The PA wave is sensed by a piezoelectric transducer (PZT) which is positioned behind the foil-covered slit in the 20- $\mu$ L absorption cell. The output terminal of the PZT is grounded through the foil and the cell body. The other terminal is connected to a BNC connector. The argon ion laser source

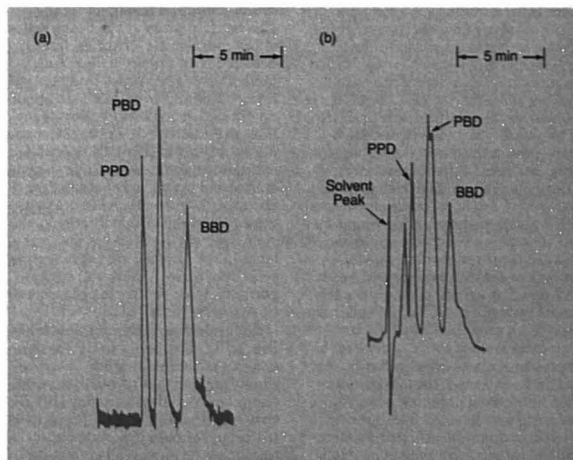
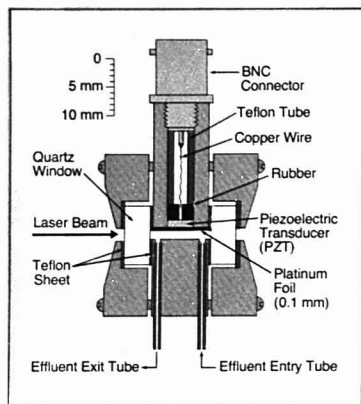


Figure 5. Simplification of chromatogram from two-photon excited fluorometric detector (a) compared to a UV absorption detector (b)

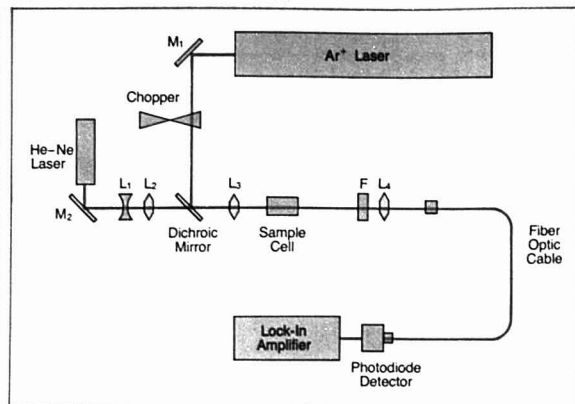
Sample contains three oxadiazoles, PPD, PBD, and BBD, plus phenol, chrysene, fluorene, and anthracene (15)



**Figure 6.** Diagram of laser-induced photoacoustic detector (17)

(488 nm) is acousto-optically modulated, and the detector signal is synchronously detected with a lock-in amplifier. Interferences from pressure fluctuations arising from the HPLC solvent pump are avoided by a judicious choice of the laser modulation frequency. In test separations of isomers of chloro-4-(dimethylamino)azobenzene (Cl-DAAB), the PA detector and a conventional UV detector (254 nm) produced comparable chromatograms. Detection limits for Cl-DAAB using the PA detector were determined to be a 25-fold improvement over the conventional UV detector.

A prototype flow cell design for LC that may be used for laser-induced PA, fluorescence, and photoionization (single- and two-photon) has been described recently (18, 19). The design is similar to the flowing droplet cell (10). The eluent stream is suspended between the column exit and a stainless steel pedestal. A quartz insulator transmits the laser-induced acoustic waves that originate in the eluent to a PZT via the pedestal. BNC connectors are incorporated into the upper end of the cell for the bias voltage and the lower end for the photocurrent and PA signal. A variety of polycyclic aromatic hydrocarbons (PAHs) and drugs have been examined using the three detection methods with ultraviolet nitrogen or excimer laser excitation. As would be expected, the lowest detection limits were produced when fluorescence was detected from species with high quantum efficiencies. Background signals from solvent contaminants were negligible in the photoionization mode, making detection possible even for molecules that gave low photoionization signals. The most at-



**Figure 7.** Diagram of thermal lensing spectrometer

$L_1$ , lens, focal length 40 mm;  $L_2$ , focal length 125 mm;  $L_3$  and  $L_4$ , focal length 100 mm; F, filter, Corning 3-69 (20)

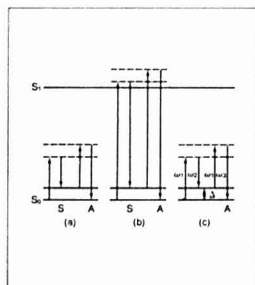
tractive feature of this detector design is that the three major processes for deactivation of the excited state can be monitored simultaneously.

The laser-induced thermal lens effect has been investigated for HPLC detection using a "pump" and "probe" configuration (20). The thermal lens is produced by the excess heat absorbed at the center of a chopped, argon ion laser beam with a Gaussian beam profile (see Figure 7). The optical path at the beam center is reduced, because of the lowered refractive index of the solution, forming a diverging "lens." The light intensity at the beam center of the collinear He-Ne probe laser is detected with a photodiode whose field of view is restricted by an optical fiber. To minimize noise due to break-up of the thermal lens by the solvent flow, the argon ion laser beam is modulated at 125 Hz. The S/N ratio is maintained although the time-dependent signal is reduced at the higher chopping frequencies. As in previous work (21), mechanical vibrations, solvent flow rate fluctuations, and turbulence in the flow cell are the major sources of noise. The overall system performance is similar to photoacoustic detectors for HPLC.

**Laser-Induced Raman Scattering.** HPLC is superior to GC for the analysis of thermally labile, nonvolatile substances, but no qualitative detector has been developed for HPLC that is comparable to a GC/mass spectrometer. Infrared absorption spectrometry provides excellent qualitative information for molecules, but quantitation is limited by low molar absorptivities. Raman spectrometry also yields information-rich vibration-

al spectra (see Figure 8a), but Raman scattering is directly related to source intensity. Therefore, visible or UV lasers produce strong Raman signals, making quantitation simple and analytically useful. Sample handling is uncomplicated because quartz or glass cells can be used.

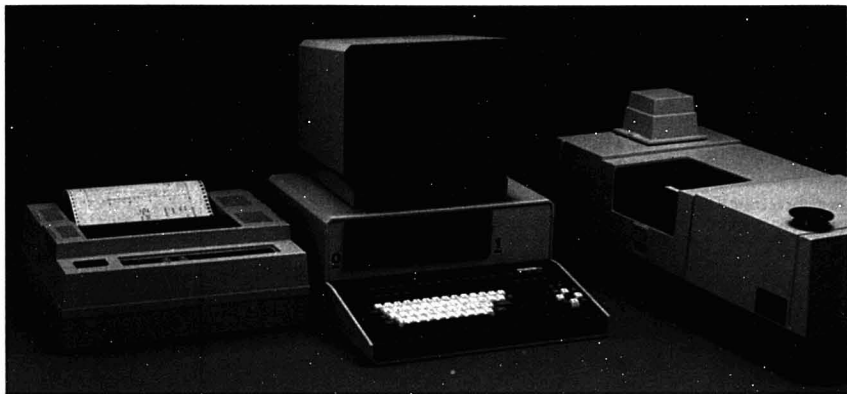
Several new embodiments of the Raman effect retain the advantages of normal (spontaneous) Raman spectrometry while providing the improved sensitivity necessary for useful chromatographic detectors. Resonance enhancement of the Raman effect occurs when the laser wavelength



**Figure 8.** Diagram of Raman scattering processes

(a) Normal Raman; (b) resonance Raman; (c) coherent anti-Stokes Raman, where  $\Delta = \omega_1 - \omega_2$  is a Raman-active molecular vibrational frequency, S = Stokes, A = anti-Stokes. Dashed lines represent virtual levels

# The FT/IR with the most features for the money just added three more.



The Perkin-Elmer Model 1500 FT/IR already goes beyond anything else in the midprice range. With a Fourier transform time at only 0.2 seconds, it's an order of magnitude faster than other systems.

Full spectra (as well as interferograms) can be monitored continuously on the screen while scanning. Data handling software is superior. What's more, continual updating with new features keeps the system expandable to fit your needs.

#### **New MCT detector and diffuse reflectance accessory.**

For example, you can now increase sensitivity up to ten times simply by adding our new mercury cadmium telluride (MCT) detector.

Combine it with the new diffuse reflectance accessory, and such difficult samples as coal powders, paint pigments, pharmaceuticals,

polymer foams, and inorganic solids can be run with an ease and sensitivity not previously considered possible.

#### **New PP-1 thermal printer-plotter.**

The new optional PP-1 thermal printer-plotter does the work of a recorder and a printer in a single unit. In less than a minute, it provides a high-quality plot of the spectrum in any format you select. At the same time, it annotates the axes and lists the scan conditions. It can also print out SEARCH and QUANT reports on the same chart along with the spectra involved.

#### **Data Station, software, graphics.**

A major advantage of the Model 1500 is the Model 3600 IR Data Station — an intelligent microcomputer. It's compatible with the most powerful applications

software anywhere: Perkin-Elmer's CDS, for processing spectra with more than 32 routines; SEARCH, for interpreting unknowns and matching with a library of nearly 3000 spectra; QUANT, for quantitating single and multiple component mixtures.

#### **Read, then invest.**

With all this, plus the use of cool detectors and the potential for even more expansion, the Model 1500 becomes your best investment in IR. For full details, call toll-free **1-800-762-4000**. Or contact your Perkin-Elmer representative or one of the offices below.

Perkin-Elmer Corp., Analytical Instruments,  
Main Ave. (MS-12), Norwalk, CT 06856  
U.S.A. Tel: (203) 762-1000 Telex 965-954  
Bodenseewerk Perkin-Elmer & Co., GmbH,  
Postfach 1120, 7770 Ueberlingen, Federal  
Republic of Germany. Tel: (07551) 811

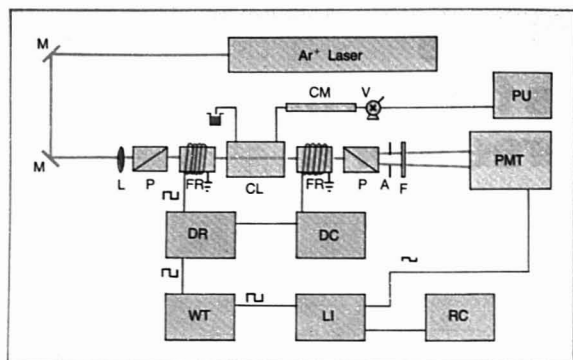
Perkin-Elmer Ltd., Post Office Lane,  
Beaconsfield, Bucks HP9 1QA, England.  
Tel: Beaconsfield (049 46) 6161



## PERKIN-ELMER

Circle 170 For Literature. Circle 171 For a Sales Call.

ANALYTICAL CHEMISTRY, VOL. 55, NO. 1, JANUARY 1983 • 27 A



**Figure 9.** Experimental arrangement for the optical activity detector

M, mirrors; P, Glan prisms; FR, Faraday rotator; CL, flow cell; A, aperture; F, filter; PMT, photomultiplier tube; DR, driver; DC, power supply; WT, wave generator; LI, lock-in amplifier; RC, recorder; PU, pump; V, injection valve; CM, column; L, collimation lens (28)

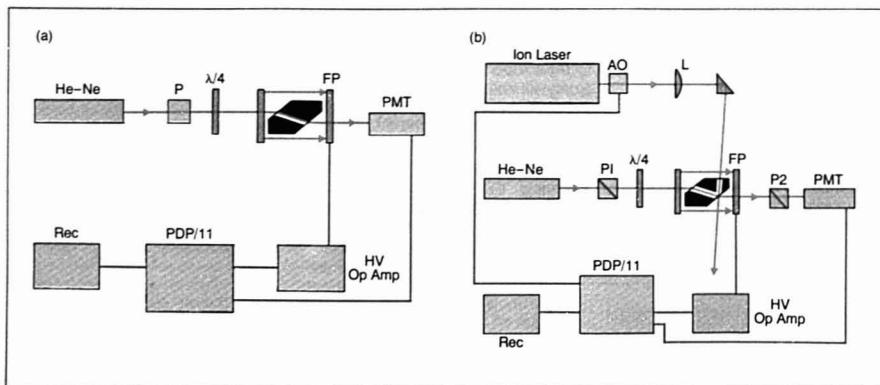
corresponds to the excitation of a vibronic level within an excited electronic state (22). RRS bands may have intensities  $10^2$ – $10^6$  times greater than NRS intensities (where only one photon may be scattered for every  $10^6$  incident photons). Because of the near-resonance excitation, the success of fluorescence discrimination may determine limits of detection (see Figure 8b). Several DAAB derivatives have been detected after HPLC using RRS excited by the 488-nm line of an argon ion laser (23). Monitoring the Raman emission continuously at a single wavelength, a  $2\text{-}\mu\text{g/mL}$  limit of detection has been determined for 2'-Cl-DAAB. Stopped-flow RRS permitted

discrimination among the individual DAAB derivatives, which are not resolved by conventional UV-VIS detection.

Ironically, the first use of Raman spectrometry for HPLC detection involved one of the newer Raman techniques, CARS (24). The generation of a CARS signal requires two lasers ( $\omega_1$  and  $\omega_2$ ). One of these lasers must be tunable; maximum flexibility is available when both are tunable. The CARS process is illustrated in Figure 8c. When the two laser beams cross in the sample at the phase-matching angle  $\theta$ , CARS emission is generated at  $\omega_3 = 2\omega_1 - \omega_2$  via a third-order nonlinear polarization (25). The

CARS technique provides much greater efficiencies than NRS (up to 1 photon scattered per 100 incident photons). A detection limit of  $1\text{ }\mu\text{g/mL}$  has been determined for trans- $\beta$ -carotene using CARS (24). Fluorescence can be rejected by detecting the "laserlike" CARS beam at an angle removed from other emission. Background emission resulting from the nonresonant, third-order susceptibility of the solvent has limited the sensitivity of CARS in solution. Two techniques, resonance enhancement and polarization, have been used to suppress the background with some success, but CARS remains marginally useful for most trace analysis. A computer-controlled system has been developed that measures the UV-VIS and fluorescence spectra of HPLC eluents, in addition to the CARS spectrum (26). Computer control is very important for the routine use of CARS because the laser frequency ( $\omega_2$ ) must be controlled, and mirrors must be adjusted to obtain the proper crossing angle after the optimum Raman excitation wavelength has been calculated from a UV-VIS spectrum. In this instrument, the UV-VIS spectrum is acquired on-line with a vidicon multichannel detector. Fluorescence detection with a xenon lamp source is incorporated to extend the capability of the instrument to trace analysis. Recently, HPLC-CARS has been used for the identification of environmental pollutants in water (27).

**Other Laser-Based Detectors.** A laser-based micropolarimeter has been interfaced to an HPLC (28). Using selected Glan prisms, selected cell-window material, and air-based Faraday rotators, extinction ratios have been obtained that are four orders of mag-



**Figure 10.** Laser-based refractive index detectors

(a) Refractive index detector: He-Ne, single-frequency laser; P, polarizer;  $\lambda/4$ , quarter wave plate; FP, interferometer; PMT, photo-multiplier tube; REC, chart recorder; (b) Absorbance detector: P1, P2, polarizers; AO, Bragg cell; L, lens (29)

# We'll take care of your trace analysis problems from AA to Zeeman.



Zeeman effect atomic absorption spectrophotometry, or ZAA, gives the analyst what he's been seeking for years: the capability of correcting accurately for very high levels of background or non-specific absorption, so important when trace elements are determined in very complex matrices.

The Zeeman/5000 is Perkin-Elmer's newest contribution to Graphite Furnace technology, a field we've been dominating for years. It combines

the HGA-500 furnace with a new approach to ZAA, TRACZ™ (Transverse AC Zeeman), providing superb background correction at levels of up to 2.0 A.

The Zeeman/5000 is an accessory to our computer-controlled Model 5000 AA spectrophotometer. It's permanently mounted to the right of the Model 5000, so you can switch from ZAA to double-beam flame atomic absorption (with UV/VIS background correction, if needed) in a second.

What's more, you can combine our Zeeman/5000 with our AS-40 Autosampler for automatic sequential determination of six elements in as many as 35 samples, including fully automatic standard addition and matrix modification.

Add our Atomic Spectroscopy Data System 10 to display and store high-resolution Graphite Furnace graphics. You'll have an outstanding tool for methods development.

The Zeeman/5000 is the perfect choice for the analysis of complex matrices. For many other applications, a combination of our HGA Graphite Furnaces with any of our AA spectrophotometers will do the job beautifully.

We'll send you all the details on how the new Perkin-Elmer Zeeman/5000 fulfills your analytical requirements. For free literature, contact your Perkin-Elmer representative or write us today.

Perkin-Elmer Corp., Analytical Instruments,  
Main Ave. (MS-12), Norwalk, CT 06856  
U.S.A. Tel. (203) 762-1000

Bodenseewerk Perkin-Elmer & Co. GmbH,  
Postfach 1120, 7770 Ueberlingen, Federal  
Republic of Germany Tel. (07551) 811

Perkin-Elmer Ltd., Post Office Lane,  
Beaconsfield, Bucks HP9 1QA, England  
Tel: Beaconsfield 6161

## PERKIN-ELMER

Circle 168 for literature. Circle 169 for a sales call.



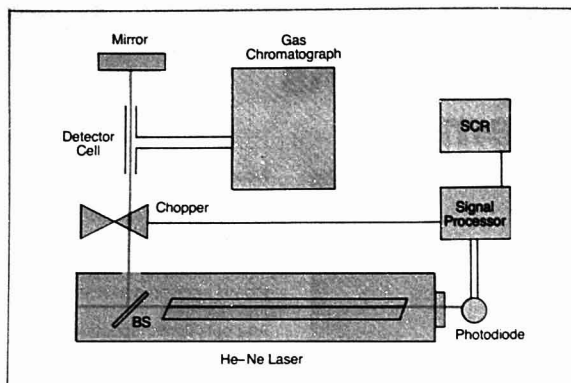


Figure 11. Diagram of double-beam He-Ne laser intracavity absorption detector. BS, beam splitter; SCR, strip chart recorder (32)

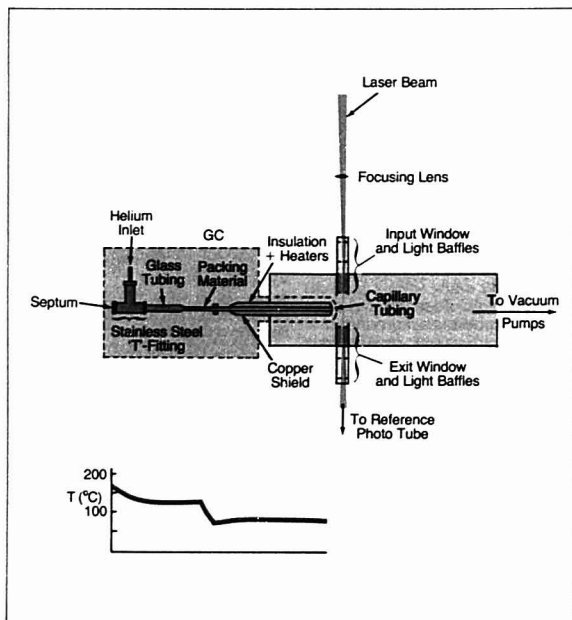


Figure 12. Diagram of the RCLIF/GC apparatus. The portion enclosed by the dotted line forms a simple GC. Temperature variation along the column is shown in the inset (34)

nitude better than standard polarimeters (see Figure 9). Most chromatographic eluents are not optically active so that this detector is very selective, with particular applicability to environmental and clinical systems. The

HPLC separation of fructose and raffinose based on optical activity has been demonstrated with a  $0.5\text{-}\mu\text{g}$  detection limit in a  $200\text{-}\mu\text{L}$  detection volume. The optically active components of human urine also have been

detected after HPLC separation.

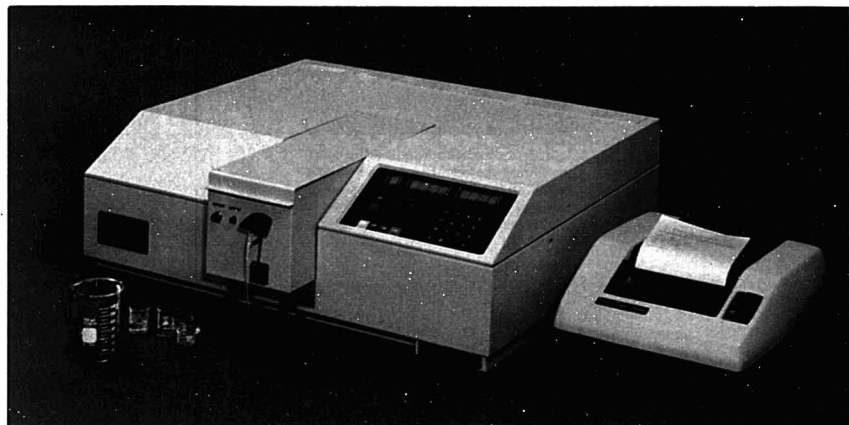
One of the most sensitive ways to measure small differences in refractive indexes is interferometry. A single-frequency laser has been used to measure the change in refractive index for a substance contained within a Fabry-Perot interferometer (29). A photomultiplier detects the transmitted light when the Fabry-Perot is scanned (see Figure 10a). The position of the maximum constructive interference is determined by a computer and converted to an analog signal that represents the change in refractive index. The additional finesse and the increased monochromaticity of the He-Ne laser provide an order-of-magnitude improvement in detection limits compared to commercial refractive index detectors. By modifying the detector cell to include a second path for an argon ion laser beam, sample absorption has been indirectly monitored as a change in refractive index due to heating of the medium (see Figure 10b). The difference in interferometric peak position before and after irradiation is plotted as an absorption chromatogram. This approach has produced limits of detection two orders of magnitude better than standard absorption detectors for HPLC.

#### Laser-Based Detectors for Chromatography

Laser-based detectors for GC have received relatively little attention because of the high resolving power of GC, which reduces the need for selective detectors, and the availability of sensitive and selective conventional detectors. Only four laser-based detectors for GC have been reported to date (30-34). Two of these will be discussed because they represent the extremes of complexity and expense. They also demonstrate the additional selectivity and sensitivity that can be provided by laser-based GC detectors.

A He-Ne laser operating simultaneously at  $3.39\text{ }\mu\text{m}$  (infrared) and  $0.63\text{ }\mu\text{m}$  (visible) has been used as a selective detector for hydrocarbons in the effluent of a GC (32). The infrared and visible laser transitions originate at the same energy level and are competitive. When a hydrocarbon enters the laser's resonant cavity, the  $3.39\text{-}\mu\text{m}$  energy is absorbed due to the C-H stretching vibration, and the visible emission is enhanced. The visible laser emission is monitored with a photodiode as a quantitative measure of the concentration of the absorbing molecule (see Figure 11). The minimum detectable concentration for propane using the double beam configuration is  $20\text{ pg/mL}$  (33), which is 25 times lower than the best value reported for a thermal conductivity detector. In practice, the detector's selectivity for

# Lambda 1- for your UV-Vis quantitative analyses. It's easy to use and starts at \$3995.\*



**Lambda 1- easy to use, with the best price/performance ratio in its class.**

Lambda 1 is designed to help solve your quantitative analysis problems. Its very logical keyboard makes it easy to use so that the large sample demands of your laboratory can be easily handled without long and costly delays. The built-in software includes all the features you require for quantitative analysis. Auto-concentration and the automatic calculation and display of the concentration factor allow for increased sample throughput and accurate results. Our unique Safe Memory feature lets you store up to nine different analytical methods, minimizing the time required for instrument setup.

**A complete range of accessories make Lambda 1 more versatile.**

A wide range of accessories further expands the use of Lambda 1 so that more specific applications can be addressed. Sippers, an automatic multi-sampler, printer and long path cell holder are only a few of the many sample handling aids available. All of these can be quickly interfaced to Lambda 1.

**Excellent optical performance for accurate/reproducible results.**

Low stray light, high resolution, a wide dynamic operating range and a unique auto-zero design provide the kind of performance you need for those demanding sample applications.

**Get more information, fast and easy with this Toll Free number.**

For more information call 800-323-7155 (in Illinois call 312-887-0770) or circle the reader service number below. If you prefer contact one of the offices below.

*\*Price U.S.A. List Only.*

Perkin-Elmer Corp. Analytical Instruments,  
Main Ave. (MS-12) Norwalk, CT 06856  
U.S.A. Tel. (203) 762-1000

Bodenseewerk Perkin-Elmer & Co., GmbH,  
Postfach 1120 7770 Ueberlingen, Federal  
Republic of Germany. Tel. (07551) 811

Perkin-Elmer Ltd., Post Office Lane,  
Beaconsfield, Bucks HP9 1QA, England  
Tel. Beaconsfield (049 46) 6161

## PERKIN-ELMER

Circle 173 for literature. Circle 174 for sales call.

hydrocarbons is modified by various substituents. The detector responds to aliphatic and aromatic hydrocarbons with aliphatic side chains, except for those substituted with halogens. The He-Ne laser intracavity absorption detector may be used without prior separation in some cases (e.g., methane in coal mines). This detector operates with nitrogen carrier gas without sacrificing sensitivity and should be useful for monitoring organic pollutants since it does not respond to water or carbon dioxide. Also, it should be possible to manufacture this detector at competitive prices.

The last method to be discussed uses the GC for quantitative sample introduction rather than separation. A GC has been coupled with a supersonic jet to resolve mixtures by rotationally cooled laser-induced fluorescence (RCLIF) (34). When a monoatomic gas seeded with molecules is allowed to expand through a supersonic jet, a molecular beam is produced in a nearly collision-free environment. The extremely low temperature of the molecular beam permits the acquisition of highly resolved laser-excited fluorescence spectra. Figure 12 shows the apparatus for RCLIF/GC. Otherwise unresolved mixtures of two isomers of methylphenylthene have been separately detected by using the appropriate excitation wavelength from a Nd:YAG pumped-dye laser. Detection limits in the picogram range have been reported. Other excitation schemes such as photoionization may be used as well. Although the laser system required for this application is complex and expensive, excellent selectivity and sensitivity are possible. The introduction of the GC simplifies the RCLIF experiment so that it may be useful for routine laboratory applications.

## Conclusions

The evolution of laser-based detectors for chromatography continues to be a dynamic process. Some of the detectors discussed here seem to be on the verge of acceptance while others require further experimental validation. The most attractive detectors for commercialization use gas lasers that are reliable, easy to use, and relatively inexpensive. Normal Raman spectroscopy has become a routine laboratory technique using this type of laser.

The success of GC/MS suggests that there may be a market for more complex and expensive laser-based detectors. Since there is a growing number of multiuser laser facilities, another approach might involve the marketing of detector/interfaces for use with the customer's laser.

The need for laser-based detectors for HPLC is unquestionable with the

trend toward improving column efficiencies via microscale instrumentation. Unparalleled growth of laser-based detectors for GC seems less likely, although gains in selectivity and sensitivity may be made here as well. Future developments in this area will probably involve the use of the GC for simple, quantitative sample introduction rather than high-resolution separation. The present state of the art suggests that laser-based detectors provide the sensitivity and selectivity necessary to augment advances in separation science.

## Acknowledgment

The author acknowledges the cooperation of the scientists whose work is reviewed here. The technical assistance of Dan Puckett and Monica Mabie is also appreciated.

## References

- Matthews, T. G.; Lytle, F. E. *Anal. Chem.* 1979, 51, 583-85.
- Gordon, J. P.; Leite, R. C. C.; Moore, R. S.; Porto, S. P. S.; Whinnery, J. R. *J. Appl. Phys.* 1965, 36, 3.
- Yeung, E. S. In "Lasers in Chemical Analysis"; Hieftje, G. M.; Travis, J. C.; Lytle, F. E., Eds.; Humana Press: Clifton, N.J., 1981; Chapter 14, pp. 273-90.
- Wright, J. C.; Wirth, M. J. *Anal. Chem.* 1980, 52, 108-95 A.
- Ouano, A. C.; Kaye, W. J. *Polym. Sci., Polym. Chem. Ed.* 1974, 12, 1151-62.
- Cazes, J. J. *Chem. Ed.* 1966, 43, A625-42.
- Kaye, W. *Anal. Chem.* 1973, 45, 221-25 A.
- Ouano, A. C. *J. Chromatogr.* 1976, 118, 303-12.
- Yeung, E. S.; Sepaniak, M. J. *Anal. Chem.* 1980, 52, 1465-70 A.
- Diebold, G. J.; Zare, R. N. *Science* 1977, 196, 1439-41.
- Hershsberger, L. W.; Callis, J. B.; Christian, G. D. *Anal. Chem.* 1979, 51, 1444-46.
- Sepaniak, M. J.; Yeung, E. S. *J. Chromatogr.* 1980, 190, 377-83.
- Folestad, S.; Johnson, L.; Joffe, B.; Galle, B. *Anal. Chem.* 1982, 54, 925-29.
- McClain, W. M. *Acc. Chem. Res.* 1974, 7, 129-35.
- Sepaniak, M. J.; Yeung, E. S. *Anal. Chem.* 1977, 49, 1554-56.
- Huff, P. B.; Tromberg, B. J.; Sepaniak, M. J. *Anal. Chem.* 1982, 54, 946-50.
- Oda, S.; Sawada, T. *Anal. Chem.* 1981, 53, 471-74.
- Voightman, E.; Jurgensen, A.; Winefordner, J. D. *Anal. Chem.* 1981, 53, 1921-23.
- Voightman, E.; Winefordner, J. W. *Anal. Chem.* 1982, 54, 1834-39.
- Buffett, C. E.; Morris, M. D. *Anal. Chem.* 1982, 54, 1824-25.
- Dovilo, N. J.; Harris, J. M. *Anal. Chem.* 1981, 53, 689-92.
- Morris, M. D.; Wallan, D. J. *Anal. Chem.* 1979, 51, 182-92 A.
- Saito, S.; Teramae, N.; Tanaka, S. *Nippon Kagaku Kaishi* 1980, 9, 1363-66.
- Rogers, L. B.; Stuart, J. D.; Goss, L. P.; Malloy, T. B., Jr.; Carreira, L. A. *Anal. Chem.* 1977, 49, 959-62.
- Harvey, A. B. *Anal. Chem.* 1978, 50, 905-12A.

- Boutlier, G. D.; Irwin, R. M.; Antcliff, R. R.; Rogers, L. B.; Carreira, L. A.; Azarraga, L. *Appl. Spectrosc.* 1981, 35, 576-81.
- Carreira, L. A. et al. In "Chemical Applications of Nonlinear Raman Spectroscopy"; Harvey, A. B., Ed.; Academic Press: New York, 1981; Chapter 8.
- Yeung, E. S.; Steenhoek, L. E.; Woodruff, S. D.; Kuo, J. C. *Anal. Chem.* 1980, 52, 1399-1402.
- Woodruff, S. D.; Yeung, E. S. *Anal. Chem.* 1982, 54, 1174-78.
- Kreuzer, L. B. *Anal. Chem.* 1978, 40, 597-606 A.
- Klimcak, C. M.; Wessel, J. E. *Anal. Chem.* 1980, 52, 1233-39.
- Parli, J. D.; Green, R. B. *Anal. Chem.* 1982, 52, 1969-72.
- Parli, J. D.; Green, R. B. "Abstracts of Papers," 185th National Meeting of the American Chemical Society, Seattle, Wash., March 1983; American Chemical Society: Washington, D.C.
- Hayes, J. M.; Small, G. J. *Anal. Chem.* 1982, 54, 1202-4.

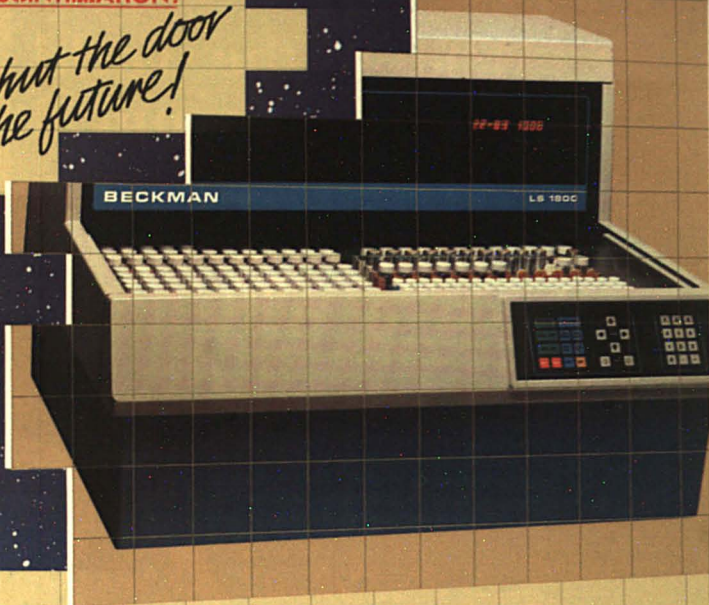
The author acknowledges the support of Matching Fund Grant 14-34-0001-1205 from the Office of Water Research and Technology, Department of the Interior, and the University of Arkansas. The support of the National Science Foundation is also appreciated. This work was presented in part during the symposium, "Routine Applications of Lasers: Present or Future," at the 9th Annual Meeting of the Federation of Analytical Chemistry and Spectroscopy Societies, Philadelphia, Pa., September 1982.



Robert Green is an associate professor of chemistry at the University of Arkansas, Fayetteville. He received a BS in chemistry from Oklahoma State University in 1966 and a PhD in chemistry from Ohio University in 1974. In the years between 1966 and 1970, he was a chemist with Monsanto Company and Jefferson Chemical Company, Inc. Green served as a National Research Council postdoctoral research associate at the National Bureau of Standards, Washington, D.C., from September 1974 to August 1976, and was an assistant professor of chemistry at West Virginia University, Morgantown, from 1976 to June 1979. His major research interest is the application of lasers to the solution of problems in analytical chemistry. Recently, Green has become interested in laser-based detectors for chromatography. Other research has involved the development and characterization of the optogalvanic effect and laser-enhanced ionization spectrometry.

## LIQUID SCINTILLATION:

*Don't shut the door  
on the future!*



Beckman's LS 1800 bench-top, rack counter system starts where the other systems stop. In its standard format, the performance and ease of use of the LS 1800 already has a "top-of-the-range" feel. But here's the difference - you can add to the LS 1800 your selection from a number of optional modules, to design exactly the LS Counter you need. As your needs change in the future, your LS 1800 can change with you.

**The top of the range, today.** Even without any additional modules, the LS 1800 is impressive. Automatic counting is a single pushbutton operation. For quick single counts, just push another button. • Rack loading for 336 standard or 648 miniature vials. • Bright, easy-to-read display of sample activity and counting time. • Built-in printer, presenting program summary, sample data and final answer, even for dual label DPM. • Three adjustable counting channels, preset to the most common isotopes, for fast, easy counting. • Fully automatic calibration in under 60 seconds. • Self-diagnostic tests, to assure you that everything is working well. • Built-in RS232 computer interface.

**The future - your choice.** Then, when you are ready, add the necessary modules to mould your LS 1800 to your exact needs.

Add Versa-Rack™, to count both mini-

vials and standard vials together, without adaptors, at the same time. Add Beckman's unique H (Horrocks) number module, to give unequalled counting precision. Add the exclusive two-phase monitor, to detect phase separation. Add multi-user programming, so you can store often-used programs. Add a 40-character alphanumeric display package to make program changes even easier. Add single and dual label DPM, digital integration, single photon monitor, 80 column printer, video display package. Add just what you need, change it when you want to. Before you shut the door on the future by deciding on a system that is less flexible, versatile and powerful, ask for full details of Beckman's LS 1800 Counter and the other counters in our 5800 range, plus our cock-tails and vials.

Write now to:

Beckman Instruments International SA,  
17, rue des Pierres-du-Niton, CH-1211  
Geneva 6, Switzerland.



# BECKMAN

Systems solving your problems

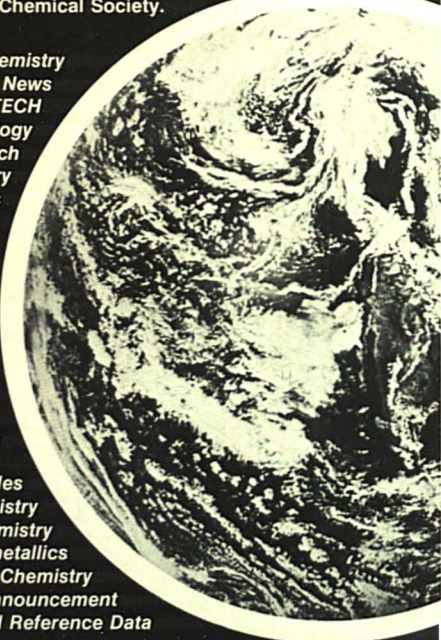


# What in the world isn't chemical

## —and how do you keep up with it all?

You keep current with developments by subscribing to the timely, authoritative, comprehensive journals published by the American Chemical Society.

*Analytical Chemistry*  
*Chemical & Engineering News*  
*CHEMTECH*  
*Environmental Science and Technology*  
*Accounts of Chemical Research*  
*Biochemistry*  
*Chemical Reviews*  
*Industrial & Engineering Chemistry*  
*—Process Design and Development*  
*Industrial & Engineering Chemistry*  
*—Product R&D*  
*Industrial and Engineering Chemistry*  
*—Fundamentals*  
*Inorganic Chemistry*  
*Journal of Agricultural & Food Chemistry*  
*Journal of the American Chemical Society*  
*Journal of Chemical & Engineering Data*  
*Journal of Chemical Information and Computer Sciences*  
*Macromolecules*  
*Journal of Medicinal Chemistry*  
*The Journal of Organic Chemistry*  
*Organometallics*  
*The Journal of Physical Chemistry*  
*ACS Single Article Announcement*  
*Journal of Physical and Chemical Reference Data*

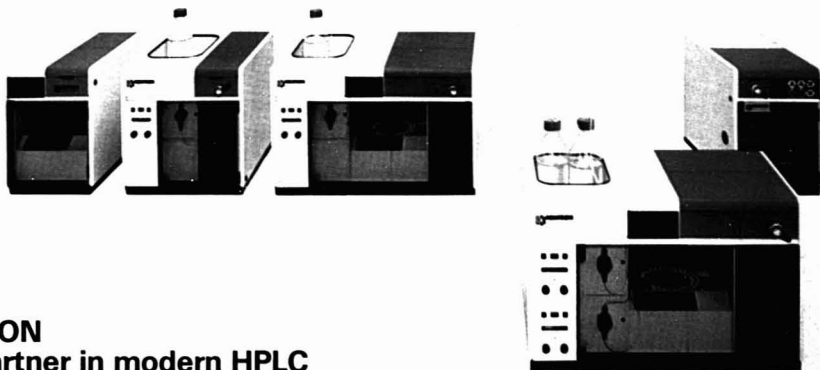


TOLL FREE: U.S. New Orders Only (800) 424-6747  
Cable Address: JIECHEM — Telex: 440159 ACSP UI or 892582 ACSPUBS

AMERICAN CHEMICAL SOCIETY PUBLICATIONS  
1155 Sixteenth Street, N.W., Washington, D.C. 20036 U.S.A.

Looking for a  
compact AND  
flexible HPLC  
instrument?

# HPLC<sup>600</sup>



**KONTRON**  
Your partner in modern HPLC



**KONTRON**  
**ANALYTICAL**

Australia (Sydney) (02) 9383433  
Austria (Vienna) (0222) 670631  
Canada (Mississauga) (416) 6781151  
France (Vélizy) (3) 9469722

Germany (Munich) (08165) 771  
Great Britain (St. Albans) (0727) 66222  
Italy (Milan) (02) 50721  
Japan (Tokyo) (03214) 5371

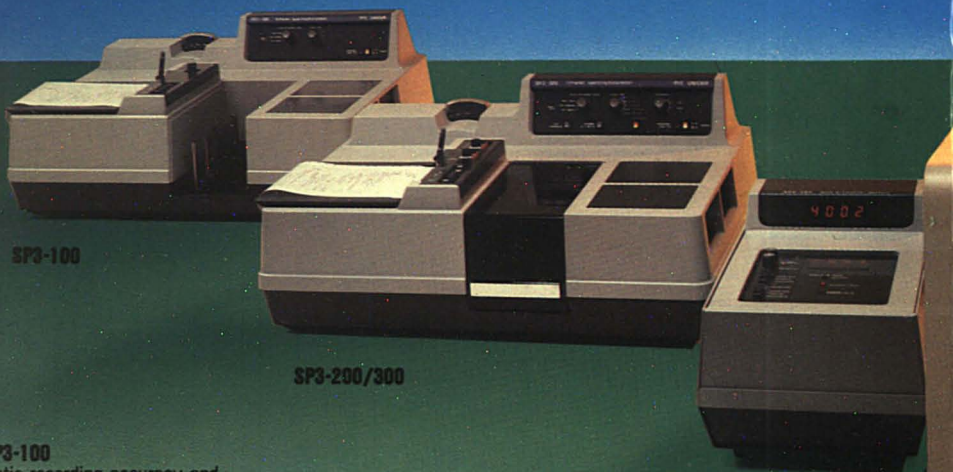
Netherlands (Maarsse) (03465) 60894  
Spain (Madrid) (01) 7291155  
Sweden (Täby) (08) 7567330  
Switzerland (Zurich) (01) 435 4111

U.S.A.: Kontron Electronics Inc., 630 Price Avenue, Redwood City/California 94063, (415) 3611012

CIRCLE 119 ON READER SERVICE CARD



# No more searching. It's Pye Unicam IR at every level.



#### **SP3-100**

Ratio recording accuracy and reproducibility, just like the others in the range. Ideal for routine laboratory and teaching applications.

#### **SP3-200/300**

Offer full flexibility for research work. The SP3-300 has an extended range, to 200 wavenumbers.

#### **SP3-050**

Data processing systems for the SP3-200/300. Option 3 will interface with laboratory computer or teleprinter.

#### **SP3-080**

The most powerful yet friendly infrared data console available. Interfaces with a video printer.

Capable of full spectrum manipulation and also infrared Library Search, Pye Unicam's latest software release.

#### **Library Search**

Software for the SP3-080 which helps identify unknown spectra more quickly and accurately than ever before. It offers you the opportunity to build up your own specialist library, as well as providing libraries of standard spectra. A numeric coding system contains up to 5,000 classes for your own information to be added to

the infrared data. So flexible is the new system, it even enables you to carry out an IR search of standard or personalised libraries using this information from other techniques.

**For further information about Pye Unicam IR spectrophotometers circle inquiry no. 70**

**For details of Pye Unicam IR data handling circle inquiry no. 71**





## LIBRARY SEARCH

### Wide LC choice

Every level of sophistication in liquid chromatography is represented in three Pye Unicam systems.

You can choose the most powerful methods development system on the market or integrated gradient and isocratic systems with a choice of detectors.

**Reader inquiry no. 72**

### STOP PRESS

Now with Ion Chromatography capability

Circle inquiry no. 83

### Revelations in AA

Pye Unicam's PU 9000 is the world's only intelligent, fully automatic, multi-element atomic absorption system. It will select and optimise conditions for all elements that can be determined by the technique, incorporates many other advances, yet is simply controlled by a single keyboard.

**Reader inquiry no. 73**

Everything you need in video atomic absorption is offered by the SP9 video AA system.

**Reader inquiry no. 74**

Circle the appropriate inquiry number for further information about Pye Unicam products.

	Inquiry No.
IR spectrophotometers	70
IR data handling	71
Liquid chromatography systems	72
PU 9000 AA system	73
SP9 video AA system	74
UV/VIS spectrophotometers	75
Gas chromatography	76
Electrochemistry instruments	77
Nuclear analysis	78

### Pye Unicam Ltd

A SCIENTIFIC AND INDUSTRIAL COMPANY OF PHILIPS  
York Street Cambridge Great Britain CB1 2PX  
Telephone (0223) 358866 Telex 817331

# PHILIPS

# Pye Unicam GC sets the parameters for value

Consider the challenge if you want the best value and choice in gas chromatography. The optimum instrument for your application.

Issue the challenge by telling Pye Unicam all about it. What you expect from the chromatograph. What you expect for your budget.





# Challenge us!

Proof that Pye Unicam GC sets the parameters will be offered by:

- The PU 4500s – the series now boasts no fewer than 10 value-for-money versions, including those for capillary and thermal conductivity, and three dedicated instruments for popular industrial applications.
- The PU 4750 headspace analyser – offering the most cost-effective solution to many problems raised by 'difficult' samples.
- An expanded series of low-cost computing integrators now offering a better choice of facilities than any competitive range.

Pye Unicam proves its case to thousands of analysts every day. Challenge us to give you the best. We guarantee no other GC manufacturer can surpass us for value, performance, choice or back-up.

First get the facts. **Circle reader inquiry no. 79** for a copy of the Pye Unicam gas chromatography range brochure – and/or **no. 80** for the new GC accessory brochure.

## Budget beaters in UV/Visible

Pye Unicam can beat any budget with its low-cost UV/VIS ranges.

Choose from four robust, easy to operate SP6 models, meter or digital, VIS or UV/VIS.

**Reader Inquiry no. 81**



For keyboard-controlled scanning at an economical price you can't better the SP7-500. It offers a built-in printer, 1st and 2nd derivative spectra, a 4-cell turret and much more.

**Reader Inquiry no. 82**

Circle the appropriate inquiry number for further information about Pye Unicam products.

**Inquiry No.**

<b>Gas chromatography range</b>	<b>79</b>
<b>Gas chromatography accessories brochure</b>	<b>80</b>
<b>SP6 UV/VIS range</b>	<b>81</b>
<b>SP7-500 UV/VIS spectrophotometer</b>	<b>82</b>

### Main Distributors

**Australia** Philips Industries SIED Ltd, 25-27 Paul Street, North Ryde, NSW. Tel: 888 8222. **Belgium** M.B.L.E. SA, 80 Rue des Deux Gares, Brussels 7. Tel: 523000. **Canada** Canadian Laboratory Supplies Ltd, 80 Juliet Road, Toronto, Ontario M8Z 2M4. Tel: 416 252 5151. **France** SA Philips Industrielle et Commerciale, 105 Rue de Paris, 93002, Bobigny. Tel: Paris 830 1111. **Holland** Philips Nederland BV, Boschweg 525, Eindhoven. Tel: 788211. **Ireland** P.J. Brennan & Co. Ltd, Unit 61, Stillorgan Industrial Estate, Sandymount Co. Dublin. Tel: 952501. **Italy** Philips S.p.A. Viale Einaudi 2, 20092 Monza. Tel: 3635233. **India** Penco Electronics & Electricals Ltd, Shivraj Estate, Block A, Dr. Ambedkar Road, Worli, Bombay 400 018. Tel: 331431. **Japan** Nihon Philips Corp., Shima Shinagawa Bldg, 7th Floor, 26-33, Tananawa 3-Chome, Minato-Ku, Tokyo 108. Tel: 448 3611. **New Zealand** Philips Electrical Industries of NZ Ltd, P.O. Box 2097, 181 Wakefield Street, Wellington. Tel: 859-859. **Portugal** Philips Portuguesa S.A.R.L., Av. Eng. Duarte Pacheco 6, Lisbon 1. Tel: 633121. **Spain** Philips Iberica SAE, Martinez Villagas 2, Madrid 27. Tel: 484 22 00. **Sweden** Svenska AB Philips, S-115 84 Stockholm. Tel: 6350000. **Switzerland** Philips AG, Alnendstrasse 140, Postfach, CH-8027 Zurich. Tel: 43211. **South Africa** South African Philips (Pty) Ltd, P.O. Box 7703, Johannesburg 2000. Tel: 8143411. **West Germany** Philips GmbH, 35 Kassel - B. Miramont 87. Tel: 0561 5010.

## Pye Unicam Ltd

A SCIENTIFIC AND INDUSTRIAL COMPANY OF PHILIPS

York Street Cambridge Great Britain CB1 2PX  
Telephone (0223) 358866 Telex 817331

# PHILIPS

# the KONTRON Double Beam UV/VIS Stars are in the ascendency

## UVIKON® 810 now from SFr. 16660,-\*



The UVIKON® 810/820 Double Beam Spectrophotometers are having so much worldwide success that KONTRON can reduce prices. NOW is the time for you to find out the reasons for the success.

 **KONTRON  
ANALYTICAL**

Austria (Vienna) (0222) 670631  
France (Montigny le Br.) (3) 0438152  
Germany (Munich) (08165) 771  
Great Britain (St. Albans) (0727) 66222

Italy (Milan)  
Japan (Tokyo)  
Netherlands (Maarsse) (03465) 60894  
Spain (Madrid)

For further information contact your local KONTRON Company or KONTRON headquarters

KONTRON AG, Analytical International,  
Bernerstrasse Süd 169, CH-8048 Zürich, Switzerland

(02) 50721  
(03) 2634801  
(03465) 60894  
(01) 7291155

Sweden (Täby) (08) 7567330  
Switzerland (Zürich) (01) 4354111  
USA (Everett/Mass.) (617) 3896400

\* UVIKON 810 DB Spectrophotometer SFr. 16660,-  
(without recorder). In some countries this price does not  
include installation, warranty and taxes. Prices subject to  
change without notice.

CIRCLE 120 ON READER SERVICE CARD

**Just published!**

Current . . . comprehensive . . . complete! An overview of developments in the past ten years. . . .

## INSTRUMENTATION IN ANALYTICAL CHEMISTRY, VOL. 2

*just  
published!*

Stuart A. Borman, Editor

Reprinted from the pages of *Analytical Chemistry*, this volume brings together articles on • **Signal Processing and Image Analysis** • **Computers** • **Atomic and Molecular Spectroscopy** • **Electroanalytical Chemistry** • **GC and LC** • **Hyphenated Methods** • **MS** • **Surface Analysis** • **NMR** • **Flow Methods** • and more.

A must for analytical chemists and all scientists who use analytical techniques in their work. **Essential reference** work for academic, government, and industrial libraries.

414 pages (1982) Clothbound US & Canada \$31.95 Export \$38.95

Special Paperbound Student Edition—Minimum Order 10 Copies

Each copy US & Canada \$14.95 Export \$17.95

Mail this card back today to order your books. Or, for faster processing, call TOLL-FREE (800) 424-4747 and charge your VISA or MasterCard.

YES, please send \_\_\_\_\_ copies of *Instrumentation in Analytical Chemistry, Vol. II*.

☐ Payment enclosed.

☐ Purchase order enclosed.

Charge my ☐ VISA ☐ MasterCard. Account No. \_\_\_\_\_

Expires \_\_\_\_\_ Interbank No. \_\_\_\_\_ (MasterCard only)

Signature \_\_\_\_\_

Ship to Name \_\_\_\_\_

Address \_\_\_\_\_

City, State, Zip \_\_\_\_\_

ORDERS MUST BE PREPAID.

13

**Just published!**

Current . . . comprehensive . . . complete! An overview of developments in the past ten years. . . .

## INSTRUMENTATION IN ANALYTICAL CHEMISTRY, VOL. 2

*just  
published!*

Stuart A. Borman, Editor

Reprinted from the pages of *Analytical Chemistry*, this volume brings together articles on • **Signal Processing and Image Analysis** • **Computers** • **Atomic and Molecular Spectroscopy** • **Electroanalytical Chemistry** • **GC and LC** • **Hyphenated Methods** • **MS** • **Surface Analysis** • **NMR** • **Flow Methods** • and more.

A must for analytical chemists and all scientists who use analytical techniques in their work. **Essential reference** work for academic, government, and industrial libraries.

414 pages (1982) Clothbound US & Canada \$31.95 Export \$38.95

Special Paperbound Student Edition—Minimum Order 10 Copies

Each copy US & Canada \$14.95 Export \$17.95

Mail this card back today to order your books. Or, for faster processing, call TOLL-FREE (800) 424-4747 and charge your VISA or MasterCard.

YES, please send \_\_\_\_\_ copies of *Instrumentation in Analytical Chemistry, Vol. II*.

☐ Payment enclosed.

☐ Purchase order enclosed.

Charge my ☐ VISA ☐ MasterCard. Account No. \_\_\_\_\_

Expires \_\_\_\_\_ Interbank No. \_\_\_\_\_ (MasterCard only)

Signature \_\_\_\_\_

Ship to Name \_\_\_\_\_

Address \_\_\_\_\_

City, State, Zip \_\_\_\_\_

ORDERS MUST BE PREPAID.

13





NO POSTAGE  
NECESSARY  
IF MAILED  
IN THE  
UNITED STATES

**BUSINESS REPLY CARD**

FIRST CLASS PERMIT NO. 10094 WASHINGTON, D.C.

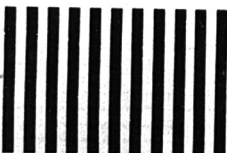
POSTAGE WILL BE PAID BY ADDRESSEE

AMERICAN CHEMICAL SOCIETY

Distribution Center, Dept. 13

1155 Sixteenth Street, N.W.

Washington, D.C. 20036



NO POSTAGE  
NECESSARY  
IF MAILED  
IN THE  
UNITED STATES

**BUSINESS REPLY CARD**

FIRST CLASS PERMIT NO. 10094 WASHINGTON, D.C.

POSTAGE WILL BE PAID BY ADDRESSEE

AMERICAN CHEMICAL SOCIETY

Distribution Center, Dept. 13

1155 Sixteenth Street, N.W.

Washington, D.C. 20036



**Just published!**

*New techniques that can save you valuable time and money!*

Essential state-of-the-art information for all scientists who use analytical techniques in their work!

## **INSTRUMENTATION IN ANALYTICAL CHEMISTRY, VOL. 2**

Stuart A. Borman, Editor

An anthology of articles on developments in analytical techniques in the past ten years—from the volumes of *Analytical Chemistry*.

**CONTENTS** Signal Processing and Image Analysis • Computers and Laboratory Data Management • Atomic and Molecular Spectroscopy • Electroanalytical Chemistry • Gas and Liquid Chromatography • Hyphenated Methods • Mass Spectrometry • Surface Analysis • Nuclear Magnetic Resonance • Flow Methods • Laboratory Instrumentation  
414 pages (1982) Clothbound  
US & Canada \$31.95 Export \$38.95  
Special Student Paperbound Edition Available—Minimum Order 10 Copies  
US & Canada \$14.95 Export \$17.95

Multi-nuclei NMR, highest field NMR, NMR in solids, and more. . .

## **NMR SPECTROSCOPY: NEW METHODS AND APPLICATIONS**

George C. Levy, Editor

Current work in new areas of NMR spectroscopy is treated in the comprehensive volume

**CONTENTS** Ultra High-Field NMR • NMR Spectroscopy at 600 MHz • Two-Dimensional Fourier Spectroscopy • Quadrupolar Metallic Nuclei • Deuterium NMR Spectroscopy • Metabolism of  $^{13}\text{C}$  Labeled Substrates • Chemical Bond Labeling and Double-Cross Polarization NMR • NMR Spectroscopy at High Pressure •  $^{13}\text{C}$  Cross Polarization Magic Angle Spinning NMR • NMR of Linear and Cyclic Peptides •  $^1\text{P}$  NMR Studies •  $^{13}\text{C}$  NMR Studies of DNA Dynamics • Photo-Chemically Induced Nuclear Polarization of Biological Molecules •  $^{13}\text{C}$  NMR Characterization of Solid Fossil Fuels • Polyester Thermoplastic Elastomers •  $^{23}\text{Na}$  NMR Studies  
388 pages (1982) Clothbound  
US & Canada \$49.95 Export \$59.95

Up-to-date research results in this emerging interdisciplinary area of chemistry. . .

## **CHEMICALLY MODIFIED SURFACES IN CATALYSIS AND ELECTROCATALYSIS**

Joel S. Milder, Editor

This book focuses on modification of materials for catalytic purposes and modification of organic and inorganic electrode materials for electrocatalytic and photoelectrochemical application.

**CONTENTS** Chemically Modified Surfaces in Catalysis • Polystyrene-divinylbenzene Supported Catalysts • Homogeneous Rhodium (I) Catalyzed Alkene Hydrogenations • Reactive Organic Functional Groups • Polypyrrole Film Electrodes • Second Order EC Catalytic Mechanism • Semiconductor Photoelectrodes • Solution Reactivity Properties • Metallopolymers on Electrode Surfaces • Chemical Modification of  $\text{TiO}_2$  Surfaces • Electrochemistry of Silane-Derivatized Indium • Improvements in Photoelectrochemical and Electrochromic Reactions • Derivatized Layered M(V) Phosphonates • Intercalation of Molecular Catalysts in Layered Silicates • Fischer-Tropsch Synthesis • Reactivity of Catalysts Derived from Organometallics • Silicrowns  
301 pages (1982) Clothbound  
US & Canada \$36.95 Export \$44.95

An invaluable resource for all who use MS in their work.

## **MASS SPECTRAL CORRELATIONS, SECOND EDITION**

F.W. McLafferty and R. Venkataraghavan, Editors

This volume is an invaluable resource for interpreting the copious spectral data generated in GC and MS investigations. Comprehensive tables show the most probable assignments for peaks in electron mass spectra of organic compounds. More than 3000 structures corresponding to 1500 elemental compounds are listed—several times the number in the first edition. Newcomers to the field will find this book indispensable. Seasoned professionals will find it a valuable timesaver in interpreting the spectrum of an unfamiliar compound when information on the history of the sample is lacking.  
124 pages (1982) Clothbound  
US & Canada \$24.95 Export \$29.95

Mail to Distribution Office Dept. 15, American Chemical Society, 1155 Sixteenth Street, N.W., Washington, D.C. 20036  
Please send me the books checked below:

Instrumentation in Analytical Chemistry,  
Vol. 2  
NMR Spectroscopy: New Methods and  
Applications  
Chemically Modified Surfaces in Catalysis  
and Electrocatalysis  
Mass Spectral Correlations, Second Edition

Quantity Price Total

\_\_\_\_\_

\_\_\_\_\_

\_\_\_\_\_

\_\_\_\_\_

\_\_\_\_\_

\_\_\_\_\_

\_\_\_\_\_

California customers add 6% state use tax: \_\_\_\_\_

**TOTAL:** \_\_\_\_\_

☐ Payment enclosed.

☐ Purchase order enclosed.

Charge my ☐ MasterCard ☐ Visa. Account No. \_\_\_\_\_

Expires \_\_\_\_\_ Interbank No. \_\_\_\_\_  
(MasterCard only)

Signature \_\_\_\_\_

Ship to Name \_\_\_\_\_

Address \_\_\_\_\_

\_\_\_\_\_

City, State, Zip \_\_\_\_\_

**ORDERS MUST BE PREPAID. PLEASE ALLOW 4-6 WEEKS FOR DELIVERY. PRICES SUBJECT TO CHANGE WITHOUT NOTICE.**  
**To charge books by phone, call (800) 424-6747.**

# Adsorbents Woelm®

*International Standard*

**for  
Chromatography**

**Active Silicas  
Active Aluminas**

**for  
CC**

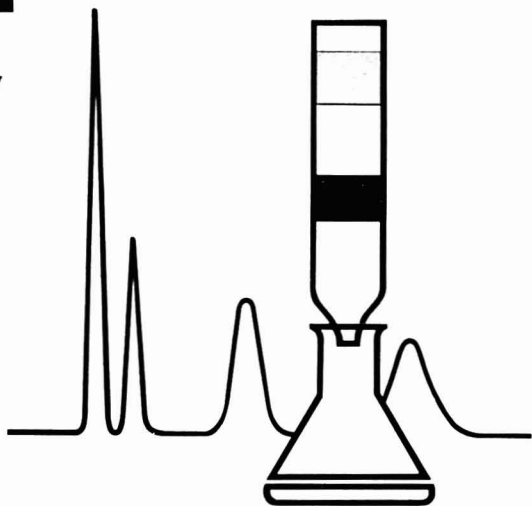
analytical  
preparative  
pilot plant

**TLC**

**Dry-Column C**

**HPLC**

high & med. pressure



## Available in

**Australia** H. B. Selby & Co. Pty. Ltd.  
352-368 Ferntree Gully Road  
Notting Hill  
Victoria  
Tel.: 544 4844

**Austria** C. Richter & Co. K.G.  
Feldgasse 19  
4600 Wels  
Tel.: 44 04

**Belgium** N. V. Pleuger S. A.  
Turnhoutsebaan 511  
2110 Wijnegem  
Tel.: 538551

**Canada** Universal Scientific, Inc.  
2070 Peachtree  
Industrial Court  
Atlanta, Georgia 30341  
Phone: 404-455-1140

**Denmark** MEDA AS  
Linde Allé 48  
2720 Vanløse  
Tel.: 74 44 00

**Finland** Lääketekniikka Oy  
Vattun:emenkuja 1  
Helsinki 20  
Tel.: 67 31 91

**France** Prolabo  
12, rue Pelée  
75011 Paris  
Tel.: (1) 355-44-88

**Germany** Woelm Pharma GmbH & Co.  
D-3440 Eschwege  
Tel.: 05651-8581

**Great Britain** Koch-Light  
Laboratories Ltd.  
Haverhill, Suffolk CB9 8PU  
Tel.: 0440-24367

**India** M/s. Sarabhai M. Chemicals  
P.O. No. 89  
Gorwa Road  
Baroda-390007  
Tel.: 88 21

**Israel** M. Kochin  
12, Shamai Str.  
Jerusalem  
Tel.: 22 28 62

**Italy** Dr. Amato & Figli r.s.l.  
Via Livorno 25  
00162 Rome  
Tel.: 42 05 06

**Japan** Wako Pure Chemical  
Industries, Ltd.  
10 Doshomachi 3-chome  
Higashi-ku  
Osaka 541  
Tel.: (06) 203-3741

**Malaysia** General Scientific Company  
SDN. BHD.  
7 Jalan 222  
Section 10 A, Petaling Jaya  
Selangor  
Tel.: 77 54 33

**Mexico** Universal Scientific, Inc.  
2070 Peachtree  
Industrial Court  
Atlanta, Georgia 30341  
Phone: 404-455-1140

**Netherlands** Pleuger Nederland  
Postbus 44  
Amstelveen 1134  
Tel.: 43 36 51

**New Zealand** Selby-Wilton Scientific, Ltd.  
410 Hutt Road  
P.O. Box 30556  
Lower Hutt  
Tel.: 69 70 99

**Portugal** Concessus S. A. R. L.  
Aparado 1455  
Lisboa 1  
Tel.: PPC 65 24 06/07

**Sweden** Flow Laboratories  
Svenska AB  
Östervägen 3  
17123 Solna  
Tel.: 08/7305575

**Switzerland** Instrumenten-Gesellschaft AG  
Räffelstraße 32  
8045 Zurich  
Tel.: 66 33 11

**USA** Universal Scientific, Inc.  
2070 Peachtree  
Industrial Court  
Atlanta, Georgia 30341  
Phone: 404-455-1140

**Woelm Pharma**

GmbH & Co. D-3440 Eschwege West-Germany  
Tel. 05651/8581

CIRCLE 215 ON READER SERVICE CARD

# Third Annual Analytical Lab Managers' Association Conference

The erosion of the scientific instrumentation base is making it difficult for the U.S. to maintain its technological edge

Obsolescence of instrumentation is a growing national problem. That was a common theme at the Third Annual Conference of the Analytical Laboratory Managers' Association (ALMA), held in late October 1982, in Madison, Wis., and hosted by Thomas Farrar, chairman of ALMA. ALMA is the new acronym replacing ULMA (University Laboratory Managers' Association), reflecting participation by industrial and government lab managers.

Analytical lab managers, mostly from academic institutions but also from industrial and government labs, met with representatives from federal and private funding agencies at the two-day conference to discuss the scope and extent of the obsolescence problem and possible solutions.

Concern was expressed that it is becoming increasingly difficult for the U.S. to maintain its overall scientific technological lead in the world because the scientific instrumentation base has been seriously eroded by a lack of modern equipment in university, government, and industrial labs.

Instrumentation costs have skyrocketed over the past decade. This has been due to inflation and to the increased adaptation of computers to instruments, which has greatly improved the capabilities of the equipment. While the increased sophistication of the instrumentation has allowed much greater efficiency, the costs of acquiring and maintaining the systems have in many cases precluded their purchase.

A conservative estimate of the cost of operating and maintaining scientific instrumentation is that it is at least 20-30% of the equipment replacement price per year. This figure includes salaries and other direct operating costs, but does not include equipment depreciation or facility overhead and utilities. It was generally agreed among conference attendees that the optimum useful life span of major research instruments is six to eight years, but as Farrar pointed out, a great deal of equipment lasts up to twice that long.

Representatives from some of the federal funding agencies [J. Talmage and F. Findeis, National Science Foundation (NSF); S. Stimler, National Institutes of Health (NIH); and J. Suttle, Department of Defense (DOD)] were well aware of and concerned about the problem. Each explained what his particular agency is doing to combat the obsolescence problem. Talmage emphasized that it is a national problem and it will take initiatives at all levels—state, local, and federal—to find innovative solutions to the key problem: lack of sufficient funding.

In response, ALMA, at its business session, voted to establish an ad hoc working group made up of people from instrument manufacturing companies, universities, industry, and the Scientific Apparatus Makers Association (SAMA). The following people were chosen to work at developing ways to generate additional funds for purchasing major research equipment: T. Farrar, University of Wisconsin; D. Grant, University of Utah; P. Llewellyn, Varian; C. Lucchesi, Northwestern University; E. Olson, Upjohn Company; J. Schaeffer, Research Corporation; and D. Upton, SAMA.

It was also agreed that ALMA and SAMA should work together to develop closer ties so that SAMA, which is a trade association representing scientific instrument manufacturers, can inform both the federal government and its own members about issues of concern to ALMA.

While NSF and NIH have managed to maintain, and in some instances increase, their instrumentation funding levels, the brightest star on the near-term horizon as far as federal funding is concerned appears to be the new DOD initiative. Suttle explained that the \$150 million five-year program is strictly limited to research equipment. Thirty million dollars per year (\$10 million each from the Army, Navy, and Air Force) will help to purchase pieces of equipment costing a minimum of \$50 000 to a maximum of \$1 million. The awardee is encouraged to

share costs whenever possible but no strict cost-sharing formula is prescribed.

Even with this welcome program the obsolescence problem will remain acute. By DOD's own estimates it would take \$1.5 to \$2 billion to fully upgrade the nation's laboratories.

A panel representing the instrument manufacturers offered for consideration a list of items that may help to minimize obsolescence in the future. High on that list was the modular approach to instrument purchases. The companies feel that modularity will allow a user to start small and add capability as funds become available.

Other suggestions were:

- Tax credits to companies to encourage new equipment donations;
- Computer networking to allow greater access to instrument data through off-line terminals;
- Lease/purchase agreements (some universities have used "creative financing" arrangements); and
- Debt financing, as hospitals have done in the past to purchase large equipment items.

Obviously there is no magic single solution to the problem. A systematic collective approach including some or all of these suggestions plus others, combined with increased government (federal and state) and private-sector funding, will help to alleviate the problem.

This year's ALMA conference will be held Oct. 20 and 21 at Purdue University. Bill Baitinger, chairman-elect of ALMA, and Jon Amy of Purdue will be hosting the conference.

The conference probably will focus on the increasing problem of finding and keeping qualified technical and scientific laboratory personnel. Topics relating to computer assistance in the management of instrumentation labs also will be included.

**Thomas Lyttle**  
Research Instrument Services Group  
Department of Chemistry  
Iowa State University  
Ames, Iowa 50011

# Taking Stock of Mass Spectrometry/Mass Spectrometry: Report of a Recent Workshop

Current MS/MS studies involve sector, quadrupole, hybrid, and Fourier transform instrument configurations

A workshop entitled "Mass Spectrometry/Mass Spectrometry: Instrumentation and Applications" was held in Chicago on Oct. 18, 1982, under the auspices of the American Society for Mass Spectrometry. The meeting, organized by Michael L. Gross of the University of Nebraska, drew 80 participants to a day of lectures and panel discussion. Different forms of MS/MS spectra as applied to a range of analytical problems were discussed. Several new instruments designed for MS/MS were introduced.

MS/MS techniques employ sequential mass analyzers to characterize ions. The first analyzer acts as a separator in selecting ions by mass/charge ratios. These *parent* ions are forced to undergo a change in mass or charge (normally by collision with a neutral target gas) to form *daughter* ions, which are analyzed in a second stage. The analogy between gas chromatography/mass spectrometry (GC/MS) and MS/MS in the analysis of mixtures is evident. A generic MS/MS spectrometer is comprised of at least two analyzers (A) and a reaction region (\*) sandwiched between the source (S) and detector (D), arranged, for example, as SA\*AD. Analyzers can be electric sectors (E), magnetic sectors (B), or quadrupole filters (Q). In Fourier transform mass spectrometry (FTMS), the analyzers are temporally rather than physically separate. The workshop was organized according to instrument configurations: sector, quadrupole, hybrid (a combination of sectors and quadrupoles), and Fourier transform instruments.

**Sector Instruments.** Presentations on sector instruments were introduced by Fred W. McLafferty of Cornell University. The original MS/MS spectrometers were reversed geometry or BE instruments, with applications in direct mixture analysis that date back to the mid-seventies. In the conventional geometry or EB arrangement, covariant scanning of the accelerating voltage and magnetic and electric fields (linked scans) establishes the re-

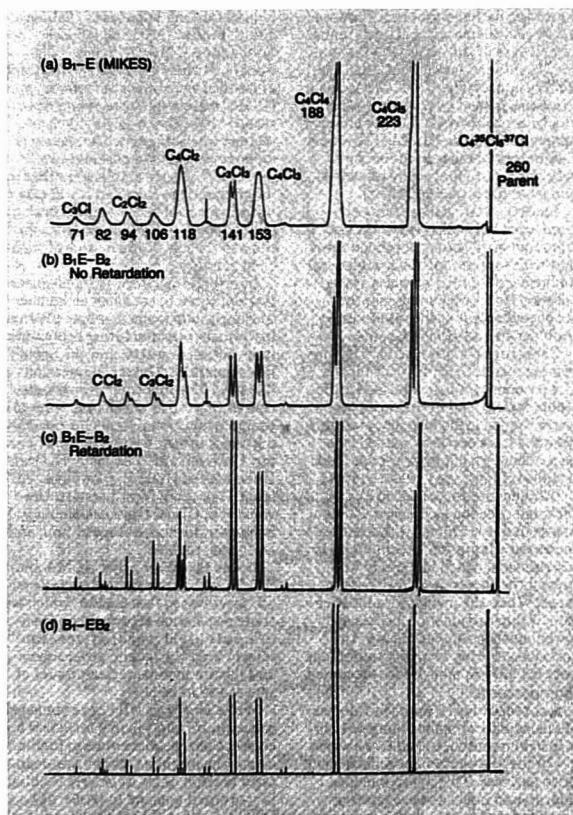


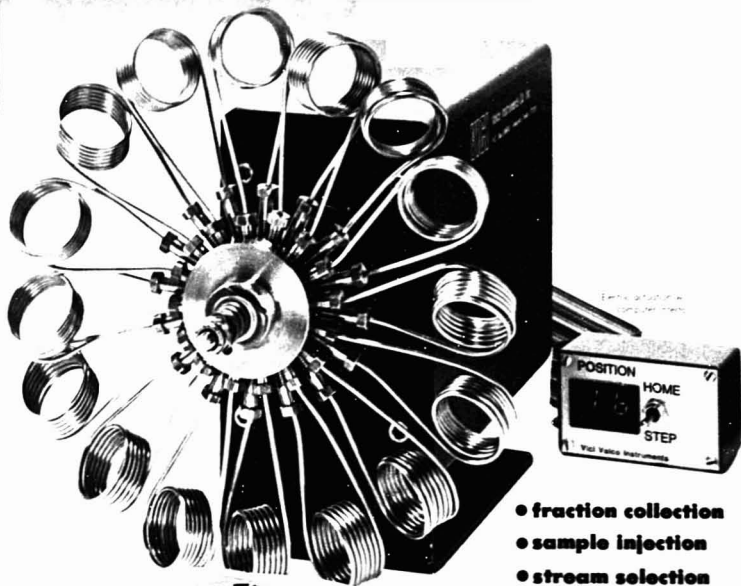
Figure 1. MS/MS spectra

An ion at  $m/z$  260 from hexachlorobutane is selected as the parent ion in this series of MS/MS experiments, which shows the increased resolution of daughter ions obtained when the collision cell in a sector instrument is held at a high voltage to retard the ion beam. (Figure courtesy of Charles Smith of VG Micromass)

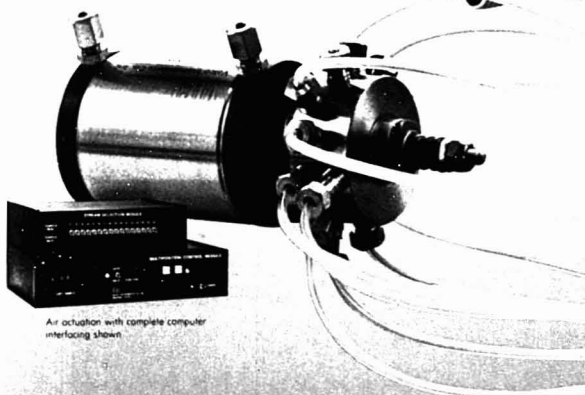
# VICI

Valco Instruments Co. Inc.

Valco Switzerland



- fraction collection
- sample injection
- stream selection
- reactor selection
- column selection



An actuation with complete computer interfacing shown

## POWERFUL NEW TOOLS FOR RESEARCH AND PROCESS CONTROL

Valco multiposition switching/sampling valves present a world of possibilities.

CIRCLE 224 ON READER SERVICE CARD

### SB Type Flowpath

Inputs dead-ended, flow when selected, or input to multiple selected outputs.



### SC Type Flowpath

All inputs to a common outlet except selected one.



### SF Type Flowpath

Each input flows to individual outlet except selected one which is diverted.



### ST Type Flowpath

Used for multi-column, multi-sampling, or multi-trap selection.





relationship between parent and daughter ions. The primary advantage of sector instruments is a large mass range (to more than 10 000) for both parent and daughter ions. A second advantage is the ability to acquire MS/MS spectra on a parent ion specified to high resolution. To achieve equivalent resolution of both parents and daughters, four-sector instruments have been assembled. An EBE instrument has been in place at Cornell for several years, and at this meeting, VG Micromass announced plans to build a BEB instrument. To date, however, high resolution for both parent and daughter ions has not been achieved.

McLafferty presented MS/MS spectra generated from parent ions of mass 1000–2000, including peptides and vitamins, and also reported investigations of the collisionally activated decomposition of even higher mass ( $C_{50}+11_2$ )<sup>+</sup> cluster ions. Syd Evans of Kratos Instruments discussed management of signal intensity in experiments with an EBE instrument. Both high-resolution MS and MS/MS are expensive in terms of signal depletion, but permit increased selectivity. Enhanced signal-to-noise ratios in MS/MS arise because of a preferential discrimination against chemical noise (signals due to mixture components other than the analyte). Charles Smith of VG Micromass discussed that firm's BEB instrument and presented data that demonstrated the effects on daughter ion resolution of ion beam retardation (Figure 1).

**Quadrupole Instruments.** The term "triple quadrupole" describes an MS/MS instrument with two quadrupoles as mass analyzers and an rf-only quadrupole as an intermediate collision region. Chris G. Enke of Michigan State University introduced this section of the program. While currently limited to a mass range of about 2000 at unit mass resolution, this specification applies to both parent and daughter ions, a capability not yet demonstrated with sector instruments. The most attractive feature of the all-quadrupole system for MS/MS has been the advanced data system, more than ever a necessary part of sophisticated MS/MS experiments. In work by Richard Yost at the University of Florida using negative ion MS/MS, trichlorophenol was identified in serum and urine extracts (a single extraction with 1 mL hexane, with 1  $\mu$ L analyzed) at levels as low as 0.25 ppb, and at sample analysis rates of up to 90/h (Figure 2). Describing similar experiments, William R. Davidson of Sciex detailed results in

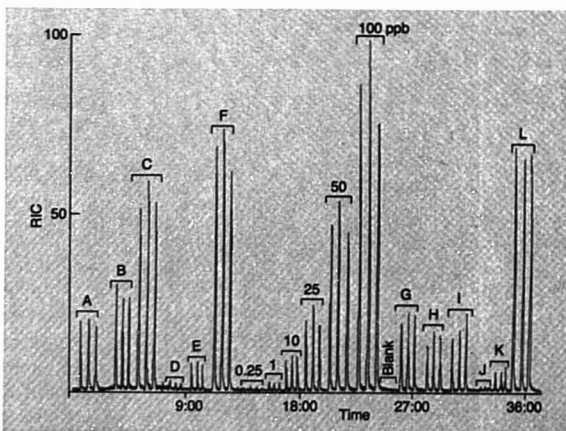
which a foodstuff contaminant, vomitoxin in wheat, was identified at the 25-pg level at a rate of 6 samples/h. This compares with 1 sample/h for a selected ion monitoring GC/MS experiment, and with the same rate for GC with electrochemical detection. All three methods gave similar quantitative results, but sample workup was minimal prior to MS/MS.

Multiple quadrupole instruments have reached their second generation. Candice Bartmann of Extranuclear Laboratories explained the data and instrument control system matched to their new QQQ mass spectrometer. A mass range to 2000 and fast scanning capabilities were described. Both Sciex (Davidson) and Finnigan/MAT (Mark Johnston and Gordon Foss) provided details about new software that controls experiments via subroutines that change scan parameters during the experiment. MS/MS spectra are obtained at rates of up to 1/s for parent ions selected after computer evaluation of the mass spectrum. Data is reconstructed using GC/MS algorithms extended to handle the different types of MS/MS scans.

**Hybrid Instruments.** MS/MS spectrometers that combine sectors and quadrupoles are termed "hybrid" instruments. As pointed out by R. Graham Cooks of Purdue University, these instruments are designed to pro-

vide the best features of both the sector and the quadrupole instruments. In their commercial forms (VG Micromass, Kratos Instruments, and Finnigan/MAT), they provide the usual capabilities of high-resolution MS in addition to features of multiple quadrupole instruments. Since these instruments have only recently been assembled, their full range of capabilities has not yet been explored. One noteworthy capability is the ability to examine collision-induced products of both high- and low-energy collisions to more completely characterize ions (especially negative ions that yield positive fragments in high-energy collisions).

Several new hybrid MS/MS instruments were announced at the meeting. Evans described the Kratos EBQ obtained by adding two quadrupoles to their MS80. The instrument is designed to provide high resolution of the parent ion using the double-focusing EB section, an efficient collision-induced dissociation process in the rf-only quadrupole, and fast MS/MS scanning with unit resolution of daughter ions to mass 2000 in the final quadrupole. Peter Dobberstein of Finnigan/MAT described an instrument of BEQ geometry based on the 8200 and 8500 series of high-resolution double-focusing instruments with similar capabilities. Data from the

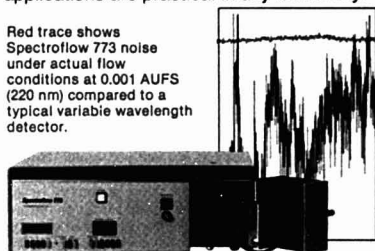


**Figure 2.** MS/MS analysis of serum and urine extracts for trichlorophenol (TCP). The analysis utilizes selected reaction monitoring of the parent ion 166<sup>+</sup> undergoing collision-induced dissociation to 160<sup>+</sup>. The standards and spiked serum/urine samples (A–L) range from 0–100 ppb; the upper level corresponds to 100  $\mu$ g of TCP per mL of sample. Note a total analysis time of 36 min for 19 samples (three replicates each). (Figure courtesy of Dean Fetterolf and Rick Yost of the University of Florida)

**High sensitivity - down to 0.001 AUFS separates the new Spectroflow 773 from the noise of the rest.**

The new Kratos Spectroflow 773 sets new standards of performance for UV-VIS variable wavelength absorbance detectors. It routinely delivers the highest sensitivity, lowest noise, and best overall performance that state of the art technology will allow. Kratos engineers combined the latest in modern technology with a thoroughly innovative design to reduce noise and drift to unprecedented levels. Now, operation at 0.001 AUFS is routine, and new levels of performance even in trace analysis, high speed LC, and microbore column applications are practical in *any* laboratory.

Red trace shows Spectroflow 773 noise under actual flow conditions at 0.001 AUFS (220 nm) compared to a typical variable wavelength detector.



The success of the Spectroflow 773 doesn't rest solely on its specifications; it also sets new standards for convenience and ease of operation: auto-zero to automatically reset the baseline at the touch of a button; front panel bulkhead flow connectors to minimize flowcell handling and simplify system plumbing; a multi-mode digital readout with self-diagnostic capabilities; adjustable time constant down to 0.045 sec.; and high speed wavelength scanning (optional) with memory correction.

Call or write to find out how the Spectroflow 773 can give you better results with any LC instrument, any LC method. Kratos Analytical Instruments, 170 Williams Drive, Ramsey, NJ 07446. (201) 934-9000. Offices in Manchester, UK, and Karlsruhe, West Germany.

**KRATOS** Analytical Instruments

**New Standards in HPLC detection.**

**If HPLC  
sensitivity  
is  
important...  
  
go with  
the proven  
leader.**

**1 1 1 1**

**NOW  
with programmable  
wavelength control  
and rapid scanning**

CIRCLE 117 ON READER SERVICE CARD

# Ultraviolet Light Sources & Products for Research . . . Industry . . . Education . . .

Shortwave UV Lamps  
Longwave UV Lamps  
Multi-Band UV Lamps  
Mid-Range UV Lamps  
Fluorescent Materials  
UV Illumination Cabinets  
UV Transilluminators  
Radiometers  
Eye/Face Protection  
Pen-Ray<sup>®</sup> Lamps  
Custom UV Light Sources  
Stable Ozone Generators  
UV Ozone Micro-Cleaner  
EPROM Erasing Equipment  
Short Arc Lamps  
Kool-Cure<sup>®</sup> UV Curing

The list is endless.

Industry, Research and  
Education have relied  
on UVP, Inc. since 1932  
for their Ultraviolet  
needs. CALL TODAY.



**UVP, Inc.**  
5100 Walnut Grove Avenue  
P.O. Box 1501  
San Gabriel, CA 91778 U.S.A.  
(213) 285-3123  
Telex: 688-461  
In Europe: UVP, Ltd.  
Science Park, Milton Road  
Cambridge CB4 4BN, England  
Tel: (0223) 355722  
Telex: 817-923 (UVPROD, G.)

CIRCLE 212 ON READER SERVICE CARD

## Focus

7070QQ from VG Micromass, configured EBQQ, was given by Smith. Parent ion resolution of several thousand was used to separate ions for MS/MS analysis.

**Fourier Transform Mass Spectrometry.** The fourth type of MS/MS instrument described was the Fourier transform mass spectrometer. This section was introduced by Gross, who detailed the separation of parent ions from daughter ions in time rather than space. Since the MS/MS experiment is executed by software, no hardware changes are required. In contrast to hybrid instruments, high resolution is available on the daughter ions, but not on the parent ions selected for dissociation. High efficiency of fragmentation and the ability to examine ions in a reaction sequence (MS/MS/MS/MS...) were demonstrated by Sahba Ghaderi of Nicolet Instruments. As in hybrids and multiquadrupole instruments, the collision energy ranges up to several hundred volts. The ability of FTMS to scan all masses simultaneously makes it compatible with pulsed ionization methods, and makes it possible to follow the time profiles of collision-induced reaction products.

**Collisionally Activated Decomposition.** The physical basis of collisionally activated decomposition, the process central to the MS/MS experiment, was described by Jean Futrell of the University of Utah. Using a crossed-beam instrument, results were obtained for polyatomic ions scattered on low-energy collision. Investigating the full range of forward and back scattering, Futrell found that many ions are scattered through large angles. Although such factors as internal energy effects, competition between various reaction channels, and the differences in energy transfer between low- and high-energy collisions have not been worked out, the process can be modeled as a vibronic excitation leading to fragmentation described by the quasi-equilibrium theory.

Breakdown curves represent mass spectra explicitly as a function of the internal energy of the fragmenting ion and are the key to understanding the decomposition process. Two methods have been developed to access this information. First, angle-resolved mass spectrometry investigates changes in the distribution of fragment ions with scattering angle in high-energy collisions. Using an electrostatic method of angular resolution, Dobberstein displayed results comparable to those obtained by photodissociation. Second, in low-energy dissociations, the kinetic energy of the parent ion controls the energy transferred to it upon collision,

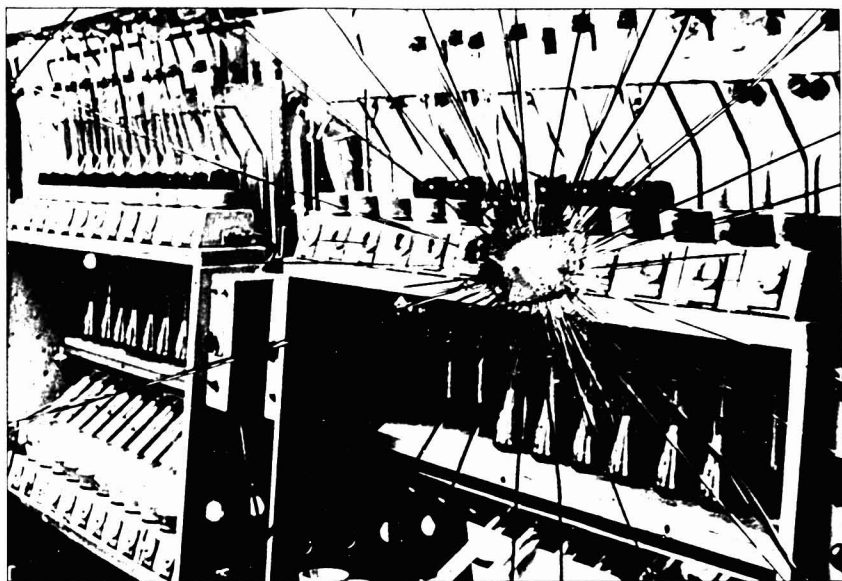
as described by Davidson. The analytical implications of the angle and energy phenomena are twofold. First, these variables must be controlled to maximize reproducibility and quantitative accuracy. Second, these data may differentiate isomeric ions not otherwise distinguished.

The workshop ended with a discussion in which questions were fielded by a panel of the speakers. Topics included quantitation by MS/MS, trade-offs between mass range and resolution, and the merits of MS/MS as compared to other analytical techniques. It was agreed that MS/MS is useful in the analyses of mixtures for targeted components; data at the parts per trillion level from the combination of capillary column gas chromatography with single reaction monitoring MS/MS were given for the determination of 2,3,7,8-tetrachlorodibenzo-dioxin in fish extracts. Examples of the MS/MS identification of new compounds in mixtures were given. There was discussion of the use of MS/MS for high mass ions generated by desorption ionization methods such as secondary ion mass spectrometry and fast atom bombardment. Several participants noted that high mass ions seem less easily dissociated upon collisional activation. Others showed spectra in which high mass ions gave MS/MS spectra interpretable in terms of the parent ion structure.

The transmission fall-off of quadrupoles for high mass ions provoked discussion. Some argued that sector instruments were absolutely necessary for transmission and resolution of higher mass ions in the MS/MS experiment; others pointed to the extended mass ranges of new quadrupole rods and the efficiency of the rf-only quadrupole collision region. Examples were given of the analysis of mixtures for particular functional groups using neutral loss MS/MS scans, taken by simultaneously varying the masses of both parent and daughter ions. New types of MS/MS scans were discussed in which associations rather than dissociations are examined. Finally, the concept of the total-loss MS/MS spectrum was introduced by Johnston. Such spectra, with a distinctive 100% fragmentation efficiency, yield no observable fragment ions, but can be obtained for infinitely high masses at infinite resolution, and should thus prove popular, if not at times unavoidable.

**Kenneth L. Busch  
R. Graham Cooks**  
Department of Chemistry  
Purdue University  
West Lafayette, Ind. 47907

# Break the habit



Get rid of broken glass, spilled chemicals and high energy bills.  
Do your "Kjeldahl" on a desktop.

We offer true Kjeldahl nitrogen analysis, as approved by AOAC, neatly performed in compact cabinets.

- Sturdy equipment, with push-button and digital display convenience, that will perform 50, 150 or 240 analyses per day.



- Small units, that will free all of your fume hoods and all but 6 square feet of your present Kjeldahl space. With our new efficient chemical scrubber, it is all a desktop job.

Our salesmen are trained experts and will demonstrate the Kjeldahl equipment in your laboratory.

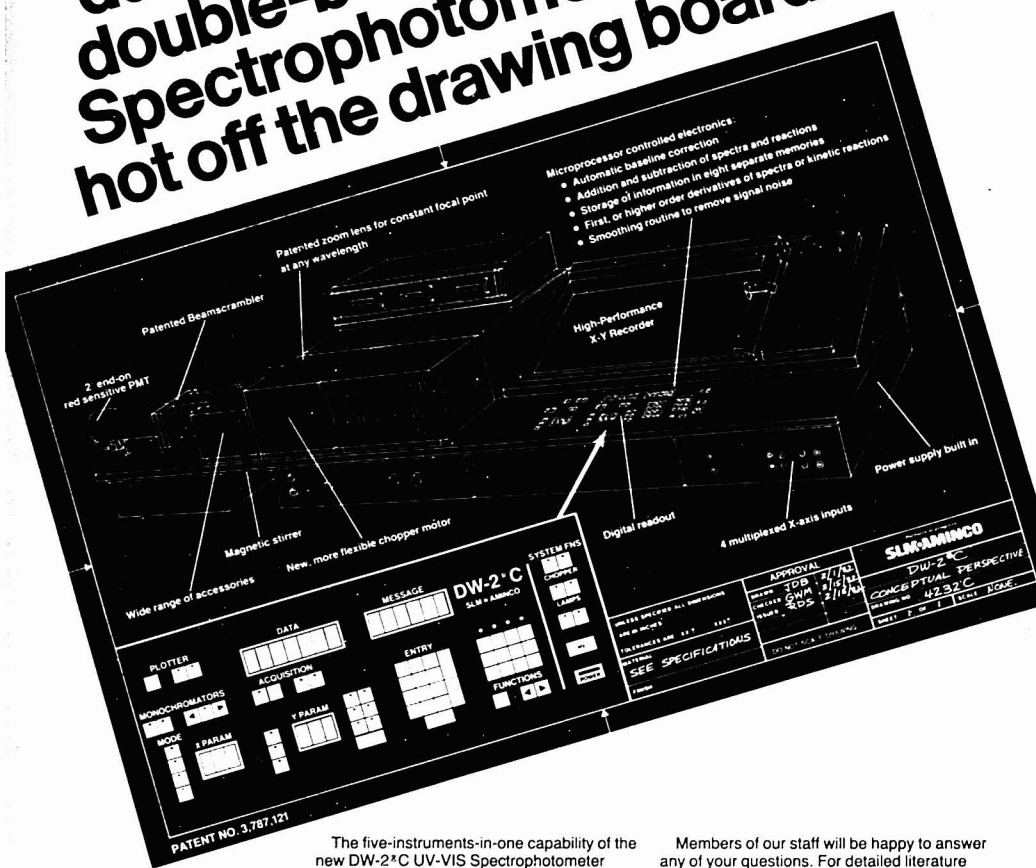
5,000 other labs have made the obvious choice.  
Contact us today for your personal demonstration.  
Call collect (703) 435-3300.



P.O. Box 405, Herndon, VA 22070, (703) 435-3300

CIRCLE 206 ON READER SERVICE CARD

# The new dual-wavelength, double-beam DW-2C UV-VIS Spectrophotometer is hot off the drawing board.



The five-instruments-in-one capability of the new DW-2C UV-VIS Spectrophotometer provides double-beam, dual-wavelength, dual-wavelength scanning, rapid kinetics, and optical derivative operations. The new built-in microprocessor controlled electronics features automatic baseline correction for even greater flexibility and ease of operation.

Members of our staff will be happy to answer any of your questions. For detailed literature and additional information about the new DW-2C UV-VIS Spectrophotometer, write SLM Instruments, Inc./American Instrument Company, 810 West Anthony Drive, Urbana, IL 61801, U.S.A. or call (800) 637-7689 toll-free. TELEX 20-6079.

Partners in progress.

## SLM-AMINCO

*Performance is the difference.*

Copyright © 1982 by SLM Instruments, Inc.

CIRCLE 194 ON READER SERVICE CARD

## ANALYTICAL CHEMISTRY Appoints New Advisory Board Members

Five new members of the Advisory Board of ANALYTICAL CHEMISTRY have been selected to serve three-year terms beginning this month. Each year the membership of the board is rotated, with the new appointees replacing those members whose terms on the board have expired.

The new members joining the board this year are: Dennis H. Evans, University of Wisconsin—Madison; Jack W. Frazer, Keithley Instruments, Inc.; Roland F. Hirsch, Seton Hall University; Herbert L. Retcofsky, Pittsburgh Energy Technology Center; and Wilhelm Simon, Swiss Federal Institute of Technology.

The members leaving the board are:

Donald D. Bly, E.I. du Pont de Nemours & Company; Georges Guiochon, Ecole Polytechnique; Bruce R. Kowalski, University of Washington; Robert A. Libby, Procter & Gamble Company; and Richard S. Nicholson, National Science Foundation.

The following 11 members will continue to serve on the board: Joel A. Carter, Oak Ridge National Laboratory; Richard S. Danchik, Aluminum Company of America; Richard Durst, National Bureau of Standards; Helen M. Free, Miles Laboratories; Shizuo Fujiwara, Chiba University; Csaba Horvath, Yale University; Wilbur Kaye, Beckman Instruments, Inc.; Thomas C. O'Haver, University of

Maryland; Janet Osteryoung, State University of New York at Buffalo; Robert E. Sievers, University of Colorado; and Rudolph H. Stehl, Dow Chemical Company.

The Advisory Board was established in the 1940s to advise the editors of the JOURNAL. It meets formally once a year at the JOURNAL's editorial offices in Washington, D.C. The board also provides guidance and advice throughout the year with regard to editorial policy and the peer review system. Board members are an invaluable link between the editors and the analytical community.

Brief biographical sketches of the new members follow.

**Dennis H. Evans** received his BS degree from Ottawa University, Ottawa, Kan., in 1960 and his MA and PhD degrees from Harvard University in 1961 and 1964, respectively. He remained at Harvard as instructor of chemistry until 1966 and then joined the faculty of the University of Wisconsin—Madison where he is now professor of chemistry. From 1977 to 1980, he was chairman of the department of chemistry, and beginning this year he will be associate dean of the College of Letters and Science. Evans's research in the areas of electroanalytical chemistry and organic

electrochemistry has been described in approximately 70 publications. He is a member of the Subcommittee on Analytical Chemistry of the ACS Examinations Committee and served as secretary-treasurer of the ACS Wisconsin Section. From 1978 to 1981, he was a member of the NSF Chemistry Division Advisory Committee, and he is currently serving on the Chemistry Research-Evaluation Panel, Air Force Office of Scientific Research. Evans has taught the ACS short course on electroanalytical chemistry and has lectured at a number of other courses given around the country.

**Jack W. Frazer** is chief executive officer of Keithley Instruments, Inc., Cleveland, Ohio. After receiving his BS degree from Hardin-Simmons University in 1948, he joined the staff of Los Alamos Scientific Laboratory. In 1953 he moved to Lawrence Livermore National Laboratory, where he remained until assuming his present position at Keithley Instruments in February 1982. Frazer's research interests include modeling of nonlinear physical and chemical processes, development of graphic techniques to aid in the evaluation of large data sets and to support modeling, automatic





characterization of multivariant non-linear (complex) chemical systems, development of self-adaptive control strategies to support experimentation, and the use of artificial intelligence for the solution of heuristic-type problems. From 1968 to 1971, Frazier served on the Instrumentation Advisory Panel of ANALYTICAL CHEMISTRY. He served as editorial advisor for *Analytica Chimica Acta* (Computer Techniques and Optimization) from 1977 to 1981, and as chairman of the ASTM E-31 Committee, Computerized Laboratory Systems, from 1970 to 1975. Frazier is recipient of the 1973 American Chemical Society Award for Chemical Instrumentation and the 1975 ASTM Award of Merit.

**Roland F. Hirsch** received his BA degree from Oberlin College in 1961 and his PhD degree from the University of Michigan in 1965. Since 1965, he has been on the faculty of Seton Hall University, where he is now associate professor of chemistry and associate dean of the College of Arts and Sciences. In 1975-76 he was a senior visitor at the Inorganic Chemistry Laboratory at Oxford University. His research interests lie in the areas of applied statistics, the use of metal ions for enhancement of selectivity in gas and liquid chromatography, and the sensing of organic ions by ion-sensitive electrodes. He has edited a book on data analysis and has published papers on a large variety of topics. He is currently serving as secretary of the American Chemical Society Division of Analytical Chemistry.

**Herbert L. Retcofsky** is chief of the Analytical Chemistry Branch at the Pittsburgh Energy Technology Center. He earned his BS degree in 1957 at California State College and his MS degree in 1965 at the University of Pittsburgh. After a year of teaching he joined the staff at the Pittsburgh Energy Technology Center, one of the U.S. Department of Energy's five energy technology centers. The standardization of methods for the routine analysis of coal-derived liquids is one of the major long-term goals of his laboratory. His principal research interest is in the application of spectral techniques, particularly infrared and magnetic resonance spectrometries, in coal research. Retcofsky has held all elective offices of the Spectroscopy Society of Pittsburgh and also served as president of the 1979 Pittsburgh Conference on Analytical Chemistry and Applied Spectroscopy. In 1981, he became the first U.S. associate editor of *Fuel*. He is recipient of the 1982 Henry H. Storch Award, pre-

sented annually by the American Chemical Society's Fuel Division for significant contributions to fundamental or engineering research on coal.

**Wilhelm Simon** received his PhD degree in 1956 from the Swiss Federal Institute of Technology (ETHZ), where he is now teaching analytical chemistry and the application of spectroscopic techniques in organic chemistry. He became Privatdozent in 1961 and Assistenz-Professor in 1965, and since 1970 has been a full professor of chemistry. In the past, Simon's research interests included the study of acid-base equilibria using glass electrodes, automation of elemental analysis, vapor pressure osmometry, pyrolysis gas chromatography, pyrolysis mass spectrometry, and other spectroscopic techniques for structural elucidation. At present, his research is focused largely on ion selectivity of organic compounds and biological systems, ion-selective sensors, and high-resolution separation techniques. Simon has written approximately 300 articles and two books. He is recipient of the Swiss Chemical Society Award and is an honorary member of the Hungarian Academy of Sciences and the Institut Grand-Ducal in Luxembourg.

### Knox to Receive Dal Nogare Award

John H. Knox will receive the 1983 Dal Nogare Award at the Pittsburgh Conference on Analytical Chemistry and Applied Spectroscopy to be held March 7-11 in Atlantic City, N.J. The award, sponsored by the Chromatography Forum of the Delaware Valley, is given annually in recognition of significant contributions to chromatographic theory, instrumentation, and applications.

Knox received his BS degree from the University of Edinburgh and his PhD degree from Cambridge University. In 1963, he earned a D.Sc. degree from the University of Edinburgh, where he is currently personal chair in physical chemistry and director of the Wolfson liquid chromatography unit.

Knox's early work involved the liquid chromatographic separation of key aldehyde intermediates and the application of gas chromatography to chlorination and combustion reactions. His interest was then drawn to the development of spherical silica gel and several bonded derivatives for liquid chromatography. Knox's current work at the Wolfson unit involves the production of novel forms of silica gel and



John Knox

porous glassy carbon; his pure research interests concern electrophoresis and endosmotically generated chromatography.

### Competition for Biochemical Analysis Prize

The German Society for Clinical Chemistry is inviting qualified researchers to compete for the 1984 Biochemical Analysis Prize. The prize is awarded every two years at the Biochemische Analytik Conference in Munich for outstanding and novel work in biochemical analysis or biochemical instrumentation, or for significant contributions to the advancement of experimental biology especially related to clinical biochemistry. The prize consists of DM 10,000 and is sponsored by Boehringer Mannheim GmbH.

Competitors for the 1984 prize should submit papers on one theme, either published or accepted for publication between Oct. 1, 1981, and Sept. 30, 1983, to: I. Trautschold, Medizinische Hochschule Hannover, Konstanty-Gutschow-Straße 8, 3000 Hannover 61, FRG. Papers must be received before Nov. 15, 1983.

### Nominations Sought for Environmental Science Award

The Central Wisconsin Section of the American Chemical Society in conjunction with Zimpro, Inc., a subsidiary of Sterling Drug, Inc., is seeking nominations for the F. J. Zimmermann Award in Environmental Science. The award, consisting of \$1000 and a plaque, is given annually to an individual whose research has had a significant impact on environmental protection.

The award announcement and presentation will be made at the 17th Great Lakes Regional Meeting to be held June 1-3, 1983, in St. Paul, Minn. The award recipient will be invited to present an overview of the scientific contributions upon which the award is based.

Any scientist residing in the U.S. is eligible for the award. Nomination forms are available from L.A. Ochrymowicz, Department of Chemistry, University of Wisconsin—Eau Claire, Eau Claire, Wis. 54701. Nomination forms and supporting documents must be received no later than Feb. 16, 1983.

## Hewlett-Packard to Contribute Analytical Instrumentation

Hewlett-Packard Company has announced that it will contribute more than \$1.3 million worth of analytical instrumentation to 75 colleges and universities across the country.

Schools were chosen on the basis of the quality of their research and research-training programs, with special consideration given to schools that actively recruit minorities for their chemistry programs. The names of the schools selected were not disclosed.

The instruments, HP 5880A gas chromatographs manufactured by the company's Analytical Group, will be equipped with capillary-column inlet systems and single-flame detectors. According to the group's general manager, Lewis E. Platt, Hewlett-Packard is trying to "help solve the ongoing problem schools have with equipment obsolescence and to help them stay current with instrumentation found in industry." The equipment contribution is part of Hewlett-Packard's corporate philanthropy program, which in 1982 included more than \$11.5 million in equipment grants to institutions of higher education.

## New NSF Program Established

A new program, Instrumentation for Materials Research (IMR), has been established within the National Science Foundation's Division of Materials Research (DMR). Proposals to be considered in the new program are those for the purchase of major instruments needed for materials research and for the development of new instruments that extend current measurement capabilities.

Proposals are encouraged from groups of researchers intending to share major items of specialized in-

strumentation, where the individual users represent diverse areas of research covered within DMR or between DMR and other NSF divisions. Proposals for individual researchers representing a single area of research will continue to be assigned to the appropriate research program within DMR unless the cost of such an award would significantly upset the balance of support within that program. Instrument development proposals with direct relevance to research areas represented within DMR are also encouraged. Such proposals may involve individual researchers or groups.

Inquiries regarding the Instrumentation for Materials Research program should be directed to the Program Director, Division of Materials Research, National Science Foundation, 1800 G St., N.W., Washington, D.C. 20550, 202-357-7570.

## Call for Papers

**25th Rocky Mountain Conference** Denver, Colo. Aug. 14-19. General papers and poster sessions in all areas of chemistry are planned along with the following specific symposia: atomic spectroscopy, chromatography, computer applications, electrochemistry, environmental, EPR, FTIR, ion chromatography, mass spectrometry, NMR, Raman and IR spectroscopy, and surface analysis. Abstracts of not more than 200 words must be submitted on a Rocky Mountain Conference or standard ACS abstract form before March 23. To obtain the abstract forms and for additional information contact Edward Brovsky, Rockwell International, P.O. Box 464, Golden, Colo. 80401; 303-497-4972.

**10th Annual Meeting of the Federation of Analytical Chemistry and Spectroscopy Societies** Philadelphia, Pa. Sept. 25-30. The scope of the meeting will encompass all phases of analytical chemistry, applied spectroscopy, chromatographic methods, and allied techniques of instrumental analysis. Prospective authors must submit the title of their presentation, current address, and telephone number by April 8 to: FACSS X Program Chairman, John O. Lephardt, Philip Morris USA, Research Center, P.O. Box 26583, Richmond, Va. 23261; 804-274-3821. After receipt of the title, authors will be asked to submit a 250-word abstract by June 10.

**20th International Symposium on Advances in Chromatography** Amsterdam, The Netherlands. Oct. 3-6. The symposium will focus on all aspects of chromatography, with special emphasis on GC, LC, and high-performance TLC. Prospective authors must submit 200-word abstracts by April 1. Address all correspondence to Albert Zlatkis, Department of Chemistry, University of Houston, Houston, Tex. 77004; 713-749-2623. Authors of accepted papers will be required to submit completed manuscripts on Oct. 3 at the meeting.

## Meetings

- **12th Annual National Measurement Science Conference and Exhibition.** Jan. 20-21. Palo Alto, Calif. Contact: Bob Weber, Lockheed Missile & Space Corp., Sunnyvale, Calif., 94046; 408-742-2957.
- **Gordon Research Conference on Electrochemistry.** Jan. 24-28. Santa Barbara, Calif. Contact: Alexander M. Cruickshank, Gordon Research Conferences, University of Rhode Island, Kingston, R.I. 02881; 401-783-4011 or 3372.
- **13th Annual Conference of the Western Spectroscopy Association.** Jan. 26-28. Pacific Grove, Calif. Contact: Mel Kronick, Applied Biosystems, 850 Lincoln Centre Dr., Foster City, Calif. 94404.
- **8th Conference of the Australian and New Zealand Society for Mass Spectrometry.** Feb. 7-11. Melbourne, Australia. Contact: The Secretary, ANZSMS Conference, Chemistry Dept., Monash University, Clayton, Victoria, Australia.
- **Second Carnegie-Mellon University Conference on Biological Spectroscopy.** Feb. 8-11. San Jose, Calif. Contact: William Derrig, IBM Instruments, Inc., Orchard Park, P.O. Box 332, Danbury, Conn. 06810.
- **Pittsburgh Conference on Analytical Chemistry and Applied Spectroscopy.** March 7-12. Atlantic City, N.J. Contact: Linda Briggs, Program Secretary, Pittsburgh Conference, 437 Donald Rd. Dept. J-005, Pittsburgh, Pa. 15235. August, p. 1046 A.
- **185th ACS National Meeting.** March 20-25. Seattle, Wash. Contact: A. T. Winstead, American Chemical Society, 1155 16th Street, N.W., Washington, D.C. 20036; 202-872-4397.
- **International Symposium on Electroanalysis in Biomedical, Environmental, and Industrial Sci-**

ences. April 5-8. UWIST, Cardiff, Wales. Contact: Short Courses Section, Electroanalytical Conference, UWIST, Cardiff CF1 3NU, Wales

■ **17th ACS Middle Atlantic Regional Meeting.** April 6-8. White Haven, Pa. Contact: N. D. Heindel, Chemistry Dept., Mudd Bldg. No. 6, Lehigh University, Bethlehem, Pa. 18015; 215-861-3470

■ **International Symposium on Ion Exchange Membranes.** April 12-13. Runcorn, Cheshire, U.K. Contact: Conference Secretariat, Society of Chemical Industry, 14/15 Belgrave Square, London SW1X 8PS, U.K.

■ **8th Annual AOAC Spring Workshop and Exposition.** April 19-21. Indianapolis, Ind. Contact: Laurence Sullivan, Indiana State Board of Health, 1330 W. Michigan St., Indianapolis, Ind. 46206; 317-633-0224, or Kathleen Fominaya, Association of Official Analytical Chemists, 1111 N. 19th St., Suite 210, Arlington, Va. 22209; 703-522-3032

■ **Advanced Analytical Concepts for the Clinical Laboratory.** April 21-22. Gatlinburg, Tenn. Contact: Carl Burtis, Chemical Technology Division, Oak Ridge National Laboratory, P.O. Box X, Oak Ridge, Tenn. 37830; 615-576-2917. November, p. 1385 A

■ **5th International Symposium on Capillary Chromatography.** April 26-28. Riva del Garda, Italy. Contact: P. Sandra, Laboratory of Organic Chemistry, University of Ghent, Krijgslaan 281 (S4), B-9000 Ghent, Belgium. October, p. 1266 A

■ **7th International Symposium on Column Liquid Chromatography.** May 2-6. Baden-Baden, West Germany. Contact: J. Wendenburg, c/o Gesellschaft Deutscher Chemiker, Varrentrappstrasse 40-42, D-6000 Frankfurt, West Germany, August, p. 1046 A

■ **Recent Advances in the Measurement of Pollutants from Ambient Air and Stationary Sources.** May 3-7. Raleigh, N.C. Contact: Seymour Hochheiser, MD 75, EPA Environmental Monitoring Systems Lab, Research Triangle Park, N.C. 27711

■ **31st Annual Conference on Mass Spectrometry and Allied Topics.** May 8-13. Boston, Mass. Contact: Judith A. Watson, ASMS, P.O. Box 1508, East Lansing, Mich. 48823; 517-337-2548

■ **1983 International Symposium on LCEC and Voltammetry.** May 15-17. Indianapolis, Ind. Contact: Kristi Kluppel, 1983 LCEC Symposium, P.O. Box 2206, West Lafayette, Ind. 47906. Tel: (317) 463-2505, Telex: 276141. December, p. 1484 A

■ **13th Annual Symposium on the Analytical Chemistry of Pollutants.** May 16-18. Jekyll Island, Ga. Contact: Elaine McGarity, U.S. Environmental Protection Agency, Environmental Research Lab, Athens, Ga. 30613

■ **5th Australian Schools/Conference on X-ray Analysis.** May 16-20. Melbourne, Victoria, Australia. Contact: Australian X-ray Analytical Association, P.O. Box 90, Parkville, Victoria 3052, Australia. September, p. 1150 A

■ **International Union of Air Pollution Prevention Associations (IUAPPA) 6th World Congress on Air Quality.** May 16-20. Paris, France. Contact: Public Relations Dept., Air Pollution Control Association, P.O. Box 2861, Pittsburgh, Pa. 15230; 412-621-1090

■ **CLEO '83—Conference on Lasers and Electro-Optics.** May 17-20. Baltimore, Md. Contact: Optical Society of America, 1816 Jefferson Pl., N.W., Washington, D.C. 20036

■ **Applications and Techniques of Modern Spectrochemistry (Atoms-83).** May 19-20. Los Alamos, N.M. Contact: L. J. Radziemski, Los Alamos National Laboratory, Group AP-4, MS J567, Los Alamos, N.M. 87545

■ **ACS Central Regional Meeting.** May 22-24. Oxford, Ohio. Contact: J. R. Gunwell, Dept. of Chemistry, Miami University, Oxford, Ohio 45056; 513-529-2813

■ **International Conference on Chromatographic Detectors.** May 30-June 3. Melbourne, Victoria, Australia. Contact: The Secretary, International Conference on Chromatographic Detectors, U of Melbourne, Parkville, Victoria 3052, Australia

■ **Budapest Chromatography Conference.** June 1-3. Budapest, Hungary. Contact: Haleem J. Issaq, NCI-Frederick Cancer Research Facility, P.O. Box B, Frederick, Md. 21701, or Tibor Devenyi, Institute of Enzymology, Hungarian Academy of Sciences, Budapest, Hungary, October, p. 1266 A

■ **17th ACS Great Lakes Regional Meeting.** June 1-3. St. Paul, Minn. Contact: M. H. Baker, Chem/Serv Inc., 207 N.W. Sixth Street, Minneapolis, Minn. 55413

■ **29th International Congress of Pure and Applied Chemistry.** June 4-12. Cologne, West Germany. Contact: W. Fritzsche, General Secretariat of the 29th IUPAC Congress, c/o Gesellschaft Deutscher Chemiker, P.O. Box 90 04 40, D-6000 Frankfurt/Main 90, West Germany

■ **66th Canadian Chemical Confer-**

**ence and Exhibition.** June 5-8. Calgary, Alberta, Canada. Contact: Arvi Rauk, M.C.I.C., Department of Chemistry, University of Calgary, Calgary, Alberta T2N 1N4, Canada or The Chemical Institute of Ottawa, 151 Slater St., Suite 906, Ottawa, Ontario K1P 5N3, Canada. October, p. 1266 A

■ **International Symposium on Drug Analysis—From Pharmaceutical Preparation to Drug Monitoring.** June 7-10. Brussels, Belgium. Contact: C. Van Kerchove, Société Belge des Sciences Pharmaceutiques-Belgisch Genootschap voor Pharmaceutische Wetenschappen, rue Archimèdesstraat 11, B-1040 Brussels, Belgium

■ **Symposium on Affinity Chromatography and Biological Recognition.** June 13-17. Annapolis, Md. Contact: Symposium Secretariat, 9650 Rockville Pike, Bethesda, Md. 20814

■ **Symposium on Chromatography and Mass Spectrometry in Nutrition Science and Food Safety.** June 20-22. Montreux, Switzerland. Contact: Symposium Secretariat, Via Erifrea, 62-20157 Milan, Italy; Tel: (02) 35.54.546, Telex: 331268 Negri 1

■ **Symposium on Computers in Chemical Analysis.** June 22. Kansas City, Mo. Contact: Kathy Greene, ASTM Publications Division, American Society for Testing and Materials, 1916 Race St., Philadelphia, Pa. 19103. November, p. 1385 A

■ **13th ACS Northeast Regional Meeting.** June 26-29. West Hartford, Conn. Contact: J. Burlew, P.O. Box 418, Glastonbury, Conn. 06033; 203-633-4133

■ **23rd Colloquium Spectroscopicum Internationale and the 10th International Conference on Atomic Spectroscopy.** June 26-July 1. Amsterdam, The Netherlands. Contact: The Secretariat 23 CSI, Organisatie Bureau Amsterdam BV, Europaplein, 1078 GZ Amsterdam, The Netherlands, May, p. 712 A

■ **3rd Symposium on Separation Science and Technology for Energy Applications.** June 27-July 1. Gatlinburg, Tenn. Contact: A. P. Malinauskas, Oak Ridge National Laboratory, P.O. Box X, Oak Ridge, Tenn. 37830. July, p. 929 A

■ **5th European Congress of Clinical Chemistry.** July 3-8. Budapest, Hungary. Contact: MOTESZ Congress Bureau, Budapest POB 32 H1361, Hungary

■ **Seventh International Symposium on Nuclear Quadrupole Resonance.** July 11-14. Kingston, Ontario, Canada. Contact: R. J. C. Brown,

Chemistry Department, Queen's University, Kingston, Ontario, Canada K7L 3N6

■ **SAC 83—International Conference and Exhibition on Analytical Chemistry.** July 17–23. Edinburgh, U.K. Contact: P.E. Hutchinson, Secretary, Analytical Division, The Royal Society of Chemistry, Burlington House, London W1V 0BN, U.K. May, p. 713 A

■ **2nd International Conference on the Clinical Chemistry and Chemical Toxicology of Metals.** July 19–22. Montreal, Canada. Contact: Secretariat COMTOX 83 (TWCO), 340 MacLaren St., Ottawa, Ontario, Canada K2P 0M6

■ **35th National Meeting of the American Association for Clinical Chemistry.** July 24–29. New York, N.Y. Contact: AACC, 1725 K St., N.W., Washington, D.C. 20006; 202-857-0717. December, p. 1484 A

■ **3rd International Conference on the Instrumental Analysis of Foods and Beverages—Recent Developments.** July 27–30. Corfu, Greece. Contact: C. J. Mussinan, IFFR&D, 1515 Highway 36, Union Beach, N.J. 07085, 201-264-4500

■ **7th Australian Symposium on Analytical Chemistry.** Aug. 21–23. Adelaide, Australia. Contact: D. Paterson, AMDEL, Flemington Rd., Frewville, South Australia 5063

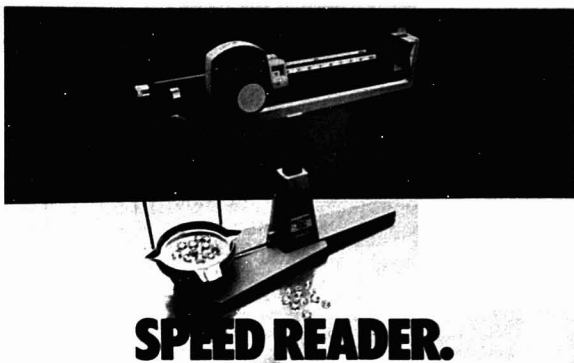
■ **186th ACS National Meeting.** Aug. 28–Sept. 2. Washington, D.C. Contact: A. T. Winstead, American Chemical Society, 1155 16th St., N.W., Washington, D.C. 20036; 202-872-4397

■ **9th International Symposium on Microchemical Techniques.** Aug. 28–Sept. 2. Amsterdam, The Netherlands. Contact: Symposium Secretariat, c/o Municipal Congress Bureau, Oudezijds Achterburgwal, 199, 1012 DK Amsterdam, The Netherlands

■ **4th Danube Symposium on Chromatography and 7th International Symposium on Advances and Applications of Chromatography in Industry.** Aug. 29–Sept. 2. Bratislava, Czechoslovakia. Contact: Jan Remen, The Analytical Section of the Czechoslovak Scientific and Technical Society, Slovnaft, 82300 Bratislava, Czechoslovakia

■ **1983 International Conference on Fourier Transform Spectroscopy.** Sept. 5–9. Durham, U.K. Contact: G. W. Chantry, Division of Electrical Science, National Physical Laboratory, Teddington, Middlesex TW11 0LW, U.K.

■ **29th IUPAC International Symposium on Macromolecules.** Sept. 5–9. Bucharest, Romania. Contact:



## SPEED READER.

The Ohaus® Dial-O-Gram® Model 310 balance gives you high accuracy and high-speed weighings at the lowest cost around—\$129.50 suggested list. Ideally suited for both lab and classroom jobs, this rugged American-made balance offers 1:31,000 resolution, a full 310 g capacity and readability of 0.01 g.

Increase your reading speed

with the Model 310. There isn't a faster, more sensitive balance for the money. Contact Ohaus or your preferred Ohaus dealer. Ohaus Scale Corporation, 29 Hanover Road, Floram Park, NJ 07932. (201) 377-9000.

**OHAS**  
**DIAL-O-GRAM**  
**MECHANICAL BALANCE**

© 1982 Ohaus Scale Corporation. Ohaus and Dial-O-Gram are trademarks of Ohaus Scale Corporation. Prices and specifications are subject to change without notice.

CIRCLE 158 ON READER SERVICE CARD

## With the new S&S Microfilter, samples make a fast 95% recovery.



The new S&S Microfilter is ideal for small sample filtration, from 20  $\mu$ l

to 2 ml, where sample loss must be minimized. Sample recovery is routinely up to 95%. Use this reusable, leak-proof microfilter in a centrifuge for the preparation of samples for HPLC, particulate removal, clarification or for sterile filtration. The S&S Microfilter (Cat. #SS009) accommodates the full range of S&S membrane filters. Contact us for more information. And start getting fast, 95% sample recovery.

## Schleicher & Schuell

Innovators in Separation Science  
Keene, N.H. 03431 (603) 352-3810

CIRCLE 193 ON READER SERVICE CARD

## Control laboratory bath temperature to $\pm 0.01^\circ\text{C}$



### with Techné Circulators and Baths

State-of-the-art solid state circuitry accounts for the reliability and outstanding temperature-control characteristics of Techné circulators and baths. The Tempunit<sup>®</sup>, with  $\pm 0.01^\circ\text{C}$

control and the Tempette<sup>®</sup> ( $\pm 0.02^\circ\text{C}$  control) are now available at new low prices. Both units have easy-to-adjust temperature-setting dials (Tempunit also has a temperature "memory"). An efficient circulating pump keeps temperature uniform throughout the bath. All units are sold through national dealers and are covered by a new two-year warranty. For full details, call or write

## Techné

Techné Incorporated  
3700 Brunswick Pike, Princeton, NJ 08540 • (609) 452-9275

CIRCLE 204 ON READER SERVICE CARD

## Low cost relief from high purity gas pains

Say good-bye to high purity gas pains. Johnson Matthey hydrogen purifiers quickly turn commercial grade hydrogen into the highest purity gas possible. And you save up to 70% in the process.

The secret is a palladium alloy diffusion membrane that blocks out all other gases and permits only ultra-pure hydrogen to pass through. The exchange is efficient, consistent and economical.

Johnson Matthey hydrogen purifiers. Available in capacities from 2 to 400 SCFH. No other product produces such high purity so economically. For additional information write: Johnson Matthey

Inc., Catalytic  
Systems Division,  
436 Devon Park  
Drive, Wayne, PA  
19087. Or call  
215-648-8500.



## JOHNSON MATTHEY

CIRCLE 115 ON READER SERVICE CARD

## Only Rabbits have better reproducibility than ALLTECH Columns



WHITE OR CALL FOR OUR NEW 320 PAGE  
CHROMATOGRAPHY CATALOG

## ALLTECH ASSOCIATES

2051 Waukegan Road • Deerfield, Illinois 60015  
(312) 941-8600

CIRCLE 5 ON READER SERVICE CARD

A STANDARD REFERENCE IN THE  
FIELD OF ANALYTICAL CHEMISTRY...

## FUNDAMENTAL REVIEWS

analytical  
chemistry

1982



Chances are you've heard a lot about this special volume. And it's no wonder! For here, in some 400 pages, are authoritative, up-to-date surveys of the most recent literature, with the outstanding work cited and digested.

Below are just a few of the areas covered in the 1982 Fundamental Reviews issue: Analytical

electrochemistry ■ Chromatography: gas, paper, thin-layer, liquid ■ Chemometrics ■ Kinetics ■ Surface analysis ■ Spectrometry: NMR, ESR, atomic, emission, IR, mass, X-ray ■ Nucleonics ■ Microscopy ■ Titrations

It's a portable library! And an enormous time-saver for any professional. Use the coupon below to order your copy today.

Distribution Center, American Chemical Society  
1155 Sixteenth Street, N.W., Washington, D.C. 20036

☐ Yes! Send me Fundamental Reviews. I enclose \$8 for each copy ordered.

Name \_\_\_\_\_

Address \_\_\_\_\_

City \_\_\_\_\_

State \_\_\_\_\_

Zip \_\_\_\_\_



**IUPAC MACRO '83, Calea Plevnei R-77131 Bucharest, Romania**

■ **2nd International Conference on Carbonaceous Particles in the Atmosphere.** Sept. 11-14. Linz, Austria. Contact: H. Puxbaum, Institute for Analytical Chemistry, Technical University of Vienna, Getreidemarkt 9, A-1060 Wien, Austria

■ **International Meeting on Chemical Sensors.** Sept. 19-22. Fukuoka, Japan. Contact: Noburu Yamazoe, Dept. of Materials Science and Technology, Graduate School of Engineering Sciences, Kyushu University, Kasuga, Kasuga-shi, Fukuoka 816, Japan

■ **12th Annual North American Thermal Analysis Society Meeting.** Sept. 25-29. Williamsburg, Va. Contact: Robert Johnson, Du Pont Central Research and Development Dept., Experimental Station, Bldg. 228, Wilmington, Del. 19898; 302-772-2198

■ **30th Canadian Spectroscopy Conference.** Oct. 6-8. Vancouver, British Columbia, Canada. Contact: Wesley Johnson, Mineral Energy, Mines, & Petroleum Resources, Par-

liament Buildings, Victoria, British Columbia, Canada; 604-387-6249

■ **Capillary Chromatography—2nd International Symposium.** Oct. 10-12. Tarrytown, N.Y. Contact: A. Zlatkis, University of Houston, Chemistry Department, Houston, Tex. 77004

■ **26th ORNL Conference on Analytical Chemistry in Energy Technology.** Oct. 11-13. Gatlinburg, Tenn. Contact: A. L. Harrod, Analytical Chemistry Division, Oak Ridge National Laboratory, P.O. Box X, Oak Ridge, Tenn. 37830

■ **Optical Society of America Annual Meeting.** Oct. 17-21. New Orleans, La. Contact: Optical Society of America, 1816 Jefferson Place, N.W., Washington, D.C. 20036; 202-223-8130

■ **18th ACS Midwest Regional Meeting.** Nov. 3-4. Lawrence, Kan. Contact: R. Givens, Department of Chemistry, University of Kansas, Lawrence, Kan. 66045; 913-864-3846, or W. Grindstaff, Southwest Missouri State University, Springfield, Mo. 65802

■ **ACS Southeastern Regional**

**Meeting.** Nov. 9-11. Charlotte, N.C. Contact: J. M. Frederickson, P.O. Box 111, Davidson, N.C. 28036; 704-892-7331

■ **9th International Congress and Exhibition for Instrumentation and Automation.** Nov. 10-16. Düsseldorf, FRG. Contact: INTERKAMA 83, Düsseldorf Messegelellschaft mbH, NOWEA, Postfach 32 02 03, D-4000 Düsseldorf 30, FRG

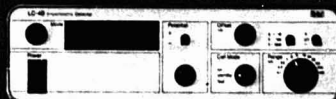
■ **39th ACS Southwest Regional Meeting.** Dec. 7-9. Tulsa, Okla. Contact: E. B. Butler, Tulsa Surchem, 4332 South Canton, Tulsa, Okla. 74135; 918-663-1877

## Short Courses

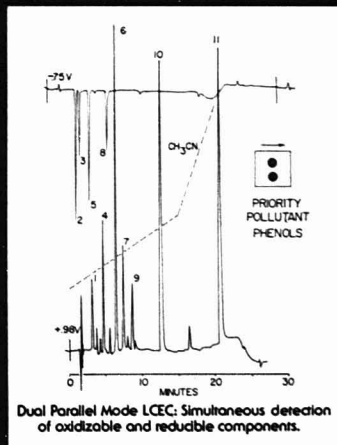
ACS courses. These new courses will be listed only once. For information on other ACS courses, see back issues and contact: Department of Educational Activities, American Chemical Society, 1155 16th St., N.W., Washington, D.C. 20036; 202-872-4508.

**Gas Chromatography, Theory & Practice**

# electrochemical detectors for liquid chromatography



**bar** bioanalytical system



CIRCLE 20 ON READER SERVICE CARD

**Blacksburg, Va. March 1-4.** Harold McNair. \$645, ACS members; \$715, nonmembers

**Microprocessors & Minicomputers: Interfacing and Applications**  
Blacksburg, Va. March 13-18. Raymond Dessy. \$665, ACS members; \$735, nonmembers

*The following courses are being offered in conjunction with the ACS National Meeting in Seattle, Wash.*

**Electronics for Laboratory Instrumentation**  
March 18-19. Howard Malmstadt, Chris Enke, Stanley Crouch. \$525, ACS members; \$595, nonmembers

**Statistics for Experimental Design**  
March 19-20. Stanley Deming, Stephen Morgan. \$395, ACS members; \$465, nonmembers

**High-Pressure Liquid Chromatography Workshop**

March 19-20. David Freeman. \$395, ACS members; \$465, nonmembers

**Column Selection in GC**  
March 19-20. Harold McNair. \$395, ACS members; \$465, nonmembers

**Laboratory Automation: Micro-, Mini-, or Midi-Computers**  
March 20-21. Raymond Dessy. \$395, ACS members; \$465, nonmembers

## We make our GC filters to get dirty.

Filters are made to get the junk out -- oxygen hidden in the carrier gas or lines, organic compounds trapped in compressed air or hydrogen. Even the best filters absorb all the junk they can and need to be changed. With conventional gas filters, that means shutting down your instrument and disconnecting the gas lines, just to change the filters.

Not so with Chrompack's Gas-Clean™ filter system! The Gas-Clean system has a specially constructed base plate which is connected to your gas line and to your chromatograph. And stays that way. The filter is attached with hand-pressure to break the seal and a simple bushing to secure the filter. A process of seconds. No need to shut down your instrument and let the column cool. No need to disconnect and flush gas lines and then reconnect. No danger of oxygen or dust contamination, thanks to specially constructed valves and dust protectors.

Filters are supposed to get dirty, so get the filters that are easy to change. Chrompack's Gas-Clean system. Call or write today for more information.



So we also make it a snap to change 'em.



Chrompack, Inc.  
P.O. Box 6795  
Bridgewater, N.J. 08807  
800-526-3687  
In NJ call:  
(201)722-8930



## For Your Information

Sybron Corporation has announced the formation of a new operating division to develop and expand its position in analytical instrumentation. The Analytical Products Division encompasses the analytical instrument business formerly part of Sybron's Taylor Instrument Company, and an organic carbon analyzer formerly offered by Sybron's Barnstead Company. The address for the division headquarters, as well as headquarters for U.S. operations, is Analytical Products Division, Sybron Corporation, 221 Rivermoor St., Boston, Mass. 02132; 617-469-3300.

**A Workshop on Analytical Chemistry Related to Canada's Nuclear Industry** will be held Oct. 24-26 on Hecia Island, Manitoba, Canada. It is open to anyone interested in either the routine or innovative analytical aspects of the uranium industry. It will emphasize small, informal discussion groups organized around a central theme. The subject matter should fit into one of the following categories: present problems, present work, or future plans and projects. Participants will be requested to forward their affiliations, areas of interest, and a brief abstract of the subject they wish to discuss by June 1. For further details, contact P. Campbell, Whiteshell Nuclear Research Establishment, Pinawa, Manitoba, Canada ROE 1L0.

The dates and application deadline for the NATO Advanced Study Institute on Chemometrics which were announced in the November NEWS section (*Anal. Chem.* 1982, 54, 1384 A) have been changed. The Study Institute will now be held Sept. 12-23 and the deadline for receipt of applications has been extended to March 31. Further information can be obtained from Bruce Kowalski, Department of Chemistry, University of Washington, Seattle, Wash. 98195.

CIRCLE 33 ON READER SERVICE CARD

# COMPUTER POWER. SUPERIOR OPTICS.

## GET ALL THE COMPUTER YOU NEED.

Our competitors are proud to offer a computer. The *Plasma-200™* ICP from Instrumentation Laboratory offers something better: a choice. In addition to the integral microcomputer that makes this instrument the most auto-



mated plasma available, IL's ICP has two different data station options to speed and simplify workflow in your lab. Our *PDS-1™* data station offers all the computer power most labs need, at a price you'll appreciate. And the *PDS-1000™* data station is built around the Pixel 100/AP™ supermicro, the most powerful, flexible microcomputer in the world.

## NO-COMPROMISE OPTICS.

An ICP is only as good as its optics. A truly superior plasma optical system would include a double monochromator to minimize stray light, automatically variable torch height for maximum emission intensity, a mercury lamp reference to continuously adjust wavelength calibration, two-channel capability to speed analysis, and a dedicated vacuum monochromator for uncompromising performance in VUV analysis. For laboratories who are

unwilling to compromise the quality of their analyses, there is only one ICP which offers those features: the IL *Plasma-200* ICP.

If you're looking at plasma emission spectrometers for your lab, compare the IL *Plasma-200* ICP. You can't buy more in an ICP.

For information call toll-free:  
**800-343-0322.**

Instrumentation Laboratory Inc.  
Analytical Instrument Division  
One Burrill Road, Andover, MA 01810



**Instrumentation  
Laboratory**

CIRCLE 111 ON READER SERVICE CARD

# YOU CAN'T BUY MORE IN AN ICP.

## Thomas Cairns

Department of Health and Human Services  
Food and Drug Administration  
Office of the Executive Director for Regional Operations  
1521 West Pico Boulevard  
Los Angeles, Calif. 90015

## W. Michael Rogers

Department of Health and Human Services  
Food and Drug Administration  
5600 Fishers Lane  
Rockville, Md. 20857

**Table I. Selective List of Environmental Laws and Significant World Events**

1962	Rachel Carson's "Silent Spring" published
1963	Clean Air Act (PI 88-206)
1965	Motor Vehicle Air Pollution Control Act (amendments to Clean Air Act, PI 89-272)
1969	Santa Barbara oil blowout Endangered Species Conservation Act (PI 91-135) National Environmental Policy Act of 1969 (PI 91-190)
1970	Earth Day initiated Environmental Protection Agency created
1972	United Nations Conference on the Environment held in Stockholm Marine Protection, Research, and Sanctuaries Act (PI 92-532)
1973	Arab oil embargo
1974	Energy Supply and Environmental Coordination Act (PI 93-319) Alaska pipeline approved by U.S. Congress Safe Drinking Water Act (PI 93-523)
1976	Toxic Substances Control Act (PI 94-469) Resource Conservation and Recovery Act (PI 94-580)
1977	Major amendment to Clean Air Act (PI 95-85) Water Pollution Control Act (PI 95-217)
1978	Major energy legislation (PI 95-617, -618, -619, -620, and -621)

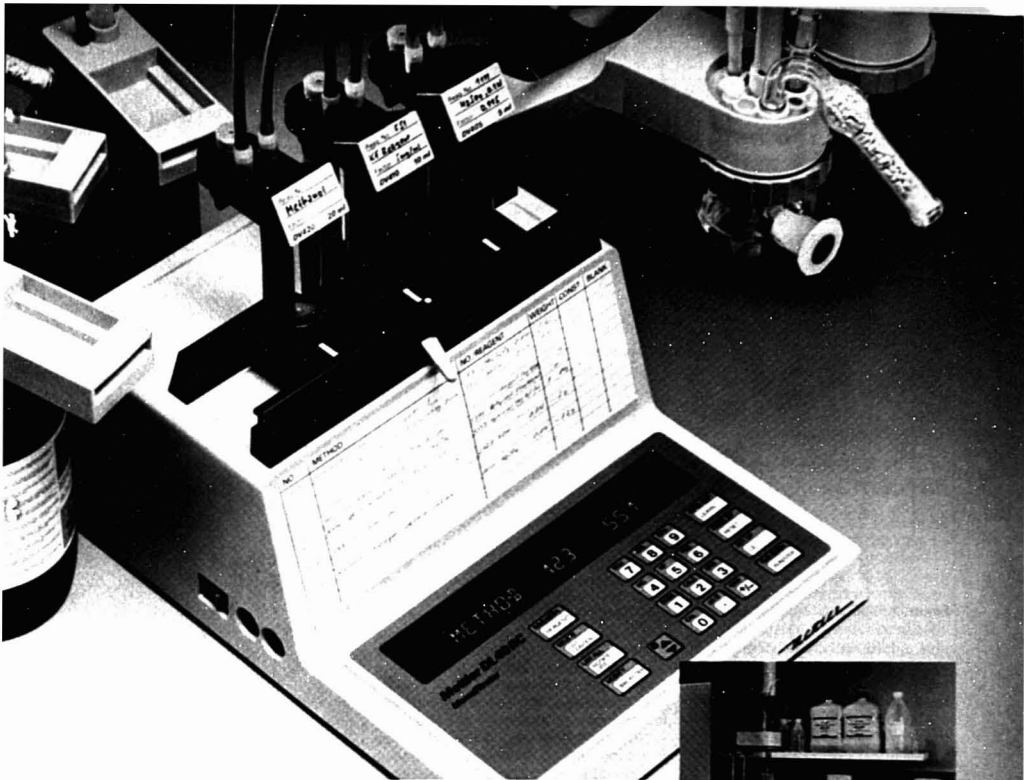
**Table II. Significant Amendments to the Federal Food, Drug, and Cosmetic Act with Key Clauses and Events**

1958	Food Additive Amendment of 1958 (PI 85-929) Delaney Amendment—409 (c) (3) (A) "... Provided, That no additive shall be deemed to be safe if it is found to induce cancer when ingested by man or animal, or if it is found, after tests which are appropriate for the evaluation of the safety of food additives, to induce cancer in man or animal ...."
1960	Color Additive Amendment (PI 86-618)
1961	Infamous Thalidomide incident in Great Britain
1962	Drug Amendments of 1962 (PI 87-781) DES proviso "... no residue ... [may be] found ... by methods of examination prescribed or approved by the Secretary ... in any edible portion of such animals ..."
1968	Animal Drug Amendment (PI 90-399)

## Acceptable Analytical Data for Trace Analysis

In several important ways, the recent symposium "Improving the Analytical Chemistry/Regulatory Interface," held at the National Bureau of Standards, Oct. 19-21, 1982, was a major milestone in the effort to come to grips with an intriguing scientific challenge and a public policy issue of profound importance. This paper was presented at the symposium to stimulate the analytical community to consider a standard protocol for quantitative trace analysis when no official methods exist.

Since the publication of Rachel Carson's "Silent Spring" in 1962, a veritable plethora of environmental laws have been passed by the U.S. Congress (Tables I and II). This intensive legislative activity has culminated in a dramatic increase in the role of analytical chemistry in the protection of the public health. Trace analysis has quickly become a buzzword of the discipline. Analytical chemistry has been elevated by the various laws to being a rate-determining element in the formulation and execution of public health initiatives. The position of analytical chemistry in the decision tree of public health protection (Figure 1) must be considered unique from several vantage points (1). Clearly the emphasis placed on trace analysis mandates technological advancements at a faster pace. Perhaps the most disturbing pressures applied by this decision tree, however, are those inadvertently applied by toxicological studies and risk assessment. Both these disciplines frequently use extrapolation methodologies. The resultant "safe" levels are often below the current level of detection and, hence, not quantifi-



## All the titration capability you need. The Mettler DL40RC MemoTitrator.

The MemoTitrator just got new remote control capability, improved software, a second titration head, an automatic sample transport module, and a new model designation: DL40RC. This single, improved instrument can handle all types of titrations. It stores up to 19 methods, performs endpoint, equilibrium and incremental titrations—links them—and prints out results in required units.

### **It's an all-purpose automatic titrator.**

Plug in the Mettler RT40 Sample Transport peripheral and you can do a series of up to 16 samples. The RT40 can accept and store

up to 50 sample weights from a connected balance.

### **It's a Karl Fischer titrator.**

The DL40RC has improved software to handle the new two-component titrants. Dual titration heads allow you to work more efficiently by switching from one head to the other.

**It's a nitrogen and protein analyzer.** You can connect a Kjeldahl/Nitrogen Analyzer to the DL40RC to quickly determine percent nitrogen or protein.

The new model DL40RC MemoTitrator is all the titration capability you need. For a demonstration or more information, complete the coupon and send it to us.

Mettler Instrument Corporation,  
Box 71, Hightstown, NJ 08520-9944,  
Phone (609) 448-3000

- ☐ Send me complete information on the new DL40RC MemoTitrator.  
☐ I'd like a demonstration

Name

Company

Address

City

State  Zip

Phone

(Area Code) (Number)

**METTLER**

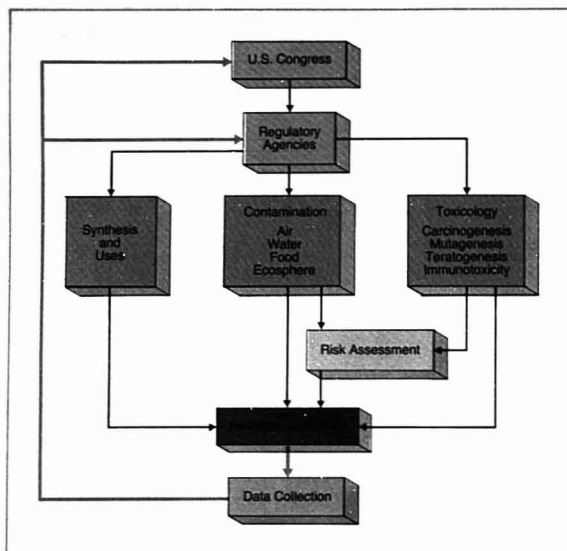


Figure 1. Role of analytical chemistry in public health protection

able. Additionally, legislative processes place a considerable burden on analytical chemistry by continual reference to "no residue" and "appropriate methods of examination." Such pressures have forced innovative technological advancements, but at increased costs. Use of advanced technology, such as gas chromatography/mass spectrometry (GC/MS) with various modes of ionization, has proved highly successful. Trace analysis has thus involved higher levels of analytical expertise and higher instrumental costs (Table III).

No mention of accuracy and precision has yet been made. Perhaps the main reason for avoiding a critical discussion of these two important criteria is that ad hoc methods developed to deal effectively with emergency situa-

tions cannot be validated by interlaboratory testing. Apart from the delay in gaining official method status, the cost of conducting such a collaborative study can be prohibitive. However, the prevailing attitude that trace analyses are more expensive (2) due to the additional analytical testing needed to generate reliability data must be balanced by a counter argument. More sophisticated instrumentation is usually necessary to implement trace analysis, but the high degree of specificity provided by such instrumentation should be sufficient to maintain an acceptable degree of reliability. Moreover, the apparent decrease in accuracy and precision at the ppm, ppb, and ppt levels should be tolerated by viewing the acquired data with different set of guidelines from that

presently employed for validated methods.

### Proposals for Acceptable Analytical Data

The situation most frequently encountered in the real world is reflected in management's expectations that the analytical chemist can respond to an immediate need by developing methodology to quantitate trace contaminants of interest. Usually no official methods exist or, if they do, the limit of detection is frequently insufficient. In the formulation of this set of proposed criteria, attention was paid to the main elements leading to general acceptance of data generated by a method:

- specificity,
- stability and recovery data,
- linearity of technique,
- variability,
- blanks,
- limit of detection,
- limit of quantitation,
- interferences,
- the analyst factor, and
- the laboratory environment.

The following guidelines are offered as a proposal in an attempt to provide a uniform acceptable approach in the design of nonofficial methods for trace analysis.

- Analytical techniques employed should be well established in the laboratory performing the trace analysis.
- A calibration curve should address at least three different concentrations about the measurement range with at least three measurements at each concentration to provide a coefficient of correlation no less than 0.94. (As a general principle, it is preferable to perform more measurements at the lower levels and fewer at the higher concentrations.) The concentration range covered must include one order of magnitude above the expected trace level and one order of magnitude below the trace level or at the limit of quantitation, whichever is greater.
- Stability and recovery experiments should be conducted in the matrix involved with a minimum of two duplicate spikes, i.e., at the level found and one-tenth of the level found or at the limit of quantitation, whichever is greater.
- Determination of the limit of detection of the method should be performed [signal-to-noise (S/N) no less than 3:1].
- Determination of the limit of quantitation of the method in the matrix used should be performed (S/N no less than 10:1).
- A blank in the matrix under study should be performed at the level found and at the noise level. If possi-

Table III. Trace Analysis and Its Technological Implications

Amount to be detected	Weight (g)	Trace contamination/g	Number of molecules *	Instrumental technique required
Milligram (mg)	$10^{-3}$	1 ppth	$10^{18}$	Titration
Microgram ( $\mu$ g)	$10^{-6}$	1 ppm	$10^{15}$	Spectrophotometric
Nanogram (ng)	$10^{-9}$	1 ppb	$10^{12}$	Gas chromatographic
Picogram (pg)	$10^{-12}$	1 ppt	$10^9$	Mass spectrometric
Femtogram (fg)	$10^{-15}$	1 ppqa	$10^6$	Mass spectrometric
Attogram (ag)	$10^{-18}$	1 ppqi	$10^3$	Yet to be discovered
(Mologram)?	$10^{-21}$	1 ppsex	$10^1$	

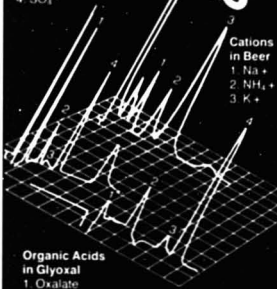
\* Based on a molecular weight of 300



# impressive ion analysis

Anions in  
Mineral Water

1. Cl<sup>-</sup>
2. NO<sub>3</sub><sup>-</sup>
3. Unknown
4. SO<sub>4</sub><sup>2-</sup>



Organic Acids  
in Glyoxal

1. Oxalate
2. Glyoxylate
3. Glycolate
4. Formate

These chromatograms dramatically show the potential of Ion Chromatography for rapid, high-sensitivity analysis of ions in complex matrices.

Wescan's single-column approach to Ion Chromatography goes beyond conventional IC to provide unprecedented savings in both initial investment and operating cost.

Let us send you the facts.

Wescan Ion  
Analyzer Systems  
as low as \$9800.  
Conductivity Detectors as  
low as \$2450.

# impressive price

## WESCAN

Ion Chromatography...  
the single-column way

Wescan Instruments, Inc.  
3018 Scott Blvd.  
Santa Clara, CA 95050  
(408) 727-3519

CIRCLE 230 ON READER SERVICE CARD

ble, the matrix should be free of the analyte being determined.

- Specificity of identification (confirmation) of the measured analyte should be provided by an alternate determinative step where possible, e.g., NMR, IR, or GC/MS. GC/MS provides the least ambiguous confirmation.

Such a set of guidelines would ensure a priori acceptance by the analytical community for only those cases where time was of the essence in responding to a contamination problem. Often it is a disparity between government, state, and industrial laboratories that causes major hurdles in reaching a consensus. While these proposed guidelines would not directly answer questions regarding absolute reliability, a quality assurance program conducted at the data-gathering laboratory site should help give credibility to the developed method, particularly if certified standards from NBS are employed. The role of NBS as an interested first party rather than the repeatedly referred to "disinterested third party" in the determination of trace organics in various matrices would be a step in the right direction.

The emphasis of this proposal centers on "acceptability" rather than method "validation" (3). Relaxing the strict standards imposed by a round-robin situation is essential to understanding the role analytical chemistry must play in trace analysis for public purposes. For the record, it is clearly understood that other considerations beyond the scientific data are sometimes included in the decision-making process, and these guidelines should not be construed so as to interfere with legal, economic, and political aspects of contamination cases under scrutiny. However, the savings in time and laboratory personnel to be gained by adoption of sound yet flexible acceptance guidelines would instill greater confidence in the analytical community and prevent protracted discussions leading to misunderstanding, confusion, and delayed consumer protection.

### Disclaimer

The views expressed are those of the authors and do not necessarily reflect the policy of the U.S. Food and Drug Administration.

### References

- (1) Cairns, T. "The Increased Role of Chemistry in Toxicology," in "The Pesticide Chemist and Modern Toxicology"; ACS Symposium 160, 1981; p. 355.
- (2) Horwitz, W. "Evaluation of Analytical Methods for Regulation of Foods and Drugs," *Anal. Chem.* 1982, 54, 67 A.
- (3) Crummett, W. B. "Guidelines for Data Acquisition and Data Quality Evaluation in Environmental Chemistry," *Anal. Chem.* 1980, 52, 2243.

## For Strength, Durability, Inertness and Reproducibility Use the New GLT Packed Column From SGE



### The New GLT™ Packed Column Has It All

**STRENGTH** The GLT Column is protected by a sleeve of stainless steel which allows the borosilicate glass lining to stand up to the toughest laboratory conditions.

**DURABILITY** The GLT effectively eliminates the problem of column fragility without sacrificing inertness.

**REPRODUCIBILITY** Through the use of consistent column packing techniques and rigorous quality control procedures, a high degree of column to column reproducibility is insured.

**INERTNESS** The GLT exhibits extremely high levels of inertness from batch to batch... at a level which is equal to the best all glass column.

For the complete GLT story contact your nearest SGE sales office.



**Head Office:**  
Scientific Glass Engineering Pty. Ltd.  
7 Argent Place, Ringwood,  
Victoria, 3134 Australia  
Tel: (03) 874-6333

**UK Sales Office:**  
Scientific Glass Engineering (U.K.)  
Ltd.  
Potters Lane, Kirt Farm  
Milton Keynes MK11 3LA  
Tel: (0908) 568844

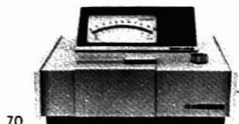
**U.S.A. Sales Office:**  
Scientific Glass Engineering Inc.  
2007 Kramer Lane, Suite 100,  
Austin, Texas 78758, U.S.A.  
Tel: (512) 837-7190

**German (BRD) Sales Office:**  
Scientific Glass Engineering GmbH.  
Fichtenweg 15,  
D-6108 Weiterstadt 1  
Tel: (06150) 40662

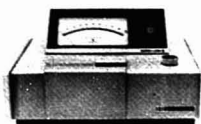
CIRCLE 195 ON READER SERVICE CARD

# Circle 27 on the reader service card for a FREE demonstration on Bausch & Lomb Spectrophotometers.

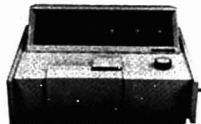
## Spectrophotometers of practical excellence



70



88



710

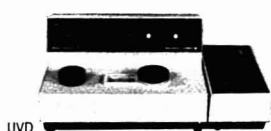
Select from three superior instruments. SPECTRONIC® 70 and 88 spectrophotometers provide wavelength ranges from 325-925nm and 8nm spectral slitwidths. SPECTRONIC 710 has 200-1000nm wavelength range, 2nm spectral slitwidth. All accept test tubes, multiple rectangular cuvettes, long-path cells. Accessory flow-thru

cell fits 88, 710. 70, big meter, only two operating controls. 88, meter readout linear in %T, C, and 2 ranges of A. 710, digital readout, simple calibration controls, FACTOR SET button to check reagent quality and instrument setup, GAIN switch for selectable sensitivity.

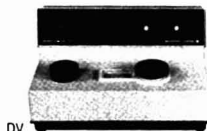
## SPECTRONIC 21—the value line of spectrophotometers



MV



UVD

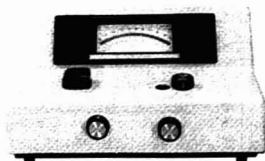


DV

Choose the best model for you and your budget. • Model MV—meter readout, visible range • Model DV—digital readout, visible range • Model UVD—digital readout, UV-visible range. Visible range models cover 340 to 1000nm. UVD covers 200 to 1000nm. All provide narrow 10nm spectral slitwidth. MV displays linear %T, nonlinear A.

Digital models offer direct readout in %T, A, and C—plus feature to check reagent quality and instrument electronic calibration. Accessory sample compartment permits multiple cuvette and long-path testing.

## SPECTRONIC 20



**SPECTRONIC 20**, the world's most widely used spectrophotometer. Over 100,000 sold. Simple, easy-to-use, 340-960nm range, 20nm spectral slitwidth.

**LIQUICELL™ Sampling Accessory** analyzes intensely colored samples without dilution. LIQUICELL replaces standard SPECTRONIC 21 sample compartment. Consists of short-path flowcell and diaphragm pump.

**SPECTRONIC 2000 UV-vis double-beam scanning spectrophotometer** reads in T, A, C, 1st and 2nd derivative. Microprocessor performs routine tasks under control of operator. Built-in programs are easily modified by operator to customize testing. LED displays, built-in printer and two types of chart recorders provide full variety of information. Wide selection of sample-handling accessories available, including microprocessor-controlled thermostatic flowcell for

## LIQUICELL™ Sampling Accessory



## SPECTRONIC 2000 UV-vis double-beam scanning spectrophotometer



kinetics. Prints test parameters after each run. Printer/recorder combination enables operator to easily, accurately interpret scans and duplicate previous test conditions. Printed messages and audible signals advise operator of invalid commands or error conditions. Digital display lets the operator see data as it is entered. Accessory p-c board contains kinetics, repeat scan, multiple wavelength-analysis programs. RS-232-C-compatible computer interface accessory permits 2-way digital communication/control with external devices.

For a free demonstration, call 800-828-6967, or in New York State, call (716) 338-8423. Or write Bausch & Lomb, Instruments & Systems Division, P.O. Box 3807, Rochester, New York 14610.

**BAUSCH & LOMB** 

2E006

CIRCLE 27 ON READER SERVICE CARD

# Space is Money

**This  
publication  
is available  
in  
Microform.**

**Call Toll Free  
800-424-6747**

for prices and information on  
American Chemical Society  
publications in microform and  
microfilm

**American Chemical Society**  
1155 16th Street, N.W.  
Washington, D.C. 20036

**JANUARY 1983**

ADVERTISED PRODUCTS:

7	8	9	10	11	12	13	14	15	16	17																																																																																																																																																																																																																																																																																																																																																																																																																																																																																																																																																																																																																																																																																																																																																																																																																																																																																																																																																																																																																																																																																																																																																																																																																																																																																																																																																																																																								
---	---	---	----	----	----	----	----	----	----	----	--	--	--	--	--	--	--	--	--	--	--	--	--	--	--	--	--	--	--	--	--	--	--	--	--	--	--	--	--	--	--	--	--	--	--	--	--	--	--	--	--	--	--	--	--	--	--	--	--	--	--	--	--	--	--	--	--	--	--	--	--	--	--	--	--	--	--	--	--	--	--	--	--	--	--	--	--	--	--	--	--	--	--	--	--	--	--	--	--	--	--	--	--	--	--	--	--	--	--	--	--	--	--	--	--	--	--	--	--	--	--	--	--	--	--	--	--	--	--	--	--	--	--	--	--	--	--	--	--	--	--	--	--	--	--	--	--	--	--	--	--	--	--	--	--	--	--	--	--	--	--	--	--	--	--	--	--	--	--	--	--	--	--	--	--	--	--	--	--	--	--	--	--	--	--	--	--	--	--	--	--	--	--	--	--	--	--	--	--	--	--	--	--	--	--	--	--	--	--	--	--	--	--	--	--	--	--	--	--	--	--	--	--	--	--	--	--	--	--	--	--	--	--	--	--	--	--	--	--	--	--	--	--	--	--	--	--	--	--	--	--	--	--	--	--	--	--	--	--	--	--	--	--	--	--	--	--	--	--	--	--	--	--	--	--	--	--	--	--	--	--	--	--	--	--	--	--	--	--	--	--	--	--	--	--	--	--	--	--	--	--	--	--	--	--	--	--	--	--	--	--	--	--	--	--	--	--	--	--	--	--	--	--	--	--	--	--	--	--	--	--	--	--	--	--	--	--	--	--	--	--	--	--	--	--	--	--	--	--	--	--	--	--	--	--	--	--	--	--	--	--	--	--	--	--	--	--	--	--	--	--	--	--	--	--	--	--	--	--	--	--	--	--	--	--	--	--	--	--	--	--	--	--	--	--	--	--	--	--	--	--	--	--	--	--	--	--	--	--	--	--	--	--	--	--	--	--	--	--	--	--	--	--	--	--	--	--	--	--	--	--	--	--	--	--	--	--	--	--	--	--	--	--	--	--	--	--	--	--	--	--	--	--	--	--	--	--	--	--	--	--	--	--	--	--	--	--	--	--	--	--	--	--	--	--	--	--	--	--	--	--	--	--	--	--	--	--	--	--	--	--	--	--	--	--	--	--	--	--	--	--	--	--	--	--	--	--	--	--	--	--	--	--	--	--	--	--	--	--	--	--	--	--	--	--	--	--	--	--	--	--	--	--	--	--	--	--	--	--	--	--	--	--	--	--	--	--	--	--	--	--	--	--	--	--	--	--	--	--	--	--	--	--	--	--	--	--	--	--	--	--	--	--	--	--	--	--	--	--	--	--	--	--	--	--	--	--	--	--	--	--	--	--	--	--	--	--	--	--	--	--	--	--	--	--	--	--	--	--	--	--	--	--	--	--	--	--	--	--	--	--	--	--	--	--	--	--	--	--	--	--	--	--	--	--	--	--	--	--	--	--	--	--	--	--	--	--	--	--	--	--	--	--	--	--	--	--	--	--	--	--	--	--	--	--	--	--	--	--	--	--	--	--	--	--	--	--	--	--	--	--	--	--	--	--	--	--	--	--	--	--	--	--	--	--	--	--	--	--	--	--	--	--	--	--	--	--	--	--	--	--	--	--	--	--	--	--	--	--	--	--	--	--	--	--	--	--	--	--	--	--	--	--	--	--	--	--	--	--	--	--	--	--	--	--	--	--	--	--	--	--	--	--	--	--	--	--	--	--	--	--	--	--	--	--	--	--	--	--	--	--	--	--	--	--	--	--	--	--	--	--	--	--	--	--	--	--	--	--	--	--	--	--	--	--	--	--	--	--	--	--	--	--	--	--	--	--	--	--	--	--	--	--	--	--	--	--	--	--	--	--	--	--	--	--	--	--	--	--	--	--	--	--	--	--	--	--	--	--	--	--	--	--	--	--	--	--	--	--	--	--	--	--	--	--	--	--	--	--	--	--	--	--	--	--	--	--	--	--	--	--	--	--	--	--	--	--	--	--	--	--	--	--	--	--	--	--	--	--	--	--	--	--	--	--	--	--	--	--	--	--	--	--	--	--	--	--	--	--	--	--	--	--	--	--	--	--	--	--	--	--	--	--	--	--	--	--	--	--	--	--	--	--	--	--	--	--	--	--	--	--	--	--	--	--	--	--	--	--	--	--	--	--	--	--	--	--	--	--	--	--	--	--	--	--	--	--	--	--	--	--	--	--	--	--	--	--	--	--	--	--	--	--	--	--	--	--	--	--	--	--	--	--	--	--	--	--	--	--	--	--	--	--	--	--	--	--	--	--	--	--	--	--	--	--	--	--	--	--	--	--	--	--	--	--	--	--	--	--	--	--	--	--	--	--	--	--	--	--	--	--	--	--	--	--	--	--	--	--	--	--	--	--	--	--	--	--	--	--	--	--	--	--	--	--	--	--	--	--	--	--	--	--	--	--	--	--	--	--	--	--	--	--	--	--	--	--	--	--	--	--	--	--	--	--	--	--	--	--	--	--	--	--	--	--	--	--	--	--	--	--	--	--	--	--	--	--	--	--	--	--	--	--	--	--	--	--	--	--	--	--	--	--	--	--	--	--	--	--	--	--	--	--	--	--	--	--	--	--	--	--	--	--	--	--	--	--	--	--	--	--	--	--	--	--	--	--	--	--	--	--	--	--	--	--	--	--	--	--	--	--	--	--	--	--	--	--	--	--	--	--	--	--	--	--	--	--	--	--	--	--	--	--	--	--	--	--	--	--	--	--	--	--	--	--	--	--	--	--	--	--	--	--	--	--	--	--	--	--	--	--	--	--	--	--	--	--	--	--	--	--	--	--	--	--	--	--	--	--	--	--	--	--	--	--	--	--	--	--	--	--	--	--	--	--	--	--	--	--	--	--	--	--	--	--	--	--	--	--	--	--	--	--	--	--	--	--	--	--	--	--	--	--	--	--	--	--	--	--	--	--	--	--	--	--	--	--	--	--	--	--	--	--	--	--	--	--	--	--	--	--	--	--	--	--	--	--	--	--	--	--	--	--	--	--	--	--	--	--	--	--	--	--	--	--	--	--	--	--	--	--	--	--	--	--	--	--	--	--	--	--	--

NEW PRODUCTS	401	402	403	404	405	406	407
408	409	410	411	412	413	414	415
416	417	418	419	420	421	422	423
424	425	426	427	428	429	430	431
432	433	434	435	436	437	438	439
440	441	442	443	444	445	446	447
448	449	450	451	452	453	454	455
456	457	458	459	460	461	462	463
464	465	466	467	468	469	470	471
472	473	474	475	476	477	478	479
480	481	482	483	484	485	486	487
488	489	490	491	492	493	494	495

VALID THROUGH  
MAY 1983

TO VALIDATE THIS CARD, PLEASE CHECK  
ONE ENTRY FOR EACH CATEGORY BELOW:

- Intensity of product need:  
☐ 1. Have salesman call  
☐ 2. Need within 6 mos.  
☐ 3. Future project

Primary field of work:

- ☐ A. Energy  
☐ B. Environmental  
☐ C. Medical/Clinical  
☐ D. Drug/Toiletries  
☐ E. Forensic/Narcotic  
☐ F. Biotechnology  
☐ G. Metals  
☐ H. Pulp/Paper/Wood  
☐ I. Soaps/Cleaners  
☐ J. Paint/Coating/Ink  
☐ K. Electrical/Electronic  
☐ L. Instrument Dev. Des.  
☐ M. Plastic/Polymer/Rub.  
☐ N. Agricultural/Food  
☐ O. Inorganic Chemicals  
☐ P. Organic Chemicals

- Primary area of employment:  
 INDUSTRIAL  
☐ A. Research/Development  
☐ B. Quality/Process Control  
 MEDICAL/HOSPITAL  
☐ C. Research/Development  
☐ D. Clinical/Diagnostic  
 GOVERNMENT  
☐ E. Research/Development  
☐ F. Regulate/Investigate  
 COLLEGE/UNIVERSITY  
☐ G. Research/Development  
☐ H. Teaching  
 INDEPENDENT/CONSULTING  
☐ I. Research/Development  
☐ J. Analysis/Testing

CIRCLE 314 FOR

SUBSCRIPTION  
FORM TO  
ANALYTICAL  
CHEMISTRY

NAME \_\_\_\_\_  
 TITLE \_\_\_\_\_  
 FIRM \_\_\_\_\_  
 STREET \_\_\_\_\_  
 CITY \_\_\_\_\_  
 STATE \_\_\_\_\_ ZIP \_\_\_\_\_  
 PHONE (\_\_\_\_) \_\_\_\_\_

**NEED MORE INFORMATION?**

**CIRCLE a key number . . .**

**SEND IN the postage paid**

**reply card . . .**

**AND GET free data on any product  
advertised in this issue. . .**



NO POSTAGE  
NECESSARY  
IF MAILED  
IN THE  
UNITED STATES

**BUSINESS REPLY CARD**

FIRST CLASS Permit #27346 Philadelphia, Pa.

POSTAGE WILL BE PAID BY ADDRESSEE

**analytical  
chemistry**

P.O. BOX #7826  
PHILADELPHIA, PA 19101





NO POSTAGE  
NECESSARY  
IF MAILED  
IN THE  
UNITED STATES

# BUSINESS REPLY CARD

FIRST CLASS Permit #27346 Philadelphia, Pa.

POSTAGE WILL BE PAID BY ADDRESSEE

**analytical**  
chemistry

P.O. BOX #7826  
PHILADELPHIA, PA 19101



**NEED MORE INFORMATION?**

**CIRCLE a key number. . .**

**SEND IN the postage paid**

**reply card. . .**

**AND GET free data on any product**

**advertised in this issue. . .**

## JANUARY 1983

ADVERTISED PRODUCTS:									
7	8	9	10	11	12	13	14	15	16
18	19	20	21	22	23	24	25	26	27
29	30	31	32	33	34	35	36	37	38
40	41	42	43	44	45	46	47	48	49
51	52	53	54	55	56	57	58	59	60
62	63	64	65	66	67	68	69	70	71
73	74	75	76	77	78	79	80	81	82
84	85	86	87	88	89	90	91	92	93
95	96	97	98	99	100	101	102	103	104
106	107	108	109	110	111	112	113	114	115
117	118	119	120	121	122	123	124	125	126
128	129	130	131	132	133	134	135	136	137
139	140	141	142	143	144	145	146	147	148
150	151	152	153	154	155	156	157	158	159
161	162	163	164	165	166	167	168	169	170
172	173	174	175	176	177	178	179	180	181
183	184	185	186	187	188	189	190	191	192
194	195	196	197	198	199	200	201	202	203
205	206	207	208	209	210	211	212	213	214
216	217	218	219	220	221	222	223	224	225
227	228	229	230	231	232	233	234	235	236
238	239	240	241	242	243	244	245	246	247
249	250	251	252	253	254	255	256	257	258
260	261	262	263	264	265	266	267	268	269
271	272	273	274	275	276	277	278	279	280
282	283	284	285	286	287	288	289	290	291
293	294	295	296	297	298	299	300	301	302
304	305	306	307	308	309	310	311	312	313

VALID THROUGH  
MAY 1983

TO VALIDATE THIS CARD, PLEASE CHECK  
ONE ENTRY FOR EACH CATEGORY BELOW:

- Intensity of product need:**
- ☐ 1. Have salesman call
  - ☐ 2. Need within 6 mos.
  - ☐ 3. Future project
- Primary area of employment:**
- ☐ A. Research/Development
  - ☐ B. Quality/Process Control
  - ☐ MEDICAL/HOSPITAL
  - ☐ C. Research/Development
  - ☐ D. Clinical/Diagnostic
  - ☐ GOVERNMENT
  - ☐ E. Research/Development
  - ☐ F. Regulate/Investigate
  - ☐ COLLEGE/UNIVERSITY
  - ☐ G. Research/Development
  - ☐ H. Teaching
  - ☐ INDEPENDENT/CONSULTING
  - ☐ I. Research/Development
  - ☐ J. Analysis/Testing
- Primary field of work:**
- ☐ A. Energy
  - ☐ B. Environmental
  - ☐ C. Medical/Clinical
  - ☐ D. Drug/Toxines
  - ☐ E. Forensic/Narcotic
  - ☐ F. Biotechnology
  - ☐ G. Metals
  - ☐ H. Pulp/Paper/Wood
  - ☐ I. Soaps/Cleaners
  - ☐ J. Paint/Coating/Ink
  - ☐ K. Electrical/Electronic
  - ☐ L. Instrument Dev./Des
  - ☐ M. Plastic/Polymer/Rub
  - ☐ N. Agricultural/Food
  - ☐ O. Inorganic Chemicals
  - ☐ P. Organic Chemicals

**CIRCLE 314 FOR  
SUBSCRIPTION  
FORM TO  
ANALYTICAL  
CHEMISTRY**

NAME: \_\_\_\_\_  
TITLE: \_\_\_\_\_  
FIRM: \_\_\_\_\_  
STREET: \_\_\_\_\_  
CITY: \_\_\_\_\_  
STATE: \_\_\_\_\_ ZIP: \_\_\_\_\_  
PHONE: (\_\_\_\_) \_\_\_\_\_

## Reagent Chemicals

**Sixth Edition  
Now Available!**

*American Chemical Society  
Specifications*



Analytical chemists — update  
your reference shelf by ordering  
this indispensable handbook of  
the latest ACS specifications.

This new 6th Edition has been improved and expanded. Eight new items appear for the first time in this valuable book — among them are three solvents especially controlled for use in the analysis of pesticides. Other important new features included in this new edition are assay limits and tests which have been established to define most of the hydrates for which monographs currently exist. The section on Definitions, Procedures, and Standards has also been extensively expanded to include many of the general procedures used in monograph tests.

Future supplements will be sent free to purchasers of this book.

### CONTENTS

Preface  
Definitions, Procedures, and Standards  
Interpretation of Requirements  
Precautions for Tests  
General Directions and Procedures  
Reagent Solutions  
Standard Solutions  
Solid Reagent Mixtures

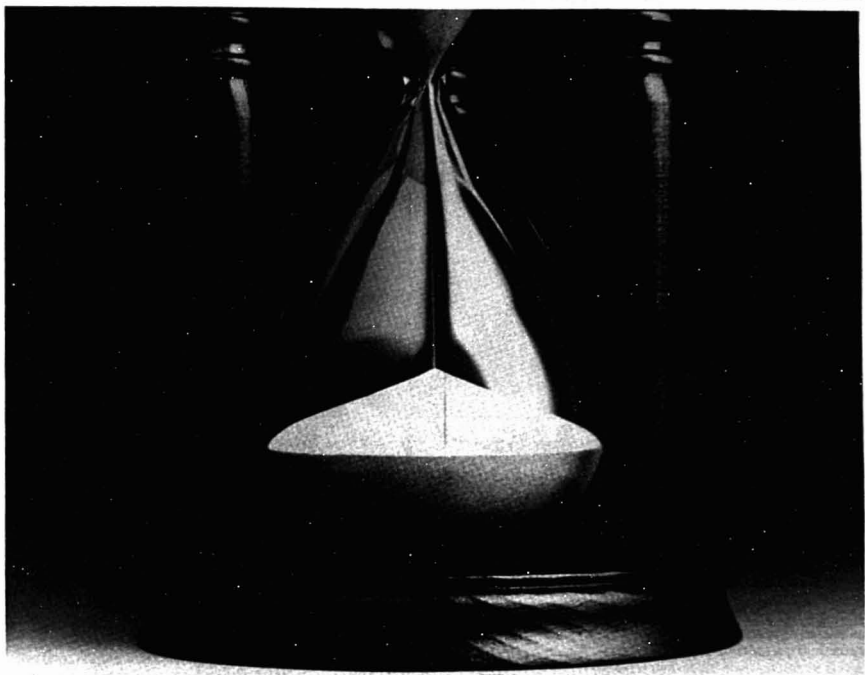
### Specifications

### Index

612 pages (1981) Clothbound \$60.00  
LC 81-8111 ISBN 0-8412-0560-4

Order from:  
SIS Dept. Box 67  
American Chemical Society  
1155 Sixteenth St., N.W.  
Washington, D.C. 20036  
or CALL TOLL FREE 800-424-6747  
and use your credit card.

NEW PRODUCTS:									
408	409	410	411	412	413	414	415	416	417
419	420	421	422	423	424	425	426	427	428
430	431	432	433	434	435	436	437	438	439
441	442	443	444	445	446	447	448	449	450
452	453	454	455	456	457	458	459	460	461
463	464	465	466	467	468	469	470	471	472
474	475	476	477	478	479	480	481	482	483
485	486	487	488	489	490	491	492	493	494



## SEND FOR THIS FREE BOOKLET WHEN YOU DON'T HAVE TIME TO EXPERIMENT.

If you're going to perform chromatography, we may be able to save you time. It's probably already been done with Florisil.

Just send for this free 80-page chromatography bibliography from Floridin. Find out how Florisil has been used to solve tough separation in column or thin layer chromatography.

The new bibliography includes Florisil's chemical composition, physical properties and adsorptivity, along with a lengthy list of chromatography procedures performed with Florisil . . .



on everything from Alkaloids to Thiosteroids.

For chromatography, consider Florisil, and send for this free bibliography. They both can save you time and money.

Write Floridin Company; Department A-1; Three Penn Center; Pittsburgh, PA 15235.  
Or call: (412) 243-7500.

**Floridin**  
A Member of the ITT System

CIRCLE 66 ON READER SERVICE CARD

PG-1105

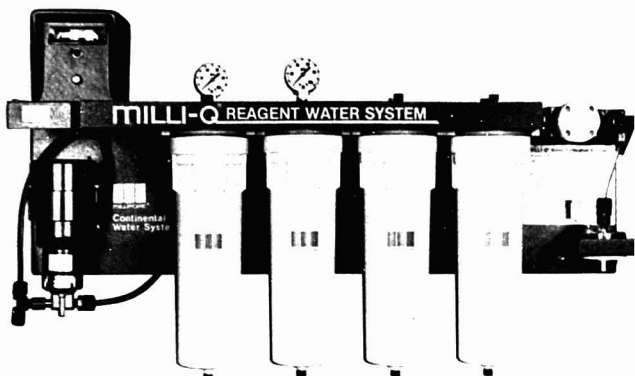
# New Products

## RIA System

NE1620 RIA Counting/Computation System consists of a 16-detector multi-well counter, 48K RAM programmable microcomputer, floppy disc, video display, and fast bidirectional line printer. At 1-min counting time, the system is capable of processing nearly 1000 samples/h. Initial software package includes provision for more than 10 different RIA data treatments, curve plotting and comparison, statistical quality control, and 16 different statistical data treatments. IN/US Service Corp. 424

## IR Training Program

The training program IR-101, "Principles of IR Quantitative Analysis," is available in either slide-tape or videotape format. It describes a systematic approach to performing quantitative analysis in solution and discusses measurement errors and their effects on precision and accuracy. Multicomponent determinations are illustrated with the analysis of a five-component mixture. Savant 408



Milli-Q HPLC-Grade Water System provides organics-free, type I reagent-grade water on demand. Based on reversed-phase elution chromatography at both 254- and 214-nm UV detection, it is consistently lower in organics than even bottled HPLC-grade water. Designed especially for critical HPLC, it is also ideal for ion chromatography, graphite oven AA spectrometry, and other critical trace analytical instrumentation. Millipore 403

## Organic Base Analysis Column

HPLC column, packed with a high-performance anion exchange resin in the sulfate form, quantitates such fermentation by-products as drugs, aromatic amines, and alkyl amines. It is used

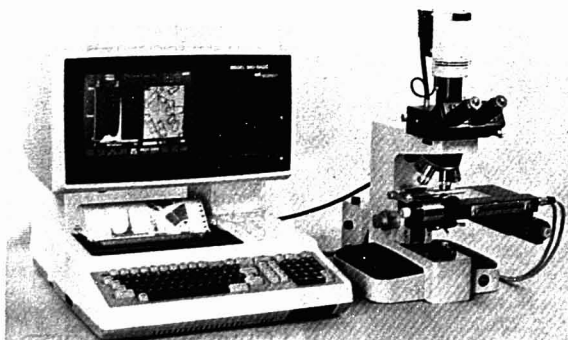
with a simple isocratic elution, and no sample preparation is required. Bio-Rad 409

## Rotary Evaporator

Rotavapor Model R-151 is a bench-top rotary evaporator with standard 10-L evaporating and receiving flasks for evaporating volumes of 10, 20, 30, or more liters. Features include electronically controlled water bath with over-temperature safety device, variable speed (10-140 rpm) sparkless induction motor, and high solvent throughput. Brinkmann Instruments Co. 410

## Electrofocusing

Immobiline System replaces conventional carrier ampholytes with immobilized pH gradients when buffering groups are covalently bound to the backbone of a polyacrylamide gel. Electrofocusing can be performed in ultranarrow gradients down to as little as 0.01 pH units/cm. Low power requirements allow gels 4-5 mm thick to be run for preparation of samples up to 100 mg. LKB 411



MPV-DADS 560 Microscope Photometer combines a modern microscope photometer MPV-Compact with a high-resolution, color-graphics computer with 64K RAM plus 48K color RAM, dual floppies, matrix printer, full ASCII keyboard, and 30 function keys. Scanning data are acquired, stored, and displayed in real time; the high-resolution image in eight colors and the histogram are displayed simultaneously. E. Leitz, Inc. 401

## Micro-Centrifuge

Model 235A Micro-Centrifuge's angled aluminum head accepts up to 16 1.5-mL sample tubes directly. A univer-



# VYDAC

## COMPLEMENTARY REVERSE PHASE MATERIALS NO RESEARCH LAB CAN AFFORD TO BE WITHOUT.



SEM photomicrograph  
of VYDAC HS silica.

**VYDAC TP 300 Angstroms**  
Spherical Silica based reverse phase

and/or

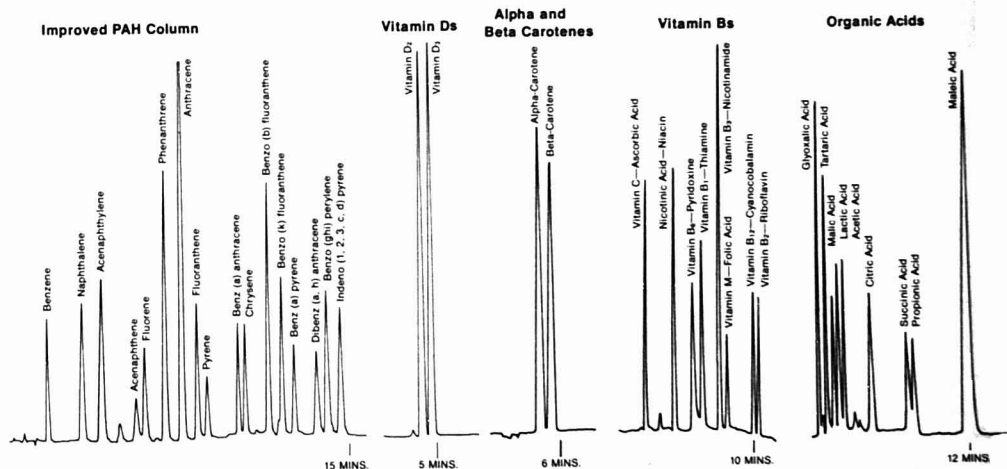
**VYDAC HS 80 Angstroms**  
Spherical Silica based reverse phase

### Applications

Polyaromatic hydrocarbons  
Vitamins D<sub>2</sub> and D<sub>3</sub>  
Large Peptides  
Proteins  
Anti-oxidants in plastics  
Vitamin A Isomers

### Applications

Nucleosides, purines, pyrimidines  
Catecholamines  
Small Peptides  
Vitamin Bs and C  
Organic Acids



Only the Separations Group offers C<sub>18</sub> reverse phase materials bonded to distinctly different spherical silica substrates yielding uniquely different selectivities for the HPLC chromatographer.

For your free copy of our "Comprehensive Guide to Reverse Phase Materials for HPLC," contact the Separations Group. Do not hesitate to call collect.

## THE SEPARATIONS GROUP

MANUFACTURERS OF VYDAC

Box 867 • 16695 Spruce St. • Hesperia, CA 92345 USA  
Telephone (619) 244-6107

SPHERICAL SILICAS and separation materials for high performance liquid chromatography since 1971

CIRCLE 191 ON READER SERVICE CARD

## New Products

sal ac motor drives the head directly, with acceleration to 13 750 rpm in less than 6 s. The screwdriver speed adjustment permits in-lab calibration (using an accessory tachometer) to meet federal requirements. Fisher Scientific Co. 412

### Gamma Counter

Auto-Gamma 5780 pipettor-compatible system holds up to 66 tip-proof, centrifuge cassettes and a maximum of 792 test tubes in sizes from 10 to 16.7 mm diameter and 50 to 100 mm tall. Featured are the PrioSTAT manual sample loader and program selectors attached to cassettes to automatically call multiuser protocols from the micro-computer memory when desired. United Technologies Packard 413

### Computer Interface pH Meters

Models 501 and 517 pH meters, which also measure mV, have parallel BCD and serial RS232 ports and a large digital LED panel display. The addressable serial port can interface up to 10 meters. A software package is offered for use with the HP Model 86 Microcomputer to implement sampling a series of meters. Eco Instruments 414

### Bioluminescence

Model 2055 toxicity analyzer system, Microtox, is a screening tool to determine the presence of toxic materials in a variety of samples that range from rinse water to hazardous spills. Instrument operation is based on measuring the influence of toxicants on the light output of a special strain of luminescent bacteria. Beckman 415

### Water Analysis System

Series 952-AD Aqua Analyzer 2 System permits more than 65 of the most important water tests to be performed even by untrained personnel. All tests are based on officially approved procedures. Only small volumes of reagents are required, and many tests take less than one minute. Hellige, Inc. 416

### Temperature Controller for Crystal Structure Analysis

Air-Stream System offers a directed air stream of 1 SCFM controllable over the range of -85 °C to +100 °C. It is useful for routine crystal structure analysis since it can be used for specimen temperature control for investigations in X-ray diffraction, NMR, ESR, optical microscopy, and IR diffraction. It has a mechanically refrigerated delivery line



**Multiprobe 600** combines scanning electron and scanning Auger microanalysis capabilities in an optimum configuration. The heart of the instrument is a vertically mounted electron optical column that includes a large-diameter cylindrical-mirror electron energy analyzer and integral, coaxial electron gun. The gun incorporates a high brightness LaB emitter and electromagnetic focusing. Accelerating voltage is variable from 1 to 25 kV. Perkin-Elmer 405

to permit air delivery to remote locations up to 10 ft without loss of efficiency. FTS Systems Inc. 417

### GPC/SEC Columns

Packed with cross-linked styrene/divinylbenzene gels in both 5- and 10- $\mu$ m gel sizes, a line of GPC/SEC columns is available that covers a broad molecular weight range. These columns are used extensively to characterize oils, resins, polymers, rubbers, and polyethylenes and for quality control of products containing these substances. IBM 418

### Dual Trace Oscilloscope

Model 530 Oscilloscope has an acceleration potential of 6 kV for bright traces and a jitterless circuit for a clear signal. A 6-in.-square CRT with internal graticule and scale illumination is stan-

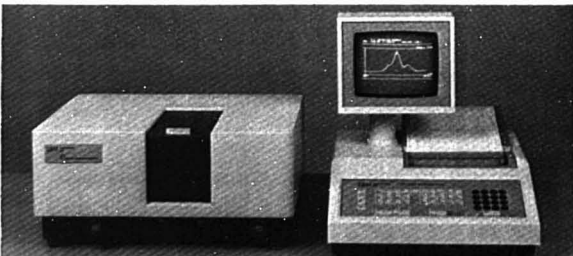
dard. An X10 horizontal-sweep magnifier increases the maximum sweep rate of 20 ns per division. Soltec Corp. 419

### UV Source

Enhanced UV source consists of a solar simulator with a dichroic mirror that selectively reflects the UV radiation and transmits most of the unwanted visible and IR radiation. It is available in 300- and 1000-W versions along with output beam sizes of 2, 4, 6, and 8 in. square. Oriol Corp. 420

### Variable Wavelength Detector

Model LC-85B UV/VIS Detector for LC provides reduced LC bandwidth made possible by a new flow cell design. The LC bandwidth with an optional 1.4  $\mu$ L flow cell is typically only 5  $\mu$ L. An 8  $\mu$ L flow cell is standard. Perkin-Elmer 422



**9400 Series UV/VIS Spectrophotometers** combine high throughput and double-beam optics with an operator console. The optical systems of the series have holographically ruled gratings and high-sensitivity photomultipliers that produce a spectral range from 195-900 nm. A digital interface gives the microprocessor control over the optics, all automated features, and displays. IBM 404



**Mead CompuChem®**  
the nation's largest, most experienced gas chromatography/mass spectrometry (GC/MS) laboratory offers you trace level analysis for:

- Hazardous Waste
- Priority Pollutants
- Toxicology
- Organics In Air
- Quality Control
- Product Evaluation



Two laboratories in Research Triangle Park, N.C. and Cary, Illinois (Chicago) provide you with rapid data turnaround and lower cost because of high capacity and specialization.

Organic and inorganic analyses are performed on a variety of matrices and a strict Quality Assurance Program ensures the highest quality data available.



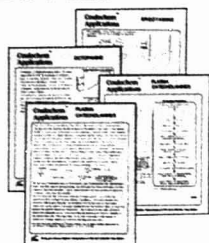
For more information on how we can meet your specific analytical requirements, please call our toll-free number: 1-800-334-8525.

**Mead  
CompuChem®**



CIRCLE 144 ON READER SERVICE CARD

## Detect Picogram Levels



### With the Coulcochem™ Electrochemical Detector

Your liquid chromatography system deserves the detector that will do justice to your separation. The Coulcochem dual electrode electrochemical detector will provide *high selectivity, greater sensitivity, and improved stability* for your biological and pharmaceutical separations. Consider:

- Greater sensitivity through unique coulometric design which allows the detector to react with virtually 100% of the sample.
- High selectivity achieved through the use of dual electrodes which eliminate mobile phase contaminants to permit interference-free measurement of the compound of interest.
- Improved stability with unique patented cell design which permits rapid equilibration, fast set up, low maintenance, and superior reproducibility.

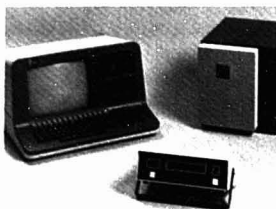
Get all the facts today. Call (617-275-0100) or write for our new Coulcochem brochure and application notes describing separations of interest to you.



45 Wiggins Avenue  
Bedford, Mass. 01730

CIRCLE 64 ON READER SERVICE CARD

## New Products



**7000 Series On-Line Near-IR Equipment** provides precise nondestructive measurement of such constituents as moisture, protein, oil, and fiber in intermittent or continuous product streams. The sensor is positioned on-line and connected to a control module that can be located up to 2000 ft away. High liquids, high oils, and true liquids can be analyzed in true transmission with NIR. Pacific Scientific 402

### Nitrogen Analyzer

System 707C Chemiluminescent Analyzer will determine total nitrogen in solids, liquids, and gases containing 50 ppb to 5% nitrogen. Analysis time is 1 min for liquids and gases and up to 10 min for solids. Antek Instruments, Inc. 421

### Chemicals

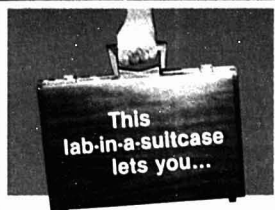
#### Iodine-125

Sodium iodide-<sup>125</sup>I is ideal for use in protein iodination procedures. The radioactivity of this product is >99.9%, and it contains less than 0.05% <sup>129</sup>I. Specific activity is approximately 17 Ci/mg iodine with no carrier added. Research Products International Corp. 425

#### Soft Agarose

SeaPrep ultralow-gelling/remelt-temperature agarose has been formulated for cloning murine hybridoma cells, general cell culture/cell electrophoresis, sol electrophoresis/centrifugation, and embedding medium for single cells in electron microscopy. Solutions remain liquid at room temperature, but gel when cooled to ≤ 15 °C (concentration dependent). FMC Corp. 427

For more information on listed items, circle the appropriate numbers on one of our Readers' Service Cards



## IDENTIFY 98% OF THE MOST COMMONLY USED METALS

**Identify virtually any alloy** commonly used by man—steels, nickel alloys, bronzes, aluminum alloys, plated metal coatings—with the Koslow #1899 Alloy ID Kit. You obtain results...

**ON SITE.** This 10-lb. lab-in-a-suitcase can be carried to the mill, stockroom, warehouse, machine shop, QA lab, construction site, scrap heap. Anywhere metals are used. You no longer have to take your sample to the lab. It's now easier to carry the lab to your work.

**QUICKLY.** Identification by chemical spot testing can be done in less than a minute per element. On raw stock. Finished parts. On scrap headed for recycling. And the results are positive and unaffected by the shape, size or physical condition of the metal.

**EASILY.** Comprehensive, step-by-step instructions are easy to follow. Kit materials are clearly identified. Even a non-technical beginner can learn to use the #1899 Kit in just a few hours.

**INEXPENSIVELY.** The #1899 contains sufficient materials for literally hundreds of tests at just pennies per test. It is the most cost/effective metal alloy identification kit available anywhere.

For full details on the versatile #1899 or any of our specific ID kits, contact Donna at Koslow Scientific Company, 75 Gorge Road, Edgewater, NJ 07020 (201) 941-4484

# **koslow**

CIRCLE 122 ON READER SERVICE CARD





## **SPEED LOAD RESOLUTION...**

...no one column can answer all these needs. But, whether it's speed, load, or resolution, Whatman has a column just right for you.

Develop your separation on an analytical column from the versatile, economical Partisil 10 family. Once developed, optimize for greater speed, load, or resolution with the appropriate Whatman LC column—there's no need to start over. Corresponding media available in all column types enable you to meet your needs without changing your methods.

Call Whatman, the column specialists. We have the selection and quality to simplify all your LC column requirements. 800-631-7290



**Whatman**

Whatman Chemical Separation Inc. 9 Bridewell Place, Clifton, New Jersey 07014

CIRCLE 241 ON READER SERVICE CARD

# Manufacturers' Literature

**Analyst.** June 1982 issue features articles on X-ray tubes, software, lab XRF, microanalysis, and industrial systems. 15 pp. Keveex Corp. 430

**Autosampler.** Booklet describes the ISIS AutoSampler, which automates sample introduction for AA or flame photometers. ISIS can collect fractions prior to sample transfer and can control accessory equipment, such as pump, diluter/dispenser, or valve, for simple processing of samples. It holds up to 114 samples in less than  $\frac{3}{4}$  sq ft of bench space. 7 pp. Isco, Inc. 431

**LC Detector.** Booklet describes the optical and electronic design features of the V<sup>4</sup> variable-wavelength LC detector, which extend the deuterium lamp life over 10 times its factory rating. Front panel controls select deuterium or tungsten-krypton lamp. 7 pp. Isco, Inc. 432

**Lab Automation System.** Publication 5953-1623 describes the computer system capabilities and peripherals available with the HP 3350 series lab automation systems. Features such as expanded memory capability and system security are discussed. The system is operational with HP's new computer languages, FORTRAN 77, MACRO/1000, and GRAPHICS/1000II. 12 pp. Hewlett-Packard 433

**Remote-Control Refrigerated Circulators.** Bulletin PB-322B describes Models KTC-2 and KTC-4, which consist of a solid-state remote-control module coupled to a modified Lauda K-2/R or K-4/R refrigerated circulator. 4 pp. Brinkmann Instruments Co. 434

**Na/K Analyzer.** Brochure describes the Model 1020 Na/K Analyzer. Revised specifications are shown, as well as new displays. The line- and battery-operated instrument measures sodium and potassium in a 100- $\mu$ L sample of whole blood, serum, or plasma in 50 s, and in a 400- $\mu$ L diluted sample of urine in 65 s. 6 pp. Orion 435

**Ludman Parallelism Interferometer.** Brochure describes the Model LPI-220P, which can interferometrically determine the parallelism and flatness of two polished surfaces, such as silicon wafers, germanium windows, and laser scan mirrors, by a real-time noncontact method. 4 pp. Space Optics Research Labs 436

**Bio-Radiations.** September 1982 issue features articles on protein assay for collagen, HPLC fatty acids analysis, a DNA electro-blot membrane, ion exchange sample preparation, and HPLC theophylline monitoring. 8 pp. Bio-Rad Labs 438

**On-Site Oil Dispersion Monitoring.** Application note describes the Model 10 field fluorometer for use on small boats near shore and on larger vessels involved in offshore work. The 12-V dc fluorometer is fitted with oil detection accessories. 11 pp. Turner Designs 439

**News & Notes for the Analyst.** October 1982 issue contains solutions to lab analysis problems, update of EPA regulations, applications, new product information, time- and money-saving tips, and features an article concerning 2,2'-bicyclicnonic acid, a compound used in the determination of trace amounts of copper in ores, metals, and other substances. 24 pp. Hach Co. 440

**NMR.** Brochure discusses a research-grade FT-NMR System and associated software from an applications standpoint. Features such as the operator console, magnet and probe assembly, and data system are described. 12 pp. Nicolet 441

**Multimeters.** Brochure describes the Series 7000 Digital Multimeters line. Handheld models with 3- $\frac{1}{2}$ -digit resolution, 4- $\frac{1}{2}$ -digit bench instruments, 5- $\frac{1}{2}$ -digit ATE units, and accessories are presented with specifications. 20 pp. Weston Instruments 442

## Catalogs

**High-Purity Materials.** Catalog lists over 2300 products and is divided into four sections: compounds, pure elements, technical and miscellaneous, and formula index. 320 pp. Aesar 445

**Chromatography.** Catalog features polar fused-silica capillaries, bonded FSOTs, FSOT columns, tuned FSOTs, and capillary connections and ferrules. 11 pp. Alltech Associates 446

**Chromatography.** Catalog includes columns, phases, and accessories for capillary gas chromatography and LC. 44 pp. Chrompack 448

**Gas Standards.** Gases and gas mixtures are offered in disposable cylinders, glass flasks, and rental cylinders. Tables provide dimensions and ordering information. 16 pp. Cryogenic Rare Gas Labs 449

**Scintillation Products.** The range of products described includes liquid scintillators, premixed concentrates, solutes and preblended solutes, solvents, incorporation aids, specialty scintillator products, vials, and standards for counters. 24 pp. Koch-Light Labs 450

**LC.** Catalog offers descriptions of LC supplies, including isocratic and gradient HPLC systems, columns, precolumns, packings, high- and low-pressure components, solvents, filters, syringes, pipets, pumps, detectors, recorders, column heaters, and accessories. 168 pp. Rainin Instrument Co. 451

**For more information on listed items, circle the appropriate numbers on one of our Readers' Service Cards**





## How to switch HPLC columns using valves.

Different analyses sometimes use different columns. But even when the same column can handle more than one kind of sample, many chemists dedicate a column to each analysis. This prolongs column life, reduces interferences, and eliminates equilibration delays.

Rheodyne's Technical Notes 4 tells how to use switching valves to connect as many as five columns to a chromatograph. Any column can be selected, while the off-line columns remain sealed at each end. The effect on resolution is shown to be negligible in most cases.

### Send for Tech Note #4

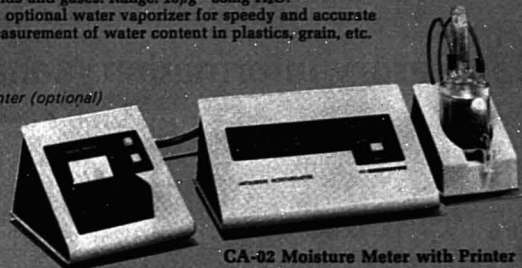
For the well-illustrated tech note, contact Rheodyne, Inc., P.O. Box 996, Cotati, California 94928, U.S.A. Phone (707) 664-9050.

**RHEODYNE**  
THE LC CONNECTION COMPANY  
CIRCLE 186 ON READER SERVICE CARD

## MCI Automatic Moisture Meter. Reliable, Fast and Easy.

Incorporates coulometry principle applied to Karl Fischer titration. Operation is full-automatic. Measuring time is shortened. Accuracy is within 5µg for 10µg-1mg H<sub>2</sub>O and within 0.5% for 1-30mg H<sub>2</sub>O. Wide-range applications include measurement of ultra-trace water content in liquids, solids and gases. Range: 10µg-30mg H<sub>2</sub>O. An optional water vaporizer for speedy and accurate measurement of water content in plastics, grain, etc.

Printer (optional)



MCI-32 Moisture Meter with Printer



MITSUBISHI CHEMICAL INDUSTRIES LIMITED

Instruments Dept., Mitsubishi Bldg., 5-2, Marunouchi 2-chome, Chiyoda-ku, Tokyo, 100 Japan Telax: J24901 Cable Address: KASEICO TOKYO

CIRCLE 143 ON READER SERVICE CARD

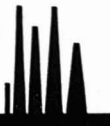


## 1983 International Symposium on LCEC and Voltammetry May 15-17, 1983 Indianapolis

with emphasis on trace determinations in environmental and industrial samples, pharmaceuticals, mechanistic electrochemistry, and new technology.

Liquid Chromatography/Electrochemistry  
Cyclic Voltammetry and ASV  
LCEC Derivatization Techniques  
Multiple Electrode Detectors  
New Electrode Materials  
Chemically Modified Electrodes  
Priority Pollutants  
Pesticides  
Forensic Analysis  
Pharmaceuticals  
Enzyme Activity Assays  
Food Additives

for more information write or call:  
1983 LCEC Symposium  
P.O. Box 2206  
West Lafayette, IN 47906 (USA)  
(317) 463-2505



CIRCLE 26 ON READER SERVICE CARD

## Laboratory Information Management Systems: Part I

It all starts with a datum point derived from a microprocessor-controlled smart instrument. It is joined by other data from automated GC, LC, mass spectrometer, and infrared instruments to form a small data stream. This merges with related data streams created by ICP and AA facilities, as well as manual test methods. Emerging from the laboratory is a torrent of data that threatens to engulf the laboratory technician and manager.

The previous pair of articles in the A/C INTERFACE series (*Anal. Chem.* 1982, 54, 1167-84 A and 1295-1306 A) dealt with local area networks (LANs), the conduits by which instruments, computers, and terminals can synergistically interact to channel data flow. Intimately related to this hardware technology is the software-dominated area of laboratory information management systems (LIMS). Together they are providing the tools to harness these data more effectively.

LIMS are the subject of the present pair of articles. This article is a tutorial dealing with the nature of LIMS, why they are needed, and how they are implemented. The second article will feature capsule reports from several different types of analytical laboratories, each presenting a different solution to the LIMS problem.

Information management systems involve some of the most complex software in existence. However, there is no excuse for the poor communication that exists between the end users of these systems, the programmers who create such systems, and the vendors who sell the developed products. The typical laboratory manager, already inundated by a flood of data

and frustrated by legal and profit imperatives, is being smothered by jargon like a torpedoed sailor under a blanket of oil. In an attempt to understand what system should be implemented in the lab, the user chokes on a stream of acronyms such as ISAM or PSAM. He or she cannot see through the films of schema definitions and cannot hear because of competitive system vendors shouting "B-tree," "plex," "hierarchy," and "relational."

An information management system is logical and highly structured. One suspects the obfuscation may be deliberate. Data General couches its business-oriented package (CEO) in terms of storing data electronically in "folders," "drawers," and "cabinets." Deletion of data is described in terms of "waste baskets" (material thrown in them can be recovered) and "shredders" (terminal destruction). The Xerox STAR video terminal actually displays replicas of documents, file folders, and drawers on the users' "electronic desk top." It should thus be possible to describe LIMS concepts in terms familiar to the analytical chemist. However, before exploring that realm, let us become convinced that we need the technology.

### What Does a LIMS Do?

It is possible to list the activities for which machine assistance would be useful from the time of sample entry into the analytical laboratory to the time of sample release.

Log-in procedures bind the sample's identity and analysis requirements with a number that will aid in retrieving information about the sample (Figure 1). These sample numbers can

be printed automatically on labels that also provide more human-oriented data about the sample and that aid in distribution of the sample throughout the laboratory (Figure 2). Since aliquoting is common, multiple copies of the label can be produced by a printer/plotter attached to the computer. Bar-coded labels can be printed and affixed, or preprinted bar-code labels can be purchased. Figure 3 shows how the vertical bars encode numbers. Labeling and bar-code identification techniques are often among the most beneficial aspects of an information management system since identification errors are drastically reduced.

As each day's samples are logged in, it is possible for a LIMS to prepare receipts for the submitter, indicating due date and estimated cost, and work lists (Figure 4), indicating a reasonable sample load and sample sequence for a given instrument. Nominal analysis times ensure that operators and instruments will not be overloaded. Even sample delivery lists can be generated. The work lists can then indicate sample location (cold room, testing rack, etc.) to expedite access. Realistic systems permit establishment of sample priorities to accommodate items that must be expedited.

The data from each analysis, as it is performed, can be captured electronically or entered manually from a video terminal. Computer-generated printed forms may be provided, each analyst filling them in and passing them to terminal operators for entry. Or video terminals can be made available to analysts for their personal entry of data. With such manual data entry it is important that the keystrokes required be minimal and user-cordial. Video-

## ANALYSIS REQUEST FORM

LAB SAMPLE # 317-5 SUBMITTER Wollenberg  
 LMS ID # \_\_\_\_\_ PROJECT # 3810  
 (to be filled in by analytical group) DATE 12/1/82

ANALYSES REQUESTED

AA Fe, Zn, Cd  
ICP P, A, Cd  
GC/MS  
LC/FLUORESCENCE  
pH  
NITRATE

PROBLEMS Check on possible  
inorganic and organic  
contaminants in feed stock  
additive

Figure 1. Analysis request form for a LIMS



Figure 2. Computer-generated sample label (adapted from Radian's SAM)

displayed forms with highlighted areas for data entry locations are one viable approach (Figure 5). A menu or list to prompt the operator is another. Bar-code readers associated with the intelligent instrument or terminal may be used to identify the sample. The analyst and the analysis he or she is performing can be recorded the same way, improving the ergonomics.

Range information on normal limits permits the operator to be alerted if results are abnormal. The alert can be overridden if the operator suspects an unusual sample. Or the procedure may be rerun if an analytical error is suspected. These editing steps are essential to keep erroneous data out of the data base. Once there, it will be almost impossible to expunge it from the system.

Along with the data, the analyst may enter free-form comments that may be useful to the requester. Privileged comments may be added that will appear only on internal laboratory reports.

The laboratory manager can request operations information about a sample at any point while it is being tested. Submission dates and completion dates are available. This sample tracking includes statistical information on all samples submitted, in-test and completed, as well as backlog profiles (Figure 6). Such operational information can be broken down into instrument, analysis type, sample type, operator, or any other category that is meaningful in running the facility.

Although each analysis carries with it the name of the analyst performing the test and the instrument used to carry out the work, it is important to have one person authorize the release of the total data set associated with a single sample. It may be advisable to resubmit samples when normal ranges have been exceeded or results from different analytical methods suggest further work. It has become common to include audit trail features in laboratory data management systems that keep track of what alterations have

been made, when, and by whom. This permits legitimate changes to be made, but makes it possible to retrace the alteration steps if legal or scientific mandates occur.

Many firms have found it inappropriate to release fragmented analytical data (sometimes even to the requester). It is too easy to jump to improper conclusions from incomplete analyses or to bias future work. Thus the access control to the various levels of information needs to be carefully considered. Who has access to what data or information when? Passwords or locks on data structures can easily define no access, or read, create, or modify status for individual users.

A well-designed system will back up (record an entire copy of its data) at appropriate points, so the system can be restored if failures occur. These copies should be kept in safe places away from the computer area. The most careful installations have backup copies stored at a different geographical site.



**Figure 3.** Bar-code

A bar-code is a set of thin bars that represent binary ones, and spaces that represent binary zeros. A series of these is used to encode a sample number. Each number is expressed as seven bars and/or spaces. There are six digits expressed to the right of a center guard space and six to the left of the guard space. Digits to the left of center begin with a binary zero and end with a one. To the right of center they begin with a one and end with a zero. The bar-code sequences used to express the same character to right and left of the center guard are the complement of each other. An optical wand may read from either direction, the attached microcomputer determining the direction of the movement from the scanned pattern. The bits are then interpreted as an Arabic number. The last digit to the right is a check sum to confirm that the other 11 digits have been read correctly. If the calculated value and the read value for this digit disagree, an error is announced at the reader.

Archiving refers to the long-term, off-line storage of data and is a separate function. It may be desirable to store only condensed information (peak area) rather than raw data in an on-line disk to conserve space. However, the raw data can be archived for subsequent retrieval by storing it on magnetic tape. Alternatively, once a report has been generated, only sample number and identity information might be maintained on-line, all chemical information being archived. In some systems, once a report is generated, the entire data set associated with a sample is archived. Each laboratory has its own use pattern for data.

The most important aspect of a LIMS is the report generation facilities it provides (Figure 7). Without a combined LAN/LIMS the analyst is doomed to become an error-prone, expensive secretary, copying data from one place to another. A well-designed LIMS provides a report program generator to allow the user to prepare programs that generate properly formatted data and text. Page headings, column headings, and columnar data formatting should be possible with a short learning curve to master the language elements involved. Word processing (text preparation) and list processing (sort, merge, and select) capabilities are built in. A math package allows the user to calculate intermediate and final values from stored raw data.

Some labs, and all quality assurance programs, require the presence of a higher level statistics and graphics

package. This permits the quality assurance manager to use data from spiked samples and standards placed in the analysis stream to evaluate trends due to instruments, reagents, or personnel. With this as a base, developing trends in raw materials, intermediates, or products can be ascertained and the statistical results presented in various graphic styles. Simple modeling programs aid this goal, allowing data to be fit to mathematical models.

#### **What Operations Should Your LIMS Perform?**

All of the above is possible with existing software packages. Some are inexpensive and can be used by the interested analytical chemist with minimal training. Others require extensive hardware, expensive software, and data management personnel to coordinate activities. The proper choice requires a clear understanding of the problems. This is where most laboratories fail. Some binary-type questions may help clarify the point:

- Do you need an operations information and/or chemical data management system? Operations information deals with sample input, output, and backlog. It is the information needed to control the day-to-day operation of the laboratory. There is no need to carry analytical data along. This simplifies the data set involved and makes searching faster. Since updating operations management systems is much faster than adding to chemical data management systems some LIMS choose to update the latter by creating

transaction files during the day and updating overnight. This presumes that instantaneous access to completed data is not necessary. Other laboratories demand concurrent updates.

- Do you require storage of analytical results or data? Some laboratories require raw, or nearly raw, data to be available at all times. Others require only condensed information derivable from the data. The latter reduces storage requirements and search times for the system. The complexity and cost of the data management system are lowered.

- Do you need to store procedures or analyses? Many production facilities and quality control laboratories need to store and update the procedures and tolerances they use for acceptance/release of material. As limits on incoming or outgoing chemicals or goods change because of supplier fluctuations, changes in regulations, or internal conditions, it is vital to keep track of these and associate the changes with a lot number.

- Are you involved with production, quality control, or research and development? The production environment is quite different from the R&D laboratory. In production, preset series of analyses are performed on batches of samples. Often the tests must be conducted repeatedly over long time periods. Sample entry into the system may need to be menu driven to match personnel capabilities. Automatic prompting is mandatory in time-scheduled reanalysis. Often the observations made on samples should be entered using menu selections to match the limited spectrum of allowed entries. The associated retrieval, statistics, and security elements must be well developed to meet the demands that will be made on the system for fiscal or legal reasons.

- Is detection or prevention of quality failure important? In some instances it is enough to detect that a product has failed. In others it is important to prevent a failure. Predictive capabilities are much more difficult to build into a system. They are a goal that will become more common as managers understand the use of computers and have access to proper modeling programs.

- Is it anticipated that changes will occur in how the data is accessed? Some data management systems permit only questions of the data that were envisaged as the data base was created. Others permit changes. There are important price/speed tradeoffs as the flexibility of a system increases.

- Is user cordiality (ease of use) or system capability important? Unfortunately these features are often inversely related.

# How To Uncover The Hidden Costs Of Chromatography.

---

**Do you realize how much lower-purity HPLC solvents might be costing you? Consider the frequent consequences.**

- ◆ **The cost to repeat separation procedures because of solvent artifacts** — this wastes analytical labor and valuable instrument time.
  - ◆ **The cost to regenerate a water deactivated column** — this causes instrument "down-time" which requires additional chromatographs to perform the same amount of work.
  - ◆ **The cost to wash off a residue-laden column** — the residue decreases column efficiency.
  - ◆ **The cost of replacing columns, filters and check valves clogged with particles** — this can increase cost from \$200-800.
  - ◆ **The cost of isolating residue from preparative peaks** — this may cause additional intermediary separations to remove unwanted contaminants.
  - ◆ **The cost of maintaining an additional inventory of several "grades" of purity (HPLC, GC, Spectro, etc.)** — the quality of high purity solvents deteriorates while on a shelf.
  - ◆ **The cost to frequently evaluate the less uniform solvents** — this diverts attention away from productive analytical time.
- Avoid these "hidden costs" and time-consuming effects from using lower purity solvents. Switch to B&J Brand High Purity Solvents. Because, when it comes to *cost and performance*, there's no comparison. B&J Brand is your best value.

Sure, less pure solvents might be cheaper. But why jeopardize your chromatography results when you use them? In the long run, lower purity solvents can cost you more because of their inconsistent quality.

Compare for yourself. If you're currently using lower purity HPLC solvents, try the highest purity solvents — B&J Brand. You'll notice the difference right away.

Then do this. Figure out your cost-benefit equation for HPLC chromatography. The answer will be pure and simple. For lower costs and better results, it's B&J Brand High Purity HPLC Solvents.

Write or call today for a free technical bulletin about B&J Brand High Purity HPLC Solvents. We'll also send you our distributor listing so you can conveniently order B&J Brand Solvents from a distributor near you.

**Avoid the hidden costs.  
Switch to B&J Brand  
High Purity Solvents.**



**BURDICK &  
JACKSON  
LABORATORIES, INC.**

1953 South Harvey Street, Muskegon, Michigan U.S.A. 49442 (616) 726-3171

A Subsidiary of Matthews-Lafferty Inc. 

CIRCLE 22 ON READER SERVICE CARD

INSTRUMENT WORK LIST			
INSTRUMENT AA-44		DATE 12/1/82	ANALYST J. Bergquist
SAMPLE #	LOCATION	ANALYSIS DESIRED	PRIORITY
1234567890	Ref. #3, Shelf 2, Tray 5	Fe, Zn, Co	Expedite
1756376520	Ref. #3, Shelf 2, Tray 5	Zn, Co	
1654329109	Ref. #3, Shelf 2, Tray 5	Fe	Expedite
1336198251	Ref. #3, Shelf 1, Tray 4	Ca, Cu	
3241117812	Ref. #1, Shelf 2, Tray 1	Pb, Cu, Zn	
7169119040	Ref. #1, Shelf 2, Tray 2	Cr, Fe, Zn	
1346118220	Ref. #1, Shelf 3, Tray 4	Mg	Expedite
1862543009	Ref. #2, Shelf 1, Tray 1	Ca, Cu, Pb, Cr	

Figure 4. Instrument work list

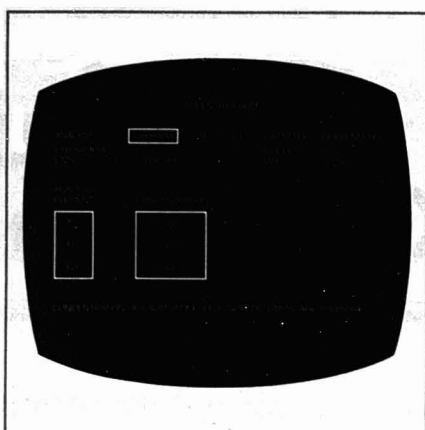


Figure 5. Video-displayed form with highlighted area for data entry

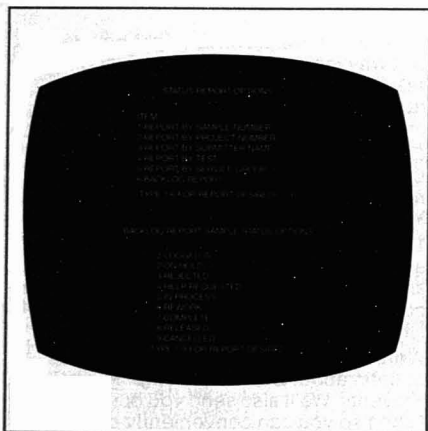


Figure 6. Typical operations report menus (adapted from Perkin-Elmer's LIMS-2000)

ANALYSIS REPORT FORM			
LAB SAMPLE #	317-5	SUBMITTER	WOLLENBERG
LIMS ID #	1234567890	PROJECT #	5010
CERTIFIED BY	PETERSEN	PHONE 5622	DATE 12/2/82
ANALYSIS		ANALYST	
AA		BERGQUIST	
Fe	3	ppm	
Zn	1	ppm	
Co	0.06	ppm	
ICP			ISHIHARA
P	12	ppm	
B	2	ppm	
Cd	0.5	ppm	
GC/MS		NO POLYBROMINATED BIPHENYL FOUND	DUEBALL
LC/FLUORESCENCE		12 ppb OF AFLATOXIN (B <sub>1</sub> , B <sub>2</sub> ) FOUND	THOMPSON
pH		4.8 USING STANDARD SLURRY TECHNIQUE	KNIFE
NITRATE		NONE DETECTED	CONDER

Figure 7. Chemical data report

- Is update of the data structure important, or is speed of retrieval vital? Unfortunately these features are always inversely related.

#### How Do LIMS Store Data?

Faced with these questions and the need for a viable system the laboratory manager is confronted with two massive structures: the vendors of hardware and software and his or her own corporate computing center. The best defense is a working vocabulary.

The concepts in data storage resemble methods traditionally used on the

printed page to store and retrieve information. Samples are submitted along with a form similar to that shown in Figure 1. The individual tests requested produce data with a structure specific to each method. Classical data storage involving work sheets in drawers or cabinets and sequenced by analytical method, sample number, date, or project number is being replaced by electronic storage on disk (Figure 8).

How can such data be stored and retrieved? Separate records could be kept for each analysis type. This ap-

proach is represented by the video display screens in Figure 9. The bench chemist sees data in this format. To prepare a report of data specifically related to sample 317-5 the separate records can be pulled and results merged. Alternatively, a single file on a sample could be kept; printing a report would entail pulling only that sample's file. That seems simpler. But suppose production asked if data were available on trends in heavy metal content, using ICP, for all samples associated with a certain project. Or suppose complaints were received



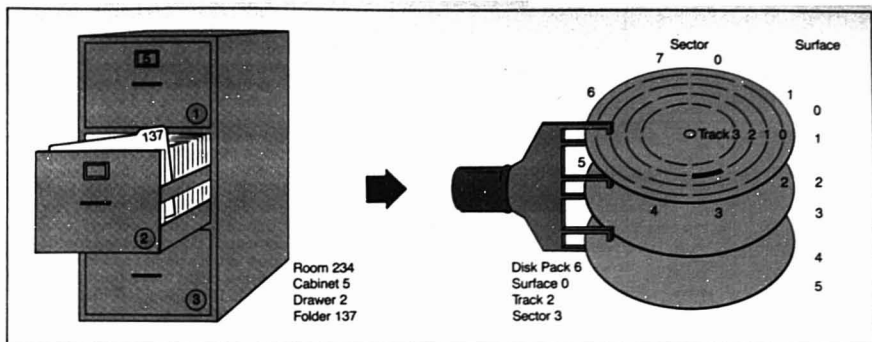


Figure 8. Classical data storage in cabinets is being replaced by electronic storage on disks

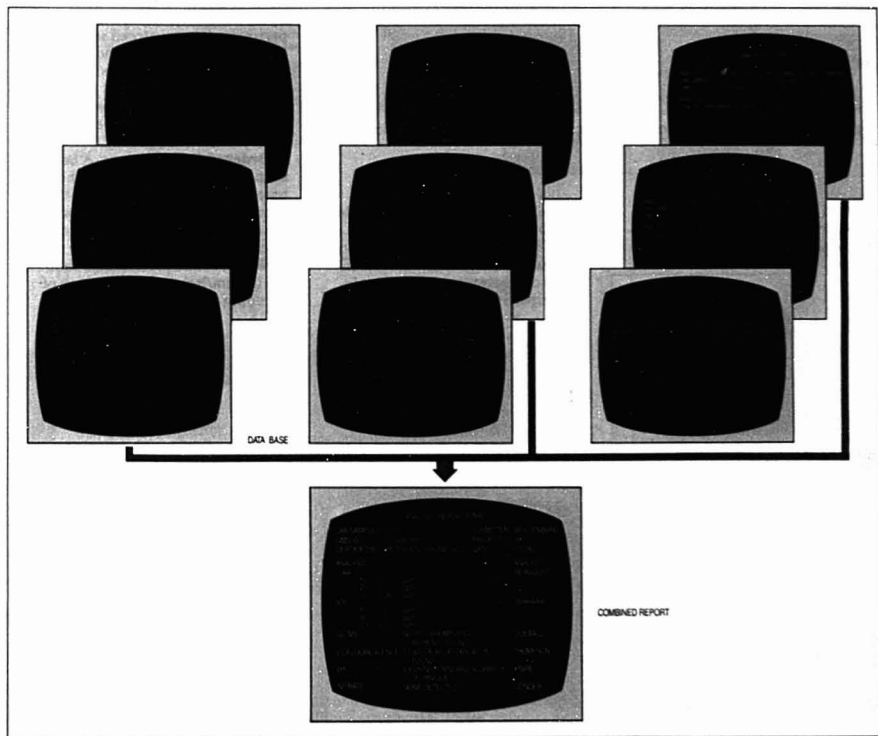


Figure 9. Data storage by analysis type

about the turnaround time for all samples submitted by a certain analyst. Appropriate structuring of the data is necessary to answer such questions and avoid long search times.

When data are stored in simple ta-

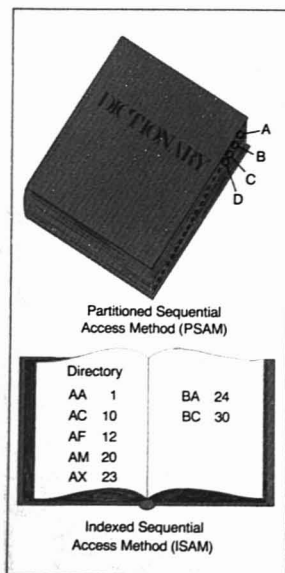
bles both status information and analytical data can be associated with each sample (Figure 10). Such tables are human-oriented and represent the classical paper approach. Information can be accessed in very different ways

depending on one's function as analyst, lab manager, or lab director. This approach posed problems in the formative years of data management because the tables often were not flat. Instead of each intersection being a

ID #	SAMPLE STATUS: PENDING COMPLETE RELEASED REPORTED DEACTIVATED	ANALYSIS	ANALYSIS STATUS: PENDING HELP RE- QUESTED REJECTED COMPLETE	SAMPLE IN	TESTS DUE	TESTS OUT	DESE- LECTED	ALLOT TRAIL	DATA
1234567890	PENDING	AA	PENDING	12/01	12/03		NO	NO	
		Fe							
		Zn							
		Cd							
		ICP	HELP REQUESTED		12/05		NO	YES	
		P							
		B							
		Cd							
		GC/MS	PENDING		12/07				
		LC/FLUORESCENCE	REJECTED						
0147598032	COMPLETE RELEASED REPORTED DEACTIVATED	pH	COMPLETE		12/02	12/02	NO	NO	4.8
		NITRATE	COMPLETE		12/02	12/02	NO	NO	NONE

Figure 10. Data stored in tables can be either status information or analytical data

Figure 11. Partitioned sequential access methods (PSAM) and indexed sequential access methods (ISAM)



simple number or phrase, a complex relationship existed. Beginning in 1970, methods were developed to convert such files into flat, two-dimensional charts involving simple relationships. Storage of information in

such relational data bases is currently an area of intense activity. We will return to them later. First, what are the alternatives commonly used?

**Sequential Access.** A common way to store data in an ordered manner is in a dictionary. This consists of the key words ordered alphabetically. When you want the data associated with a key word, you thumb into the dictionary to the appropriate letter and scan the list sequentially. The "Oxford English Dictionary" provides convenient thumb tabs to expedite entry into the proper area. Some dictionaries might have a small index to indicate the pages where first and second letters change. These are partitioned sequential access methods (PSAM) and indexed sequential access methods (ISAM) (Figure 11). They allow you to use sample number or date to locate the disk area where pertinent data are stored sequentially. You go to that location and read sequentially until the desired sample is recovered. If a word needs to be inserted or deleted it is necessary to move all of the dictionary entries beyond that location point.

**Ordered Index Access.** A better solution involves structuring the data base in a more complex way at the outset. Indexes can be kept in which the submitters' names are alphabetized. Next to each name can be an ordered list of sample numbers submitted by him/her, and the location of that data on the disk. This ordered

INDEX		THESAURUS	
CHAPTER-PAGE		INFORMATION	
ABORT	7-5	COMPUTER DATA	348.19
ACTIVATE	3-27	KNOWLEDGE	474.1
ADD	2-6	ENLIGHTENMENT	555
CLEAR	3-4	MANAGEMENT	
DEACTIVATE	3-26	OPERATION	163.1
		HANDLING	663.2
		USE	663.8
		GUARDIANSHIP	697.2
		SYSTEM	
		ORDER	59.1
		PLAN	652.1
		WAY	655.1

Figure 12. Ordered index and inverted list

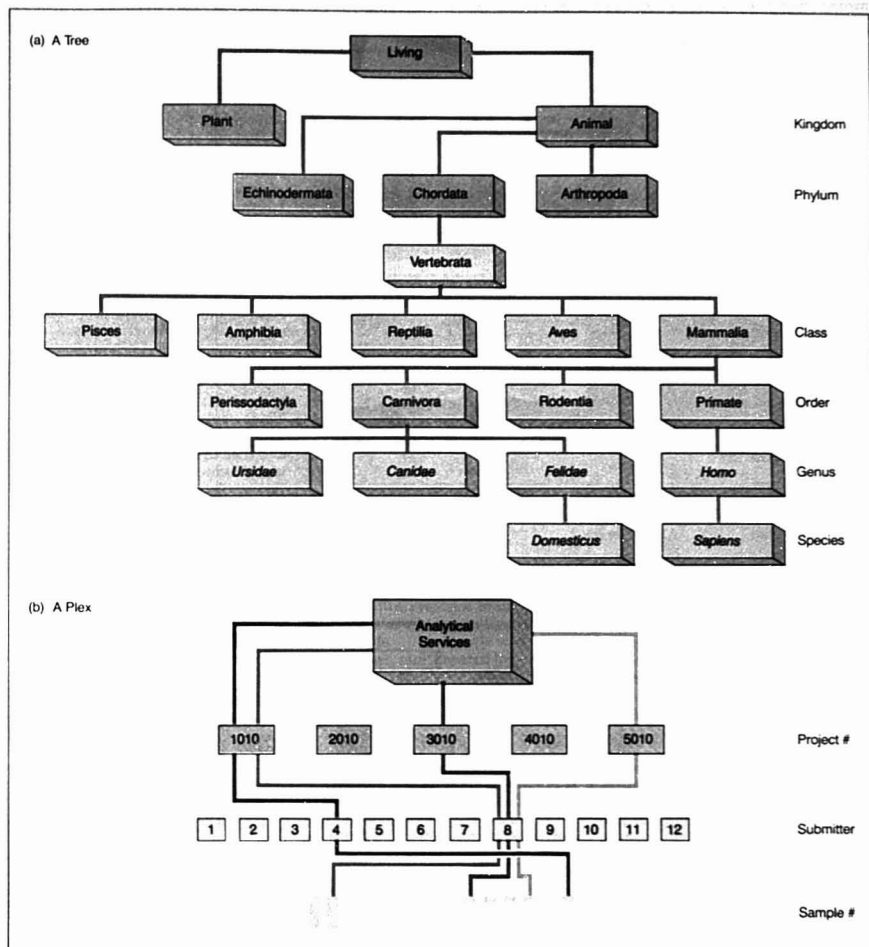


Figure 13. A tree and a plex

index access method involves rewriting only the index as changes are made (Figure 12). The main data files need not be altered. A good analogy is a three-ring notebook to which pages of information are added as required. Appropriate additions are made to an index. The main file is unordered. Only the index is ordered.

**Inverted List.** Multiple indexes might be involved. These might include lists of *submitters*, their associated sample numbers, and location of related data; *project numbers* and their associated sample numbers; *analysts' names* and the samples they

have run. We have moved away from storing data in a way that used a key word (sample number) to access a file containing information on project number, analyst, and results, to a method that has separate files for each of these attributes. These separate files for submitters, project numbers, and analysts are associated with lists of sample numbers and disk location where analytical results may be found. A thesaurus is an example of such an approach (Figure 12). Each word has associated with it a list of related words and the location where information on them can be found. This method

makes it easy to respond quickly to questions like: What analyses have been run by analyst A on project 5010? What samples have been run for submitter B on project 5010?

This method is called an inverted list or inverted file approach, since it reverses the normal procedures. These systems retrieve information very rapidly, but update slowly. As information is added to the data system, each inverted file must be updated appropriately.

**Trees.** The Linnean classification is a hierarchical approach to classification. Each level becomes more specific

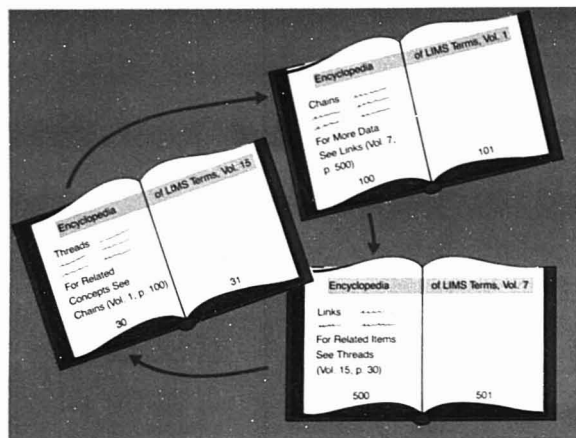


Figure 14. Threaded list

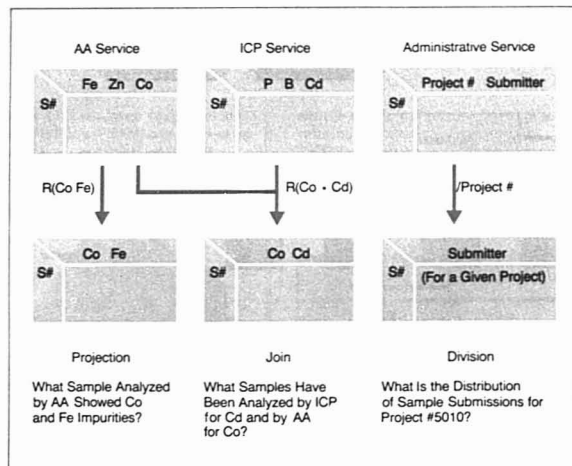


Figure 15. A relational data base

about the nature of the organism being identified (Figure 13a). Consider also a genealogical tree where only the male side is presented. Laboratory data can be handled in tree form where there is a parent/offspring relationship between classification elements. It is easy to add things. Search times do tend to become long as the number of levels in the tree grow.

**Plex.** A genealogical tree in which both mother and father are considered, and in which intermarriage/di-

vorce/remarriage occurs makes the simple tree more complex. The relationship is called a plex (Figure 13b). A laboratory information management system that stores data in a hierarchical approach, i.e., project number, submitter, and sample number, can actually be a plex since each submitter can have many projects as a parent. Handling plex structures requires storing the data in quite a different form, often invoking a complex set of internal pointers to thread the data.

**Threaded-List Data Storage.** An encyclopedia is a threaded set of data. Embedded in each entry on a subject are pointers to other volumes and subjects that have related data (Figure 14). To find all of the data associated with a given subject requires beginning at one end and following the thread. Threads update quickly but retrieve slowly. Some threads run in multiple dimensions, forward and backward, so searches can be in either direction.

**Relational Data Bases.** The data structures described up to this point allow the user to ask only those questions of it that were conceived at design time when the data base was structured. Relational data bases are not so constrained. Techniques of relational algebra and calculus have been developed that make it possible to create and use such data bases. These permit the user to imagine the data to be comprised of flat tables, and then to join, project, and otherwise manipulate the tables to produce the correlations or comparisons needed (Figure 15). These new relations, often called VIEWS, did not originally exist; however, they were present as virtual entities. Once abstracted they can be manipulated or stored as real entities. This encourages "what-if?" type questions. The current implementations are for large machines or for use on personal computers. The former speaks to the interest the professional community has in the concept, the latter to the fact that it could be done on laboratory-sized machines with proper pressure from the scientific community. Growth in the laboratory area can be expected. It is possible to take many of the storage methods previously described and make them appear "relational-like" to the user. With such approaches prospective users should investigate the flexibility of the final system. How relational is a relational-like data base?

**Hashing.** As the amount of data grows, another data management problem develops—managing the indexes to the data. Indexes to data, often called directories, can appear like our telephone directories, i.e., ordered lists partitioned for sequential search (Figure 16). Indexes can also appear as tree-shaped directories. Another approach is like the Chinese telephone directories. Family names are made up of a series of brush strokes. This collection is called an ideogram. The names in the Chinese directory are arranged by the number of brush strokes in the ideogram (Figure 16). It is possible to convert keywords like submitter, project, etc. to numbers. This is done by a process called hashing. All alphanumeric expressions that "hash" to the same

U.S. Telephone Directory			
Name	Telephone #		
Yumas	639-5850		
Yunanavattana	352-8963		
Zabec	951-1365		
Zaboski	552-4102		
Zaborskie	552-4096		

Ordered Directory			
#	Strokes	Idiogram	Pinyin
4	王		Wang
8	刘		Liu
7	汪		Wang
10	唐		Tang

Chinese Telephone Directory			
#	Strokes	Idiogram	Pinyin
4	王		Wang
8	刘		Liu
7	汪		Wang
10	唐		Tang

Hashed Directory			
#	Strokes	Idiogram	Pinyin
4	王		Wang
8	刘		Liu
7	汪		Wang
10	唐		Tang

Figure 16. An ordered directory and a hashed directory

number are stored in a separate area along with the location on the disk containing the relevant information. Hashing is commonly used to speed up access to information.

#### Who Supplies LIMS?

A variety of commercial LIMS packages are available from main-frame vendors and systems houses. The view of LIMS presented at the beginning of this article is actually a synthesis of various products currently in use in many analytical laboratories: LIMS-2000 (Perkin-Elmer), System-2000 (Intel), CALS/LBGR and LBDMS (Computer Inquiries Systems), IMAGE (Hewlett-Packard), Datatrive and MUMPS (Digital Equipment Corp.), SAM (Radcan Corp.), RS/1 with RDE and Sample Tracking Options (Bolt, Beranek and Newman), RDM (Interactive Technologies), and LABMAN (Spectrogram). They variously use simple trees, inverted files in conjunction with multiple threaded lists, a tree-structured ISAM approach, and a hashed access to a multikeyed tree structure. Installation costs of these systems range from \$50 000 to \$500 000, but pay-back periods of 18 months are often encountered.

#### What Should You Expect and Avoid in a LIMS?

With the fundamentals in place, what are reasonable expectations for a LIMS?

- Some prime rules: No more than a month should be required to become a skilled programmer of the system; no more than a day should be required to

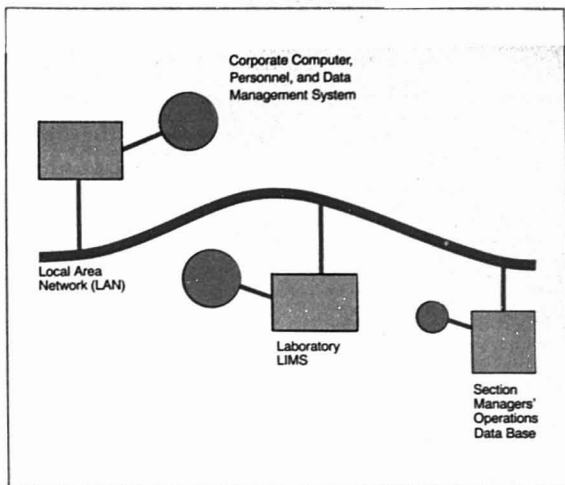


Figure 17. Distributed data management

learn to use the system; response to moderately complex queries should be a few minutes; response to simple form and status requests should be a few seconds.

- Elaborate, multilayered log-on procedures should not be required.
- Repetitive entry of name, analysis type, and sample ID should not be required. The manufacturing industry now uses bar-codes routinely in production; so should the laboratory.
- Long queue lines for data entry at a few terminals must be avoided.
- Manual data entry should have good HELP functions available on the video screens so that recourse to an operating manual is not necessary. Some systems provide multiple-level HELP commands to provide the novice with detailed examples and experienced users with brief reminders.
- For experienced analysts, alternate data entry pathways should be available to avoid repetitive waiting for menus to be searched for and printed.
- Data should be capable of being selected/deselected for use in statistics or reports. Entire records should be capable of being activated/deactivated. This does not throw data away; it does allow the scientist to use only appropriate data.
- With a LIMS users should be able to back out of situations they may have created that are incorrect. The system should back itself off from contentions that have locked the system, and backup (copying) should be periodic and ritual. Required archiv-

ing must be automatic. Many of the current LIMS fail in these vital areas.

- Since most users will not know what they want to do with a data system until they begin to use it, the ability to implement change quickly and frequently is a necessity. Nonprocedural, user-cordial languages are available to permit this feature. Currently we face a conservatism and a hesitation to accept this change among computing center personnel and laboratory instrument designers. The language Nomad (National CSSS), running on large machines, has demonstrated the ability to create user-driven software in environments where applications development has been largely without programmers. The classical approach involving a long, detailed specifications study, with early signoff by the prospective user and subsequent implementation by isolated computing center personnel, must be replaced by a more flexible pilot development/change approach. Resistance to these new languages can be overcome with the simple realization that maintenance costs of a piece of software rise with time, as does rewriting the application in a more easily maintained language. The slope of the latter is lower. At the point where the costs of the systems cross, it is better to switch rather than fight.
- As LANs develop and it becomes possible to support distributed data bases, even greater changes in our use of the virtual file cabinet will be seen (Figure 17). Distributed data bases in

the business sector already exist, e.g., Datatrive. In such networked data bases it is possible to concatenate relational requests made on data in the local computer with other relational requests that involve data on remote machines. Only relevant material is transmitted along the net to the requesting unit. Many managers find the combination of the "what-if?" capabilities of relational data bases and the local security of distributed data management compelling. Intel has announced an iDIS hardware/software system that supports multiple users enjoying full-function relational access to System-2000 operating on a larger computer. Two time-share vendors of production-oriented data management systems already support small microcomputers at the individual user sites (General Electric, Comshare). If true distributed data management develops in this sector, smaller labs may find this approach attractive.

### How Do You Implement a LIMS?

With a working vocabulary in hand how does an analytical chemist go about implementing a LIMS?

- *In-house analysis of the problem and user preeducation.* Time spent analyzing the informational and psychological needs of users should focus on the normal flow of laboratory information. Laboratory managers' views of detailed laboratory operation may be oversimplified or erroneous. The technicians and section managers should be heavily consulted. The time to co-opt user support is at this point, making the user part of the decision-making process, or at least aware of the factors involved. This intimate contact with the user should continue during the entire development phase. Ego-less decisions and solutions that do not utilize the ability of LIMS to be centers of power structures are facets of successful implementations.
- *Turnkey vs. customized.* Unless you are very lucky, or you have a very simple operations information system in mind, some customization of an existing system will be necessary.
- *In-house or systems house?* Packages are available that provide in-house programmers with a set of powerful tools that allow development of applications programs in a reasonable time frame. It is possible to employ a systems house to customize software for you, developing it in-house or delivering and installing the system after generation elsewhere. Finally, computer vendors will often customize software for you. In any case, it is essential that some of your personnel develop expertise in any installed system so that your organization is capable of extending and supporting the

system. As part of any purchase agreement insist on source code for sections of the system that you have any thought of altering. Sign nondisclosure agreements if necessary. Where work is performed by outside personnel, it should be made clear initially what freedom the vendor has to use the developed software elsewhere.

- *Choosing hardware.* Although the ideal installation involves software that would run on any reasonable machine, most LIMS will run on only one type of computer. Datatrive, MUMPS, RS/1 (RDE/STO), RDM, and LABMAN run on Digital Equipment Corporation hardware. LIMS-2000 runs on Perkin-Elmer Interdata equipment, IMAGE, CALS/LBMGR, and LBDMS on Hewlett-Packard systems, and SAM on Data General computers. Documented assurances that new generations of hardware will not engender expensive software relicensing costs are essential. As the data base grows, it may be necessary to install not only more disks but different types of disks, terminals, printers, or other peripherals. The better information management systems are hardware-independent at this level. Another important feature to evaluate is field service support.

- *Compatibility.* LIMS that run under standard operating systems provide many software development tools that are essential if additions and modifications are implemented. Data files created can be accessed by programs written in other languages, and the files can be exchanged between computers relatively easily. For example, LABMAN and RDM run under DEC's RT-11 or RSX-11M operating systems. Some systems houses provide software front ends or handshakes between traditional data management systems from computer vendors and their own LIMS. For example, Bolt, Baranek and Newman is developing access methods to Datatrive for RS/1. Where users will be responsible for applications software development the drop-off between the powerful data management command language and the next level of programming language should be small. Thus, although RS/1 is written in C to take advantage of the full power of the DEC VAX computer, the user sees either the high-level command language or a cordial RPL (research programming language). Many scientists would find a direct, precipitous drop to languages like FORTRAN, C, or APL shattering.

- *Networking.* Networking software should support communication from the LIMS host to larger computers. The LIMS should also support satellite computers for real-time data collection or as ancillary data entry

points. Terminals at any level should have transparent access to computational facilities above them.

- *System benchmarking.* Comparison shopping is essential. Actually working with a system already installed at another location or, less satisfactory, interacting with a demonstration system at a vendor sales center is essential. Benchmarking is difficult at best. Try to compare systems with similar CPU capabilities, disk size, data base size, and number of active users.

- *Cost/benefit analysis and planning.* In preparing cost/benefit analyses it is seldom advisable to use arguments based on reducing staff. Sample throughput, the quality of data produced, and the ability to abstract information previously lost in manual manipulations are cogent arguments. More efficient use of instruments and analysts is achievable. Realistic PERT charts prevent prospective users and management from losing their faith in the project.

- *Start-up.* Credibility is most easily lost during the start-up phase. Good documentation and training of initial users characterize successful installations. These implementations have been done in stages so the problems that develop are localized, small, and quickly fixed. Manual entry services usually precede the more difficult real-time data capture services. Parallel manual backup is suggested during any initial phase. Eugene Schneider of Ralston Purina, a pioneer in the area, suggests "the project team must be highly visible and responsive to the requests and needs of the lab personnel during this time... then... be prepared for requests for new and increased functions for the LIMS... It is a natural outgrowth of the acceptance of the system by its users."

The area is just maturing. Vendor interest is high. The informed chemist has an opportunity and a responsibility to affect the market place by articulate input to prospective vendors. This tutorial was intended to give the analytical chemist a vocabulary and philosophy. The next A/C INTERFACE will contain a series of capsule reports describing how various chemists have successfully implemented a laboratory information management system.

### Acknowledgment

Many of the philosophies developed in this article are the result of a series of discussions with David Hooley of the Standard Oil of Ohio Research Laboratories, Cleveland, Ohio. Szulin Chen, a graduate student in the VPI & SU Chemistry Department, provided the information on Chinese telephone directories and the ideograms.



Tygon.<sup>®</sup>  
Laboratories have placed  
their confidence in Tygon  
for over 40 years.



This is Tygon laboratory tubing. It is specifically formulated for use in the laboratory. Tygon laboratory tubing safely handles an exceptionally wide range of chemicals, yet offers outstanding flexibility and long service life. But Tygon offers more. Tygon is used with confidence. Confidence that your analyses of gases or solutions will not be affected. Confidence that your results will be reproducible. Confidence that Tygon laboratory tubing is, in fact, specifically formulated for lab use, and has been for over 40 years.

For literature and additional information, contact Norton Specialty Plastics Division/Industrial Products, P.O. Box 350, Akron, Ohio 44309, or call (216) 673-5860.

**NORTON**

CIRCLE 153 ON READER SERVICE CARD

# DEFINITIVE REFERENCE RESOURCES

## ☐ PETROANALYSIS '81

**ADVANCES IN ANALYTICAL CHEMISTRY IN THE PETROLEUM INDUSTRY—PROCEEDINGS OF THE INSTITUTE OF PETROLEUM, LONDON, 1982**  
 Edited by G. B. Crump, Shell Research Limited  
 Reviews progress in the analysis of petroleum, its products and related materials from both marketing and environmental perspectives. It demonstrates how new and emerging techniques (particularly when coupled with computers and microprocessors) allow petroleum analysts to solve complex problems more quickly and precisely.  
 (0 471-26217-X) 1982 416 pp. \$83.95

## ☐ ESSENTIAL OILS ANALYSIS BY CAPILLARY GAS CHROMATOGRAPHY AND CARBON-13 NMR SPECTROSCOPY

V. Formáček, Bruker Analytische Messtechnik GmbH, Rheinstetten/Karlsruhe, and K.-H. Kubeczka, Lehrstuhl für Pharmazeutische Biologie der Universität Würzburg  
 A complete guide to capillary gas chromatographic and carbon-13 NMR spectroscopic methods for the analysis of industrial oils, perfumes, and flavors. Presents gas chromatograms and corresponding data tables providing instant access to the qualitative and quantitative composition of the oils studied.  
 (0 471-26218-8) 1982 400 pp. \$89.95

## ☐ TECHNIQUES IN LIQUID CHROMATOGRAPHY

Edited by C. F. Simpson, Chelsea College, University of London  
 Experts in the field examine the theory and application of liquid chromatography techniques and offer ways to eliminate everyday problems. Includes a large number of experiments to familiarize readers with current methodologies.  
 (0 471-26220-X) 1982 464 pp. \$44.95

## ☐ THERMAL ANALYSIS

Edited by Bernard Miller, Textile Research Institute

International experts in the field present a collection of state-of-the-art papers on theory and instrumentation, inorganic chemistry, metallurgy, earth science and ceramics, organic chemistry, biological and medical science, polymer science, applied science and industrial applications. Two Volume Set.  
 (0 471-26243-9) 1982 832 pp. \$90.00

## ☐ QUANTITATIVE CHEMICAL ANALYSIS: A LABORATORY MANUAL, 4th EDITION (ELLIS HORWOOD SERIES IN ANALYTICAL CHEMISTRY)

R. A. Chalmers and M. S. Cresser, both of the University of Aberdeen  
 This invaluable manual offers a wide range of experiments for use in laboratory work in analytical chemistry. It presents numerous experiments that illustrate theoretical concepts, and outlines the reasons why procedural details must be followed — highlighting the errors that occur when they are changed.  
 (0 470-27228-7) Due January, 1983 approx. 420 pp. \$79.95 (tentative)

## ☐ QUALITY MEASURING INSTRUMENTS IN ON-LINE PROCESS ANALYSIS

David Huskins, W. G. Engineering Design Limited

Dealing with a wide spectrum of quality measuring instruments, this text reviews their use in measuring such attributes as viscosity, density, and boiling point. The author provides theoretical descriptions and discusses the applications and effectiveness of each piece of equipment in detail.  
 (0 470-27521-9) 1982 455 pp. \$102.95

## ☐ SEPARATION AND PRECONCENTRATION METHODS IN INORGANIC TRACE ANALYSIS (ELLIS HORWOOD SERIES IN ANALYTICAL CHEMISTRY)

Jerzy Minczewski, Jadwiga Chwastowska, both of Warsaw Technical Univ., and Rajmund Dybczynski, Institute of Nuclear Research, Warsaw  
 The first book devoted solely to separation and preconcentration methods of trace amounts of elements. It provides a sound theoretical pathway for understanding basic principles underlying modern separation methods together with trace-element oriented examples of application.  
 (0 470-27169-8) 1982 543 pp. \$95.00

## ☐ TRACE-ORGANIC SAMPLE HANDLING METHODOLOGICAL SURVEYS—SUB-SERIES (A): ANALYSIS, VOLUME 10

Edited by E. Reid, Institute of Industrial & Environmental Health & Safety, University of Surrey  
 Expert investigators offer practical guidance to new cutting-edge techniques for detecting organic compounds in a variety of raw samples. Contributions detail time-accurate, useful measurement, with special emphasis on obtaining pharmacologically relevant measurements on blood samples.  
 (0 470-27071-3) 1981 383 pp. \$109.95

## John Wiley & Sons, Inc.

Indicate the book(s) which you wish to examine free for thirty days and mail this ad to:



Dept. 3-9500  
 John Wiley & Sons, Inc.  
 605 Third Avenue  
 New York, New York 10158

☐ **PAYMENT ENCLOSED** + applicable sales tax. John Wiley pays postage/handling. NOTE: We usually ship within 10 days. If payment accompanies order and shipment cannot be made within 90 days, full payment will be refunded. Foreign payment must be made in U.S. currency by U.S. bank draft, international money order or UNESCO coupons.

☐ **BILL ME** + postage handling. If order totals \$75 or more 25% partial payment must be enclosed.

NAME \_\_\_\_\_

ADDRESS \_\_\_\_\_

CITY \_\_\_\_\_ STATE \_\_\_\_\_ ZIP \_\_\_\_\_

For special discounts on bulk purchase by business, industrial or governmental organizations of any book in this ad, write or call Susan Kantrowitz (collect) 212-867-9800.

Prices subject to change without notice; slightly higher in Canada. IN CANADA: John Wiley & Sons, Canada, Ltd. 22 Worcester Road, Rexdale, Ontario.

3-9500

CIRCLE 238 ON READER SERVICE CARD

## A Field unto Itself

**General Handbook of On-Line Process Analyzers.** D. J. Huskins. 239 pp. John Wiley & Sons Inc., 605 Third Ave., New York, N.Y. 10016. 1982. \$84.95

*Reviewed by Martin Frant, Foxboro Analytical, Burlington Center, 78 Blanchard Rd., P.O. Box 435, Burlington, Mass. 01803*

The field of on-line analyzers is quite literally a field unto itself. Most analytical chemists (and, on occasion, some laboratory instrument manufacturers) have assumed that to put a laboratory analytical instrument on-line requires only a large box into which the instrument is placed; they have not recognized that this is an entirely different technical area. It is one in which most of the instruments are

*Most analytical chemists have assumed that to put a laboratory analytical instrument on-line requires only a large box into which the instrument is placed . . .*

based on principles similar to those used in the laboratories, but the design, construction, operation, and user expectations are all very different. In the foreword, R. S. Medlock quotes the author of the book as saying that "there are many good specialist books on the various analytical techniques and methods, but only a few which have been written to describe process analyzers." This certainly has been true, and this book provides an interesting glimpse into that world.

The author has undertaken a monumental task in attempting to write a complete handbook of on-line process analyzers—if I may use the term—single-handedly. He has divided it into five smaller volumes: the current volume, a general handbook providing background information; a volume on quality-measuring instruments (consistency, viscosity, vapor pressure, flash point, dissolved oxygen, etc.); optical methods (emission, ultraviolet,

infrared, colorimetry, X-ray diffraction, etc.); electrical and magnetic methods (dielectric constant, ion-selective electrodes, flame ionization analyzers, mass spectrographs, NMR, etc.); and a separate volume devoted to on-line gas chromatographs. Clearly, this is a very large field to cover.

The rationale for the choice of material for the separate volumes is not too clear. The groupings selected are convenient as a way of classifying analyzers, but sometimes lead to awkwardness as well. Thus, flame and photoionization analyzers are considered in one volume (electrical), while flame and photoionization detectors are in another (gas chromatography). On the other hand, electron capture detectors are in the electrical volume, not the gas chromatography one. For readers who want a quick reference to find out the operating principles or the availability of a particular type of instrument, the organization matters very little, particularly if they have bought all of the volumes as they appear. If, as is suggested in the first volume, the book is aimed at the plant instrument engineer, then an organization based on type of sample (aqueous liquids, gases, solids dissolved in liquids, etc.) might have been more helpful, since most plants have one type of problem or another. The problem of analyzer selection to solve a particular problem has been recognized by a cross-index in the first volume, but the index only references chapters and does not provide much comparative guidance. Perhaps, more extensive tables could be provided in a subsequent volume.

The first volume, however, can stand by itself and will be quite useful to someone starting out in this field, or to laboratory analysts who want a better appreciation of the state of process analyzer art and the complexity, precautions, and decisions it requires. The individual chapters are relatively concise (Huskins covers sample handling and conditioning in 80-odd pages; for a complete book on the same topic, see: "Sampling Systems for Process Analyzers"; Cornish, D. C.; Jepson, G.; Smurthwaite, M. J.; But-

terworth: London, 1981; 453 pp.), but they are nonetheless very informative and helpful. The chapters are filled with tables, equations, nomographs, and typical examples that are practical and useful. Among the topics covered in the first volumes are most of the general ones—symbols and graphics, calculation of concentrations, errors, calibration, sample handling, enclosures, maintenance and availability, and a variety of analyzer case histories to show how analyzers are placed and used in different processes.

In summary, the author clearly writes from firsthand experience, and this volume should be of value to everyone working in this field. I look forward to seeing the others.

**Origins of Clinical Chemistry—The Evolution of Protein Analysis.** Louis Rosenfeld. xviii + 356 pp. Academic Press Inc., 111 Fifth Ave., New York, N.Y. 10003. 1982. \$38

*Reviewed by Nathan Gochman, Beckman Instruments, Inc., Clinical Systems Division, P.O. Box 428, 200 South Kraemer Blvd., Brea, Calif. 92621*

We tend to think of clinical chemistry as a relatively modern field, with its "origins" dating back to the introduction of automated analytical equipment in the 1950s. However, as Louis Rosenfeld quickly makes us realize, the historical development of clinical chemistry could easily be said to begin with the study of urine in the 17th century. The relationship between variations in chemical constituent concentrations of body fluids and human health is clearly a centuries-old endeavor. Rosenfeld's book, as the subtitle implies, is especially directed toward protein analysis but covers a wide spectrum of related topics. Chapters are included on: colloidal state, origins of organic chemistry, Kjeldahl method, protein fractionation, colorimetry, ultracentrifuge, electrophoresis, immunochemistry, proteins in urine and cerebrospinal fluid, fibrinogen, and radioimmunoassay.

# How to get a headstart on new projects.



There's a lot of information scattered around the world that can help you, if only you can find it. That's the job for Lockheed's Dialog, the world's leading online information retrieval system.

This computerized sleuth puts you in instant touch with more than 130 databases and provides abstracts of journal articles, conference papers, research reports, patents and news stories—and all of this information goes back 15 years.

Dialog covers virtually every field, from alkaloids to polymers to zinc.

All you need to use Dialog is a standard computer terminal and a telephone. Your library probably subscribes to Dialog.

Involved in some phase of a new project? Better get involved first with Dialog. It can save you time, money and effort—and lots of each.

For more information, contact Dialog Information Services, Dept. 25, 3460 Hillview Ave., Palo Alto, CA 94304. Call toll-free (800) 227-1927. In California, call (800) 982-5838.

**Lockheed Dialog**  
CIRCLE 127 ON READER SERVICE CARD

## Books

The book is liberally sprinkled with photographs of pioneer investigators, historical vignettes, and illustrations of apparatus—both ancient and modern. There are extensive references to the original literature where additional details on particular subjects may be obtained. The author writes in a scholarly, but nevertheless entertaining manner that makes reading his book a delightful and informative experience.

I would certainly recommend this book to practitioners of clinical chemistry, other chemists interested in protein analysis, and to undergraduate, graduate, and medical students interested in the background of this modern health discipline.

## Books Received

**Chromatographic Separation and Extraction with Foamed Plastics and Rubbers.** G. J. Moody, J. D. R. Thomas, vi + 139 pp. Marcel Dekker Inc., 270 Madison Ave., New York, N.Y. 10016. 1982. \$29.75

**Analytical Profiles of Drug Substances.** Vol. 11. Klaus Florey, Ed. x + 665 pp. Academic Press, 111 Fifth Ave., New York, N.Y. 10003. 1982. \$39

**Organic Acids in Man.** R. A. Chalmers, A. M. Lawson. xii + 523 pp. Methuen Inc., 733 Third Ave., New York, N.Y. 10017. 1982. \$59.95

**Chemistry of Heterocyclic Compounds in Flavors and Aromas.** G. Vernin, Ed. 375 pp. John Wiley & Sons Inc., 605 Third Ave., New York, N.Y. 10016. 1982. \$89.95

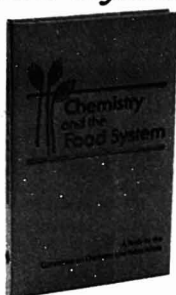
**Clustering of Large Data Sets.** Jure Zupan. xviii + 122 pp. Research Studies Press, John Wiley & Sons, Inc., 605 Third Ave., New York, N.Y. 10158. 1982. \$31.35

**Coal and Coal Products: Analytical Characterization Techniques.** E. L. Fuller, Ed. 326 pp. American Chemical Society, 1155 16th St., N.W., Washington, D.C. 20036. 1982. \$42.95

**Applied Electron Spectroscopy for Chemical Analysis.** Hassan Windawi, Floyd F.-L. Ho, Eds. ix + 213 pp. John Wiley & Sons, Inc., 605 Third Ave., New York, N.Y. 10016. 1982. \$45

**Writing a Successful Grant Application.** Liane Reif-Lehrer. vii + 100 pp. Science Books International, Inc., 51 Sleeper St., Boston, Mass. 02210. 1982. \$9.50 (paper), \$16 (cloth)

# Chemistry and the Food System



## A Study Report by the ACS Committee on Chemistry and Public Affairs

Vital reading for everyone concerned with this important public policy issue.

This report describes how a range of chemical substances—including fertilizers, pesticides, plant growth regulators, drugs to control animal diseases, and nutritional supplements—have clearly provided benefits in the production, storage, and processing of foods from both plants and animals.

Attendant benefits, disadvantages, problems, and risks are all fully discussed with the aim of providing public policy makers with the necessary information and recommendations needed in their formulation of public policy.

## CONTENTS

Summary and Recommendations: Fertilizers, Pest Control, Crop, Animal, and Fish Production, Additives in Foods, Handling and Storing of Fresh Foods, Preserving and Processing of Foods, Fortification of Foods with Micronutrients, Fabricated Foods, Special Dietary Foods, Unconventional Sources of Food and Feed, Assuring the Wise Use of Chemicals Production of Food: Crop, Animal, and Fish Production Handling, Storing, Preserving, and Processing of Foods: Additives in Food, Handling (Transporting and Preprocessing) of Foods, Storing Fresh Foods, Preserving and Processing of Traditional Foods, Including Convenience Foods, Fortification of Foods with Vitamins, Minerals, and Amino Acids, Fabricated Foods, Special Dietary Foods Unconventional Sources of Food and Feed: Single-Cell Protein, Wastes, Synthetic Fats and Carbohydrates Assuring the Wise Use of Chemicals: Evaluation of Safety, Incentives for the Use of Chemicals, Evaluating Benefits and Risks Under the Law, Public Reaction and Public Confidence, Chemistry as a Tool

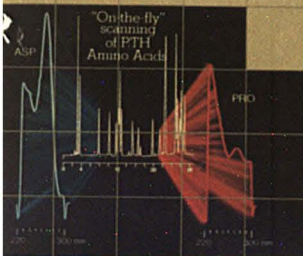
138 pages (1980) Hardback \$15.00  
LC 80-11194 ISBN 0-8412-0557-4  
138 pages (1980) Paperback \$9.00  
LC 80-11194 ISBN 0-8412-0563-9

Order from:  
SIS Dept. Box 06  
American Chemical Society  
1155 Sixteenth St., N.W.  
Washington, D.C. 20036  
or CALL TOLL FREE 800-424-6747  
and use your credit card.



GOAL:

*Reveal  
hidden  
HPLC peaks*



Model 165 multichannel, rapid-scanning UV-Vis Detector sheds light on those unknown HPLC peaks.

This revolutionary instrument utilizes a patented servo-driven monochromator for simultaneous monitoring of any two previously selected wavelengths from 190 to 700 nm.

A third channel then provides you with a real time analog plot of the absorbance ratio

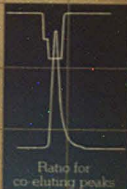
of these two wavelengths. You have the power to identify peaks independent of retention times and co-eluting

peaks that might otherwise be mistaken for a single component. That's efficiency.

But the Model 165's detecting capacity doesn't stop there. It's "on-the-fly" scanning of any or all peaks aids in wavelength selection for optimum detectability and wavelength ratios. You get UV spectral scans without stop flow analysis.

And for easy user-interface, the Model 165's software-based minicontroller puts all this power right in the palm of your hand.

Now that Beckman has revealed the Model 165 Detector, let the Model 165 reveal all those peaks you've been missing. Write Beckman Instruments, Inc., Scientific Instruments Division, 1716 Fourth Street, Berkeley, CA 94710, and request brochure #7388A. Or call (415) 527-5900 and ask to see your Beckman representative.



**BECKMAN**

CIRCLE 18 ON READER SERVICE CARD

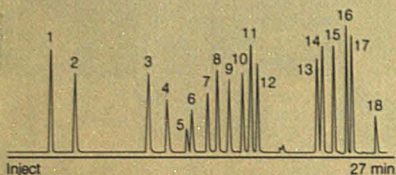


# Only Waters<sup>TM</sup> this much advanced

## Breakthrough in automated derivatization technology.

### 50 picomoles each component

1. Aspartic Acid 2. Glutamic Acid 3. Asparagine 4. Serine
5. Glutamine 6. Histidine 7. Glycine 8. Threonine 9. Arginine
10. Alanine 11. Amino Butyric Acid 12. Tyrosine
13. Methionine 14. Valine 15. Phenylalanine
16. Isoleucine 17. Leucine 18. Lysine



### High-speed pre-column derivatization and analysis of primary amino acids with unparalleled sensitivity.

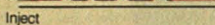
Waters eliminates the need for manual pre-column derivative formation by automating metering, mixing, timing the reaction, injecting and separating derivatized samples. This breakthrough technology gives you all the reproducibility and ease of automation plus high-speed, high-resolution chromatography. Ask for Bulletin #101.

## Microbore for both isocratic and gradient analyses.

Column:  
Waters  
Microbore  
μ BONDAPAK<sup>®</sup>  
Phenyl  
2mm x 30cm

Column:  
Waters  
μ BONDAPAK<sup>®</sup>  
Phenyl 3.9mm x  
30cm

1. Hydrocortisone
2. Cortisone
3. Corticosterone
4. Hydrocortisone acetate
5. Cortisone acetate



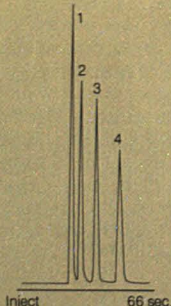
### This microbore separation of steroids shows a four-fold increase in sensitivity with a Waters system.

Waters systems give you microbore sensitivity for your sample limited applications. And you have the versatility to switch to any analytical to milligram scale prep application without system modification. Ask for Bulletin #102.

## High-speed HPLC with high resolution.

Column:  
Waters Z-Module<sup>®</sup>  
Radial  
Compression  
Separation  
System with  
Radial-PAK 5 μ  
C<sub>18</sub> cartridge

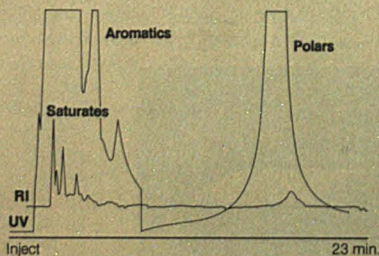
1. Methylparaben
2. Ethylparaben
3. Propylparaben
4. Butylparaben



### A 66-second separation of parabens with a Waters system.

Combining advanced systems design with innovative radial compression column technology allows you to achieve high-speed HPLC without sacrificing resolution. Ask for Bulletin #103.

## Extended capabilities in compound isolation and purification.



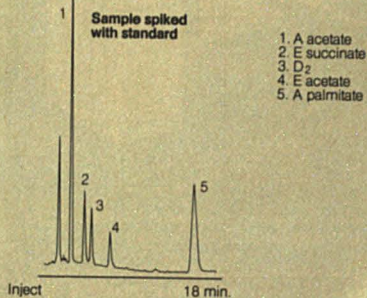
### Preparative separation of crude oil to fractionate saturates, aromatics and polars.

Waters systems with new solvent delivery capability—flow rates from 10 microliters to 45 milliliters per minute—combined with a wider range of columns give you expanded preparative capabilities. Ask for Bulletin #107.



# systems offer HPLC capability:

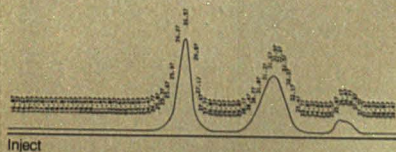
### Automatic Peak Identification



Automatic sample spiking with vitamin A acetate to verify retention time and elution order.

Waters systems let you verify the identity of peaks of interest by determining the true elution order and retention times of corresponding standards within the sample matrix. This new, fully automated technique is based on the automatic addition of standards into the sample matrix prior to analysis. Ask for Bulletin #105.

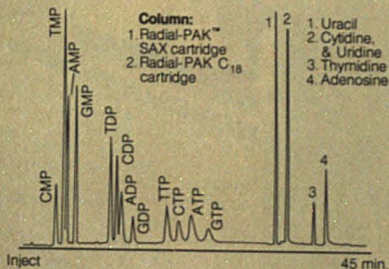
### GPC and LC Data Reduction



Determination of molecular weight distribution of the polymer (GPC) and quantitative determination of the additives by weight-percent (LC) in a single analysis.

This unique Waters systems capability gives you both GPC and LC data reduction in a single analysis for the most complete information about your sample. Ask for Bulletin #106.

## Multi-dimensional HPLC



**Fully automated high resolution separation of nucleotides, nucleosides and bases in a single chromatographic analysis.**

Unique Waters systems capability utilizes different column selectivities—ion exchange and reverse phase—to separate highly complex samples with widely varying characteristics in a single run. Ask for Bulletin #104.

**Push the limits of your chromatography further than ever before with a Waters HPLC system.**

These are just a few examples of how Waters systems combine sophisticated instrumentation with innovative chemistry to bring you advanced HPLC capabilities. And we back that up with: the best application support, service and training in the industry. Call or write today. We'll prove it.

# Waters

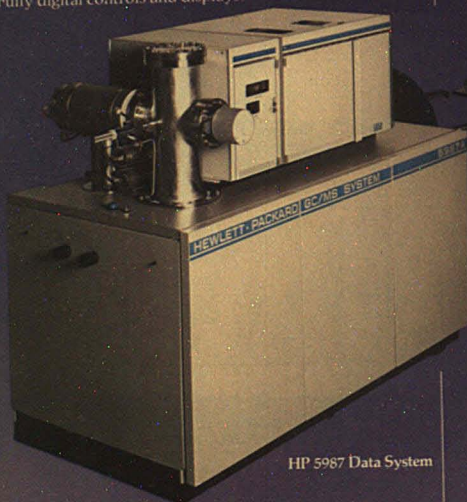


**Waters**, the Liquid Chromatography People  
34 Maple St./Milford, MA 01757/(617) 478-2000

CIRCLE 234 ON READER SERVICE CARD

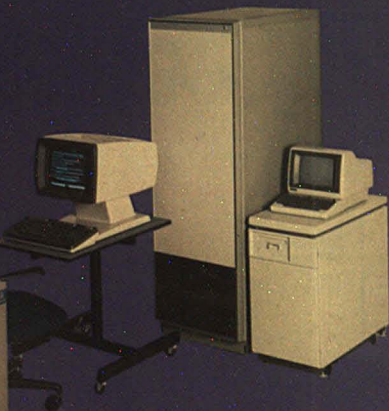


- Easily adaptable to adding enhancements such as FAB, DCI and DLI-LCMS.
- Advanced vacuum system for exceptionally reliable operation with autoranging pressure readout.
- Second-generation hyperbolic quadrupole rods enhance high mass sensitivity.
- Entire system optimized for capillary operation, utilizing versatile HP 5880A Gas Chromatograph.
- Fast scanning speed and wide dynamic range.
- Fully digital controls and displays.



HP 5987 Data System

- Multi-tasking allows simultaneous operation of up to 2 GC/MS systems and 6 graphics terminals.
- Softkeys and forms mode for rapid, friendly input.



- Separate microcomputer controls GC/MS, freeing CPU for data reduction and analysis.
- Easy key word programming provides greatly increased flexibility and power in processing data and producing reports.
- 70,000-compound data base.

## The new HP 5987A GC/MS can identify any of 70,000 components—as they elute.

But it doesn't stop there. The HP 5987A GC/MS even has a program that can analyze your data to come up with the probable identity of components whose spectra are not in the data base! The HP 5987A combines the capabilities of a new, top-of-the-line GC/MS with the HP 1000 Computer then adds powerful software options to create an analytical system of unparalleled user-friendliness and resourcefulness.

The many hardware and software options designed into the HP 5987A let you easily custom-tailor its operation to solve even your most complex analysis

problems. It saves you effort. It increases the accuracy and sophistication of your results. It increases the productivity of your laboratory. It has to be seen to be believed.

If you don't need the full capabilities of the HP 5987A, the same user-friendly flexibility is available at lower cost in the new HP 5996A GC/MS.

For the whole, amazing story call your local Hewlett-Packard sales office and ask for an Analytical representative or write: Hewlett-Packard Co., Analytical Group, 1820 Embarcadero Rd., Palo Alto, CA 94303.

When performance must  
be measured by results



**HEWLETT  
PACKARD**

A004202

Circle 96 for literature. Circle 97 for a HP representative to call.

J. F. McClelland

Ames Laboratory-USDOE  
Iowa State University  
Ames, Iowa 50011

# Photoacoustic Spectroscopy

The use of photoacoustic<sup>a</sup> spectroscopy to obtain optical absorption spectra of solid and fluid substances has attracted considerable interest in the analytical community since the mid-1970s. The method has a number of appealing characteristics. In principle, UV, visible, and IR spectra can be measured—often with little or no sample preparation—over substantial analyte concentration ranges. This can be done without experiencing difficulties with collection and detection of optical radiation often common to re-

flection and transmission spectroscopies because the photoacoustic signal is generated by the sample and no photodetector is employed. A schematic of a typical experimental setup is shown in Figure 1.

Photoacoustic measurements providing these advantages are based on a single generation sequence involving optical absorption in the sample under study, followed by conversion of the absorbed energy into heat. The subsequent heat-induced thermal expansion in the sample and adjacent media produces a photoacoustic signal when the incident beam intensity is modulated at a frequency in the acoustic range. The photoacoustic signal mag-

nitude is linearly dependent on the sample's optically absorbing analyte concentrations over substantial ranges, provided that proper measurement conditions and data analysis methods are used, as explained later in the article.

Two types of photoacoustic measurements will be discussed here that are applicable to important sample classes in chemical analysis. The first deals with light-scattering solid or semisolid samples and the second with weakly absorbing fluids. These measurements do not encompass the full range of methods and applications currently being explored in photoacoustic spectroscopy, but they have

<sup>a</sup> The term optoacoustic rather than photoacoustic is favored by some authors to describe essentially the same phenomenon.

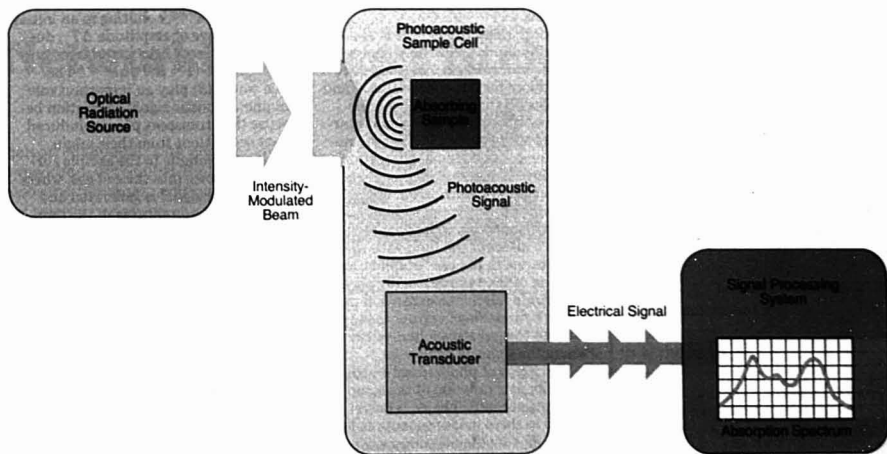
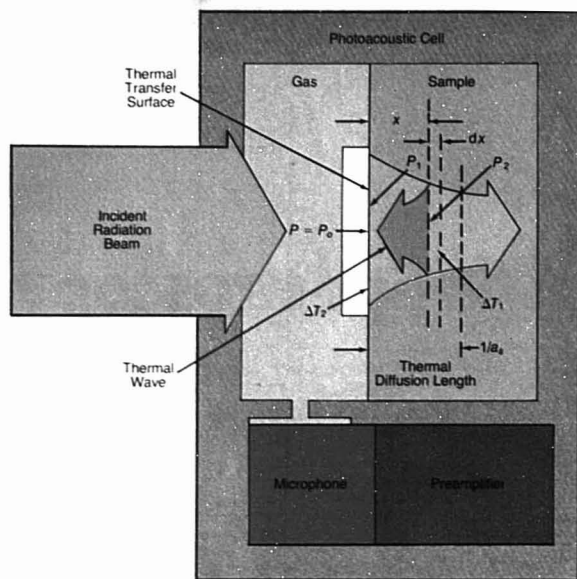


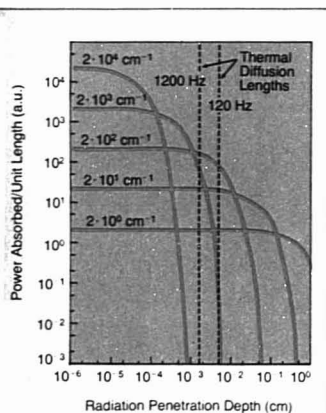
Figure 1. Schematic of a photoacoustic spectrometer

The actual components used depend on the sample type and spectral range of the measurement



**Figure 2.** Schematic of the one-dimensional photoacoustic signal generation model

The optical power just inside the sample surface and at a depth  $x$  is given by  $P_1 = (1 - R)P_0$  and  $P_2 = (1 - R)P_0e^{-\alpha x}$ , respectively. The initial thermal wave amplitude,  $\Delta T_1$ , generated in layer  $dx$  is proportional to  $(1 - R)P_0\alpha e^{-\alpha x}$ . After propagation to the thermal transfer surface the amplitude  $\Delta T_2$  is proportional to  $(1 - R)P_0\alpha e^{-(1+\alpha_s)x}$ .



**Figure 3.** Plots of power absorbed per unit length vs. radiation penetration depth for  $\alpha$  values from two to  $2 \times 10^4 \text{ cm}^{-1}$

A penetration depth of  $10^{-6} \text{ cm}$  can be considered essentially to correspond with the thermal transfer surface of the sample shown in Figure 2

received the most attention for analytical determinations and have reached a level of development where they are becoming useful analytical tools for chemists.

In both cases the sample is sealed in a small-volume cell with windows for optical transmission and a sensitive transducer for signal detection. Fluid samples fill the entire cell volume while solids are placed in a transparent gas atmosphere that fills the remaining volume. Signal generation from fluid samples is due to the expansion and pressurization of the fluid following absorption of radiation. The acoustic signal produced is sensed via direct contact of the fluid with the transducer. In the case of solids, expansion of the sample usually plays a minor role relative to expansion produced by heat flowing from the sample into the gas atmosphere of the cell where the signal is detected.

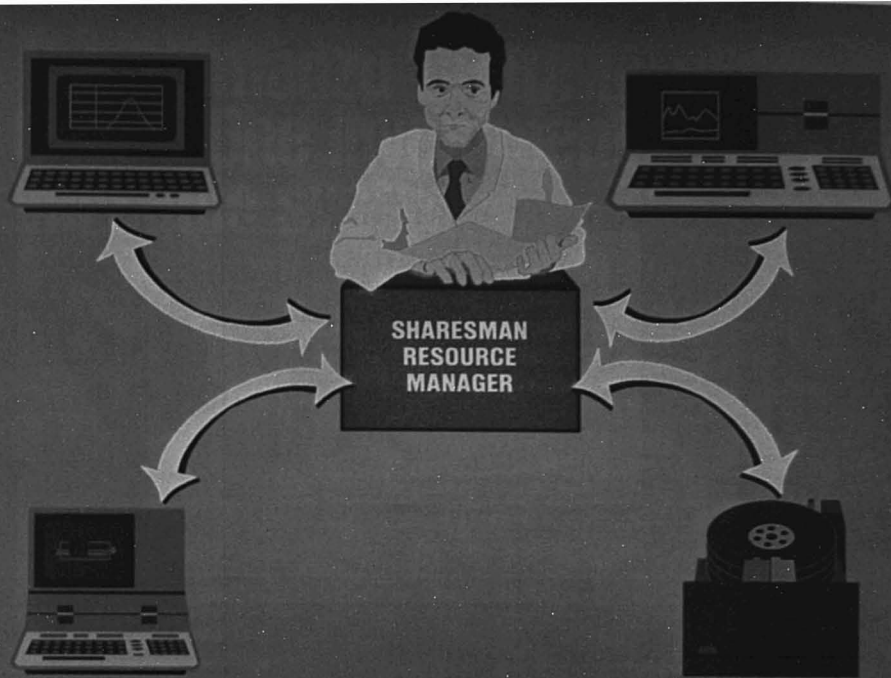
The range of photoacoustic signal linearity as a function of the sample's absorption coefficient,  $\alpha$ , is determined in these measurements at low values of  $\alpha$  by the measurement's background signal interference, which is primarily due to spurious photoacoustic signal generation by radia-

tion absorbed in cell windows and walls. Specific methods for controlling this problem are dictated by the type of cell involved.

Photoacoustic characterizations of fluid absorption do not usually involve measuring samples with high enough values of  $\alpha$  to experience nonlinearity at the upper end of the absorption range measured. This is because samples of interest are weakly absorbing substances due to an inherent advantage of photoacoustic over transmission spectroscopy for such samples (1). This advantage is gained because the photoacoustic signal scales linearly with  $\alpha$  for weakly absorbing samples and avoids the problem encountered in transmission spectroscopy of having to accurately determine a very small difference between two large signals in order to calculate  $\alpha$ .

In contrast to the situation with fluids, signal nonlinearity or saturation with more strongly absorbing solid samples can be a serious problem in photoacoustic measurements. The physical basis for loss of signal sensitivity to increases in  $\alpha$  can be understood by studying the signal generation process with a one-dimensional model (2) illustrated in Figure 2. The schematic shows a monochromatic radiation beam of power,  $P_0$ , incident on a sample contained in a photoacoustic cell. The sample's surface reflectivity,  $R$ , reduces the power just inside the surface of the sample to a value of  $(1 - R)P_0$ . Absorption of radiation causes an additional reduction at a depth  $x$  in the sample to a value of  $(1 - R)P_0e^{-\alpha x}$ .

The power that can be converted into heat in layer  $dx$  is proportional to  $(1 - R)P_0\alpha e^{-\alpha x}$ , resulting in an initial thermal wave of amplitude  $\Delta T_1$ , due to absorption of light in the layer proportional to  $(1 - R)P_0\alpha e^{-\alpha x}$ . Thermal waves (3) play an important role in photoacoustic signal generation because they transport photon-induced heat oscillations from their origin within the sample to the sample surface and hence into the cell gas, where the acoustic signal is generated and detected. The amplitude of the thermal wave decays as it propagates to the thermal transfer surface with a coefficient,  $\alpha_s$ . This results in a value at the surface,  $\Delta T_2$ , proportional to  $(1 - R)P_0\alpha e^{-(1+\alpha_s)x}$ . The actual temperature oscillation produced in the gas is due to thermal waves launched by all of the light-absorbing layers of the sample within approximately a thermal diffusion length (given by  $1/\alpha_s$ ) of the thermal transfer surface. Thermal waves generated in this region make the primary heat contribution to the gas relative to those generated deeper in the sample due to the decay phenomenon.



## Networking comes to chromatography.

Nelson Analytical, with another software innovation, introduces the SHARESMAN resource manager, and brings the bounty of networking to the analytical laboratory. Up to eight local chromatography data systems, with as many as 10 chromatographs in each system, can now share each others results, along with methods, programs and raw data, producing maximum productivity among systems.

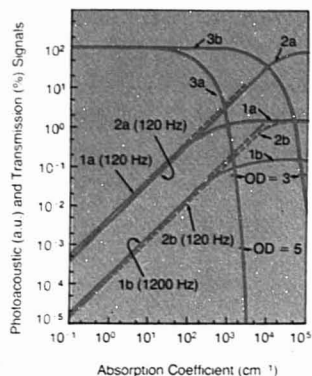
SHARESMAN links any of Nelson Analytical's data systems



based on the HP Series 200 computers, the Model 16, the Model 26 or the Model 36. It gives you the cost savings of using large discs (up to 64 MB) rather than individual smaller Winchester on each system. And the network accommodates an X-Y plotter as well.

Best of all, the entry cost for all this enhanced capability is small, essentially the cost of a single chromatography data system, which can later be added to without obsolescence. Write to 10061 Bubb Road, Cupertino, CA 95014 or call (408) 725-1107

**nelson ANALYTICAL**

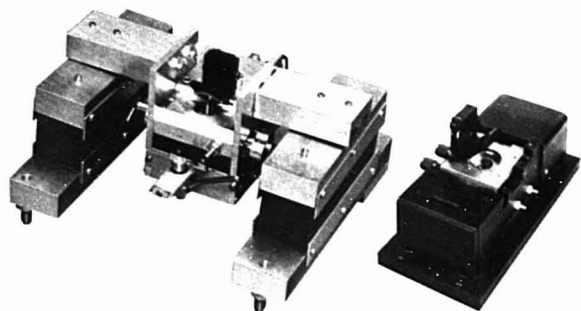


**Figure 4.** Photoacoustic and transmission signals

The signals are plotted as a function of sample absorption coefficient,  $\alpha$ , for various conditions of sample thickness and modulation frequency

Figure 3 is useful in explaining the important details of the photoacoustic signal's dependence on  $\alpha$ . It shows plots of power absorbed per unit length in the sample as a function of radiation penetration depth for a range of  $\alpha$  values increasing from  $2 \text{ cm}^{-1}$  to  $2 \times 10^4 \text{ cm}^{-1}$ . The figure shows that the absorbed power distribution shifts more into the thermally active region defined by the thermal diffusion length as  $\alpha$  increases from  $2 \text{ cm}^{-1}$  to  $20 \text{ cm}^{-1}$ . The resulting linear change in photoacoustic signal is shown in curves 1a (120-Hz modulation frequency) and 1b (1200 Hz) of Figure 4. An additional increase in  $\alpha$  from  $20 \text{ cm}^{-1}$  to  $200 \text{ cm}^{-1}$  causes a similar shift shown in Figure 3 and signal increases for curves 1a and 1b. It is evident, however, that nonlinearity is beginning to appear, especially in curve 1a, and this can be qualitatively explained by noting that the  $\alpha = 200 \text{ cm}^{-1}$  curve in Figure 3 has decayed significantly at the 120-Hz diffusion length. This decay reduces the effectiveness of the shift effect in signal generation. This reduction of effectiveness for redistribution of the absorbed power becomes more significant in going from  $\alpha = 200 \text{ cm}^{-1}$  to  $2000$  and  $20,000 \text{ cm}^{-1}$  with full saturation having occurred for both 120- and 1200-Hz signals at the higher  $\alpha$  value.

Close examination of Figure 3 in terms of the interaction between the thermal diffusion lengths and power absorption curves as  $\alpha$  increases pro-



**Figure 5.** Photoacoustic cells

Cell (a), for condensed samples, was designed and constructed at the Ames Laboratory. Cell (b) is manufactured by EG&G Princeton Applied Research, Princeton, N.J.

vides a qualitative understanding of the delay in saturation observed in Figure 4 for curve 1b relative to 1a. Figures 3 and 4 also illustrate the rationale for using the thermal diffusion length as the estimate of sampling depth in photoacoustic measurements. This consideration is the basis for photoacoustic depth profiling of materials having absorption properties that vary with distance into the sample. For instance, if the subsurface layer between the 120- and 1200-Hz diffusion length lines in Figure 4 has an absorption spectrum different from that of the material closer to the surface, the spectrum of the subsurface layer can be determined by subtracting normalized spectra taken at the 120- and 1200-Hz modulation frequencies.

The one-dimensional model of photoacoustic signal generation discussed above can be put into quantitative terms by solving the appropriate differential equation (4, 5). The signal expression obtained is valid for an idealized parallel-faced sample such as shown schematically in Figure 2 and has proven very useful in setting experimental conditions and interpreting results. Important assumptions used in the calculation include non-radiative decay of optically excited states on a time scale that is fast relative to the modulation period and an absence of multiple reflections and light-scattering effects.

The expression obtained for the photoacoustic signal magnitude and phase (relative to the incident beam waveform) has a rather complicated form (5) that can be simplified for

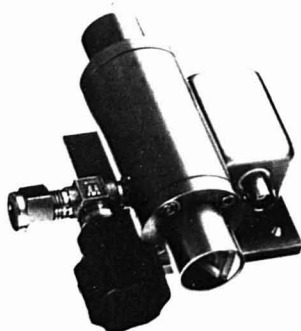
special cases (6-9). The most common case for "as received samples" is when the sample thickness is considerably larger than the thermal diffusion length,  $1/a_s$ , and optical decay length,  $1/\alpha$ . In this case signal magnitude,  $q_1(\lambda)$ , and phase,  $\psi_1(\lambda)$ , are given by:

$$q_1(\lambda) = k(1-R)(P_0(\lambda) \cdot \alpha(\lambda)/a_s)(2/((\alpha(\lambda)/a_s + 1)^2 + 1))^{1/2} \quad (1)$$

and

$$\psi_1(\lambda) = \tan^{-1}(1 + 2a_s/\alpha(\lambda)) \quad (2)$$

where  $\lambda$  denotes the wavelength of incident radiation and  $k$  is a constant



**Figure 6.** Photoacoustic cell for gas analysis from Burleigh Instruments, Inc., Fishers, N.Y.



# The Shimadzu CHROMATOPAC C-R2A. One investment buys two versatile systems.



## CHROMATOPAC C-R2A Data Processor



As an integrator, the Shimadzu chromatopac C-R2A(X) is designed with functions, features and capability to make it the ideal instrument for advanced chromatography—both GC and LC.

As a computer using Basic language programming, it is designed to put a host of capabilities at your fingertips—including complex calculations, the smooth handling of program data and control of your Shimadzu GC-9A or LC-4A system.

As one of the world's most advanced data processors, its performance capability is out-

standing in more than a few applications:

- User-defined Basic language programming can be used to establish a fully automated GC or LC system in which all parameters, data time programs and operational sequences can be predetermined.
- With the optional INP-R2A 2-Channel Interface, you can simultaneously process and record output signals from two detectors.
- Max. 20K byte memory can handle up to 5000 peaks (Chromatopac C-R2AX) and the thermal printer-plotter can record graphic as well as alphanumeric data.

• Write today for more information on these and other Shimadzu instruments.



**SHIMADZU**  
SCIENTIFIC INSTRUMENTS, INC.

SHIMADZU SCIENTIFIC INSTRUMENTS, INC.  
9147 Red Branch Road, Columbia, Md 21045 U.S.A. Phone: (301) 997-1227 Fax: (301) 730-1290  
SHIMADZU (EUROPA) GMBH  
Acker Strasse 111, 4030 Düsseldorf, F.R.G. Germany Phone: (0211) 666371 Telex: 08586839  
SHIMADZU CORPORATION INTERNATIONAL MARKETING DIV.  
Shinjuku-Mitsui Building 1-1 Nishishinjuku 2-chome, Shinjuku-ku, Tokyo 160 Japan  
Phone: Tokyo 03-346-5641 Telex: 0232-3291 SHMDT J

CIRCLE 187 ON READER SERVICE CARD



Figure 7. Photoacoustic spectrometer pictured with a Commodore PET computer, floppy disc drive, and printer. The spectrometer is manufactured by EDT Research, 14 Trading Estate Rd., Great Western Trading Estate, Park Royal, London NW10 7LW, England.

depending on thermal and dimensional properties of the sample cell and gas, as well as the microphone sensitivity. Equation 1 was used to calculate curves 1a (1b) with  $a_s = 200 \text{ cm}^{-1}$  (630  $\text{cm}^{-1}$ ) and  $R = 0$ .

The dotted-line linear extensions of these curves are obtained by combining Equations 1 and 2 (9) to give:

$$q_{11}(\lambda) = q_1(\lambda) \left( \frac{\cos^2(\psi_1(\lambda))}{1 + 1/2} \right)^{1/2} \quad (3)$$

which substantially extends the linearity range of the measurement. The limitation on linearity extension using Equation 3 is imposed by how accurately the phase,  $\psi_1(\lambda)$ , can be determined. Accuracies of several tenths of a degree are specified for state-of-the-art lock-in amplifiers, making extensions as shown in Figure 4 realistic. It is of interest to make a comparison with the transmission signal, given by  $T(\lambda) = (1 - R(\lambda))^2 e^{-\alpha(\lambda)l/a_s}$ , that would be obtained with a sample thickness equal to the photoacoustic sampling depth as defined by the thermal diffusion length,  $1/a_s = 1/200 \text{ cm}^{-1} = 0.5 \times 10^{-3} \text{ cm}$ . The transmission signal is given by curve 3a, again assuming that  $R = 0$ . Comparison of curves 1a and 3a shows that a spectrophotometer would have to be able to measure an optical density (OD) of approximately five to provide transmission data equivalent to the photoacoustic data of curve 1a. This result demonstrates the capability of photoacoustic measurements to determine optical densities beyond the range of most spectrophotometers and to do so without the need to prepare thin-section samples, which is often impractical.

Light-scattering effects common to many samples can be accounted for by modifying Equations 1 and 2 (9) using Kubelka's theory for the optical properties of light-scattering materials (10). The modification is required because light scattering causes a higher

intensity and subsequent power absorption near the illuminated surface of the sample than is predicted by the  $P_0 e^{-\alpha x}$  expression used in the model discussed above. When the modification is made, Equations 1 and 2 contain additional reflectance and scattering coefficients (9). Burggraf and Leyden have demonstrated that the resulting equations for the photoacoustic signal magnitude and phase can be used to obtain a linear signal dependence on  $\alpha(\lambda)$  that is corrected for nonlinearity and light-scattering effects (9).

A second important sample type to be discussed is the case of samples that are thin, rather than thick as discussed above, relative to the optical and thermal decay lengths. In this case photoacoustic measurements have significant advantages over transmission and reflection spectroscopy because they have the potential of providing, in most cases, a signal proportional to  $\alpha(\lambda)$  without dependence on any other optical property, including scattering coefficients (11). In contrast, transmission determinations of  $\alpha(\lambda)$  based on the expression  $T = (1 - R)^2 e^{-\alpha l}$  ( $l$  is the sample thickness) are often confounded by scattering effects or by spectral structure in the sample's reflectivity,  $R$ , which is usually not known. Analysis of specular or diffuse reflectance data to obtain  $\alpha(\lambda)$  is also subject to difficulties due to the complicated equations involved and to theoretical and experimental difficulties in dealing with real samples.

Examples of this type of thin sample include thin layers of fine particles or nonspecular films that may originally exist in this state or that can be prepared to fit these conditions. For these samples, the photoacoustic signal magnitude,  $q_2(\lambda)$ , and phase,  $\psi_2$ , are given, respectively, by:

$$q_2(\lambda) = k P_0(\lambda) \alpha(\lambda) l \cdot (2b^2 + 2b a_s l + a_s^2 l^2)^{-1/2} \quad (4)$$

and

$$\psi_2 = \tan^{-1} (1 - (a_l + b)/b) \quad (5)$$

where  $l$  is the sample thickness and  $b$  is a constant dependent on thermal properties of the sample and cell gas. Equations 4 and 5 are derived assuming that the sample is self-supporting or supported on a low thermal mass substrate backed by cell gas and that  $e^{-\alpha l} = 1 - \alpha l$ .

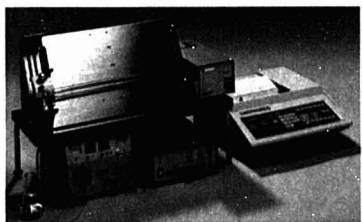
Curve 2a in Figure 4 is plotted from Equation 4 with  $l = 10^{-4} \text{ cm}$ , 120-Hz modulation frequency, and  $a_s = 200 \text{ cm}^{-1}$  as in the earlier calculation for a thick sample (curve 1a). The signal magnitude is nearly equal to that shown with curve 1a below  $\alpha = 100 \text{ cm}^{-1}$  and becomes considerably higher above this value due to more efficient transfer of heat into the gas in this region. The linearity range of curve 2a can be seen to compare favorably with the linear extension of curve 1a obtained using Equation 3.

Equations 4 and 5 cannot be used in a manner analogous to the combination of Equations 1 and 2 to extend the range of linearity. However, extension of linearity to higher values of  $\alpha$  can be accomplished by reducing the sample thickness,  $l$ , for instance, by grinding finer powders. Curve 2b is plotted to illustrate how the signal level changes for a thin sample when it is supported by a thick rather than thin transparent substrate. The advantages of a low thermal mass substrate are evident by comparing curves 2a and 2b. Curve 3b shows the transmission signal behavior for a sample of the same thickness as that used to calculate curves 2a and 2b. No advantage is gained by the photoacoustic method in terms of measuring high optical densities, but insensitivity to reflection and scattering effects is highly significant for determining  $\alpha(\lambda)$  values accurately and for maximum spectral contrast since scattering effects degrade spectra by lowering absorption peaks and raising valleys (11).

In some cases the physical properties of the sample or instrumental limitations make it impossible to avoid signal saturation using the methods discussed above. It is still possible in the signal saturation regime with thick samples to obtain spectral information of potential analytical value. This information is similar to that of specular reflectance spectroscopy due to the photoacoustic signal's sensitivity in that case to the reflected beam fraction,  $R(\lambda)$ . This is because the fraction of the incident beam in a photoacoustic measurement that enters the sample and contributes to the signal is proportional to a factor given by  $(1 - R)$ , as discussed earlier. This factor weights the signal under all conditions with thick samples but assumes

# Shimadzu gives the LC concept broader dimensions.

## LC-5A High Performance Liquid Chromatograph



If you do a lot of LC work, you may want to reduce solvent consumption, or perhaps obtain a higher number of theoretical plates. If so, you ought to consider the advantages of SHIMADZU's new LC-5A Microbore Column Liquid Chromatograph.

For instance:

- Pump capacity can be varied from 1-9900  $\mu\text{l}/\text{minute}$ , while the total system dead volume is only 2 l.
- With the 1 mm diameter microbore column you can do the same work as a conventional LC with 5% the solvent.
- The greater efficiency of the microbore column lets you reach theoretical plate numbers as high as 300,000.
- Standard and reverse phase model columns are available in 25, 50 and 100cm lengths, and can be combined up to 1000cm without reducing efficiency.

• Write today for more information on these and other Shimadzu Instruments.



**SHIMADZU**  
SCIENTIFIC INSTRUMENTS, INC.

**SHIMADZU SCIENTIFIC INSTRUMENTS, INC.**

9147 Red Branch Road, Columbia, Md. 21045 U.S.A. Phone (301)997-1227 Fax (301)730-1290

**SHIMADZU (EUROPA) GMBH**

Acker Strasse 111, 4000 Düsseldorf F.R. Germany Phone (0211)666371 Telex 08586839

**SHIMADZU CORPORATION INTERNATIONAL MARKETING DIV.**

Shinjuku-Mitsui Building, 1-1, Nishishinjuku 2-chome, Shinjuku-ku, Tokyo 160 Japan

Phone Tokyo 03-346-5641 Telex 0232-3291 SHIMDT J

CIRCLE 188 ON READER SERVICE CARD

a special significance in the full signal saturation regime with opaque samples because then there is no other explicit optical property term in the photoacoustic signal expression to account for signal changes (12). In this regime, photoacoustic methods can supply information directly complementary to that of reflectance (13) that can also be used to eliminate the often unwanted signal dependence on the  $(1 - R)$  factor in Equation 1. However, this will not always be permitted due to limitations imposed by instrumental capabilities and sample properties.

## Instrumentation

Practical photoacoustic measurements have historically depended and continue to depend to a considerable degree on instrumental capabilities. The rather demanding requirements placed on instrumentation are due to inherent characteristics of both the signal generation process and the difficult-to-handle samples often chosen for photoacoustic analysis. Measurements on condensed substances encounter signal-to-noise (S/N) limitations primarily due to impedance mismatches at steps in the signal generation sequence, such as the transfer of heat at the sample-gas interface. In the case of fluids, the low absorption usually involved in measuring dilute concentrations of interest leads again to a small fraction of incident power being converted into signal. For this reason high-power optical radiation sources are needed to obtain acceptable S/N levels. The noise contributions to the signal must also be carefully controlled to best utilize the photoacoustic method. These contributions are due primarily to light source instability, acoustic pickup through the atmosphere and support structure, and electrical interference.

The three principal instrument components of a photoacoustic spectrometer include the light source and intensity modulator; the sample cell; and the signal processing and analysis system. These components have benefited greatly in the last 10 years by incorporating new developments such as low  $f$ -number monochromators, Fourier transform spectrometers, lasers, high-sensitivity microphones, lock-in amplifiers, and other computer-based signal processing systems. The main area of instrumentation development specific to photoacoustic measurements has been concerned with sample cells and their associated acoustic detectors.

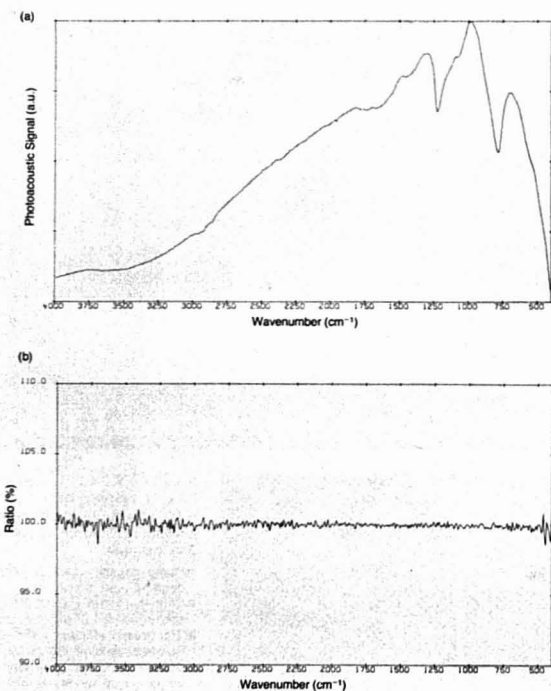
Cells optimized for measurements on condensed samples have small-volume chambers for the sample, typically well under  $1 \text{ cm}^3$ , to enhance the

signal amplitude (the signal is inversely proportional to chamber volume). A sensitive (typically  $50 \text{ mV/Pa}$ ) microphone detector is mounted directly in front of a low-noise preamplifier and coupled to the chamber in a manner that provides a nonresonant acoustic response over the modulation frequency range of interest. Signal enhancement via a resonant cell, although initially thought attractive, is generally impractical for quantitative measurements because chamber resonance characteristics depend on properties of the sample and cell gas. An additional problem with resonant cells has been the distortion of signal phase information that complicates signal processing.

Optical design considerations of particular significance in quantitative measurements include having dimensions of the incident beam focal spot consistent with minimal cell volume

and controlling the fate of radiation after it has interacted with the sample. It is important that this radiation have minimal secondary interaction with the chamber walls or the sample because spurious signals will be produced that are difficult to interpret. These effects have been effectively dealt with by using transparent materials and appropriate chamber geometries (14).

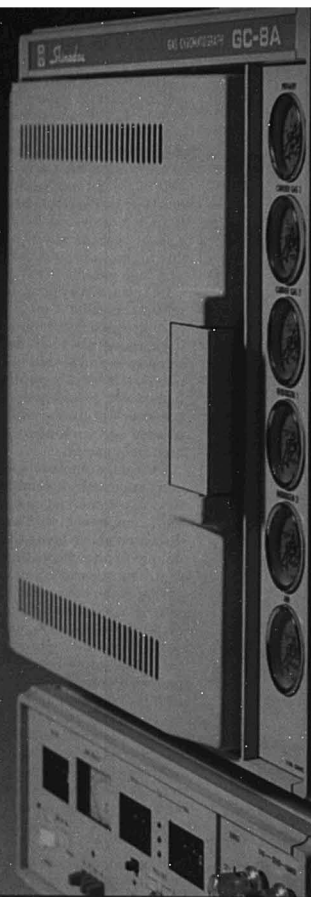
Other important cell considerations include means to control the chamber gas type and purity as well as the operating temperature and pressure. When He gas is used in the cell, rather than air, the signal magnitude is increased by approximately a factor of two, in most cases due to better thermal coupling properties. Gas purity in the sample chamber is a particularly important and often difficult condition to achieve for IR measurements because signal generation by radiation



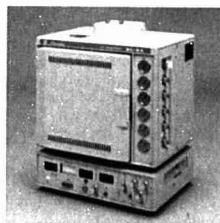
**Figure 8. Source spectra**

Spectrum (a) is due to the optical characteristics of the FTIR spectrometer source and optics. It was acquired with a carbon black sample by averaging 128 scans of the interferometer at  $8 \text{ cm}^{-1}$  resolution and plotted without spectral smoothing. Spectrum (b) is the result of ratioing two spectra of the type shown in (a) to determine the noise level of the FTIR-photoacoustic cell system (no noise corresponds to a straight line). The peak-to-peak noise shown here is well below 1% in the  $2000 \text{ cm}^{-1}$  region.

# Shimadzu breaks the cost barrier of high quality GC.



## GC-8A Series Gas Chromatograph



At Shimadzu it's a cardinal belief that all GC instruments, whether used for R&D or routine control tests, should be of high technical quality. As a result, Shimadzu's GC-8A Series is designed to be the best possible basic GC equipment with ready-to-go when you need them features that include:

- Great economy in cost, maintenance and size
- Digital dial temperature setting, and digital temperature programming (GC-8AP Series)
- An on-column, on-detector system, and cylindrical collector type FID (FID models)

- Constant current type TCD (TCD models)
- Convenient maintenance check system

When you want the best, basic GC performance, think SHIMADZU.

• Write today for more information on these and other Shimadzu instruments.



**SHIMADZU**  
SCIENTIFIC INSTRUMENTS, INC.

**SHIMADZU SCIENTIFIC INSTRUMENTS, INC.**  
9147 Red Branch Road, Columbia, Md 21045, U.S.A. Phone (301) 997-1227 Fax (301) 730-1290  
**SHIMADZU (EUROPA) GMBH**  
Acker Strasse 111, 4000 Düsseldorf, F.R.G. Germany Phone (0211) 666371 Telex 08568839  
**SHIMADZU CORPORATION INTERNATIONAL MARKETING DIV.**  
Shinjuku-Mitsui Building 1-1 Nishishinjuku 2-chome, Shinjuku-ku, Tokyo 160, Japan  
Phone Tokyo 03-346-5641 Telex 0232-3291 SHMDT J

CIRCLE 189 ON READER SERVICE CARD

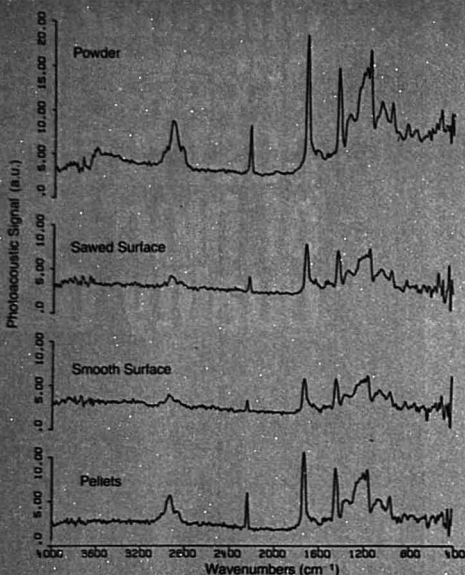


Figure 9. Photoacoustic spectra of nitrile plastic samples with different surface morphologies

Reprinted from Reference 19, with permission

absorbed in water vapor or  $\text{CO}_2$  is very efficient, and trace amounts can cause serious interferences. In some cases, spectral subtraction rather than elimination of residual gases is a practical solution to this problem.

Laboratory and commercially built cells with some of the features discussed above are shown in Figure 5. These cells are designed to have the beam incident from above to allow samples such as powders to be held by gravity. The cells have vibration isolators to reduce structure-borne noise, which is an especially important consideration in FTIR measurements because synchronous amplification is not used. The cell in Figure 5a is designed to operate in an evacuated FTIR spectrometer and may be baked out under vacuum preparatory to loading surface-sensitive samples under glove box conditions.

Photoacoustic cells for fluids (15, 16) are designed for low-absorption gas or liquid samples that fill the sample chamber volume. The most sensitive measurements on liquids have been reported in work by Patel and Tam (15) at Bell Laboratories. They use pulsed-laser excitation directed

along a cylindrical cell axis. Their laboratory-constructed cell has a chamber of polished stainless steel to reduce background absorption and is closed by quartz windows. The cell volume for liquids can be considerably larger (several  $\text{cm}^3$ ) than would be appropriate for condensed samples because the signal depends, due to an inertial confinement effect common to pulsed excitation, on the laser beam diameter and detector distance from the beam axis rather than on cell volume (15). The detector used in these measurements is a miniature hydrophone located in the chamber wall with a time response capable of resolving the excitation response pulse. This allows spurious photoacoustic background signals originating from window and wall absorption to be gated out by the amplifier. Measurements of very low absorbance, in the  $10^{-6}$ – $10^{-7}$  range, have been possible with signal discrimination. Cells for these measurements are not the author's knowledge currently commercially available but the key component, a miniature hydrophone, can be purchased from several firms (15).

A commercial nonresonant pho-

toacoustic cell for gases has recently become available for general use with modulated CW laser excitation. The cell, pictured in Figure 6, is also of stainless steel construction and is evacuated prior to filling. It is not designed to be used in a flow-through configuration such as might be desirable in gas chromatography detection, but laser intracavity operation has been demonstrated. This resulted in a signal enhancement by a factor of 10 due to the additional laser power available relative to extracavity operation. Intracavity operation is an important consideration in terms of generating signal levels above the noise background when very low absorption samples are measured (17). Unfortunately, it is usually impractical to use high-power pulsed lasers with gases because of problems with signal transmission and microphone response at high frequencies.

Currently, photoacoustic spectrometers are usually assembled from a variety of commercial and laboratory-built components with sample cells as discussed above being the main item unique to photoacoustic instrumentation. The one exception known to the author is the commercial UV-VIS-near IR spectrometer and computer system pictured in Figure 7. This xenon lamp-monochromator-based unit has a single-beam source-compensated optical system with six selectable modulation frequencies in a range from 10 to 240 Hz. The instrument is designed with RS232 and IEEE-488 computer interface options. Software has been developed by the manufacturer for instrument control and data analysis tasks.

## Applications

The potential uses of photoacoustic spectroscopy in chemical analysis encompass a wide range of sample types that might be associated with the food, pharmaceutical, coal, semiconductor, and coatings industries, or with biomedical, environmental, or energy research. Most of the activity in these and other areas falls essentially into two categories—differentiated by whether or not the application is in the user or research stage. The first applications area to be discussed, FTIR measurements, is from the first category and has a number of nonspecialist users, especially in qualitative analysis, while the second area, chromatography applications, is currently primarily a research area, but has future general-user potential.

Photoacoustic mid-IR spectra of condensed substances are best obtained using an FTIR instrument with a photoacoustic cell accessory because the low power available from dispersive instruments makes it difficult to



# The LC Connection

## Injectors.Valves.Filters.Columns.Good advice.

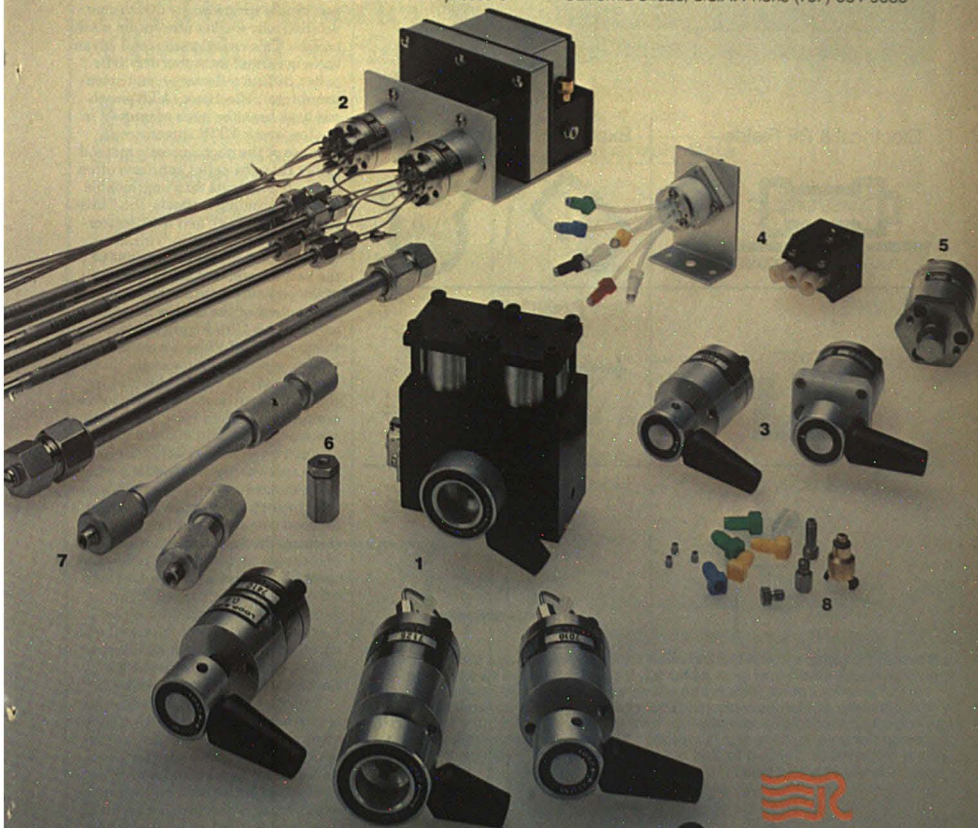
When you use HPLC, make the important connection, Rheodyne. Our components both simplify your work and extend the capabilities of your system. Just check our connections.


**1. Sample Injectors.** The Model 7125 injects either a fully-loaded or partially-loaded sample loop. Other injectors include the pneumatically-actuated 7126, the 7410 for microsamples and the 7010 for full-loop loading only. **2. Column selection valve.** Model 7066 selects one of up to five columns. **3. Switching valves.** Type 70 Valves switch flow for backflushing, sample enrichment, sample cleanup, etc. **4. Solvent switches.** Low-cost Teflon valves switch low-pressure

streams. **5. Pressure relief valve.** Model 7037 protects equipment from overpressure. **6. Column inlet filter.** The 7302 keeps particles from damaging columns. **7. Columns.** Guard, presaturator and analytical columns. **8. Fittings.**

As for good advice, you'll do better HPLC if you ask us for free copies of Technical Notes 1, 2, 3 and 4. They contain practical how-to-do-it information for both the beginner and the experienced chromatographer.

For Tech Notes and product literature, please address Rheodyne, Inc., P.O. Box 996, Cotati, California 94928, U.S.A. Phone (707) 664-9050



  
**RHEODYNE**  
THE LC CONNECTION COMPANY  
CIRCLE 165 ON READER SERVICE CARD

# SCIENTISTS:

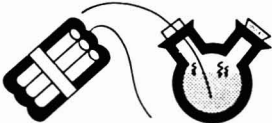
This inert  
optical fiber probe  
measures temperatures in  
amazing places



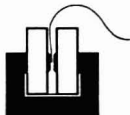
## Electrical & RF Fields



## Explosive Environments



## NMR/ESR



## Very Small Volumes



## Thermal Gradients



## Hostile Environments



Beyond the capabilities of thermometers, thermocouples and thermistors are environments where you have never been able to measure temperature. But now our slender optical fiber probe allows you to reach into hostile, corrosive environments where conventional sensors cannot go. Let us provide you with previously unobtainable temperature data in the range of  $+20^{\circ}\text{C}$  to  $+240^{\circ}\text{C}$  ... using our unique, patented Fluoroptic™ Thermometry technique. Call us for more information ... or just to find out why we won two "Product of the Year" awards in our very first year!

## LUXTRON

Fluoroptic™ Temperature Sensing  
1060 Terra Bella Avenue, Mountain View, California 94043  
Phone (415) 962-8110, Telex 348-399 KARMIGA

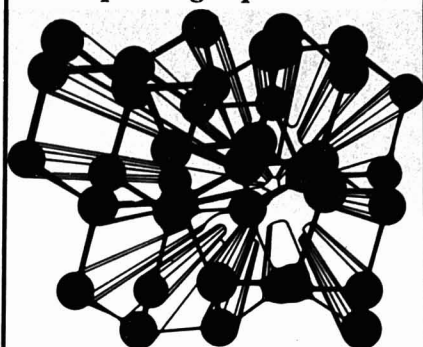
CIRCLE 126 ON READER SERVICE CARD

achieve an acceptable S/N ratio. Photoacoustic cells are available from FTIR instrument manufacturers and other companies mentioned in this article. The quality of FTIR results is most dependent on the sample cell performance. The FTIR instrument is usually a secondary factor, provided that it has (as most do) an incident beam power in the range of tens of milliwatts and mirror velocities as low as approximately  $5 \times 10^{-2}$  cm/s. The latter implies acceptable optical modulation frequencies between 50 and 500 Hz in the 400 to 4000  $\text{cm}^{-1}$  wave-number range. Under these conditions a well-designed cell should give a source power spectrum and noise performance comparable to that shown in Figure 8 and allow spectrum acquisition in several minutes.

Signal saturation is usually less of a problem in the IR region than in UV and visible spectroscopy due to characteristically weaker absorption mechanisms. This consideration and advantages in certain instances over KBr pellet, diffuse reflectance, and attenuated total reflectance (ATR) methods have been the basis of interest in photoacoustic FTIR spectroscopy. The use of the photoacoustic method rather than the pellet approach often prevents problems with ungrindable samples, grinding artifacts, the Christiansen effect (18), and light scattering. Spectra reported by Vidrine of Nicolet Instruments provide one of the best examples of the insensitivity of the photoacoustic method to the morphology of the sample in qualitative analysis (19). Figure 9, which shows results of Vidrine's work, is convincing evidence of how easily IR absorption spectra can be obtained by the photoacoustic method without the sample preparation required for pellet spectroscopy. Additional advantages also can be realized relative to reflectance spectroscopies, especially when samples have a low diffuse reflectance component or properties incompatible for good contact with ATR sampling surfaces. Figure 10a shows KBr pellet, photoacoustic, and diffuse reflectance spectra of Pittsburgh seam coal measured by Solomon's group at Advanced Fuel Research (20). A photoacoustic spectrum of improved quality taken at Advanced Fuel Research with a cell developed at the Ames Laboratory is shown in Figure 10b.

The combination of photoacoustic spectroscopy and chromatography is attractive because problems with poor selectivity often inherent in absorption spectroscopy are reduced by separation of constituents. Photoacoustic quantification of constituents can be more sensitive or less involved than conventional chromatographic detection methods. The first use of photo-

*An Expanding Experience . . .*



## **. . . The American Chemical Society**

**F**or over 100 years the American Chemical Society has added more publications, new services, scores of local sections, divisions by the dozen, and over 120,000 unique members. Some are Nobel Laureates, some have just received their degrees.

Today, we would like to add *you*.

We think you would enjoy association with experienced chemical scientists who take their profession seriously.

You can start today by becoming a member or national affiliate of the Society.

The benefits are immediate:

- reduced fees at meetings
- weekly issues of C&EN
- member rates on ACS journals
- local section activities
- 31 specialized divisions
- employment aids
- group insurance plans

Send the coupon below today for an application, or call (202) 872-4437.

**Yes, I am interested in joining the ACS. Please send information and an application.**

Name

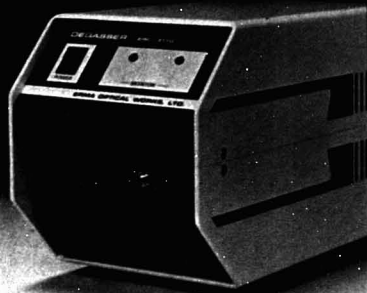
Address

City  State  Zip/Country

Phone (  )

**American Chemical Society  
Membership Development**  
1155 Sixteenth Street, N.W. Washington, D.C. 20036

## **Innovative On-Line HPLC Degasser**



**ERC-3000 series**

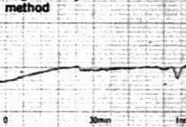
- No change in the mixture ratio of solvent because of the membrane separation system
- Safety and no change of solvent because of no heating of process.

### **Comparison Data**

**Degassed by ERC-3110**

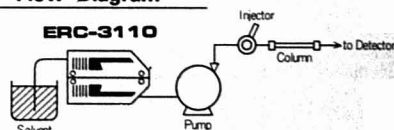


**Degassed by conventional method**



- Solvent: Distilled water
- Detector: ERC-7510 ( $0.25 \times 10^{-5}$  RIU/FS)

### **Flow Diagram**



*Under patent application in several countries*

**For more information, contact**

## **ERMA OPTICAL WORKS, LTD.**

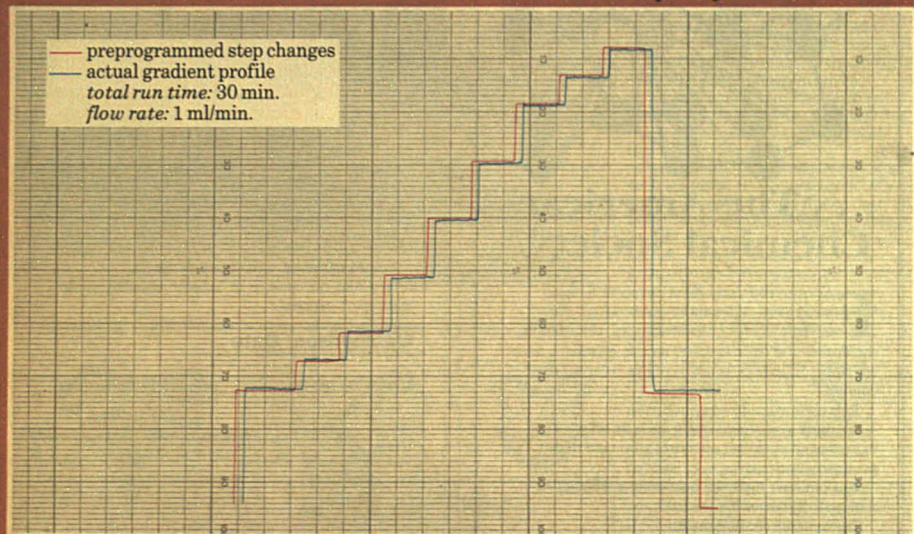
Scientific Instruments Department  
2-4-5, Kaiicho, Chiyoda-ku  
Tokyo, 101 Japan  
Telex: J25301 ERMAWORK  
Cable: ERMAWORKS TOKYO

CIRCLE 63 ON READER SERVICE CARD



# Distinguished for accuracy

## the new LKB Solvent Delivery System



The new LKB 2152 HPLC Controller is designed to operate together with LKB 2150 HPLC Pumps to produce the smoothest, most accurate and reproducible gradients obtainable today. Even at the extremes of solvent composition, where very low flow rates are required, an LKB solvent delivery "team" ensures precision. When it comes to microbore and capillary HPLC applications, this new system is ideal.

The 2152 Controller is also a state-of-the-art central microprocessor unit for complete HPLC system control. It can be used to control an autosampler, column

oven or valves. It even enables precise volume fraction collection and volumetric calibration of the recorder chart speed during gradient elution. And it is the only HPLC controller which offers exact synchronization of your gradient profile and chromatogram.

The 2152 HPLC Controller is designed with particular concern for accurate and efficient methods development. A variety of sophisticated features such as editing, file storage, scaling functions, flow-programming and link-file capabilities make the 2152 the controller of choice for methods research.

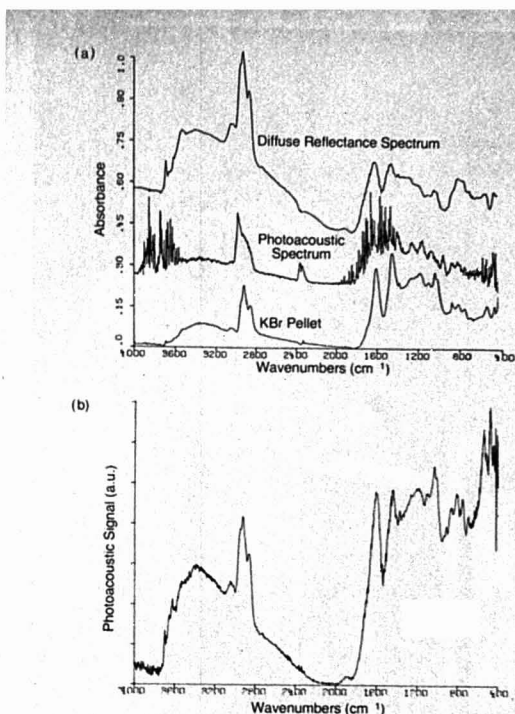


For full facts on the new LKB HPLC Controller, don't hesitate to contact your local LKB representative.



Head office: LKB-Produkt AB, Box 305, S-161 26 Bromma, Sweden. Tel. 09-99 00 40, telex 10492  
Main US sales office: LKB Instruments, Inc. 8319 Gaither Road, Gaithersburg, Maryland 20877. Tel. 301-963-3200, telex 160870 (dom.), 64634 (intern.)  
UK sales office: LKB Instruments Ltd., 232 Addington Road, S. Croydon, Surrey CR2 8YD, England. Tel. 01-657 8822, telex 264414  
Other sales offices in: Athens (for Middle East), Copenhagen, Ghent, Zoetermeer, Hong Kong, Luzern, Munich, Paris, Rome, Turku, Vienna

CIRCLE 125 ON READER SERVICE CARD



**Figure 10.** Photoacoustic spectra

(a) Comparison of FTIR spectra of a Pittsburgh seam coal obtained by diffuse reflectance, photoacoustic, and KBr pellet methods, reprinted from Reference 20 with permission. (b) Photoacoustic spectrum of the same coal taken with a photoacoustic cell developed at the Ames Laboratory

photoacoustic spectroscopy in chromatographic detection involved gas chromatography (21), but more recent activity has involved high-performance liquid (HPLC) and thin layer (TLC) chromatography.

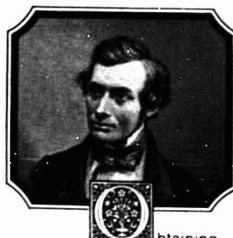
Sawada's group at the University of Tokyo has developed a photoacoustic cell for measurements on HPLC effluents and compared its performance to a UV absorption detector for trace analysis (22). Their cylindrical cell is similar to Patel and Tam's cell in that it has a stainless steel chamber closed by quartz windows but differs significantly in volume, flow-through design, and excitation mode. The chamber volume has been reduced to 20  $\mu$ L for the chromatographic application and has inlet and outlet ports for the effluent flow. It is excited by a 500-mW CW argon ion laser beam at 488 nm

modulated at approximately 4 kHz. This frequency provides the best S/N ratio in the presence of acoustic noise from the HPLC pump. The signal is detected by a piezoelectric transducer disk coupled to the side of the cell by an acoustic window sealed with platinum foil.

In tests on a group of isomers of chloro-4-(dimethylaminolazobenzene (Cl-DAAB), photoacoustic detection sensitivity showed a 25-fold improvement over the UV detector without compromising chromatogram bandwidth or reproducibility. Sawada has suggested that additional sensitivity improvements may be possible using the pulsed excitation approach of Patel and Tam.

Photoacoustic analysis of thin-layer chromatograms was initially demonstrated as a qualitative method (23)

*"If only I'd known about Scott!"*



obtaining pure gases for his experiments on diffusion must not have been easy for Thomas Graham. Far better for him to have opened the Scott Specialty Gases Buying Guide!

Today's chemist is more fortunate. He need only look in the latest edition of the Scott Buying Guide to find an exceptionally valuable source of information on hydrogen, nitrogen, oxygen, argon, helium, methane, air and other gases for use as carriers and fuels in gas chromatography.



Far more than a mere listing of cylinder sizes and gas purities, the new application guide section provides recommendations for virtually every user of specialty gases. Specific instruments and applications are covered in detail. The Scott GC Specialty Gases Buying Guide is an indispensable document for every worker in GC. Request your new edition now.

**New edition of Scott Specialty Gases Buying Guide just published — get your copy today!**



**Scott Specialty Gases**  
a division of Scott Environmental  
Technology Inc.

Plymouthville, PA • 215-766-8861  
San Bernardino, CA • 714-887-2571  
Houston, TX • 713-537-8512  
Troy, MI • 313-589-2950

21A

CIRCLE 190 ON READER SERVICE CARD



## ***The real payoff from this new Mettler is productivity.***

The new Mettler AE electronic analytical balances aren't just a little bit faster than your mechanical balances. They're three to four times faster. Why? Because most of the work is preprogrammed for you by AE's tiny but mighty brain. This faster speed translates directly into significant increases in your productivity.

### ***Productivity comes naturally.***

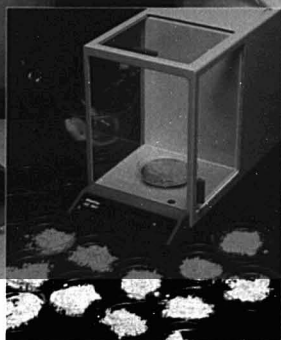
AE balances are so easy to work with your productivity will just naturally get better. The AE is ready when you are. There's no warmup. No dial switching. No micrometer adjustments. No swinging pans to cope with. The AE's

top-loading weighing pan is stable and only 55 mm above the lab bench surface. This makes repeated weighings a lot less tiring, so the work goes faster. The exclusive Mettler DeltaDisplay speeds up weighing-in procedures by automatically adjusting to your pouring speed until the target weight is reached.

### ***Practically runs itself.***

And the wonder of it all is that everything happens automatically. With a touch of the control bar. Calibrating. Setting tare. Even adjusting for environmental factors that could make other balances unstable.

CIRCLE 138 ON READER SERVICE CARD



**The AE163:** 162 g readable to 0.1 mg or 31 g readable to 0.01 mg. **The AE160:** 162 g readable to 0.1 mg.

### ***At an affordable price.***

For even greater productivity, you can use a Mettler optional data output to connect the AE balance with a computer or other electronic peripheral equipment. Best of all, the benefits of this new Mettler can be yours at a price that's about the same as today's mechanical balances.

For more information write or call:  
Mettler Instrument Corporation,  
Box 71, Hightstown, NJ 08520.  
Phone (609) 448-3000.

**METTLER**



and more recently for quantitative determinations (9, 24, 25). The method's capability for spectroscopic analysis of non specular surfaces and surface sensitivity (due to higher efficiency of heat transfer from the sample's surface vs. its bulk) are exploited in this application. Work to date has demonstrated that measurements can be made directly on TLC plates or on material removed from the plate (24).

Additional refinements of the method to simplify or, in some cases, initiate quantitative TLC analysis seem practical. Fishman and Bard at the University of Texas recently developed a photoacoustic cell that can be placed directly on a TLC plate (26). The cell is excited via a fiber-optic-linked source with a spectral range covering the visible and parts of the UV and near IR.

## Conclusion

Photoacoustic spectroscopy has developed to the stage where it is practical for general analytical users as a qualitative mid-IR technique applicable to difficult samples that are incompatible with conventional IR methods. In the context of photoacoustic research, quantitative potential has been demonstrated in some IR measurements and in other applications such as chromatography detection. Additional developments in the areas of instrumentation, sample preparation/calibration methodology, and data acquisition and analysis are necessary to realize the full potential of the method. Current research in photoacoustics and related areas is addressing these needs. For instance, new theoretical progress on the complex but important problem of photoacoustic signal generation in light-scattering samples such as powders will serve as a foundation for improved sample preparation and data interpretation (9, 11). In the future, photoacoustic measurements can be expected to be practical for additional applications due to the widening spectral range of lasers and the increasing capability of data analysis routines to extract more information from spectra (27).

## Acknowledgment

Thanks are due to M. K. Iles and S. W. Veysey for research assistance and to E. L. DeKalb, V. A. Fassel, W. J. Haas, and R. N. Kniseley for comments on this article. The provision of photographs and product information by photoacoustic instrument firms is gratefully acknowledged.

## References

- (1) Harris, T. D. *Anal. Chem.* 1982, 54, 741 A.
- (2) McClelland, J. F.; Kniseley, R. N. *Appl. Phys. Lett.* 1976, 28, 467.

- (3) McDonald, F. A. *Am. J. Phys.* 1980, 48, 41.
- (4) Parker, J. G. *Appl. Opt.* 1973, 12, 2974.
- (5) Rosencwaig, A.; Gersho, A. *J. Appl. Phys.* 1976, 47, 64.
- (6) Poulet, P.; Chamberon, J.; Unterreiner, R. *J. Appl. Phys.* 1980, 51, 1738.
- (7) Teng, Y. C.; Royce, B. S. *H. J. Opt. Soc. Am.* 1980, 70, 557.
- (8) Roark, J. C.; Palmer, R. A.; Hutchison, J. S. *Chem. Phys. Lett.* 1978, 60, 112.
- (9) Burggraf, L. W.; Leyden, D. E. *Anal. Chem.* 1981, 53, 759.
- (10) Kubelka, P. *J. Opt. Soc. Am.* 1948, 38, 448.
- (11) Yasa, Z. A.; Jackson, W. B.; Amer, N. M. *Appl. Opt.* 1982, 21, 21.
- (12) McClelland, J. F.; Kniseley, R. N. *Appl. Opt.* 1976, 15, 2658.
- (13) Baldassarre, L.; Cingolani, A. *Solid State Commun.* 1982, 44, 705.
- (14) McClelland, J. F.; Kniseley, R. N. *Appl. Opt.* 1976, 15, 2967.
- (15) Patel, C. R. N.; Tam, A. C. *Rev. Mod. Phys.* 1981, 53, 517.
- (16) Voightman, E.; Jurgensen, A.; Winefordner, J. *Anal. Chem.* 1981, 53, 1442.
- (17) Stella, G.; Gelfand, J.; Smith, W. H. *Chem. Phys. Lett.* 1976, 39, 146.
- (18) Laufer, G.; Huneke, J. T.; Royce, B. S. H.; Teng, Y. C. *Appl. Phys. Lett.* 1980, 37, 517.
- (19) Vidrine, D. W. *Appl. Spectrosc.* 1980, 34, 314.
- (20) Solomon, P. R.; Carangelo, R. M. *Fuel* 1982, 61, 663.
- (21) Kruzezer, L. B. *Anal. Chem.* 1978, 50, 597 A.
- (22) Oda, S.; Sawada, T. *Anal. Chem.* 1981, 53, 471.
- (23) Rosencwaig, A.; Hall, S. S. *Anal. Chem.* 1975, 47, 548.
- (24) Castleden, S. L.; Elliott, C. M.; Kirkbright, G. F.; Spillane, O. E. *M. Anal. Chem.* 1979, 51, 2152.
- (25) Ashworth, C. M.; Castleden, S. L.; Kirkbright, G. F. *Anal. Proc.* 1981, 18, 14.
- (26) Fishman, V. A.; Bard, A. J. *Anal. Chem.* 1981, 53, 102.
- (27) Hruschka, W. R.; Norris, K. H. *Appl. Spectrosc.* 1982, 36, 261.

This work was supported by the U.S. Department of Energy, Contract W-7405-Eng-82, Division of Basic Energy Sciences, Budget Code KC-03-02-03, and in part by IBM Instruments.



J. F. McClelland received a BS in physics from Dickinson College, and earned his physics PhD at Iowa State University. He has worked at the National Bureau of Standards and Honeywell Electro-Optics Center, and is currently an associate physicist at the Ames Laboratory of Iowa State University. His current research interests include photoacoustic spectroscopy and thermal wave microscopy.

# Whatman 800-631-7290 For Prompt Total Service

Chromatographers need more than quick delivery of supplies. They also need prompt, reliable technical service to help gain the most from their laboratory.

That's why Whatman will now market and distribute its chromatography products directly.\*

We have expanded our team of highly skilled technical field representatives supported by a technical staff and shipping expeditors. This will assure prompt delivery and in-depth technical support.

For all your LC, TLC, and AIEC product needs, call Whatman direct:

## 800-631-7290.

It's the one source for prompt delivery... and responsive technical support.

\*Whatman TLC products will continue to be distributed by The Ansco Co. Inc., Bodman Chemicals and Pierce Chemical Co.; and Whatman AIEC products by Pierce Chemical Co.



**Whatman**  
Whatman Chemical Separation Inc.  
9 Bridwell Place, Clifton, New Jersey 07014  
Tel 201-773-5800 • Telex 133426

CIRCLE 240 ON READER SERVICE CARD

# LABORATORY SERVICE CENTER

## CLASSIFIED SECTION

POSITIONS OPEN

DL- $\alpha$ -Alanine • DL- $\beta$ -Amino-n-butyric Acid •  $\epsilon$ -Amino-n-Caproic Acid  
p-Aminohippuric Acid • Bicine • 1-Bromonaphthalene • iso-Caproic Acid  
Cinchophen • Dibenzoylmethane • 1,4-Dichlorobutane • 1,3-Dimethylurea  
Gallate • Glutaric Acid • Lactic Acid • L-Malic Acid • Malonic Acid  
Maltose • Mercuric Potassium Iodide • N-Methylformamide • Orcinol  
Ninhydrin • o-Nitrobenzaldehyde • Phenylthiourea • Propyl Butyrate  
Quinalizarin • Sodium Pyruvate • Sodium Tetrathionate • Succinimide  
Tetramethylammonium Chloride & Hydroxide • Vanillic Acid • Xylitol

Write for our Products List of over 3000 chemicals

Tel: 516-273-0900 • TOLL FREE: 800-645-5566

TWX: 510-227-6230

### EASTERN CHEMICAL

A Division of UNITED-GUARDIAN, INC.

P. O. Box 2500

DEPT. AC

SMITHTOWN, N. Y. 11787

## LABORATORY MULTI-MILL

PULVERISES ANALYTICAL SAMPLES.

Ideal for use in mining, geology, agriculture, forestry, etc.



- 80 samples simultaneously.
- Highest productivity/operator hour.
- Each sample 1 to 150 grams.
- No heavy handling.
- No dust. Easy to clean.
- Patented worldwide.

### ROCKLABS

P.O. BOX 18142 AUCKLAND, NEW ZEALAND.  
TELEPHONE (09) 574 698 TELEX NZ65550



## USE LABORATORY SERVICE CENTER

CUSTOM PURCHASE OF ORGANIC COMPOUNDS

Prep-Scale Gel  
Permeation  
Chromatography

L. C. Services Corporation

225 Widenow Street  
Woburn, MA 01801

(617) 938-1700

## West Germany

Specialist in HPLC to supervise a group of scientists and technicians developing assays for drugs and their metabolites in biological samples. This group is also responsible for the assay of such samples arising from studies of these drugs in man. Relocation to Germany is required. Send resume and salary requirements in confidence to Pharmaconsult, Inc., Box 559, New Vernon, New Jersey 07976.

## CLASSIFIED ADVERTISING RATES

Rate based on number of insertions used within 12 months from date of first insertion and not on the number of inches used. Space in classified advertising cannot be combined for frequency with ROP advertising. Classified advertising accepted in inch multiples only.

Unit 1-T 6-T 12-T 24-T 48-T 72-T  
1 inch 117 109 104 95 90 83  
(Check Classified Advertising Department for rates if advertisement is larger than 10")  
SHIPPING INSTRUCTIONS: Send all material to

Analytical Chemistry  
Classified Advertising Department  
25 Sylvan Rd. South, P.O. Box 231  
Westport, CT 06881

## INDEX TO ADVERTISERS IN THIS ISSUE

CIRCLE INQUIRY NO.	ADVERTISERS	PAGE NO.	CIRCLE INQUIRY NO.	ADVERTISERS	PAGE NO.
5	*Alltech Associates Cromad	50A	64	ESA James F. Balderson & Associates	68A
3	Analytichem International Forsythe Advertising, Inc.	15A	65	*Erba Instruments, Inc. TMK, Inc.	19A
27	*B&L/Instrument & Systems Div. Blair Advertising	58A	63	*Erma Optical	101A
28	*Beckman Instruments International	32B	66	*Floridin Company Marsteller, Incorporated	61A
18	*Beckman/Allex LaPointe, Schott & Smith, Inc.	85A	68	*GFS Chemical Company	19A
20, 26	*Bioanalytical Systems Kissinger Advertising Associates	51A, 69A	69	*Gilsen Medical Electronics LaPointe, Schott & Smith, Inc.	1A
24	*Brinkman Instruments Div. of Sybron Corporation Lavey/Wolff/Swift	OBC	100	*Hamilton Company Mealer & Emerson	24A
22	*Burdick & Jackson Nordstrom/Cox Marketing	73A	96-97	*Hewlett-Packard Company Pinne, Garvin & Hock, Inc.	88A
33	Chrompack Lohmeyer Simpson Communications, Inc.	52A	98	*Hitachi, Ltd.	108A
xx	*Cole-Parmer Instrument Co.	76B-76C	111	*Instrumentation Laboratory Aries Advertising, Incorporated	53A
60	*Dionex Corporation Baxter, Gurian & Mazzell, Inc.	7A	115	*Johnson Matthey, Incorporated Al Paul Leffon Company, Inc.	50A
62	*Dynatech Labs, Incorporated Ehrlich, Manes & Associates	23A	xx	*Kevex Corporation LaPointe, Schott & Smith, Inc.	IFC
			119-120	*Kontron, Ltd.	32D, 32I
			122	*Koslow Scientific Company K M & S Advertising	68A

# INDEX TO ADVERTISERS IN THIS ISSUE

CIRCLE INQUIRY NO.	ADVERTISERS	PAGE NO.	CIRCLE INQUIRY NO.	ADVERTISERS	PAGE NO.
117	*Kratos Analytical Instruments TMK, Inc.	41A	224	*Valco Instruments Technical Advertising Associates	39A
125	LKB Biochrom Ltd.	102A	218-219	*Varian Moran, Lanig & Duncan	17A
127	Lockheed McCann-Erickson, Inc.	84A	232, 234	Waters Associates Mintz & Hoke, Inc.	4A-5A, 86A-87A
128	Luxtron	100A	230	*Wescan Instruments LaPointe, Schott & Smith, Inc.	57A
141-142	*Matheson Kenyon Hoag Associates	12A, 13A	240-241	*Whatman Chemical Separation, Inc. RS Design	67A, 105A
144	*Mead CompuChem Hodskins Simone & Searls Adv.	65A	236	*Whatman Lab Products J. S. Lanza & Associates, Inc.	9A
138-139	Mettler Instruments McKinney, Inc.	55A, 104A	238	John Wiley & Sons 605 Advertising Group	82A
143	*Mitsubishi Chemical Ind., Ltd. Global Advertising	69A	* See ad in ACS Laboratory Guide ** Company so marked has advertisement in Foreign Regional edition only. Advertising Management for the American Chemical Society Publications		
155	Nelson Analytical Moran Lanig & Duncan Advertising	91A	CENTCOM, LTD.		
153	*Norton Specialty Plastics Div. Scott & Associates	81A	Thomas N. J. Koerwer, President Benjamin W. Jones, Vice President James A. Byrne, Vice President Robert L. Voepel, Vice President Alfred L. Gregory, Vice President Joseph P. Stenza, Production Director Clay S. Holden, Vice President		
158	*Ohaus Scale Corporation Jarman, Spitzer & Felix	49A	25 Sylvan Rd. South P.O. Box 231 Westport, Connecticut 06881 (Area Code 203) 226-7131		
168-171	*Perkin-Elmer Corporation Marquardt & Roche	27A, 29A	ADVERTISING SALES MANAGER James A. Byrne		
173-174	Perkin-Elmer/Oak Brook Div.	31A	ADVERTISING PRODUCTION MANAGER Barbara Aufderheide		
163	*Pharmacia G&C Advertising	14A	SALES REPRESENTATIVES		
165	Philips Analytical X-Ray STG Marketing	18A	Philadelphia . . . Dean A. Baldwin, Jerry Naab, CENTCOM, LTD., GSB Building, Suite 425, 1 Belmont Avenue, Bala Cynwyd, Pa. 19004. Telephone: 215-667-9666		
70-78, 79-82	*Pye Unicam, Ltd. R. Connors Publicity	32E-32F 32G-32H	New York . . . Dean A. Baldwin, Don Davis, CENTCOM, LTD., 60 East 42nd St., 212-972-9660, New York, N.Y. 10165		
185-186	*Rheodyne, Inc. Bonfield Associates	69A, 99A	Westport, CT . . . Don Davis, CENTCOM, LTD., 25 Sylvan Rd. South, P.O. Box 231, Westport, Ct. 06881. Telephone: 203-226-7131		
194	SLM/AMINCO Grubb, Graham & Wilder, Inc.	44A	Cleveland . . . Bruce E. Poorman, CENTCOM, LTD., 17 Church St., Berea, Ohio 44017, 216-234-1333		
193	*Schleicher & Schuell, Inc. Jarman, Spitzer & Felix	49A	Chicago . . . Bruce E. Poorman, CENTCOM, LTD., 540 Frontage Rd., Northfield, Ill. 60093, 312-441-6383		
195	Scientific Glass Engineering Arden Advertising	57A	Houston . . . Dean A. Baldwin, CENTCOM, LTD., 215-667-9666		
190	Scott Specialty Gases The Matlin Company	103A	San Francisco, CA . . . Paul M. Butts, CENTCOM, LTD., Suite 112, 1499 Bayshore Hwy, Burlingame, CA 94010. Telephone: 415-682-1218		
191	*The Separations Group LaPointe, Schott & Smith, Inc.	63A	Los Angeles . . . Clay S. Holden, CENTCOM, LTD., Newton Pacific Center, 3142 Pacific Coast Highway, Suite 200, Torrance, CA 90505, 213- 325-1903		
187-189	Shimadzu Scientific Instruments, Inc. General Advertising Agency	93A, 95A, 97A	Boston, MA . . . Don Davis, CENTCOM, LTD. Telephone: 203-226-7131		
206	Tecator, Inc.	43A	Atlanta, GA . . . Don Davis, CENTCOM, LTD. Telephone: 203-226-7131		
204	*Techne, Incorporated Brunswick Advertising	50A	Denver . . . Clay S. Holden, CENTCOM, LTD., 213-325-1903		
203	Thermolyne (Sybron) Stephan & Brady, Inc./Adv.	11A	United Kingdom Reading, England . . . Malcolm Thiele, Technomedia Ltd., Wood Cottage, Shurlock Row, Reading RG10 0QE. Berkshire, England. Telephone: 0734-343302		
212	Ultra-Violet Products UVP, Inc. Marketing Services	42A	Lancashire, England . . . Technomedia Ltd., c/o Meconomics Ltd., Meco- nomics House, 31 Old Street, Ashton Under Lyne, Lancashire, England. Telephone: 061-308-3025		
215	Universal Scientific	36A	Continental Europe . . . Andre Jamar, Rue Mallat 1, 4800 Verviers, Belgium. Telephone: (087) 22-53-85, Telex #49263		
			Tokyo, Japan . . . Shigao Aoki, International Media Representatives Ltd., 2-29 Toranomon, 1-Chome Minato-ku Tokyo 105 Japan. Telephone: 502- 0656		

# THE SECRET IS OUT...

*For Years Hitachi Users Have Had The Advantage of Working with Our Reliable, Innovative Chromatographs.*

*The Newest Member of Our Family,*

*The Model 655 HPLC is so Good We Want to Share It with You.*

The MODEL 655 HPLC pump is easy to operate and easy to maintain. All wetted parts are right up front. Flow is pulseless and compressibility compensation is automatic. Delivery is precise; typically, RSD of retention times is less than 0.25%.

**Model 655**



To truly reveal the highest performance of the 655 pump a sensitive, stable detector is required. The MODEL 638-41 UV detector is the perfect complement to our newest pump. This detector offers excellent signal to noise characteristics and pushbutton autozero.

**Model 638-41**



Our HPLC products offer the same ease of use, quality, and reliability we build into all Hitachi products.

Reliability is our most important specification.



**HITACHI**

SCIENTIFIC INSTRUMENTS  
NISSEI SANGYO AMERICA, LTD.  
460 East Middlefield Road, Mountain View,  
CA 94043 U.S.A. Tel: (415) 969-1100  
CIRCLE 98 ON READER SERVICE CARD

• NISSEI SANGYO CO., LTD.  
Japan: (03) 504-7111

EDITOR: GEORGE H. MORRISON

EDITORIAL HEADQUARTERS

1155 Sixteenth St., N.W.  
Washington, D.C. 20036  
Phone: 202-872-4570 Teletype: 710-8220 151

Executive Editor: Josephine M. Petruzzelli

Managing Editor: Barbara Cassatt

Associate Editor: Stuart A. Borman

Assistant Editors: Marcia S. Cohen,

Rani A. George

Production Manager: Leroy L. Corcoran

Art Director: John V. Sinnott

Staff Artist: Linda M. Mattingly

Copy Editor: Gail M. Mortenson

Circulation Manager: Cynthia G. Smith

Journals Dept., Columbus, Ohio

Associate Head: Marianne Brogan

Associate Editor: Rodney L. Temos

Advisory Board: Joel A. Carter, Richard S.

Danchik, Richard Durst, Dennis H. Evans,

Jack W. Frazer, Helen M. Free, Shizuo Fuji-

wara, Roland F. Hirsch, Csaba Horvath, Wilbur

I. Kaye, Thomas C. O'Haver, Janet Oster-

young, Herbert L. Retcofsky, Robert E. Siev-

ers, Wilhelm Simon, Rudolph H. Stehl

Instrumentation Advisory Panel: Edward M.

Chait, M. Bonner Denton, Raymond E. Dessy,

Larry R. Faulkner, Martin S. Frant, Michael L.

Gross, Fred E. Lytle, Curt Reimann, Andrew

T. Zander

Contributing Editors, A/C Interface: Raymond

E. Dessy, The Analytical Approach: Jeanette

G. Grasselli

The Analytical Approach Advisory Panel: Ed-

ward C. Dunlop, Robert A. Hofstadter, Wilbur

D. Shultz

Regulatory Affairs, Analytical Division Com-

mittee: Fred Freeberg (Chairman)

Published by the  
AMERICAN CHEMICAL SOCIETY

1155 16th Street, N.W.

Washington, D.C. 20036

Books and Journals Division

Director: D. H. Michael Bowen

Journals: Charles R. Bertsch

Production: Elmer Pusey, Jr.

Marketing & Sales: Claud K. Robinson

Research and Development: Seidon W.

Tarrant

Manuscript requirements are published in the

January 1983 issue, page 171. Manuscripts for

publication (4 copies) should be submitted to

ANALYTICAL CHEMISTRY at the ACS Washington

address.

The American Chemical Society and its editors

assume no responsibility for the statements and

opinions advanced by contributors. Views ex-

pressed in the editorials are those of the editors

and do not necessarily represent the official

position of the American Chemical Society.

## Software and Analytical Instrumentation

Recently, a matter of serious concern associated with the software used in analytical instrumentation was brought to our attention by a reader. Following a recent ASTM symposium that highlighted the lack of openness on the part of vendors who provide such software, this correspondent was given the task of alerting editors of scientific journals to this developing problem.

Our inquiry into the matter confirms the serious nature of the situation. Many instrument vendors will not share software with purchasers. Some will not even share the algorithm that describes what the software does. Vendors seem sensitive to users and competitors sharing software with each other in an unregulated manner. The problem involves documentation, the electronically readable form of software, human-readable forms of the same material, and the algorithm.

Raymond Dessy, our contributing editor for A/C INTERFACE, does not believe that user pirating is a problem for software in PROM (programmed by the vendor prior to sale) or for software distributed on magnetic media. Too much specific ancillary hardware is involved, which is intimately associated with the software, to make user duplication worth the effort. Furthermore, duplication can be made difficult to impossible by using encrypting techniques, or by writing special enabling data in the intersector gaps of disks. Licensing agreements and nondisclosure agreements signed by the user provide a final legal barrier.

Under the latter conditions, controller and interface vendors will share printed circuit schematics with purchasers. It seems reasonable then to expect instrument vendors to share algorithms with users who want to be sure that the invisible data treatment being applied is appropriate to their requirements. Even source codes should be shared where specific needs warrant it. After all, computer vendors do provide source codes for many aspects of operating systems when users wish to modify them for special purposes.

With respect to the commercial competitor, certainly retroengineering is always possible. However, the time and expense involved are considerable. The distributors of business, personal, and hobby software protect themselves by the methods mentioned, and then maintain their competitive edge by developing new generations of products, rather than compulsively worrying about protecting the last release.

With the increasing computer sophistication of analytical chemists, deciding which instrument to buy may well hinge on the quality of the software provided by the manufacturer. This important problem will be explored more fully in a forthcoming pair of articles in A/C INTERFACE.

*G. H. Morrison*



# Separation of Sulfite, Sulfate, and Thiosulfate by Ion Chromatography with Gradient Elution

Thomas Sundén,\* Mats Lindgren, and Anders Cedergren

Department of Analytical Chemistry, University of Umeå, S-901 87 Umeå, Sweden

Darryl D. Slemmer

Exxon Nuclear Idaho Company, Inc., P.O. Box 2800, Idaho Falls, Idaho 83401

A simple gradient apparatus, consisting of a peristaltic pump in addition to a standard high-pressure pump, is described. The device is used to make a single-run ion chromatographic separation of sulfite, sulfate, and thiosulfate in less than 15 min. This separation required a step gradient with 4.8 mM  $\text{NaHCO}_3$ /4.7 mM  $\text{Na}_2\text{CO}_3$  as start eluent and 6.9 mM  $\text{NaHCO}_3$ /8.6 mM  $\text{Na}_2\text{CO}_3$  as final eluent when two ( $4 \times 50$ ) mm Dionex anion precolumns in series were used as separator. The eluent compositions were simplex optimized.

Ion chromatography (IC) (1) has been shown to be a suitable analytical technique for determination of sulfur anions such as sulfite, sulfate, and thiosulfate. One of the major problems concerned with these analyses is that the retention time for thiosulfate is unacceptably long when determined under the same ion chromatography (IC) conditions as for sulfite/sulfate.

Holcombe et al. (2) have reported IC determinations of these sulfoxo ions, but two separate IC runs with different eluents for sulfite/sulfate and thiosulfate, respectively, were required. Trujillo et al. (3) reported on the use of a very short column with high eluent flow rate to elute thiosulfate in about 4 min. However, this short retention time for  $\text{S}_2\text{O}_3^{2-}$  caused the other anions present, such as  $\text{F}^-$ ,  $\text{Cl}^-$ ,  $\text{NO}_2^-$ ,  $\text{NO}_3^-$ ,  $\text{PO}_4^{3-}$ , and  $\text{SO}_4^{2-}$  to elute as a single peak. As a consequence, two separate IC runs are required for the sulfite, sulfate, and thiosulfate analyses. Gjerde et al. (4, 5) have shown chromatograms with thiosulfate and sulfate well separated, with a retention time for thiosulfate of about 12 min. However, their tabulated retention times for sulfite and sulfate indicate poor separation of these ions.

The purpose of this paper was to investigate the possibility of separating sulfite, sulfate, and thiosulfate in an acceptable time in a single IC run.

## EXPERIMENTAL SECTION

**Instrumentation.** A diagram of the complete ion chromatograph is presented in Figure 1. The system consisted of the following parts: (1) a Constametric III Pump (Laboratory Data Control) which delivers the eluent at a constant flow rate through the sample loop, the analytical column, the suppressor column and the conductivity cell; (2) a stepper motor driven peristaltic pump P-1 (Pharmacia Fine Chemicals) used to generate gradients in eluent strength, the pump speed was controlled by a homemade variable frequency sweep generator (F.S.G.); (3) a sample injection valve (Rheodyne 70-10) with 50-, 100-, or 200- $\mu\text{L}$  sample loops; (4) two plastic ( $4 \times 50$ ) mm anion precolumns (Dionex Corp., catalog no. 030825) were coupled in series to serve both as pre-column and analytical column; (5) a laboratory made ( $5.7 \times 300$ ) mm glass column packed with Amberlite AG, 100-200 mesh (Serva AG), in the hydrogen form serves as suppressor column, the suppressor was regenerated with 0.5 M  $\text{H}_2\text{SO}_4$ ; (6) a Conducto Cell with Conducto Monitor (LDC) to serve as the detector; (7)

a Vitatron two-channel recorder to trace the chromatograms.

**Chemicals.** All solutions were prepared in doubly deionized water using reagent grade chemicals. The sulfite standard solutions were prepared from  $\text{HOCH}_2\text{SO}_3\text{Na}$  (98% Aldrich) in order to avoid oxidation to sulfate (6).

The sodium hydrogen carbonate and disodium carbonate solutions, of equal molarity (e.g., 5 mM), for the gradient elution experiments were prepared in the following manner: (1) 1000 mL of 5 mM  $\text{NaHCO}_3$  was made by using the dried salt (Merck p.a.). (2) This solution was divided in two equal parts. One was set aside and the other was converted to carbonate by replacing 500  $\mu\text{L}$  of the solution with a 500- $\mu\text{L}$  aliquot of 5.00 M  $\text{NaOH}$ .

**The Gradient System.** There are two ways of effecting gradient elution in liquid chromatography, viz., (i) high-pressure mixing and (ii) low pressure mixing. The former, conventional approach requires two high-pressure pumps and a solvent programmer. An alternate, less expensive, approach requires only one high-pressure pump.

To create the gradient, this system uses a peristaltic pump in addition to the high-pressure liquid chromatography (HPLC) pump. This peristaltic pump (P-1) is connected to the suction side of the HPLC pump. When P-1 is off, only eluent A (see Figure 1) is pumped through the chromatograph. But when P-1 is on, it will force eluent B into a mixing "tee" at the suction side of the HPLC pump. Therefore, the rate of the two eluents (A/B) reaching the column will vary depending on the pumping rate of P-1. Since P-1 is driven by a stepper motor its speed depends only of the driving frequency of the motor.

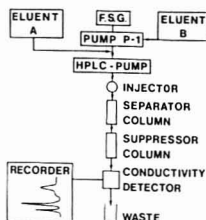
The frequency sweep generator makes it possible to increase and decrease the motor speed as a function of time.

The frequency sweep generator consists of two main parts, a ramp generator and a voltage-to-frequency converter. The ramp generator produces a voltage ramp with adjustable, positive and negative, slopes. There is also a possibility to hold the output (and thus the output frequency) at any desired value between 0 and +5 V dc.

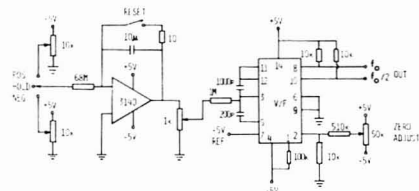
The circuit diagram of the frequency sweep generator is shown in Figure 2.

## RESULTS AND DISCUSSION

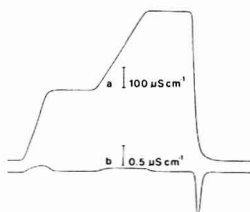
**The Gradient System.** The initial aim of this work was to make a gradient elution with no base line shift. This is achieved by starting the gradient with hydrogen carbonate and finishing it with carbonate of the same molar concentration. By this procedure the carbonic acid concentration in the detector should be constant during the whole gradient run. Figure 3 shows a gradient, with 5 mM  $\text{NaHCO}_3$  as eluent A (see Figure 1) and 5 mM  $\text{Na}_2\text{CO}_3$  as eluent B, as it appears on top of the separator column. The line below is the detector base line. The disturbances in the base line, which originate from the separator column, are positive and negative carbonate peaks (humps). These peaks arise from the variations in the ionic strength, for example, when the eluent is changed from 5 mM hydrogen carbonate to 5 mM carbonate. The double negatively charged carbonate ion causes a temporary increase in the carbonic acid concentration in the detector when two hydrogen carbonate ions are replaced by one carbonate ion



**Figure 1.** Schematic diagram of the ion chromatograph.



**Figure 2.** Circuit diagram of the frequency sweep generator: V/F, Datel VFO-1.



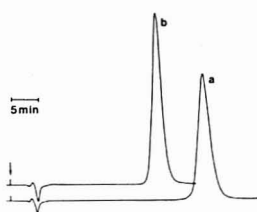
**Figure 3.** (a) Typical gradient as it appears on top of the separator column and (b) detector response during the gradient: eluent A, 5 mM  $\text{NaHCO}_3$ ; eluent B, 5 mM  $\text{Na}_2\text{CO}_3$ .

at the amino groups in the separator resin. In order to minimize base line shift, due to small differences in  $\text{HCO}_3^-/\text{CO}_3^{2-}$  concentrations, special care in making the eluents was necessary. The recommended procedure is described in the Experimental Section.

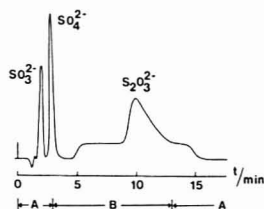
The higher eluting strength of carbonate compared with hydrogen carbonate gives rise to a decrease in retention time of about 25% for, e.g., sulfate (Figure 4). This difference in retention times might be sufficient for certain applications, but the effect is not adequate in the case of strongly retarded anions such as thiosulfate.

The increase in pH when going from hydrogen carbonate to carbonate makes it possible to control the charge of, e.g., phosphate and thus its retention time. If, for example, nitrate and phosphate coelute with an eluent of a pH where  $\text{HPO}_4^{2-}$  exists, you are able to change the pH of the eluent so  $\text{PO}_4^{3-}$  elutes with a longer retention time than nitrate. This is simply and quickly done with the equipment and the type of eluents described herein. The fact that these eluents give the same carbonic acid concentration in the detector causes no base line shift when changing eluent pH. Moreover, the possibility of altering the pH without long waiting times is useful in method development work.

In order to resolve sulfite, sulfate, and thiosulfate in a reasonable time, we had to abandon this initial approach. A much greater change in eluent ionic strength during the IC



**Figure 4.**  $\text{SO}_4^{2-}$  eluted with (a) 5 mM  $\text{NaHCO}_3$  and (b) 5 mM  $\text{Na}_2\text{CO}_3$ ; flow, 1.4 mL  $\text{min}^{-1}$ ; columns, (4  $\times$  50) + (4  $\times$  250) mm Dionex anion separators (catalog no. 030825 and 030827) and (5.7  $\times$  300) mm Amberlite AG suppressor.



**Figure 5.** Chromatogram of  $\text{SO}_3^{2-}$ ,  $\text{SO}_4^{2-}$ , and  $\text{S}_2\text{O}_3^{2-}$  with step gradient and the best eluent composition found by simplex optimization: eluent A, 4.8 mM  $\text{NaHCO}_3$ /4.7 mM  $\text{Na}_2\text{CO}_3$ ; eluent B, 7.2 mM  $\text{NaHCO}_3$ /9.1 mM  $\text{Na}_2\text{CO}_3$ .

Table I. Simplex Optimization Facts

variables	[NaHCO <sub>3</sub> ] <sub>A</sub> , [Na <sub>2</sub> CO <sub>3</sub> ] <sub>A</sub> , [NaHCO <sub>3</sub> ] <sub>B</sub> , [Na <sub>2</sub> CO <sub>3</sub> ] <sub>B</sub>
total eluent flow	3.4 mL min <sup>-1</sup>
eluent B flow <sup>a</sup>	3.0 mL min <sup>-1</sup>
separator column	2 Dionex precolumns (4 × 50) mm in series
suppressor column	(5.7 × 300) mm Amberlite AG, 100–200 mesh
sample loop	200 µL
sample	50 ppm SO <sub>3</sub> <sup>2-</sup> , 25 ppm SO <sub>3</sub> <sup>1-</sup> ,

<sup>a</sup> Peristaltic pump was turned on 3 min after injection.

run apparently was necessary, to shorten the time between the elution of sulfate and thiosulfate.

Studies showed that steep gradients were required to fulfill the above mentioned requirements, and in practice, a limiting step gradient, controlled only by the mixing of the two eluents, was employed. However, to find the best conditions for this eluent change, a simplex optimization of the eluent composition was done. When we switch on the peristaltic pump at a certain time after the injection, an eluent change will occur after approximately 2 min of delay as shown as a base line shift on the recorder.

**Simplex Optimization.** A function minimization with four variables was done with the simplex method (7). The variables were  $\text{NaHCO}_3$  and  $\text{Na}_2\text{CO}_3$  concentrations in eluent A and eluent B, respectively. The function to be minimized was the sum of three terms, namely, the thiosulfate retention time, an estimate of the separation between sulfite and sulfate, taken as the distance from the base line to the valley between the peaks, and an estimate of the separation of the sulfate peak from the base line shift due to eluent change.

The chromatographic specifications are given in Table I. The best result obtained with this formulated function is shown in Figure 5.

Although the retention time for thiosulfate is 10 min, the total time for a full cycle, including restabilization of the base line with eluent A, is about 15 min. This is mainly due to the tailing of the thiosulfate peak and to a lesser extent depending on the restabilization of the base line, which requires approximately 1 min.

In order to decrease the severe tailing of the thiosulfate peak, experiments were performed with  $\text{B}_2\text{O}_3^{2-}$  in both eluents as a modifier. However, the extent of tailing was not reduced and the sulfite/sulfate separation deteriorated. It is possible that the severe tailing of this peak not only is due to adsorption effects in the separator column but also is caused by decomposition of thiosulfate when it is acidified in the suppressor column. This, however, is not confirmed.

The use of eluents with concentrations high enough to elute thiosulfate in about 10–12 min shortens the lifetime of the suppressor column. To cope with this problem, it is possible to use two suppressors in parallel, alternatively using one while regenerating the other. Another possibility is the use of the hollow fiber suppressor, with continuous regeneration, recently described by Stevens et al. (8).

Note: Eluent suppression ion chromatography is covered

by patents in several countries.

## ACKNOWLEDGMENT

The authors wish to thank Lars Lundmark and Svante Jonsson for the electronic and mechanical constructions.

## LITERATURE CITED

- (1) Small, H.; Stevens, T. S.; Bauman, W. C. *Anal. Chem.* **1975**, *47*, 1801–1809.
- (2) Holcombe, L. J.; Jones, B. F.; Ellisworth, E. E.; Meserole, F. B. In "Ion Chromatographic Analysis of Environmental Pollutants"; Ann Arbor Science: Ann Arbor, MI, 1979; Vol. 2, pp 401–412.
- (3) Trujillo, F. J.; Miller, M. M.; Skogerboe, R. K.; Taylor, H. E.; Grant, C. L. *Anal. Chem.* **1981**, *53*, 1944–1946.
- (4) Gjerde, D. T.; Fritz, J. S.; Schmuckler, G. J. *Chromatogr.* **1979**, *186*, 509–519.
- (5) Gjerde, D. T.; Schmuckler, G.; Fritz, J. S. *J. Chromatogr.* **1980**, *187*, 35–45.
- (6) Lindgren, M.; Cedergren, A.; Lindberg, J. *Anal. Chim. Acta* **1982**, *141*, 279–286.
- (7) Neider, J. A.; Mead, R. *Computer J.* **1965**, *7*, 308–313.
- (8) Stevens, T. S.; Davis, J. C.; Small, H. *Anal. Chem.* **1981**, *53*, 1488–1492.

RECEIVED for review July 26, 1982. Accepted September 29, 1982.

# Determination of Cyanide, Sulfide, Iodide, and Bromide by Ion Chromatography with Electrochemical Detection

Roy D. Rocklin\* and Edward L. Johnson

Dionex Corp., 1228 Titan Way, Sunnyvale, California 94086

Cyanide, sulfide, iodide, and bromide are separated and detected by using ion chromatography (IC) and electrochemical detection via a silver working electrode. The detection limits are 2 ppb, 30 ppb, 10 ppb, and 10 ppb, respectively. Cyanide and sulfide can be determined simultaneously, as well as with other anions commonly determined by IC. Cyanide contained in Cd and Zn complexes is quantitatively determined as total "free" cyanide, while cyanide contained in Ni and Cu complexes is only partially determined as "free" cyanide. The strongly bound cyanide in Au, Fe, or Co complexes is not detected.

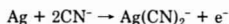
Although ion exchange techniques can easily separate cyanide or sulfide from a host of common anions, their detection via common methods such as conductivity is very poor. During an IC analysis, the weakly acidic species HCN and  $\text{HS}^-$  are formed in the anion suppressor column. Unlike the halogen acids, they are not detected by the conductivity detector due to their low dissociation and, therefore, low conductivity. This inability to detect cyanide and sulfide has prevented the exploitation of the separating power of ion chromatography (1) for the determination of these ions.

In all the analytical methods so far developed for cyanide and sulfide, removing interferences is a necessary first step when analyzing most samples. In addition to interfering with each other, other species interfering with cyanide and sulfide determination include the halogens, thiocyanate, and thiosulfate. The traditional wet chemical analytical method for cyanide, including the removal of interferences, involves precipitating sulfide with cadmium ion, filtering, acidifying,

and distilling the sample (2). The cyanide is trapped in a sodium hydroxide solution, which is usually assayed by argentometric titration, by spectrophotometry, or by an ion selective electrode. The entire process takes approximately 2 h. Samples which can be analyzed directly without distillation are those which are known not to contain significant quantities of interfering species. Sulfide is usually determined by precipitating sulfide with zinc ion, filtering, and then acidifying the precipitate. This solution can be assayed by iodometric titration, spectrophotometry (methylene blue method) or by an ion selective electrode. This procedure takes approximately  $1\frac{1}{2}$  h per sample.

Electrochemical methods for cyanide determination include amperometry (3–5) and polarography (6). Sulfide can be determined by cathodic stripping voltammetry (7). The polarographic method (6) can determine cyanide or sulfide when in the presence of the other; however, iodide and thiosulfate interfere.

Recently Pihlar and Kosta (8, 9) developed an electrochemical method for cyanide analysis by using flow injection analysis (FIA). The method is based on the ability of a silver working electrode in an amperometric electrochemical flow-through cell to produce a current. The reaction for cyanide is



The main conclusions from the work of Pihlar and Kosta are as follows:

- (1) Current is directly proportional to cyanide ion concentration.
- (2) The electrode maintains the same sensitivity over long periods of time; i.e., it is not poisoned.

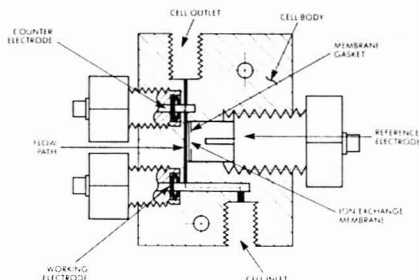
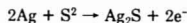


Figure 1. Diagram of amperometric flow-through cell.

(3) Sulfide interference is still a problem.

Similar reactions occur for sulfide and the halogens; however, the products are precipitates rather than a soluble complex.



In this paper, the results of placing an ion exchange column in front of the electrochemical detector are presented. Cyanide and sulfide are separated and thus are determined simultaneously. Although bromide and iodide can be determined by IC with conductivity detection, the use of electrochemical detection results in greater selectivity as well as increased sensitivity.

#### EXPERIMENTAL SECTION

All chromatography was performed on a Dionex System 2010 (P/N 35201) ion chromatograph. Unless otherwise specified, the sample loop size was 50  $\mu\text{L}$  and the eluent flow rate was 2.5 mL/min. Cyanide and sulfide were separated on an HPIC-AS4 (P/N 35311) anion exchange column using an eluent consisting of 14.7 mM ethylenediamine, 10 mM  $\text{NaH}_2\text{BO}_3$  (prepared from  $\text{H}_3\text{BO}_3$  and  $\text{NaOH}$ ), and 1.0 mM  $\text{Na}_2\text{CO}_3$ . The eluent pH is 11.0. Chromatography of iodide was performed by using an HPIC-AS1 (P/N 30827) column with an eluent consisting of 20 mM  $\text{NaNO}_3$ . Chromatography of bromide was performed using an HPIC-AS3 (P/N 30985) column with an eluent consisting of 2 mM  $\text{Na}_2\text{CO}_3$ .

Electrochemical detection was performed with an Ion-Chrom/Amperometric Detector (P/N 35221). The cell (Figure 1) consists of a silver rod working electrode 1.3 cm long  $\times$  0.178 cm in diameter, an Ag/AgCl reference electrode separated from the flowing stream by a Nafion cation exchange membrane, and platinum counterelectrode. (Nafion is a registered trademark of E. I. du Pont de Nemours & Co.) The cell geometry is based on one previously reported in the literature (10). The working electrode was occasionally cleaned by mechanical polishing. The applied potential was 0 V for cyanide and sulfide, 0.20 V for iodide, and 0.30 V for bromide.

Cyanide standard solutions were prepared from a 1000 ppm NaCN (Mallinckrodt, Paris, KY) stock solution, standardized by argentometric titration. Sulfide standards were prepared by diluting 21%  $(\text{NH}_4)_2\text{S}$  (J. T. Baker, Phillipsburg, NJ).  $\text{K}_3\text{Fe}(\text{CN})_6$ ,  $\text{K}_3\text{Co}(\text{CN})_6$ , and CuCN were purchased from Alfa Products (Danvers, MA).  $\text{K}_2\text{Zn}(\text{CN})_4$  and  $\text{KAu}(\text{CN})_2$  were purchased from Pfaltz and Bauer (Stamford, CT).  $\text{Ni}(\text{CN})_4^{2-}$  was prepared from NaCN and  $\text{Ni}(\text{CH}_3\text{COO})_2$  (Matheson, Norwood, OH).  $\text{Cd}(\text{CN})_4^{2-}$  was prepared from 1000 ppm solutions of CdCl<sub>2</sub> (Alfa) and NaCN. Copper cyanide solutions were prepared by adding stoichiometric quantities of NaCN to a  $1.0 \times 10^{-6}$  M CuCN solution.

#### RESULTS AND DISCUSSION

**Applied Potential.** Figure 2 shows the dependence of current response on applied potential ( $E_{\text{app}}$ ). As the potential is increased from negative to positive, the peak height increases as the diffusion controlled plateau is reached. Beyond this

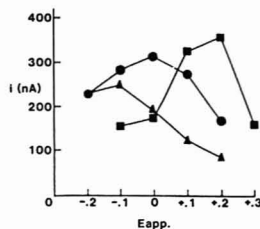


Figure 2. Dependence of current response on  $E_{\text{app}}$  for 1 ppm cyanide (dots), 500 ppb sulfide (triangles), and 5 ppm iodide (squares).

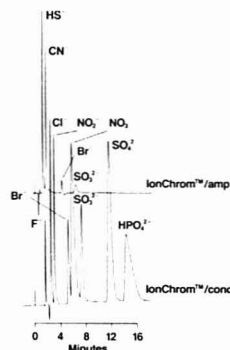


Figure 3. Simultaneous analysis by using electrochemical and conductivity detection. Concentrations are 300 ppb sulfide, 500 ppb cyanide, 1 ppm fluoride, 4 ppm chloride, 10 ppm nitrite, 10 ppm bromide, 25 ppm nitrate, 30 ppm sulfite, 25 ppm sulfate, and 50 ppm phosphate.

potential, peak height decreases as other reactions compete with the one of interest, probably oxidation of silver to form an oxide or hydroxide, thus poisoning the electrode surface (11).

**Simultaneous Multianion Analysis.** Electrochemical detection can be used in conjunction with conductivity detection to determine, in a simultaneous analysis, ions detectable by either method. This is accomplished by placing the electrochemical detector between the separator and suppressor columns of the ion chromatograph. The electrochemical detector must be placed before the suppressor column, as the suppressor's purpose is to lower the conductivity by decreasing the concentration of the supporting electrolyte. The separation of a 10 anion standard is shown in Figure 3. Sulfide, cyanide, bromide, and sulfite are detected at the silver electrode, while nitrite, nitrate, phosphate, and sulfate produce no response. Due to the low dissociation of  $\text{H}_2\text{S}$  and HCN following protonation by the suppressor column, they are not detected by the conductivity detector.

The major advantage of chromatography over other analytical methods is its ability to separate interferences. With one exception, the determination of one of the four ions is not affected by the presence of the others. For example, a solution containing 2500 times as much chloride as bromide has little effect on the determination of bromide (Table I), even though chloride elutes first. Since  $E^\circ$  for the oxidation of Ag to AgCl is positive of  $E^\circ$  for the oxidation of Ag to AgBr, at a potential just on the diffusion controlled plateau for bromide, the current response for bromide will be much greater than that

Table I. Determination of 1 ppm Cyanide in the Presence of Sulfide

amt of added $S^{2-}$ , ppm	recovery of $CN^-$ , %, $\pm 2\%$
0	100
0.10	109
1.00	112
10.0	104

Table II. Determination of 400 ppb Bromide in the Presence of Chloride

amt of added $Cl^-$ , ppm	recovery of $Br^-$ , %, $\pm 2\%$
0	100
10	104
100	100
1000	115 <sup>a</sup>

<sup>a</sup> The 1000 ppm chloride solution contains 50 ppb bromide, accounting for 12.5% of the 15% excess.

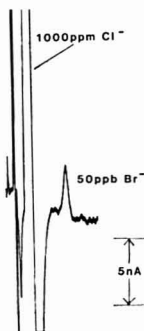


Figure 4. Determination of 50 ppb bromide in 1000 ppm chloride from reagent grade NaCl (Baker). A 100- $\mu$ L sample loop was used.

for chloride. This can be exploited in order to determine small quantities of bromide in a large excess of chloride; a difficult process using other methods of analysis due to the similar chemical properties of the two halides. The determination of 50 ppb bromide present in 1000 ppm of reagent grade chloride is shown in Figure 4. The large negative dip following the chloride peak is caused by the reduction of the AgCl deposited on the electrode. Since there is no longer chloride in the solution next to the electrode (as it has all eluted), and since the applied potential is below the diffusion controlled plateau, AgCl reduction is favored in order to satisfy the Nernst equation. A small dip following the bromide peak can also be seen.

The determination of cyanide is affected by the presence of sulfide in the sample, as shown in Table II. Since sulfide elutes before cyanide (Figure 3), cyanide does not interfere with the analysis of sulfide. The addition of 0.1 ppm sulfide enhances the cyanide peak by 9%. This effect can be minimized or eliminated by using the standard addition method or by matching the cyanide standards as closely as possible to the sample. For example, if the sample is known to contain approximately 100 ppb sulfide, then this amount should be added to the standards.

**Reproducibility.** The reproducibility of peak heights for repeated injections of the four ions is generally 1%, however the first injection of a series usually produces a peak a few

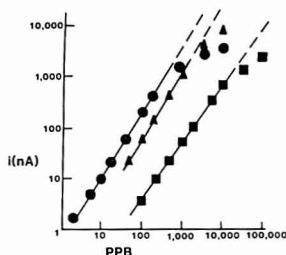


Figure 5. log (current) vs. log (concentration) for cyanide (dots), sulfide (triangles), and iodide (squares).

percent lower than the subsequent injections. This effect is most pronounced for sulfide, which produces an initial peak as much as 10% lower than the subsequent peaks. In actual use, errors in concentration measurements can be reduced or eliminated by making two or three injections until the peak height is reproducible.

Extremely small quantities of sulfide (<20 ppb) also produce irreproducible peaks, often disappearing entirely. As this problem is independent of the applied potential and is not noticed in FIA experiments, it is thought to be caused by chemical reactions occurring in the column.

It is interesting that the deposition of a layer of  $Ag_2S$  or  $AgX$  on the working electrode surface does not poison the electrode, since we have seen no evidence of a decrease in peak height caused by a build up of silver sulfide or halide. Shimizu, Aoki, and Osteryoung (12) have noted that the rate of oxidation of a rotated silver disk electrode in the presence of sulfide is limited by the diffusion of sulfide ions to the electrode, as long as less than  $0.08 C cm^{-2}$  of charge has passed. This charge, equivalent to about 700 monolayers, is considerably in excess of the integrated current from a 1 ppm sulfide peak, about  $10^{-6} C cm^{-2}$ . Cyanide forms a soluble product and cannot form a layer (13).

**Linearity and Sensitivity.** Calibration curves for cyanide, sulfide, and iodide are shown in Figure 5. In general, plots of the log of peak height as a function of the log of concentration are linear at low concentration. At high concentrations, an increase in concentration produces a smaller increase in current as shown by the plateau for each ion. This plateau (also observed in FIA studies) is caused by uncompensated resistance in the cell. The upper limit of linearity can be extended by increasing the applied potential or by decreasing the size of the injection loop. With a 100- $\mu$ L injection loop, the detection limit for cyanide is 2 ppb, for sulfide 30 ppb, for iodide 10 ppb, and for bromide, 10 ppb. The detection limits reported here are approximately 2 orders of magnitude lower than those reported with the use of gold or mercury working electrodes (5).

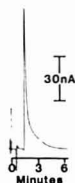
**Analysis of Metal Cyanide Complexes.** The cyanide in inorganic cyanides can be present as both complexed and free cyanide. In order to study the chromatography of metal cyanides, we prepared and assayed solutions of cadmium, zinc, copper, nickel, gold, iron, and cobalt cyanides. Table III lists the percentage of total cyanide detected.

The results suggest that the complex cyanides can be grouped into three categories depending on the cumulative formation constant and stability of the complex. Category 1 includes the weakly complexed and labile (14) cyanides  $Cd(CN)_2$  ( $\log \beta_4 = 18.78$ ) (15) and  $Zn(CN)_2$  ( $\log \beta_4 = 16.7$ ). These complexes completely dissociate under the chromatographic conditions used; the cyanide being indistinguishable from free cyanide.



Table III. Percentage of Total Cyanide in Metal Complexes Determined as "Free" Cyanide

metal complex	$\log \beta_1^a$	%
$\text{Cd}(\text{CN})_4^{2-}$	18.8	102
$\text{Zn}(\text{CN})_4^{2-}$	16.7	102
$\text{Ni}(\text{CN})_4^{2-}$	31.3	81
$\text{Cu}(\text{CN})_3^{2-}$	30.3	52
$\text{Cu}(\text{CN})_2^-$	28.6	42
$\text{Cu}(\text{CN})_2^-$	24.0	38
$\text{Au}(\text{CN})_2^-$	38.3	0
$\text{Fe}(\text{CN})_6^{3-}$	42	0
$\text{Co}(\text{CN})_6^{3-}$	64 <sup>b</sup>	0

<sup>a</sup> Formation constants from ref 15. <sup>b</sup> From ref 16.Figure 6. Chromatogram of  $1.0 \times 10^{-5} \text{ M Cu}(\text{CN})_3^{2-}$ .

Category 2 includes the moderately strong cyanide complexes  $\text{Ni}(\text{CN})_4^{2-}$  ( $\log \beta_4 = 31.3$ ) and  $\text{Cu}(\text{CN})_4^{2-}$  ( $\log \beta_4 = 30.3$ ). Although the complexes are labile, they are retained on the column and slowly dissociate during the chromatography. This slow dissociation produces tailing which lasts for several minutes as the free cyanide elutes and is detected. The chromatography of  $\text{Cu}(\text{CN})_3^{2-}$  is shown in Figure 6 and can be compared to the cyanide peak in Figure 3. As the results presented in Table III demonstrate, the tailing and the non-quantitative recovery of cyanide preclude the use of direct injection to determine total cyanide in samples containing copper or nickel. These samples may be analyzed after acid distillation and caustic trapping. The cyanide in the caustic solution can then be determined by ion chromatography with electrochemical detection.

Category 3 includes those cyanides which are inert and therefore totally undissociated, such as  $\text{Au}(\text{CN})_2^-$  ( $\log \beta_2 =$

38.3),  $\text{Fe}(\text{CN})_6^{3-}$  ( $\log \beta_6 = 42$ ), and  $\text{Co}(\text{CN})_6^{3-}$  ( $\log \beta_6 = 64$ ) (16). No free cyanide was detected for these complexes. Although these complexes do not elute under the chromatographic conditions used, they can be eluted and determined by using different chromatographic conditions and conductivity detection (17).

Samples containing both free cyanide (or weakly complexed cyanide) and strongly complexed cyanide can be analyzed for free cyanide by direct injection. The determination of total cyanide (both free and strongly complexed) requires distillation of the sample with caustic trapping.

## ACKNOWLEDGMENT

The authors thank Dennis C. Johnson for his help and advice.

**Registry No.** NaCl, 7647-14-5;  $\text{Cd}(\text{CN})_4^{2-}$ , 16041-14-8;  $\text{Zn}(\text{CN})_4^{2-}$ , 19440-55-2;  $\text{Ni}(\text{CN})_4^{2-}$ , 48042-08-6;  $\text{Cu}(\text{CN})_4^{2-}$ , 19441-11-3;  $\text{Cu}(\text{CN})_3^{2-}$ , 16593-63-8;  $\text{Cu}(\text{CN})_2^-$ , 18973-62-1; Ag, 7440-22-4.

## LITERATURE CITED

- (1) Pohl, C. A.; Johnson, E. L. *J. Chromatogr. Sci.* **1980**, *18*, 442.
- (2) "Standard Methods for the Analysis of Water and Wastewater", 15th ed.; APHA, AWWA, WPCF, 1980.
- (3) McCloskey, J. A. *Anal. Chem.* **1981**, *33*, 1842.
- (4) Miller, G. W.; Long, L. E.; George, G. M.; Skes, W. L. *Anal. Chem.* **1984**, *36*, 980.
- (5) Bond, A. M.; Heritage, I. D.; Wallace, G. G.; McCormick, M. J. *Anal. Chem.* **1982**, *54*, 582.
- (6) Canterford, D. R. *Anal. Chem.* **1975**, *47*, 88.
- (7) Shimizu, K.; Osteryoung, R. A. *Anal. Chem.* **1981**, *53*, 588.
- (8) Phiar, B.; Kosta, L. *Anal. Chim. Acta* **1980**, *114*, 275.
- (9) Phiar, B.; Kosta, L.; Hristovskij, B. *Talanta* **1979**, *26*, 805.
- (10) Lown, J. A.; Koile, R.; Johnson, D. C. *Anal. Chim. Acta* **1980**, *116*, 33.
- (11) Hampson, A. N.; Macdonald, K. I.; Lee, J. B. *J. Electroanal. Chem.* **1973**, *45*, 149.
- (12) Shimizu, K.; Aoki, K.; Osteryoung, R. A. *J. Electroanal. Chem.* **1981**, *129*, 159.
- (13) Shimizu, K.; Osteryoung, R. A. *Anal. Chem.* **1981**, *53*, 2351.
- (14) Ford-Smith, M. H. "The Chemistry of Complex Cyanides"; Her Majesty's Stationary Office: London, 1964.
- (15) "Lang's Handbook of Chemistry", 11th ed.; Dean, J. A., Ed. McGraw-Hill: New York, 1973.
- (16) Martell, A. E.; Calvin, M. "Chemistry of Inorganic Compounds"; Prentice Hall: Englewood Cliffs, NJ, 1952.
- (17) Fitchett, A. W.; Johnson, E.; Pohl, C. to be presented at the Pittsburgh Conference in Applied Spectroscopy and Analytical Chemistry, Atlantic City, NJ, March 1983.

RECEIVED for review June 28, 1982. Accepted September 27, 1982.

# Dual Electrode Liquid Chromatography Detector for Thiols and Disulfides

Laura A. Allison and Ronald E. Shoup\*

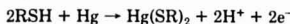
Bioanalytical Systems Inc., Research Laboratories, 1205 Kent Avenue, West Lafayette, Indiana 47906

Thiols and disulfides were determined simultaneously by using liquid chromatography/electrochemistry (LCEC) with thin-layer dual mercury amalgam electrodes in the series mode. After liquid chromatographic separation of all species, disulfides were first converted to the corresponding thiols at an upstream electrode at  $-1.0$  V vs. Ag/AgCl. Both thiols and disulfides were then detected as thiols downstream at  $+0.15$  V via their catalytic oxidation of the mercury surface. Only the downstream electrode current need be monitored. The high selectivity of the mercury surface-specific detector reaction ensures a low probability of interferences. Cysteine, glutathione, penicillamine, and the pure disulfides were used as test solutes. The dual electrode detector has been applicable to the determination of oxidized and reduced glutathione in human blood and citrus leaf homogenate.

There continues to be wide interest in the fate of thiols in various biological and chemical systems. For example, in plant and animal systems the tripeptide glutathione ( $\gamma$ -glutamyl-cysteinylglycine) is found principally as the reduced form (GSH), although both disulfides (GSSG or GSSR) and protein adducts (GSSP) are also important. Due to its ubiquitous occurrence in nature, physiologists have expended much effort in studying the function of GSH and its metabolites in cell biochemistry. Also, sulfhydryl-containing pharmaceuticals such as captopril and penicillamine are partially metabolized to disulfides.

While numerous methods for the determination of thiols have been reported, few have described procedures for the simultaneous determination of both oxidized and reduced thiols. One approach (1, 2) is to perform wet chemical steps in which the thiol and disulfide are separated into fractions, the disulfide is chemically reduced, and then the thiol content of each fraction determined colorimetrically via a coupling reagent such as Ellman's reagent, 3,3'-dithiobis[6-nitrobenzoic acid]. The bench chemistry is tedious but reasonably sensitive. Recently liquid chromatography coupled to postcolumn mixing has been employed to detect thiols in this manner (3), and both thiols and disulfides have been detected by using a two-stage solid-phase postcolumn reactor employing similar chemistry (4).

Liquid chromatography coupled to amperometric detection was first proposed for thiols by Rabenstein and Sætre (5), who used a mercury pool electrode. The detector reaction is indirect and based on the oxidation of mercury in the presence of certain species such as thiols, chelons, and halide ions



The detector may be poised at very low potential, typically  $+0.1$  V vs. Ag/AgCl, in contrast to the  $+0.9$  to  $1.0$  V potentials required for direct oxidation of thiol to the disulfide on a carbon surface. Bergstrom et al. (6) refined this approach for the therapeutic agent penicillamine by employing a mercury film on gold surface (eventually creating an amalgam). They

demonstrated sample detection limits of approximately  $10^{-7}$  M.

To determine both thiols and disulfides, Rabenstein and Sætre performed off-line bulk electrolyses of plasma samples over mercury pool electrodes to convert penicillamine disulfide to penicillamine (7). Injections were made before and after electrolysis, and the increase in the penicillamine peak height was attributed to the disulfide. Eggl and Asper (8) further elaborated on this theme by inserting an on-line column electrode of amalgamated silver particles between the column and detector to quantitatively reduce disulfides to thiols prior to entering a mercury pool electrode of Rabenstein's design.

Our experience with Hg/Au detector electrodes for liquid chromatography (9) and more recently with multiple electrode LCEC (10, 11) prompted us to investigate the use of a dual electrode thin-layer cell for the simultaneous determination of thiols and disulfides. While similar in philosophy to that of Eggl and Asper, the proposed cell has very low dead volume and is ideally suited to high-speed LC separations. Two mercury film electrodes are utilized, in a series arrangement, analogous to the scheme devised by MacCrehan and Durst (12). After the LC separation, the eluate passes over the upstream electrode, held at  $-1.0$  V vs. Ag/AgCl, to reductively cleave disulfides to thiols. All thiols, whether present naturally or as upstream conversion products, are detected conventionally downstream at  $+0.15$  V vs. Ag/AgCl. The upstream electrode serves as a unique postcolumn reactor of negligible dead-volume, since the conversion takes place in the thin layer, on the electrode surface.

In this report, we evaluate the suitability of this detector configuration for thiols and disulfides. Its application to the measurement of these compounds in plant tissue and human blood will be demonstrated.

## EXPERIMENTAL SECTION

**Apparatus.** A Bioanalytical Systems LC-154 liquid chromatograph with tandem LC-4B amperometric controllers was modified to exclude oxygen from the system. All Teflon tubing was replaced by stainless steel. The mobile phase was heated to  $50^\circ\text{C}$  for 30 min in a reflux condenser and continuously bubbled with nitrogen to maintain an oxygen-free atmosphere (13). The reflux apparatus served as the mobile phase reservoir and remained under positive  $\text{N}_2$  pressure to exclude oxygen at all times.

Both single and dual mercury-gold detectors were used. The single electrode detector was of the conventional thin-layer amperometric design (14), with a single circular gold electrode. The dual electrode detector cell consisted of two circular gold electrodes, each 3.2 mm in diameter. The electrodes were positioned in series in the thin-layer flow channel, separated by a distance of approximately 0.6 mm. The mercury/gold surface was prepared by placing mercury onto the highly polished gold surface. After waiting 2-3 min, the excess mercury was removed with the edge of a card and the surface firmly wiped with a laboratory tissue. A properly prepared surface should have a dull sheen. Excess mercury is indicated by reflective region(s) and should be removed by further smoothing. The auxiliary electrode was directly across from the working electrode(s), and two TG-5M gaskets (BAS) defined the thin-layer channel, which was 254  $\mu\text{m}$  thick. The Ag/AgCl reference electrode was positioned downstream in the

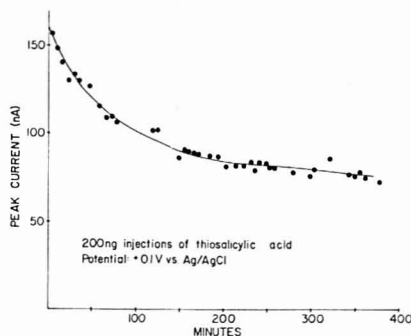


Figure 1. Hg/Au electrode response during equilibration of the amalgam.

conventional manner. The dual LC-4B controllers provided the equivalent of a four-electrode potentiostat.

For the separations, the mobile phase was generally a combination of 0.10 M monochloroacetate (pH 3.0) and an organic solvent, usually  $\text{CH}_3\text{OH}$  (Mallinckrodt) or  $\text{CH}_3\text{CN}$  (Baker, Resi-Analyzed grade). Specific mixtures will be noted in the text and captions. A Biophase ODS 5 $\mu$  column ( $250 \times 4.6$  mm, BAS) with a 5  $\mu$ m diameter spherical particle size provided the separations. The flow rate was 1.5 mL/min.

Sample extracts were filtered prior to injection with centrifugal Microfilters (BAS) and RC-58 regenerated cellulose membranes (0.20  $\mu$ m).

Bulk electrolyses were carried out over a mercury pool electrode in a conventional dual side-arm electrolysis cell. A Bioanalytical Systems DCV-5 potentiostat provided potential control and current output, which was integrated for  $n$  values with a prototype BAS LC-26 integrator. Cyclic voltammetry was carried out with a CV-1B unit (BAS) and a Hg/Au voltammetry electrode (p/n MF2014, BAS) prepared as described above. All potentials are vs. an Ag/AgCl/3 M NaCl reference electrode (p/n MF2020, BAS).

**Reagents.** Standards of various thiols and disulfides were dissolved in 0.1% (w/v)  $\text{Na}_2\text{EDTA}$  solution and refrigerated. For the glutathione (GSH) in blood assay, 20 mg of GSH was dissolved in 100 mL of  $\text{Na}_2\text{EDTA}$  solution (final concentration, 0.67 mM).

**Sample Preparation.** The assay in blood was as follows: 0.8 mL of 0.1%  $\text{Na}_2\text{EDTA}$  solution and 20  $\mu$ L of fresh blood were combined in a 5-mL centrifuge tube, causing the erythrocytes to lyse. At least one sample was spiked with 20  $\mu$ L of the 0.67 mM GSH standard solution. Two hundred microliters of 0.2 M  $\text{HClO}_4$  was then added, and the tube was vortexed briefly. After standing 10 min to precipitate proteins, the sample was centrifuged for 10 min at 1600g, and the supernatant was decanted into a Microfilter and centrifuged again prior to injection.

For plant sample preparation, 5 g of fresh citrus leaf tissue was chopped and homogenized in 75 mL of methanol. The homogenate was filtered and extracted with petroleum ether to remove chlorophyll. Residual petroleum ether was removed by vacuum aspiration. For liquid chromatographic experiments, the homogenate was then evaporated to dryness under nitrogen and re-constituted in an equal volume of mobile phase.

## RESULTS AND DISCUSSION

**Single Electrode Evaluation.** Before dual electrode experiments were attempted, the reliability of a single electrode thiol determination was established. Thiosalicylic acid and *N*-acetylcysteine were used as test solutes. The gold electrode substrate was polished in stages to a mirrorlike finish with a 0.5- $\mu$ m alumina slurry. Following the application of the mercury, there is a period of equilibration, during which time the electrode response is rapidly changing and the electrode is unsuitable for use (Figure 1). This stabilization occurs

Table I. Reproducibility of *N*-Acetylcysteine Peak Heights

mobile phase	ng/inj.	N	av peak height, nA	% rel dev
40% $\text{CH}_3\text{CN}$ :60% 0.1 M monochloroacetate, pH 3.0	200	42	205.2	0.6
5% $\text{CH}_3\text{OH}$ :95% 0.1 M monochloroacetate, pH 3.0	100	18	89.5	1.5

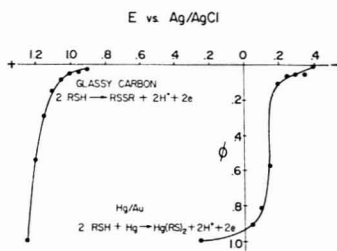


Figure 2. Hydrodynamic voltammograms of *N*-acetylcysteine on both glassy carbon and Hg/Au electrodes: mobile phase, 95% 0.1 M monochloroacetate, pH 3.0/5% methanol.  $\phi$  is the ratio of the peak current to the limiting current. For glassy carbon, a diffusion-limited response was not obtained, and  $\phi$  was calculated as the ratio of the peak current to the current response at +1.25 V.

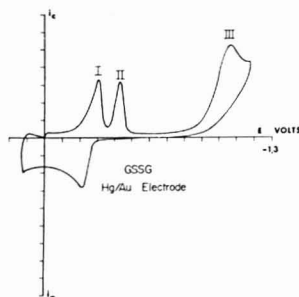
independently of the environment of the electrode and no potential need be applied to achieve it, causing speculation that a purely physical amalgamation process is responsible.

Once equilibrated, the reproducibility of the Hg/Au electrode was evaluated by using *N*-acetylcysteine as test solute in two different mobile phases at +0.1 V (Table I). This experiment was designed to determine if a high percentage of organic solvent was required to "wash" mercury-thiol complexes from the electrode surface. From Table I, the results indicate that the electrode was reproducible by using either high or low solvent concentrations. Average lifetimes of Au/Hg surfaces were from 2 to 3 weeks. When resurfacing became necessary, a gradual decrease in response was observed and the electrode, upon inspection, had a gold tint. Although additional mercury could be applied directly to the old amalgam as directed above, the maximum sensitivity was obtained by freshly polishing the used electrode to expose a new gold "mirror" prior to amalgamation.

Rigorous deoxygenation of the mobile phase was required for two reasons: (1) dissolved oxygen oxidizes thiols on-column, leading to poor reproducibility, and (2) reduction of dissolved oxygen causes a high negative residual current. After deoxygenation, the residual current at +0.1 V was about -10 nA or less. Sample deoxygenation was not attempted or necessary for single electrode studies.

Although carbon surfaces may be used to oxidize thiols directly (15), the elimination of several interferences could be accomplished by operating at much lower potential on mercury (Figure 2). Substances such as uric acid, plant phenolics, and ascorbate are not detected by using Hg instead of glassy carbon.

**Voltammetry of RSSR.** To utilize the detection of thiols on a mercury amalgam electrode as an indirect means of measuring disulfides, we investigated the electrochemistry of glutathione disulfide. In the dual electrode thin-layer detector, it was essential to demonstrate that free GSH could be re-



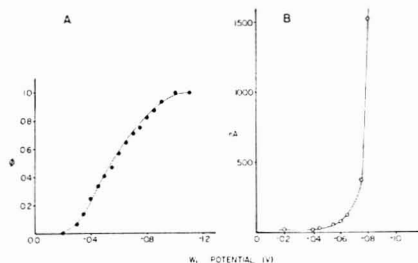
**Figure 3.** Cyclic voltammogram of GSSG in 0.1 M monochloroacetate, pH 3.0, using an Hg/Au electrode: initial potential, 0.0 V; scan rate, 20 mV s<sup>-1</sup>; vertical axis, 2  $\mu$ A/division.

leased at the upstream electrode for subsequent detection downstream at +0.15 V as shown above.

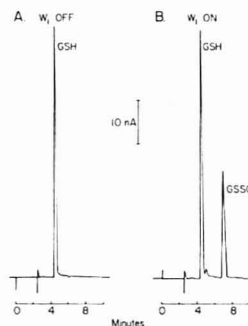
The reduction of oxidized glutathione on mercury was recently studied by Sakane et al. (16); similar studies were reported earlier (17, 18). A cyclic voltammogram of GSSG initiated at 0.0 V in the negative direction shows three distinct reduction peaks (Figure 3). Peaks I and II resemble adsorption waves, while peak III is diffusion-controlled. These results are identical with those of Sakane et al., who suggested that the first peak represented the reduction of adsorbed GSSG to free GSH, while the third peak derived from the reduction of free GSSG to GSH. It is interesting to note that the second peak at -420 mV eventually disappears upon subsequent cycles, with a corresponding increase in peak I.

Bulk electrolysis of a  $1.6 \times 10^{-6}$  M GSSG solution in the pH 3.0 buffer at -1.1 V was carried out to identify reaction products. To detect GSSG as GSH in the dual electrode scheme, it was necessary to prove that GSH was indeed released in the process occurring at peak 3. After a 2-h exhaustive electrolysis, the GSSG standard was injected into the LC; only one peak, corresponding to GSH, was detected, indicating the formation of free thiol. Integration gave an  $n$  value of 2.09 at -1.1 V, for the process  $\text{GSSG} + 2e^- + 2\text{H}^+ \rightarrow 2\text{GSH}$ . Lowering the electrolysis potential to -0.9 V was inadequate.

**Dual Hg Amalgam Detector.** The mercury/gold detector was extended from single to dual electrode for measurement of disulfides, using GSSG as a model compound. GSSG standards were injected onto the LCEC system to determine the optimum operating potential for the upstream electrode. The downstream electrode potential was fixed at +0.15 V and the potential of the upstream electrode was changed with each injection (Figure 4A). It was necessary to set the upstream electrode potential at -1.0 V or greater, in order to achieve a maximal level of upstream reduction to the sulfhydryl. These results are consistent with those of the bulk electrolysis experiment. The high negative potential required for this reduction makes direct detection of GSSG intractable for trace determinations, as the residual current becomes concomitantly very high (Figure 4B). Reliable measurements could not be obtained even for high nanomole amounts of GSSG injected. Alternatively, at a potential of +0.15 V, the downstream electrode has a negative residual current of only 0 to 10 nA, and measurements are easily made. The primary advantage of the series dual electrode approach is this ability to employ the upstream electrode as a "generator" electrode, essentially ignoring the unwieldy background current and other problems associated with the high potential. The downstream electrode is then the "detector" electrode, providing quantitative in-



**Figure 4.** (A) Peak height responses at downstream electrode (+0.15 V) as a function of applied potential at upstream electrode. Each point represents the mean of two injections, 200 ng of GSSG.  $\phi$  is defined as in Figure 2. (B) Residual current at upstream mercury/gold electrode as a function of applied potential.



**Figure 5.** Response of downstream electrode (+0.15 V) to a standard solution containing GSH and GSSG and (A) upstream electrode OFF and (B) upstream electrode ON (-1.0 V): mobile phase, 99% 0.1 M monochloroacetate, pH 3.0/1% methanol.

formation in a single output for both thiols and disulfides.

Deoxygenation of mobile phase was found to be of even greater significance with the dual electrode detector. It was also necessary to deoxygenate samples when lower analyte concentrations required high gain detection. Evidently, the extremely high negative potential of the upstream electrode causes the entire detector to become more sensitive to dissolved oxygen effects. Mercury surfaces in the dual mode demonstrated a usable lifetime dependent on the applied potential. The upstream electrode, which operated at -1.0 V, usually required resurfacing after about 10 days of operation. The downstream electrode behaved as the single electrode, with resurfacing after approximately 3 weeks. It should be noted that the upstream electrode can be "rejuvenated" by applying mercury to the old amalgam surface without repolishing. This is possible due to the fact that the upstream electrode is strictly used as a generator of detectable species. Resurfacing of the downstream electrode in this manner is not recommended, as noise levels may be increased.

Linearity of the dual mercury/gold detector was demonstrated for GSH over the range of 10-800 pmol injected (slope, 108 pA/pmol; y intercept, -2.0 pA; correlation coefficient, 0.9994). GSSG also showed a linear response from 10 to 800 pmol (slope, 38 pA/pmol; y intercept, -0.45 pA; correlation coefficient, 0.9990). Minimum detectable quantities ( $S/N$  of 3) were 3.5 pmol for GSH and 5.7 pmol for GSSG. A single injection is sufficient to individually measure both thiols and

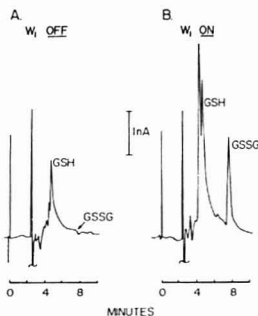


Figure 6. Downstream electrode chromatograms of citrus leaf homogenate with (A) upstream electrode OFF and (B) upstream electrode ON ( $-1.0$  V). Mobile phase was as given in Figure 5.

disulfides in a given sample, provided that they are chromatographically separated (Figure 5B). Each compound is detected as free thiol at the downstream electrode, but they are presented to this electrode resolved in time and are thus detected separately.

In the course of experiments with the dual detector, it was observed that the precision of detector response for disulfides was consistently greater than that for thiols. This phenomenon was determined to be a result of adsorption of thiols onto the upstream mercury surface and was effectively eliminated by inclusion of a nonretained thiol within each injection. This thiol "conditions" the upstream mercury surface prior to the peaks of interest, resulting in reproducible detector response.

A certain amount of qualitative information is available by using this detector arrangement. The downstream mercury/gold electrode at a potential of  $+0.15$  V is extremely specific, detecting only sulfhydryls, halide and similar ions, and chelating agents. In addition to this inherent specificity, the dual detector system provides the option of selecting for or against disulfide detection. This is illustrated by Figure 5, which shows chromatograms of a standard solution containing GSH and GSSG. When the upstream electrode is on, both compounds are detected (Figure 5B); only GSH is observed with the upstream electrode off (Figure 5A). Such an ability can be advantageous when analyzing a complex sample containing several thiols and disulfides. It represents a rapid and simple method of qualitatively isolating disulfides from thiols, further confirming peak assignments and integrity. Also, the detection of unsymmetrical, or mixed, disulfides should be feasible with the dual detector. Although standards were not available for verification, an unknown disulfide peak was observed to appear over time in standard solutions containing both cysteine and glutathione. This disulfide peak had a retention time different from those of the symmetrical disulfides of cysteine and glutathione and was probably the mixed disulfide.

**Applications of the Dual Detector.** In plants, studies on the role of GSH and GSSG in temperature hardiness require measurement of their levels in various tissues. Present methodology for these determinations requires a considerable analysis time and effort (19). The filtered citrus leaf homogenate is passed through an ion-exchange column to retain glutathione (both oxidized and reduced forms) and cysteine. The eluent from this column is divided and separate analyses are performed for each analyte of interest. Total thiol levels can be determined colorimetrically with derivatization while specific GSH and GSSG levels must be measured by using time-consuming enzymatic methods.

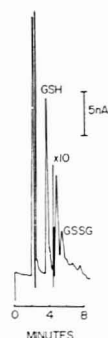


Figure 7. Downstream electrode chromatogram of whole blood filtrate, with upstream electrode ON ( $-1.0$  V). Mobile phase was as given in Figure 5.

The dual detector is well-suited to this application; reconstituted homogenates can be directly injected, Figure 6. GSH and GSSG in the homogenate were calculated at  $6.5 \mu\text{M}$  and  $1.8 \mu\text{M}$ , respectively. There is evidence in the sample chromatogram of at least one disulfide in addition to GSSG, since the peak eluting prior to GSH is not observed with the upstream electrode turned off. The quality of analytical data provided by this approach is much higher than that obtained with the more lengthy procedures. Chromatographic retention times provide added confidence in peak integrity, and detection limits in preliminary work suggest an improvement of several orders of magnitude.

GSH and GSSG concentration in human blood can be readily determined by use of the detector. The chromatogram shown (Figure 7) represents a blood sample containing  $1.1 \text{ mM}$  GSH and  $1.8 \mu\text{M}$  GSSG. The sample was diluted approximately 50-fold prior to injection, as GSH levels were known to be quite high. For determinations of GSSG, it would be preferable to decrease the dilution volume, producing a more concentrated sample. The base line disturbance at 4.7 min occurs in every blood sample; its retention time may be manipulated by mobile phase variations.

## CONCLUSIONS

The series dual mercury/gold detector for liquid chromatography represents a significant improvement in analytical methodology for the determination of disulfides and thiols. The simplicity of design and low dead volume make it readily applicable to existing liquid chromatographic methods. Sample cleanup can be extremely simple because of the high degree of specificity inherent in the detector.

Some caution should be exercised in generalizing this detection scheme to all disulfides. Successful detection of a disulfide at trace levels requires the molecule to undergo a facile reduction at the upstream electrode. Factors which may influence this upstream reaction include diffusion coefficient, reduction potential, and steric shielding of the disulfide functionality.

Experimentation is now progressing toward developing improved chromatographic separations for mixtures of thiols and disulfides, as well as investigating the detection of different disulfide-containing compounds.

## ACKNOWLEDGMENT

The authors wish to thank Judy Keddington and Joseph Bougher for their excellent technical assistance, Charles L. Guy and John V. Carter of the Department of Horticultural



Science and Landscape Architecture at the University of Minnesota, St. Paul, for providing the plant tissue homogenates, and Linda Baker for her expert assistance typing the manuscript.

Registry No. GSSG, 27025-41-8; N-acetylcysteine, 616-91-1.

### LITERATURE CITED

- (1) Elman, G. H. *Arch. Biochem. Biophys.* **1959**, *82*, 70-77.
- (2) Fowler, B.; Robins, A. G. *J. Chromatogr.* **1972**, *72*, 105.
- (3) Beales, D.; Finch, R.; McLean, A. E. M. *J. Chromatogr.* **1981**, *226*, 498-503.
- (4) Studebaker, J. F.; Slocum, S. A.; Lewis, E. L. *Anal. Chem.* **1978**, *50*, 1500-1503.
- (5) Rabenstein, D. L.; Saetre, R. *Anal. Chem.* **1977**, *49*, 1036-1039.
- (6) Bergstrom, R. F.; Kay, D. R.; Wagner, J. G. *J. Chromatogr.* **1981**, *222*, 445-452.
- (7) Saetre, R.; Rabenstein, D. L. *Anal. Chem.* **1978**, *50*, 276-280.

- (8) Eggl, R.; Asper, R. *Anal. Chim. Acta* **1978**, *101*, 253-259.
- (9) Allison, L. A.; Keddington, J., unpublished results.
- (10) Shoup, R. E.; Mayer, G. S. *Anal. Chem.* **1982**, *54*, 1164-1169.
- (11) Mayer, G. S.; Shoup, R. E., accepted for publication in *J. Chromatogr.*
- (12) MacCrab, W. A.; Dursi, R. A. *Anal. Chem.* **1981**, *53*, 1700-1704.
- (13) LC-48 Manual, Bioanalytical Systems Inc., 1982, Sections 5, 6.
- (14) Kissinger, P. T. *Anal. Chem.* **1977**, *49*, 447A-456A.
- (15) Mefford, I.; Adams, R. N. *Life Sci.* **1978**, *23*, 1167-1174.
- (16) Sakane, Y.; Matsumoto, K.; Ohtsuka, R.; Osajima, Y. *Nippon Kagaku Kaishi* **1982**, (1), 81-86. *Chem. Abstr.* **1982**, *96*, 76374c.
- (17) Starkovich, M. T.; Bard, A. J. *J. Electroanal. Chem.* **1977**, *75*, 487.
- (18) Maesre-Ducarmois, C. A.; Patriarche, G. J.; Vandenbalck, J. L. *Anal. Chim. Acta* **1974**, *71*, 165.
- (19) Guy, C. L.; Carter, J. V. "Plant Cold Hardiness and Freezing Stress", Li, P. H., Sakai, A., Eds.; Academic Press: New York, 1982.

RECEIVED for review August 2, 1982. Accepted September 28, 1982.

## Addition of Complexing Agents in Ion Chromatography for Separation of Polyvalent Metal Ions

Gregory J. Sevenich\* and James S. Fritz

Ames Laboratory and Department of Chemistry, Iowa State University, Ames, Iowa 50011

The scope of ion chromatography with a conductivity detector has been expanded to include several additional divalent metal ions and the trivalent lanthanide cations. A complexing anion is incorporated in the eluent which increases the number of metal ions that can be separated and improves the sharpness of the eluted peaks. Further selectivity is obtained by adding a complexing reagent to the sample and then eluting with an eluent containing ethylenediammonium tartrate. This technique provides a rapid and highly selective method for separating and determining magnesium, calcium, and strontium in various samples.

Chromatographic methods for the separation of inorganic cations have tended to be rather time-consuming and often have not employed automatic detection of eluted peaks. In 1975 Small, Stevens, and Bauman (1) invented a clever dual-column method for the separation of inorganic cations that uses a conductivity detector. This system is excellent for separation of the alkali metal ions and the alkaline earth cations, but its scope is limited because the hydroxide-form suppressor column would precipitate most polyvalent metal cations. Fritz, Gjerde, and Becker (2) developed a single-column method for cation chromatography that uses a conductivity detector and permits the separation of additional inorganic cations. They established the principle that a decrease in conductance, as well as an increase in conductance, can be used for detection and quantitative estimation of eluted ions. Other modern methods of inorganic ion-exchange chromatography have been reviewed in a recent book (3).

Complexing eluents have been used in many published methods to achieve more selective chromatographic separations of metal ions, but the presence of a complexing agent often makes detection of the metal ions difficult. However, Elchuk and Cassidy have obtained excellent chromatographic separation of the lanthanides with  $\alpha$ -hydroxyisobutyric acid using postcolumn derivatization and spectrophotometric detection (4). Conductivity detectors have been improved greatly

in recent years and have the advantage of providing sensitive and "universal" detection of ions in solution. However, the conductivity detector has not been previously used in ion chromatography in conjunction with a complexing eluent.

In the present work eluents containing the ethylenediammonium cation and either tartrate or hydroxyisobutyrate as the complexing anion have been used for separation of polyvalent metal cations. The use of a complexing agent in the eluent improves the sharpness of separations and broadens the scope of cation chromatography with a conductivity detector. The eluted metal ions are only partly complexed and are mostly in solution as cations. As in our previous work (2), the eluted ions have a lower equivalent conductance than the eluent cation and thus appear as peaks of lower conductance. In some cases an additional complexing reagent, such as EDTA, is added to the sample (but not to the eluent) to increase the selectivity of the chromatographic separations.

### EXPERIMENTAL SECTION

**Apparatus.** The instrument used was described previously (2) and consists of a Model 396 Milton Roy minipump, Rheodyne Model 7010 sample injection valve equipped with a 100- $\mu$ L sample loop, a low-capacity cation-exchange column, a Model 213 conductivity detector from Wescan Instruments (Santa Clara, CA), and a strip chart recorder. All fittings in contact with the eluent were either Teflon, Kel-F, or stainless steel. The column, detector, and eluent were each located in a styrofoam-lined cabinet to minimize temperature effects. All chromatograms were obtained at room temperature. Flow rates were 0.85 mL/min, flow rates much higher than this gave pressures approaching the limits of the fittings.

**Cation Exchange Column.** The column is of thick-walled glass and measured 350 mm in length with a 2 mm i.d. The column was packed with a gel-type resin with a particle size of 20  $\mu$ m. The resin was lightly sulfonated to give a low cation-exchange capacity. This material was obtained by special order from Benson Co. (Reno, NE) and was packed by use of a balanced density slurry method.

**Eluents.** Reagent grade ethylenediamine was used after redistillation. Reagent grade tartaric acid and  $\alpha$ -hydroxyisobutyric acid were used as received. All eluents were prepared in distilled-deionized water and filtered through a 0.45- $\mu$ m membrane

filter before use. The pH of each eluent was adjusted with either perchloric acid or sodium hydroxide, depending on the pH desired.

**Sample Solutions.** All samples were prepared from reagent grade salts and dissolved in distilled-deionized water. Solutions for quantitative work were standardized by EDTA titration.

Lanthanide samples were obtained courtesy of J. E. Powell, Ames Laboratory. All lanthanides were received as the oxides and were at least 99.95% pure.

**Samples Masked with EDTA.** Samples were prepared by mixing appropriate amounts of Mg(II), Ca(II), Sr(II), and interfering-ion solutions. Enough EDTA was added to completely mask the excess metal ions. The pH of each solution was monitored and adjusted to be about 3.6 while adding the EDTA. The usable pH range was about 3.5–4.0. At higher pH values Mg(II), Ca(II), and Sr(II) are significantly complexed with complete loss of the peaks at a pH around 5. At lower pH values the EDTA precipitates. The solution can be made basic to redissolve the precipitated EDTA and then reacidified without affecting the results.

In samples containing Fe(III), hydrolysis occurred at pH values above 2.0. However the large formation constant of the iron(III)–EDTA complex permitted a pH of 1.7 without any precipitation.

The solutions were diluted to give final concentrations of Mg(II), Ca(II), and Sr(II) of  $1.0 \times 10^{-4}$  M. The EDTA concentration was 0.01 M.

Interfering metal ions tested included Al(III), Cu(II), Fe(III), Ni(II), Pb(II), and Zn(II). Amounts in 1-, 10-, and 100-fold molar excess were examined. At 1-fold excess no real interference existed in most cases so this concentration was not examined.

## RESULTS AND DISCUSSION

The system used was similar to that previously described (2) for the separation of divalent metal cations on a low-capacity cation-exchange resin with an ethylenediammonium salt as the eluent, except that a complexing anion was incorporated in the eluent to modify the elution behavior of sample ions. Of several complexing reagents tried, tartrate was the most successful, although  $\alpha$ -hydroxyisobutyrate (HIBA) was also useful for some separations. With complexing eluents it was found that better results were obtained with a resin of somewhat higher exchange capacity (0.059 mequiv/g) than that used in the earlier work (0.017 mequiv/g).

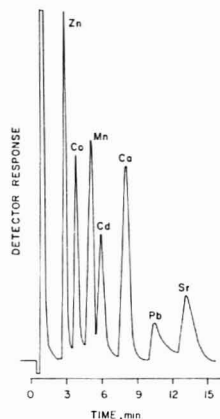
With eluents containing approximately equal molar concentrations of ethylenediammonium cation and tartrate anion, well-formed peaks were obtained for each of the following metal cations: Ba(II), Ca(II), Cd(II), Ce(III), Co(II), Dy(III), Er(III), Eu(III), Fe(II), Gd(III), Ho(III), La(III), Lu(III), Mg(II), Mn(II), Nd(III), Ni(II), Pb(II), Pr(III), Sm(III), Sr(II), Tb(III), Tm(III), Yb(III), and Zn(II). The retention times varied sufficiently to suggest that good separation of mixtures would be possible. The retention times decreased with increasing pH owing to the greater complexing ability of tartrate at higher pH. A practical upper limit of approximately pH 5 was established because the protonation of ethylenediamine is incomplete at higher pH values. The lower end of the practical pH range was found to be approximately pH 3. At more acidic pH values much of the complexing ability of tartrate is lost and the detection sensitivity for metal cations is significantly lower because of the higher background conductance.

Eluents containing ammonium tartrate and no ethylenediammonium salt were ineffective for elution of the metal cations studied. It appears that the elution mechanism is a combination of the mass action "pushing" effect of the ethylenediammonium cation and the weakly complexing or "pulling" effect of the tartrate anion.

The effect of various ratios of tartrate to ethylenediammonium ion molar concentration was studied. The retention times, shown in Table I decrease as more tartrate is used in the eluent. The most dramatic changes are in the elution of lead(II), which is very strongly retained when no

**Table I. Adjusted Retention Times ( $t'_R$ ) (in Minutes) of Metal Ions for Constant Ethylenediamine Concentration ( $2.0 \times 10^{-3}$  M), Constant pH (4.50), and Varied Tartrate Concentration**

metal ion	tartrate concentration, M $\times 10^3$					
	0.0	1.0	2.0	3.0	4.0	5.0
Mg <sup>2+</sup>	2.8	2.9	2.8	2.8	2.9	2.8
Zn <sup>2+</sup>	3.2	2.6	2.0	1.6	1.5	1.4
Ni <sup>2+</sup>	3.4	3.0	2.4	2.0	1.8	1.6
Mn <sup>2+</sup>	4.3	4.0	3.8	3.7	3.6	3.5
Cd <sup>2+</sup>	5.2	5.0	4.5	4.0	4.0	3.7
Sr <sup>2+</sup>	11.2	11.0	10.3	9.7	9.6	9.1
Pb <sup>2+</sup>	41.2	12.7	7.8	5.7	4.9	4.1

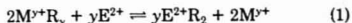


**Figure 1.** Separation of Zn(II) (10.3 ppm), Co(II) (9.1 ppm), Mn(II) (16.0 ppm), Cd(II) (16.1 ppm), Ca(II) (17.1 ppm) (16.0 ppm), and Sr(II) (20.3 ppm): eluent,  $1.5 \times 10^{-3}$  M ethylenediamine,  $2.0 \times 10^{-3}$  M tartrate, pH 4.0.

tartrate is present but elutes much more rapidly when tartrate is added to the eluent.

**Separations with Ethylenediammonium Tartrate.** By use of conditions suggested by these preliminary experiments, several nice separations of metal ion mixtures were obtained with eluents containing ethylenediammonium tartrate. Figure 1 shows the separation of several divalent cations in less than 15 min. The rather difficult separation of cadmium(II) and manganese(II) is demonstrated in Figure 2. It is even possible to separate several of the individual rare earth cations, as demonstrated in Figure 3.

**Theoretical Considerations.** The effect of elution parameters can be shown more precisely than was done in the earlier experiments. The cation-exchange equilibrium is represented by



where  $E^{2+}$  represents the eluent cation (ethylenediammonium),  $M^{2+}$  represents the sample metal ion, and the subscript on R represents the number of exchange sites on the resin used by the ion. The selectivity coefficient,  $K_M^E$ , for this reaction is

$$K_M^E = \frac{[E^{2+}R_2]^y [M^{2+}]^2}{[E^{2+}]^y [M^{2+}R_y]^2} \quad (2)$$

At low loading of sample ion, the resin capacity/2 is ap-

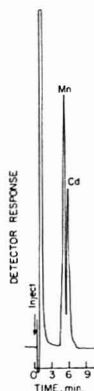


Figure 2. Separation of 20 ppm Mn(II) and 20 ppm Cd(II). Conditions are the same as those given in Figure 1.

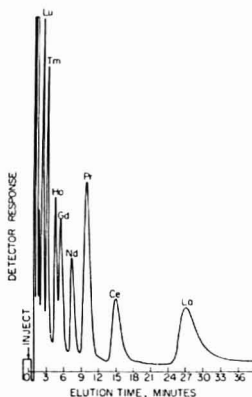


Figure 3. Separation of Lu(III), Tm(III), Ho(III), Gd(III), Nd(III), Pr(III), Ce(III), and La(III). All concentrations are 20 ppm except Pr(III) (30 ppm): eluent,  $2 \times 10^{-3}$  M ethylenediamine,  $2 \times 10^{-3}$  M tartrate, pH 4.5.

proximately given by  $[E^{2+}R_2]$ . The capacity factor,  $k$ , is equal to the ratio  $[M^{2+}R_2]/[M^{2+}]$ . Thus the equation can be written

$$K_M^E = \frac{[\text{cap}/2]^y}{[E^{2+}]^y k^2} \quad (3)$$

The adjusted retention time for an eluted peak ( $t'$ ) is equal to  $t_0 k$ , where  $t_0$  is the retention time of a nonsorbed substance. Substituting  $t'/t_0$  for  $k$  and taking the log of each term gives

$$\log t' = \frac{y}{2} \log \left( \frac{\text{cap}}{2} \right) + \log t_0 - \frac{y}{2} \log [E^{2+}] - 1/2 \log K_M^E \quad (4)$$

In eluents containing a complexing anion such as tartrate, some of the metal cation will be in solution as a neutral or anionic complex. The effect of this complexing on the exchange equilibrium can be calculated by methods worked out primarily by Ringbom (5). We substitute  $[M']\alpha_M$  for  $[M^{2+}]$

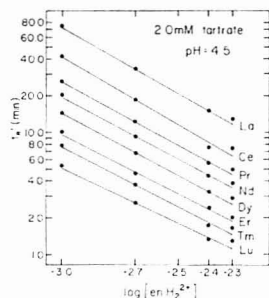


Figure 4. Plot of the logarithm of the adjusted retention time vs. the logarithm of the eluent concentration for several representative lanthanides. Both the pH and the tartrate concentration are held constant.

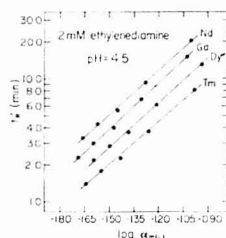


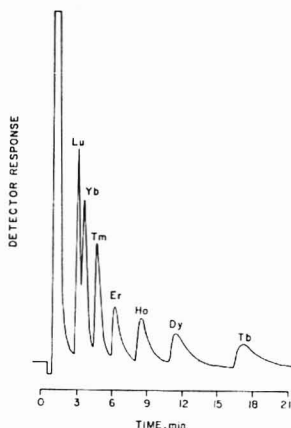
Figure 5. Plot of the logarithm of the adjusted retention time for several representative lanthanides vs. the logarithm of the fraction of that same metal as free metal cations. Both the ethylenediammonium ion concentration and the pH are held constant.

in eq 2, where  $[M']$  is the sum of free and complexed metal in solution and  $\alpha_M$  is the fraction of the metal in solution that exists as the free cation. The capacity factor,  $k$ , is now the ratio of  $[M^{2+}R_2]$  to  $[M']$ . Continuing the derivation as before, we obtain an equation that is identical with eq 4, but with an additional term containing  $\alpha_M$ .

$$\log t' = \frac{y}{2} \log \alpha_M + \frac{y}{2} \log \left( \frac{\text{cap}}{2} \right) + \log t_0 - \frac{y}{2} \log [E^{2+}] - 1/2 \log K_M^E \quad (5)$$

The validity of eq 4 was tested by measuring the adjusted retention times of a number of cations at constant tartrate and pH but at varying concentrations of ethylenediammonium cation in the eluent. As shown in Figure 4, linear plots were obtained. The theoretical slope for a  $3+$  cation is  $-1.5$ , but the experimental values for the rare earth ions in the figure were slightly below  $-1.0$ . However, the experimental slopes for divalent metal ions such as cadmium, magnesium, calcium, manganese, strontium, and zinc averaged about  $-0.9$  or slightly lower. This is in fairly good agreement with the theoretical slope of  $-1.0$ .

Linear plots were also obtained in every case when the concentration of tartrate in the eluent was varied and the log of adjusted retention time was plotted against  $\log \alpha_M$  (see eq 5 and Figure 5). The slopes of the rare earth cations varied slightly but most were around  $1.2$  compared with a theoretical slope of  $1.5$ . From the values of  $\alpha_M$  in Figure 5, it can be seen that about 90% or more of the lanthanide sample ions are complexed. However, 50% or less of divalent sample ions are



**Figure 6.** Separation of the seven heaviest lanthanides using  $\alpha$ -hydroxyisobutyrate eluent. All metal ion concentrations are 10 ppm. Eluent is  $4.0 \times 10^{-3}$  M ethylenediamine and  $3.0 \times 10^{-3}$  M  $\alpha$ -hydroxyisobutyrate, pH 4.5.

complexed in the mobile phase. These complexing conditions are mild compared to older methods, but complexing is sufficient to sharpen most of the peaks considerably.

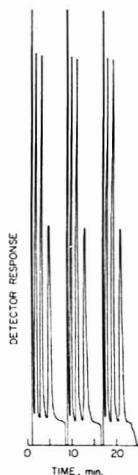
**Eluents Containing  $\alpha$ -Hydroxyisobutyrate.** Success with tartrate as a complexing eluent anion suggested the use of  $\alpha$ -hydroxyisobutyrate, especially for separation of the rare earths. The use of such eluents showed no particular advantage over tartrate for chromatography of divalent metal ions, but separation of several individual rare earth cations was successful. Figure 6 shows a separation of the seven heaviest rare earths using an eluent of ethylenediammonium  $\alpha$ -hydroxyisobutyrate. The tailing of the later peaks suggests that the complexing-decomplexing equilibrium probably is slow.

**Quantitative Measurements and Detection Limits.** Plots of either peak height or peak area with ethylenediammonium tartrate eluents gave linear calibration curves for magnesium(II) over a concentration range of 1.0–15.0 ppm, for calcium(II) over a range of 2.0–30.0 ppm, and for zinc(II) over a range of 2.0–14.0 ppm. Other metal cations behave similarly with both tartrate and  $\alpha$ -hydroxyisobutyrate eluents. Figure 7 shows the excellent reproducibility obtained for a rapid separation of magnesium, calcium, and strontium.

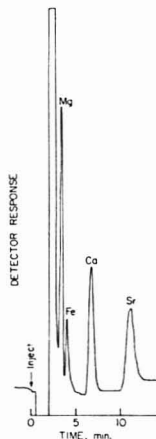
Quantitative measurements are not limited to the concentration ranges mentioned above. The detector sensitivity can be adjusted to work in different concentration ranges. The practical detection limit of this system is 49 ppb of magnesium and 80 ppb of calcium, which represents only 200 pmol of each metal ion.

**Use of Masking Reagents.** In work with eluents containing a complexing anion it became apparent that the complexed metal moves rapidly through the column under conditions where strong complexing occurs. If a selective complexing reagent could be employed, it should be possible to elute the strongly complexed metal ions quite rapidly and then to separate the remaining cations with the ethylenediammonium tartrate eluent described above. A further requirement would be that the auxiliary complexing agent must work in the 3 to 5 pH range needed for the eluent.

Simple calculations showed that EDTA does not complex metal ions significantly such as magnesium(II) and calcium(II)

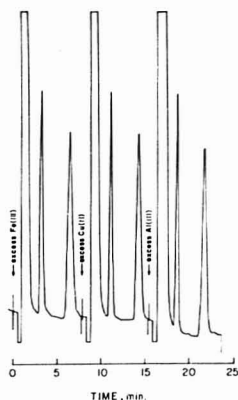


**Figure 7.** Rapid separation of Mg(II), Ca(II), and Sr(II) for successive injections of the same solution. Each metal is  $5.0 \times 10^{-4}$  M. Eluent is  $4.0 \times 10^{-3}$  M ethylenediamine and  $3.0 \times 10^{-3}$  M tartrate, pH 4.5.



**Figure 8.** Injection of Mg(II), Ca(II), and Sr(II) ( $1.0 \times 10^{-4}$  M each) in 100X excess of Fe(III). A sufficient amount of EDTA (0.01 M) was added to complex the Fe(III) present. Chromatographic conditions  $2.0 \times 10^{-3}$  M ethylenediamine and  $2.0 \times 10^{-3}$  M tartrate, pH 4.5; sample pH is 1.7. The Fe peak present is an Fe(II) impurity.

at pH 4 but it does complex many metal cations that form more stable EDTA complexes. Therefore, experiments were performed in which EDTA is added to the metal ion sample and the column was eluted with ethylenediammonium tartrate as before. The amount of EDTA used was more than enough to complex the metal ions present, but an unduly high concentration of EDTA was avoided. The results obtained show that conditions can easily be established whereby magnesium and the alkaline earth cation peaks are hardly affected but metal ions that form stable EDTA complexes at about pH 4



**Figure 9.** Determination of Mg(II) and Ca(II) ( $2.0 \times 10^{-4}$  M each) in a 50-fold excess of Fe(III), Cu(II), and Al(III). Each sample had EDTA added to mask the interfering metal. Sample pH was as follows: Fe(III), 1.7; Cu(II), 3.7; Al(III), 3.7. Eluent was  $2.0 \times 10^{-3}$  M ethylenediamine and  $2.0 \times 10^{-3}$  M tartrate, pH 4.5.

**Table II.** Chromatographic Separation of 20  $\mu$ mol of  $Mg^{2+}$ ,  $Ca^{2+}$ , and  $Sr^{2+}$  from a Large Excess of Foreign Metal Ion Using EDTA Masking

foreign metal ion	molar excess	recovery, %		
		Mg <sup>2+</sup>	Ca <sup>2+</sup>	Sr <sup>2+</sup>
Al <sup>3+</sup>	10x	102.5	101.7	99.5
	100x	107.4	108.1	102.0
Co <sup>2+</sup>	10x	100.1	99.0	97.7
	100x	107.3	97.9	95.8
Cu <sup>2+</sup>	10x	99.4	98.2	96.4
	100x	104.0	103.1	92.3
Fe <sup>3+</sup>	10x	99.8	96.7	96.0
	100x	107.0	96.5	96.6
Ni <sup>2+</sup>	10x	102.5	102.8	102.1
	100x	105.2	104.2	98.8
Pb <sup>2+</sup>	10x	99.5	98.3	97.3
	100x	107.8	104.9	97.5
Zn <sup>2+</sup>	10x	100.9	98.1	96.4
	100x	106.0	104.9	102.3

are rapidly eluted. the EDTA, being added only to the sample and not to the eluent, also moves rapidly through the column and appears as part of the initial peak, or pseudopeak.

Samples containing a large excess of iron(III) give extremely wide "pseudopeaks", when the ethylenediammonium tartrate

is used. This excess of iron(III) in a sample of magnesium, calcium, and strontium will totally obscure the magnesium peak while calcium and strontium appear on the tail of the "pseudopeak". Figure 8 shows a chromatogram of the same sample in which EDTA is added to complex the iron(III). The additional peak is from an iron(II) impurity in the iron(II) solution used. Work thus far indicated that any metal ion that has an EDTA formation constant of about  $10^{15}$  or higher should be masked effectively by adding EDTA to the sample. Figure 9 shows a nice separation of magnesium and calcium in samples containing a large excess of aluminum(III), copper(II), or iron(III).

Quantitative data are presented in Table II for recovery of magnesium, calcium, and strontium from a much larger concentration of selected metal ions using masking with EDTA. Although a 100-fold molar excess causes slightly high results in several cases, the results are definitely good enough to show that this is a very useful and selective method for quantitative determination of magnesium, calcium, and strontium.

## ACKNOWLEDGMENT

The authors wish to thank D. T. Gjerde for his consultation and advice and J. Benson for supplying the cation exchange resins used in this work.

**Registry No.** Ca, 7440-70-2; Mg, 7439-95-4; Sr, 7440-24-6; Pr, 7440-10-0; Ba, 7440-39-3; Cd, 7440-43-9; Ce, 7440-45-1; Co, 7440-48-4; Dy, 7429-91-6; Er, 7440-52-0; Eu, 7440-53-1; Fe, 7439-89-6; Gd, 7440-54-2; Ho, 7440-60-0; La, 7439-91-0; Lu, 7439-94-3; Mn, 7439-96-5; Nd, 7440-00-8; Ni, 7440-02-0; Pb, 7439-92-1; Sm, 7440-19-9; Tb, 7440-27-9; Tm, 7440-30-4; Yb, 7440-64-4; Zn, 7440-66-6; ethyl, 107-15-3; tartaric acid, 87-69-4;  $\alpha$ -hydroxyisobutyric acid, 79-31-2.

## LITERATURE CITED

- (1) Small, H.; Stevens, T. S.; Bauman, W. C. *Anal. Chem.* **1975**, *47*, 1801.
- (2) Fritz, J. S.; Gjerde, D. T.; Becker, R. M. *Anal. Chem.* **1980**, *52*, 1519.
- (3) Fritz, J. S.; Gjerde, D. T.; Pohlandt, C. "Ion Chromatography"; Alfred Huthig: Heidelberg, 1982.
- (4) Elchuk, S.; Cassidy, R. M. *Anal. Chem.* **1979**, *51*, 1434.
- (5) Ringbom, A. "Complexation in Analytical Chemistry"; Wiley-Interscience: New York, 1963.

RECEIVED for review July 30, 1982. Accepted October 1, 1982. Operated for the U.S. Department of Energy by Iowa State University under Contract No. W-7405-ENG-82. This work was supported by the director of Energy Research, Office of Basic Energy Sciences. This work was presented at the 24th Annual Rocky Mountain Conference, Aug 1-5, 1982, Denver, CO.



# Phenyl-Modified Kel-F as a Column Packing for Liquid Chromatography

Richard W. Siergle and Neil D. Danielson\*

Department of Chemistry, Miami University, Oxford, Ohio 45056

Phenyl Kel-F is prepared by reacting Kel-F 6061 (100% poly(chlorotrifluoroethylene)) and phenyllithium in THF under helium. From IR and elemental analysis data, substitution of the chlorine in the polymer for phenyl groups is the primary reaction occurring. Electron microscopy of the phenyl Kel-F shows a definite increase in surface porosity. Various chromatographic parameters such as the reduced plate height, sample capacity, column porosity, and permeability indicate phenyl Kel-F is pellicular in nature. On the basis of selectivity data, the retention mechanism is found to be solvophobic in nature. The retention order of various functionalized benzenes is identical with that found for C-18 silica. Applications of phenyl Kel-F for the separation of mixtures containing chlorophenols, *N*-alkyl anilines, and aromatic hydrocarbons are demonstrated.

In the reversed-phase mode of high-performance liquid chromatography (HPLC), the solid support used most often is silica chemically modified with a hydrocarbon moiety. Reversed-phase packings have been shown to be highly efficient and versatile for a large variety of separations. However, routine use of silica-based HPLC packings with either low or high pH mobile phases is difficult. At pH values less than 2, hydrolysis of siloxane bonds can occur, while above pH 7, dissolution of the silica is possible. A nonpolar rigid support possessing reasonable surface area and chemical stability would widen the pH range of aqueous solutions available for reversed-phase separations.

A variety of materials have been investigated as alternative packing materials to silicated silica. The XAD resins have been studied extensively for use as reversed-phase HPLC packings (1-3). In addition, various carbonaceous packings have been prepared and characterized for HPLC. Guiochon and co-workers (4, 5) have found that carbon black, after graphitization and pyrolytic deposition of various hydrocarbons, was then useful as an HPLC packing. Porous carbon packings prepared by high temperature heat treatment of active carbon or coke were found to have good stability, high surface area, and a hydrophobic surface (6). The fluorocarbon polymers Teflon and Kel-F, after reduction to carbon using lithium amalgam, have also been utilized as HPLC packing materials (7, 8). The presence of oxygenated reactive sites such as hydroxyls lessened the nonpolar character of these materials (8, 9). However, after chlorination of the surface followed by functionalization of the carbon particles using a Grignard reaction, improved reversed-phase properties of reduced Kel-F carbon were demonstrated (8). Recently, it has been reported that carbon prepared from the reduction of Teflon can be heat-treated in an inert atmosphere to reduce the oxygen content (10). All of these carbon packings require lengthy and involved reaction conditions and/or extensive heat treatments.

Recent work in this laboratory has indicated that Kel-F (poly(chlorotrifluoroethylene)) particles can be derivatized with either organolithium or organomagnesium reagents under relatively mild conditions (11). The organic functional groups

replaced chlorine atoms and formed a carbon-carbon bond with the polymer. The potential of *n*-butyl Kel-F as an HPLC packing has been previously demonstrated (12). However, a detailed chromatographic study of functionalized Kel-F has not been carried out. The present paper describes the preparation of phenyl-modified Kel-F particles by using phenyllithium as the organic modifier. Fundamental chromatographic properties of this packing such as reduced plate height and sample capacity were investigated. The dependence of solute retention with type and composition of mixed solvents was also investigated. Utility of phenyl Kel-F for the separation of various aromatic hydrocarbon mixtures is also presented.

## EXPERIMENTAL SECTION

**Preparation of Column Packings.** Kel-F 6061 (100% poly(chlorotrifluoroethylene)), a white powder of 80-100 mesh, was obtained from A. M. Plastics (Rockaway, NJ) and jet ground (Alnor Inc., Camden, NJ) to obtain particles less than 325 mesh. Elutriation (3) in 2-propanol was used to obtain a size distribution of 15-35  $\mu$ m as determined by light microscopy for 90% of the particles. These particles were filtered and dried before derivatization. Seven grams of Kel-F in 100 mL of dry THF (gold label, Aldrich Chemical Co.) was heated to 50 °C and purged with helium for 30 min. Thirty milliliters of 1.95 M phenyllithium (Aldrich Chemical Co.) was added dropwise and the mixture was refluxed for 3 h with constant stirring. For termination of the reaction, 3-5 mL of water was carefully added dropwise. The product was filtered and washed with hexane, acetone, 2-propanol, water, and methanol. The dry product was brown.

BN-X35, a neutral poly(styrene-divinylbenzene) resin with particles <30  $\mu$ m, was obtained from Alltech Associates. Particle size was checked by sieving through a 325 mesh screen and fines were removed by sedimentation in methanol.

Elemental analyses (C, H, and Cl) were performed by Atlantic Microlab Inc. (Atlanta, GA). The fluorine determination was provided by Galbraith (Knoxville, TN). Photomicrographs were taken with a Coates and Welter Model 106 scanning electron microscope. Surface area measurements were calculated from the BET adsorption isotherm of nitrogen.

**Chromatographic Procedures.** Fines in the phenyl Kel-F were removed by repetitive sedimentation in methanol. With a slurry of the desired packing in methanol, stainless steel columns 150  $\times$  4.1 mm i.d. were packed at a pressure of 60 MPa (6.9 MPa = 1000 psi) using a Model 10-600-30 pneumatic amplifier pump (SC Hydraulic Engineering Corp., Los Angeles, CA) and a high-pressure slurry packer (Alltech, Deerfield, IL). Most of the chromatographic measurements were made with two Altex Model 110A pumps (Berkely, CA) equipped with an Altex Model 420 gradient programmer and Model 153 photometric detector (254 nm). Sample injections of 20  $\mu$ L were made with a Rheodyne Model 7120 loop injector. An IBM 9533 liquid chromatograph (Hartford, CT) was used to generate the data in Figures 5 and 6. Peaks were recorded on an Omniscribe Model B-5000 recorder (Houston Instruments, Austin, TX). All solvents used as mobile phases were degassed by purging with helium. Methanol and acetonitrile were "Distilled-in-Glass" quality (Burdick and Jackson). A PRP-1 column (Hamilton Co. Reno, NV) and IBM C-18 and phenyl columns were used to generate the data in Table III. Column efficiency data were reported as plate height,  $H$ , or as reduced plate height,  $h$ , where  $H = L/N$ ,  $h = H/d_p$ , and  $N = 5.54(t_R/w_{1/2})^2$ . Retention data were reported as capacity factors,

Table I. Addition of Phenyl Groups to Kel-F Based on C, H, and Cl Elemental Analysis

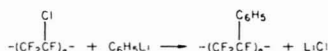
element	% derivatization <sup>a</sup>	mmol of phenyl/g of packing <sup>b</sup>
C	29.4	2.3
H	30.7	2.4
Cl	32.9	2.5

<sup>a</sup> Due to the change in molecular weight of the polymer upon derivatization, the amount of phenyl coverage was determined by first calculating the percent derivatization. Using 100 units for convenience: % elemental analysis = [(wt element in 100 monomer units)/(total wt 100 monomer units)] × 100. In 100 monomer units: wt F = 300(atomic wt F); wt Cl = (100 - X)(atomic wt Cl); wt C = (200 + 6X)(atomic wt C); wt H = 5X(atomic wt H); where X = % derivatization. The total weight of 100 monomer units is the sum of these four terms. <sup>b</sup> The amount of phenyl coverage was calculated by using an average formula weight of the derivatized Kel-F: mol of phenyl/g of packing = X/[X(formula wt of Phenyl Kel-F monomer) + (100 - X)(formula wt of Kel-F monomer)].

$k'$ , where  $k' = (t_R - t_0)/t_0$ . The reduced velocity was calculated by using the method described by Snyder (13) where  $\mu = (1.8 \times 10^3)C^*Ld_p/t_0$  where  $C^* = 0.635$  for biphenyl. The abbreviations  $L$ ,  $d_p$ ,  $t_R$ ,  $t_0$ , and  $w_{1/2}$  correspond to the column length, particle diameter, retention time, retention time of nitrate, and the peak width at half height, respectively. The column permeability,  $\phi$ , and the total porosity,  $\epsilon_{tot}$ , were calculated as indicated by Bristow and Knox (14).

## RESULTS AND DISCUSSION

**Characterization of Phenyl Kel-F.** Phenyl-modified Kel-F was qualitatively identified by infrared spectrometry. Absorption bands at 3059  $\text{cm}^{-1}$  and 3028  $\text{cm}^{-1}$  and overtones in the 2000–1660  $\text{cm}^{-1}$  range clearly indicated the presence of substituted aromatic groups. Two characteristic bands at 758  $\text{cm}^{-1}$  and 697  $\text{cm}^{-1}$  confirmed the presence of monosubstituted benzene. Quantitative information about the amount of phenyl derivatization was obtained from elemental analysis. Unreacted Kel-F was 21.3% C, 0% H, 30.6% Cl, and 48.1% F (by difference) in composition. Elemental analyses of  $35.1 \pm 1.2\%$  C,  $1.2 \pm 0.1\%$  H, and  $18.3 \pm 1.4\%$  Cl were indicated for three batches of the polymer product. Table I lists the changes in C, H, and Cl content produced by the reaction assuming a 1:1 substitution of chlorine for phenyl. The average extent of derivatization and the amount of phenyl groups attached to Kel-F were  $31.0 \pm 1.8\%$  and  $2.4 \pm 0.1$  mmol/g, respectively. The close agreement of phenyl coverage indicated by the individual elements is strong evidence that phenyl substitution was the primary reaction occurring.



The reaction between phenyllithium and Kel-F was believed to proceed by a one-electron exchange mechanism. A more detailed discussion of the reaction mechanism will be published elsewhere (11).

Derivatization of the polymer particles was accompanied by an increase in surface area from 1.5 to 10.5  $\text{m}^2/\text{g}$ . The reason for this surface area increase was revealed by both light and electron microscopy. Light microscopy of the phenyl Kel-F packing indicated a particle range from 5 to 36  $\mu\text{m}$ . For the 83 particles measured, the average particle diameter was  $20 \pm 7 \mu\text{m}$ . It appears that the organolithium reaction does increase the number of small particles which could contribute to a higher surface area. An electron micrograph of undervatized Kel-F is shown in Figure 1. Essentially the polymer particles appear smooth and nonporous. However a marked

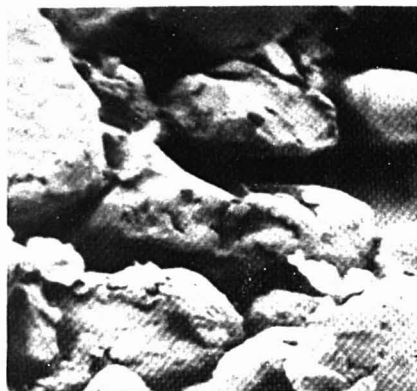


Figure 1. Scanning electron micrograph of Kel-F 6061, 1 cm =  $3.9 \times 10^{-6}$  m.

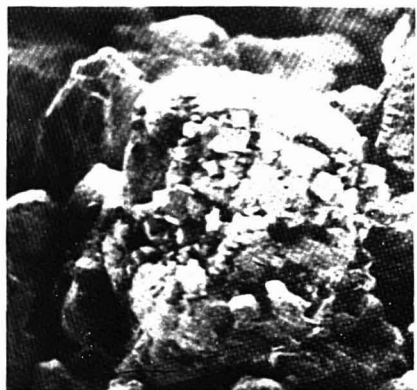


Figure 2. Scanning electron micrograph of phenyl Kel-F, 1 cm =  $3.9 \times 10^{-6}$  m. The cubic crystals are believed to be LiF.

increase in porosity was noted for the phenyl Kel-F particles (Figure 2). This type of etching has also been reported for the reaction of sodium with poly(tetrafluoroethylene) (15). This process can cause loss in fluorine and indeed crystals of LiF on the phenyl Kel-F were confirmed by powder X-ray diffraction. However, organic fluorides are considered to be less reactive than organic chlorides (16) and displacement of fluorine was not likely to be substantial. This conclusion was confirmed by an elemental analysis value for fluorine of 41.2%.

Derivatization of Kel-F with phenyl groups as found for *n*-butyl Kel-F cannot be strictly a surface phenomenon because of the high millimoles of phenyl/gram of packing as compared to the surface area. Swelling of Kel-F by the solvent THF during the course of the reaction may be the primary factor. Hydrocarbon solvents such as ethers and various chlorinated solvents have been shown to swell Kel-F particles particularly at elevated temperatures. In addition, chemical permeability of Kel-F films by diethyl ether was found to be substantially higher than other hydrocarbon solvents (17).

**Chromatographic Properties of Phenyl Kel-F.** Figure 3 illustrates the influence of phenyl modification on the

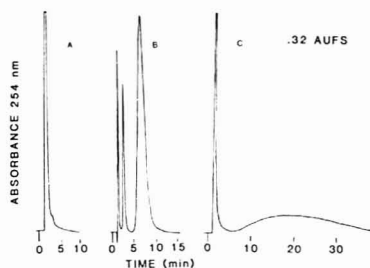


Figure 3. Chromatograms of a mixture containing *p*-nitroaniline (0.3 mg/mL), toluene (0.3 mg/mL), and phenanthrene (1.0 mg/mL) on 15 cm  $\times$  4.1 mm i.d. columns of undervivatized Kel-F (A), phenyl Kel-F (B), and BN-X35 poly(styrene-divinylbenzene) resin (C): mobile phase, 85:15 (v/v) methanol-H<sub>2</sub>O for (A) and (B); mobile phase, 75:25 (v/v) methanol-H<sub>2</sub>O for (C); flow rate, 1.0 mL/min.

chromatographic properties of Kel-F. Unmodified Kel-F was unable to separate a test mixture of *p*-nitroaniline, toluene, and phenanthrene. Under identical conditions a phenyl Kel-F column easily separated the three components. Peak asymmetry (measured at 10% peak height) was found to be acceptable, with values of 1.20 for toluene and 1.26 for phenanthrene. A third chromatogram of the test mixture is shown with a column packed with BN-X35. The water content of the mobile phase was increased slightly to adjust the retention of phenanthrene to that found with the phenyl Kel-F column. Although phenanthrene was still separated, *p*-nitroaniline and toluene remained unresolved. The better separation capability of phenyl Kel-F as compared to BN-X35 may be due to the more hydrophobic nature of the fluorocarbon polymer.

Column efficiency was studied using biphenyl as the solute ( $k' = 11.8$ ) and a plot of  $\log h$  vs.  $\log \nu$  was generated. A minimum  $H$  value of 0.11 mm corresponding to 8800 plates/m was calculated. The corresponding reduced plate height of 5.7 occurred at a reduced velocity of 19.7 (0.3 mL/min). However, the flow rate could be varied in the range from 0.3 to 0.6 mL/min with only a 25% loss in plates. This reduced plate height was higher than what is theoretically predicted by the Knox equation for "good" pellicular columns ( $h = 4.9$  at  $\nu = 100$ ), but it is comparable to reduced plate heights reported for carbon absorbents (6, 7, 10). The phenyl Kel-F column also produced a plate count somewhat higher than that found by Roos (18) for columns packed with an ether modified pellicular packing. The plate number was essentially independent of temperature from 25 to 55 °C. However, a linear decrease of  $k'$  for biphenyl from 2.9 to 1.9 was observed as the temperature of the column was increased from 25 to 55 °C.

Sample capacity was determined with toluene as the solute. Figure 4 illustrates the decrease in capacity factor with increasing sample size. The maximum linear sample capacity,  $\theta_{0.1}$ , is defined at the point where  $k'$  had decreased 10% (14) and was determined to be about 100  $\mu\text{g/g}$  of packing. This value is low compared to pellicular silica; however, it is impressive considering the moderate surface area of the particles. Corasil II, a representative pellicular packing, has a sample capacity of 400  $\mu\text{g/g}$  of packing and a surface area of 25  $\text{m}^2/\text{g}$ .

The mechanical stability of phenyl Kel-F was quite good. Column packing was performed at high pressures (60 MPa). A back-pressure of 3.4 MPa developed using a 1% acetic acid-water mobile phase at a flow rate of 5.7 mL/min. Prolonged use of highly viscous (greater than 1.4 cP) mobile phases occasionally caused the column bed to compact with a corresponding increase in back-pressure. The permeability,

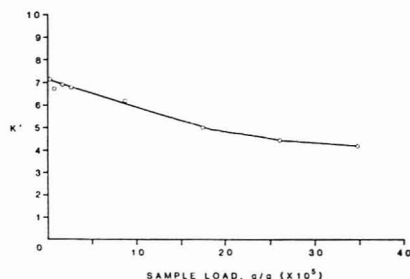


Figure 4. Effect of sample size on retention of toluene: mobile phase, 85:15 (v/v) methanol-water; flow rate, 0.8 mL/min.

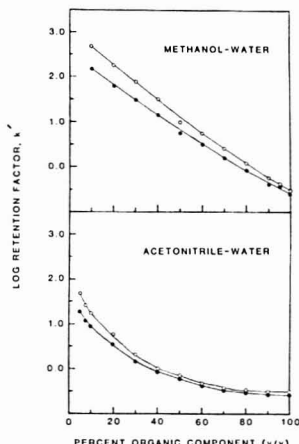


Figure 5.  $\log k'$  vs. the percent organic modifier in an aqueous mobile phase for methanol and acetonitrile. Solutes are benzyl alcohol (●) and phenylethanol (○).

$\phi$ , and the total porosity,  $\epsilon_{\text{tot}}$ , were calculated to be 547 and 0.41, respectively. Spherical pellicular packings have typical flow resistance factors of 250–350. The slightly higher value obtained for phenyl Kel-F may be due to the irregular shape of the particles (19). Pellicular particles have been reported previously to have porosity values of about 0.4 (14). It appears in general that phenyl Kel-F has similar properties to pellicular packings.

The dependence of solute retention with type and composition of mixed solvents was investigated with phenyl Kel-F. Plots of  $\log k'$  for benzyl alcohol and phenylethanol as a function of organic volume fraction for methanol in water and acetonitrile in water are shown in Figure 5. Both  $\log k'$  plots were similar to those found previously using *n*-alcohols and C-18 derivatized silica (20). For methanol-water, the plots were linear with corresponding  $k'$  values ranging from about 570 for 10% methanol to 2 for 70% methanol. At 100% water, essentially irreversible adsorption of the solutes was noted. Above 70% methanol, a very slight flattening of the curve occurred for both solutes. The following relationship could be useful for the prediction of  $\log k'$  of the mixed solvent.

$$\log k'_{\text{mix}} = V_{\text{H}_2\text{O}}(\log k'_{\text{H}_2\text{O}}) + V_{\text{methanol}}(\log k'_{\text{methanol}})$$

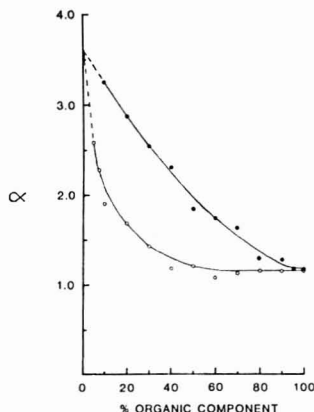


Figure 6. Methylene group selectivity ( $\alpha$ ) vs. the percentage of organic solvent in the mobile phase for methanol (●) and acetonitrile (○).

where  $V$  is the volume fraction of each solvent in the mobile phase. In contrast, for acetonitrile/water, the plots were curved with corresponding  $k'$  values ranging from about 40 for 5% acetonitrile to 3 for 80% acetonitrile. Above 65% acetonitrile, the  $k'$  value remained relatively constant. The rapid decrease of  $\log k'$  to a plateau value with increasing acetonitrile content in the mobile phase can be attributed to the greater enrichment of the stationary phase by acetonitrile as compared to methanol. Yonkers et al. (21) have noted the increase in percent acetonitrile adsorbed by a C-18 stationary phase was about twice as great as the increase in percent methanol when the composition of the mobile phase changed from 100% water to 80/20% water/organic. Increasing the organic solvent composition in the mobile phase further resulted in a linear increase in the percent methanol in the stationary phase while the percent acetonitrile remained fairly constant. The phenomenon of hydrophobic expulsion of the organic solvent from the mobile phase is well-known for  $n$ -alkyl bonded silica and is undoubtedly occurring with phenyl Kel-F as well (22).

The effect of the methylene group selectivity,  $\alpha$ , as a function of percent methanol and acetonitrile composition in the mobile phase is shown in Figure 6. Extrapolation of both curves to 100% water indicated a  $y$  intercept of 3.7. This value agreed well with the methylene increment of 4.0 reported for  $n$ -alcohols taken on a C-18 column. Previously it has been noted that the value of the methylene group selectivity was quite constant regardless of the class of compound (20). At the 100% organic content, the magnitude of  $\alpha$  for both acetonitrile and methanol converged to a value of about 1.1. This number was similar to 1.5 which had been found previously by using a C-18 column (21). The curves in Figure 6 strongly resembled surface tension vs. percent organic composition plots (23). A direct relationship between  $\log \alpha$  and the surface tension of the mobile phase has been substantiated by Riley et al. (24) for a variety of group selectivities using both methanol and acetonitrile. A plot of  $\log \alpha$  vs. the surface tension of methanol/water was linear to about 70% water before slightly leveling off toward the surface tension of 100% water. The plot of  $\log \alpha$  vs. the surface tension of acetonitrile/water was linear throughout the solvent composition range. Extrapolation of the line to 100% water indicated a  $\log \alpha$  of 0.52 corresponding to an  $\alpha$  value of 3.3. These results show that the reversed-phase mechanism for phenyl Kel-F

Table II. Capacity Factor ( $k'$ ) and Hydrophobic Selectivity ( $\alpha^*$ ) Data for Various Functionalized Benzenes

compound no.	functional group	$k'$	$\alpha^*$
1	-CONH <sub>2</sub>	0.30	0.01
2	-CH <sub>2</sub> OH	1.12	0.05
3	-(CH <sub>2</sub> ) <sub>2</sub> OH	1.61	0.06
4	-OH	1.81	0.07
5	-NH <sub>2</sub>	2.33	0.09
6	-CH <sub>2</sub> NH <sub>2</sub>	8.16	0.33
7	-CHO	8.19	0.33
8	-CN	11.6	0.47
9	-NO <sub>2</sub>	20.3	0.82
10	-OCH <sub>3</sub>	23.8	0.96
11	-H	24.8	1.0

$\alpha^* = k'$  of functionalized benzene/ $k'$  of benzene. Mobile phase, 30:70 acetonitrile:water; pH 3.4.

follows the solvophobic theory generally accepted for  $n$ -alkyl, derivatized silica packings.

Further characterization of the hydrophobic selectivity,  $\alpha^*$ , for phenyl Kel-F was carried out with a variety of functionalized benzenes. Capacity factors and  $\alpha^*$  data for 11 compounds are shown in Table II. Similar data have been reported previously by Tanaka et al. (25) using the same mobile phase on a C-18 column. Three significant points can be made when comparing the phenyl Kel-F and the C-18 data. First, the retention order of these compounds on phenyl Kel-F and C-18 columns was identical. This result provides additional evidence to the fact that the retention mechanism on phenyl Kel-F and C-18 were similar in nature. Second, for compounds 7-11, the  $k'$  values obtained with phenyl Kel-F were about 3 to 4 times larger than the corresponding C-18 capacity factors. Higher  $k'$  values are typical of other carbonaceous stationary phases such as pyrocarbon modified carbon black (26). The high  $k'$  values were evidence that the polymer backbone did contribute to retention. Since the phenyl groups are slightly more polar than the C-18 groups, the relative retention would be expected to be less on a phenyl column if the polymer backbone did not contribute to retention. Finally, when the  $\alpha^*$  values were compared, another significant difference between columns was seen. The solutes which were retained the longest on both columns (compounds 8-10) have very similar  $\alpha^*$  values. However, the  $\alpha^*$  values for solutes such as 1-4 were about 3 times greater on the C-18 column than on the phenyl column. This increased relative retention was most probably due to hydrogen bonding between the silanol groups on the silica and the functional groups of the solutes. In general, it appears that phenyl Kel-F shows good selectivity in separating nonpolar solutes. However, C-18 silica can retain moderately polar solutes better than phenyl Kel-F.

Additional evidence supporting the role of residual silanols in the retention of solutes is provided by the data in Table III. The capacity factors of toluene and  $\alpha,\alpha,\alpha$ -trifluorotoluene were measured on phenyl Kel-F, PRP-1, C-18 silica, and phenylsilica columns. Toluene was retained longer than  $\alpha,\alpha,\alpha$ -trifluorotoluene on both polymeric packing materials while the retention order was reversed on the silica-based packings. Apparently the presence of residual silanols on the silica allowed sufficient hydrogen bonding to occur with the fluorines of trifluorotoluene causing the longer retention of this compound.

Finally several applications showing the potential of phenyl Kel-F as a HPLC column packing have been carried out. Figure 7 demonstrates the selectivity of phenyl Kel-F for various aromatic and polyaromatic solutes. At mobile phase compositions greater than 60% water, irreversible retention of the solutes took place. The separation of various alkyl-substituted anilines is shown in Figure 8. The use of a high

Table III. Capacity Factor ( $k'$ ) for Toluene and  $\alpha,\alpha,\alpha$ -Trifluorotoluene as a Function of Column Packing<sup>a</sup>

column type	$k'$	
	toluene	$\alpha,\alpha,\alpha$ -trifluorotoluene
phenyl Kel-F <sup>c</sup>	7.3	6.7
PRP-1 <sup>d</sup>	8.8	6.9
C-18 silica <sup>e</sup>	6.7	8.2
phenylsilica <sup>f</sup>	1.4 (4.6) <sup>b</sup>	1.6 (8.5) <sup>b</sup>

<sup>a</sup> Mobile phase, 50:50 acetonitrile:water. <sup>b</sup> Mobile phase, 20:80 acetonitrile:water. <sup>c</sup> Column 4.1 × 150 mm packed with 20- $\mu$ m phenyl Kel-F. <sup>d</sup> Column 4.1 × 150 mm packed with 10- $\mu$ m poly(styrene-divinylbenzene) resin. <sup>e</sup> Column 4.5 × 250 mm packed with 5- $\mu$ m C-18 silica. <sup>f</sup> Column 4.5 × 250 mm packed with 5- $\mu$ m phenylsilica.

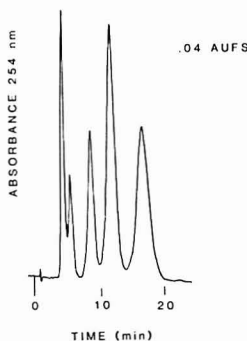


Figure 7. Chromatogram of benzene (120  $\mu$ g/mL), toluene, biphenyl, naphthalene, and phenanthrene (all 80  $\mu$ g/mL): mobile phase, 65:35 (v/v) methanol:water; flow rate, 0.8 mL/min.

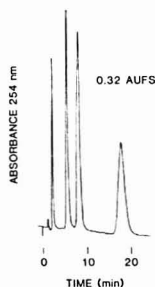


Figure 8. Chromatogram of aniline, *N*-ethylaniline, *N,N*-dimethylaniline, and *N,N*-diethylaniline: mobile phase, 55:45 (v/v) acetonitrile:0.01 M borate buffer, pH 10; flow rate, 0.7 mL/min. Each solute concentration was 80  $\mu$ g/mL.

pH mobile phase well above the  $pK_a$  values of the solutes helped provide excellent resolution for the four amines. Separation of various chlorophenols is shown in Figure 9. In this case, use of a high pH mobile phase was desirable to enhance the UV absorbance of the compound class (27). Future work planned is to take advantage of the capability of group functionalization possible with phenyl Kel-F. Preparation of sulfonated and quaternary ammonium deriv-

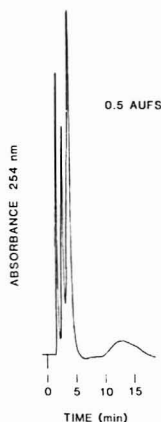


Figure 9. Chromatogram of *p*-chlorophenol, 2,4-dichlorophenol, 2,4,6-trichlorophenol, and 2,3,4,6-tetrachlorophenol: mobile phase, 88:12 (v/v) 0.05 M borate buffer, pH 10.4/3 mM tetrabutylammonium hydrogen sulfate-acetonitrile; flow rate, 0.7 mL/min. Each solute concentration was 100  $\mu$ g/mL.

atives of phenyl Kel-F for use in ion exchange chromatography should be straightforward.

#### ACKNOWLEDGMENT

The authors thank T. K. Wilson of Miami University and D. Lauderbach of the Armco Steel Corp. for assistance with the electron microscopy and the surface area data, respectively.

#### LITERATURE CITED

- (1) Fritz, J. S.; Willis, R. B. *J. Chromatogr.* **1973**, *79*, 107.
- (2) Kroeff, E. P.; Pietrzyk, D. J. *Anal. Chem.* **1978**, *50*, 502.
- (3) Baum, R. G.; Sastre, R.; Cantwell, F. F. *Anal. Chem.* **1980**, *52*, 15.
- (4) Colin, H.; Eon, C.; Guiochon, G. *J. Chromatogr.* **1978**, *119*, 41.
- (5) Colin, H.; Eon, C.; Guiochon, G. *J. Chromatogr.* **1978**, *122*, 223.
- (6) Unger, K.; Roumeliotis, P.; Mueller, H.; Goetz, H. *J. Chromatogr.* **1980**, *202*, 3.
- (7) Pitzak, Z.; Dousek, F. P.; Jansta, J. *J. Chromatogr.* **1978**, *147*, 137.
- (8) Zwier, T. A.; Burke, M. F. *Anal. Chem.* **1981**, *53*, 812.
- (9) Riggs, W. M.; Dwight, D. W. *J. Electron Spectrosc. Relat. Phenom.* **1974**, *5*, 447.
- (10) Smolkova, E.; Zima, J.; Dousek, F. P.; Jansta, J. *J. Chromatogr.* **1980**, *191*, 61.
- (11) Danielson, N. D.; Taylor, R. T.; Huth, J. A.; Siegle, R. W.; Galloway, J. G.; Papernan, J. B., Miami University, Oxford, OH, Sept 1981, unpublished work.
- (12) Huth, J. A.; Danielson, N. D. *Anal. Chem.* **1982**, *54*, 930.
- (13) Snyder, L. R. *J. Chromatogr. Sci.* **1977**, *15*, 441.
- (14) Bristow, P. A.; Knox, J. H. *Chromatographia* **1977**, *10*, 279.
- (15) Cagle, C. V. "Handbook of Adhesive Binding"; McGraw-Hill: New York, 1973; Chapter 19.
- (16) Wakefield, B. J. "The Chemistry of Organolithium Compounds"; Pergamon Press: Oxford, 1974; p 22.
- (17) Mark, H. F.; Gaylord, N. G.; Bikales, N. M., Eds. "Encyclopedia of Polymer Science and Technology"; Wiley (Interscience): New York, 1967; Vol. 7, p 181.
- (18) Roos, R. W. *J. Chromatogr. Sci.* **1978**, *14*, 505.
- (19) Snyder, L. R.; Kirkland, J. J. "Introduction to Modern Liquid Chromatography"; Wiley-Interscience: New York, 1979; p 37.
- (20) Karger, B. L.; Galt, J. R.; Hartkopf, A.; Weiner, P. H. *J. Chromatogr.* **1976**, *128*, 65.
- (21) Yonkers, C. R.; Zwier, T. A.; Burke, M. F. *J. Chromatogr.* **1982**, *241*, 257.
- (22) McCormick, R. M.; Karger, B. L. *Anal. Chem.* **1980**, *52*, 2249.
- (23) Horvath, Cs.; Melander, W. *J. Chromatogr. Sci.* **1977**, *15*, 393.
- (24) Riley, C. M.; Tomlinson, E.; Jeffries, T. M. *J. Chromatogr.* **1979**, *185*, 197.
- (25) Tanaka, N.; Goodell, H.; Karger, B. L. *J. Chromatogr.* **1978**, *158*, 233.
- (26) Colin, H.; Ward, N.; Guiochon, G. *J. Chromatogr.* **1978**, *149*, 169.
- (27) Lee, D. P. *J. Chromatogr. Sci.* **1982**, *20*, 203.

RECEIVED for review March 25, 1982. Resubmitted August 27, 1982. Accepted September 20, 1982. This work was

supported in part by grants from the Faculty Research Committee of Miami University, the Research Corporation, and the donors of the Petroleum Research Fund, administered by the American Chemical Society. Infrared spectra were taken on a Perkin-Elmer Model 680 spectrometer funded by the National Science Foundation through Grant TFI-8022902.

Donation of the 9533 liquid chromatograph by IBM to the Chemistry Department is appreciated. R. W. Siegiej gratefully acknowledges support provided by a Dissertation Fellowship from Miami University. This work was presented at the 183rd American Chemical Society Meeting, Las Vegas, NV, March 30, 1982.

## Liquid Chromatography/Proton Nuclear Magnetic Resonance Spectrometry Average Composition Analysis of Fuels

James F. Haw,<sup>1</sup> T. E. Glass, and H. C. Dorn\*

Department of Chemistry, Virginia Polytechnic Institute and State University, Blacksburg, Virginia 24061

The use of a NMR spectrometer as a continuous flow liquid chromatographic detector (LC/<sup>1</sup>H NMR) generates a proton spectrum of each hydrocarbon class present in the sample. A detailed set of equations is presented which permits LC/<sup>1</sup>H NMR integration data from petroleum fuels to be interpreted as an average composition for each chromatographic fraction. Quantities calculated for each aromatic fraction include: the number average molecular weight, average degree of substitution on aromatic rings, the absolute number of moles of each structural type of carbon, an average structure (devoid of stereoisomer information), the total number of moles of carbon in each chromatographic fraction, and numerous other properties of interest in fuel characterization. The method is demonstrated for artificial fuels of known composition, for two experimental aviation fuels, and for a fuel blending stock sample which had been fully characterized at an independent laboratory by gas chromatography and GC/MS. The LC/<sup>1</sup>H NMR average composition method is shown to be very accurate for the monocyclic aromatic (substituted benzenes and tetralins) and dicyclic aromatic (substituted naphthalenes and acenaphthenes) fractions of petroleum fuels. Average molecular weights for these fractions can be routinely determined at an accuracy of  $\pm 4$  daltons. The other quantities are also determined at a high degree of accuracy. The applicability of the LC/<sup>1</sup>H NMR method to the aliphatic fraction of fuel samples is restricted by difficulties in accounting for quaternary carbons and cycloalkanes.

Often in fuel analysis it is unnecessary (even undesirable) to identify and quantify every component. In these cases, certain average compositional data (vide infra) may be related to desirable or undesirable properties of the sample. A familiar average compositional datum is aromaticity which is easily measured via <sup>13</sup>C NMR. Identification and quantitation of every compound also permit aromaticity to be calculated. This also provides a great deal of additional information, often obtained at great expense. This paper delineates systematic methodology for determining average compositional data for the aromatic fractions of low boiling fuels. Inherent in the determination of average compositional data are the following questions. How much information can be extracted reliably from a spectrum with as little a priori knowledge as possible?

To what extent can the method be made independent of crude correlations derived from a limited set of test samples? Can a method be developed that is reliant on only one measuring device rather than on a collection of different instruments?

In considering which instrumental method is most appropriate for petroleum fuel analysis, the following considerations apply. The resulting information must unambiguously correlate with structure. In other words, a peak in a certain position must indicate a specific structural unit and no other. Furthermore, the intensity (or area) of each peak must be directly proportional to the relative population of that structural unit in the sample. The proportionality should be linear to avoid the need for calibration curves. In addition, the proportionality should be independent of the remainder of the structure. For this reason infrared absorption data are unsuitable.

All of the above requirements are readily met by proton NMR spectrometry. With careful attention to experimental parameters, <sup>13</sup>C NMR is also a suitable candidate. Other techniques (e.g., mass spectrometry) have greater sensitivity for trace constituents, but since average composition is desired here, the sensitivity of modern NMR spectrometers is entirely adequate. The scheme presented here is based totally on the use of <sup>1</sup>H NMR analysis of several easily obtained liquid chromatographic fractions. The option of using one piece of <sup>13</sup>C NMR data (aromaticity of the bulk sample) to derive additional information is also discussed.

NMR has been of interest to fuel chemists ever since early high-resolution instruments became available. Since this time, several "average structure" schemes using NMR in association with other techniques have been developed. For the most part, these techniques have been proposed for total aromatic cuts (obtained by open column liquid chromatography on silica gel). These methods will not be reviewed in detail since this has been done by Clutter et al. (1). Each method does have limitations which deserve mentioning. In 1958, Williams (2) reported a method for determining an average structure for fuel cuts. Quantitative <sup>1</sup>H NMR, elemental analysis, molecular weight data, other mass spectral data, and semiempirical correlations based on a poorly defined quantity (branchiness index) were used as input data for calculations that gave the average numbers of each carbon type in a hypothetical average molecule. Williams was severely limited by existing instrumentation, but his work was very impressive for its time. Proceeding in a similar vein, Brown and Ladner (3, 4) were able to interpret <sup>1</sup>H NMR spectra of soluble coal-derived samples in terms of an average structure framework. Knight (5) employed <sup>13</sup>C NMR, <sup>1</sup>H NMR, average molecular weight

<sup>1</sup>Present address: Department of Chemistry, Colorado State University, Ft. Collins, CO 80523.



data (from mass spectrometry or VPO), and elemental analysis to arrive at an average structure. This method has some nice features since the carbon backbone is examined directly. But like many of these methods, it requires a rather large and diverse quantity of data to be acquired. Clutter et al. (1) developed a method based solely on  $^1\text{H}$  NMR spectrometry. In order to calculate average parameters for monocyclic and bicyclic aromatics, certain assumptions are made which are of questionable validity. For example, monocyclic and bicyclic aromatic ring protons are determined from one spectrum, with a dividing line at 7.05 ppm. Our fuel samples rarely show any hint of a valley at or near this dividing line, even at 200 MHz. They further assumed that the average number of alkyl substituents on benzene rings was identical with the average number of substituents on naphthalene rings. This assumption is necessary to solve their equations. The fraction of monocyclic aromatics is then calculated by an iterative process based on these assumptions. This method may give good results (or at least show trends) for certain sets of samples. But for experimental fuels (which may be doped with additives to alter performance) the calculated values may be in considerable error. The above methods suffer because they were developed for the analysis of fractions containing the total aromatic content of the fuel. The need to somehow estimate the relative proportion of compounds of different classes (e.g., substituted benzenes and substituted naphthalenes) complicates the calculation process.

Modern normal-phase liquid chromatography is readily able to separate low boiling fuels into distinct hydrocarbon classes. Aliphatics, monocyclic aromatics, bicyclic aromatics, and tricyclic aromatics readily may be collected as separate fractions with the total separation requiring between 5 and 30 min (depending on choice of column, solvent, and flow rate). A suitable solvent is 1,1,2-trichlorotrifluoroethane which is less expensive than most chromatographic solvents and yields no proton signals. Chloroform-*d* may be used as a polar additive at little additional cost. This permits fractions collected from the chromatographic column to be submitted directly for  $^1\text{H}$  NMR analysis without the manipulation difficulties and potential sample loss problems associated with LC solvent removal and subsequent uptake in a deuterated solvent. The high sample load capacity of semipreparative HPLC columns and the high sensitivity of modern spectrometers permit the total analysis to be done with a single injection of 100  $\mu\text{L}$  or less. Much smaller injections can be made at the cost of lower signal to noise or increased spectral acquisition time.

## EXPERIMENTAL SECTION

A series of seven model mixtures, designed to resemble typical fuel samples, were prepared from reagent grade chemicals. One of these (a standard model mixture used frequently in this lab, designated "model C") was prepared by mixing 13.29 g of *n*-butylbenzene, 18.47 g of *n*-pentane, 10.16 g of *m*-xylene, 13.07 g of tetralin, 95.70 g of *n*-nonane, 56.20 g of hexadecane, 200.40 g of isooctane, 43.65 g of *n*-hexane, 85.67 g of dodecane, and 12.80 g of naphthalene. The remaining six model mixtures were prepared by adding known quantities of an additional compound to model C. Two National Aeronautic and Space Administration experimental fuel samples were supplied by the Air Force Aero Propulsion Laboratory (Wright-Patterson Air Force Base, OH) for analysis. The two NASA fuels were designated NASA-Lewis 3S and NASA-Lewis 3B. In addition, one Naval Research Laboratory (NRL) sample (81-3, a blending stock of alkylbenzenes) is reported. All samples were subjected to on-line LC/ $^1\text{H}$  NMR analysis without pretreatment.

A Whatman Magnum-9 silica gel-PAC column (500 mm  $\times$  9 mm i.d.) was used for all separations. The packing in this column is silica gel derivatized to introduce amino and cyano functionalities to the surface. Retention of aromatic hydrocarbons on this column is generally superior to silica gel columns. A special

activation sequence was used to remove polar compounds (e.g., methanol) from the column. These polar compounds slowly bleed off with nonpolar solvents and create large background signals in the proton spectra. The following sequence completely removes this background: 50 mL of 10% acetonitrile-*d*<sub>3</sub> (99% *d*, Aldrich) in chloroform-*d* (99.8% *d*, Aldrich) was followed by 60 mL of chloroform-*d*. The chromatographic solvent, 97.5% 1,1,1-trichlorotrifluoroethane (Miller-Stephenson Chemical Co.) and 2.5% chloroform-*d*, was then pumped through the column. Column equilibration was generally achieved after 60 mL. A second source of background is particular to semipreparative LC columns. Large internal diameter columns do not completely flush the alkane fraction due to partially stagnant regions near the inlet, outlet, and wall. In terms of LC/ $^1\text{H}$  NMR this effect can result in a very small amount of aliphatic material being present in the spectra of the aromatic fractions. For fuels of low aromaticity, the signal is intense enough to make the measurement of  $\text{CH}_2$  and  $\text{CH}_3$   $^1\text{H}$  integrals for alkyl aromatics erroneously high. A correction for our column was determined by injecting a very low aromaticity fuel and measuring the relative aliphatic signal intensities in each file. This tailing problem is apparently not present in analytical scale columns which have smaller internal diameters.

The chromatographic solvent contained 0.05% (v/v) hexamethyldisiloxane (HMDS, Merck) as a chemical shift and quantitation reference. The solvent was not degassed since dissolved oxygen reduces proton spin-lattice relaxation time values to several seconds. A Waters M-45 pump equipped with a needle valve to create a 1000 psi back-pressure was used. The M-45 pump requires back-pressure to activate its pulse dampener. A Valco injector equipped with a 100- $\mu\text{L}$  sample loop was used. A 1-mL rinse of solvent followed by 1 mL of sample was used to ensure that the sample loop was thoroughly flushed. All samples were injected neat. A guard column was used as a matter of course.

A Jeol FX-200 nuclear magnetic resonance spectrometer equipped with an Oxford 4.7-T superconducting solenoid magnet (54 mm bore) was used to obtain  $^1\text{H}$  spectra at 199.50 MHz. A floppy disk system was used for data storage and each diskette had sufficient storage for 58 (1024 point) LC/ $^1\text{H}$  NMR spectra. A flow cell designed for quantitative work was used for all analyses. This cell is described in detail in ref 10. Further details on flow probe design may be found in ref 8. The average composition equations were incorporated in a BASIC program which was run on a Hewlett-Packard HP-85. A copy of this program is available upon request.

Aromaticity was measured from  $^{13}\text{C}$  spectra obtained at 50 MHz.  $\text{Tris}(\text{acetylacetonato})\text{chromium(III)}$ ,  $\text{Cr}(\text{acac})_3$ , was added to each sample to reduce  $^{13}\text{C}$  spin-lattice relaxation times for aromaticity measurements. Gated decoupling was used for NOE suppression. Long pulse delays were also used to further ensure quantitative  $^{13}\text{C}$  spectra. All  $^{13}\text{C}$  spectra were run under conventional (spinning) conditions in 10-mm sample tubes.

## RESULTS AND DISCUSSION

Our laboratory is currently interested in several applications of NMR of flowing systems, principally the use of NMR as an on-line, continuous flow HPLC detector (6-9). The equations in our average composition method are applicable to both fraction collection (off-line) and directly coupled systems (on-line LC/ $^1\text{H}$  NMR). Most laboratories will prefer to use the off-line approach, at least until a commercial flow probe becomes available. Whichever approach is used, the effort spent in the preliminary separation step is a small price for the resulting more explicit and reliable calculations (vide infra).

For the purposes of this paper, the average composition of a low boiling fuel sample is defined in the following manner. For each hydrocarbon class, the absolute moles of each distinct carbon type (with associated hydrogens) in a specified aliquot is determined. An example of a distinct carbon type is an unsubstituted aromatic ring carbon (which has one associated hydrogen). Substituted aromatic ring carbons (having no associated hydrogen) clearly constitute a separate type of carbon. Having determined the number of moles of each carbon type in a fuel aliquot, it may be possible to normalize



Table I. Definitions of Representative Symbols<sup>a</sup>

$H^x_r$	<sup>1</sup> H NMR integrated area for the reference peak (HMDS) of the aliphatic monocyclic aromatic or bicyclic aromatic fractions (x = a, m, or d (aliphatic, monocyclic aromatic, or bicyclic fraction))
$H^a_{CH}$	<sup>1</sup> H NMR integrated area for methine groups (R <sub>1</sub> C-H) in the alkane fraction
$H^a_{CH_2}$	<sup>1</sup> H NMR integrated area for methylene groups (R-CH <sub>2</sub> -R) in the alkane fraction
$H^a_{CH_3}$	<sup>1</sup> H NMR integrated area for methyl groups (R-CH <sub>3</sub> ) in the alkane fraction
$H^x_{Ar}$	<sup>1</sup> H NMR integrated area for aromatic hydrogens in the monocyclic aromatic or bicyclic aromatic fraction (x = m or d)
$H^x_{arom}$	<sup>1</sup> H NMR integrated area for aliphatic ring hydrogen α to aromatic rings (e.g., α-methylene hydrogen in tetralin) in the monocyclic or bicyclic aromatic fractions (x = m or d)
$H^x_{αCH_2}$	<sup>1</sup> H NMR integrated area for aliphatic methylene hydrogen α to aromatic rings (e.g., methylene group in ethylbenzene) for the monocyclic or bicyclic aromatic fractions (x = m or d)
$H^x_{αCH_3}$	<sup>1</sup> H NMR integrated area for aliphatic methyl hydrogen α to aromatic rings (e.g., methyl groups for toluene and/or β-methylnaphthalene) for the monocyclic or bicyclic aromatic fractions (x = m or d)
$H^x_{>α}$	<sup>1</sup> H NMR integrated area for aliphatic hydrogen groups not adjacent to aromatic rings (i.e., greater than α) for the monocyclic or bicyclic aromatic fractions (x = m or d)
$C^x_{un}$	moles of unsubstituted aromatic carbon for the monocyclic or bicyclic aromatic fractions (x = m or d) <sup>b</sup>
$C^x_{sub}$	moles of substituted aromatic carbon for the monocyclic or bicyclic aromatic fractions (x = m or d)
$C^x_{αCH_3}$	moles of methyl carbon α to aromatic rings (x = m or d)
$C^m_{CH_2}$	moles of methylene carbon α to aromatic rings (x = m or d)
$C^m_{arom}$	moles of aliphatic ring carbon α to monocyclic aromatic rings (e.g., α-methylene carbons in tetralin)
$C^x_{CH_2>α}$	moles of aliphatic methylene carbon not bonded to aromatic rings (i.e., greater than α)
$C^x_{CH_3>α}$	moles of terminal chain methyl carbon not bonded to aromatic rings (i.e., greater than α)
$C^d_{BH}$	moles of bridgehead carbon for the bicyclic aromatic fraction (i.e., $C^d_{BH} = 2.0$ )
$C^x_{total}$	the total carbon in a given fraction (i.e., alkane, monocyclic, or bicyclic fraction)
$ADS^x$	the average degree of aromatic substitution for the monocyclic or bicyclic fractions
$MW^x$	the number average molecular weight for the monocyclic or bicyclic fraction
$f_a$	the carbon aromaticity for the total sample (i.e., the total aromatic carbon ( $C_{Ar(total)}$ ) divided by total carbon ( $C_{total}$ ))
$f_a^x$	the partial carbon aromaticity contribution for the monocyclic aromatic or bicyclic aromatic fractions (i.e., $f_a = f_a^m + f_a^d$ )
$F^x$	the fraction of total carbon in each chromatographic fraction (i.e., $F^x_{total} + F^m_{total} + F^d_{total} = 1$ )

<sup>a</sup> See Figure 1 for further clarification of symbols and Figures 2-4 for defined <sup>1</sup>H NMR integration regions. <sup>b</sup> If the carbon types indicated below have a superscript asterisk (e.g.,  $*C^m_{un}$ ), this denotes the number of each carbon type in the hypothetical average molecule.

used to indicate that separate, but analogous, terms exist for the two fractions (i.e., x = m or d). For some quantities (e.g., average molecular weight) this is not possible and separate equations are presented.

Two common problems with previous average composition methods have been relating proton integrals to carbon content and normalizing the data to an average molecule. In the LC/<sup>1</sup>H NMR method, the number of aromatic ring carbons is known for both of the aromatic cuts. The existence of an aromatic ring proton implies the existence of an unsubstituted aromatic ring carbon. Likewise, the existence of three αCH<sub>3</sub> protons implies the existence of an α carbon and a substituted aromatic ring carbon. These absolute mole values are obtained via the product of the reference response factor with the appropriate proton integration value weighted for proton/carbon ratio (e.g., for an αCH<sub>2</sub> group, 2 mol of protons in the αCH<sub>2</sub> region implies the existence of 1 mol of α carbons). Unsubstituted aromatic ring carbons are given by eq 2.

$$C^x_{un} = K(V^x)H^x_{Ar} \quad x = m \text{ or } d \quad (2)$$

Substituted aromatic ring carbons are given by eq 3.

$$C^x_{sub} = K(V^x) \left( \frac{H^x_{αCH_3}}{3} + \frac{H^x_{αCH_2}}{2} + \frac{H^x_{arom}}{2} + H^x_{αCH} \right) \quad (3)$$

At 200 MHz and above, the various α proton types are sufficiently spectrally resolved that quantities such as  $C^x_{αCH_3}$  may be separately defined (Table I and eq 4). In a similar manner, equations for  $C^x_{αCH_2}$ ,  $C^x_{arom}$ , and  $C^x_{αCH}$  can be easily written except with denominators of 2, 2, and 1, respectively.

$$C^x_{αCH_3} = K(V^x)H^x_{αCH_3}/3 \quad (4)$$

For the monocyclic fraction, normalization is obtained via the following equation. The number of carbons of each type in the "average structure" of the monocyclic aromatic fraction is obtained by dividing the absolute number of moles of each carbon type by the appropriate normalization constant and reference response factor. This is illustrated by eq 6 for  $*C^m_{un}$ . The asterisk denotes the number of each carbon type ( $*C^m_{un}$ ) in the hypothetical average molecule instead of the absolute number of moles of carbon ( $C^m_{un}$ ) in the injected sample.

$$N^m = [C^m_{Ar(total)}]/6 \quad (5)$$

$$*C^m_{un} = C^m_{un}/N^mK(V^m) \quad (6)$$

For the bicyclic fraction (here assumed to be naphthalenes and acenaphthenes), the normalization constant is given by the following equation.

$$N^d = (C^d_{un} + C^d_{sub})/8 \quad (7)$$

The normalized bicyclic fraction carbon types are obtained by analogy to eq 6. Naphthalene molecules also contain two bridgehead carbons.

$$C^d_{BH} = \frac{1}{4}[C^d_{un} + C^d_{sub}] \quad (8)$$

$$*C^d_{BH} = C^d_{BH}/K(V^d)N^d = 2 \quad (9)$$

The region of the proton spectra of the monocyclic and bicyclic fractions upfield of 2 ppm contains all alkyl chain protons at positions β, γ, δ, and higher with respect to the aromatic ring. Division of this region into distinct subregions (e.g., βCH<sub>3</sub>) is impractical for most fuel samples. The region  $H^x_{>α}$  is instead integrated as a whole and equations for  $*C^x_{CH_2>α}$  and  $*C^x_{CH_3>α}$  have been derived.

$$*C^{\alpha}_{CH_2>\alpha} = ADS^{\alpha} - *C^{\alpha}_{\alpha CH_3} - *C^{\alpha}_{\alpha ring} \quad (10)$$

$$*C^{\alpha}_{CH_2>\alpha} = \frac{H^{\alpha}_{>\alpha}}{2N^{\alpha}} - \frac{3}{2}[*C^{\alpha}_{CH_3>\alpha}] \quad (11)$$

These equations assume that no branching exists beyond the  $\alpha$  position. Experience in our laboratory indicates that this is a reasonable assumption for aviation fuels. Alkyl substitution on aromatics tends to take the form of  $n$ -alkyl and tetralin. Similarly, we frequently ignore the  $\alpha_{CH_3}$  region. Even if branching is present beyond the  $\alpha$  position, the accuracy of the average properties calculated below (e.g., average molecular weight) will be unaffected. The absolute number of moles of alkyl carbon in positions greater than  $\alpha$  (e.g.,  $*C^{\alpha}_{CH_3>\alpha}$  and  $*C^{\alpha}_{CH_2>\alpha}$ ) can be calculated directly from  $*C^{\alpha}_{CH_3>\alpha}$  and  $*C^{\alpha}_{CH_2>\alpha}$ , respectively.

$$C^{\alpha}_{CH_3>\alpha} = *C^{\alpha}_{CH_3>\alpha} N^{\alpha} K(V^{\alpha}) \quad (12)$$

$$C^{\alpha}_{CH_2>\alpha} = *C^{\alpha}_{CH_2>\alpha} N^{\alpha} K(V^{\alpha}) \quad (13)$$

The total number of moles of aromatic carbon in the monocyclic aromatic fraction and the total number of moles of carbon (alkyl plus aromatic) in this fraction are calculated via eq 14 and 15, respectively.

$$C^m_{Ar(total)} = C^m_{un} + C^m_{sub} \quad (14)$$

$$C^m_{total} = C^m_{Ar(total)} + C^m_{\alpha CH_3} + C^m_{\alpha CH_2} + C^m_{\alpha CH} + C^m_{\alpha ring} \quad (15)$$

The average molecular weight of the compounds in this fraction may also be calculated.

$$\begin{aligned} \overline{MW}^m = & 13 * C^m_{un} + 12 * C^m_{sub} + 15 * C^m_{\alpha CH_3} + 14 * C^m_{\alpha CH_2} \\ & + 13 * C^m_{\alpha CH} + 14 * C^m_{\alpha ring} + 14 * C^m_{CH_2>\alpha} + 15 * C^m_{CH_3>\alpha} \end{aligned} \quad (16)$$

This follows in a straightforward manner. Since the number of carbons of each type in the "average molecule" is determined, the weight in daltons of every carbon (and associated hydrogens) can be summed. The result is the number average molecular weight rather than the less useful weight average (1). Total absolute moles of dicyclic aromatic ring carbon and total absolute moles of all carbon in the dicyclic aromatic chromatographic fraction can now be calculated.

$$C^d_{Ar(total)} = C^d_{un} + C^d_{sub} + C^d_{BH} \quad (17)$$

$$C^d_{total} = C^d_{Ar(total)} + C^d_{\alpha CH_3} + C^d_{\alpha CH_2} + C^d_{\alpha CH} + C^d_{\alpha ring} \quad (18)$$

The average molecular weight of this fraction now follows as before.

$$\begin{aligned} \overline{MW}^d = & 13 * C^d_{un} + 12 * C^d_{sub} + 12 * C^d_{BH} + 15 * C^d_{\alpha CH_3} + \\ & 14 * C^d_{\alpha CH_2} + 13 * C^d_{\alpha CH} + 14 * C^d_{\alpha ring} + 14 * C^d_{CH_2>\alpha} + \\ & 15 * C^d_{CH_3>\alpha} \end{aligned} \quad (19)$$

For fuel samples, one of the most commonly measured average compositional properties is the carbon aromaticity ( $f_a$ ). It is defined as the numerical ratio of aromatic ring carbons to total carbons in the sample. It is conveniently (and most directly) measured by  $^{13}C$  NMR. The conditions necessary for obtaining quantitative  $^{13}C$  spectra are now well understood (10, 11). If the aromaticity is known for the sample, the partial aromaticities for the monocyclic and dicyclic fractions may be calculated assuming the absence of tricyclic aromatics. The partial aromaticities are defined such that their sum is equal to the total aromaticity.

$$f_a = f_a^m + f_a^d \quad (20)$$

$$f_a = (f_a) \left[ \frac{C^{\alpha}_{Ar(total)}}{C^m_{Ar(total)} + C^d_{Ar(total)}} \right] \quad (21)$$

The fraction of total carbon in each chromatographic peak (relative to the entire sample) may now be calculated. The values for the monocyclic and dicyclic fractions are obtained explicitly. The value for the aliphatic fraction is obtained by difference and will be in error if there are appreciable amounts of latter eluting materials (e.g., phenanthrenes) or noneluted polars (e.g., phenols).

$$F^{\alpha}_{total C} = (f_a) \left( \frac{C^{\alpha}_{total}}{C^{\alpha}_{Ar(total)}} \right) \quad (22)$$

And for the aliphatic peak

$$F^{\alpha}_{total C} = 1 - F^m_{total C} - F^d_{total C} \quad (23)$$

In the above discussion, it has been assumed that the dicyclic fraction is composed exclusively of alkylnaphthalenes and acenaphthene. Coal-derived fuel samples can contain some biphenyl derivatives, usually as minor constituents of the dicyclic fraction. Compounds of these types have elution characteristics similar to alkylnaphthalenes (8). Acenaphthenes will not introduce error. The  $\alpha CH_2$  proton signal of acenaphthene has a unique chemical shift so an explicit treatment analogous to that for tetralins (via  $C^d_{ring}$ ) is possible. Biphenyls can introduce error, but only for normalized compositional data. For naphthalene, eight protons imply the existence of ten carbons. For biphenyl, ten protons imply the existence of twelve carbons. If a dicyclic fraction is 100% biphenyl, eq 2 will give the correct value for  $C^d_{un}$ . Equation 8 will give a value for  $C^d_{BH}$  that will be 25% too high. The error in  $C^d_{Ar total}$  will only be 4%. The fraction of substituted sites for dimethylbiphenyl (0.2) will be correctly calculated but the calculated  $ADS^d$  will be 20% low. The normalization equation for dicyclics (eq 7) should have a denominator of ten for biphenyls rather than eight which was derived for naphthalenes. Computations of normalized average composition (e.g.,  $ADS^d$  and  $\overline{MW}^d$ ) data via the above equations are typically ~20% low for pure biphenyl fractions. Biphenyls are typically <15% of the dicyclic fraction of aviation fuel samples so the actual error is quite small. In addition, it may be possible to chromatographically resolve substituted biphenyls from the substituted naphthalenes, which represents the most straightforward solution to this problem.

One may at this point wonder if any direct information may be deduced from the aliphatic fraction. Referring to Figure 2, it can be noted that a reasonable demarcation exists between methyl, methylene, and methine protons. It is easy to proceed in a manner similar to that for the aromatic fractions and arrive at average compositional data. Two serious precautions must be mentioned. Cycloalkane protons produce signals inconsistent with the  $CH_3$ ,  $CH_2$ , and  $CH$   $^1H$  spectral regions characteristic of normal and branched alkanes. If cycloalkanes are present in substantial quantities, considerable error will result in the following analysis. Reference spectra of cycloalkanes suggest that the three integration windows will typically "see" a large amount of  $CH_2$  with roughly equal amounts of  $CH$  and  $CH_3$ . Thus, if cycloalkanes are at low levels, the resulting analysis will have little error.

The second problem concerns quaternary carbons. In this scheme, the existence of a certain proton resonance is used to imply the existence of a certain carbon type. A quaternary carbon has no directly attached protons and is, therefore, "invisible" to  $^1H$  NMR. Substituted aromatic ring carbons have no directly attached protons. But the existence of a clearly resolved proton resonance on the  $\alpha$  carbon implies the

**Table II.** Comparison of Known and Measured Average Degree of Substitution (ADS), Average Molecular Weight Data, and Total Carbon Ratio for Models as Determined by LC/<sup>1</sup>H NMR<sup>a</sup>

model	monocyclic aromatic fraction		dicyclic aromatic fraction		C <sup>m</sup> <sub>total</sub> /C <sup>d</sup> <sub>total</sub>
	ADS <sup>m</sup>	MW <sup>m</sup>	ADS <sup>d</sup>	MW <sup>d</sup>	
model C	1.76 (1.66)	124.9 (124.4)	0.12 (0)	130.6 (128.2)	2.83 (2.75)
model C (27.47 g) + m-xylene (0.02 m)	1.84 (1.86)	113.4 (113.9)	0.01 (0)	131.5 (128.2)	6.19 (5.94)
model C (27.47 g) + n-butylbenzene (0.02 m)	1.29 (1.28)	132.2 (130.1)	0.04 (0)	131.8 (128.2)	7.60 (7.60)
model C (27.47 g) + tetralin (0.02 m)	2.05 (1.86)	130.3 (128.9)	0.04 (0)	128.4 (128.2)	7.06 (6.74)
model C (27.47 g) + cumene (0.04 m)	1.13 (1.18)	119.6 (121.2)	0.03 (0)	128.3 (128.2)	9.91 (9.95)
model C (27.47 g) + decalin (0.02 m)	1.57 (1.66)	124.2 (124.4)	0.05 (0)	129.2 (128.2)	3.16 (2.75)
model C (27.47 g) + 2,3-dimethylnaphthalene (0.0056 m)	1.64 (1.66)	118.6 (124.4)	1.04 (1.06)	142.4 (142.8)	1.29 (1.30)

<sup>a</sup> The values determined by LC/<sup>1</sup>H NMR without parentheses are directly compared with the known values obtained from composition data (in parentheses).

existence of a substituted ring carbon. If *tert*-butylbenzene is a prominent constituent of fuel samples, not only will the determination of  $\alpha$  carbons be in error but the normalization for monocyclic aromatics will also be in error since the ring carbons would be miscounted. We have not observed tertiary alkyl substitution on aromatic rings, so this is not a problem. Highly branched alkanes generally improve fuel performance data (e.g., high octane number). Quaternary carbon containing molecules are more likely to be present in the alkane fraction of fuels. In eq 24, a term has been included for quaternary carbon (expressed as a fraction of methyl carbon). This term is included for completeness since some workers may have a priori information on the nature of the alkane fraction. This is particularly true if a compound such as isooctane has been added to improve fuel performance.

The normalization factor is first determined

$$N^a = \frac{H^a_{CH_3} - 3H^a_{CH}}{6} - \frac{[F_{quat}(^aH_{CH})]}{3} \quad (24)$$

The last term in the above equation is the correction for quaternary carbons, which is (in general) not known. Absolute moles of each carbon type are now calculated (e.g., eq 25). Similar equations hold for the C<sup>m</sup><sub>CH<sub>3</sub></sub> and C<sup>m</sup><sub>CH</sub> terms with denominators of 2 and 1, respectively. An average molecule

$$C^a_{CH_3} = H^a_{CH_3}K(V^a)/3 \quad (25)$$

may now be constructed by normalization as before. The average molecular weight is then calculated.

$$\overline{MW}^a = \frac{15^a C^a_{CH_3} + 14^a C^a_{CH_2} + 13^a C^a_{CH} + 12 F_{quat}(^a C_{CH_3})}{C^a_{total}} \quad (26)$$

Because of pitfalls outlined above in obtaining average compositional data for the alkane fraction, eq 24–26 should be used with caution. In principle, an aromaticity value could be calculated (independent of <sup>13</sup>C NMR) at this point. In practice, it is much safer to directly measure aromaticity (via <sup>13</sup>C NMR) since this will keep errors in the aliphatic fraction determination from affecting the much more rigorous treatment of the aromatic fractions.

In Table II we report average degree of substitution (ADS<sup>m</sup>), average molecular weight (MW<sup>m</sup>), and ratios of total carbon (C<sup>m</sup><sub>total</sub>/C<sup>d</sup><sub>total</sub>) for seven model mixtures. These values are compared with the known values calculated from the known compositions. The comparison is excellent. The other average composition values are also in very close agreement with the known values. The measured ADS<sup>d</sup> for samples containing no dicyclic compound other than naphthalene has an average of 0.05. This illustrates the problem of spectral background creating small integrals in regions where no sample is present.

**Table III.** Naval Research Laboratory Data

Monocyclic Aromatic Fraction of Fuel 81-3  
GC/MS Identification  
GC Quantitation

component	wt % of fraction
ethylbenzene	0.7 ± 0.08
p- and m-xylene	9.0 ± 0.5
o-xylene	16.6 ± 1.0
isopropylbenzene	0.9 ± 0.07
n-propylbenzene	3.1 ± 0.2
methylstyrene (isomer unknown)	20.6 ± 1.2
1,3,5-trimethylbenzene	9.4 ± 0.7
1-methyl-2-ethylbenzene	4.7 ± 0.3
1,2,4-trimethylbenzene	29.9 ± 2.1
1,2,3-trimethylbenzene	5.0 ± 0.4
total	99.0 ± 1.0

This could be partially solved by determining background corrections. The background problem is most apparent in the chromatographically broad dicyclic peak which has the lowest concentration. Some of the background arises from a certain arbitrariness in measuring integrals for cases of very low signal to noise. The average molecular weight data (MW<sup>d</sup>) matches the known values very closely. The measured ratio of total carbon in the monocyclic aromatic peak to total carbon in the dicyclic peak (C<sup>m</sup><sub>total</sub>/C<sup>d</sup><sub>total</sub>) is compared with the known ratio. The agreement is surprisingly close since this measurement is based on every integration from the two fractions and so includes all cumulative errors. Since the dicyclic fraction is much smaller than the monocyclic fraction, a small absolute error in determining the dicyclic carbons will produce a large error in the ratio.

A very strong verification of the LC/<sup>1</sup>H NMR average composition method was provided by the Naval Research Laboratory (12). Unknown to our laboratory, GC/MS had been used by the NRL to identify every aromatic compound in sample 81-3. Each component in this sample was also quantitated by GC. The results of this analysis are presented in Table II. This analysis was possible since blending stock 81-3 is considerably less complex than typical fuel samples. Knowing the exact composition, the average compositional data were readily calculated for the monocyclic aromatics. Table III shows the comparison between the NRL GC/GC/MS results and our laboratories LC/<sup>1</sup>H NMR results. The agreement is excellent. It is clear that the flow NMR measurements are very accurate. These data suggest that the LC/<sup>1</sup>H NMR average composition equations are correct and fully applicable to the monocyclic aromatic content of these fuels. There is some overlap between the H<sup>m</sup><sub>αCH<sub>3</sub></sub> and H<sup>m</sup><sub>αring</sub>

Table IV. Comparison of LC/NMR and GC/MS for Monocyclic Fraction of Fuel 81-3

property	NRL GC/MS	VPI LC/NMR
MW <sup>m</sup>	116.3	116.5
$f_a^m$	0.677	0.682
*C <sup>m</sup> <sub>un</sub>	3.60	3.64
*C <sup>m</sup> <sub>oCH<sub>3</sub></sub>	2.12	2.07
*C <sup>m</sup> <sub>oCH<sub>2</sub></sub>	0.291	0.278
*C <sup>m</sup> <sub>oCH</sub>	0.009	0.0007
*C <sup>m</sup> <sub>oring</sub>	0.00	0.013
*C <sup>m</sup> <sub>CH<sub>2</sub>&gt;α</sub>	0.031	0.108
*C <sup>m</sup> <sub>CH<sub>3</sub>&gt;α</sub>	0.309	0.279
ADS <sup>m</sup>	2.39	2.36

regions at 200 MHz. This overlap accounts for the shift in \*C<sup>m</sup><sub>oCH<sub>2</sub></sub> vs. \*C<sup>m</sup><sub>oring</sub>. This error is propagated into \*C<sup>m</sup><sub>CH<sub>2</sub>>α</sub> vs. \*C<sup>m</sup><sub>CH<sub>3</sub>>α</sub>, since \*C<sup>m</sup><sub>oring</sub> is used to determine the number of alkyl chains not terminated by methyl groups. The overlap between  $H^m$ <sub>oring</sub> and  $H^m$ <sub>oCH<sub>2</sub></sub> should be reduced at 360 MHz. The reliability of these measurements will, therefore, be improved by using a higher field spectrometer.

The spectra in Figures 2, 3, and 4 are from the three fractions of NASA-Lewis 3B. Data acquisition was initiated at the onset of the aliphatic peak, as monitored by the RI detector. Data on the aliphatic fraction were collected for 5.8 min (5.6 mL). During this time, the aliphatic peak passed the flow cell. The monocyclic and dicyclic files each represent 9.7 min (9.3 mL). The experimental conditions were identical for all samples. The spectra of the other fuel show obvious differences from NASA-Lewis 3B.

The average compositional data for the monocyclic fraction of the two fuels are shown in Table V. Sample 3S has the lower average molecular weight (MW<sup>m</sup> = 113.3) and average degree of substitution (ADS<sup>m</sup> = 2.15). It should also be noted that 5% of the benzene rings in this sample are tetralins or indans. Most of the substitution is in the form of methyl groups (\*C<sup>m</sup><sub>oCH<sub>3</sub></sub> = 1.71). The relative proportion of long chain alkyl groups is low (\*C<sup>m</sup><sub>oCH<sub>2</sub>>α</sub> = 0.043, \*C<sup>m</sup><sub>oCH<sub>3</sub>>α</sub> = 0.33).

Fuel 3B is very different with respect to the monocyclic aromatic fraction. It has the higher average molecular weight (MW<sup>m</sup> = 153.9) and a higher average degree of substitution (ADS<sup>m</sup> = 2.81). A total of 21% of the molecules in this fraction are tetralins or indans. Although methyl substitution is still prominent (\*C<sup>m</sup><sub>oCH<sub>3</sub></sub> = 1.57), longer alkyl chains are also quite prominent (\*C<sup>m</sup><sub>CH<sub>2</sub>>α</sub> = 1.82, \*C<sup>m</sup><sub>CH<sub>3</sub>>α</sub> = 0.811). The average compositional data for the dicyclic (naphthalene) fractions of these fuels are very similar.

The total moles of carbon in each fraction (C<sup>total</sup>, C<sup>m</sup><sub>total</sub>, and C<sup>d</sup><sub>total</sub>) are presented for each sample. Also presented are: aromaticities ( $f_a$ ), partial aromaticities ( $f_a^m$ ,  $f_a^d$ ), total moles of aromatic ring carbon (C<sup>Ar(total)</sup>, C<sup>Ar(total)</sup>), and fraction of total carbon in each LC peak (F<sup>a</sup><sub>total</sub>, F<sup>m</sup><sub>total</sub>, F<sup>d</sup><sub>total</sub>). These data also illustrate the stark contrast between 3S and 3B. Sample 3S has a higher level of both monocyclic and dicyclic aromatics (F<sup>m</sup><sub>total</sub> = 0.573, F<sup>d</sup><sub>total</sub> = 0.217). In contrast, sample 3B has the lowest levels of both monocyclic and dicyclic aromatics (F<sup>m</sup><sub>total</sub> = 0.192, F<sup>d</sup><sub>total</sub> = 0.136). Sample 3S contains a large quantity of relatively simple monocyclic aromatics (e.g., xylenes), and sample 3B contains a small quantity of more complex monocyclic aromatic compounds (e.g., tetralins, polysubstitution, longer chain alkyl groups). It is particularly interesting that the fraction of total carbon in the naphthalene fraction differs significantly in these two samples. It should also be noted that sample 3S was also subjected to GC/MS analysis. Biphenyls and acenaphthenes were not detected in these samples at levels above 5% (vide supra).

Substituted phenanthrenes were not included in the analytical scheme for the fuels discussed above; however, they are occasionally present in our samples at detectable levels. The same LC/<sup>1</sup>H NMR average compositional formalism is applicable given adequate signal to noise. In principle, mixtures of many types could be characterized by a formalism analogous to the one developed here for fuel samples.

Although the results of only two actual fuels are reported in this paper, it should be mentioned that we have analyzed ~75 other fuels by this approach.

## CONCLUSIONS

The LC/<sup>1</sup>H NMR average composition formalism demonstrates that a considerable amount of information can be extracted from <sup>1</sup>H NMR spectra of mixtures. A key requirement is that some information must be known about the class of compounds composing each mixture. In this formalism, hydrocarbon classes separated by normal phase liquid chromatography constitute the mixtures. The knowledge of compound class (e.g., monocyclic aromatic hydrocarbons) permits the spectral data to be interpreted explicitly as average compositions for each class.

The LC/<sup>1</sup>H NMR method allows carbon framework data to be obtained indirectly via the proton spectra and elution volumes. Direct observation of the carbon framework (via <sup>13</sup>C NMR) should also remain a fruitful area of fuel characterization research. Spectral editing pulse sequences (13-15), with or without prior chromatographic fraction collection, are potential avenues of research. In the LC/<sup>1</sup>H NMR average composition treatment of the alkane fraction, a critical problem is the determination of quaternary carbons. Spectral

Table V. Average Structural Parameters for NASA Fuels 3S and 3B

Monocyclic Aromatic Fraction										
sample	*C <sup>m</sup> <sub>un</sub>	*C <sup>m</sup> <sub>sub</sub>	*C <sup>m</sup> <sub>oCH<sub>3</sub></sub>	*C <sup>m</sup> <sub>oCH<sub>2</sub></sub>	*C <sup>m</sup> <sub>oCH</sub>	*C <sup>m</sup> <sub>aring</sub>	*C <sup>m</sup> <sub>CH<sub>2</sub>&gt;α</sub>	*C <sup>m</sup> <sub>CH<sub>3</sub>&gt;α</sub>	ADS <sup>m</sup>	MW <sup>m</sup>
3S	3.85	2.15	1.71	0.320	0.008	0.106	0.043	0.328	2.15	113.3
3B	3.19	2.81	1.57	0.777	0.034	0.423	1.82	0.811	2.81	153.9
Dicyclic Aromatic Fraction										
sample	*C <sup>d</sup> <sub>un</sub>	*C <sup>d</sup> <sub>sub</sub>	*C <sup>d</sup> <sub>BH</sub>	*C <sup>d</sup> <sub>oCH<sub>3</sub></sub>	*C <sup>d</sup> <sub>oCH<sub>2</sub></sub>	*C <sup>d</sup> <sub>CH<sub>2</sub>&gt;α</sub>	*C <sup>d</sup> <sub>CH<sub>3</sub>&gt;α</sub>	ADS <sup>d</sup>	MW <sup>d</sup>	
3S	5.98	2.02	2.00	1.90	0.117	0.001	0.117	2.02	158.1	
3B	6.27	1.73	2.00	1.61	0.117	0.079	0.117	1.73	155.2	
Absolute Number of Moles and Fractional Aromaticity Data										
sample	alkanes		alkyl aromatics				naphthalenes			
	C <sup>a</sup> <sub>total</sub>	F <sup>a</sup> <sub>total</sub>	C <sup>m</sup> <sub>Ar(total)</sub>	C <sup>m</sup> <sub>total</sub>	f <sup>a</sup> <sub>m</sub>	F <sup>m</sup> <sub>total</sub>	C <sup>d</sup> <sub>Ar(total)</sub>	C <sup>d</sup> <sub>total</sub>	f <sup>a</sup> <sub>d</sub>	F <sup>d</sup> <sub>total</sub>
3S	0.00262	0.210	0.00314	0.00446	0.403	0.573	0.00139	0.00169	0.179	0.217
3B	0.00483	0.672	0.00063	0.00120	0.101	0.192	0.000714	0.00085	0.114	0.136



editing sequences could permit direct measurement of this quantity.

### LITERATURE CITED

- (1) Clutter, D. R.; Petrakis, L.; Stenger, R. L., Jr.; Jensen, R. K. *Anal. Chem.* 1972, 44, 1395-1405.
- (2) Williams, R. B. *ASTM Spec. Tech. Publ.* 1958, STP 224, 168-194.
- (3) Brown, J. K.; Ladner, W. R.; Sheppard, N. *Fuel* 1959, 39, 79-88.
- (4) Brown, J. K.; Ladner, W. R. *Fuel* 1959, 39, 87-98.
- (5) Knight, S. A. *Chem. Ind.* 1967, 1920-1923.
- (6) Haw, J. F.; Glass, T. E.; Hausler, D. W.; Motell, E.; Dorn, H. C. *Anal. Chem.* 1980, 52, 1135-1140.
- (7) Haw, J. F.; Glass, T. E.; Dorn, H. C. *Anal. Chem.* 1981, 53, 2327-2332.
- (8) Haw, J. F.; Glass, T. E.; Dorn, H. C. *Anal. Chem.* 1981, 53, 2332-2336.
- (9) Haw, J. F.; Glass, T. E.; Dorn, H. C. *J. Magn. Reson.* 1982, 49, 22-31.
- (10) Dorn, H. C.; Wootton, D. L. *Anal. Chem.* 1976, 48, 2146-2148.
- (11) Gray, G. A. *Anal. Chem.* 1975, 47, 545A-564A.
- (12) Hardy, Dennis; Hazlett, R. N., Naval Research Laboratory, private communication, 1981.
- (13) Burum, D. P.; Ernst, R. R. J. *Magn. Reson.* 1980, 39, 163-168.
- (14) Bendall, M. R.; Doddrell, D. M.; Pegg, D. T. *J. Am. Chem. Soc.* 1981, 103, 4603-4605.
- (15) Cookson, D. J.; Smith, B. E.; White, N. J. *Chem. Soc., Chem. Commun.* 1981, 12-13.

RECEIVED for review February 6, 1982. Resubmitted July 26, 1982. Accepted September 21, 1982. This work was supported by the Naval Research Laboratory (Washington, DC) and the United States Air Force Aero Propulsion Laboratory (Wright-Patterson Air Force Base, OH). J. F. Haw holds a Virginia Mining and Minerals Resources and Research Institute Fellowship.

## Determination of Vasodilators and Their Metabolites in Plasma by Liquid Chromatography with a Nitrosyl-Specific Detector

Wing C. Yu\* and E. Ulku Goff

Thermo Electron Corporation, Analytical Instruments, 101 First Avenue, Waltham, Massachusetts 02254

A specific and sensitive method for the determination of the nitrate esters of glycerol, isosorbide, and pentaerythritol has been developed. The instrumentation involves high-performance liquid chromatography (HPLC) interfaced to a nitro/nitrosyl-specific detector (TEA analyzer). The lower limit of detection of the method is 0.1 ng for each of glycerol trinitrate (GTN) and pentaerythritol tetranitrate (PETN) and 0.2 ng for isosorbide dinitrate (ISDN). At the 5 ng level, the relative standard deviations are  $\pm 4.1\%$ ,  $\pm 2.2\%$ , and  $\pm 7.3\%$  for GTN, PETN, and ISDN, respectively. The isocratic conditions developed by using HPLC/TEA provide a useful tool for the routine analysis of plasma or blood samples in bioavailability studies.

Organic nitrate esters such as glycerol trinitrate (GTN), isosorbide dinitrate (ISDN), and pentaerythritol tetranitrate (PETN) have been widely used as vasodilators in the treatment of angina pectoris. Despite many publications, the pharmacokinetics of these drugs and their metabolites in humans are not well established, posing questions as to the efficacy and efficiency of the formulated drug. The problem is due, in part, to the limitation of available analytical instrumentation for detecting low levels of the drugs and their metabolites in circulating blood.

A survey of analytical techniques that have been used in the determination of these compounds include spectrophotometry (1), polarography (2), carbon-14 radioactivity labeling (3-5), thin-layer chromatography (6, 7), gas chromatography (8-12), liquid chromatography (13-16), and digital plethysmography (17). Of these techniques, gas chromatography coupled with electron capture detection is most commonly used. Electron capture, though sensitive, suffers from lack of reproducibility, detector contamination, and excessive retention times for the separation of some metabolites. Also, special techniques must be employed to maintain linearity of the detector response.

Recent advances in high-performance liquid chromatography (HPLC) offer another approach in the determination of these thermally unstable compounds. The use of the UV detector in conjunction with normal- or reversed-phase HPLC is a logical choice.

However, in a matrix as complex as blood or plasma where the levels of therapeutic drug and metabolites are present at the low parts per billion range, the UV detector cannot properly fulfill the need because of its relative lack of specificity and limited sensitivity.

For enhanced sensitivity and selectivity, specific detectors have to be used. Lafleur (18) et al. recently used a nitrosyl-specific detector, the TEA analyzer, in the identification of explosives at trace levels by interfacing it with high-performance liquid chromatography (HPLC/TEA). Spangord (19) et al. also reported on the application of HPLC/TEA in the determination of nitroglycerin and its metabolites in blood. Both methods utilized solvent programming techniques. In this report we describe an analytical method for the selective and sensitive determination of glycerol trinitrate, isosorbide dinitrate, pentaerythritol tetranitrate, and their metabolites, in plasma by HPLC/TEA using isocratic conditions.

### EXPERIMENTAL SECTION

**Equipment.** The high-performance liquid chromatograph was constructed by combining a solvent pump (Altex, Model 110) with an injector (Waters Associates, Model U6K). The columns used were 10  $\mu$ m Ultrasil NH<sub>2</sub>, 25 cm long by 4.6 mm i.d. (Altex), and 10  $\mu$ m  $\mu$ Bondapak CN, 30 cm long by 3.9 mm i.d. (Waters Associates).

The detector was a TEA Model 502 analyzer (Thermo Electron). Data acquisition was achieved with System I computing integrator (Spectra-Physics).

**Chemicals.** The HPLC solvents, methylene chloride, chloroform, methanol, ethyl acetate, and isooctane, were distilled in glass (Burdick and Jackson). Sep-PAK C<sub>18</sub> cartridges (Waters Associates) and 0.5- $\mu$ m Millex-SR filters (Millipore) were used.

**HPLC Procedure.** Isocratic conditions were employed for the analysis of the vasodilators and their metabolites. The Ultrasil

Table I. HPLC Retention Data for Nitrate Esters on NH<sub>2</sub> Column

retention time, s	compound	chemical identity	no. of NO <sub>2</sub> groups	no. of OH groups
169	ISDN	1,4:3,6-dianhydro-D-glucitol dinitrate	2	0
197	GTN	glycerol trinitrate	3	0
205	PETN	2,2-bis(nitroxymethyl)-1,3-propanediol 1,3-dinitrate	4	0
217	2-ISMN	isorbide 2-mononitrate	1	1
229	1,2-DNG	glycerol 1,2-dinitrate	2	1
293	1,3-DNG	glycerol 1,3-dinitrate	2	1
293	PETRIN	2-(hydroxymethyl)-2-(nitroxymethyl)-1,3-propanediol dinitrate	3	1
295	5-ISMN	isorbide 5-mononitrate	1	1
467	2-MNG	glycerol 2-mononitrate	1	2
510	PEDN	2,2-bis(hydroxymethyl)-1,3-propanediol 1,3-dinitrate	2	2
533	1-MNG	glycerol 1-mononitrate	1	2

NH<sub>2</sub> column was used for the separation of each vasodilator from its metabolites. The mobile phase was isooctane/methylene chloride/methanol in the ratio of 80:13:7. Solvent flow rate was maintained at 2.0 mL/min. The  $\mu$ Bondapak CN column was used for the separation of isoribide dinitrate, glycerol trinitrate, and pentaerythritol tetranitrate from each other, with a mobile phase of isooctane/chloroform/methanol in the ratio of 75:20:5 and a flow rate of 1.5 mL/min.

The TEA analyzer was operated at a pyrolyzer temperature of 500 °C. The carrier gas was nitrogen at a flow rate of 20 mL/min. Ozone was generated by passing oxygen to the ozonator, at 5 mL/min. The reaction chamber was operated at 0.6 torr. The cryogenic traps were maintained at -78 °C with an ethanol-solid carbon dioxide slush bath. Attenuation was set at  $\times 16$ .

**Sample Preparation.** Fresh frozen plasma was thawed in lukewarm water. Aliquots of 5 mL of plasma were pipetted into screw-capped culture tubes. The tubes were fortified with various levels of glycerol trinitrate, isoribide dinitrate, and pentaerythritol tetranitrate. Eight milliliters of ethyl acetate was added to the plasma and the mixture was vortexed for 1 min, sonicated for 5 min, and centrifuged at 2000 rpm for 10 min. The clear supernatant was transferred into another culture tube and the extraction was repeated twice, first with 8 mL of ethyl acetate and then with 6 mL of ethyl acetate. The combined supernatant was clarified through a Sep-PAK C<sub>18</sub> cartridge and Millex-SR filter connected in series. The filtrate was concentrated by a gentle stream of nitrogen of 35 °C to approximately 0.2 mL. Aliquots of 25  $\mu$ L were injected for HPLC/TEA analysis.

## RESULTS AND DISCUSSION

Figure 1 shows the isocratic separation of each of the nitrate esters from their metabolites, using an NH<sub>2</sub> column. Although the separation of nitrate esters of pentaerythritol has been reported previously using a solvent programming technique (18), the present chromatographic conditions represent a more realistic approach to routine analysis of a large number of samples. With this new method, the chromatographic analysis can be completed in approximately 10 min.

Table I shows the HPLC retention data for nitrate esters of glycerol, isoribide, and pentaerythritol. The retentivity of these compounds on the NH<sub>2</sub> column varies widely with the number of nitro groups and the number of hydroxyl groups on the molecule, with the hydroxyl group exhibiting the predominant effect. The relative retention times of these compounds provide a useful guide for selecting an internal standard which would not interfere with the separation of the compounds of interest. As an example, we selected glycerol 2-mononitrate as an internal standard for a study involving isoribide dinitrate and mononitrates.

The three parent compounds, isoribide dinitrate, glycerol trinitrate, and pentaerythritol tetranitrate have similar retention times on the NH<sub>2</sub> column, since the nitro groups exhibit little polarizing effects on the molecules. For better separation of these compounds, a  $\mu$ Bondapak CN column was

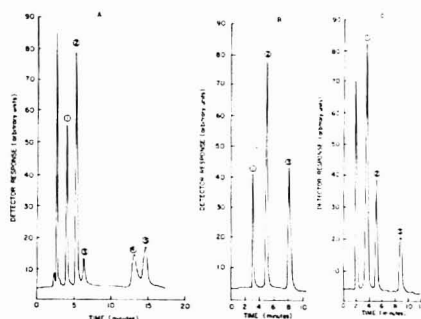


Figure 1. HPLC/TEA analysis of: (A) nitrate esters of glycerol, (1) GTN (2.5 ng), (2) 1,3-DNG (3.7 ng), (3) 1,2-DNG (0.7 ng), (4) 2-MNG (2.2 ng), (5) 1-MNG (4.4 ng); (B) nitrate esters of isoribide, (1) ISDN (4 ng), (2) 2-ISMN (10 ng), (3) 5-ISMN (10 ng); (C) nitrate esters of pentaerythritol, (1) PETN (5 ng), (2) PETRIN (4.6 ng), (3) PEDN (14 ng).

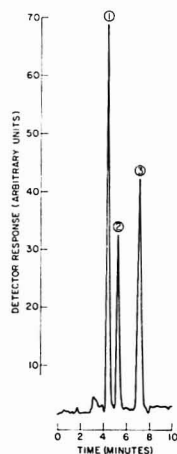


Figure 2. HPLC/TEA analysis of (1) isoribide dinitrate, 10 ng, (2) glycerol trinitrate, 5 ng, and (3) pentaerythritol tetranitrate, 10 ng. used with a mobile phase of isooctane/chloroform/methanol (75:20:5). Figure 2 shows a chromatogram of 10 ng of iso-

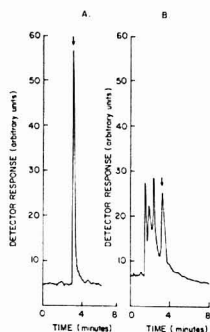


Figure 3. HPLC/TEA analysis of plasma sample fortified with glycerol trinitrate at 3 ppb level: (A) glycerol trinitrate, 2 ng; (B) spiked plasma.

Table II. Recovery of Vasodilators Added to Plasma

ppb added	mean recovery, % ( $\pm$ std dev, $n = 4$ )		
	GTN	ISDN	PETN
1	54.0 $\pm$ 4.0	75.5 $\pm$ 6.4	67.0 $\pm$ 3.8
5	64.5 $\pm$ 6.6	62.0 $\pm$ 4.0	62.8 $\pm$ 3.7
10	77.4 $\pm$ 5.6	80.3 $\pm$ 5.0	67.0 $\pm$ 2.2
20	74.3 $\pm$ 6.7	69.0 $\pm$ 5.0	71.0 $\pm$ 1.2
40	82.0 $\pm$ 8.8	80.0 $\pm$ 4.8	63.3 $\pm$ 4.4
80	80.8 $\pm$ 5.1	64.7 $\pm$ 5.3	72.0 $\pm$ 3.7
overall mean ( $n = 24$ )	72.0 $\pm$ 11.8	71.2 $\pm$ 8.1	67.2 $\pm$ 4.6
$r$	0.9997	0.9929	0.9981

sorbide dinitrate, 5 ng of glycerol trinitrate, and 10 ng of pentaerythritol tetranitrate.

The TEA analyzer has been shown to be a nitrosyl-specific detector, with a linear and dynamic range greater than 6 orders of magnitude (20). For complex matrices such as blood, plasma, or urine, the detector screens out compounds that do not contain nitrosyl groups, thus simplifying the chromatography and data interpretation. Furthermore, for the nitrate esters, the detector response has been shown to vary linearly with the number of nitrosyl-containing functional groups (18). This feature provides an added advantage over other detectors when quantitating a nitrate ester and its metabolites with a known number of nitrosyl groups, even in the absence of authentic standards. The current method has a lower limit of detectability of 0.1 ng for both glycerol trinitrate and pentaerythritol tetranitrate, and 0.2 ng for isosorbide dinitrate at a signal to noise ratio of 3 to 1. This level of sensitivity should be adequate for drug bioavailability studies where less than 1 ppb sensitivity is required. New technologies in HPLC with 3- $\mu$ m column packing materials resulting in over 120,000 theoretical plates/m should further enhance the sensitivity of the method.

To demonstrate the feasibility of the HPLC/TEA method for the determination of nitrate esters, plasma samples were fortified at various levels with glycerol trinitrate, isosorbide dinitrate, and pentaerythritol tetranitrate. Figures 3 and 4 show the typical chromatograms obtained from spiked plasma. The recovery of these nitrate esters from 1 ppb to 80 ppb is summarized in Table II. Although higher recoveries have been reported with other solvents such as petroleum spirit (21), hexane (13), or benzene (22), those extraction procedures were limited to the parent nitrate ester and involved tedious repetitive extractions. The use of ethyl acetate, in addition

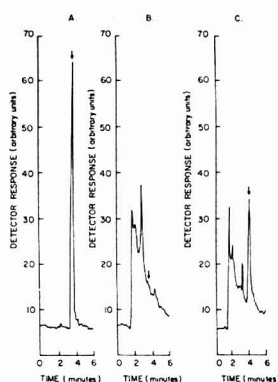


Figure 4. HPLC/TEA analysis of plasma sample fortified with isosorbide dinitrate at 5 ppb level: (A) isosorbide dinitrate, 5 ng; (B) blank plasma; (C) spiked plasma.

Table III. Precision of HPLC-TEA

com- pound	amt in- jected, ng	response $\bar{X}^a$	std dev <sup>b</sup>	% RSD <sup>c</sup>
GTN	1.0	$5.28 \times 10^5$	0.12	2.3
	5.0	$2.77 \times 10^6$	0.11	4.1
	20.0	$1.16 \times 10^7$	0.04	3.5
	50.0	$2.65 \times 10^7$	0.09	3.4
ISDN	1.0	$1.41 \times 10^5$	0.12	8.6
	5.0	$8.25 \times 10^5$	0.61	7.3
	20.0	$3.25 \times 10^6$	0.21	6.5
	50.0	$1.62 \times 10^7$	0.12	7.4
PETN	1.0	$4.41 \times 10^5$	0.25	5.9
	5.0	$2.04 \times 10^6$	0.04	2.2
	20.0	$7.85 \times 10^6$	0.34	4.3
	50.0	$2.08 \times 10^7$	0.05	2.4

<sup>a</sup>  $\bar{X}$  = mean value for five determinations, arbitrary units.

<sup>b</sup> Standard deviation. <sup>c</sup> Relative standard deviation expressed as a percent.

to its ability to simultaneously extract the more polar lower nitrates, is also believed to have a quenching effect on the enzyme which may otherwise degrade the nitrate ester drug, eliciting erroneous results.

Table III summarizes the precision data for GTN, PETN, and ISDN at 1-ng, 5-ng, 20-ng, and 50-ng injection levels, expressed as relative standard deviations (RSD). At the 5-ng injection level, the relative standard deviations are  $\pm 4.1\%$ ,  $\pm 2.2\%$ , and  $\pm 7.3\%$  for GTN, PETN and ISDN, respectively.

During the sample workup procedure, the extract was further clarified by the use of Sep-PAK  $C_{18}$  cartridge to remove many of the proteins, glucuronides, and lipids. This is particularly useful in working with blood samples where the interfering compounds and pigments are retained, resulting in prolonged HPLC column life, and ultimately lower operating cost per sample.

#### ACKNOWLEDGMENT

The isosorbide 2-mononitrate and isosorbide 5-mononitrate were kindly provided by John Markis of Beth Israel Hospital, Boston, MA. We thank Brian Challis and David Fine for many helpful discussions. The Northeast Region Blood Services of Red Cross is gratefully acknowledged for providing fresh frozen plasma samples.

Registry No. ISDN, 87-33-2; GTN, 55-63-0; PETN, 78-11-5; 2-ISMN, 16106-20-0; 1,2-DNG, 621-65-8; 1,3-DNG, 623-87-0;

PETRIN, 1607-17-6; 5-ISMN, 16051-77-7; 2-MNG, 620-12-2; PEDN, 1607-01-8.

# LITERATURE CITED

- (1) Pristera, F.; Hallik, M.; Castelli, A.; Fredericks, W. *Anal. Chem.* **1960**, *32*, 495.
- (2) Whitnack, G. C.; Mayfield, M. M.; Gantz, E. S. C. *Anal. Chem.* **1965**, *37*, 899.
- (3) Di Carlo, F. J.; Crew, M. C.; Sklow, N. J.; Coutinho, C. B.; Nonkin, P.; Simon, F.; Bernstein, A. J. *Pharmacol. Exp. Ther.* **1976**, *153*, 254.
- (4) Di Carlo, F. J.; Crew, M. C.; Haynes, L. J.; Melgar, M. D.; Gala, R. L. *Biochem. Pharmacol.* **1968**, *17*, 2179.
- (5) Reed, D. E.; Akester, J. M.; Prather, J. F.; Tuckosh, J. R.; McCurdy, D. H.; Yeh, C. J. *Pharmacol. Exp. Ther.* **1977**, *202*, 32.
- (6) Crew, M. C.; Gale, R. L.; Haynes, L. J.; Di Carlo, F. J. *Biochem. Pharmacol.* **1971**, *20*, 3077.
- (7) Crew, M. C.; Melgar, M. D.; Di Carlo, F. J. *J. Pharmacol. Exp. Ther.* **1975**, *192*, 218.
- (8) Roseel, M. T.; Bogaert, M. G. J. *Chromatogr.* **1974**, *64*, 364.
- (9) Davidson, I. W. F.; Di Carlo, F. J.; Szabo, E. I. *J. Chromatogr.* **1971**, *57*, 345.
- (10) Assinder, D. F.; Chasseaud, L. F.; Taylor, T. J. *Pharm. Sci.* **1977**, *66*, 775.
- (11) Yap, P. S. K.; McNiff, E. F.; Fung, H. L. *J. Pharm. Sci.* **1978**, *67*, 583.
- (12) Armstrong, J. A.; Marks, G. S.; Armstrong, P. W. *Mol. Pharmacol.* **1980**, *19*, 112.
- (13) Chandler, C. D.; Gibson, G. R.; Boleter, W. T. *J. Chromatogr.* **1974**, *100*, 185.
- (14) Chin, D. A.; Prue, D. G.; Michelucci, J.; Kho, T.; Warner, C. R. *J. Pharm. Sci.* **1977**, *66*, 1143.
- (15) Baake, D. M.; Carter, J. E.; Amann, A. H. *J. Pharm. Sci.* **1977**, *66*, 1143.
- (16) Crouthamel, W. G.; Dorsch, B. J. *Pharm. Sci.* **1979**, *68*, 481.
- (17) Hanemann, R. E.; Erb, R. J.; Stoltman, W. P.; Bronson, E. C.; Williams, E. J.; Long, R. A.; Hull, J. H.; Starbuck, R. R. *Clin. Pharmacol. Ther.* **1981**, *35*.
- (18) Lafleur, A. L.; Morriseau, B. D. *Anal. Chem.* **1980**, *52*, 1313.
- (19) Spangord, R. J.; Keck, R. G. *J. Pharm. Sci.* **1980**, *69*, 444.
- (20) Fine, D. H.; Rufe, F.; Lieb, D.; Rounbehler, D. P. *Anal. Chem.* **1975**, *47*, 1188.
- (21) Doyle, E.; Chasseaud, L. F.; Taylor, T. *Biopharm. Drug Dispos.* **1980**, *1*, 141.
- (22) Malbica, J. O.; Monson, K.; Nelson, K.; Sprissler, R. *J. Pharm. Sci.* **1977**, *66*, 365.

RECEIVED for review June 24, 1982. Accepted October 4, 1982.

## Determination of Phencyclidine and Phenobarbital in Complex Mixtures by Fourier-Transformed Infrared Photoacoustic Spectroscopy

M. G. Rockley,\* M. Woodard, H. H. Richardson, D. M. Davis, N. Purdie, and J. M. Bowen

Department of Chemistry, Oklahoma State University, Stillwater, Oklahoma 74078

Fourier-transformed infrared photoacoustic spectroscopy has been used to quantitate the amounts of controlled substances (phencyclidine and phenobarbital) in substrates such as lactose and parsley. Quantitation to 1% accuracy is demonstrated, although saturation effects might be exhibited in some of the spectra.

Every conceivable analytical technique has been applied to the difficult problem of drug analysis (1). Because drugs are minor constituents in rather complex mixtures, a primary requirement in almost every analysis is to first effectively separate the mixture and, in so doing, concentrate the drug so that it has a concentration which exceeds the limits of detection of the method to be used. Qualitative identification is readily accomplished by the many chromatographic procedures either alone or in tandem with mass spectrometry or, in some cases, by spot tests. Quantitation is less readily accomplished and frequently requires compound derivatization and repeated instrument calibration.

Innovative techniques which can simplify the analytical protocol either by requiring less stringent separation needs or by eliminating subsequent sample preparation steps are valuable in that time, a precious commodity in clinical and criminalistic laboratories, is saved. A recent innovation, for example, is the application of circular dichroism spectropolarimetry (2) to the direct analysis of drugs.

A rapidly emerging technique which has the potential to expedite analysis is photoacoustic spectroscopy (PAS) (3, 4). Its use in the ultraviolet spectral range was described in the early literature and, more recently, reports have appeared for the application of PAS in the mid-infrared range by both dispersive (5-9) and Fourier-transformed methods (FTIR-

PAS) (10-13). The advantages of FTIR-PAS over dispersive methods are well delineated in these articles. They include speed of analysis, high incident power (useful for PAS studies), and frequency multiplexing. The disadvantages of FTIR-PAS are that the sampling depth varies with frequency, there is some difficulty in knowing exactly what to use as a power correcting reference spectrum, and the thermal and optical properties of the samples control the frequency dependence of the PAS signal strength. These difficulties have been discussed in some detail by Krishnan (14) and by Royce et al. (15). These advantages notwithstanding, it was felt that for routine quantitative and qualitative analysis the currently used methods of FTIR-PAS analysis would prove to be a significantly useful tool in the modern forensic analysis laboratory by virtue of the speed of analysis, use of commercially available components, and other features described below.

In this paper we describe the direct quantitative determination of phenobarbital and phencyclidine (PCP) using FTIR-PAS. Sample mixtures, in powdered solid form, were all in-house preparations and were tested for both the qualitative and quantitative capabilities of the method.

### EXPERIMENTAL SECTION

The samples were prepared gravimetrically and made somewhat homogeneous in composition by shaking for 5 min in a Wiggle-bug. Reference FTIR-PAS spectra of the pure components of the various mixtures were stored on disk for subsequent subtraction as will be explained below.

PCP was phencyclidine hydrochloride obtained from NIDA via Research Triangle Institute. Parsley was from a local grocery store. This mixture was coground. Phenobarbital was from Sigma. Lactose was from Aldrich.

The procedure for analysis of the FTIR-PAS spectra has been described elsewhere. There were essentially no new features with the exception of some minor modifications to the cell design. The cell used for these experiments incorporated a Bruel and Kjaer

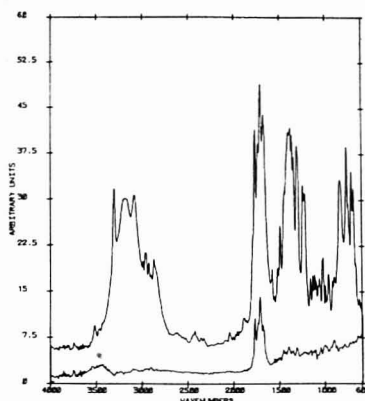


Figure 1. Top spectrum is that of ca. 10 mg of pure phenobarbital with 2000 scans at  $8\text{ cm}^{-1}$  resolution, corrected by reference to a carbon-black spectrum. Bottom spectrum is the residual spectrum from 2000 scans at  $8\text{ cm}^{-1}$  resolution of 12.1% by weight phenobarbital in lactose after subtracting the spectra of the pure components in a 0.12 to 0.88 ratio of phenobarbital to lactose.

4175 0.5-in. foil electret microphone with a 2642 preamplifier and a 2610 battery operated power supply, all of these components being available off the shelf from Bruel and Kjaer. The preamplifier was sealed with rubber cement to prevent acoustic noise pickup from the room. The spectra were all ratioed against a carbon black standard. Since this work was completed, it has emerged in studies by others (16) that carbon black is not such a good reference for FTIR-PAS spectral measurements because it has several spectral features which are not intense but nevertheless present. Because the cell constructed here indicated the presence of no acoustic resonances over the range of audio modulation frequencies present in the FTIR beam, the spectra would just as easily have been corrected for source power variations with wavelength by ratioing to the standard DTGS detector response. An excellent description of the problems associated with spectral correction of FTIR-PAS spectra has been recently published by Royce et al. (15). Therefore, besides band intensity problems associated with specular reflectance and saturation, the pure component spectra reported here have some band intensity errors which may be as much as 5% of the total band intensity. However, while this means that the spectra reported here cannot be used for study of absolute band intensities, they can be used for quantitative purposes because the same reference carbon-black spectrum was used to correct all spectra measured. As a result, the relative errors in using the spectral subtraction methods outlined below prove to be negligible and have not been considered further for the purposes of this work.

Two-component mixtures were made with the compositions of these mixtures being made known to the individual running the FTIR-PAS spectra. In this way a so-called calibration line was inferred. The calibration line was prepared by subtracting the spectra of the individual pure components from the spectra of the mixture and repeating the process until the flattest possible base line was obtained, as shown by Figure 1 for the case of 12.1% by weight phenobarbital in lactose.

Following the experimental derivation of a calibration line or curve (for all cases studied here the set of points was well correlated with a straight line) a few samples ("blinds") were analyzed in which the concentration was known to the preparator but not to the analyst. Those points are represented by a "U" prefix in Tables I and II.

## RESULTS AND DISCUSSION

An illustration of some typical spectra is given in Figure 1 for the case of a 12% by weight phenobarbital in lactose

Table I. Analysis of Phenobarbital<sup>a</sup>

sample	% calcd	% given
1	8.4	7.5
2	19.2	19.8
3	26.7	27.1
4	40.8	40.7
5	36.8	37.1
U1	12.0	12.3
U2	10.8	9.9
U2	10.0	9.9
U3	11.3	12.3
U3	12.8	12.3
U4	12.2	10.7
U5	36.8	39.9

<sup>a</sup> Calculated (by FTIR-PAS) and given weight percentages of phenobarbital in lactose. U1-U5 are "unknowns" with typical precisions of independent measurements of the same sample as indicated.

Table II. Analysis of Phencyclidine<sup>a</sup>

sample	% calcd	% given
1	4.0	4.1
2	9.6	9.7
3	7.2	7.1
5	3.4	3.3
6	12.2	12.2
U1	13.8	14.9
U2	8.8	6.0
U3	14.5	17.9
U4	5.8	3.5
U5	14.3	13.1

<sup>a</sup> Calculated (by FTIR-PAS) and given weight percentages of PCP on parsley. Typical sample weights were about 10<sup>4</sup> mg.

system. The top spectrum is that of 10 mg of pure phenobarbital. The bottom spectrum is that which remains after  $0.12 \times$  the pure lactose spectrum and  $0.88 \times$  the pure phenobarbital spectrum are subtracted from the spectrum of the 12.1% by weight phenobarbital in lactose mixture. It can be seen that the base line is essentially flat with the notable exception of the band at ca.  $1700\text{ cm}^{-1}$ . The flatness of this base line was estimated by eye and was not further analyzed by any computer algorithm, although with the purchase of suitable software this could also have been done. After several trials it was determined that the band at  $1700\text{ cm}^{-1}$  which remains outstanding after spectral subtraction of the component spectra is not quantitatively related to the amount of phenobarbital in the mixture. While the exact cause of this outstanding feature has not been determined here, it is hypothesized that it could be due to a number of different phenomena. It could be that the pure component spectrum of phenobarbital was measured with a sample which had a slightly different grain size distribution than that present in the mixtures. In such a case, the amount of reflected light might be different at that particular band. That is, the phenomenon would correspond to some sensitivity of the photoacoustic spectrum to the amount of reflected light, especially for the case of intense transitions where the amount of scattered or reflected light will be greatest. Another possible cause for this phenomenon which also could be explained on the basis of variations in the distribution of grain sizes is the occurrence of saturation (14, 16). Since the presence of saturation in the generation of the photoacoustic signal is dependent on the ratio of the thermal to the optical thickness of the sample, the appearance of this anomaly in band intensity could be associated with differing amounts of signal saturation present in the pure and mixed samples for absorption into this particular band. As to whether or not either

of these two reasons is correct requires the analysis of a series of samples in which the grain size distribution of the pure and mixed samples are tightly specified. Even then it is not clear that the relative surface areas for the two samples would be the same. Nevertheless, it might be that the amplitude of this anomalous feature would decrease with decreasing grain size in which case at least one of these two proposed origins might apply. A third reason may be associated with photometric nonlinearity for intense bands. Finally, it is possible that Kubelka-Munk corrections, which are necessary to correct band intensities for reflectivity variations, might prove useful in distinguishing saturation from reflection problems.

Despite these difficulties, the relative compositions of the various mixtures were obtained by spectral subtraction procedures. Adequate subtraction was inferred by assessing the flatness of the subtracted spectral base line in regions outside of those containing intense features. Table I contains the results obtained for the analysis of phenobarbital and lactose. In all cases for the phenobarbital and lactose system the measured weight percentages are accurate to within 1% and have a precision of better than 1% as shown by multiple but independent analyses of the same unknowns. For the two measurements of the same unknown, two independent samples were obtained from the container of sample provided.

The PCP on parsley system was analyzed in similar fashion and the data are described in Table II. The accuracy of the measured results here is not quite as good as for the case of phenobarbital and lactose. That is to be expected, however, since the samples of PCP on parsley cannot be made nearly as homogeneous as the phenobarbital and lactose system.

As a result, sampling errors become more significant. The presence of two strong bands centered at  $1600\text{ cm}^{-1}$  and  $1100\text{ cm}^{-1}$  in the spectrum of parsley could not be subtracted totally from the spectra of the mixtures, indicating the presence of the saturation and reflectivity problems also apparent in the phenobarbital-lactose system. The parsley was also incompletely dried. This resulted in the introduction of significant quantities of water vapor into the PAS cell, despite the presence of molecular sieves in the sample compartment. It is clear that the quantitative determination and qualitative analysis of these intractable drug mixtures are feasible by FTIR-PAS over the range of concentrations studied here. However, it is also apparent that, because of saturation and reflectance effects, technical improvements in the methodology

(an example might be careful spectral reflectance corrections) must be introduced before very complex multicomponent solid samples can be analyzed with ease. These phenomena manifest themselves in the difficulty associated with quantitation but will be less important in qualification.

In conclusion, the data presented here demonstrate the feasibility of rapid quantitative analysis of difficult samples (e.g., PCP on parsley) commonly encountered in the forensic laboratory. It is to be stressed that the samples are not adulterated in any way. It is therefore clear that this technique has qualitative and quantitative analytical capabilities. In addition to finding use in the forensic laboratory, it may find use wherever quantitation of solid mixtures is required such as in the analysis of food additives or pharmaceuticals and pesticides on grains.

#### ACKNOWLEDGMENT

We thank the National Institute for Drug Abuse and the Research Triangle Institute for providing the standard samples.

Registry No. phencyclidine, 77-10-1; phenobarbital, 50-06-6; lactose, 63-42-3.

#### LITERATURE CITED

- (1) Clarke, E. G. C. "Isolation and Identification of Drugs"; The Pharmaceutical Press: London, 1978; Vol. 1.
- (2) Bowen, J. M.; Crone, T. A.; Head, V. L.; McMorrow, H. A.; Kennedy, P. K.; Purdie, N. J. *Forensic Sci.* **1981**, *26* (4), 664-670.
- (3) Rosenzweig, A. "Photoacoustics and Photoacoustic Spectroscopy"; Wiley-Interscience: New York, 1980; p 309.
- (4) Pao, Y. H. "Photoacoustic Spectroscopy and Detection"; Academic: New York, 1977; p 244.
- (5) Low, M. J. D.; Parodi, G. A. *Spectrosc. Lett.* **1978**, *11*, 581.
- (6) Low, M. J. D.; Parodi, G. A. *Infrared Phys.* **1980**, *20*, 333.
- (7) Low, M. J. D.; Parodi, G. A. *Appl. Spectrosc.* **1980**, *34*, 76.
- (8) Low, M. J. D.; Parodi, G. A. *J. Mol. Struct.* **1980**, *61*, 119.
- (9) Low, M. J. D.; Parodi, G. A. *Spectrosc. Lett.* **1980**, *13*, 663.
- (10) Rockley, M. G. *Chem. Phys. Lett.* **1979**, *69*, 455.
- (11) Vidrine, D. W. *Appl. Spectrosc.* **1980**, *34*, 313.
- (12) Lauter, G.; Huneke, J. T.; Royce, B. S. H.; Teng, Y. C. *Appl. Phys. Lett.* **1980**, *37*, 617.
- (13) Rockley, M. G.; Devlin, J. P. *Appl. Spectrosc.* **1980**, *34*, 407.
- (14) Krishnan, K. *Appl. Spectrosc.* **1981**, *35*, 549.
- (15) Teng, Y. C.; Royce, B. S. H. *Appl. Opt.* **1982**, *21*, 77.
- (16) Riseman, S. M.; Eyring, E. M. *Spectrosc. Lett.* **1981**, *14* (3), 163-185.

RECEIVED for review July 21, 1982. Accepted October 4, 1982.  
Supported in part by ARO Contract No. DAAG 29 81 K009  
and in part by NSF Grant No. CHE-7909388



# Sequential Determination of L-Lactate and Lactate Dehydrogenase with Immobilized Enzyme Electrode

Fumio Mizutani,\* Kanji Sasaki, and Yukio Shimura

Research Institute for Polymers and Textiles, 1-1-4 Yatabe-Higashi, Tsukuba, Ibaraki 305, Japan

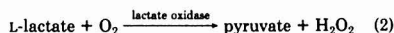
An L-lactate selective electrode consisting of an immobilized lactate oxidase layer and a Clark oxygen electrode is used for the sequential determination of L-lactate and lactate dehydrogenase (LDH) in the same sample. L-Lactate ( $5 \times 10^{-4}$  to  $5 \times 10^{-2}$  M in the final concentration) is determined from the decrease in the electrode current after the addition of the sample to a buffer solution. LDH (1–300 IU/L in the final activity) is then determined from the decreasing rate of the current which is induced by the enzymatic L-lactate production after the addition of pyruvate and NADH to the sample-containing solution. The sequential determination is completed within ca. 7 min. The precisions are 1.4% for L-lactate and 2.8% for LDH. The electrode can be used for more than 2 weeks and 140 sequential determinations. Its application for human sera is also described.

Lactate dehydrogenase (E.C. 1.1.1.27, L-lactate:NAD<sup>+</sup> oxidoreductase, abbreviated LDH) catalyzes the L-lactate producing reaction



Total LDH activity in serum is of clinical importance in differentiating disorders, such as acute myocardial infarction, congestive heart disease, pernicious anemia, and hepatitis. Although some spectrophotometric methods (1–5) have been proposed for the routine assay of LDH, electrochemical monitoring of the enzyme has the advantage of providing simple and rapid assays. Smith and Olson (6) have described an electrochemical method which is based on the amperometric detection of an NADH-coupled reaction, but the method requires an electrode system with a particular and complex structure.

An enzyme electrode is considered convenient because of its simple structure and also because of its substrate specificity (7, 8). Recently, Karube et al. (9) have reported an amperometric L-lactate sensing electrode consisting of a Clark oxygen electrode and an immobilized layer of lactate oxidase (L-lactate:oxygen oxidoreductase) which catalyzes the reaction



The electrode is expected to be applicable to the determination of LDH by monitoring the catalytic production rate of L-lactate, i.e., based on the procedure of "amperometric rate assay" (10, 11). Further, application of the electrode provides the method for sequential determination of L-lactate and LDH in a sample; before the determination of LDH in a sample-containing solution, L-lactate in the same solution can be measured by the same electrode. The determination of L-lactate in serum is also clinically important, e.g., abnormally high levels of L-lactate produced by slight exertion are indicative of anoxia which includes congestive heart disease, coronary artery disease, and pneumonia. Therefore, sequential determination is very useful for clinical laboratories. In this

paper, such a new application of the enzyme electrode is described.

## EXPERIMENTAL SECTION

**Materials.** The enzymes used were lactate oxidase (from *Pediococcus* sp., 17 IU/mg, Toyo Jozo), LDH (E.C. 1.1.1.27, from hog muscle, 550 IU/mg, Böhringer Mannheim), and glutamate pyruvate transaminase (E.C. 2.6.1.2, from pig heart, 80 IU/mg, Böhringer Mannheim). Commercially available lyophilized human sera were used (Böhringer Mannheim or Ortho Diagnostics). Pyruvate (as sodium salt), L-lactate (as lithium salt), NADH, and NAD<sup>+</sup> were obtained from Sigma Chemical Co. and were used without further purification. KH<sub>2</sub>PO<sub>4</sub> and K<sub>2</sub>HPO<sub>4</sub> were reagent grade and were used as received. Deionized and twice-distilled water was used for all experiments.

**Assembly of the Enzyme Electrode System.** An enzyme solution (200  $\mu$ L, containing 40 IU of lactate oxidase in 0.1 M phosphate buffer, pH 7.0) was dropped onto a porous filter membrane (Millipore, Type GS, 25-mm diameter) which was placed on the Teflon membrane of a Clark oxygen electrode (Ishikawa Manufacturing, battery type with a platinum cathode of 12-mm diameter). The filter membrane was covered with a dialysis membrane (Visking, 40 mm diameter) and then the three membranes were fastened with rubber rings so that the enzyme was trapped in the filter membrane which was sandwiched between two other membranes. The enzyme electrode thus prepared was immersed in 0.1 M phosphate buffer solution (10 mL, pH 5.5–7.7) in a cylindrical cell (volume ca. 30 mL). The solution was saturated with air by blowing it onto the surface at a flow rate of ca. 100 mL/min while stirring magnetically. Temperature of the solution was kept at  $25.0 \pm 0.1^\circ\text{C}$ . The current from the enzyme electrode was recorded on a recorder (Yokogawa Electric Works, Model 3066) through a 2-k $\Omega$  resistance. The enzyme electrode was stored in 0.1 M phosphate buffer solution (pH 7.0) at  $5^\circ\text{C}$  when not in use.

**Procedures.** For the determination of L-lactate in the sample, the decrease in the electrode current as the result of the decrease in dissolved oxygen associated with the addition of the sample to the buffer solution (eq 2) was measured. For the (sequential) determination of LDH, pyruvate and NADH were added to the sample-containing buffer solution after the electrode current reached a steady-state value, and the decrease in the current caused by their addition was recorded. NADH should not be added to the buffer solution before the addition of the sample when it contains L-lactate in addition to LDH, since an excessive decrease in the electrode current against the concentration of L-lactate in the sample is brought about by the circulating enzymatic reactions between L-lactate and pyruvate: pyruvate is produced via the oxidation of L-lactate with the immobilized lactate oxidase (eq 2), and the pyruvate thus produced is reoxidized to L-lactate with LDH in the sample in the presence of NADH (eq 1). Therefore, the LDH reaction was initiated by the final addition of NADH in the present electrode system.

**Assays of L-Lactate and LDH.** L-Lactate and LDH were respectively assayed by the method of Noll (12) and of Henry et al. (2). A Hitachi Model 323 spectrophotometer was used for these assays.

## RESULTS AND DISCUSSION

**Response for L-Lactate.** Figure 1 shows response curves of the enzyme electrode at different L-lactate concentrations at pH 7.4. The current began to decrease several seconds after the addition of L-lactate and restored a steady-state value

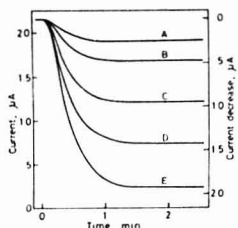


Figure 1. Typical response curves of the enzyme electrode at pH 7.4 to (A) 0.1 mM, (B) 0.2 mM, (C) 0.4 mM, (D) 0.6 mM, and (E) 0.8 mM L-lactate.

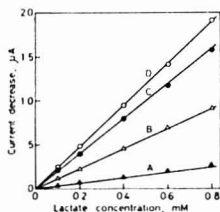


Figure 2. Relationships between the current decrease and the concentration of L-lactate at pH 7.4. The times after the addition of L-lactate are (A) 10 s, (B) 20 s, (C) 40 s, and (D) 2 min (steady state).

within ca. 1.5 min. Figure 2 shows the relationships between the current decrease (the difference between the currents before and after the addition of the sample) and L-lactate concentration at intervals of 10 s, 20 s, 40 s, and 2 min (in steady state) after addition of the substrate. Linear relationships were obtained for all intervals up to the concentration being 0.8 mM. Therefore, the current decrease,  $\Delta i$  (in  $\mu A$ ), can be expressed as

$$\Delta i = 23.7c[1 - f(t)] \quad (3)$$

where  $c$  is the concentration of L-lactate (in mM) and  $f(t)$  is a (concentration-independent) function which monotonously decreases with time from unity at  $t = 0$  to zero at  $t \geq 1.5$  min. The result from digital simulation concerning an amperometric enzyme electrode has indicated that a linear relationship between  $\Delta i$  and  $c$  is given at any interval as in eq 3 when the activity of the immobilized enzyme is very high (13).

The minimum concentration of L-lactate which could be determined was ca. 5  $\mu M$  (signal in steady-state to noise, 5; pH 7.4). The relative standard deviation was 1.4% for 10 successive measurements of the current decrease in steady-state on 0.2 mM L-lactate at pH 7.4.

The current decrease for L-lactate was almost independent of pH between 6.0 and 7.5. Hence, further experiments were carried out at pH 7.4, i.e., LDH's optimum pH for the production of L-lactate (2, 14). Karube et al. (9) have also reported that the optimum pH of the electrode was around 7.

**Response for LDH.** Addition of NADH to the buffer solution containing LDH and pyruvate caused a decrease in the current as shown in Figure 3; the current decreased linearly with time at least from 1.5 to 4 min after the addition of NADH. The rate of current decrease in the linear region is expected to be proportional to the activity of LDH as in the cases described previously (10, 11). Since the rate of current decrease depended on the concentrations of both pyruvate and NADH in addition to the activity of LDH, the effect of their concentrations on the rate was firstly examined to obtain the optimal condition for the enzyme assay. Figure 4 shows

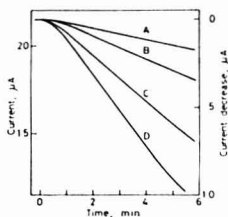


Figure 3. Typical response curves of the enzyme electrode after the addition of 0.8 mM NADH to the buffer solution (pH 7.4) containing 1.0 mM pyruvate and LDH. LDH activities are (A) 14 IU/L, (B) 28 IU/L, (C) 56 IU/L, and (D) 84 IU/L.

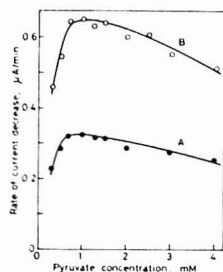


Figure 4. Relationships between the rate of current decrease and pyruvate concentration at pH 7.4 and NADH concentration 0.8 mM. LDH activities are (A) 14 IU/L and (B) 28 IU/L.

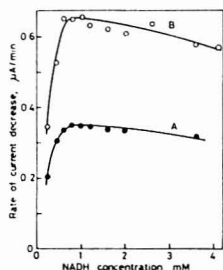


Figure 5. Relationships between the rate of current decrease and NADH concentration at pH 7.4 and pyruvate concentration 1.0 mM. LDH activities are (A) 14 IU/L and (B) 28 IU/L.

the change in the rate of current decrease against the change in the concentration of pyruvate at a fixed NADH concentration of 0.8 mM for LDH-containing solutions with the activities of 14 and 28 IU/L. For both LDH activities, maximum rates are given in the range of pyruvate concentration from 0.6 to 1.5 mM. Figure 5 shows the effect of the concentration of NADH on the rate of current decrease at a fixed pyruvate concentration of 1.0 mM for the same LDH-containing solutions as given in Figure 4. The NADH concentrations between 0.5 and 1.5 mM give maximum rates. Therefore, the concentrations of pyruvate and NADH were adjusted to 1.0 and 0.8 mM, respectively. The optimal concentrations of both substances in the present system are fairly higher than those for a conventional method, i.e., the method which involves spectrophotometric monitoring of the decreasing rate of NADH (1, 2, 14); Bergmeyer and Bernt (14)

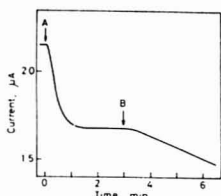


Figure 6. Typical response curve of the enzyme electrode for a sample containing both L-lactate (0.2 mM in the final concentration) and LDH (28 IU/L in the final activity): (A) time when the sample is added to the buffer solution (pH 7.4), (B) time when pyruvate (1.0 mM) and NADH (0.8 mM) are successively added to the sample-containing buffer solution.

have described that the optimal concentration ranges of pyruvate and NADH are 0.3 to 0.6 mM and 0.05 to 0.5 mM, respectively, for the method. However, the reason for the inconsistency between the optimal condition for the present method and that for the spectrophotometric one (1, 2, 14) has not yet been known.

The rate of current decrease in the linear region,  $\Delta i/\Delta t$  (in  $\mu\text{A}/\text{min}$ ), was proportional to the activity of LDH,  $a$  (in IU/L), up to 300 IU/L

$$\Delta i/\Delta t = 0.0232a \quad (4)$$

A very similar relationship between  $\Delta i/\Delta t$  and  $a$  to eq 4 can be derived from eq 3 by introducing the transfer function of the electrode system. Namely, the electrode response for LDH is predictable from that for L-lactate as follows. The current decrease against L-lactate (eq 3) is the output from the electrode system corresponding to the input of the L-lactate concentration which is expressed as  $cu(t)$  ( $u(t)$  is the function) in the bulk of the solution. Hence, the transfer function,  $G(s)$ , is given as

$$G(s) = \mathcal{L}[23.7c(1 - f(t))]/\mathcal{L}[cu(t)] = 23.7[1 - \mathcal{L}[f(t)]] \quad (5)$$

where  $\mathcal{L}[\ ]$  denotes the Laplace transform and  $s$  is a parameter. The activity of a IU/L LDH is the value which causes a L-lactate-producing rate of a  $\mu\text{M}/\text{min}$  at 25 °C under optimal conditions (14). Thus the bulk concentration of L-lactate (input) produced with LDH at  $t$  min after the enzymatic reaction being initiated is expressed as  $10^{-3}at$  mM. The current decrease (output),  $\Delta i$ ,  $\mu\text{A}$ , corresponding to the above input is given as

$$\Delta i = \mathcal{L}^{-1}[G(s) \cdot \mathcal{L}[10^{-3}at]] = 0.0237a \left\{ t - \int_0^t f(t) dt \right\} \quad (6)$$

where  $\mathcal{L}^{-1}[\ ]$  is the inverse Laplace transform. Since  $\int_0^t f(t) dt$  becomes constant for  $t \geq 1.5$  min,  $\Delta i$  vs.  $t$  curve becomes linear with its slope being  $0.0237a$   $\mu\text{A}/\text{min}$ . This value is very close to the slope of  $0.0232a$   $\mu\text{A}/\text{min}$  written in eq 4. It is indicated from the above result, concerning the determination of LDH, that only a calibration curve for L-lactate is required and that the calibration for LDH itself can be omitted. This is practically useful, especially for carrying out the sequential determination of L-lactate and LDH, which is described in the following sections.

The minimum activity of LDH which could be determined was ca. 1 IU/L (signal at 4 min after the addition of NADH to noise, 5). The relative standard deviation was 2.6% in 10 successive measurements of the rate of current decrease on a constant activity of LDH (28 IU/L).

**Sequential Determination of L-Lactate and LDH.** Figure 6 shows a typical response curve of the enzyme elec-

Table I. Comparison of Results Obtained for L-Lactate and LDH in Serum

serum no.	concn of L-lactate in serum, mM		activity of LDH in serum, IU/L	
	present method	spectrophotometric method (12)	present method	spectrophotometric method (3)
1	1.37	1.41	138	137
2	3.33	3.15	349	340
3	1.57	1.48	240	248
4	2.10	2.27	414	407
5	1.73	1.67	315	334
6	1.37	1.34	199	193
7	1.52	1.44	166	170

trode, where a sample containing both L-lactate (0.2 mM in the final concentration) and LDH (28 IU/L in the final activity) was added to the buffer solution and, after 3 min, 1.0 mM pyruvate and 0.8 mM NADH were successively added to the sample-containing buffer solution. The current decrease before the addition of NADH and the rate of current decrease 1.5 to 4 min after the addition are considered to correspond to the concentration of L-lactate and the activity of LDH, respectively. The current decrease for L-lactate at a fixed concentration of 0.2 mM did not change in the presence of LDH within its activity range of 0 to 300 IU/L. The rate of current decrease for LDH at a fixed activity of 28 IU/L was not affected appreciably by the coexisting L-lactate within the concentration range of 0 to 0.5 mM; the LDH rate measurement gave the exact activity of the enzyme when the electrode current is more than  $10 \mu\text{A}$  before the measurement. A discernible lowering of the rate against the LDH activity (more than ca. 5% in relative response) is brought about when the L-lactate concentration is more than 0.5 mM. The sequential determination of L-lactate and LDH can be, therefore, carried out with adequate precision when the concentration of L-lactate is smaller than 0.5 mM.

**Application and Stability of the Enzyme Electrode.** The present sequential determination method was applied for human serum, and the obtained L-lactate concentration and LDH activity were compared with the results obtained by the method of Noll (12) and of Henry et al. (2) each to each. In the present method, 0.5 mL of serum was added to 9.5 mL of the buffer solution. The obtained results, summarized in Table I, agreed satisfactorily for both L-lactate and LDH; the correlation coefficients between the present method and the conventional methods (2, 12) were 0.988 for L-lactate and 0.995 for LDH concerning the seven samples given in Table I.

When the enzyme electrode once used for the sequential determination of L-lactate and LDH in serum was rinsed in water and then dipped in the buffer solution without serum, the current returned to its initial level within 2 min. Therefore, the total cycle time per sequential determination of serum was less than 10 min.

The long-term stability of the enzyme electrode was examined; the sequential determination of L-lactate (0.2 mM) and LDH (28 IU/L) in a solution was carried out 10 times a day, every day for 3 weeks. Average values of both the current decrease (in steady state) for L-lactate and the rate of current decrease for LDH in 10 successive measurements did not reduce even after 2 weeks as shown in Figure 7. The reduced responses after more than 2 weeks are considered attributable to slow denaturation of the immobilized enzyme. Some contamination of the enzyme by bacteria or fungi might also be responsible for the reduced responses, although their growth was not obviously detected.

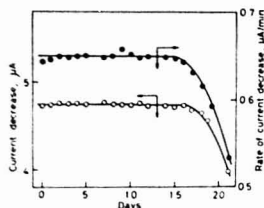


Figure 7. Long-term stability of the enzyme electrode. The current decrease (in steady-state) for L-lactate (0.2 mM) and the rate of current decrease for LDH (28 I.U./L) in a solution are sequentially measured as shown in Figure 6. Each average value for 10 successive measurements per day is plotted against days after the preparation of the enzyme electrode.

#### ACKNOWLEDGMENT

The authors are grateful to Toyo Jozo Co. for supplying lactate oxidase.

Registry No. LDH, 9001-60-9; L-lactate, 79-33-4; lactate oxidase, 9028-72-2.

#### LITERATURE CITED

- (1) Wroblewski, F.; La Due, J. S. *Proc. Soc. Exp. Biol. Med.* **1955**, *90*, 210-213.
- (2) Henry, R. J.; Chiamori, N.; Golub, O. J.; Berkman, S. *Am. J. Clin. Pathol.* **1960**, *34*, 381-396.
- (3) Cabaud, P. G.; Wroblewski, F. *Am. J. Clin. Pathol.* **1958**, *30*, 234-236.
- (4) Morgenstern, S.; Flor, R.; Kesseler, G.; Klein, B. *Anal. Biochem.* **1985**, *13*, 149-161.
- (5) Zimmerman, R. L., Jr.; Gullbault, G. G. *Anal. Chim. Acta* **1972**, *58*, 75-81.
- (6) Smith, M. D.; Olson, C. L. *Anal. Chem.* **1974**, *46*, 1544-1547.
- (7) Gullbault, G. G. "Handbook of Enzymatic Methods of Analysis"; Marcel Dekker: New York, 1976; pp 460-510.
- (8) Carr, P. W.; Browers, L. D. "Immobilized Enzyme in Analytical and Clinical Chemistry"; Wiley: New York, 1980; pp 197-310.
- (9) Karube, I.; Matsunaga, T.; Teraoka, N.; Suzuki, S. *Anal. Chim. Acta* **1980**, *119*, 271-275.
- (10) Mizutani, F.; Tsuda, K.; Karube, I.; Suzuki, S.; Matsumoto, K. *Anal. Chim. Acta* **1980**, *118*, 65-71.
- (11) Mizutani, F.; Tsuda, K. *Anal. Chim. Acta* **1982**, *139*, 359-362.
- (12) Noll, F. *Biochem. Z.* **1966**, *346*, 41-49.
- (13) Mell, D. L.; Maloy, J. T. *Anal. Chem.* **1975**, *47*, 299-307.
- (14) Bergmeyer, H. U.; Bent, E. In "Method of Enzymatic Analysis", 4th ed.; Bergmeyer, H. U., Ed.; Verlag Chemie-Academic Press: New York and London, 1974; Vol. 2, pp 574-579.

RECEIVED for review July 21, 1982. Accepted October 4, 1982.

## Determination of Molecular Weight Distribution of Aromatic Components in Petroleum Products by Chemical Ionization Mass Spectrometry with Chlorobenzene as Reagent Gas

L. Wayne Steck

Chemical Thermodynamics Division, Center for Chemical Physics, National Bureau of Standards, Washington, D.C. 20234

A chemical ionization mass spectrometric technique for direct determination of the molecular weight distributions of the major aromatic components in liquid fuels and other petro-products is discussed. The basic mechanism involves selective charge exchange reactions between chlorobenzene cations and the substituted benzenes and naphthalenes present in the sample. Chlorobenzene also serves as the solvent for the fuel, and screening of successive samples can be carried out with a 3-min turn-around time. Depending upon conditions, the paraffinic components present in the fuel are absent in the resulting mass spectrum.

In spite of the vigorous growth in the application of chemical ionization (CI) mass spectrometry for analytical purposes (1), most of the attention has focused on the utilization of GC/MS techniques. With respect to the specific problem of oil and petroproduct analysis by CI, studies which involve the introduction of unfractionated bulk samples directly into the mass spectrometer (other than GC/MS) have been restricted to the OH<sup>-</sup> screening of aromatics (2) and the screening of organo sulfur compounds using triple quadrupole MS (3). The present study was undertaken to develop rapid CI methods, requiring no prior sample treatment, which could provide quantitative information concerning aromatic components in liquid fuels and petroproducts. The basic method utilizes an

appropriate solvent(s) for the untreated sample as the source of the reagent ions for the measurement.

#### EXPERIMENTAL SECTION

All measurements were carried out with the NBS high-pressure photoionization mass spectrometer, which was modified for this study by incorporating a 0-5-kV electron gun to provide electron impact ionization under typical analytical CI conditions. Unless otherwise indicated, all spectra were recorded by using this auxiliary gun at source temperatures of 150-200 °C (423-473 K). Samples for study were syringe-injected and vaporized into a 3-L evacuated Pyrex reservoir (450 K) which was interfaced to the mass spectrometer via a micrometering valve. The other essential features of the system have been described previously (4).

#### RESULTS AND DISCUSSION

**Solvent Selection.** The selection of solvents for use as sources of reagent ions was based on the satisfaction of the following criteria:

- (1) It must be a reasonably volatile liquid in which the important components of the sample are soluble.
- (2) It must not fragment extensively following electron impact ionization under CI conditions.
- (3) The ion(s) produced initially from the solvent either must be unreactive toward the solvent vapor or must react in a well-specified manner giving a relatively simple, well-characterized, and reproducible reagent ion spectrum.
- (4) The solvents must be relatively free of those impurities which are likely to be significant components in the samples

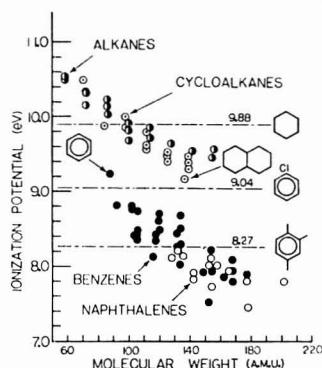


Figure 1. Ionization potentials of certain classes of organic molecules as a function of their molecular weight. Some specific molecules are included for reference.

to be screened and be readily available and in a condition to be used essentially as supplied (no elaborate purification required).

(5) The products of the CI interactions must be unreactive toward the bulk solvent vapor.

(6) The reagent ions must react with each sample component to give, ideally, product ions which are characteristic of that particular component and are easily related to the neutrals from which they were derived. In order to simplify the interpretation, we decided to restrict the solvent(s) to those which give reagent ions which react to yield the corresponding molecular ion ( $M^+$ ) of the component via a charge transfer mechanism:

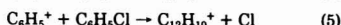
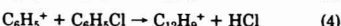


Figure 1 displays the ionization energies or ionization potentials (IP's) of several classes of organic molecules as a function of their molecular weight. Some specific molecules are identified for reference. The important feature of Figure 1 is the gap which exists between the IP's (5) of aliphatic and aromatic hydrocarbons. With the exception of benzene (IP = 9.24 eV), the IP's of aromatic hydrocarbons are all  $\leq 8.82$  eV (toluene). On the other hand, the lowest reliable IP which has been determined for a saturated hydrocarbon is that of *trans*-decalin, 9.14 eV. Therefore a careful search was made for solvents which have IP's  $\leq 9.1$ –9.2 eV, since, to a first approximation, the resulting molecular ions should react only with the aromatic components in liquid fuels.

Benzene, although it has been successfully used as a reagent gas in GC/MS applications (6, 7), as well as toluene and the xylenes (IP's 8.48–8.58 eV) were all found to be unsuitable due to relatively high impurity levels ( $>1$  part in  $10^4$ ) of higher molecular weight alkyl-substituted benzenes, rendering them useless for the screening of lighter fuels. Heterocyclics, such as substituted pyridines, which have appropriate IP's and are relatively stable toward ionic fragmentation following electron impact ionization, undergo protonation and cannot participate in reaction 1. Some olefins, such as cyclohexene (IP = 8.95 eV) were also investigated but were found to fragment excessively and produce condensation ions which were totally unreactive.

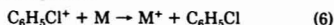
The primary solvent eventually chosen was reagent grade chlorobenzene. It has an appropriate IP (9.04 eV), is free from impurities which would mask  $M^+$  ions from aromatics, and is an excellent solvent for fuels and petroproducts. At CI

pressures in excess of 35–40 mtorr of pure chlorobenzene at 150–200 °C, the following mass spectrum is obtained (normalized to  $m/z$  112,  $C_6H_5^{35}Cl^+ = 100$ ):  $m/z$  112, 100;  $m/z$  113, 11.1;  $m/z$  114,  $C_6H_5^{37}Cl^+$ , 32.5;  $m/z$  115, 5.0;  $m/z$  128,  $C_{10}H_8^+$ , 6.0;  $m/z$  152,  $C_{12}H_8^+$ , 4.1;  $m/z$  153,  $C_{12}H_9^+$ , 11.6; and  $m/z$  154,  $C_{12}H_{10}^+$ , 5.6. The higher mass peaks result from the following reactions involving fragment ions:



With the exception of the primary product ions at  $m/z$  128 (same as naphthalene) and  $m/z$  154 (same as ethanonaphthalenes), there are no peaks in the reagent ion spectrum which would mask signals from major aromatic components in petroproducts. Approximately 85% of the total ionization is in the molecular ion,  $C_6H_5Cl^+$  ( $m/z$  112–115).

**Sensitivity Measurements.** The utility of  $C_6H_5Cl^+$  ( $CB^+$ ) as a reagent ion depends critically upon its reactivity toward various classes of organic compounds. Therefore an extensive evaluation of the process



was carried out to define the relative sensitivities for different types of M (the relative sensitivity for molecules  $M_1$  and  $M_2$  is defined as the ratio of the intensities or peak heights of the corresponding molecular ions,  $M_1^+$  and  $M_2^+$ , obtained in equimolar mixtures of  $M_1$  and  $M_2$  in chlorobenzene) under CI conditions. These measurements were completed as follows:

(1) mixtures of known composition of three or four compounds (minimum stated purity, 96%) having different molecular weights were prepared and diluted to approximately 1 part in  $10^4$ – $10^5$  of CB.

(2) A 100- $\mu$ L portion of this mixture was then injected into the sample reservoir and the leak rate adjusted to maintain a total pressure of 0.1 torr in the CI chamber.

(3) The composite spectrum was then recorded (usually three or four scans) and inspected to verify that the expected  $M^+$  ions were the only products of the CI reaction. The chamber pressure was then decreased by a factor of 2 (three more scans) and then increased by a factor of 4 (three more scans), and the relative  $M^+$  peak heights compared to ensure that no secondary reactions were occurring in the ion source.

(4) The inlet reservoir was then evacuated, followed by the injection of a different mixture containing one component in common with the prior sample. The scanning sequence was repeated, and a network of relative sensitivities assembled by cross-comparison of many such mixtures containing different additives.

Conditions were always adjusted to provide a composite mass spectrum in which the sum of the intensities of the  $M^+$  ions was  $\leq 10\%$  of the intensity of  $CB^+$  at the time of the determination. This was also the case during the screening of fuel and petroproduct samples. Higher conversions ( $>10\%$ ) to  $M^+$  ions sometimes gave a distorted spectrum due to consecutive charge exchange reactions involving  $M^+$  ions and M-type neutrals present in the mixtures.

The  $CB$  CI sensitivities for a variety of substituted benzenes and naphthalenes, as well as some substituted indans and tetralins, plotted as a function of the molecular weight of M, are shown in Figure 2 (see legend for class identification). All values are normalized to  $m/z$  142 from 1-methylnaphthalene = 1.00. The pseudomonotonic decrease in apparent sensitivity vs. molecular weight, which is clearly evident in the alkylbenzene data, is ascribed to detector response characteristics rather than an actual reduced reactivity of  $CB^+$  toward the

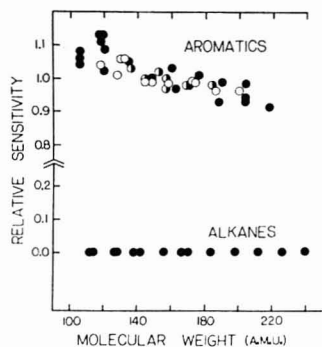
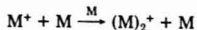


Figure 2. Relative sensitivities in chlorobenzene CI toward aromatic and aliphatic hydrocarbons: (●) alkylbenzenes, including indans and tetralins; (○) phenylolefins; (◐) substituted naphthalenes.

higher molecular weight members of given families of hydrocarbons. This is assumed to be true since the electron multiplier, which is of the Cu-Be dynode-type, exhibits a response which is approximately proportional to the inverse of the square root of the mass of the impacting ion for hydrocarbon ions.

There are two very important features of Figure 2. Firstly, it would appear that different families of substituted aromatics do not show significantly different relative sensitivities as a function of molecular weight when  $CB^+$  is used as the reagent ion. This implies that charge exchange to give  $M^+$  is taking place at every encounter, and since the relative collision coefficients between any given ion and any neutral can be predicted (8) to within a few percent (assuming a prior knowledge of the polarizability and dipole moment of the neutral), it would appear that the relative sensitivity for any given fuel component could be calculated directly without any experimental information. However, this assumes that the only product of the reaction is  $M^+$  derived from the neutral  $M$ . When the charge transfer reaction becomes highly exothermic, it is possible that the resulting ion will retain sufficient internal energy to undergo dissociation ( $M^{+*} \rightarrow A^+ + B$ ), causing a reduced sensitivity at the  $m/z$  value associated with  $M^+$  and a more complex CI spectrum. Although dissociative charge transfer was not observed under CI conditions for any of the molecules investigated, it may be manifested in the more exothermic reactions involving higher molecular weight substituted aromatics, which are expected to have still lower IP's. In this context it is appropriate to mention that clustering reactions involving ionized product ions ( $M^+$ ) and the solvent (S), to yield  $MS^+$ -type ions, were undetectable. This was to be expected since (i) we use relatively low partial pressures of S (the conversion to  $MS^+$  involves third-order kinetics) and (ii) it is well-established (9) that the three-body rate coefficients for production of association ions involving two molecular species of significantly different IP's are generally orders of magnitude lower than the corresponding resonance case



The other important feature of Figure 2 is the fact that no signals were detected at any  $m/z$  values from any acyclic alkane or substituted cyclohexane investigated. These included linear and branched alkanes up to heptadecane, and alkylcyclohexanes up to bicyclohexyl. Again, this was anticipated since the IP of chlorobenzene (9.04 eV) is expected to

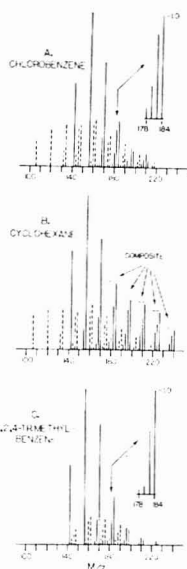


Figure 3. (A) Charge exchange CI spectrum of a no. 4 fuel oil using chlorobenzene. Substituted benzenes are indicated by broken lines. (B) Charge exchange CI spectrum of the same no. 4 fuel oil using cyclo- $C_6H_{12}^+$  as the reagent ion. See text for meaning of composite peaks. (C) Charge exchange CI spectrum of the same no. 4 fuel oil using (1,2,4-trimethylbenzene) $^+$  as the reagent ion. See text for meaning of enlarged portions of spectra 3A and 3C.

be below that of the majority of the saturated hydrocarbons expected to be present in liquid fuels.

**Sample Screening.** The major features in the CI spectra of a no. 4 fuel oil using different solvents are given in Figure 3. Figure 3A gives the net pattern (ions from CB have been subtracted) obtained with CB. The measurement conditions were 0.5% (v/v) of the oil in CB, 100  $\mu$ L of the mixture injected into the inlet reservoir, CI chamber pressure of 50 torr, and 150  $^{\circ}$ C. Peaks having the appropriate masses for substituted benzenes and naphthalenes are indicated by broken and solid lines, respectively. The spectrum of this same oil using cyclo- $C_6H_{12}^+$  as the reagent ion is given in Figure 3B. This measurement was made by photoionization (4), instead of electron impact, and is presented here only for comparison. The IP of cyclo- $C_6H_{12}$  is 9.88 eV, which lies above those expected for higher molecular weight aliphatics (see Figure 1). Therefore, the cyclo- $C_6H_{12}^+$  CI spectrum contains composite peaks including contributions from substituted naphthalenes and aliphatics (indicated by brackets in Figure 3B) having the same nominal  $m/z$  values. Note that those lower molecular weight aliphatic components with molecular weights between 100 and  $\sim$ 160 amu's, although also having IP's < 9.88 eV, do not contribute measurably to the composite spectrum. This due to the fact (10) that rate coefficients for charge exchange decrease when the exothermicity of the overall reaction is low (difference in IP's). Reference to Figure 1 indicates that this is the case for lower molecular weight aliphatics, resulting in a drastically reduced sensitivity for these molecules.

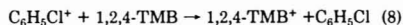
To a first approximation, the chlorobenzene CI spectrum may be taken as the actual molecular weight profile of the



major aromatic components in the particular fuel (after correcting for relative sensitivities). This is certainly true for the substituted benzenes. However, as mentioned earlier, the IP's of the great majority of aliphatic hydrocarbons have not been measured, and essentially no information is available concerning bicyclic molecules, including spiro compounds and terpenes. Even when IP's have been reported, we have found in some cases that rearrangement ions are produced in the CB CI of bridged hydrocarbons even though the overall reaction is highly endothermic as written. For example, the reported IP of norbornane ( $C_7H_{12}$ ) is 9.80 eV, indicating that electron exchange involving  $CB^+$  would be endothermic by at least 0.7 eV. However, we have found (11) that the reaction

$$C_6H_5Cl^+ + C_7H_{12}(\text{norbornane}) \rightarrow C_7H_{12}^+ + C_6H_5Cl \quad (7)$$

is relatively efficient. This is due to the fact that isomerization of  $C_7H_{12}$  occurs in the ion-molecule collision complex to yield one or more diolefinic ions having IP's much less than the IP of CB, 9.04 eV. Consequently, the reaction goes to completion in spite of the apparent endothermicity. Obviously, one cannot rule out similar rearrangement processes in higher molecular weight cyclics, including cyclohexanes, particularly at the elevated temperatures associated with the screening of heavier fuels. Taken together, these reactions would generate ions in the CI spectrum having the same nominal  $m/z$  values as alkanos and alkenonaphthalenes. Furthermore, although processed fuels derived from petroleum are usually low in olefins, this class of compounds, having IP's in the range of 8.5–9.0 eV, would also appear at these same nominal  $m/z$  values and distort the composite spectra associated with bridged naphthalenes. In order to assess such contributions, we have utilized an addition solvent, 1,2,4-trimethylbenzene (1,2,4-TMB), which has an IP of 8.27 eV, placing it far below those anticipated for any olefin irrespective of the degree of unsaturation. This value also places it above all naphthalenes (see Figure 1). Figure 3C gives the CI spectrum of the same no. 4 fuel oil using 1,2,4-TMB $^+$  as the reagent ion. This measurement was made by taking the original solution of the fuel oil in chlorobenzene, adding 5% (v/v) of 1,2,4-TMB, and scanning the spectrum under the same conditions as those given for Figure 3A. The addition of 1,2,4-TMB serves a 2-fold purpose. The molecular ion, 1,2,4-TMB $^+$ , assumes the role of major reagent ion via interception of  $CB^+$



and the neutral 1,2,4-TMB present in the mixture reacts with any ions having IP's > 8.27 eV which might have been generated initially by the interactions of  $CB^+$  with fuel components. Comparison of Figure 3A and Figure 3C reveals a complete elimination of all signals from lower molecular weight benzenes using 1,2,4-TMB, which is consistent with the IP data of Figure 1. The relative intensities of the higher molecular weight benzene derivatives are also somewhat reduced. Although the general profiles of the naphthalene manifolds are similar (solid lines), close inspection of the relative intensities of "naphthalenic" peaks having the same carbon number reveals a significant reduction in the signals at those  $m/z$  values which might include contributions from rearrangement (olefinic) ions. For example, one of the groupings, indicated by the arrows and enlargements on 3A and 3C,

includes  $m/z$  178, 180, 182, and the base peak, 184, which is uniquely associated with butyl-, methylpropyl-, etc., naphthalenes having the empirical formula  $C_{14}H_{18}$  in both spectra. The pure naphthalene profile within this manifold (3C) has the following distribution for  $m/z$  178, 180, 182, and 184 (taking 184 = 1.00): 0.05, 0.08, 0.64, and 1.00. The corresponding distribution in 3A is 0.11, 0.33, 0.82, and 1.00. Consequently rearrangement and/or olefinic ions increase the relative signals at those  $m/z$  values associated with bridged naphthalenes by more than 60% in this particular manifold. In view of this, we suggest that two separate CI spectra of the same sample are required to define a molecular weight profile for aromatic components in fuels and petroproducts (both CB and 1,2,4-TMB). For qualitative screening, as in forensic applications, CB CI is sufficient. We should mention that spectra such as 3A and 3C are routinely recorded here with a 3-min turn-around time between injection of successive samples. Assuming that the mass spectrometer is preset to scan the  $m/z$  range of interest several times within approximately 1 min, the limiting factor is only the time required to evacuate the inlet reservoir and inject a new sample diluted in the proper solvent(s).

We have also found that perdeuterionaphthalene,  $C_{10}D_8$ , can be used as an internal standard to define the actual concentrations of classes of aromatic components in petroproducts. The molecular ion,  $C_{10}D_8^+$ , occurs at  $m/z$  136, which is clean in the pure solvent spectra. Therefore, a solution of  $C_{10}D_8$  in CB of known concentration (usually one part in  $10^4$ ) can be used as the medium for preparing samples for analysis in which the volume dilution of the unknown is accurately controlled. The resulting signal at  $m/z$  136, which is negligible in neat fuels, can be compared with any other features associated with substituted benzenes or naphthalenes which appear in the resultant spectrum. Following any corrections for relative response (Figure 2) and assuming that the entire mass range has been scanned, one can directly calculate the total aromatic content of the unknown.

**Registry No.**  $CB^+$ , 55450-32-3; PhCl, 108-90-7;  $C_6H_{12}^+$ , 34473-67-1;  $C_6H_{12}$ , 100-82-7; 1,2,4- $Me_3C_6H_3$ , 95-63-6; 1,2,4- $Me_3C_6H_3^+$ , 65018-34-0;  $C_{10}D_8$ , 1146-65-2.

## LITERATURE CITED

- (1) Symposium on Positive and Negative Chemical Ionization, 29th Annual Conference on Mass Spectrometry, Minneapolis, MN, May 1981, Paper No. FAMOB1 through FAMOB15.
- (2) Sieck, L. W.; Jennings, K. R.; Burke, P. D. *Anal. Chem.* **1979**, *51*, 13.
- (3) Hunt, D. F.; Shebanowitz, J. Presented at the 29th Annual Conference on Mass Spectrometry, Minneapolis, MN, May 1981; p 655, paper no. RPC15.
- (4) Sieck, L. W. *Anal. Chem.* **1979**, *51*, 128.
- (5) Levin, R. D.; Lias, S. G.; "Ionization Potential and Appearance Potential Measurements, 1971–1981," NSRDS-NBS Series, No. 71, 1982.
- (6) Hatch, F.; Munson, M. S. B. *Anal. Chem.* **1977**, *49*, 731.
- (7) Subba Rao, S. C.; Fenselau, C. *Anal. Chem.* **1978**, *50*, 511.
- (8) Chesnavich, W. J.; Su, T.; Bowers, M. T. "Kinetics of Ion-Molecule Reactions"; Ausloos, P., Ed.; Plenum Press: New York, 1979; p 165.
- (9) Meot-Ner (Mautner), M.; Hamlet, P.; Hunter, E. P.; Field, F. H. *J. Am. Chem. Soc.* **1978**, *100*, 5466.
- (10) Lias, S. G.; Ausloos, P.; Horvath, Z. *Int. J. Chem. Kinet.* **1976**, *8*, 725.
- (11) Meot-ner (Mautner), M., NBS, unpublished results.

RECEIVED for review July 14, 1982. Accepted September 16, 1982. This work was supported by the Office of Basic Energy Sciences, U.S. Department of Energy.

# Characterization of the Microstructure and Macrostructure of Coal-Derived Asphaltenes by Nuclear Magnetic Resonance Spectrometry and X-ray Diffraction

I. Schwager,<sup>1</sup> P. A. Farmanian,<sup>2</sup> J. T. Kwan,<sup>3</sup> V. A. Weinberg, and T. F. Yen\*

School of Engineering, University of Southern California, University Park, Los Angeles, California 90007

Structural characterization studies have been carried out on coal-derived asphaltenes from five major demonstration processes in the United States: PAMCO SRC, Catalytic Inc. SRC, HRI H-Coal, Synthoil, and FMC-COED. Elemental, molecular weight, proton nuclear magnetic resonance, and functional group analyses have been used to calculate average molecular properties of the asphaltenes. The macrostructure and crystallite parameters of these asphaltenes were studied by X-ray diffraction methods. A combined NMR-X-ray procedure was used to estimate the size of the average aromatic structural unit and the number of such aromatic structural units per molecule.

The three direct general processes for converting coals to liquid fuels which have received the most attention in the United States are catalyzed hydrogenation, solvent refining, and staged pyrolysis (1, 2). All of these processes result in coal liquids which contain a fraction known as asphaltene in addition to coal oils. Asphaltenes are defined operationally as the benzene soluble and pentane insoluble part of coal liquid. This fraction consists of highly functionalized, highly aromatic, high molecular weight molecules of the coal-liquefaction products.

The purpose of this work is to characterize coal-derived asphaltenes obtained from a wide range of coal liquefaction processes in terms of micro- and macrostructures by use of nuclear magnetic resonance, X-ray diffraction, and other analytical techniques. The study of the composition and structural character of the nitrogen- and oxygen-containing asphaltene compounds present in the liquids is important in understanding problems associated with coal liquid use such as air pollution, health hazards, refining conditions and catalysts, and precursors of useful chemicals.

## EXPERIMENTAL SECTION

Coal-derived asphaltenes were separated by solvent fractionation from coal liquids produced in five major demonstration liquefaction processes: Synthoil, HRI H-Coal, FMC-COED, Catalytic Inc. SRC, and PAMCO SRC (3). Elemental analyses were carried out with standard procedures by the ELEK Microanalytical Laboratories, Torrance, CA, and Huffman Laboratories, Wheatridge, CO. Molecular weights were determined in our laboratory with a Mechrolab Model 301A vapor pressure osmometer. In normal runs, six to eight concentrations, over the range 4-39 (g/L) were employed in the solvents benzene and tetrahydrofuran for extrapolation to infinite dilution (4).

The amount of phenolic oxygen in the asphaltenes was determined by a silylation procedure. Trimethylsilyl ethers of asphaltenes were synthesized by refluxing the asphaltene with

excess 1,1,1,3,3,3-hexamethyldisilazane (HMDS) and catalytic amounts of trimethylchlorosilane and pyridine in benzene (5). After removal of liquids by rotary evaporation, the silyl derivatives were freeze-dried from benzene and dried under vacuum to constant weight. The number of trimethylsilyl groups introduced was determined by proton NMR analysis (6) after the silyl derivative was checked by infrared spectrometry in dilute solution to ensure complete removal of hydroxyl groups.

The fraction of pyrrole-type nitrogen was determined by a combined gravimetric-infrared method. Separation of nonbasic, pyrrole-type, nitrogen-containing asphaltenes was carried out by solvent elution chromatography on silica gel with benzene followed by further treatment with methyl iodide to remove any residual basic compounds. The methylations were carried out in benzene with a large excess (35:1) of methyl iodide. The reaction solutions were refluxed for 1 week, and any benzene-insoluble product was removed by filtration. The benzene-soluble products were recovered by freeze drying the concentrated benzene solutions. These asphaltenes, which contain essentially no basic (pyridine-like) nitrogen, were then used to establish an infrared correlation between the absorptivity of the N-H stretch and the weight percent pyrrolic nitrogen (7).

Proton NMR spectra were run on a Varian T-60 spectrometer. Chloroform-*d* (99.8%) with or without 1% Me<sub>2</sub>Si was used as solvent. X-ray diffraction measurements were made on finely ground powders with a General Electric XRD-6 X-ray diffractometer with a Cu K $\alpha$  radiation source. The X-ray techniques used to obtain the reduced intensity were those described previously (8).

## RESULTS AND DISCUSSION

**NMR Analysis.** High-resolution proton nuclear magnetic resonance spectrometry was first used by Brown and Ladner (9) for structural characterization of coal pyrolysis products. Other workers have extended this type of analysis to coal extracts (10) and coal hydrogenation products (11-17). A recently published comparison between  $f_i$  values determined from <sup>13</sup>C NMR spectra and those estimated from <sup>1</sup>H NMR data demonstrated that the use of the <sup>1</sup>H NMR method is reasonably reliable for coal-derived materials (18). The proton NMR spectrum of a typical coal asphaltene is shown in Figure 1. The centers of absorption for different types of protons are marked with arrows:  $\delta = 7.25$ , H<sub>ar</sub> = aromatic protons;  $\delta = 2.40$ , H<sub>a</sub> = protons  $\alpha$  to aromatic rings;  $\delta = 1.58$ , H<sub>N</sub> = naphthenic protons;  $\delta = 1.25$ , H<sub>R</sub> = methylenic protons;  $\delta = 0.9$ , H<sub>SM</sub> = saturated methyl protons. Brown-Ladner analysis requires that the three areas of absorption centered at  $\delta = 7.3$ , 2.4, and 1.2 ppm be assigned to aromatic ring hydrogens (H<sub>ar</sub>), aliphatic hydrogens adjacent to aromatic rings (H<sub>a</sub>), and aliphatic hydrogens not adjacent to aromatic rings (H<sub>N</sub>). The separation point between the H<sub>a</sub> and H<sub>N</sub> protons was chosen at  $\delta = 1.73$  ppm. Because hydrogen bonded phenolic OH resonances are also believed to be shifted under the aromatic envelope (19, 20), it is necessary to take into consideration the OH concentration in order to correct the H<sub>a</sub> value. The modified Brown-Ladner equations are used for calculations (21) in this paper.

The average molar properties of the asphaltene microstructures, obtained from elemental analyses, molecular weight

<sup>1</sup> Present address: Filtrol Corporation Technical Center, 3250 E. Washington Blvd., Los Angeles, CA 90023.

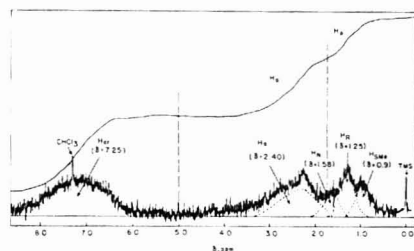
<sup>2</sup> Present address: Ralph M. Parsons Co., 100 W. Walnut St., Pasadena, CA 91124.

<sup>3</sup> Present address: Union Oil Co. of California Research Center, 376 S. Valencia Ave., Brea, CA 92621.

Table I. Average Molar Properties of Asphaltenes<sup>a</sup>

	Synthoil	HRI H-Coal	FMC-COED	PAMCO SRC	Cat. Inc. SRC
mol formula	$C_{40.9}H_{32.1}N_{0.70}O_{1.36}$	$C_{31.6}H_{23.8}N_{0.56}O_{1.52}$	$C_{26.1}H_{24.1}N_{0.33}O_{2.20}$	$C_{26.4}H_{29.1}N_{0.56}O_{1.47}$	$C_{23.6}H_{28.2}N_{0.45}O_{1.39}$
mol wt <sup>b</sup>	561	492	382	502	486
$H^*_{ar}$ <sup>c</sup>	30.5	43	32	39	44.3
$H^*_{\alpha}$	42	36	40	38	36
$H^*_{\theta}$	25	18	21	20	16
$f_a$	0.71	0.78	0.72	0.76	0.79
$H_{aru}/C_{ar}$	0.67	0.69	0.79	0.68	0.67
$\sigma$	0.45	0.35	0.48	0.38	0.34
$r_s$	8.8	6.7	7.0	7.2	6.5
$n$	1.6	1.5	1.5	1.5	1.4
$C_A$	29.2	27.8	18.7	27.7	28.3
$R_A$	5.9	5.3	3.0	5.4	5.7
$OH/O_{total}$	0.64	0.56	0.78	0.60	0.75
$NH/N_{total}$	0.53	0.55	0.28	0.74	0.58

<sup>a</sup> Brown-Ladner method  $x = y = 2$ . <sup>b</sup> Extrapolated infinite dilution values measured in THF. <sup>c</sup>  $H^*_{ar} = H^*_{ar}(obsd) - OH/H$ .

Figure 1. <sup>1</sup>H NMR spectrum of PAMCO SRC asphaltene.

determination, and NMR are presented in Table I. Hydroxylic oxygen and pyrrolic nitrogen values obtained as described earlier are also included. Nonhydroxylic ether oxygen, and basic pyridine-like nitrogen may be calculated by difference from total oxygen and nitrogen except for the FMC-COED asphaltene where IR absorption bands were observed at 3400  $cm^{-1}$  and 1650  $cm^{-1}$ , which may be assigned to the NH and C=O stretches of amide groups. The average coal-derived asphaltenes generally have number-average molecular weights in the 400–550 range and are highly aromatic species having from 71% to 79% of their carbon as aromatic carbon. The average aromatic ring systems, deduced from Haru/Car values, range from about 2 to 4. These molecules are moderately substituted with 34% to 48% of the available aromatic edge carbons being substituted. Saturated substituents are small; the average number of carbons atoms per saturated substituent is between 1.4 and 1.6. The fraction of O as OH ranges from 0.56 to 0.78 and the fraction of N as pyrrolic NH from 0.28 to 0.74. These  $OH/O_{total}$  values are more reliable than those reported previously (15, 16) due to the more rigorous silylation procedure used and the use of proton NMR analysis (6) instead of the direct silicon analysis method (5).

**X-ray Diffraction Analysis.** X-ray diffraction methods developed by Warren (22), Franklin (23, 24) and Diamond (21, 25) have been used by many workers to study the structure of coal (26–28), carbon black structures (29), small aromatic systems in noncrystalline polymers (30), petroleum asphaltenes (8), pitch fractions (31, 32) and oil shale kerogen (33). X-ray analysis was done for the asphaltenes. A typical corrected asphaltene X-ray diffraction curve, plotted on the basis of reduced intensities, is shown in Figure 2. The overlapping peaks in the low angle region, i.e.

$$(\sin \theta)/\lambda = 0.05\text{--}0.20 \quad (1)$$

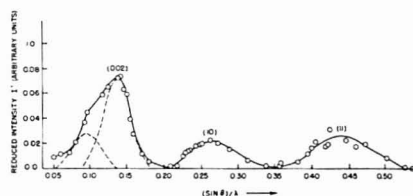


Figure 2. X-ray diffraction pattern of Catalytic Inc. SRC asphaltene.

encompass both the  $\gamma$  and the (002) bands. The (002) band is generally accepted as representing the spacing between the layers of a condensed aromatic system, whereas the  $\gamma$  band is believed to represent the packing distance of saturated structures such as aliphatic chains or condensed saturated rings. The peaks in the high angle region at  $(\sin \theta)/\lambda = 0.25$  and 0.425 can be indexed as the (10) reflection and the (11) reflection, respectively. These bands correspond to the first and second nearest neighbors in ringed compounds, and the shapes of the bands have been studied theoretically (21, 34).

An X-ray diffraction method, previously used to investigate the structure of petroleum asphaltenes (6) was employed to determine the crystallite parameters of these coal-derived asphaltenes. The repeat distance, representing the spacing between aromatic sheets,  $d_m$ , was calculated from the maximum of the (002) band by the Bragg relation

$$d_m = \lambda / (2 \sin \theta) \quad (2)$$

The repeat distance representing the spacing between saturated structures,  $d_s$ , was calculated similarly from the maximum of the  $\gamma$  band. The average size of the aromatic clusters perpendicular to the plane of the sheet,  $L_c$ , was calculated from the width of the (002) band at half maximum by use of the Scherrer crystallite size formula (35)

$$L_c = 0.45 / B_{1/2} \quad (3)$$

where  $B_{1/2}$  is the width of the band at half maximum expressed in terms of  $(\sin \theta)/\lambda$ . The number of aromatic sheets associated in a stacked cluster,  $M$ , may be calculated from the values of  $L_c$  and  $d_m$

$$M = (L_c / d_m) + 1 \quad (4)$$

The average layer diameter of the sheets,  $L_a$ , was evaluated by a procedure developed by Yen and co-workers (8) which makes use of Diamond's computed intensities of X-rays dif-

Table II. Asphaltene X-ray Crystallite Parameters

asphaltene	$L_a^a$	$L_c^b$	$d_m^c$	$d_\gamma^d$	$M^e$
Synthoil	10.3	12.2	3.7	5.4	4.3
HRI H-Coal	8.2	13.6	3.6	4.4	4.8
FMC-COED	8.0	10.6	3.6	4.9	3.9
PAMCO SRC	10.0	12.1	3.6	5.1	4.3
Cat. Inc. SRC	9.4	10.6	3.6	5.2	3.9

<sup>a</sup>  $L_a$  = diameter of aromatic sheet +  $\alpha$  carbons of side chains, from Diamond's curve (11) band,  $\text{\AA}$ . <sup>b</sup>  $L_c$  = diameter of the aromatic clusters perpendicular to the plane of the sheets,  $\text{\AA}$ . <sup>c</sup>  $d_m$  = interaromatic layer distance,  $\text{\AA}$ . <sup>d</sup>  $d_\gamma$  = interchain or internaphthene layer distance,  $\text{\AA}$ . <sup>e</sup>  $M$  = average number of aromatic sheets associated in a stacked cluster.

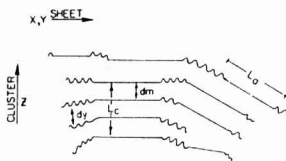


Figure 3. Cross-sectional view of asphaltene model: (---) represents the zigzag configuration of a saturated carbon chain or naphthenic ring(s); (—) represents the edge of flat sheets of condensed aromatic ring(s).

fracted from randomly oriented perfect aromatic molecules of varying sizes using the Debye radial distribution function (36). Yen and co-workers tested their procedure on both the (10) and (11) bands with a model blend and found that the (11) band afforded better agreement. Therefore, we have calculated  $L_a$  values from the correlation curve between the width of half maximum of the (11) band and Diamond's data.

The resulting X-ray crystallite parameters, presented in Table II, may be used to derive hypothetical cross-sectional model structures for coal-derived asphaltenes (Figure 3). Condensed aromatic sheets are postulated to be stacked on top of each other with the sheets parallel and with aliphatic chains or naphthenic rings protruding from the edges. The results indicate that the average interlayer distance,  $d_m$ , ranges from 3.6 to 3.7  $\text{\AA}$ , the average interchain distance,  $d_\gamma$ , is between 4.4 and 5.4  $\text{\AA}$ , and the average stack height of the aromatic clusters perpendicular to the plane of the sheets,  $L_c$ , ranges between 10.6 and 13.6  $\text{\AA}$ . The average effective number of aromatic sheets associated in a stacked cluster is between 3.9 and 4.8. The average layer diameter of the sheets generally falls between 8.0 and 10.3  $\text{\AA}$  when the (11) band is used in conjunction with Diamond's curve.

**Combined X-ray-NMR Analysis.** The average layer diameter of the sheets,  $L_a$ , is one of the most important structural parameters. Although  $L_a$  is generally considered to be the diameter of the aromatic sheet, this is only strictly correct for wholly aromatic molecules. For such systems, which are kata-condensed,  $L_a$  is related to the number of carbons per aromatic structural unit,  $C_{Au}$ , by the following equation (37):

$$C_{Au} = (L_a + 1.23)/0.615 \quad (5)$$

However, the aromatic systems in coal liquid fractions contain some heteroatoms in place of carbons and contain some rings which may be partially or completely saturated. Therefore, the dimensions of the sheet may be considered to include heteroatoms and  $\alpha$  carbons of side chains which are also restricted to the plane of the sheet. In order to correct the above equation for the latter effect, it is necessary to multiply  $L_a$

Table III. Asphaltene Structural Parameters Calculated from X-ray and NMR Data

asphaltenes	$L_a^a$	$L_a^{*b}$	$C_{Au}^c$	$N^d$
Synthoil	10.3	7.9	14.9	2.0
HRI H-Coal	8.2	6.6	12.7	2.2
FMC-COED	8.0	5.8	11.5	1.6
PAMCO SRC	10.0	7.9	14.9	1.9
Cat. Inc. SRC	9.4	7.6	14.4	2.0

<sup>a</sup>  $L_a$  = X-ray diameter of the aromatic sheet +  $\alpha$  carbons of side chains,  $\text{\AA}$ , from Diamond's curve (11) band. <sup>b</sup>  $L_a^*$  =  $L_a[C_A/(C_A + R_S)]$ . <sup>c</sup>  $C_{Au}$  = aromatic carbons per structural unit =  $(L_a^* + 1.23)/0.615$ . <sup>d</sup>  $N$  = number of aromatic structural units per molecule =  $C_A/C_{Au}$ .

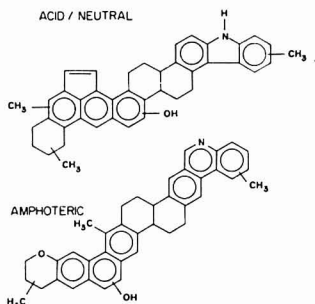


Figure 4. Hypothetical average structures of acid/neutral and amphoteric Synthoil asphaltene molecules.

by the factor  $C_A/(C_A + R_S)$  which may be obtained from the preceding NMR analysis. The structural parameter  $C_{Au}$  may be divided into the total number of aromatic carbons per molecule,  $C_A$ , to obtain the number of aromatic structural units per molecule,  $N$ .

$$N = C_{Au}/C_A \quad (6)$$

The results of such calculations are presented in Table III. For asphaltenes the results agree with those previously deduced from NMR alone. The  $C_{Au}$  values are generally close to 14 except for FMC-COED which is 11.5. These values are close to the number of aromatic carbons present in a three-ring kata system such as anthracene or phenanthrene. The number of structural units per molecule is close to two for all the asphaltenes except the FMC-COED asphaltene which has an  $N$  value of 1.6.

The  $N$  values of a variety of coal-derived liquid products were determined and found to have  $N$  values close to 2. These include not only the asphaltenes but the carbenes and carboids as well (38). Recently Charlesworth (39) proposed a number of structures for coal-derived asphaltenes from Australia. His proposed structures also have  $N$  values of approximately 2. These data indicate that these coal derived molecules are ratio condensed systems.

**Hypothetical Average Structures.** By combining the structural information obtained by NMR and functional group analyses (Table I) with that obtained by the X-ray method (Table III), it is possible to derive hypothetical average structures for asphaltene molecules. Examples of such molecules, for Synthoil asphaltene, are shown in Figure 4. A comparison of the hypothetical structures shown in Figure 4 is presented in Table IV. The results are seen to agree reasonably well in most cases.

Table IV. Comparison of Average Molecular Parameters for Synthol Asphaltene

	experimentally determined	from hypothetical average structures	
		amphoteric	acid/neutral
mol formula	$C_{41}H_{33}N_{0.7}O_{1.4}S_{0.07}$	$C_{33}H_{33}N_1O_2S_0$	$C_{41}H_{33}O_1S_0$
mol wt	561	549	559
$H^*_{ar}$	0.31	0.29	0.30
$H^*_a$	0.42	0.40	0.43
$H^*_o$	0.25	0.29	0.27
$f_a$	0.71	0.69	0.68
$H_{ar}/C_{ar}$	0.67	0.71	0.66
$a$	0.45	0.47	0.47
$R_S$	8.8	9	9
$n$	1.6	1.5	1.6
$C_A$	29.1	28	28
$R_A$	5.9	6	7
$C/H$	1.16	1.11	1.11
$\alpha\text{-CH}_3^a$	1.93	2	2
$\gamma\text{-CH}_3^a$	1.31	1	1
$C_{Au}^b$	14.9	14	14.5
$N^b$	2.0	2	2

<sup>a</sup> Determined from  $^{13}C$  NMR analysis. <sup>b</sup> From X-ray-NMR analysis—considering aromatic ring nitrogen as carbon.

## CONCLUSION

One of the useful conclusions is that the higher-molecular weight functions of coal liquid products always appear to have their aromatic portions divided into 2 parts ( $N = 2$ ). This will automatically cause their aromatic portion to be keta rather than peri in nature.

By using these analytical methods and correlations, it is possible to obtain average macro- and microstructural parameters for complex mixtures such as coal liquid asphaltenes. These parameters allow construction of an hypothetical average molecule for the mixture. However, it must be emphasized that values obtained are only average values. It is unlikely that any one molecule in the mixture will actually have the hypothetical structure. But knowledge of the kinds of molecules found in these complex mixtures will aid in the understanding of the physical and chemical behavior of the coal liquefaction product.

## ACKNOWLEDGMENT

The authors wish to thank the FMC Corporation, Hydrocarbon Research Inc., Catalytic Inc., PAMCO, and the Pittsburgh Energy Technology Center of DOE for generously supplying samples of their coal liquid products.

## LITERATURE CITED

- Burke, D. P. *Chem. Week* 1974, 115, 38.
- Cochran, N. P. *Sci. Am.* 1978, 234, 24.
- Schwager, I.; Yen, T. F. *Fuel* 1978, 57, 100.
- Schwager, I.; Lee, W. C.; Yen, T. F. *Anal. Chem.* 1977, 49, 2363.
- Friedman, S.; Zahn, C.; Kaufman, M.; Wender, J. *Fuel* 1961, 40, 38.
- Schweighardt, F. K.; Retcofsky, H. L.; Friedman, S.; Hough, M. *Anal. Chem.* 1978, 50, 368.
- Schwager, I.; Yen, T. F. *Anal. Chem.* 1979, 51, 569.
- Yen, T. F.; Erdman, J. G.; Pollack, S. *Anal. Chem.* 1961, 33, 1587.
- Brown, J. K.; Ladner, W. R. *Fuel* 1960, 39, 87.
- Retcofsky, H. L.; Friedel, R. A. In "Spectrometry of Fuels"; Friedel, R. A., Ed.; Plenum Press: New York, 1970; Chapters 6-8.
- Makawa, Y.; Ueda, S.; Hasegawa, Y.; Nakata, Y.; Yakoyama, S.; Yoshida, Y. *Prepr. Pap.—Am. Chem. Soc., Div. Fuel Chem.* 1975, 20 (3), 1.
- Yakoyama, S.; Bodily, D. M.; Wiser, W. H. *Prepr. Pap.—Am. Chem. Soc., Div. Fuel Chem.* 1976, 21 (7), 77.
- Yakoyama, S.; Bodily, D. M.; Wiser, W. H. *Prepr. Pap.—Am. Chem. Soc., Div. Fuel Chem.* 1978, 21 (7), 84.
- Woolsey, N.; Battsberger, R.; Klumb, K.; Sterberg, V.; Kaba, R. *Prepr. Pap.—Am. Chem. Soc., Div. Fuel Chem.* 1976, 21 (7), 33.
- Schwager, I.; Farmanian, P. A.; Yen, T. F. *Prepr., Div. Pet. Chem., Am. Chem. Soc.* 1977, 22 (2), 677.
- Schwager, I.; Farmanian, P. A.; Yen, T. F. "Analytical Chemistry of Liquid Fuel Sources"; Uden, P. C., Siglla, S., Jensen, H. B., Eds.; American Chemical Society: Washington, DC, 1978; ACS Adv. Chem. Ser., Chapter 5.
- Cantor, D. M. *Anal. Chem.* 1978, 50, 1185.
- Retcofsky, H. L.; Schweighardt, F. K.; Hough, M. *Anal. Chem.* 1977, 49, 585.
- Schweighardt, F. K.; Friedel, R. A.; Retcofsky, H. L. *Appl. Spectrosc.* 1978, 30, 291.
- Taylor, S. R.; Galya, L. G.; Brown, B. J.; Li, N. C. *Spectrosc. Lett.* 1976, 9, 733.
- Diamond, R. *Acta Crystallogr.* 1957, 10, 129.
- Warren, B. E. *Phys. Rev.* 1941, 59, 693.
- Franklin, R. E. *Acta Crystallogr.* 1950, 3, 107.
- Franklin, R. E. *Proc. R. Soc. London* 1951, 209, 196.
- Diamond, R. *Acta Crystallogr.* 1958, 11, 129.
- Curtz, L.; Hirsch, P. B. *Philos. Trans. R. Soc. London, Ser. A* 1960, 252, 557.
- Ergun, S. *Fuel* 1958, 37, 365.
- Ergun, S.; Tiensu, V. H. *Fuel* 1959, 38, 64.
- Alexander, L. E.; Sommer, E. C. *J. Phys. Chem.* 1956, 60, 1646.
- Ruland, W. *Acta Crystallogr.* 1959, 12, 679.
- Shiraihi, M.; Kobayashi, K. *Bull. Chem. Soc. Jpn.* 1973, 46, 2573.
- Yanada, Y.; Furuta, T.; Samada, Y. *Anal. Chem.* 1976, 48, 1637.
- Yen, T. F. In "Science and Technology of Oil Shale"; Yen, T. F., Ed.; Ann Arbor Science: Ann Arbor, MI, 1976.
- Ergun, S.; Donaldson, W.; Smith, R. W., Jr. *Bull.—U.S., Bur. Mines* 1975, no. 620.
- Klug, H. P.; Alexander, L. E. "X-Ray Diffraction Procedure"; Wiley: New York, 1954; p 538.
- Debye, P. *Ann. Phys.* 1915, 46, 809.
- Yen, T. F.; Erdman, J. G. *Prepr., Div. Pet. Chem., Am. Chem. Soc.* 1962, 7 (3), 99.
- Yen, T. F. "Chemistry and Structure of Coal-Derived Asphaltenes and Preasphaltenes"; National Technical Information Service: Washington, DC, 1980; DOE Report No. FE 2031-14.
- Charlesworth, J. M. "4th Australian Workshop on Coal Hydrogenation"; Richmond, Victoria, 1979; pp V13-V15.

RECEIVED for review August 4, 1982. Accepted September 29, 1982. This research was supported by the United States Department of Energy under Contract No. DE-AC-22-76ET10626.

# Molar Absorptivities of Ultraviolet and Visible Bands of Ozone in Aqueous Solutions

Edwin J. Hart<sup>1</sup>

Hahn-Meitner-Institut für Kernforschung Berlin GmbH, Bereich Strahlenchemie, D-1000 Berlin 39, Germany

K. Sehested and J. Holman

Accelerator Department, Risø National Laboratory, DK 4000 Roskilde, Denmark

The molar absorptivities of aqueous ozone solutions are reported for the wavelength ranges 190–300 nm and 350–900 nm. At the maxima of these bands,  $\epsilon_{260}(\text{O}_3) = 3292 \pm 70 \text{ M}^{-1} \text{ cm}^{-1}$  and  $\epsilon_{500}(\text{O}_3) = 5.1 \pm 0.1 \text{ M}^{-1} \text{ cm}^{-1}$ . The analyses for ozone were carried out by absorbance measurements of the gas at 253.7 nm and by oxidation of ferrous sulfate in sulfuric acid solution followed by back-titration of excess ferrous ion with potassium permanganate. Spectrophotometric analysis of ferric ion was also used at low ozone concentrations. A stoichiometric ratio,  $\text{Fe}^{3+}/\text{O}_3$ , of  $1.996 \pm 0.036$  was found. The visible spectrum of aqueous  $\text{O}_3$  is compared with that of ozone gas.

A reliable determination of the molar absorptivity  $\epsilon(\text{O}_3)$  of the 260-nm band of aqueous ozone solutions is difficult to make because of the volatility, instability, and the lack of an acceptable analytical method for aqueous  $\text{O}_3$  solutions. Recent published values vary from 2600 (1) to 3600  $\text{M}^{-1} \text{ cm}^{-1}$  (2) with two intermediate values at 2900  $\text{M}^{-1} \text{ cm}^{-1}$  (3, 4). Two sources of error exist, namely, the measurements of ozone concentration and optical density of an unstable solution. In view of the importance of ozone in environmental chemistry, in chemical research, and in industrial applications such as the treatment of wastewater (5) and the purification of drinking water (4), a more precise analytical method for the analysis of ozone in aqueous solutions is needed. Optical density measurements at the strong 260-nm band provide a suitable and simple physical method for the estimation of ozone. A new value for  $\epsilon_{260}(\text{O}_3)$  is reported.

Two general chemical methods have been used for the measurement of ozone concentration in aqueous solutions. These are (a) the liberation of  $\text{I}_2$  from KI solution followed by titration with sodium thiosulfate (6) or by the measurement of  $\text{I}_3^-$  absorbance at 350 nm (7) and (b) the oxidation of  $\text{Fe}^{2+}$  in excess  $\text{FeSO}_4$  in acidic solution followed by back-titration with  $\text{KMnO}_4$  (1). These authors also report that the iodide method is pH dependent but at pH 9.0 agreement between the  $\text{I}^-$  and  $\text{Fe}^{2+}$  methods was obtained. By use of syringes (8, 9) for the containment of the ozone solution and thereby avoiding ozone losses from the solutions through contact with air, the reproducibility of the determinations may be appreciably improved. Results are reported for the analysis of ozone by measurement of  $\text{Fe}^{2+}$  consumption in sulfuric acid solutions. A preliminary test of the  $\text{I}^-$  method proved it to be less reliable than the  $\text{Fe}^{2+}$  method so we report only our  $\text{Fe}^{2+}$  results. We also determined the stoichiometric ratio,  $\text{Fe}^{3+}$  formed per ozone molecule consumed, by shaking a known amount of  $\text{O}_3$  gas with  $\text{FeSO}_4$  solution. The amount of  $\text{O}_3$  gas

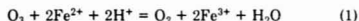
was measured by its absorbance at 253.7 nm. A technique is described for obtaining up to 0.015 M  $\text{O}_3$  solutions. The spectrum of  $\text{O}_3$  in the 350–900-nm range is also given.

## EXPERIMENTAL SECTION

(1) **Materials.** Deionized, Millipore-filtered water ( $R_{\text{H}_2\text{O}} > 18 \text{ M}\Omega$ ), found to be the equivalent of triply distilled water, and/or triply distilled water were used in the preparation of all solutions. The chemicals potassium iodide, potassium permanganate, ferrous sulfate, sodium oxalate, potassium acid phthalate, and acetic and sulfuric acids were each of reagent grade and used without further purification. These chemicals were used in the analytical procedures described below.

The  $\text{O}_3$  was prepared from Linde cylinder  $\text{O}_2$ , first dried by passing through 35–70 mesh silica gel (Merck), and then through an Ozonisorb Modell V (Erwin Sander). The rate of  $\text{O}_2$  flow was adjusted to about 500  $\text{cm}^3/\text{min}$ . The  $\text{O}_3$  generated was adsorbed on the silica gel in a  $16 \times 4.5 \text{ cm}$  diameter tube maintained at  $-78^\circ \text{C}$  with a  $\text{CO}_2$ -acetone mixture (10–12). Relatively high concentrations of  $\text{O}_3$  in aqueous solutions were then obtained by the slow elution of the adsorbed  $\text{O}_3$  with He or  $\text{CO}_2$  at atmospheric pressure. The eluted  $\text{O}_3$  was passed through nylon tubing into ice-cooled 100-mL syringes containing 20 mL of 0.001 to 0.01 M acetic acid. With  $\text{CO}_2$  elution, 0.01–0.015 M  $\text{O}_3$  solutions may be obtained. These solutions were then diluted up to 100-fold in calibrated syringes, and the  $\text{O}_3$  concentration was measured by the  $\text{FeSO}_4$  methods described below. Because of the inherent instability of aqueous  $\text{O}_3$  (4), these stock solutions were stored in 100-mL syringes in ice water. **CAUTION:** Ozone gas at atmospheric pressure is extremely dangerous but explosions may be avoided by diluting the gas with He, Ar,  $\text{O}_2$ ,  $\text{N}_2\text{O}$ , or  $\text{CO}_2$ . Elution of  $\text{O}_3$  from our trap with He, Ar, or  $\text{O}_2$  poses no hazard since typical  $\text{O}_3$  concentrations are in the range of 0.0002–0.0005 M indicating dilution factors of about 20. However elution with  $\text{N}_2\text{O}$  or  $\text{CO}_2$  provides a gas composition in the range of 50 to 100% pure  $\text{O}_3$ . Passage of  $\text{O}_3$  gas at these concentrations into ice-cooled syringes by the above technique has resulted in no explosions although a violent explosion did occur when this mixture of gas was passed into a dry syringe.

(2) **Analytical Procedures.** The oxidation of  $\text{FeSO}_4$  by  $\text{O}_3$  in sulfuric acid solution provides a satisfactory chemical method for  $\text{O}_3$  analysis (1). For low  $\text{O}_3$  concentrations, the  $\text{O}_3$  was slowly injected into magnetically stirred 0.001 M  $\text{FeSO}_4$  in 0.8 N  $\text{H}_2\text{SO}_4$ . The resulting  $\text{Fe}^{3+}$  concentration was determined spectrophotometrically at the 304 nm  $\text{Fe}^{3+}$  absorption maximum (13). At higher  $\text{O}_3$  concentrations, the  $\text{O}_3$  solution was added to stirred 0.01 M  $\text{FeSO}_4$  and excess  $\text{Fe}^{2+}$  back-titrated with standardized 0.005 N  $\text{KMnO}_4$  (1). All  $\text{O}_3$  solution transfers were made with calibrated syringes provided with an attached 8-cm capillary tube. The overall reaction is



Although the oxidation of  $\text{Fe}^{2+}$  by  $\text{O}_3$  according to reaction 1 is reported to be quantitative (1), the exact stoichiometry becomes an important factor in the measurement of the absorptivity of  $\text{O}_3$  in aqueous solutions. In order to determine the suitability of this reaction for the analysis of  $\text{O}_3$ , we have reacted a known quantity of gaseous  $\text{O}_3$  with  $\text{FeSO}_4$  in order to determine the

<sup>1</sup> Present address: 2115 Hart Road, Port Angeles, WA 98362.



Table I. Determination of  $\text{Fe}^{3+}/\text{O}_3$  Stoichiometry

$A(\text{O}_3)/\text{cm}$	vol, mL		$A(\text{Fe}^{3+})/\text{cm}$	$[\text{Fe}^{3+}] \times 10^4 \text{ M}$	$[\text{O}_3] \times 10^4 \text{ M}$	$\text{Fe}^{3+}/\text{O}_3$
	$\text{Fe}^{2+}$	$\text{O}_3$				
Series A						
1.108	51	300.8	<i>a</i>	754.0	375.3	2.010
1.084	51	300.8	<i>a</i>	736.6	367.2	2.007
1.407	50	300.8	<i>a</i>	932.7	476.6	1.958
1.866	50	300.8	<i>a</i>	1333.3	633.1	1.957
2.060	50	300.8	<i>a</i>	1400.5	697.8	2.008
0.611	50	300.8	<i>a</i>	407.6	207.0	1.970
0.617	50	300.8	<i>a</i>	407.1	209.0	1.949
1.218	50	300.8	<i>a</i>	828.9	412.6	2.010
1.552	50	300.8	<i>a</i>	1055.9	525.6	2.010
Series B						
0.065	31	37	0.114	51.8	22.02	1.973
0.122	21	51	0.437	199.0	41.33	1.984
0.1335	21	45	0.425	193.5	45.22	1.998
0.152	19	44	0.532	242.2	51.49	2.032
0.160	30	40	0.316	143.8	54.20	1.991
0.120	21	44	0.375	170.7	40.72	2.002
0.132	30	35	0.237	108.0	44.58	2.078
0.1595	25	54	0.519	236.2	54.03	2.025
0.0477	30	50	0.1205	54.8	16.16	2.036
0.1510	31	28	0.1953	88.9	51.15	1.926

<sup>a</sup> Absorbance of  $\text{Fe}^{3+}$  was not measured.

$\text{Fe}^{3+}/\text{O}_3$  ratio. The methods used are described below.

The absolute amount of gaseous  $\text{O}_3$  may be calculated from its absorbance at 253.7 nm since its absorptivity,  $2954 \text{ M}^{-1} \text{ cm}^{-1}$ , is accurately known (14) at this wavelength. This value has recently been verified (15). Earlier reported values range from 2984 to  $3026 \text{ M}^{-1} \text{ cm}^{-1}$  (16–20). A value recently used for the ozone absorptivity at 254.0 nm is  $3003 \text{ M}^{-1} \text{ cm}^{-1}$  (21).  $\text{O}_3$  generated by the ozonizer was passed successively through a 2-L flask, a calibrated reaction flask (series A), and finally a 1.00-cm absorption cell. The absorbance was continuously monitored at 253.7 nm and after steady-state conditions prevailed, the  $\text{O}_3$  in the flask was sealed off and a calibrated volume of 0.01 M  $\text{FeSO}_4$  added from a 50-mL syringe. The sealed flask was shaken for 60 s and the solution drawn back into the syringe. Once again the  $\text{O}_3$  treated  $\text{FeSO}_4$  was added to the flask, swirled around to ensure uniformity and finally withdrawn for analysis. An aliquot portion of the solution was analyzed with standard 0.0100 N  $\text{KMnO}_4$ . In series A, column 5 of Table I, the total  $\text{Fe}^{3+}$  formed from the  $\text{O}_3$  used is reported. The ratio,  $\text{Fe}^{3+}/\text{O}_3$ , averages  $1.987 \pm 0.027$  for this series.

In series B of Table I, the test of the stoichiometry was carried out at  $\text{O}_3$  concentrations a factor of 10 less than those in series A; consequently, the technique was modified. In this series the  $\text{O}_3$  was passed through a 10.00-cm optical cell until a steady absorbance reading at 253.7 nm was obtained. At this point a measured volume of gaseous  $\text{O}_3$  was run into a 100-mL syringe and a measured volume of 0.001 M  $\text{FeSO}_4$  in 0.8 N  $\text{H}_2\text{SO}_4$  added. This mixture was shaken for 60 s and the  $\text{Fe}^{3+}$  determined spectrophotometrically as described above. The ratio,  $\text{Fe}^{3+}/\text{O}_3$ , averages  $2.0045 \pm 0.0413$  for this series.

We conclude, from the results of Table I that 2.00  $\text{Fe}^{3+}$  form for every  $\text{O}_3$  molecule reacted thereby confirming the stoichiometry of reaction 1. The overall average of our data of Table I is  $1.996 \pm 0.036$ . And if the two extreme values, 2.077 and 1.925, of series B are deleted, this overall average narrows down to  $1.995 \pm 0.026$ .

(3) **Absorption Spectra.** The absorbance measurements and the spectrum of  $\text{O}_3$  were obtained on a Varian SuperScan 3 recording spectrophotometer. The absorbance at 260 nm was taken on identical samples of each of the standardized  $\text{O}_3$  solutions given in Table II. These absorbance measurements were made in 2, 10, or 50 mm cuvettes at a spectrometer cavity temperature of 20 °C. Because of the instability of neutral  $\text{O}_3$  solutions, the most reliable measurements were made with acetic acid stabilized solutions. Little or no decay took place during the time of the measurement in  $\text{O}_3$  solutions stabilized by 1 to 10 mM acetic acid. At these concentrations acetic acid was shown to have no effect on  $\epsilon_{260}(\text{O}_3)$  or on the visible spectrum in the 360–700-nm wave-

length range. In the absence of stabilizer, either acetic or sulfuric acids, decay of  $\text{O}_3$  was too rapid to obtain satisfactory readings.

## RESULTS AND DISCUSSION

Since  $\text{O}_3$  is a volatile, thermally unstable and reactive gas, its analysis, especially in aqueous solution, is difficult as has been pointed out by a number of authors (1, 3, 6, 7). Ozone in neutral solution has a half-life of 50 min and a decay rate that is between zero and first order in  $\text{O}_3$  concentration (4). Furthermore its decomposition is catalyzed by glass surfaces and impurities in the water. Because of these two factors, considerable variation in the value of  $\epsilon(\text{O}_3)$  at 260 nm has been reported. Without careful attention to details, variations of 50% or more in  $\epsilon_{260}(\text{O}_3)$  may be found.

The results obtained by spectrophotometry of the  $\text{Fe}^{3+}$  ion and by the back-titration of excess  $\text{Fe}^{2+}$  are presented in Table II. The average value of  $\epsilon(\text{O}_3)$  and its standard deviation for each series of runs is given. The  $\text{KMnO}_4$  back-titration of excess  $\text{Fe}^{2+}$  is quantitative and a reliable method for the determination of  $\text{Fe}^{3+}$ . The spectrophotometry of the  $\text{Fe}^{3+}$  ions depends on its molar absorptivity, a property that is temperature dependent. The absorptivity used for calculating the  $\text{Fe}^{3+}$  data of Tables I and II is  $2197 \text{ M}^{-1} \text{ cm}^{-1}$  for the  $\text{Fe}^{3+}$  ion at 304 nm (13). Therefore for the determination of  $\epsilon(\text{O}_3)$ , we consider the first two groups of measurements less reliable than the remaining  $\text{KMnO}_4$  back-titration groups.

Fifty eight analyses of  $\text{O}_3$  by back-titration are given in Table II. Overall,  $\epsilon_{260}(\text{O}_3)$  averages  $3312 \pm 125 \text{ M}^{-1} \text{ cm}^{-1}$ . Our technique of carrying out the determinations improved with time as is illustrated by the lower four groups which show an average value of  $3292 \pm 70 \text{ M}^{-1} \text{ cm}^{-1}$ . And our last group gives an average of  $3292 \pm 23 \text{ M}^{-1} \text{ cm}^{-1}$  based on our experimental result that 2.00  $\text{Fe}^{2+}$  are oxidized per  $\text{O}_3$  decomposed. We conclude that an acceptable  $\epsilon_{260}(\text{O}_3)$  is  $3300 \text{ M}^{-1} \text{ cm}^{-1}$ . This value is practically midway between the values of 2900 (3, 4) and  $3600 \text{ M}^{-1} \text{ cm}^{-1}$  (2) already reported.

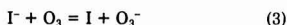
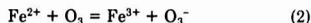
While the stoichiometry of the  $\text{Fe}^{2+}$  reaction with  $\text{O}_3$  is well established, its detailed mechanism is uncertain. However, it is known that  $\text{O}_3$  reacts with organic molecules by two different mechanisms (4). In acidic media the pathway leads to selective ozonization whereas in alkaline solutions OH radicals become the dominant oxidizing species. In the present

Table II. Summary of Ozone Molar Absorptivity Measurements at 260 nm

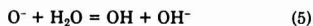
method	sys-tem	no. of sam-ples	$\epsilon(\text{O}_3)$
spectrophotometric	Fe <sup>3+</sup>	8	3340 ± 146
spectrophotometric	Fe <sup>3+</sup>	5	3211 ± 40
KMnO <sub>4</sub> back-titration	Fe <sup>2+</sup>	6	3183 ± 115
KMnO <sub>4</sub> back-titration	Fe <sup>2+</sup>	12	3329 ± 205
KMnO <sub>4</sub> back-titration	Fe <sup>2+</sup>	7	3421 ± 84
KMnO <sub>4</sub> back-titration	Fe <sup>2+</sup>	5	3308 ± 46
KMnO <sub>4</sub> back-titration	Fe <sup>2+</sup>	6	3319 ± 140
KMnO <sub>4</sub> back-titration	Fe <sup>2+</sup>	5	3330 ± 50
KMnO <sub>4</sub> back-titration	Fe <sup>2+</sup>	11	3316 ± 44
KMnO <sub>4</sub> back-titration	Fe <sup>2+</sup>	6	3292 ± 23

reactions it is likely that the primary step is one of electron transfer from Fe<sup>2+</sup> to O<sub>3</sub> as has been proposed in the case of the I<sup>-</sup> reaction (7). These authors explain the stoichiometry of the I<sup>-</sup> reaction (2I<sup>-</sup>/O<sub>3</sub>) with O<sub>3</sub> by this mechanism. And by postulating the intermediate formation of HO<sub>3</sub>, they account for the enhanced yield of I<sub>2</sub> in acid solutions. Thus it is important to utilize conditions favorable for the quantitative oxidation of the Fe<sup>2+</sup> and I<sup>-</sup> ions by O<sub>3</sub>.

Recent work (22) has confirmed the earlier conclusion (4) that OH radicals form in alkaline O<sub>3</sub> solutions. Furthermore it is highly likely that OH radicals form whenever an electron is transferred from either Fe<sup>2+</sup> or I<sup>-</sup> to O<sub>3</sub> by the reactions



And because of the well-established (23) equilibrium reactions



the OH radical may be an intermediate species in reaction 1. If this is the case, it is important to adjust the solution parameters so that they are favorable for its reaction with Fe<sup>2+</sup> and not with the substrate. For example, under our titration conditions for the FeSO<sub>4</sub> determination, the acetic acid present intercepts less than 1% of the OH radicals formed by reactions 4 and 5 (24).

The O<sub>3</sub> solution must be rapidly mixed with the Fe<sup>2+</sup> solution in order to avoid O<sub>3</sub> decomposition by OH radicals. In this instance, reaction of OH with O<sub>3</sub> is favored by a factor of 10 because  $k(\text{OH} + \text{O}_3)$  (25) is 10-fold greater than  $k(\text{OH} + \text{Fe}^{2+})$  (24). Consequently it is important to maintain a factor of about 100 in relative Fe<sup>2+</sup>/O<sub>3</sub> concentrations during the titration in order to ensure reaction of OH with Fe<sup>2+</sup> and not with O<sub>3</sub>.

The effect of wavelength on  $\epsilon(\text{O}_3)$  is given in Table III. These  $\epsilon(\text{O}_3)$  values are based on a relative absorbance ratio of 646 for the 260- and 590-nm bands. Our  $\epsilon_{600}(\text{O}_3)$  of 5.1 M<sup>-1</sup> cm<sup>-1</sup> agrees exactly with an earlier value published by Taube (2).

The spectrum of the aqueous O<sub>3</sub> band centered at 588 nm is shown in Figure 1. A qualitative tracing of the gaseous O<sub>3</sub> band run in a 10-cm cell is also given for comparison. The spectrum and absorption coefficients of the Hartley (260 nm) and Chappius (600 nm) bands of gaseous O<sub>3</sub> have already been reported (14). It is interesting to note that the aqueous 260-nm band is shifted to the red; the aqueous 590-nm band is shifted to the blue relative to that of O<sub>3</sub> gas.

Table III. Effect of Wavelength on the Molar Absorptivities of the Ozone Bands Centered at 260 and 588 nm

ultraviolet band		visible band	
wave-length, nm	$\epsilon(\text{O}_3)$ , M <sup>-1</sup> cm <sup>-1</sup>	wave-length, nm	$\epsilon(\text{O}_3)$ , M <sup>-1</sup> cm <sup>-1</sup>
300	287	900	0.00
290	764	800	0.143
280	1695	700	0.932
270	2738	650	2.37
260	3300	600	4.81
259	3300	590	5.11
250	2961	588	5.12
240	2067	580	5.06
230	1292	550	4.30
220	842	500	1.79
210	689	450	0.38
200	685	400	0.047
190	931	380	0.036 <sup>a</sup>
		350	0.61

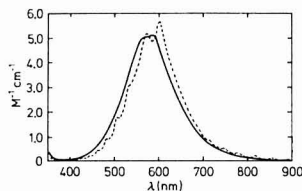


Figure 1. Absorption spectra of the visible bands of aqueous and gaseous ozone: (solid line) O<sub>3</sub> in 0.01 M acetic acid; (dotted line) qualitative spectrum of O<sub>3</sub> gas.

#### ACKNOWLEDGMENT

The research on the molar absorptivity of O<sub>3</sub> was carried out at the Hahn-Meitner Institut und the research on stoichiometry at the Riso National Laboratory. E.H. is grateful to E. Darnstadt for technical assistance and to several staff members of Bereich Strahlenchemie for help in equipping a laboratory for these ozone studies. We thank H. Corfitzen for standardization of the KMnO<sub>4</sub> solutions.

Registry No. O<sub>3</sub>, 10028-15-6; FeSO<sub>4</sub>, 7720-78-7.

#### LITERATURE CITED

- (1) Ingols, R. S.; Fetner, R. H.; Eberhardt, W. H. *Adv. Chem. Ser.* **1959**, *21*, 102-107.
- (2) Taube, H. *Trans. Faraday Soc.* **1957**, *53*, 656-665.
- (3) Kilpatrick, M. L.; Herrick, C. C.; Kilpatrick, M. J. *Am. Chem. Soc.* **1956**, *78*, 1784-1789.
- (4) Hoigne, J.; Bader, H. In "Organometals and Organometalloids. Occurrence and Fate in the Environment"; Brinckman, F. E.; Bellama, J. M., Eds.; American Chemical Society: Washington, DC, 1976; ACS Symp. Ser. No. 82, p. 292.
- (5) Murphy, J. S.; Orr, J. R. "Ozone Chemistry and Technology, A Review of the Literature 1964-1974"; Franklin Institute Press: Philadelphia, PA, 1975; pp. 392.
- (6) Birdsall, C. M.; Jenkins, A. C.; Spadinger, E. *Anal. Chem.* **1952**, *24*, 662-664.
- (7) Boyd, A. W.; Willis, C.; Cyr, R. *Anal. Chem.* **1970**, *42*, 670-672.
- (8) Hart, E. J.; Gordon, S.; Thomas, J. K. *J. Phys. Chem.* **1964**, *68*, 1271-1274.
- (9) Michael, B. D.; Hart, E. J. *J. Phys. Chem.* **1970**, *74*, 2878-2884.
- (10) Cook, G. A.; Kiffer, A. D.; Klumpp, C. V.; Malik, A. H.; Spence, L. A. *Adv. Chem. Ser.* **1959**, *21*, 44-52.
- (11) Rosen, D. I.; Cool, T. A. *J. Chem. Phys.* **1973**, *59*, 6097-6103.
- (12) Zahniser, M. S.; Kaufman, F.; Anderson, J. G. *Chem. Phys. Lett.* **1976**, *37*, 226-231.
- (13) Frické, H.; Hart, E. J. "Radiation Dosimetry"; Attix, H.; Roessch, W. G., Eds.; Academic Press: New York, 1966; Chapter 12.
- (14) Griggs, M. J. *Chem. Phys.* **1968**, *49*, 857-859.
- (15) Autholtz, D. C.; Croce, A. E.; Troe, J. J. *Phys. Chem.* **1982**, *86*, 696-699.
- (16) Inn, E. C. Y.; Tanaka, Y. *J. Opt. Soc. Am.* **1953**, *43*, 870.
- (17) Becker, J. H.; Schurath, U.; Seltz, H. *Int. J. Chem. Kinet.* **1974**, *6*, 725.

- (18) Hearn, A. G. *Proc. Phys. Soc., London* 1961, 78, 932.  
 (19) DeMore, W. B.; Raper, O. J. *Phys. Chem.* 1964, 68, 412.  
 (20) Cline, M. A. A.; Coxon, J. A. *Proc. R. Soc. London, Ser. A* 1968, 303, 207.  
 (21) Paur, R. J. *NBS Spec. Publ. (U.S.)* 1977, No. 464, 15, 16.  
 (22) Forni, L.; Bahnmann, D.; Hart, E. J. *J. Phys. Chem.* 1982, 86, 255-259.  
 (23) Belski, B. H. J.; Gebicki, J. M. "Advances in Radiation Chemistry"; Burton, M.; Magee, J. L., Eds.; Wiley-Interscience: New York, 1970; Vol. 2, p. 177.  
 (24) Dorfman, L. M.; Adams, G. E. *Natl. Stand. Ref. Data Ser. (U.S. Natl. Bur. Stand.)* 1973, NSRDS-NBS 46.

(25) Bahnmann, D.; Hart, E. J. *J. Phys. Chem.* 1982, 86, 252.

RECEIVED for review July 22, 1982. Accepted September 23, 1982. E.H. wishes to thank the Alexander von Humboldt-stiftung, Bad Godesberg, D-5300 Bonn 2, West Germany, for a Senior U.S. Scientist Award and the Hahn-Meitner-Institut für Kernforschung Berlin GmbH, Berlin, West Germany, for laboratory facilities.

## Cross-Correlation Analysis of Molecular Fluorescence Spectra

Marilyn A. Stadallus and Harvey S. Gold\*

Department of Chemistry, University of Delaware, Newark, Delaware 19711

A new computational method for the identification of fluorescence spectra has been developed utilizing cross-correlation analysis of molecular fluorescence spectra. The spectra are obtained with conventional instrumentation and then transformed to relative time-space by using fast Fourier transform procedures. This method is applicable to a wide variety of species with overlapping fluorescence spectra. The procedure has been tested upon a representative series of polycyclic aromatic hydrocarbons and has proven to be successful for the identification of both isolated and overlapped multicomponent mixtures.

Polycyclic aromatic hydrocarbons (PAH) have been established to be a serious health threat due to their carcinogenic and mutagenic properties. They are found primarily in the residue of various combustion products (soot, coal tar, and some smoke condensates) and materials derived from petroleum and coal. The composition of these mixtures may include 100 to 200 unique PAH species. The separation and identification of such mixtures have been carried out by using reversed-phase high-performance liquid chromatography (HPLC) in conjunction with direct insertion probe mass spectrometry (1).

Molecular fluorescence is well-suited to the identification of the components of a mixture of PAH's due to its selectivity and high sensitivity. The major impediment to this approach is the inherent broad-band nature of conventional ambient temperature fluorescence spectroscopy, which results in nonoptimal differentiation among similar compounds and frequently to severe overlap in multicomponent systems. Several techniques have been proposed as solutions to this problem. The Shpol'skii effect utilizes an *n*-alkane matrix at temperatures below 80 K in order to reduce the spectral linewidth to that of the vibrational levels in the ground state (2). O'Haver and co-workers have employed derivative spectroscopy to enhance minor spectral features in the emission spectrum (3).

Christian and co-workers (4) have published extensively on the use of videofluorimeters to identify fluorescence spectra. Despite the high information density of the resulting excitation-emission spectra, unique identification of mixture components using principal component and factor analysis remains elusive when high interspecies correlation is present. Faulkner and co-workers (5) have relied upon analysis of conventional

fluorescence spectra to compare selected features of an unknown spectrum against the first 1000 fluorescence spectra in the Sadtler collection. Identification was based upon an index of similarity, incorporating parameters such as peak locations, intensities, and excitation maximum. Another approach subjected a digitized spectrum to a fast Fourier transform algorithm (6) and utilized a dissimilarity index which reflected differences in the real and imaginary parts of the Fourier component of the excitation and emission spectra of both an unknown and a reference spectrum. Gold and co-workers explored the use of decomposition analysis to identify electronic spectra, particularly of PAH (7). While overcoming the necessity to use specialized equipment, decomposition analysis has difficulty differentiating among highly correlated spectra; this was recently contrasted with several principal component analysis procedures (8).

While each of these approaches can be made to work in particular cases, none of them has achieved a level of universality. The ideal electronic spectral characterization procedure would produce a compact and unique set of numerical parameters for each species. Further, the characterization procedure would not be affected by overlapped spectra when mixtures were considered.

Computer file-searching algorithms generally subject an unknown digitized spectrum to an encoding process and directly compare the resulting parameters to a collection of known compounds stored in an encoded library file. Statistically significant matches are reported, but loss of spectral information during the encoding process is a common limitation.

An IR search system utilizing direct comparison of interferograms of an unknown chromatographic peak produced by a GC/FTIR against a library of known compounds was reported by Isenhour (9). Powell and Hieftje (10) developed an IR search system based upon cross-correlation in which the complete cross-correlation was calculated between each unknown and every member of the library file.

In the present study, a computer file-search procedure is introduced which identifies the digitized fluorescence spectrum of an unknown species (or of a mixture) with the aid of the Cooley-Tukey fast Fourier transform (FFT) algorithm (11). The program performs a preliminary search which isolates reference spectra which possess a high degree of similarity to the unknown species. Final identification utilizes cross-correlation of the unknown with those reference compounds isolated in the initial test. The details of this procedure and

its application to a library of some 200 fluorescence spectra are discussed below.

### EXPERIMENTAL SECTION

A Hitachi MPF-44B fluorescence spectrometer was used to obtain excitation and emission spectra. Spectral quality cyclohexane (MCB) was used as the solvent for all of the polycyclic aromatic hydrocarbon species (all reagent grade or better) that were studied.

**Computational Procedure.** The cross-correlation of two functions  $A(f)$  and  $B(f)$  may be represented as  $A(f) \cdot B(f)$  and is defined mathematically by the integral (12)

$$C_{AB}(\nu) = A(f) \cdot B(f) = \lim_{F \rightarrow \infty} \frac{1}{2F} \int_{-F}^{+F} A(f)B(f \pm \nu) df \quad (1)$$

where  $\nu$  represents the relative displacement between the two wave forms being compared. Implementation as a computer algorithm has been described previously (13).

For convenience, the Cooley-Tukey FFT algorithm was used to compute the discrete FT of the digitized spectrum. The FFTC and FFTCC subroutines of the International Mathematical and Statistical Library (IMSL) were employed to perform forward and inverse FT operations in this study. Details of the general cross-correlation procedure are discussed by Horlick and Hieftje (12) and graphically depicted by Isenhour and co-workers (14).

This procedure is incorporated in a FORTRAN program entitled SIPS (spectral identification program system), which is used to determine the extent to which an unknown and a reference spectrum are correlated. The unknown and reference spectra are properly termed "power spectra" since they encode data as optical power per unit bandwidth (15). The power spectrum (or spectral density)  $I_A(\omega)$  is defined as (16)

$$I_A(\omega) = \frac{1}{2\pi} \int_{-F}^{+F} dt e^{-i\omega t} (A^*(0)A(t)). \quad (2)$$

Fourier inversion of (2) leads to an expression for the so-called time-correlation function in terms of the power spectrum (16)

$$\langle A^*(0)A(t) \rangle = \int_{-F}^{+F} d\omega e^{i\omega t} I_A(\omega) \quad (3)$$

The time-correlation function is the first-order electric-field autocorrelation function and may properly be referred to as an interferogram. Popular usage is to refer to the time-correlation function as the "time-domain spectrum" and to its Fourier pair, the power spectrum, as the "frequency-domain spectrum" (14).

Examination of eq 1 shows that if two spectra are identical, the largest value of  $A(f) \cdot B(f)$  will be obtained when  $\nu = 0$ , that is, when every point is multiplied by itself. This is a special case of cross-correlation and is termed autocorrelation. If  $A(f)$  and  $B(f)$  are not identical, the maximum correlation value may be shifted some distance (in  $\nu$  units) from  $\nu = 0$ . The criterion of a match is therefore the absolute magnitude of  $A(f) \cdot B(f)$  at  $\nu = 0$ .

SIPS normalizes the value at  $\nu = 0$  to the largest point in the cross-correlation function. A value of 1.000 is obtained if perfect correlation exists between the unknown and a particular reference spectrum. Compounds that fluoresce in the same wavelength region will often exhibit a high degree of correlation when judged utilizing this criterion. A second criterion employs the absolute value of the function at  $\nu = 0$  for further discrimination. The input reference spectrum is first normalized and the intensity at each point is squared. The sum of these squares (SUMSQ), computed over the interval from 12 800 to 38 500  $\text{cm}^{-1}$ , for each spectrum is stored in the library as an additional parameter. Whenever an unknown spectrum contains a component that matches a reference spectrum, the absolute value at  $\nu = 0$  divided by the number of discrete digitized points,  $N$ , will be equal to SUMSQ. Perfect correlation will result in this (viz.  $C_{AB}(0)/N$ ) dividing being equal to 1.000.

The calculation of a complete cross-correlation of the unknown against each reference spectrum in the library would require a large amount of computer time. Therefore, a partial cross-correlation (PCC) is initially used to determine the degree of similarity prior to calculating the complete cross-correlation (CCC). The data for the PCC calculation are contained in the complex array that results from implementing the simple product

$\bar{A}(\tau) \cdot B^*(\tau)$  where the bars indicate Fourier transformation. If the FT of the unknown spectrum is multiplied by the complex conjugate of itself, the real components of the resulting complex array contain only positively signed components. As the reference spectrum becomes increasingly unlike the unknown spectrum, the negative component increases in magnitude. The presence of negative components at this point is caused by spectral dissimilarities between the unknown and a particular reference species. A rejection factor empirically based upon the magnitude of this negative component limits the computational time required for the analysis since the CCC is carried out only for those reference spectra which give PCC values more positive than this rejection factor.

**Search Implementation.** The 200 PAH reference spectra were originally collected at the Argonne National Laboratory, stored on magnetic tape, and subsequently published by Berlan (17). A magnetic tape copy of the library, containing excitation and emission spectra, was obtained from Berlan for use. Due to systematic errors in the tape records, some data reconstruction was required. The emission spectra were separated from the excitation spectra and the two halves stored in two library files. SIPS presently utilizes the emission library exclusively.

Both library files contain aromatic compounds that vary in complexity. Each spectrum was digitized at a constant 100- $\text{cm}^{-1}$  interval. When required, spectra in wavelength units were converted to  $\text{cm}^{-1}$  (an energy unit) with SPECSOLV, a FORTRAN program previously described (18). Distinct library spectra were coadded to generate pseudounknown bicomponent mixtures for use in this study. In each instance, the resulting spectrum was adjusted to fill a sampling window from 12 800 to 38 500  $\text{cm}^{-1}$ . Regions having zero intensity were assigned a base line value of  $1.000 \times 10^{-6}$ . Spectra acquired in this laboratory were processed in an identical manner.

When a discrete CCC is performed on the unknown and one of the reference spectra, both of equal length, an artificial period is imposed upon each. This period is constant since it depends upon the length of the data record. The correlation function can be distorted by "end effects" which arise from the improper overlap of one period with another when one spectrum is shifted with respect to the other.

Bendat and Piersol have shown that end effects do not significantly influence the correlation values near zero displacement ( $\nu = 0$ ), provided that the correlation function decays rapidly (19). Powell and Hieftje (10) ignored the use of zero filling, without affecting the reliability of a search system used to identify infrared spectra using CCC values near zero displacement. SIPS relies primarily upon CCC values near  $\nu = 0$ , so zero filling has not been employed, although partial zero filling has been used so that each spectrum spans the same wavenumber region and is represented by 265 data points. A two-point linear interpolation doubles the point density prior to transformation to the complementary time domain. The sequential steps of SIPS are illustrated in Figure 1.

### RESULTS AND DISCUSSION

Fluorescence spectra of three common PAH's (anthracene, naphthalene, and 3,4-benzophenanthrene) are shown in Figure 2. The partial cross-correlation (PCC) of anthracene with itself is shown in Figure 3A. A key feature of Figure 3A is the absence of any negative components. In contrast, Figure 3B shows the characteristic negative component that results from the PCC of anthracene with naphthalene. The magnitude of the negative component in this PCC is a reflection of the differences that exist in the anthracene and naphthalene spectra. This conclusion is easily reached by looking specifically at the input spectra of these species. If the spectrum of anthracene is compared with a spectrum that fluoresces in the same wavelength region and has similar spectral features (that is, a more highly correlated spectrum), the result is a decrease in the magnitude of the negative component. This "magnitude" refers to the negative values of a PCC which are summed and eventually compared to a rejection factor established in SIPS. As the unknown is compared sequentially with the reference spectra stored in the library file, SIPS will calculate the complete cross-correlation only if the magnitude

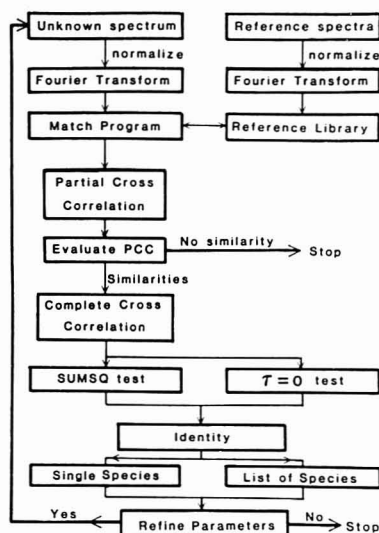


Figure 1. Block diagram of the operation of SIPS (spectral identification program system).

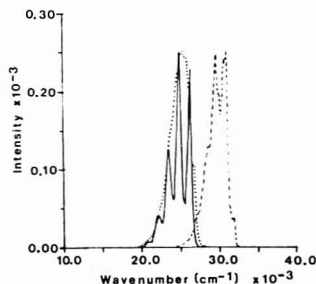


Figure 2. Input fluorescence spectra: anthracene (—), naphthalene (---), and 3,4-benzophenanthrene (-·-) after digitization at constant wavenumber interval.

of the negative component is smaller than the rejection factor. The illustration in Figure 4 graphically depicts complete cross-correlation.

Figure 4A shows anthracene cross-correlated with naphthalene. Note that the curve is asymmetric and that the maximum is shifted away from  $\nu = 0$ . This asymmetry and the displacement from  $\nu = 0$  clearly demonstrate that these two spectra are not identical. If anthracene is cross-correlated with itself, as shown in Figure 4B, the curve is symmetric with a maximum at  $\nu = 0$ , but the asymmetry of the curve is still apparent. SIPS does not currently utilize the symmetry information contained in these plots since this feature is ambiguous when studying multicomponent systems whose component spectral features overlap.

The second criterion relies upon the fact that the value at  $\nu = 0$  divided by  $N$  should equal SUMSQ. Table I presents

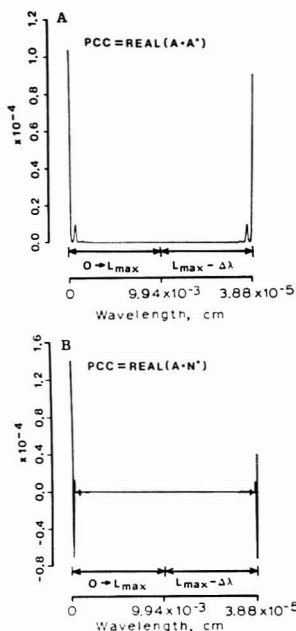


Figure 3. Results of the partial cross-correlation (PCC) of (A) anthracene with anthracene and (B) anthracene with naphthalene. The left portion of the abscissa to the midpoint (inclusive) extends from 0 to  $L_{max}$  where  $L_{max} = [(N-1)/2(E_{max} - E_{min})]$ . The right portion of the abscissa extends from  $(L_{max} - \Delta\lambda)$  to  $\Delta\lambda$  where  $\Delta\lambda = [(N-1)/N(E_{max} - E_{min})]$ .  $E_{max}$  and  $E_{min}$  have units of energy in the context of this study.

Table I. Illustration of the Result of Complete Cross-Correlation (CCC) of a Pseudoknown with a Small Set of Library Spectra, the Unknown Was Anthracene

library species	correlation parameter	
	CR1	CR2
anthracene	1.0000	1.0000
3,4-benzophenanthrene	0.9987	0.6084
naphthalene	0.0274	0.0197

data for the correlation of anthracene with itself, with 3,4-benzophenanthrene, and with naphthalene. The value obtained at  $\nu = 0$  relative to the maximum in the complete cross-correlation function is reported as criterion 1 (CR1), while the comparison based on the value at  $\nu = 0$  is referred to as criterion 2 (CR2). With these three spectra as a small library file, anthracene is clearly the correct match.

When anthracene is compared to a library file containing 200 reference spectra, the number of potential matches increases. Table II lists the most probable spectral matches in the order that they were found. When one looks at the correlation values CR1 and CR2, anthracene is the best choice for a match. Deuterated anthracene has very similar spectral features and emission wavelength region, so that the relatively high correlation values which were obtained are not unexpected.

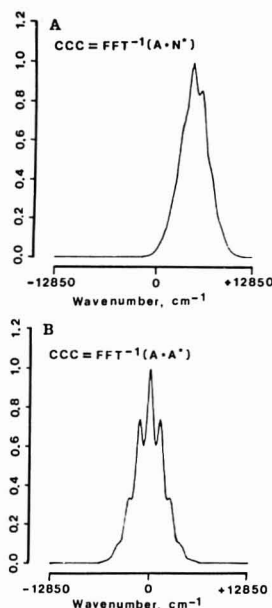


Figure 4. Plots of the complete cross-correlation (CCC) of (A) anthracene with naphthalene and (B) anthracene with anthracene.

Table II. Results of a Complete Library Search (200 Species) for the Identity of an Unknown Compound (Anthracene), the Most Probable Matches Are Listed Below

library species	reported correlation parameters	
	CR1	CR2
anthracene	1.0000	1.0000
deuterated anthracene	0.9918	1.0000
3,4-benzophenanthrene	0.9987	0.6084
benzidine	0.9995	0.5971
sodium salicylate	0.9832	0.5369
tetramethyl- <i>p</i> -octaphenyl	0.9811	0.5455
tetramethylphenylene-diamine	0.9557	0.5640

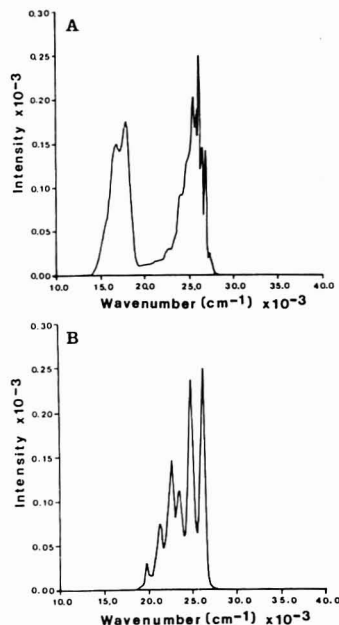


Figure 5. Input fluorescence spectra of binary mixtures of fluorescent species: (A) pyrene/rubrene and (B) anthracene/peryene.

The identification of a bicomponent mixture is easily carried out if the spectrum has minimal or, of course, zero overlap. This is the case for anthracene/peryene and rubrene/pyrene, respectively. The input spectra for these mixtures are shown in Figure 5. Note that the fluorescence intensities of the components in each mixture are not identical.

Table III contains the output correlation values for both mixtures. Each component of the mixture is identified individually and sequentially, although the initial analysis may reveal the identity of each component. The CR1 and CR2 values are used to select a particular reference spectrum as the "best" match. This reference spectrum is then subtracted from the input spectrum and the resultant spectrum is reevaluated as a unique unknown. The identity of the second component is confirmed by this process.

Table III. Results of a Library Search for the Identity of Components of Binary Mixtures of Fluorescent Species<sup>a</sup>

first search				second search		
unknown mixture	library species found	correlation parameter		library species found	correlation parameter	
		CR1	CR2		CR1	CR2
pyrene/rubrene	pyrene <sup>b</sup>	1.000	1.011	rubrene	1.000	1.001
	3,4-benzophenanthrene	0.9783	0.6619	rubicene	0.9983	0.8829
	deuterated anthracene	0.9549	0.8818			
anthracene/peryene	peryene <sup>b</sup>	0.9984	1.0000	anthracene	1.000	0.9785
	anthracene	0.9715	1.022	deuterated anthracene	0.9924	0.9820
	deuterated anthracene	0.9598	1.026	3,4-benzophenanthrene	0.9963	0.5934
	2-aminoanthracene	0.9526	0.6946	pyrene	0.9525	0.8713

<sup>a</sup> The most probable identities of the unknowns are shown initially and after mathematical removal of one species (second search). <sup>b</sup> Library species selected as match following first search. This species was mathematically subtracted prior to second search.



Table IV. Results of a Library Search for the Identity of the Components of a Binary Mixture of Fluorescent Species<sup>a</sup>

		first search				second search	
		correlation parameter				correlation parameter	
unknown mixture	library species found	CR1	CR2	library species found	CR1	CR2	
pyrene/chrysene	chrysene <sup>b</sup>	0.9978	1.141	3,4-benzophenanthrene	1.000	0.6477	
	pyrene	0.9934	1.009	pyrene	0.9910	0.9411	
	2-phenylphenanthrene	0.9943	0.7733	9-methylanthracene	0.9588	0.8007	
	4,4-di( <i>n</i> -butoxy)-1,1-binaphthyl	0.9904	0.6185				
	1,4-diphenylnaphthalene	0.9706	0.5950				

<sup>a</sup> The most probable identities of the unknowns are shown initially and after mathematical removal of one species (second search). This table illustrates the case of severe overlap. <sup>b</sup> Library species selected as match following first search. This species was mathematically subtracted prior to second search.

In the case of the rubrene/pyrene mixture, pyrene is clearly the best match. Pyrene is also the major fluorescent component of the mixture. The second search easily identifies rubrene. In the anthracene/erylene mixture, perylene is identified as the best match, but anthracene also appears as a potential component. After subtraction of perylene, anthracene is confirmed as the other component in the second search. Deviations of the CR1 and CR2 values from unity result from the slight overlap between the two individual spectra, but this does not prohibit successful identification.

A bicomponent mixture whose superimposed spectra have a high degree of overlap is considered next. As shown in Figure 6, chrysene and pyrene fluoresce in essentially the same region. With increasing overlap, the number of potential matches increases and the correlation values CR1 and CR2 deviate from unity. This arises since the relative intensities of the component peaks in the unknown spectrum are altered, as a result of overlapping spectral bands, with respect to the individual species in the reference library. In addition, the unknown bicomponent spectrum may have aggregate features similar to unique single component reference spectra stored in the library.

SIPS lists the reference spectra which have CR1 values greater than 0.9500 and then relies upon the user to assist in the evaluation of the data. On utilization of the chrysene/pyrene mixture as a representative unknown, the reference spectrum that had the largest CR1 value was chrysene (0.9978). The correlation values for 2-phenylphenanthrene, pyrene, and 4,4-di(n-butyl)-1,1-bisnaphthyl were 0.9943, 0.9934, and 0.9904, respectively. These values indicate that the spectral features of the unknown have the largest degree of similarity when compared with the reference spectrum of chrysene. The unknown might indeed be thought to contain pyrene, 2-phenylphenanthrene, or 4,4-di(n-butyl)-1,1-bisnaphthyl since the CR1 values for these compounds are high. Reliance upon the CR2 parameter in this case must be done carefully since the large degree of spectral overlap for this mixture causes the peaks to merge and to change intensity, thereby causing the absolute magnitude at  $\nu = 0$  to increase. Consequently in the case of highly overlapped spectra, the ratio between the value at  $\nu = 0$  and variable SUMSQ, corresponding to a reference spectrum that is a component of the unknown mixture, will be greater than unity.

Chrysene and pyrene both have CR2 values greater than unity, while 2-phenylphenanthrene and 4,4-di(n-butyl)-1,1-bisnaphthyl do not. This evidence strongly suggests that both chrysene and pyrene are present in the unknown mixture. If chrysene is chosen as a match, a second search which subtracts the chrysene spectrum and reanalyzes the resultant spectrum as a unique unknown is carried out. The CR1 and CR2 values tabulated in Table IV confirm the presence of pyrene in the sample. Although 3,4-benzophenanthrene has an exceptionally

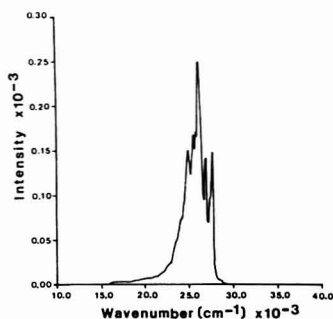


Figure 6. Input fluorescence spectrum of a mixture of pyrene and chrysene.

good CR1 value of 1.000, the CR2 value of 0.6477 is much smaller than 1.00 and therefore allows this species to be eliminated from consideration.

Spectra acquired in this laboratory were satisfactorily identified by use of SIPS when the unknown and reference spectra were well-behaved in the sense of not exhibiting concentration quenching. Mixtures were also identified properly when all species were individually well-behaved. Under these conditions, identification of real mixtures resulted in search patterns essentially unchanged from those shown for the synthetic mixtures of Tables III and IV. In some cases (substituted naphthalenes for instance), the results using emission spectra are unsatisfactory; work is ongoing to incorporate excitation spectra into the search scheme in an attempt to reduce the number of spurious identifications.

Identification of conventional molecular fluorescence spectra via cross-correlation benefits from an encoding process which allows for full data retention. Previous work (6) has shown that the higher frequency harmonics present in the transformed spectra can be removed without any substantive loss of spectral information, and ongoing work in this laboratory seeks to incorporate such data compression.

File searching of fluorescence spectra is plagued by the irreproducibility of fluorescence spectra from one instrument to another. Data obtained in various laboratories (17, 20) indicate that spectra cannot be adequately corrected by reliance upon a series of standard spectra. Yim and Faulkner (6, 21) have shown that point by point division of an unknown spectrum by the spectrum of a standard material can be beneficial.

The lack of comparability among spectra collected on different instruments has hindered the development of

fluorescence file searching routines. Conversely, this absence has diminished the need to develop standard protocols for fluorescence instrumentation. This interface between the requirements of the collection and identification of fluorescence spectra promises to be a challenging area for future investigation.

The FORTRAN code for SIPS compiles and runs under the TOPS-10 operating system on the University of Delaware Computer system DEC-10 system. Source listings are available from the author. Portability is restricted by the IMSL subroutine calls and by use of DELPLOT for hard-copy graphics output.

### ACKNOWLEDGMENT

The assistance of Cecil Dybowski and the insights he provided regarding the broader aspects of Fourier transforms is gratefully acknowledged. The cooperation and help of Isadore Berlman in making available a computer-readable library file of spectra aided this work immeasurably.

**Registry No.** Anthracene, 120-12-7; 3,4-benzophenanthrene, 195-19-7; naphthalene, 91-20-3; deuterated anthracene, 54261-80-2; benzidine, 92-87-5; sodium salicylate, 54-21-7; tetramethyl-*p*-octaphenyl, 83399-67-1; tetramethylphenylenediamine, 27215-51-6; pyrene, 129-00-0; perylene, 198-55-0; 2-aminoanthracene, 613-13-8; rubrene, 517-51-1; chrysene, 218-01-9; 2-phenylphenanthrene, 4325-77-3; 4,4-di(*n*-butoxy)-1,1-bisphenyl, 4499-67-6; 1,4-diphenylnaphthalene, 796-30-5.

### LITERATURE CITED

- (1) Hirata Y.; Novotny, M.; Peaden, P. A.; Lee, M. L. *Anal. Chim. Acta* **1981**, *127*, 55-61.

- (2) Shpol'skii, E. V. *Sov. Phys.-Usp. (Engl. Transl.)* **1962**, *5*, 522-531.
- (3) Green, L. G.; O'Haver, T. C. *Anal. Chem.* **1974**, *46*, 2191-2196.
- (4) Warner, I. M.; Christian, G. D.; Davidson, E. R.; Callis, J. B. *Anal. Chem.* **1977**, *49*, 564-573.
- (5) Miller, T. C.; Faulkner, L. R. *Anal. Chem.* **1976**, *48*, 2083-2088.
- (6) Yin, K. W. K.; Miller, T. C.; Faulkner, L. R. *Anal. Chem.* **1977**, *49*, 2069-2074.
- (7) Gold, H. S.; Rechsteiner, C. E.; Buck, R. P. *Anal. Chim. Acta* **1977**, *95*, 51-58.
- (8) Stadalus, M. A.; Gold, H. S. *Federation of Analytical Chemistry and Spectroscopy Societies Meeting*, Philadelphia, PA, Sept 1981; paper 62.
- (9) Small, G. W.; Rasmussen, G. T.; Isenhour, T. L. *Appl. Spectrosc.* **1979**, *33*, 444-450.
- (10) Powell, L. A.; Hietje, G. M. *Anal. Chim. Acta* **1978**, *100*, 313-327.
- (11) Cooley, J. W.; Tukey, J. W. *Math. Comput.* **1965**, *19*, 297-309.
- (12) Horlick, G.; Hietje, G. M. In "Contemporary Topics in Analytical and Clinical Chemistry"; Hercules, D. M., Hietje, G. M., Snyder, L. R., Evenson, M. A., Eds.; Plenum: New York, 1978; Vol. III.
- (13) Horlick, G. *Anal. Chem.* **1973**, *45*, 319-324.
- (14) Lam, R. B.; Wieboldt, R. C.; Isenhour, T. L. *Anal. Chem.* **1981**, *53*, 889A-901A.
- (15) Marshall, A. V. In "Fourier, Hadamard, and Hilbert Transforms in Chemistry"; Marshall, A. G., Ed.; Plenum: New York, 1982.
- (16) Berne, B. J.; Pecora, R. "Dynamic Light Scattering"; Wiley: New York, 1976.
- (17) Berlman, I. B. "Handbook of Fluorescence Spectra of Aromatic Molecules"; Academic Press: New York, 1971.
- (18) Gold, H. S.; Rechsteiner, C. E.; Buck, R. P. *Anal. Chem.* **1976**, *48*, 1540-1546.
- (19) Bendat, J. S.; Piersol, A. G. "Random Data: Analysis and Measurement Procedures"; Wiley-Interscience: New York, 1971.
- (20) Demas, J. N.; Crosby, G. A. *J. Phys. Chem.* **1971**, *75*, 991-1024.
- (21) Yin, K. W. K. Ph.D. Dissertation, University of Illinois at Urbana-Champaign, Urbana, IL, 1978.

RECEIVED for review May 17, 1982. Accepted September 24, 1982. Partial support of this research was provided by the American Cancer Society under Grant IN-159.

## Determination of Salicylic Acid in Aspirin Powder by Second Derivative Ultraviolet Spectrometry

Keisuke Kitamura\* and Ryo Majima

Kyoto College of Pharmacy, 5 Nakaguchi-cho, Misasagi, Yamashina-ku, Kyoto 607, Japan

The second derivative spectrum of salicylic acid showed a trough at 292 nm and a satellite peak at 316 nm. When large amounts of aspirin coexisted, the trough disappeared but the height of the satellite peak ( $D_1$ ) was not altered even at an aspirin concentration 20 000 times that of salicylic acid (corresponding to salicylic acid content of 0.005 %). A plot of 25 sets of  $D_1$  values and salicylic acid concentrations (1.00-10.02  $\mu\text{g/mL}$ ) gave a straight line (correlation coefficient = 0.9999) and relative standard deviation ( $s/\bar{x}$ ) for a slope of 1.2%. A typical assay result for commercial aspirin powder was that the content of salicylic acid was  $0.0361 \pm 0.0005$  % (at the 95 % confidence limit) with  $s/\bar{x}$  of 1.2% for five measurements.

It has been shown that the application of derivative techniques to spectrophotometry is very useful when there exists signal overlapping or interferences (1-3). Moreover, the experimental procedure is simple and time-saving. Despite these advantages, however, few applications of derivative spectrophotometry have been published (4-7).

This paper describes an application of second derivative UV spectrometry to permit a simple and rapid assay of sal-

icylic acid in aspirin powder. As salicylic acid, the major decomposition product of aspirin, irritates the digestive system, the limit of salicylic acid content in aspirin powder is prescribed to be 0.1% by the Pharmacopeias (8, 9). But the assay for aspirin powder described in them is qualitative. There have been some reports on the assay for salicylic acid of 0.1 % content level in aspirin by gas-liquid chromatography (GLC) (10), liquid chromatography (11), and high-performance liquid chromatography (12). Although the retention times of salicylic acid were within 10 min in every one of these chromatographic methods (10-12), time-consuming chromatographic conditioning was essential for all of them and chemical derivatization was necessary for the GLC method (10).

### EXPERIMENTAL SECTION

**Solvent and Chemicals.** A 1 % chloroacetic acid-ethanol solution was used as solvent. Salicylic acid was twice recrystallized from hexane, and standard salicylic acid solutions of various concentrations were prepared by dilution of a stock solution with the solvent. Salicylic acid free aspirin was obtained by twice recrystallization of aspirin from acetone.

**Preparation of Assay Solutions.** Assay solutions were prepared immediately before measurement. A 150-mg sample of aspirin powder was dissolved in the solvent to bring the mixture to 25.0 mL.

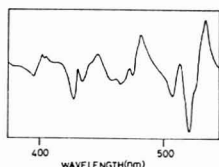


Figure 1. Second derivative spectrum of a didymium filter.

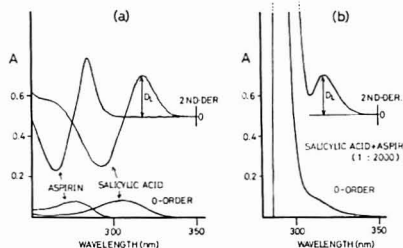


Figure 2. Absorption (zero order) and second derivative spectra of salicylic acid ( $3.0 \mu\text{g/mL}$ ) and aspirin ( $12.1 \mu\text{g/mL}$ ) (a) and the spectra of their mixture in the concentration ratio of 1:2000 (b).

**Second Derivative UV Spectrometry.** A differentiator was constructed with electronic derivative circuits (1, 13). Three circuits having varied differential time constants (2.7, 8.2, and 22.0 s) were incorporated and any one of them could be selected by switching. The differentiator was connected to a double-beam scanning spectrophotometer, Shimadzu UV-210A. The derivative spectra were obtained at a slit width of 1 nm, a scanning speed of 120 nm/min, and a time constant of 22.0 s.

## RESULTS AND DISCUSSION

**Second Derivative Spectrum of a Didymium Filter.** Figure 1 shows a second derivative spectrum of a didymium filter measured under the same derivative conditions employed for the assay of salicylic acid (see Experimental Section). The positions of troughs in the second derivative spectrum were shifted along the scanning direction (toward short wavelength) by about 10 nm relative to corresponding peaks in nonderivative absorption spectrum. The spectrum may serve as a certain index when the derivative conditions are referred to other derivative devices or methods.

**Absorption (Zero Order) and Second Derivative Spectra of Salicylic Acid, Aspirin, and Their Mixture (1:2000).** The absorption spectra of salicylic acid ( $3.0 \mu\text{g/mL}$ ) and aspirin ( $12.1 \mu\text{g/mL}$ ) are depicted at the bottom of Figure 2a. Since the concentration of aspirin was not much higher than that of salicylic acid, the zero-order spectrum of aspirin showed no absorption at the  $\lambda_{\text{max}}$  of salicylic acid (302 nm). Thus the concentration of salicylic acid in a mixture with a comparable amount of aspirin could be determined from the absorbance at 302 nm without any interference of aspirin signal. However, since the content of salicylic acid in aspirin powder is prescribed not to exceed 0.1% (8, 9), the concentration of aspirin would be considerably higher than 1000 times that of salicylic acid in practical cases. The zero-order spectrum of a mixture of salicylic acid and a great quantity of aspirin (about 2000 times of salicylic acid) is illustrated in the lower part of Figure 2b. The salicylic acid signal was severely interfered with by a large aspirin band, so that the determination of salicylic acid by conventional absorption spectrometry would not be feasible.

The upper spectra in Figure 2a illustrated the second derivative spectra of salicylic acid and aspirin, respectively. The

spectrum of salicylic acid showed a trough at 292 nm and a satellite peak at 316 nm, and the spectrum of aspirin showed a trough at 264 nm and a satellite peak at 284 nm. It was apparent from comparing the zero order and second derivative spectra in Figure 2a that the detection power for both salicylic acid and aspirin was enhanced by differentiation. The limit of detection for salicylic acid in the second derivative spectrum was about  $0.12 \mu\text{g/mL}$ , since the height of trough-to-peak was almost equivalent to twice of peak-to-peak noise at this concentration.

The second derivative spectrum for the mixture of salicylic acid and aspirin (1:2000) is shown in the upper part of Figure 2b. On account of the large satellite peak of aspirin, the trough of salicylic acid at 292 nm disappeared but the satellite peak of salicylic acid at 316 nm seemed to be reproduced. If the height of the satellite peak measured with respect to the derivative zero, denoted by  $D_L$  in Figure 2, would not be affected by coexisting aspirin, it could be used for the quantitative determination of salicylic acid in aspirin powder.

**Effect of Coexisting Aspirin on  $D_L$  Values.** The influence of aspirin signal on  $D_L$  values could be known by comparing the  $D_L$  values of a solution of salicylic acid alone with that of a solution having the same salicylic acid concentration but containing large amounts of aspirin. For this purpose salicylic acid free aspirin was needed, since if aspirin added to a salicylic acid solution contained salicylic acid originally, the amount of salicylic acid in the solution would be increased and the results could not be reliable. Salicylic acid in aspirin was removed by recrystallization. When the second derivative spectrum of highly concentrated aspirin solution (6 mg/mL) did not show any signal at 316 nm ( $D_L = 0$ ), the aspirin was considered salicylic acid free. Among the several recrystallization solvents (benzene, chloroform, dioxane, isopropyl alcohol), only acetone could give salicylic acid free aspirin.

One more problem which would make results uncertain was the hydrolysis of aspirin to salicylic acid in the sample solution during the experiment. When a second derivative spectrum of salicylic acid free aspirin in ethanol (6 mg/mL) was measured repeatedly at intervals of a few minutes, the recorded line at 316 nm gradually raised from the base line due to the formation of salicylic acid by the hydrolysis of aspirin. In order to suppress the hydrolysis of aspirin, acid-containing ethanol could be used as solvent (14). Three kinds of acid, phosphoric acid (85%), acetic acid, and chloroacetic acid were tested. A 60-mg sample of salicylic acid free aspirin was dissolved in 10 mL of ethanol which contained one of these acids with 1% concentration and the second derivative spectrum was taken repeatedly for 1 h with some time intervals. The plot of the obtained  $D_L$  values against the time (0–60 min) yielded a straight line for each acid. The comparison of the suppression effect of each acid was carried out by using slopes of the lines. The results summarized in Table I showed that the hydrolysis of aspirin was most effectively suppressed in 1% chloroacetic acid-ethanol solvent, since the slope of this solvent was about one-seventh that of ethanol. Though the hydrolysis of aspirin could be suppressed to some extent by using this solvent, it was still recommended for higher accuracy that the experimental procedure, from dissolution of aspirin to measurement of spectrum, was to be accomplished within 15 min. Since the time necessary for one scanning was about 1.5 min, measurement of spectrum for a sample could be repeated five times in 15 min.

The influence of aspirin signal on  $D_L$  value was investigated at three different salicylic acid concentrations of 5.0, 1.0, and  $0.3 \mu\text{g/mL}$  and the amount of aspirin incorporated was 0–6 mg/mL. The measurement of spectrum was repeated five times for each samples and the mean value of five  $D_L$  values

**Table I. Suppression Effects of Acids on Aspirin Hydrolysis in Ethanol Solution**

acid added	concn in ethanol, %	slope, <sup>a</sup> mm/h
none		15.1
phosphoric acid (85%)	1	10.0
acetic acid	1	5.2
chloroacetic acid	1	2.1

<sup>a</sup> The slope was obtained from the plot of  $D_L$  values against time. Derivative conditions are given in the Experimental Section.

**Table II. Effect of Aspirin Concentration on the Height of Second Derivative Satellite Peak of Salicylic Acid ( $D_L$ )**

salicylic acid concn, $\mu\text{g/mL}$	amt of aspirin added, mg/mL	fraction of salicylic acid, %	$D_L$ , <sup>a</sup> mm
5.014	0.0	100.0	40.41
	6.01	0.0834	40.07
1.003	0.0	100.0	8.28
	6.14	0.0163	8.29
0.301	0.0	100.0	2.42
	6.15	0.0049	2.46

<sup>a</sup> Mean value of the five duplicate measurements.

was taken. The results are shown in Table II. At every salicylic acid concentration, there could not be seen any effect of the coexisting aspirin on  $D_L$  values, even where the amount of aspirin incorporated was more than 20000 times that of salicylic acid (corresponding to salicylic acid fraction of 0.0049%).

**Calibration Curve for Salicylic Acid.** To obtain a calibration curve for salicylic acid, the second derivative spectra of standard salicylic acid solutions were taken for five varied concentrations (1.002–10.015  $\mu\text{g/mL}$ ). The spectrum was measured five times for each concentration, so that 25 sets of  $D_L$  values ( $y$ ) and salicylic acid concentrations ( $x$ ) were obtained. The correlation coefficient between  $y$  and  $x$  was calculated to be 0.9999 and a plot of  $y$  against  $x$  yielded a good straight line which intercepted the origin. The slope was 8.01 mm/( $\mu\text{g/mL}$ ) with a relative standard deviation ( $s/x$ ) of 1.2%. These corresponded to the confidence limits of  $8.01 \pm 0.04$  mm/( $\mu\text{g/mL}$ ) at the 95% level. The salicylic acid concentration  $x$   $\mu\text{g/mL}$  could be calculated from  $1/\text{slope} \times D_L$ , that is

$$x = 0.125 \times D_L \quad (1)$$

Accuracy of the second derivative method for salicylic acid was calculated by eq 2, using the data of the calibration curve

$$\% \text{ accuracy} = (\bar{x} - \bar{\bar{x}}) / \bar{x} \times 100 \quad (2)$$

where  $\bar{x}$  is the prepared concentration of salicylic acid in a standard solution and  $\bar{\bar{x}}$  is the mean value of the salicylic acid concentrations calculated by eq 1 for each five  $D_L$  values. As the results in Table III show, good accuracy was proved for the second derivative method at every salicylic acid concentration.

**Assay of Commercial Aspirin Powders.** Three kinds of commercially obtained aspirin powders A, B, and C were assayed and the results are listed in Table IV. The salicylic acid content of the aspirin powders tested fell well within 0.1%. The statistical calculations of the assay results showed satisfactory precision of the derivative method.

In conclusion, it was demonstrated that the second derivative UV spectrometry could permit a simple and time-saving assay of salicylic acid in aspirin powder which had sufficiently

**Table III. Accuracy in Second Derivative UV Spectrometric Determination of Salicylic Acid**

salicylic acid concn, $\mu\text{g/mL}$	$\bar{x}$ <sup>b</sup>	% accuracy $100(\bar{x} - \bar{\bar{x}})/\bar{x}$
1.002	1.004	0.20
2.003	2.004	0.05
3.005	2.994	-0.37
5.008	5.024	0.32
10.015	10.031	0.16

<sup>a</sup> Prepared value. <sup>b</sup> Mean value of five  $\bar{x}$ 's calculated from  $D_L$  values using eq 1.

**Table IV. Assay Results of Salicylic Acid in Commercial Aspirin Powders**

sam- ple	salicylic acid		
	aspirin concn, mg/mL	content, %	
A	6.060	2.16	0.0356
	5.976	2.15	0.0360
	6.092	2.18	0.0358
	5.924	2.15	0.0363
	6.040	2.22	0.0367
B	6.248	2.38	0.0381
	5.928	2.24	0.0378
	6.032	2.26	0.0375
	6.100	2.30	0.0377
	5.968	2.20	0.0369
C	5.980	1.56	0.0261
	5.992	1.64	0.0274
	5.996	1.59	0.0265
	6.084	1.65	0.0271
	6.154	1.68	0.0273

<sup>a</sup> Confidence limits at 95% level. <sup>b</sup> Relative standard deviation.

good accuracy and precision. The method could have a possibility of application to the similar problem of determining very small amounts of impurity in pure chemicals.

#### ACKNOWLEDGMENT

The authors thank M. Takagi for her assistance with the experiments.

**Registry No.** Salicylic acid, 69-72-7; aspirin, 50-78-2.

#### LITERATURE CITED

- Talsky, G.; Mayring, L.; Kreuzer, H. *Angew. Chem., Int. Ed. Engl.* **1978**, *17*, 785-874.
- O'Haver, T. C. *Anal. Chem.* **1979**, *51*, 91A-100A.
- Fell, A. F. *UVG Bull.* **1980**, *8*, 5-31.
- Fell, A. F. *Proc. Anal. Div. Chem. Soc.* **1978**, *15*, 260-267.
- Such, V.; Traveset, J.; Gonzalez, R.; Gelpi, E. *Anal. Chem.* **1980**, *52*, 412-419.
- Fell, A. F.; Davidson, A. G. *J. Pharm. Pharmacol., Suppl.* **1980**, *32*, 97P.
- Fell, A. F.; Jarvie, D. R.; Stewart, M. J. *Clin. Chem. (Winston-Salem, N.C.)* **1981**, *27*, 286-292.
- "Pharmacopoeia of the United States XX"; United States Pharmacopoeial Convention, Inc.: Rockville, MD, 1980; p 56.
- "Pharmacopoeia Japonica Edito Deca"; Ministry of Health and Welfare: Tokyo, Japan, 1980; p 41.
- Patel, S.; Perrin, J. H.; Windheuser, J. J. *J. Pharm. Sci.* **1972**, *61*, 1974-1976.
- Baum, R. G.; Cantwell, F. F. *J. Pharm. Sci.* **1978**, *67*, 1066-1069.
- Gupta, V. D. *J. Pharm. Sci.* **1980**, *69*, 113-115.
- Green, G. L.; O'Haver, T. C. *Anal. Chem.* **1974**, *46*, 2192-2196.
- Martin, A. N.; Swarbrick, J.; Cammarata, A. "Physical Pharmacy", 2nd ed.; Lea & Febiger: Philadelphia, PA, 1969; p 388.

RECEIVED for review June 23, 1982. Accepted September 28, 1982. Financial support of this research was provided by Kyoto College of Pharmacy. This research was presented in preliminary form at the 102th Annual Meeting of Pharmaceutical Society of Japan, Osaka, April 1982.

# Spatial Discrimination in Spark Emission Spectrochemical Analysis

John P. Walters\*<sup>1</sup> and William S. Eaton<sup>2</sup>

Department of Chemistry, University of Wisconsin, Madison, Wisconsin 53706

An adjustable wave form spark source and argon flow jet are used to produce a positionally stable spark train. The image of the spark is relayed to an intermediate focal plane containing masks of varying diameters. Background, plasma, and ionized electrode emissions are minimized by positioning the mask in front of the central core of the discharge, leaving simpler spectra with less noise to enter the spectrometer. Three- to ten-fold improvements in signal/noise are reported for common impurities in commercial aluminum alloys. It is shown that lost signal due to masking can be recovered by rotating the disk sample and increasing the repetition rate of the source.

The signal and background levels in a positionally stabilized spark discharge can be decoupled. The discharge displays radial structure, with many of the common analytical lines emitting in its radial wings (1). Much of the background and its noise is, however, confined more to the central core, along and coaxial with the interelectrode axis. If the light observed from the discharge is restricted to that originating in the outer radial regions, the spectra are simpler, the lines narrower, and the signal to noise ratios higher than observed if all of the radiation is detected.

There is additional information in the time domain (2, 3). The analytical signals tend to maximize when the time derivative of the discharge current is negative, while background and plasma ion noise signals tend to maximize when it is positive. Example spectroscopic data showing these characteristics of a positionally stable spark have been published, along with evidence and ideas on their physical causes (4).

When either spatial or temporal discrimination is used in observing the radiation emitted from a positionally stable spark train, some usable signal is lost. This occurs mainly because the separation in time or space between signal and noise is not abrupt, but rather continuously melds from region to region (5). This need not be a fatal flaw to the discrimination technique if the losses can be compensated by a real increase in the amount of useful signal generated by the spark. We have shown this to occur when the repetition rate of the spark source is increased (6) and the early times in the burn monitored (7). Thus, by combination of higher repetition rates with techniques that use more of the electrode surface to give the equivalent of observation early during a burn, spatial or temporal discrimination will show real improvements as mentioned, without significant analytical system losses.

To illustrate the discrimination technique, experiments were conducted with conservative equipment and straightforward procedures. These methods obviously would not be used in a production situation. For example, for exploration of all effects of parameter changes knowledgeably, data were recorded photographically, with darkroom procedures suffi-

ciently standardized to allow day-to-day reproducibility on the order of 5% or less. To produce the discharge train and cover a wide range of repetition rates, we modified an air-interrupter spark source (8) to produce a pulsating, unidirectional current wave form. To stabilize the discharge positionally, we directed argon coaxially with the interelectrode axis, from anode to cathode, using a simple nozzle (9-11).

To capitalize on the increased sampling efficiency that occurs during the first portions of a burn with a positionally stable spark discharge (7), without actually time-resolving the photographically-detected spectra, we rotated the aluminum cathode at ~4 rpm during the exposure. This provided a continually refreshed electrode surface, giving the same performance spectroscopically as is observed during the first few seconds of a burn to a stationary electrode attacked by a positionally stable spark. This also allowed a primitive averaging of the radial inhomogeneities in the electrode (12-14). Then a modest adjustment in the repetition rate was done to accent the electrode signal over the background, again due to enhancements in the sampling efficiency (6, 7).

Spectral lines for analysis were selected from temporally and radially resolved spectra, obtained from instrumentation that allowed high-fidelity acquisition of such multidimensional spectra (15). All analytical data were acquired in a time-integrated mode. To verify that the line intensities detected in this mode were responsive to the spark source parameters (16), we measured the time integral of the current wave form as a function of changes in the source inductance. Then, the line intensities for selected test lines from the cathodic electrode were also measured as a function of increasing source inductance. Correlation between these data was used to signal proper correspondence between the spark source and electrode sampling. In all, the spark source, while conservative in comparison to present computer-controlled electronic units (17), was well behaved.

In this paper, the above introductory remarks will be amplified with experimental parameters. Then data taken with aluminum electrodes sparked in argon will be presented to illustrate the points made. We will also show spectra and microscope data that address the issue of increased current efficiency relative to electrode sampling. Following this, we will show the improvement in spectral simplification and in signal to noise ratios that result from optically masking the central core of the discharge.

## EXPERIMENTAL SECTION

The apparatus consisted of a modified (8) air-interrupter spark source, a conventional arc-spark stand containing an electrode rotator assembly, a quartz transfer lens, a concave grating eagle spectrograph, conventional darkroom equipment, a recording densitometer, and an assortment of conventional electronics and electrode preparation devices. A complete set of experimental parameters for the above is given in Table I.

Electrodes were prepared by machining disks of aluminum to the proper circular shape and then drilling and tapping a small hole in their center. One surface was then turned to a smooth finish. The disk was then mounted on a rotating arbor in the spark stand as shown in Figure 1. The disk was cathodic with respect to the tungsten pin counterelectrode. The counterelectrode was

<sup>1</sup>Present address: Department of Chemistry, St. Olaf College, Northfield, MN 55057.

<sup>2</sup>Present address: Rockwell International, P.O. Box 27930, Denver, CO 80227.

Table I. Experimental Parameters

source: National Spectrographic Laboratories, KE-1234, modified as per ref 8	
capacitance	0.012 $\mu$ F
spark power	10
resistance	0 added
inductance, L1	56 $\mu$ H
inductance, L2	variable, 5–40 $\mu$ H
oscilloscope	Tektronix 547/1A1
current monitor	Pearson, Type 110, current transformer into 1 M $\Omega$
spark stand: Spex Industries, Inc., No. 9010 arc/spark stand	
electrode gap	3 mm typ
cathode electrode	aluminum flat (see Figure 1)
anode electrode	3% thoriated tungsten (see Figure)
gas	argon
flow rate	0.6 L/min
cathode rotation	4 rev/min
spectrograph: Baird-Atomic RDRS Mod. 6X-1, 3.0 m Eagle Mount	
slit width	0.050 mm
spectra/plate	28, with 2.5 mm plate aperture
grating angle	3°
grating mask	1.8 cm height
wavelength range	2400–5100 Å
dispersion	5.5 Å/mm, first order
emulsion: Kodak, type SA-1, 4 × 10 glass plates	
development	Kodak, D-19, 4 min
stop	Kodak stop, 30 s
fix	Kodak fix, 10 min
wash	deionized water, 30 min
processor	Jarrell-Ash Model 34-301
calibration	Baird-Atomic seven-step sector, 3-A DC iron arc
densitometer	
	Baird-Atomic, recording, Model RC-2, operated as per
	slit height 1 mm
	slit width 0.007 mm
	scan rate 0.0055 mm/s

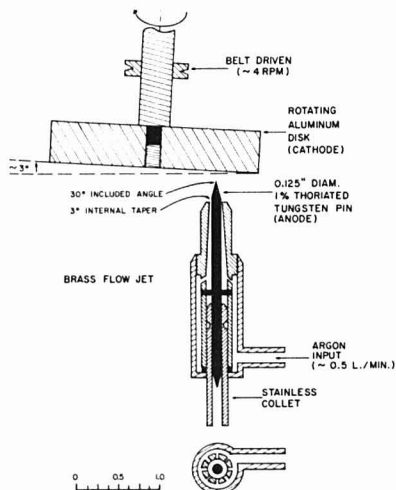


Figure 1. Electrode configuration and nominal experimental parameters for producing stable spark discharges.

mounted to a jet assembly, through which argon was delivered coaxially with the tungsten pin. The pin was held in a collet and

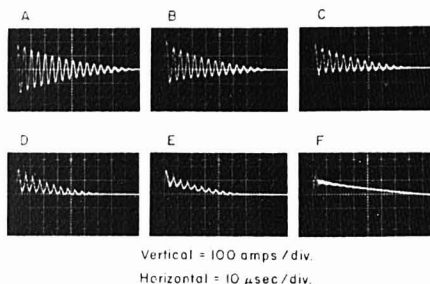


Figure 2. Current wave forms produced from the source described in ref 8 under the following parameters. L1 = 56  $\mu$ H & L2 as per: (A) residual, (B) 0.1  $\mu$ H, (C) 2.2  $\mu$ H, (D) 6.0  $\mu$ H, (E) 10  $\mu$ H, (F) 88  $\mu$ H.

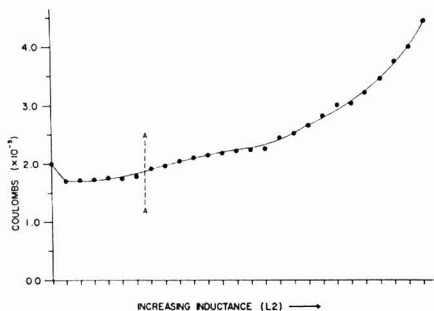


Figure 3. Coulombs per spark for current wave forms varying from fully oscillatory (left of line A–A) to fully unidirectional (right of line A–A). For the oscillatory discharges the coulombs apply only to half cycles where the aluminum electrode in Figure 1 was cathodic.

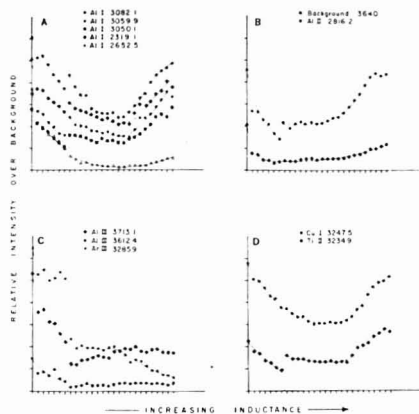
centered in the jet with three screws at 120° separations, such that it could be replaced periodically. With this configuration and the air-interrupter spark source, the discharge was sufficiently stable to produce a burn between 2 and 3 mm in diameter at electrode separations between 2 and 4 mm. The gas flow was adjusted about a nominal value of 0.5 L min<sup>-1</sup> to produce optimum stability.

The spark source parameters were fixed, except for the wave-shaping inductance L2 (18). This was adjusted to produce the wave forms shown in Figure 2. The current was measured with a Pearson Electronics Model 110 current transformer into a Tektronix type 547/1A1 oscilloscope/plug-in combination. These wave forms were selected as working standards to be used for all measurements. They allow the range of charge shown in Figure 3 to be delivered to the aluminum electrode. The aluminum and selected impurity lines that were chosen to monitor signal to background changes with respect to spatial discrimination are indicated in Figure 4. It is evident that they are all responsive to the changes in current wave form in reasonable proportion to the changes in the number of coulombs delivered to the electrode (19–21).

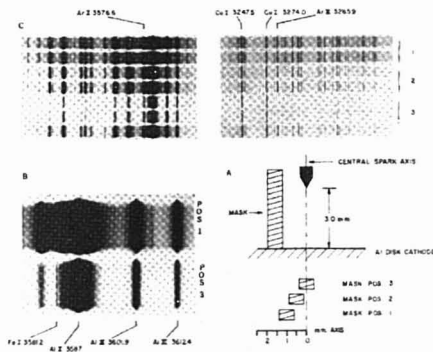
Optical discrimination is accomplished by placing one or another of a series of copper wires at Sirks focus in front of and parallel to the spectrograph slit and then focusing an image of the positionally stable spark channel on the wire using a 20-cm focal length biconvex quartz lens. Corrections for chromatic aberration were not made (22). The experiment as executed is shown schematically in inset A of Figure 5.

A wire having a preselected diameter between 0.5 and 2.5 mm is placed between the spectrograph entrance slit and the spark gap, in line with the spark and to one side of the optical axis. The electrode is started rotating and the spark started. After five to





**Figure 4.** Relative intensities of selected spectral lines in response to the same changes in source inductance L2 as reported in Figure 3. Matrix and sample impurity lines in insets A, B, and D respond to the coulombs delivered to the aluminum electrode; background, Al III, and Ar III lines do not (insets B and C).

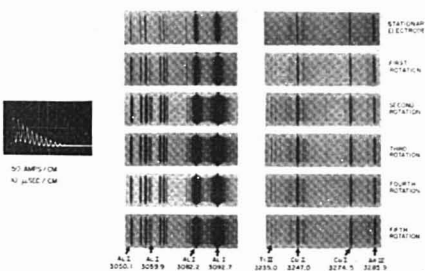


**Figure 5.** Illustration of the masking experiment (inset A) and the changes in detected spectra that result from different mask positions. Spectral simplification for two mask positions is shown in inset B. Background reduction for three mask positions is shown in inset C. The current wave form is D in Figure 2.

six full revolutions, the emission from the spark has stabilized (see Figure 6). The shutter to the spectrograph is then opened and an exposure taken. The spectrograph camera is then racked to a new position, and the identical run repeated with a new electrode mounted in the stand.

After each pair of exposures, the mask is shifted in position by at least one diameter closer to the optical axis, and the same complete exposure routine is repeated. A set of exposures usually is taken, corresponding to moving the mask completely through coincidence with the optical axis. Spectra similar to those in Figure 5 result, where each two positions on the plate correspond to duplicate runs at one mask position. A few lines are identified in Figure 5 to illustrate the more obvious spectral simplification that results when the mask has been moved to a position directly coincident with the spark channel.

Proper darkroom and densitometer procedures are essential, since each masking experiment may require as many as a separate set of plates per parameter change. A Jarrell-Ash 34-300 photoprocessor was used to develop the plates according to the pa-



**Figure 6.** Nonmasked spectra observed as the aluminum cathode shown in Figure 1 rotated under the positionally stable spark. Masking experiments are begun after the third or fourth rotation. See ref. 7.

rameters in Table I. After being washed, each plate was carefully wiped with photographic sponges dipped in Kodak PhotoFlo 200 wetting solution, and dried under gentle heat to a spot-free condition. For quantitation, a conventional seven-step sector method of emulsion calibration (23) was used to convert  $T$  to relative intensity. Each development was done on two plates at the same time, and each pair of plates was calibrated before quantitation.

### CALIBRATION

Two parts of the experiment were calibrated before spatial discrimination work was begun. The first part was to verify for the matrix lines of aluminum that there was a correspondence between the total amount of charge delivered to the electrode and the integrated line intensities, both in terms of the number of coulombs per spark (i.e., the area of the current wave form) and in terms of the number of sparks per second per exposure (i.e., the repetition rate). This is necessary to allow normalization of spectra that have different degrees of spatial discrimination, so that when a particular signal to noise ratio is observed, it also is known what fraction of the total intensity changes that have occurred can be compensated via spark source adjustment.

The spark source was calibrated by photographing the current wave forms of interest, graphically measuring their area, and then plotting that area against the relative value of the inductance L2 that was used to produce the different wave forms. When the discharge was oscillatory, only the area of the half cycles when the aluminum electrode was cathodic was measured. Then the same changes in inductor L2 were used to prepare a series of time integrated spectra. Lines were identified in these spectra that were expected to be useful in the discrimination studies as indexes of the amount of "signal" present, i.e., the analytical signal of choice due to the electrode material as opposed to the plasma lines and continuous background. The intensities of these lines were measured and plotted as a function of the same relative value of the inductor L2.

The source data are shown in Figure 3. The abscissa is not linear, and should be interpreted only in terms of the data shown in Figure 4, where relative line intensities over background are plotted against the same set of source inductances. Data to the left of the vertical dotted lines in both figures correspond to an oscillatory discharge, while data to the right correspond to a pulsating unidirectional current wave form. Correlation plots were not made of the line intensities directly against number of coulombs because the discontinuity that occurs when the wave form changes from oscillatory to unidirectional changes the physical nature of the discharge as well as the current wave form (18).

The data in Figure 4 for the unidirectional current wave forms indicate that most Al I line intensities respond to in-

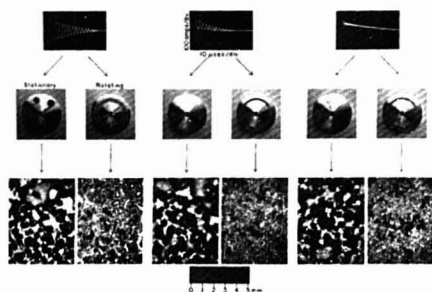


Figure 7. Microscopic comparison of turned aluminum cathode surface erosion by the spark current wave forms shown when the electrode is rotated during an exposure and held still. See also ref. 7.

creases in the area of the current wave form (e.g., inset A), as do selected Al II, Ti II, and Cu I lines (insets B and D). Background does not, at least to the same degree as the above lines, nor do the selected set of Al and Ar III lines shown in inset C. We conclude from these data that any signal lost in a discrimination experiment could at least be partially recovered by increasing the number of coulombs delivered to the sample electrode via adjustments in the source wave-shaping inductor L2.

Because there were cases when it was not desirable to change the current wave form, a second calibration experiment was done on the spark source to determine how time integrated line intensities could be increased by adjustment in spark source repetition rate. Because the literature precedent is against this as an effective parameter for such adjustments (24, 25), we report here our first investigations on microscopic electrode erosion patterns produced by different current wave forms. The data in Figure 7 show differences in electrode erosion that result on an aluminum cathode held stationary under a positionally stable spark compared to one that is rotated at approximately 4 rpm for three different wave forms. The "puddled" appearance of the stationary electrode is clear, as is its traceability to a lack of electrode rotation, rather than a unique current wave form (26).

We have shown that when an electrode has this "puddled" appearance (7), the emitted light is both noisier and of lower intensity than when the electrode surface erosion has a more granular appearance. Further, we have shown (6) that under the conditions that produce the granular erosion, the spark source repetition rate is effective as a parameter that affects time integrated line intensities. These independent observations are verified here by comparing the effect of repetition rate on the intensities of selected lines for stationary and rotating electrodes.

The data in Figure 8 show the effect of source repetition rate on line intensities over background for a stationary electrode. It is evident that the main effect of increasing the repetition rate in this case is to increase the intensity of the spectral noise, i.e., the Ar III, Ar II, and background radiation. The matrix and analytical impurity lines respond only sluggishly if at all to the increased repetition rate. However, as shown in Figure 9, the situation is much different when the electrode is rotated. In that case, the analytical line intensities over background increase with increases in source repetition rate at least as much as the plasma and background radiation, and in some cases to a greater degree. This represents a real increase in available signal. From these data, and our previous work, we conclude that there has been a real increase in the sampling efficiency.

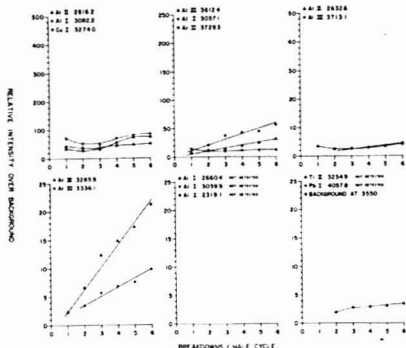


Figure 8. Effect of spark source repetition rate on selected plasma and aluminum cathode electrode lines for a nonrotating electrode.

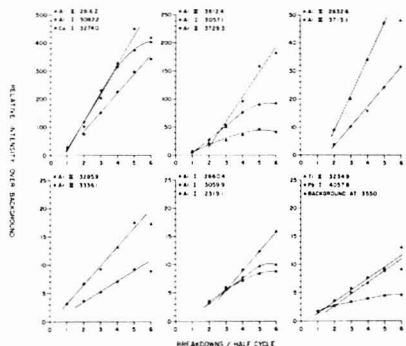


Figure 9. Effect of spark source repetition rate on the lines shown in Figure 8 for a rotating electrode.

From these two calibration experiments, it is reasonable to expect total light losses from spatial discrimination to be recoverable, at least in part, via adjustment of either the spark current wave form or the spark source repetition rate, both of which are quite simple to accomplish in recent all electronic (17), computer-controlled units (27). It remains then to illustrate the gains to be made by such discrimination.

#### SPATIAL DISCRIMINATION

The results to be expected from a spatial discrimination experiment can be anticipated by observing the time and space resolved emission spectra from the positionally stable discharge. Such spectra, produced by a discharge train with the current wave form shown in Figure 11, are shown in Figure 10. The instrumentation used to photograph the spectra has been presented (15). The optical window through which the spatial discrimination was obtained was placed at two distances up from the aluminum cathode surface (0.5 and 1.2 mm). These are the "axial slices" from within which the emission is radially resolved. This resolution gives structure along the length of the spectral lines. Each spectrum is stroboscopically photographed at a particular time after discharge ignition and, thus, at some particular instantaneous current value.

It is evident by inspection that much of the noise radiation in Figure 10 is at a maximum in the central radial regions of

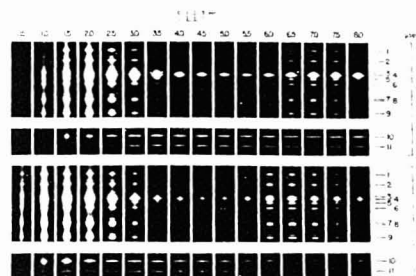


Figure 10. Time and space resolved spectra for two axial displacements from the aluminum cathode surface taken with the instrumentation described in ref 15. Marked lines are identified in Table II. The vertical spark interelectrode axis follows the horizontal (wavelength) axis of each spectrum. The right-hand scale shows the radial extent of the emission. Numbers to the right of each spectrum are the time in microseconds after current onset, relative to the current wave form in Figure 11.

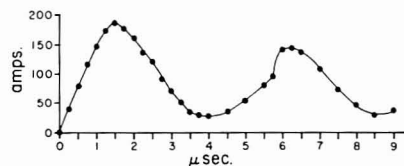


Figure 11. Discharge current wave form used to produce the spectra shown in Figure 10. Spark source and parameters used are described in ref 18 (mostly) and 15.

the spark gap, at times when the current is peaking. This includes background as well as the Al III and Ar II radiation. Analytically useful signals, such as the no. 10 and 11 Al I lines, emit into the discharge wings and at times when the current is minimizing. Thus, by visual inspection alone, we expect that optically masking the core regions of the discharge should diminish the amount of plasma and background radiation entering the spectrometer, and the amount of internally scattered light as well, while still retaining a significant amount of that emitted in the low-energy analytical lines. Less obvious, but still to be expected, would be narrower line widths for the analytical lines. Inspection of Figure 10 suggests a major portion of the large line widths associated with spark spectra compared to other discharges (28) arises from broadening in the spark channel. By masking this region, we expect the wing radiation, when time integrated, to produce a narrower line.

The best visual verification of the above points is obtained by masking with a very large mask. Effects are then accentuated more dramatically than with smaller, perhaps more optimal, sizes. Such masking is shown in Figure 12. In comparing inset A and B, note that the lines indicated by arrows are of about equal intensity in inset A, while they are not in inset B. Both lines are from the same stage of ionization but from different elements. In insets C and D, the difference in background intensity is clear, as is that for the Ar II lines. The Mg II lines in inset D are preserved under masking, since they have far radial emission (29), but some of the other analytical lines are not, such as no. 2, 3, 7, and 9 in inset B. There clearly is an optimum mask diameter.

For reduction in the plasma emission relative to the background emission, there is no advantage to a mask diameter greater than (approximately) 1.6 mm, as indicated in

Table II. Line Identification for Figure 10

line no.	species	wavelength, Å
1	Al III	3612.4
2	Al III	3601.6
3	Ar II	3588.4
4	Al II	3587 mix
5	Ar II	3582.4
6	Ar II	3576.6
7	Ar II	3561.0
		3562.2
8	Ar II	3559.5
9	Ar II	3545.6
10	Al I	3092.8
	Ar II	3093.0
11	Al I	3082.2

Table III. Line Identification for Figure 12

line no.	species	wavelength, Å
1	Mg II	2790.8
2	Mg II	2795.5
3	Mg II	2798.1
4	Mg II	2802.7
5	Al II	2816.2
6	Ar II	3545.6
7	Ar II	3559.5
8	Ar II	3561.0
		3562.2
9	Ar II	3576.6
10	Cr I	3578.7
11	Fe I	3581.2
12	Ar II	3582.4
13	Al II	3587 mix
14	Ar II	3588.4
15	Cr I	3593.5
16	Al III	3601.6
17	Cr I	3605.3
18	Al III	3612.4

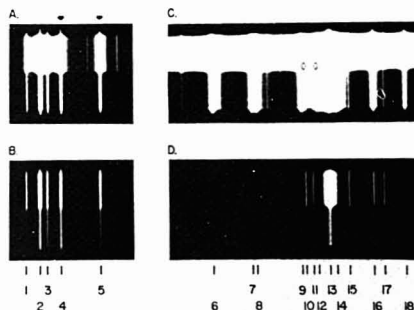
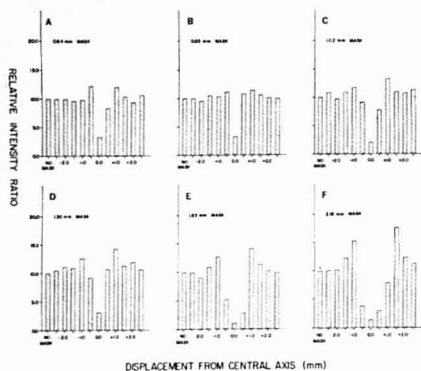


Figure 12. Spectral effects of masking the central core of the discharge with a 2.2 mm diameter mask. Numbered lines are identified in Table III. Insets A and C are two-step filtered spectra with the mask at position 1 in Figure 5. Insets B and D are with the mask at position 3.

Figure 13. Even for masks as small as 0.6 mm, the plasma radiation is reduced by more than a factor of 2 relative to the background when the center core is optically blocked. On the basis of just these data, it would be best to use the smallest mask practical, since this would reduce the total amount of usable signal available to a lesser degree. There is however another advantage to using the larger mask.

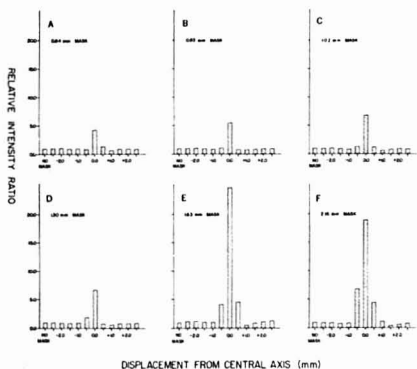
The relative amount of radiation in the analytical lines compared to that in the plasma lines does maximize with mask size, as shown in Figure 14 for the aluminum matrix lines, in

Ar I 3285.9 / BKG 3270



**Figure 13.** Relative intensity ratios of plasma emission as indexed by Ar III lines to background for various diameter masks. The mask was moved across the discharge interelectrode axis in 11 steps as illustrated in Figure 5. Refer to the "no mask" position for normalization. Emulsion types and exposure times per spectrum are as follows: SA-1 and 50 s for insets A-C, SA-1 and 90 s for inset D, SA-3 and 90 s for inset E, and SA-3 and 165 s for inset F.

Al I 3082.2 / Ar I 3285.9

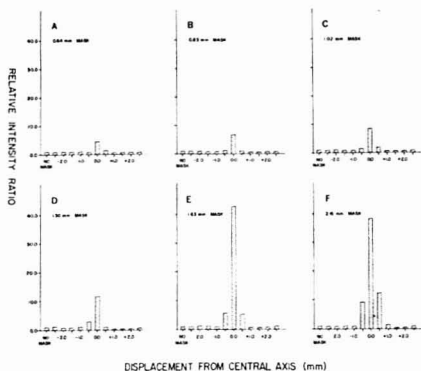


**Figure 14.** Relative intensity ratios of neutral-atom electrode lines to plasma emission for various diameter masks, emulsion and exposure parameters as per Figure 13.

Figure 15 for a lead impurity in the aluminum, and in Figure 16 for a copper impurity. There is greater advantage obtained with a larger mask for copper, primarily because the radial excursion of the copper line investigated is greater than for the lead or aluminum lines. This then is compared to the enhancement in signal to background ratios for the same lines in Figures 17-19. Improvements as high as a factor of 5 are again seen for the larger masks.

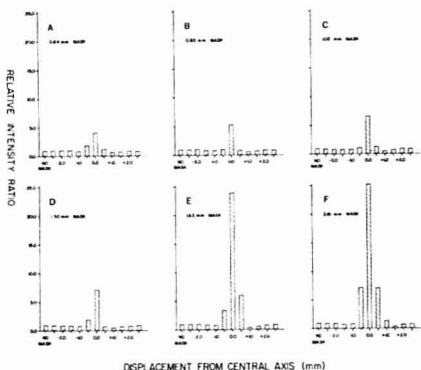
Since the study was done photographically, we cannot comment on how the precision varies with mask diameter. There were no noticeable changes in the linearity of test working curves for the lines shown here (see, for example, Figure 20), but this must be viewed only as a preliminary observation. Far more needs to be done to comment with authority on the long term reliability of working curve linearity and precision using an optically masked system. However,

Pb I 4057.8 / Ar I 3285.9



**Figure 15.** Relative intensity ratios of a neutral-atom lead impurity line in aluminum to plasma emission for various diameter masks, emulsion and exposure parameters as per Figure 13.

Cu I 3274.0 / Ar I 3285.9



**Figure 16.** Relative intensity ratios of a neutral-atom copper impurity line in aluminum to plasma emission for various diameter masks, emulsion and exposure parameters as per Figure 13.

the reduction in background is evident, and the spectra in Figure 5 show how this can be used to great advantage in pulling an iron line (Fe I 3581.2 Å) out of a region of the spectrum rendered virtually useless by the argon plasma emission.

## CONCLUSIONS

Even a modest amount of practical experience in emission spectrometry using spark excitation will caution against making a single technique or device the central focus of a spark-based analytical method. Certainly, this is the case for spatial discrimination by optical masking. In fact, there are cogent arguments against using it in an analytical method at all, such as the degree of discharge stabilization it could require to achieve some prescribed precision in a working method. However, we feel that there will be overriding values to the approach that will justify such efforts as are needed for its practical implementation. Those values will likely arise from its combined use with other techniques to produce a better

Al I 3082.2 / BKG 3087

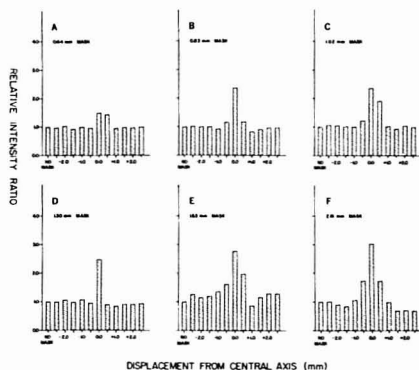


Figure 17. Relative intensity ratios of neutral-atom electrode lines to background for various diameter masks, emulsion and exposure parameters as per Figure 13.

Cu I 3274.0 / BKG 3270

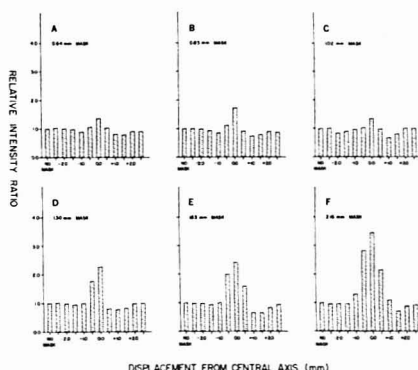


Figure 19. Relative intensity ratios of a neutral-atom copper impurity line in aluminum to background for various diameter masks, emulsion and exposure parameters as per Figure 13.

Pb I 4057.8 / BKG 4060

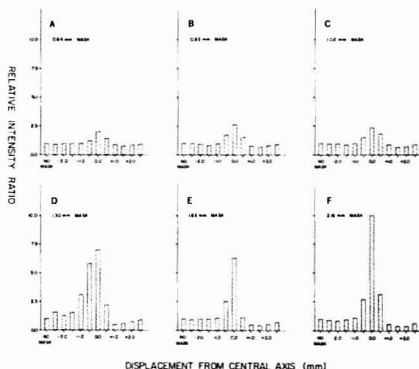


Figure 18. Relative intensity ratios of a neutral-atom lead impurity line in aluminum to background for various diameter masks, emulsion and exposure parameters as per Figure 13.

overall analytical result. These other techniques have been developed but have been reported separately, and with some fragmentation. This paper is well concluded by mentioning how they all could work together to give much better total system performance than we have come to expect from the spark.

When the discharge channel is masked, as shown here, we expect better signal to noise in the method, along with the narrower lines and simpler spectra. But, we also expect lower total flux, and thus longer exposures. To compensate for this, we suggest that the repetition rate of the spark source be increased. This can now be done with electronic ease (30), since the technology is available by using microcomputers to fire the source and with fiber optic links and simpler electronic spark source circuitry to just about eliminate the last of the real problems with radiofrequency interference.

As the repetition rate of the spark source is increased, the first emission from the train of sparks making up a single exposure will peak earlier, requiring only a second or so to

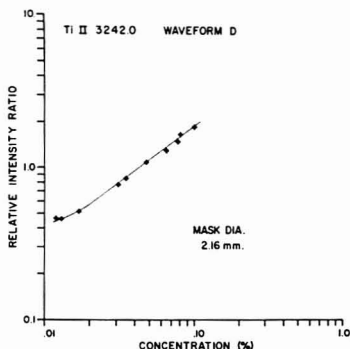


Figure 20. Example working curve for a titanium impurity in aluminum using spatial discrimination. The internal standard line was Al I 3082.2 Å. The current wave form is shown in Figure 2, inset D.

gather most of the useful signal (31). This will reduce the exposure time and, if the time at which the peak occurs is monitored, give good diagnostic information about the matrix condition of the analytical sample. Using the area under this transient peak as the analytical signal will reduce the total exposure time needed to register a spectrum (32). To take best advantage of this, we recommend that the number of burns per sample be increased up to 50 or so (instead of two or three) so that the final answer reported reflects that statistical composition of the alloy (12). Then, the increased signal to noise that comes from masking can be combined with the better statistics and increased matrix knowledge to also give better accuracy. By proper analysis of the multiple burn pattern, better precision can also result (33). An on-line microcomputer can be used to move the electrode under the stable spark to produce such a grid of burns over the surface, as well as to handle the increased amount of information produced and processing needed.

Where the electrode is difficult to attack, we again recommend adjusting the power delivered to the sample, through both the repetition rate and the instantaneous current within a single discharge. If, to cause good sampling, the instanta-

neous current within a single spark becomes so high that the signal to noise benefits gained through spatial discrimination are defeated (34), we recommend synchronously time gating the detector integrator circuit during the valleys of the current wave form (35). The same microcomputer that is used to fire the spark and move the electrode can also do this, even though the situation today is economically such that it is quite sensible to design for several machines being active at once (36). The signal to noise can then be increased again, further compensating for the higher background that would come from using higher power on more difficult sampled alloys.

The net picture here then is one of substantial enhancements in overall analytical performance, all based on prior experimental research and all possible at expected modest cost due to the simpler electronic, computer-controlled spark sources presently possible. We look forward to reporting the first results of such combined techniques in the near future.

#### ACKNOWLEDGMENT

The assistance of Robert J. Lang and Robert M. Schmelzer in instrument fabrication is appreciated, as is that of Patricia Brinkman in financial management.

#### LITERATURE CITED

- (1) Sacks, R. D.; Walters, J. P. *Anal. Chem.* **1970**, *42*, 61.
- (2) Walters, J. P.; Malmstadt, H. V. *Anal. Chem.* **1965**, *37*, 1484.
- (3) Walters, J. P. *Anal. Chem.* **1968**, *40*, 1540.
- (4) Walters, J. P. *Science* **1977**, *198*, 787.
- (5) Scheeline, A.; Walters, J. P. In "Contemporary Topics in Analytical and Clinical Chemistry"; Hercules, D. M., Hietje, G. M., Snyder, L. R., Evenson, M. A., Eds.; Plenum Press, New York, Vol. 4, pp 295-372.
- (6) Washburn, D. N.; Walters, J. P. *Anal. Chem.* **1981**, *53*, 1644.
- (7) Ekimoff, D.; Walters, J. P. *Anal. Chem.* **1981**, *53*, 1644.
- (8) Walters, J. P. *Appl. Spectrosc.* **1977**, *31*, 36.
- (9) Walters, J. P.; Goldstein, S. A. *ASTM Spec. Tech. Publ.* **1973**, *STP 540*, 45-71.
- (10) Thackeray, D. P. C. *Nature (London)* **1957**, *180*, 913.
- (11) van der Piepen, H.; Schroeder, W. W. *J. Phys. D* **1972**, *5*, 2190.
- (12) Olesik, J. W. Ph.D. Thesis University of Wisconsin, 1982.
- (13) Olesik, J.; Walters, J. P. *Appl. Spectrosc.*, in press.
- (14) Walters, J. P.; Goldstein, S. A.; Eaton, W. S. U.S. Patent 3 815 995, June 1, 1974.
- (15) Klueppel, R. J.; Coleman, D. M.; Eaton, W. S.; Goldstein, S. A.; Sacks, R. D.; Walters, J. P. *Spectrochim. Acta, Part B* **1978**, *33B*, 1.
- (16) Walters, J. P. *Appl. Spectrosc.* **1972**, *26*, 17.
- (17) Barnhart, S. G.; Farnsworth, P. B.; Walters, J. P. *Anal. Chem.* **1981**, *53*, 1432.
- (18) Walters, J. P. *Anal. Chem.* **1988**, *40*, 1672.
- (19) Takahashi, T. *Bunko Kenyu* **1988**, *15*, 164.
- (20) Hirokawa, K.; Goto, H. *Spectrochim. Acta, Part B* **1970**, *25B*, 419.
- (21) Strasheim, A.; Blum, F. *Spectrochim. Acta, Part B* **1971**, *26B*, 685.
- (22) Farnsworth, P. B.; Walters, J. P. *Anal. Chem.* **1982**, *54*, 885.
- (23) Mika, J.; Torok, T. "Analytical Emission Spectroscopy—Fundamentals"; Crane, Russell & Co.: New York, 1974; p 423.
- (24) Kuznetsova, L. A.; Petrova, N. G.; Podmoshenskaya, S. F. *Zh. Prikl. Spektrosk.* **1976**, *24*, 576.
- (25) Holler, P.; Thoma, C.; Brost, U. *Spectrochim. Acta, Part B* **1972**, *27B*, 365.
- (26) Yamano, T.; Matsushita, S. *Spectrochim. Acta, Part B* **1972**, *27B*, 27.
- (27) Mathews, S. M.; Walters, J. P. *Appl. Spectrosc.*, in press.
- (28) Fassel, V. A. *Science* **1978**, *202*, 183.
- (29) Klueppel, R. J.; Walters, J. P. *Spectrochim. Acta, Part B* **1980**, *36B*, 431.
- (30) Mathews, S. M. Ph.D. Thesis University of Wisconsin, 1982.
- (31) Ekimoff, D. Ph.D. Thesis University of Wisconsin, 1981.
- (32) Washburn, D. N. Ph.D. Thesis University of Wisconsin, 1981.
- (33) Holt, G.; Strasheim, A. *Appl. Spectrosc.* **1980**, *14*, 64.
- (34) Goldstein, S. A. Ph.D. Thesis University of Wisconsin, 1973.
- (35) Barnhart, S. G.; Walters, J. P. U.S. Patent Appl., 1982.
- (36) Walters, J. P. 2nd Chemical Congress, North America, ACS, Las Vegas, NV, Aug 1982.

RECEIVED for review July 16, 1982. Accepted October 1, 1982.  
We acknowledge the continual support of the National Science Foundation during the time that this work was done and as its initial results were independently verified under Grants GP-13975, GP-35602X, CHE76-17557, CHE77-05294, and CHE79-15195.

## Analysis of Pharmaceuticals by Fluorine-19 Nuclear Magnetic Resonance Spectrometry of Pentafluoropropionic Anhydride Derivatives

Gary E. Zuber,\* David B. Stalger, and Richard J. Warren

Smith Kline & French Laboratories, P.O. Box 7929, Philadelphia, Pennsylvania 19101

A quantitative method for the fluorine-19 NMR analysis of pentafluoropropionic anhydride derivatized pharmaceuticals is presented. The procedure is based upon chromatographic derivatization methods. Reactions were carried out in deuterated chloroform using approximately 50 mg of sample. The samples analyzed were bulk pharmaceutical materials and drug dosage forms containing hydroxyl and amino groups. In some cases, the catalyst pyridine at a reaction temperature of 55 °C was used to shorten the reaction times and to assure complete derivatization. This fluorine derivatization technique results in fluorine-19 NMR spectra of pharmaceuticals which are greatly simplified in comparison to their more complex proton spectra. The major advantage of the method is the speed with which the analysis can be carried out since most derivatizations are completed in 10 min. The broad application of this technique to pharmaceutical analysis is reported along with accuracy and precision data.

The quantitative analysis of pharmaceuticals as commonly done by gas chromatography is often a time-consuming and

difficult procedure (1). The use of proton nuclear magnetic resonance (NMR) for drug determinations is sometimes limited due to the complex NMR spectrum of some molecules. Consequently, we decided to develop an analytical procedure using fluorine derivatization of drugs containing active hydrogens and subsequent analysis of their fluorine-19 NMR spectra.

Fluorinated derivatives are extensively used in analyses by gas chromatography (GC) and mass spectrometry (MS) (2-5), but their application in quantitative fluorine-19 NMR spectrometry, especially for pharmaceutical analyses, has been somewhat limited. A great deal of work has been done with hexafluoroacetone (HFA) and fluorine NMR to quantitate and characterize active hydrogen compounds (6-9). Since this initial work, some recent applications in the areas of food and coal product analysis have been made (10, 11). The disadvantage associated with these HFA methods is that they require the use and storage of a reagent gas which is a potential toxicity hazard. In addition, fluorine-19 NMR analysis of trifluoroacetyl derivatives has been used to determine organic compounds and also some biologically related materials (12-17). Trifluoroacetyl derivatives can be formed by using



a variety of different derivatization reagents, the most popular ones being trifluoroacetyl chloride and trifluoroacetic anhydride. Use of trifluoroacetyl chloride still requires the possibly undesirable storage of this reagent gas, and the use of volatile trifluoroacetic anhydride also requires careful reagent storage.

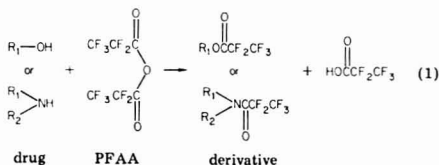
The method presented here was based upon information and techniques found within these previous NMR, GC, and MS studies. We adapted the fluorinated anhydride derivatization methods used in GC/MS for use in a suitable fluorine-19 NMR method. The derivatization reagent chosen for use was pentafluoropropionic anhydride. This reagent is readily available and is less volatile than trifluoroacetic anhydride, thus allowing for easier storage. The formation of pentafluoropropionyl derivatives also has another advantage in that in most cases each derivatization reaction results in a derivatized drug which yields a fluorine NMR where quantitation is possible in both the CF<sub>3</sub> and CF<sub>2</sub> regions of the spectra. Consequently, an internal check of integral accuracy is present. This is not the case when trifluoroacetyl derivatives are formed. This technique was designed to avoid any preliminary preparation steps so that accurate and precise results could be quickly obtained. In addition, it was felt that quantitative analyses of anhydride derivatives by fluorine-19 NMR spectrometry should be possible even for complex drug mixtures provided that the components of the derivatized mixture yield well-separated adduct signals.

## EXPERIMENTAL SECTION

**Apparatus.** The instrument used was a Perkin-Elmer R32 equipped with a fluorine-19 accessory. The instrument operates at a magnet field strength of 21.1 kG with resonance frequencies for fluorine-19 at 84.6 MHz and proton at 90 MHz. All spectra were obtained at a 100-ppm sweep width initially and also a 10-ppm sweep width for quantitation. A 180-s sweep rate was used for the integrations. Samples were each run at various spin rates in order to eliminate any chance of interference from spinning side bands.

**Reagents.** Pentafluoropropionic anhydride (PFAA) was obtained from Pierce Chemicals, Rockford, IL. The free acid content of these anhydrides is reported as being 1% or less. The anhydride reagent was kept under nitrogen and in a refrigerator between use to prevent any decomposition. The solvent used for all analyses was deuteriochloroform (minimum isotopic purity 99.6 atom % D) which was obtained from Merck and Co., Rahway, NJ. The internal standard used was trifluoroacetanilide (purity = 99.9% by GC) which was obtained from BDH Chemicals, Poole, England. All of the pharmaceuticals analyzed were of the highest purity. All other chemicals were high-grade commercial products and were used without further purification.

**Procedure.** In cases not requiring catalysis, approximately 50 mg of the sample and 30 mg of the internal standard were weighed into a 5-mL vial. This mixture was then dissolved with 0.5 mL of deuteriochloroform and transferred to a 5-mm NMR tube. An excess amount of the derivatization reagent (PFAA) was then introduced, and the reaction was allowed to proceed for 10 min at room temperature. Equation 1 illustrates the basic reaction. After this reaction period, the resultant mixture was



analyzed by fluorine-19 NMR at sweep widths of 100 and 10 ppm. The results were then analyzed, and additional reaction time was allowed if necessary.

In cases (e.g., phenols and some amines) where a simple catalyst was required, an excess amount of either 1.0 M triethylamine or

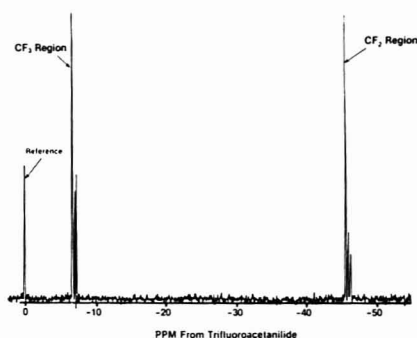


Figure 1. Fluorine-19 NMR spectrum of derivatized cholesterol in CDCl<sub>3</sub> (sweep width = 100 ppm).

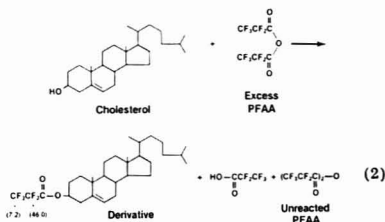
pyridine in deuteriochloroform was added immediately following the addition of PFAA.

In cases which required both pyridine and heat, an excess amount of 1.0 M pyridine was added to the NMR tube containing the sample, reference, and PFAA. This tube was then placed in a water bath kept at about 55 °C for the proper reaction period (usually 10 min) and then analyzed by fluorine-19 NMR.

After the initial fluorine-19 NMR analyses were made, each sample was washed with a saturated sodium bicarbonate solution to eliminate any excess PFAA and pentafluoropropionic acid present. Each sample was then reanalyzed under the same NMR conditions previously described.

## RESULTS AND DISCUSSION

An example of a typical reaction between the drug cholesterol and PFAA appears below.



The numbers in parentheses represent the chemical shifts in parts per million upfield from the reference trifluoroacetanilide.

Figure 1 shows a 100-ppm fluorine-19 NMR spectrum of derivatized cholesterol. This spectrum is first order with quantitation possible either in the CF<sub>3</sub> region (-6.8 to -7.4 ppm) or in the CF<sub>2</sub> region (-45.6 to -46.4 ppm). Figure 2 is a 10-ppm expansion of the reference and both the CF<sub>3</sub> and CF<sub>2</sub> signal regions of the cholesterol derivative. Signal a at -7.2 ppm represents the CF<sub>3</sub> group of the cholesterol derivative and signal b at -46.0 ppm the CF<sub>2</sub>. Each of these signals was integrated five times vs. the reference standard trifluoroacetanilide. The results were then analyzed by means of the following basic equation.

$$\frac{\text{integration (sample)}}{\text{integration (std)}} \times \frac{\text{wt (std)}}{\text{wt (sample)}} \times \frac{\text{equiv wt (sample)}}{\text{equiv wt (std)}} \times 100\% = \% \text{ determined} \quad (3)$$

In cases where both the CF<sub>3</sub> and CF<sub>2</sub> signals of the derivative

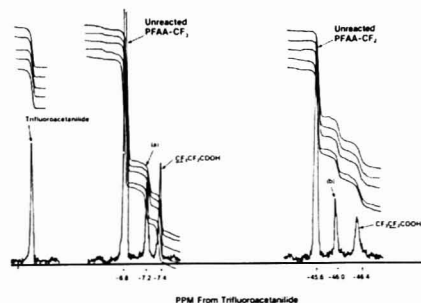


Figure 2. A 10-ppm expanded fluorine-19 NMR spectrum of derivatized cholesterol in  $\text{CDCl}_3$  (integral sweep rate = 80 s).

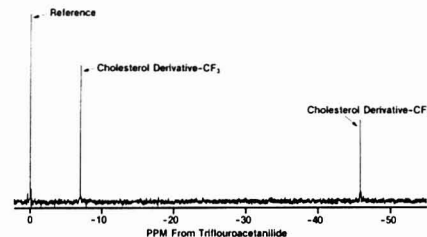


Figure 3. Fluorine-19 NMR spectrum of derivatized cholesterol in  $\text{CDCl}_3$  after a sodium bicarbonate wash (sweep width = 100 ppm).

are observed, both are individually quantitated vs. the reference and the results averaged. The relative standard deviation for each analysis was calculated by means of the following:

$$\frac{\text{std dev}}{\text{av integration}} \times 100\% = \text{rel std dev} \quad (4)$$

Figure 2 also illustrates the  $\text{CF}_3$  and  $\text{CF}_2$  signals for the unreacted PFAA reagent present with chemical shifts of -6.8 ppm and -45.6 ppm, respectively. The signals at -7.4 and -46.4 ppm represent the respective  $\text{CF}_3$  and  $\text{CF}_2$  groups of pentafluoropropionic acid which is a byproduct of the anhydride reaction.

Signal assignments were made on the basis of reference spectra of pentafluoropropionic acid, pentafluoropropionic anhydride, and a derivatized cholesterol sample which had been washed with saturated sodium bicarbonate. Figure 3 shows a 100-ppm fluorine-19 NMR spectrum of derivatized cholesterol which has been subjected to a bicarbonate wash to eliminate the excess PFAA and pentafluoropropionic acid interfering signals. The sodium bicarbonate wash resulted in a more simplified spectrum which was much easier to analyze. In Figure 3, the two derivative signals which remain have chemical shifts of -7.2 ppm and -46.0 ppm and represent the respective  $\text{CF}_3$  and  $\text{CF}_2$  groups of the cholesterol derivative.

**Alcohols.** Table I illustrates the quantitative results obtained for six pharmaceuticals containing OH groups. The steroid cholesterol, alkaloid oxycodone, and menthol all undergo complete derivatization within 10 min. The alkaloid bulbocapnine which possesses a phenolic OH function requires the presence of the catalyst pyridine for a rapid and complete derivatization reaction. The presence of a base such as pyridine enhances reactivity by serving as an acid acceptor in the derivatization reaction (18). The steroid mestranol

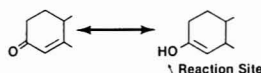
Table I. Quantitative Results for Alcohols

pharmaceutical	% determined	rel std dev	reaction time	catalyst
cholesterol (-OH)	99.8	1.8	10 min	none
norethindrone (2-OH)	94.3	1.4	1 day	none
mestranol (-OH)	96.5	2.3	1 day	none
menthol (-OH)	97.2	2.5	10 min	none
oxycodone (-OH)	99.8	1.7	10 min	none
bulbocapnine (PhOH)	97.5	1.9	10 min	pyridine

Table II. Chemical Shifts for PFAA Derivative of Pharmaceuticals (Alcohols)

Drug Name	Structure	Peak Position (PPM)	
		$\text{CF}_3$	$\text{CF}_2$
1 Cholesterol		-7.20	-46.0
2 Mestranol		-6.90	-45.7
3 Norethindrone		-6.92	-45.6
4 Menthol		-7.05	-45.6
5 Oxycodone		-7.10	-45.8
6 Bulbocapnine		-6.37	-

possesses a cyclic OH group at the C-17 position which is sterically hindered by the close proximity of an alkene group. Consequently, the reaction of this compound at this site takes 24 h to near completion. It was also found that 2.0 M pyridine and heat did not catalyze this reaction to any significant extent. The steroid norethindrone possesses two reaction sites which undergo derivatization at different rates. As in mestranol, a slow reacting sterically hindered OH group which requires 24 h for derivatization is present at the C-17 position. In addition, an active hydrogen site is present at the C-3 position in norethindrone. Keto-enol tautomerization of this C-3 carbonyl as seen below results in the formation of a fast reacting OH group.



The resultant active hydrogen found here reacts almost immediately with the anhydride reagent.

Table II illustrates that the chemical shifts for the  $\text{CF}_3$  groups of these alcohol derivatives all are within the range of -6.90 to -7.20 ppm with the exception of oxycodone (-6.37 ppm). The  $\text{CF}_2$  group derivative signals were unobservable for mestranol, norethindrone, oxycodone, and bulbocapnine prior to washing with sodium bicarbonate and were believed to be overlapped by either the excess PFAA signal or the pentafluoropropionic acid signal. After bicarbonate washing, the mestranol and norethindrone signals did become observable, but the fluorine-19 NMR spectra obtained for the derivatized alkaloids, oxycodone and bulbocapnine, indicated that these compounds decomposed in the presence of sodium bicarbonate. Sodium bicarbonate washing of cholesterol and

Table III. Quantitative Results for Amines

pharmaceutical	% determined	% precision	reaction time, min	catalyst
propylhexedrine (-NH <sub>2</sub> )	98.3	2.1	10	pyridine + $\Delta$
phentermine (-NH <sub>2</sub> )	98.3	0.9	10	pyridine + $\Delta$
benzocaine (-NH <sub>2</sub> )	98.9	1.6	10	none

Table IV. Chemical Shifts For PFAA Derivatives of Pharmaceuticals (Amines)

Drug Name	Structure	Peak Position (PPM)	
		CF <sub>3</sub>	CF <sub>2</sub>
1. Propylhexedrine		-6.20	-38.9
2. Phentermine		-5.82	-40.8
3. Benzocaine		-6.85	-46.2

menthol did eliminate the interfering signals without causing derivative decomposition.

**Amines.** Table III illustrates the quantitative results obtained for three pharmaceuticals containing NH<sub>2</sub> groups. The aromatic amine benzocaine was found to react rapidly with no catalysis required. The aliphatic amine propylhexedrine was found to react to the 80% level after a reaction time of 24 h both without a catalyst and with the catalyst triethylamine present. With 1.0 M pyridine added to the reaction mixture, a near complete (95%) reaction was achieved after 24 h. Finally, it was found that the addition of both pyridine and heat (55 °C) drove the reaction to completion within 10 min. On the basis of this information, the aliphatic amine phentermine was completely derivatized within 10 min by using the same established reaction conditions.

Table IV illustrates that all of the chemical shifts for the CF<sub>3</sub> groups of these derivatized amines are within the broad range of -5.82 to -6.85 ppm. The CF<sub>2</sub> signals which were all observable are within a range of -38.9 to -46.2 ppm. All of these derivatized amine compounds underwent apparent decomposition when washed with saturated sodium bicarbonate.

**Drug Mixture.** Table V illustrates the results obtained for a derivatized drug mixture of propylhexedrine and menthol. Menthol was found to undergo rapid and complete derivatization under all reaction conditions. Propylhexedrine, however, requires the presence of 1.0 M pyridine and a reaction temperature of 55 °C to be completely derivatized. Once the proper catalyzed reaction conditions are established, quantitation of both drugs is possible in both the CF<sub>3</sub> and CF<sub>2</sub> signal regions. Accurate and precise results are possible because of the large chemical shift differences between the derivative signals of propylhexedrine and menthol. The CF<sub>3</sub> signals for propylhexedrine and menthol were at -6.20 and -7.10 ppm, respectively, and the CF<sub>2</sub> signals at -38.9 and -45.8 ppm, respectively. Whenever this type of derivative signal separation is encountered, this technique can be used to

Table V. <sup>19</sup>F NMR Analysis of a Standard Derivatized Mixture of Propylhexedrine and Menthol

reaction conditions	milligrams of propylhexedrine		milligrams of menthol	
	actual	NMR method (% determined)	actual	NMR method (% determined)
24 h with 1.0 M pyridine present	51.0	50.3 (98.6)	53.0	53.1 (100.2)
10 min with 1.0 M pyridine present and heat	51.4	50.8 (98.8)	50.6	50.9 (100.5)

readily analyze drug mixtures.

## CONCLUSIONS

The above results demonstrate that a variety of different pharmaceutical types can be rapidly quantitated by fluorine-19 NMR analysis of their pentafluoropropionic anhydride derivatives. This method was shown to be applicable to simple alcohols and amines as well as complex drugs such as steroids and alkaloids. Steroids and alkaloids which normally give highly complex proton NMR spectra can be derivatized quickly under the proper reaction conditions and their simplified fluorine-19 NMR spectra used for accurate quantitations.

This method of analyzing pure drugs and drug mixtures offers many advantages over previous analytical techniques. The analysis offers the advantages of speed, specificity, and accuracy (a relative standard deviation always less than 2.5%).

**Registry No.** PFAA, 356-42-3; cholesterol, 57-88-5; mentranol, 72-33-3; norethindrone, 68-22-4; menthol, 1490-04-6; oxycodeone, 76-42-6; bulbocepinine, 298-45-3; propylhexedrine, 101-40-6; phentermine, 122-09-8; benzocaine, 94-09-7.

## LITERATURE CITED

- (1) Internal communication; Gas Chromatography Section; Smith Kline & French Laboratories, 1981.
- (2) Ehrsson, H.; Walle, T.; Brostell, H. *Acta Pharm. Suec.* **1971**, *8*, 319-328.
- (3) Walle, T.; Ehrsson, H. *Acta Pharm. Suec.* **1971**, *8*, 27-38.
- (4) Walle, T.; Ehrsson, H. *Acta Pharm. Suec.* **1970**, *7*, 389-406.
- (5) Ervik, M.; Walle, T.; Ehrsson, H. *Acta Pharm. Suec.* **1970**, *7*, 625-634.
- (6) Leader, G. R. *Anal. Chem.* **1970**, *42*, 16-21.
- (7) Leader, G. R. *Anal. Chem.* **1973**, *45*, 1700-1706.
- (8) Ho, F. F.-L. *Anal. Chem.* **1974**, *46*, 496-499.
- (9) Ho, F. F.-L.; Kohler, R. R. *Anal. Chem.* **1974**, *46*, 1302-1304.
- (10) Gaffield, W.; Lundin, R. E. *J. Assoc. Sci. Publ.* **1978**, *19*, 87-95.
- (11) Bartle, K. D.; Matthews, R. S.; Stadelhofer, J. W. *Appl. Spectrosc.* **1980**, *34*, 615-617.
- (12) Ida, T.; Tamura, T.; Matsumoto, T. *Nihon Daigaku Kagakubu Kyo, Bunru*, **A 1980**, *21*, 223-226.
- (13) Brown, W. E.; Seamon, K. B. *Anal. Biochem.* **1978**, *87*, 211-222.
- (14) Sleevi, P.; Glass, T. E.; Dorn, H. C. *Anal. Chem.* **1979**, *51*, 1931-1934.
- (15) Manatt, S. L. *J. Am. Chem. Soc.* **1966**, *88*, 1323-1324.
- (16) Manatt, S. L.; Lawson, D. D.; Ingham, J. D.; Rapp, J. D.; Hardy, J. D. *Anal. Chem.* **1968**, *38*, 1063-1065.
- (17) Voelter, W.; Brietmaier, W.; Jung, G.; Bayer, E. *Org. Mag. Reson.* **1970**, *2*, 251.
- (18) "Pierce Handbook and General Catalog"; Pierce Chemical Co.: Rockford, IL, 1979-1980; p 189.

RECEIVED for review August 10, 1981. Resubmitted August 24, 1982. Accepted September 27, 1982. Presented in part at the 1981 Pittsburgh Conference on Analytical Chemistry and Applied Spectroscopy in Atlantic City, NJ, March 11, 1981.

# Standards for Nanosecond Fluorescence Decay Time Measurements

Roger A. Lampert, Leslie A. Chewter, and David Phillips\*

Davy Faraday Research Laboratory, The Royal Institution, 21 Albemarle Street, London W1X 4BS, United Kingdom

Desmond V. O'Connor

Institute for Molecular Sciences, Myodaiji, Okazaki 444, Japan

Anthony J. Roberts

Unilever Research Laboratories, Port Sunlight, Merseyside, United Kingdom

Stephen R. Meech

Department of Chemistry, Wayne State University, Detroit, Michigan 48202

With a synchronously pumped dye laser as excitation source for fluorescence decay time measurements with single-photon counting detection, a critical reevaluation of literature fluorescence decay parameters for "standard" compounds is made and new standards are proposed for lifetime measurements. These are 2,5-diphenyloxazole (PPO), 1-cyanonaphthalene, 1-methylindole, 3-methylindole, 1,2-dimethylindole, and *N,N*-dimethyl-1-naphthylamine, in cyclohexane, hexane, or ethanol solution, covering an emission wavelength range of 330 to 440 nm and decay time range of 1.28 to 18.23 ns. Anthracene in solution may also be used as a standard if care is taken with purification and the concentration is known. Quinine bisulfate should not be used as a decay time standard. 1-Cyanonaphthalene provides a convenient standard for gas-phase experiments.

Fluorescence decay times represent an additional, relatively easily measured parameter with which to characterize molecular fluorescence.

Perhaps the most widely used source of single-exponential lifetime data is Birk's "Photophysics of Aromatic Molecules" (7), published in 1970. Without wishing to detract from the reputation of this monumental work, we believe that many of the lifetimes listed therein, although undoubtedly the most accurate available at the time of publication, have since been shown to be seriously in error. The fact is that relatively crude techniques for lifetime measurements were still in operation at the time the book was written and the author's declared intention was merely to classify the reported data. Similarly many workers standardize the performance of SPC equipment against lifetime data given in Berlman's "Handbook of Fluorescence Spectra of Aromatic Molecules" (2). Since these lifetimes were measured many years ago with a relatively old fashioned pulse sampling oscilloscope technique, it is not surprising that many of them are inaccurate.

Any compound with a single exponential decay will serve as a lifetime standard. However, for the sake of convenience the compound should also be easily purifiable and have a known single exponential decay time, independent of excitation and emission wavelength, in an easily purifiable solvent. Among the most commonly used standards are *p*-bis(2-phenyloxazolyl)benzene (POPOP), 2,5-diphenyloxazole (PPO), anthracene, and quinine bisulfate. Quoted lifetimes for POPOP in cyclohexane do not show much variation (3, 4) but

for the other three compounds the literature values for the decay times contain some serious discrepancies, as shown in Table I (5-27). Thus quinine sulfate in 1 N or 0.1 N H<sub>2</sub>SO<sub>4</sub> is commonly regarded as having a single exponential decay time of about 19 ns. Recently we have shown that it has, in fact, a double exponential decay that is strongly dependent on temperature and emission wavelength (28).

We believe there is a case for a critical new evaluation of decay time data, and in this report we describe a single-photon counting instrument of high sensitivity and time resolution, list a number of parameters, some of them very seldom applied to this technique, by which least-squares fitting procedures can be judged, and finally propose a set of standard compounds with single-exponential decay times which can serve as calibrants for standard nanosecond measurements.

While the decay times of many compounds show only very slight, if any, dependence on excitation and emission wavelength and are relatively insensitive to change in temperature, we believe that the precise conditions under which a decay time is measured should always be specified, as is now common for quantum yield determinations. Moreover it is advisable always to remove oxygen from organic solvents since the possibility of reversible charge transfer complex formation in the excited state cannot be ruled out.

## EXPERIMENTAL SECTION

**The Instrument.** A diagram of the time-resolved fluorescence spectrometer employed for the measurements reported in this paper is shown in Figure 1. Sample excitation in the wavelength range 290-315 nm was achieved with a frequency doubled, cavity dumped, mode-locked synchronously pumped dye laser system. In this a 15-W argon-ion laser (Spectra-Physics Model 171) was mode locked using an acoustooptic device (Spectra-Physics Model 342) providing pulses of around 100 ps fwhm (full width at half maximum intensity), at a repetition rate of 82 MHz, and with an average power of 420 mW. These pulses were used to excite Rhodamine 6G dye in ethylene glycol in a jet stream dye laser (Spectra-Physics Model 375) the normal end mirror of which had been removed and the cavity length extended to match that of the ion laser. Under these conditions the laser was found to mode lock, producing pulses at a repetition rate of 82 MHz. For most photophysical systems, this pulse rate was too fast to allow total system relaxation between excitation events and, consequently, an acoustooptic cavity dumper (Spectra-Physics Model 344) was used to output pulses at a lower rate (single shot—4 MHz). A limited tunability, 570-640 nm, was available by using a multilayer broad band tuning wedge (Spectra-Physics Model 570) incorporated in the dye laser cavity. For wavelengths outside this region

Table I. Some Single Exponential Decay Times Measured Since 1970

compound	solvent	concn, M	$\lambda$ , nm		$T$ , °C	$\tau_F$ , ns	method of data analysis	ref
			excitation	emission				
quinine sulfate	0.1 N $H_2SO_4$	$10^{-6}$			room	19.4	moments	5
	0.1 N $H_2SO_4$				room	20	oscilloscope	6
	0.1 N $H_2SO_4$	$10^{-4}$			room	19.4	moments	7
	0.1 N $H_2SO_4$				room	18.8	log plot	8
	1 N $H_2SO_4$	$10^{-3}$	257	470	room	19.3	fourier transform	9
anthracene	1 N $H_2SO_4$	$10^{-3}$			room	$a$	least squares	10
	cyclohexane (degassed)	$10^{-3}$	365	>400	20	$6.80 \pm 0.07$	least squares	11
			257	440	room	$4.79 \pm 0.05$	least squares	12
		$10^{-4}$	365	>400	20	$6.01 \pm 0.06$	least squares	11
		$4 \times 10^{-5}$	365	400	20	5.20	least squares	11
		$2 \times 10^{-5}$	365		25	5.2	least squares	11
			340	>405*	room	5.28	least squares	3
			355	415	room	$5.03 \pm 0.07$	least squares	4
		$2.7 \times 10^{-5}$	340	405*	25	$5.22 \pm 0.04$	least squares	14
		$2 \times 10^{-5}$	340	405*	room	5.16	least squares	15
		$2 \times 10^{-5}$	340	405*	room	5.14	least squares	16
		$9.52 \times 10^{-6}$	365	>400	20	$5.42 \pm 0.04$	least squares	11
		$10^{-6}$	365	>400	20	$5.15 \pm 0.05$	least squares	11
	cyclohexane (undegassed)	$5 \times 10^{-6}$			room	3.97	least squares	17
	cyclohexane (undegassed)		308	410	room	4.1	least squares	18
	cyclohexane (undegassed)		355	415	room	$3.99 \pm 0.03$	least squares	4
	ethanol (degassed)	$2 \times 10^{-5}$	365	405*	25	5.0	least squares	13
	ethanol (degassed)		355	415	room	$5.06 \pm 0.05$	least squares	4
	ethanol (degassed)		257	400	room	5.67	Fourier	9
9-cyanoanthracene	benzene (degassed)				25	3.6	least squares	19
	benzene (degassed)	$8 \times 10^{-5}$			room	$4.00 \pm 0.05$	moments	7
	cyclohexane (degassed)		257	440	room	$12.8 \pm 0.1$	least squares	12
	cyclohexane (degassed)		355	415	room	$12.8 \pm 0.2$	least squares	4
	cyclohexane (degassed)		340	405*	room	1.13	least squares	3
POPOP	cyclohexane (degassed)		355	415	room	$1.10 \pm 0.02$	least squares	4
	cyclohexane <sup>b</sup> (degassed)	$10^{-5}$	310	370	room	1.27	least squares	20
PPO	cyclohexane (degassed)				room	1.36	c	21
	methanol (undegassed)		568		room	0.54	least squares	22
rose bengal	methanol (undegassed)				room	0.60	least squares	23
	ethanol (undegassed)	$10^{-6}$	580		room	2.85	moments	24
rhodamine B	ethanol (undegassed)	$10^{-6}$	580		room	$2.88 \pm 0.06$	moments	25
	ethanol (undegassed)							
1-cyanonaphthalene	hexane (degassed)	$2 \times 10^{-5}$	280	325	25	18.26	least squares	26
	hexane (degassed)	$2 \times 10^{-5}$			25	19.8	least squares	27

<sup>a</sup> Single exponential lifetime not found. <sup>b</sup> Not specified whether solvent is degassed. <sup>c</sup> Not specified but probably moments.

alternative laser dyes could be employed. With careful alignment average powers in excess of 50 mW could be obtained with a pulse repetition rate of 4 MHz. The pulses were found to have an autocorrelation width of ca. 6 ps measured using a scanning autocorrelator (Spectra-Physics Model 409). Pulses were also monitored by using fast photodiodes (Hewlett-Packard 4220 in a home-built mount, Spectra-Physics Model 403B). Frequency doubling into the 290–315-nm range was achieved by using temperature and angle tuned ADP crystals (J. K. Lasers) mounted at a beam waist formed between two 10-cm focal length lenses. The relatively low pulse peak intensities resulted in a small second harmonic generation efficiency and consequently residual un-

doubled light was removed with a Corning 7-54 filter. For stability the laser system was mounted on a mechanically isolated optical table (Newport Research Corp.) and operated in a temperature-controlled environment ( $20 \pm 1^\circ\text{C}$ ).

The sample was contained in a 1-cm<sup>2</sup> quartz cuvette. Fluorescence was monitored at right angles to the excitation path through a Hilger-Watts 0.33-m D330 monochromator by a fast photomultiplier (Philips XP2020Q) mounted in a homemade voltage divider. The fluorescence resolution was typically 1–2 nm. In order to totally exclude scattered excitation light, it was found necessary to incorporate a Schott WG345 cutoff filter before the monochromator.

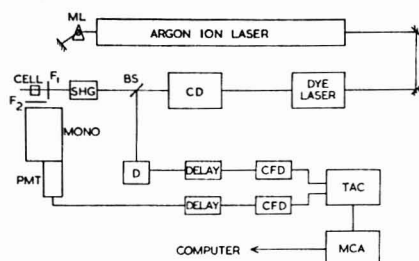


Figure 1. Time-resolved fluorescence spectrometer: ML, mode locker; CD, cavity dumper; BS, beam splitter; D, photodiode; SHG, frequency doubling crystal; F<sub>1</sub>, Corning 7-54 filter; F<sub>2</sub>, Schott WG 345 filter; MONO, monochromator; PMT, photomultiplier tube; CFD, constant fraction discriminator; TAC, time-to-pulse height converter; MCA, multichannel analyzer.

Conventional single photon counting detection methods were employed for decay time measurements (29). The "time zero" reference signal, corresponding to the laser pulse, was provided either from a fast photodiode monitoring a fraction of the excitation beam or from a TTL logic pulse generated from the cavity dumper and synchronized with the pulse train. Both methods were found to be adequate and, in general, the latter was used for convenience. In order to utilize the full potential of the 4 MHz excitation rate, the time-to-pulse-height converter (Ortec Model 457) was operated in an inverted configuration, the voltage ramp being initiated by a signal from the photomultiplier and terminated by the laser pulse (30). Pulse pile-up effects were avoided by ensuring that the ratio of laser pulses to detected fluorescence was greater than 200:1. Ortec Model 934 constant fraction discriminators were used in order to (a) provide suitable voltage signals for the time-to-pulse height converter and (b) eliminate background counts from the photomultiplier. Data from the time-to-amplitude converter were stored in a Canberra series 30 multichannel analyzer using 512 channels for each data set. Data were output from this to a Perkin-Elmer 7-32 computer for analysis.

It is worthwhile listing the possible sources of error in a single-photon counting experiment. When a true fluorescence decay profile is to be determined by means of the time-correlated single photon counting technique, two experimental time profiles are measured: (a) that of the scattered excitation function distorted by the measuring system and (b) that of the sample fluorescence, also distorted by the measuring system. If certain conditions are satisfied the observed fluorescence decay,  $I(t)$ , is a convolution of the true decay,  $G(t)$ , and the measured excitation function,  $P(t)$ , i.e.

$$I(t) = \int_0^t P(t') G(t - t') dt' \quad (1)$$

or

$$I(t) = P(t) \otimes G(t) \quad (2)$$

When  $I(t)$  and  $P(t)$  are known  $G(t)$  may be determined by a variety of techniques (7). The most commonly met errors are as follows:

(i) The excitation function,  $P(t)$ , is really a convolution of the true pumping function,  $E(t)$ , with the photomultiplier response,  $H(t)$ , and the response of the electronics,  $K(t)$

$$P(t) = E(t) \otimes H(t) \otimes K(t) \quad (3)$$

Similarly eq 2 can be written

$$I(t) = E(t) \otimes G(t) \otimes H(t) \otimes K(t) \quad (4)$$

If long-term drift causes  $P(t)$  to vary between the two experiments (a) and (b),  $E(t)$  will not be the same in eq 3 and 4 with resulting errors in deconvolution.

(ii)  $H(t)$ , the response of the photomultiplier, is dependent on the area of the photocathode illuminated. Therefore if this area

is different in experiments (a) and (b),  $H(t)$  in eq 3 and 4 is different.

(iii)  $H(t)$  may also depend on the wavelength of the incident photons (31). If experiments (a) and (b) are performed at different wavelengths  $H(t)$  in (3) and (4) may be different, i.e.,  $H(\lambda_e, t) \neq H(\lambda_o, t)$  ( $\lambda_e$  = excitation wavelength,  $\lambda_o$  = emission observation wavelength). If this problem is solved by performing experiments (a) and (b) at the same wavelength,  $E(t)$  in eq 3 and 4 may be different i.e.,  $E(\lambda_e, t) \neq E(\lambda_o, t)$ .

(iv) Poor adjustment of electronic components may cause errors. In particular a maladjusted voltage divider in the fluorescence photomultiplier, a high discriminator level on the single photon pulses, and pulse pile-up can all distort the measured decay curves, sometimes in a very subtle way. For instance, occasions may arise when successful deconvolution as indicated by some simple criterion (e.g., the reduced  $\chi^2$  in least-squares fitting) has been achieved but when the recovered lifetime is in error. Excessive discrimination of the PM pulses, with consequent bias toward multiphoton pulses, may have this effect.

(v) Fluorescence from impurities may contribute to the observed decay. In the present experiments (v) was removed by careful purification of materials, (iv) was avoided by very careful tuning of the detection system, and (i), (ii), and (iii) were dealt with by the method of data analysis outlined below.

**Data Analysis.** Decay curves were first assumed to follow the equation

$$I(t) = \int_0^{t+\delta} P(t') G(t + \delta - t') dt' \quad (5)$$

in which  $\delta$  is taken to represent a shift in the zero time between excitation function and decay curve. This shift may result from drift in the pump pulse profile or, as is usually assumed, from a variation in the average transit-time spread of electrons in the photomultiplier tube with wavelength (9, 31). It is usually of little practical importance which of these two causes gives rise to observed shifts, although it should be realized that in instruments where the excitation function is measured at the emission wavelength, the need for a shift requires rather more justification than is usually given. What is of the utmost importance, however, is the correlation of the shift with a short lifetime that may be present in the decay (32). We believe that this correlation gives serious trouble only when the second lifetime is subnanosecond and its preexponential factor is negative (28). Methods for deconvolving such decays have been described for measurements where the shift is due to the photomultiplier response (4, 21) and to exciting light drift (17). If it is known that the excitation source is very stable, eq 5 may be used with a value of  $\delta$  determined from the wavelength characteristics of the photomultiplier response (33). Unfortunately complete exciting light stability is not always present and we have not yet, therefore, adopted as routine the use of a constant value of  $\delta$  determined by the difference between excitation and observation wavelengths.

Deconvolution of fluorescence decay curves has been discussed in detail in two fairly recent publications (3, 34). Both discussions recommended least-squares iterative reconvolution and this method was adopted for the present results. With this technique the data points with the highest number of counts are more heavily weighted; moreover any section of the decay curve may be excluded from the analysis, a feature especially useful if distortions are present in the data. If the sample decay is a single exponential,  $G(t)$  is given by

$$G(t) = a_1 \exp(-t/\tau_1) \quad (6)$$

and in order to linearize the fitting function (35), eq 5 is expanded to first order in a Taylor's expansion as a function of the parameters  $a_1$  and  $a_2$ . A linear least-squares search is then carried out to find values of the parameter increments  $\delta a_1$  and  $\delta a_2$  that minimize the reduced  $\chi^2$ , given by

$$\chi^2_r = \frac{\sum_{i=n_1}^{n_2} w_i [Y(t_i) - I(t_i)]^2}{n_2 - n_1 + 1 - p} \quad (7)$$

where  $w_i$ , the weighting factor, is the reciprocal of the number of counts  $Y(t_i)$  in channel  $i$ ,  $n_1$  and  $n_2$  are the first and last channels of the section of the decay to be analyzed, and  $p$  is the number



Table II. Lifetimes of Standard Compounds Measured in the Present Study

compound	solvent	$\lambda(\text{emission}),$ nm	$\tau_F, \text{nm}$	$\chi^2_\nu$	DW
PPO	cyclohexane (degassed)	440	1.42	1.10	1.8
PPO	cyclohexane (undegassed)	440	1.28	1.17	1.8
anthracene	cyclohexane (degassed)	405	5.23	1.11	1.8
anthracene	cyclohexane (undegassed)	405	4.10	1.09	2.0
1-cyanonaphthalene	hexane (degassed)	345	18.23	1.10	1.9
1-cyanonaphthalene	gas phase <sup>a</sup>	345	24.1	1.27	1.8
1-methylindole	cyclohexane (degassed)	330	6.24	1.09	1.9
3-methylindole	cyclohexane (degassed)	330	4.36	1.01	1.9
3-methylindole	ethanol (degassed)	330	8.17	1.30	1.6
1,2-dimethylindole	ethanol (degassed)	330	5.71	0.97	1.8
DMNA	$\text{CH}_2\text{Cl}_2$	375	2.40	1.1	2.0

<sup>a</sup> Vibrationally relaxed with latm cyclohexane vapor at 188 °C.

of fitting parameters (two for a single exponential fit). The search for the minimum in  $\chi^2_\nu$  is performed according to Marquadt's technique (36).

When the minimum in  $\chi^2_\nu$  has been reached it is vitally important to have reliable criteria by which the fit can be judged. The actual value of  $\chi^2_\nu$  is initially a good diagnostic in many cases. This value should be close to 1; values of  $\chi^2_\nu$  much less than 1 are symptomatic of poor statistics whereas values much in excess of 1 indicate a poor fit. If all distorted data are to be rejected we would accept results for which  $\chi^2_\nu$  is less than 1.2, whereas if some level of distortion must be tolerated, fits with values of  $\chi^2_\nu$  less than 1.4 may be acceptable if they are justified by some other criteria. Since acceptable values of  $\chi^2_\nu$  are sometimes obtained for poor fits, it is usual to inspect a plot of the weighted residuals for nonrandom fluctuations. The weighted residual in channel  $i$  is given by

$$r_i = \sqrt{w_i}(Y(t_i) - I(t_i)) \quad (8)$$

It is generally less difficult to detect small deviations of the fitted from the observed curve in a plot of  $r_i$  vs. channel number rather than in the more traditional visual inspection of the two curves  $Y(t_i)$  and  $I(t_i)$ . An even more sensitive plot is that of the autocorrelation function of the weighted residuals. The correlation of the residual in channel  $i$  with the residual in channel  $i + j$  is summed over a number of channels,  $m$ , and normalized, i.e.

$$C_{ij} = \frac{\frac{1}{m} \sum_{i=n_1}^{n_1+m-1} r_i r_{i+j}}{\frac{1}{n_3} \sum_{i=n_1}^{n_2} r_i^2} \quad (9)$$

In this expression  $n_3 = n_2 - n_1 + 1$ , the total number of channels in the section of the decay used in the fit. An upper limit, usually  $n_{3/2}$  (10), is put on  $j$  so that the number of terms,  $m = n_3 - j$ , summed in the numerator is sufficient to give proper averaging. According to eq 9  $C_{00} = 1$ . In a successful fit  $C_{ij}$  for  $j \neq 0$  is randomly scattered about zero although, because of the finite value of  $m$ , some high-frequency low-amplitude fluctuations are generally observed. These are clearly distinguishable from the type of correlation indicative of an incorrect fitting function or of distorted data (32).

Judgements based on inspection of the aforementioned plots are subject to the inevitable bias associated with subjective tests. Consequently we calculate the Durbin-Watson parameter (37, 38), DW, which is, in our opinion, more sensitive than  $\chi^2_\nu$  to small nonrandom oscillations in the residuals. DW is calculated according to the equation

$$\text{DW} = \frac{\sum_{i=n_1+1}^{n_2} (r_i - r_{i-1})^2}{\sum_{i=n_1}^{n_2} r_i^2} \quad (10)$$

Acceptable values for DW have been tabulated for up to 100 data points and five fitting parameters. Extrapolation of the tables to more data points is quite straightforward. On the basis of our

experience we conclude that single exponential fits yielding values of DW greater than 1.65 are generally successful. The corresponding values for double and triple exponential fits are 1.75 and 1.8, respectively. In addition we calculate a skewness factor, SK, given by

$$\text{SK} = \sqrt{\frac{n_3}{\sum_{i=n_1}^{n_2} (r_i - r)^3}} \sum_{i=n_1}^{n_2} (r_i - r)^3 \quad (11)$$

and a kurtosis factor,  $K$ , given by

$$K = \frac{n_3 \sum_{i=n_1}^{n_2} (r_i - r)^4}{\left[ \sum_{i=n_1}^{n_2} (r_i - r)^2 \right]^2} \quad (12)$$

In these equations  $r$  is the mean of the weighted residuals. For normally distributed residuals SK has a mean of zero and a standard deviation of  $(6/n_3)^{1/2}$ , while  $K$  has a mean of 3 and, for large  $n_3$ , a standard deviation of  $(24/n_3)^{1/2}$ . Although we calculate these parameters routinely they are difficult to interpret and therefore we find them less useful than the Durbin-Watson parameter.

A very useful test, particularly when there is doubt about the suitability of a chosen fitting function is variation of the fitting range. Variation in the recovered parameters when channels representing earlier times are included in the fit is indicative of an incorrect fitting function. Usually, but not always, instrumental distortions affecting the early time data points lead to nonnormally distributed residuals but the same values for the recovered parameters irrespective of the fitting range.

**Materials.** In general we follow standard procedures for purification of chemicals. Purity of fluorescing compounds is tested for lifetime measurements using the exponentiality and constancy of measured decay as a test. Solvents are judged to be pure when they show no fluorescence at any wavelength when excited with any of the available laser lines. In this section we briefly indicate the purification techniques adopted.

1-Methylindole was vacuum distilled. 1,2-Dimethylindole was vacuum sublimed. 3-Methylindole was recrystallized three times from cyclohexane. PPO was purchased from Fluka Chemicals and was used without further purification. *N,N*-Dimethyl-1-naphthylamine (DMNA) was vacuum distilled. Quinine bisulfate was recrystallized three times from water. 1-Cyanonaphthalene purchased, with a stated purity of 99%, as red crystals from Fluka Chemicals was vacuum sublimed three times, after which the substance was white. However, fluorescing impurities were still present but were noticeable only in the gas-phase decay curve. They were removed by recrystallization from hexane followed by further vacuum sublimation. We are extremely grateful to J. O. Williams, University College of Wales, Aberystwyth, for the donation of a sample of ultrahigh purity, multiply zone refined anthracene.

Cyclohexane was passed down a column containing equal amounts of basic alumina and silica gel. Hexane, purchased as spectrograde hexanes from Aldrich, was fractionally distilled.

Ethanol was purified by the method described by Weissberger and Proskauer (39). Water was triply distilled. Sulfuric acid was BDH "Aristar" grade. Dichloromethane was fractionally distilled.

Solutions were outgassed with a freeze-pump-thaw technique capable of evacuation to better than  $10^{-6}$  torr. Gas-phase samples of 1-cyanonaphthalene were prepared by introduction of a solution of known concentration to a closed 1-cm quartz cuvette, thorough outgassing, and heating in a modified Oxford Instruments DN704 oven (40).

## RESULTS AND DISCUSSION

In Table II are recorded single exponential decay times measured on the instrument described above. For these measurements the excitation wavelength was 300 nm and the temperature, unless otherwise stated, was 20 °C.

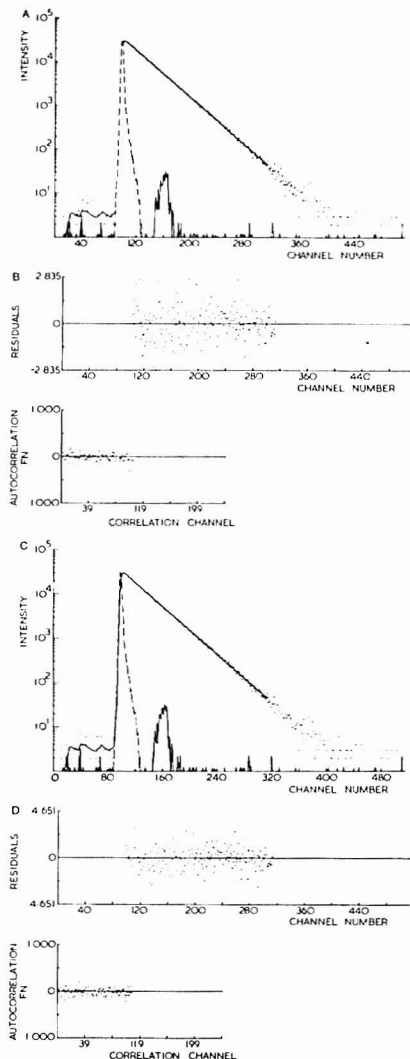
Concentrations in all solutions were less than  $10^{-5}$  M. The values of  $\chi^2$ , and of DW given are for fitting over the whole curve using a variable shift. In all cases the lifetime value did not depend on the section of the curve chosen for analysis.

Quinine bisulfate, a very popular lifetime standard, is not included in the table. We have been unable to measure single exponential decay kinetics from this compound in 1 N or 0.1 N sulfuric acid (28). In fact the decay is strongly dependent on observation wavelength and temperature and these factors render the compound unsuitable as a standard.

PPO in undegassed cyclohexane would appear to be a suitable standard when lifetimes in the region of 1 or 2 ns are to be measured. Our value for its lifetime, 1.27 ns, is independent of emission wavelength and agrees quite well with the measurement of Birch and Imhof, Table I (20). As already stated we recommend that organic solvents should be degassed for lifetime measurements. Our value for the decay time of PPO in degassed cyclohexane is 1.42 ns compared to 1.36 ns measured by Wahl et al. (21) Table I. The discrepancy, although not great, is perhaps slightly outside the experimental error associated with present day instruments and may be due to different analysis techniques. A distinctly pleasing attribute of commercially available PPO is that it requires no further purification.

Anthracene, on the other hand, is difficult to purify, a fact that may explain the variations in the measured lifetimes listed in Table I, although reabsorption effects also render the measured decay time very sensitive to concentration of anthracene used (11). The  $\tau_f$  value given in Table II, 5.23 ns, is in good agreement with four of the previous measurements in Table I and is probably accurate to within 50 ps. We use the decay curve of this compound to illustrate the quality of the fitting we achieve with our SPC instrument. In Figure 2A are shown the excitation function, anthracene decay curve, and the decay calculated by convolution of the pump pulse with parameters recovered from a fit over the decaying portion of the experimental curve. The lifetime calculated from this fit was 5.22 ns with  $\chi^2 = 1.04$  and DW = 1.84. Plots of the weighted residuals and autocorrelation function of the fit are shown in Figure 2B. While the residuals are distributed randomly, the autocorrelation function shows the low amplitude oscillations characteristic of a good fit. In Figure 2C are plotted the same excitation function and decay curve with, this time, a convolved curve, derived from a fit over all the experimental data. The zero times of the excitation function and decay curve have been shifted by 0.115 ns to obtain this fit, for which the lifetime is 5.23 ns,  $\chi^2 = 1.10$  and DW = 1.79. The plots of weighted residuals and autocorrelation function of weighted residuals, shown in Figure 2D, are also indicative of a good fit.

Emission from anthracene was observed at 405 nm, 105 nm to the red of excitation. In accordance with the rule of thumb of Robbins et al. (33) we expect a shift of about 1 ps/nm for the XP2020Q photomultiplier. We obtained, in fact, a shift of 115 ps for 105 nm. However, the results in Table III for



**Figure 2.** Decay of anthracene ( $10^{-5}$  M) in degassed cyclohexane solution at 20 °C: (a) and (c), (broken line) instrument response function, (points) observed decay curve, (line) calculated curve derived from fitting over decay only (a) and over whole curve with shift of 115 ps (c); (b) and (d), plots of weighted residuals and autocorrelation function of weighted residuals resulting from fitting over decay only (b) and over whole curve with shift (d).

the compound DMNA in dichloromethane indicate that this shift is not constant. There are two likely causes for the observed zero-time shifts between excitation function and decay curve. One is a slight instability in the laser pulse and the other is a variation of the response function of the pho-

Table III. Lifetime Data for the Fluorescence of *N,N*-Dimethyl-1-naphthylamine (DMNA) in Dichloromethane Solution Measured at Different Wavelengths (Excitation Wavelength, 300 nm)

$\lambda$ (observn), nm	region of fit	shift, ps	$\tau_F$ , ns	$\chi_p^2$	DW
375	decay		2.40	1.1	2.1
	whole curve	-8	2.40	1.1	2.1
425	decay		2.39	1.1	1.9
	whole curve	+8	2.38	1.2	1.8
475	decay		2.42	1.1	1.9
	whole curve	+41	2.42	1.1	1.9

tomultiplier with wavelength. Luckily the simple linear shift in the data analysis routine completely corrects for both effects but, since the amount of instability in the pump pulse may vary, we are not justified in choosing a fixed value of the shift depending on the wavelength difference between excitation and observation. In the use of anthracene as a standard, care must be taken with concentration and viscosity of solution, since these affect the measured decay time (11).

1-Cyanonaphthalene has proved a good acceptor molecule in exciplex studies (40). We have given the lifetime of this compound in the relaxed vapor as a standard for gas-phase measurements in which distortions such as scattered light may be significant. An atmosphere of cyclohexane was used as a vibrational relaxer and the cyanonaphthalene was present at a concentration of  $10^{-6}$  mol dm $^{-3}$ . It is generally acknowledged that purity requirements are more severe in gas phase than in solution phase measurements. Our experience with cyanonaphthalene bears out this belief. When the compound was sublimed three times under vacuum, a dilute hexane solution had a fluorescence decay that could be fit by a single exponential function. The only possible indication of residual impurities was a slight wavelength dependence in the lifetime with a longer value obtained at longer wavelengths. In the gas phase, however, the decay had a small contribution of fluorescence from a short-lived (around 2 ns) species and could not be fit by a single exponential. Further purification, as outlined above, eliminated the short-lived species and led to single component decay kinetics with the lifetime at 188 °C given in Table II.

Indoles have long been of interest as potential probes in biological studies. The fluorescence of the substituted indoles listed in Table II is only slightly displaced energetically from absorption. They have reasonably short single exponential decay times and their decay curves should be analyzable without having recourse to a shift.

DMNA has been used to test the hypothesis that the wavelength dependence of the response of the photomultiplier gives rise to a simple shift between instrument response function and decay curve. We show the results of this test in Table III. It will be seen that a negative shift is needed to fit the whole curve collected at 375 nm. As the observation wavelength is increased the expected positive shift is found with good  $\chi_p^2$  and DW values for fitting over the whole curve. We conclude, therefore, that for single exponential decays the wavelength dependence of the photomultiplier response can indeed be corrected for using a simple linear shift even when

some small pump pulse instabilities are present.

It is to be hoped that the full outline of the experimental and data handling techniques given in this paper, and the results quoted in Table II, will be of use to users of single-photon counting techniques for fluorescence decay.

**Registry No.** 2,5-Diphenyloxazole, 92-71-7; 1-cyanonaphthalene, 86-53-3; 1-methylindole, 603-76-9; 3-methylindole, 83-34-1; 1,2-dimethylindole, 875-79-6; *N,N*-dimethyl-1-naphthylamine, 86-56-6; quinine bisulfate, 549-56-4; anthracene, 120-12-7.

## LITERATURE CITED

- (1) Birks, J. B. "Photophysics of Aromatic Molecules"; Wiley-Interscience: New York, 1970.
- (2) Berlman, I. B. "Handbook of Fluorescence Spectra of Aromatic Molecules"; Academic Press: London, 1965.
- (3) O'Connor, D. V.; Ware, W. R.; Andre, J. C. *J. Phys. Chem.* **1979**, *83*, 1333.
- (4) Rayner, D. M.; McKinnon, A. E.; Szabo, A. G.; Hackett, P. A. *Can. J. Chem.* **1976**, *54*, 3246.
- (5) Yguerabide, J. In "Methods in Enzymology"; Hirs, C. H. W., Timasheff, S. N., Eds.; Academic Press: New York, 1972; Vol. 26.
- (6) Chen, R. F. *J. Res. Natl. Bur. Stand., Sect. A* **1972**, *76*, 593.
- (7) Schuyler, R.; Isenberg, I. *Rev. Sci. Instrum.* **1971**, *42*, 813.
- (8) Lopez-Delgado, R.; Tramer, A.; Munro, I. H. *Chem. Phys.* **1974**, *5*, 72.
- (9) Wild, U. P.; Holzwarth, A. R.; Good, H. P. *Rev. Sci. Instrum.* **1977**, *48*, 1621.
- (10) Harris, C. H.; Selinger, B. K. *Aust. J. Chem.* **1979**, *32*, 2111.
- (11) Blatt, E.; Treloar, E. F.; Ghiggino, K. P.; Gilbert, R. G. *J. Phys. Chem.* **1981**, *85*, 2810.
- (12) Ghiggino, K. P.; Roberts, A. J.; Phillips, D. J. *Phys. E* **1980**, *13*, 446.
- (13) Ware, W. R.; Lewis, C. J. *Chem. Phys.* **1973**, *57*, 3546.
- (14) Hül, M. H.; Ware, W. R. *J. Am. Chem. Soc.* **1976**, *98*, 4718.
- (15) Nemzek, T. L., Ph.D. Thesis, University of Minnesota, 1975.
- (16) O'Connor, D. V. Ph.D. Thesis, University of Western Ontario, 1977.
- (17) Hazan, G.; Grinvald, A.; Maytal, M.; Steinberg, I. Z. *Rev. Sci. Instrum.* **1974**, *45*, 1602.
- (18) Lampert, R. A. Ph.D. Thesis, University of Southampton, 1982.
- (19) Ware, W. R.; Holmes, J. D.; Arnold, D. R. *J. Am. Chem. Soc.* **1974**, *96*, 7851.
- (20) Birch, D. J. S.; Imhof, R. E. *Rev. Sci. Instrum.* **1981**, *52*, 9.
- (21) Wahl, Ph.; Auchet, J. C.; Donzel, B. *Rev. Sci. Instrum.* **1974**, *45*, 28.
- (22) Spears, K. G.; Cramer, L. E.; Hoffland, L. D. *Rev. Sci. Instrum.* **1978**, *49*, 255.
- (23) Fleming, R. G.; Beddard, G. S. *Opt. Laser Technol.* **1978**, *10*, (Oct), 257.
- (24) Koester, V. J.; Dowben, R. M. *Rev. Sci. Instrum.* **1978**, *49*, 1186.
- (25) Harris, J. M.; Lytle, J. E. *Rev. Sci. Instrum.* **1977**, *48*, 1469.
- (26) O'Connor, D. V.; Ware, W. R. *J. Am. Chem. Soc.* **1979**, *101*, 121.
- (27) Ware, W. R.; Watt, D.; Holmes, J. D. *J. Am. Chem. Soc.* **1974**, *96*, 7853.
- (28) O'Connor, D. V.; Meech, S. R.; Phillips, D. *Chem. Phys. Lett.* **1982**, *88*, 22.
- (29) Ware, W. R. In "Creation and Detection of the Excited State"; Lammela, A. A., Ed.; Marcel Dekker: New York 1971; Vol. 1A, p 213.
- (30) Ghiggino, K. P.; Phillips, D.; Salisbury, K.; Swords, M. D. *J. Photochem.* **1977**, *7*, 141.
- (31) Isenberg, I. *J. Chem. Phys.* **1973**, *59*, 5696.
- (32) Grinvald, A. *Anal. Biochem.* **1976**, *75*, 260.
- (33) Robbins, R. J.; Fleming, G. R.; Beddard, G. S.; Robinson, G. W.; Thistlethwaite, P. J.; Wolfe, G. J. *J. Am. Chem. Soc.* **1980**, *102*, 6271.
- (34) McKinnon, A. E.; Szabo, A. G.; Miller, D. R. *J. Phys. Chem.* **1977**, *81*, 1564.
- (35) Bevington, P. R. "Data Reduction and Error Analysis for the Physical Sciences"; McGraw-Hill: New York, 1969.
- (36) Marquardt, D. W. *J. Soc. Ind. Appl. Math.* **1963**, *11*, 431.
- (37) Durbin, J.; Watson, G. S. *Biometrika* **1950**, *37*, 409.
- (38) Durbin, J.; Watson, G. S. *Biometrika* **1951**, *38*, 159.
- (39) Weissberger, A.; Proskauer, F. "Organic Solvents: Physical Constants and Methods of Purification"; Oxford, Clarendon Press (1935).
- (40) Chewter, L.; O'Connor, D. V.; Phillips, D. *Chem. Phys. Lett.* **1981**, *84*, 39.

RECEIVED for review May 28, 1982. Accepted September 20, 1982. The authors thank the SERC, the Royal Society, and the U.S. Army European Research Office for financial support.

# Solvent Extraction of Oil-Sand Components for Determination of Trace Elements by Neutron Activation Analysis

F. S. Jacobs and R. H. Filby\*

Nuclear Radiation Center and Department of Chemistry, Washington State University, Pullman, Washington 99164-1300

Instrumental neutron activation analysis was used to measure the concentrations of 30 elements in Athabasca oil sands and oil-sand components. The oil sands were separated into solid residue, bitumen, and fines by Soxhlet extraction with toluene. Bitumen extracts contained finely divided mineral matter that was only partially removed by centrifugation of the toluene-bitumen extract. The mineral content of the extracted bitumen was dependent on the treatment of the oil sand prior to extraction. The geochemically important and organically associated trace element contents of the bitumen (and asphaltene) were determined by subtracting the mineral contributions from the total measured concentrations. The method allows analysis of the bitumen without the necessity of ultracentrifugation or membrane filtration, which might remove geochemically important components of the bitumen. The method permits classification of trace elements into organic and inorganic combinations.

The abundances of certain trace elements, particularly Ni and V, in crude oils are geochemically significant and provide information on the origin, migration, and maturation, of petroleum (1-3). Knowledge of trace element contents is also important for the processing of crudes and in designing demetallation processes to remove metals that act as catalyst poisons (4, 5). Oil sands (or tar sands) are sandstone deposits whose interstices contain viscous to solid bitumen which cannot be recovered by conventional primary oil-well production methods (6). Oil-sand bitumens are chemically similar to heavy crude oils and normally contain higher concentrations of metals than conventional crudes. The high concentrations of Ni, V, and other metals are of concern in the upgrading of oil-sand bitumen to synthetic crudes and products (7).

Determination of trace elements in oil-sand bitumen involves sampling problems other than those encountered in conventional crude oil analysis, because the bitumen must be extracted from the rock matrix which consists predominantly of coarse-grained quartz ( $\text{SiO}_2$ ) and finer-grained clay minerals (illite and kaolinite) together with minor amounts of other minerals (6). Soxhlet extraction with benzene or toluene is normally used (7) for laboratory extraction of oil-sand bitumen because of the solubility of the bitumen in these solvents. Recent work (8), however, has shown that complete extraction is observed only for oil sands containing greater than 7 wt % bitumen and low fines contents. Oil sands with high concentrations of finely divided mineral matter (e.g., clay minerals) and less than 7% bitumen show incomplete recovery by Soxhlet extraction due to adsorption of polar bitumen components on fine-grained minerals. Other solvent extraction methods (9) and hot-water extraction methods have been reported (10) but are not suitable for trace element analysis.

Instrumental neutron activation analysis (INAA) has been used to determine trace elements in crude oils (11-13) because of its high sensitivity, freedom from matrix effects, and simplicity of sample preparation prior to analysis. The method cannot be applied directly, however, to the analysis of oil sand

bitumen which must be extracted from the impregnated rock. Solvent extraction, however, may result in the coextraction of finely divided mineral matter, mostly clay minerals, which will bias the measured trace element content. Only the trace element component that is complexed to, or inherently part of, the bitumen matrix is geochemically meaningful and it is necessary either to remove, or correct for, entrained mineral matter. Also, the use of large solvent/sample volume ratios may require correction of measured trace element contents for solvent blank values (14). Particulate matter in extracted bitumen can be partly removed by centrifuging the bitumen extract, but some particulates remain in suspension. This suspension (or colloid) may be stabilized by interaction with polar bitumen components, e.g., porphyrins, naphthenic acids, etc., and organic matter adsorbed on the fines has been reported by Majid et al. (8). High speed centrifugation or ultracentrifugation cannot be used because the higher molecular weight components of asphaltene, which contain a significant fraction of some trace metals (15), and adsorbed polar components may be removed. Filtration by inert membranes with pore sizes small enough to remove clay minerals ( $<1 \mu\text{m}$ ) results in rapid clogging of the membrane and cannot be used for routine bitumen demineralization.

The distribution of trace elements among petroleum components, i.e., maltenes (oils + resins) and asphaltene, is also of geochemical significance (7). For conventional crude oils, asphaltene is separated from maltenes by precipitation with a large excess of *n*-pentane (16) or *n*-heptane (17). Selucky et al. (18) have described a procedure for the sequential solvent extraction of maltenes and asphaltene of oil-sand bitumens that has been modified for trace element analysis by Jacobs (7). Similar problems with coextraction of mineral matter in this separation scheme were observed (7).

This paper describes a solvent extraction procedure for extraction of oil-sand bitumen, maltenes, and asphaltene for trace element determination by INAA. Corrections are made for extraction blanks and for residual particulate material to give inherent trace element contents of the bitumen and its components.

## EXPERIMENTAL SECTION

**Sample Preparation.** The Athabasca oil sand, obtained as a grab sample, was visually heterogeneous with distinct nodules and intercalating lenses of shaly material in the bulk bituminous sand. One sample (designated Athabasca I) was ground in a Spex tungsten carbide ball mill for 30 min in order to homogenize the sample and another sample (Athabasca II) was sampled without homogenization. Fifty-gram aliquots of oil sand were placed in cellulose extraction thimbles (Whatman, 33 mm  $\times$  94 mm) and extracted with 200 mL of toluene (Baker reagent) for 12 h until the liquid siphoning to the flask was clear. The sand was dried at 100 °C. The toluene extract was centrifuged at 3000 rpm for 30 min to remove particulate material (particle size  $<2 \mu\text{m}$ ). The fines were washed twice with 50 mL of tetrahydrofuran (THF) and the washings combined with the toluene extract. A total of 1798 g of Athabasca II oil sand was extracted with the 200 mL solvent. The corresponding weight for Athabasca I, oil sand was 226 g. The fines were oven-dried at 110 °C for 2 h. The maltenes component of the bitumen was extracted with *n*-pentane (Baker

**Table I. Primary Standards Used for Instrumental Neutron Activation Analysis**

elements	materials used as primary standard
Ti, V, Cl, Se, Ba, Sm, Br, Ga, Th, Se, Na, La, Mn, Ce	NBS Coal SRM 1632 <sup>a</sup>
Al, Mg, Mo, Sr, Ni, Se, Rb, Co	NBS Fly Ash SRM 1633 <sup>a</sup>
Cu, As, Sb, K, Hg, Cr, Zn	NBS Orchard Leaves SRM 1571 <sup>a</sup>
Hf, Zr, Rb, Fe, Ta, Eu	USGS Standard Rock GSP-1 <sup>b</sup>

<sup>a</sup> U.S. National Bureau of Standards Standard Reference Materials. <sup>b</sup> U.S. Geological Survey Standard Rock.

reagent) for 30 h at 30 °C in a Soxhlet extractor. After extraction of the maltenes, the asphaltenes were extracted in a similar manner with toluene for 12 h at 110 °C. The toluene extract was centrifuged at 2400 rpm for 2 h and decanted; the residue was washed twice with THF and the washings were combined with the asphaltenes solution. The bitumens, maltenes, and asphaltenes were recovered by solvent evaporation in a rotary evaporator at 40 °C.

**Determination of Trace Elements by INAA.** Aliquots weighing 200–400 mg for raw oil sand, 100–200 mg for oil sand solids, 50–150 mg for asphaltenes and fines, and 500–900 mg for bitumen and maltenes were placed in 0.4-dram polyethylene vials. The vials were heat-sealed and sealed in 2-dram polyethylene vials for irradiation. Trace element standards were prepared in the same manner. Standards used include U.S. National Bureau of Standards (NBS) Standard Reference Materials (SRM's) Coal (SRM 1632), Fly Ash (SRM 1633), and Orchard Leaves (SRM 1571) and the U.S. Geological Survey rock standards GSP-1 (grandodiorite), BCR-1 (basalt), PCC-1 (peridotite), and DTS-1 (dunite). The reference standards SRM 1632, 1633, and 1571 and PCC-1 and DTS-1 were used as primary standards for some elements, and as checks on the analytical data for others. The elements for which these materials were used as primary standards are shown in Table I. All containers with which the analyzed or separated samples came into contact were previously soaked in THF (reagent grade) for 24 h and then in 35% HNO<sub>3</sub> for the same length of time before washing with double-distilled water and acetone.

Samples and standards were irradiated in the Washington State University TRIGA III-fueled research reactor in an average thermal neutron flux of  $6 \times 10^{15}$  neutrons cm<sup>-2</sup> s<sup>-1</sup>. Two irradiation times were used depending on the half-life of the induced radionuclide as shown in Table II. Special care was taken to ensure that the irradiation geometry was the same for the small volume solid samples and standards and the larger volume bitumens and maltenes.  $\gamma$ -ray spectrometry using Ge(Li) detectors interfaced to an ND 6620 spectrometer (Nuclear Data) was used for radionuclide measurement. Postirradiation decay times and approximate counting times are shown in Table II. Reduction of  $\gamma$ -ray spectra to  $\gamma$ -ray peak areas and elemental concentrations was carried out by using the SPANAL program (19) or the FOURIER program (20) in the Washington State University Amdahl 470 computer. Appropriate corrections were made for decay during counting by using the method of Hoffman and Van Camerik (21), overlapping  $\gamma$ -ray peak corrections (e.g., <sup>76</sup>Se/<sup>203</sup>Hg, <sup>64</sup>Cu/<sup>24</sup>Na),

and for differences in integrated neutron exposure between samples and standards. Details of the  $\gamma$ -ray spectrometry and data reduction procedures have been presented elsewhere (22), with minor changes and modifications as indicated here. The elemental concentrations determined for bitumen, maltenes, and asphaltenes were corrected for contributions from the extracting solvent (blank), using the method described by Jacobs et al. (14).

## RESULTS AND DISCUSSION

The concentrations of 30 elements in Athabasca I and II oil sand components are shown in Table III. These concentrations reported have been corrected for extraction solvent blanks which were negligible for all elements (14). Except for Ni and V, there are large differences in trace element contents between bitumens I and II. The fact that both bitumens contain similar concentrations of Ni and V which are known to be present either as Ni<sup>2+</sup> and VO<sup>2+</sup> metalloporphyrins (1) or as nonporphyrin complexes in asphaltene moieties (6) suggests that the bitumens have similar trace element contents. The large differences in trace element contents between the two bitumens therefore appear to be due to the presence of entrained mineral matter and thus the measured trace element concentrations do not represent the inherent concentrations in the oil-sand bitumen. The weight percentages of bitumen in the Athabasca I and II samples are similar (10.8% and 11.0%, respectively) but the coextracted fines content in Athabasca I is much larger than in Athabasca II (2.2% and 0.2%, respectively). Thus the homogenization of Athabasca I oil sand prior to extraction of bitumen resulted in a much larger amount of fine-grained mineral matter being coextracted with the bitumen. Also, the higher concentrations of such elements as Al and K, which are important clay mineral constituents, in Athabasca I bitumen compared to Athabasca II suggest that the former retains a greater amount of entrained mineral material. The fines from both Athabasca samples have similar compositions with the mean major element concentrations being 12.3% Al, 2.7% Fe, 1.7% K, and 0.8% Ti. The data are consistent with a mixture of silica plus kaolinite, nominally Al<sub>2</sub>Si<sub>4</sub>O<sub>10</sub>(OH)<sub>8</sub> (Al = 21%), and illite, nominally K<sub>0.2</sub>Al<sub>4</sub>(Si<sub>6.5</sub>Al<sub>0.5</sub>)O<sub>20</sub>(OH)<sub>4</sub> (Al = 15–20%, K = 0–9%), which are the major clay minerals in the Athabasca oil sand (7) and which were identified by X-ray diffraction as the major mineral species in the extracted fines. Finely divided mineral matter entrained in the bitumen is probably colloidal illite and kaolinite with minor amounts of SiO<sub>2</sub>.

Because K forms no geochemically important organic complexes in petroleum it is assumed that all the K in the bitumen is present as mineral matter. Any K contained in the water film surrounding the sand grains would be present as KCl which would be distributed among the solid components when the water evaporated during Soxhlet extraction. Negligible amounts of KCl would dissolve in toluene during the extraction and appear as bitumen-soluble K species. Assuming the mineral matter in the fines to have the same elemental composition as that retained in the bitumen, except perhaps for Si, the computed concentrations of retained particulates in Athabasca bitumens I and II are 3.54 wt % and 0.25 wt %, respectively. The inherent concentration of an element in the bitumen [X]<sub>MF</sub> may be calculated thus

**Table II. Irradiation, Decay, and Counting Times for Instrumental Neutron Activation Analysis**

nuclide measured and half-life range	irradiation time	decay time	counting time
<sup>24</sup> Al, <sup>27</sup> Mg, <sup>51</sup> Ti, <sup>123</sup> V ( $t_{1/2}$ = 2.3–8.8 min)	3–5 min	1 min	150–180 s
<sup>35</sup> Cl, <sup>55</sup> Mn ( $t_{1/2}$ = 35–160 min)	3–5 min	30 min	1000 s
<sup>76</sup> As, <sup>82</sup> Br, <sup>64</sup> Cu, <sup>72</sup> Ga, <sup>81</sup> K, <sup>140</sup> La, <sup>99</sup> Mo– <sup>99m</sup> Tc, <sup>23</sup> Na, <sup>152</sup> Sm ( $t_{1/2}$ = 10–70 h)	8 h	36 h	4000 s
<sup>131</sup> Ba, <sup>141</sup> Ce, <sup>88</sup> Co, <sup>51</sup> Cr, <sup>152</sup> Eu, <sup>59</sup> Fe, <sup>181</sup> Hf, <sup>190</sup> Hg, <sup>57</sup> Co (for Ni), <sup>86</sup> Rb, <sup>125</sup> Sb, <sup>46</sup> Sc, <sup>76</sup> Se, <sup>89</sup> Sr, <sup>182</sup> Ta, <sup>160</sup> Tb, <sup>233</sup> Pa (for Th), <sup>65</sup> Zn, <sup>90</sup> Zr ( $t_{1/2}$ > 4 days)	8 h	21 days	80000 s

Table III. Measured Trace Element Concentrations (in  $\mu\text{g g}^{-1}$ ) in Athabasca Oil-Sand Components,  $[X]_A$ , and Mineral-Free Concentrations,  $[X]_{MF}$ 

element	Athabasca I			Athabasca II	
	bitumen (10.75%) <sup>a</sup> [X] <sub>A</sub>	finer (2.23%) <sup>a</sup> [X] <sub>F</sub>	mineral-free bitumen [X] <sub>MF</sub>	bitumen (10.98%) <sup>a</sup> [X] <sub>A</sub>	finer (0.21%) <sup>a</sup> [X] <sub>F</sub>
Al	3190 ± 300 <sup>b</sup>	113000 ± 7100 <sup>b</sup>	<1000	274 ± 16 <sup>b</sup>	133000 ± 9200 <sup>b</sup>
As	0.56 ± 0.06	6.3 ± 0.4	0.341 ± 0.061	0.146 ± 0.014	15.4 ± 0.05
Ba	8.4 ± 2.7	472 ± 2	<6	2.9 ± 1.2	464 ± 76
Ce	2.50 ± 0.34	91.8 ± 2.0	<0.9	0.22 ± 0.03	102 ± 12
Cl	23.3 ± 3.1	109 ± 3	19.4 ± 3.2	13.8 ± 2.9	<20
Co	4.39 ± 0.20	34000 ± 280	3.19 ± 0.22	0.24 ± 0.03	22.9 ± 3.1
Cr	4.60 ± 0.37	93.1 ± 1.3	1.31 ± 0.45	0.85 ± 0.07	117 ± 18
Cs	0.23 ± 0.02	5.9 ± 0.1	<0.05	0.02 ± 0.001	5.9 ± 0.8
Eu	0.04 ± 0.005	1.4 ± 0.05	<0.02	0.007 ± 0.001	1.4 ± 0.2
Fe	1030 ± 70	26600 ± 180	<200	242 ± 17	27500 ± 4100
Ga	1.30 ± 0.2	20.1 ± 0.5	0.58 ± 0.18	0.360 ± 0.051	28.7 ± 1.9
Hf	0.39 ± 0.02	7.72 ± 0.02	0.12 ± 0.03	0.046 ± 0.007	8.8 ± 1.2
K	594 ± 45	16800 ± 30	0	<44.3 ± 2.9	17200 ± 64
La	1.64 ± 0.12	49.2 ± 1.2	<0.4	0.17 ± 0.02	62.3 ± 0.8
Mn	18.4 ± 1.6	520 ± 74	<7	4.76 ± 0.21	733 ± 19 <sup>c</sup>
Mo	NM <sup>d</sup>	NM <sup>d</sup>		7.2 ± 1.8	<20
Na	149 ± 10	2750 ± 7	52 ± 12	21.2 ± 3.0	2110 ± 13
Ni	68.1 ± 8.0	52.0 ± 7.7	66.3 ± 8.0	71 ± 16	69 ± 17
Rb	5.7 ± 1.1	57 ± 14	3.71 ± 1.2	1.72 ± 0.13	65 ± 22
Sb	0.05 ± 0.009	0.58 ± 0.05	0.03 ± 0.01	0.025 ± 0.002	1.0 ± 0.3
Sc	0.48 ± 0.02	12.7 ± 0.2	<0.1	0.19 ± 0.01	14.1 ± 0.2
Se	0.61 ± 0.06	27.1 ± 0.3	0.51 ± 0.06	0.34 ± 0.03	3.1 ± 0.7
Sm	0.20 ± 0.03	5.82 ± 0.09	<0.07	0.03 ± 0.006	8.4 ± 0.5
Sr	5.0 ± 0.5	160 ± 19	<3	3.0 ± 0.2	183 ± 3
Ta	0.22 ± 0.01	15.6 ± 0.3	<0.04	0.004 ± 0.001	1.5 ± 0.2
Tb	0.023 ± 0.008	0.71 ± 0.12	<0.02	0.007 ± 0.001	0.68 ± 0.5
Th	0.56 ± 0.04	12.7 ± 0.2	<0.1	0.11 ± 0.01	14.0 ± 2
Ti	183 ± 37	6830 ± 580	<100	<80	9690 ± 2200
V	144 ± 19	142 ± 16	139 ± 19	170 ± 5	194 ± 24
Zr	9.80 ± 3.4	219 ± 9	<7	2.81 ± 0.78	254 ± 83
replicates	n = 6	n = 2		n = 6	n = 2

element	Athabasca II					
	mineral-free bitumen		maltenes		asphaltenes	
	[X] <sub>MF</sub> <sup>c</sup>	% [X] <sub>MF</sub>	[X] <sub>MF</sub> <sup>c</sup>	% [X] <sub>MF</sub>	[X] <sub>MF</sub> <sup>c</sup>	% [X] <sub>MF</sub>
Al	<80		2		<2	
As	0.11 ± 0.01	73	0.09 ± 0.01	99	0.357 ± 0.035	67
Ba	<3		<0.01		8 ± 2	62
Ce	<0.1		<0.005		<0.5	
Cl	13.8 ± 2.9	100	NM <sup>d</sup>		NM <sup>d</sup>	
Co	0.18 ± 0.03	75	0.056 ± 0.002	98	1.02 ± 0.08	80
Cr	0.55 ± 0.09	65	0.17 ± 0.03	97	3.0 ± 0.5	70
Cs	<0.01		<0.001		<0.03	
Eu	<0.004		0.002 ± 0.0004	96	0.020 ± 0.002	55
Fe	171 ± 21	71	139 ± 4	99	720 ± 60	70
Ga	0.296 ± 0.05	80	<0.04		1.11 ± 0.1	77
Hf	0.02 ± 0.01	51	<0.001		0.12 ± 0.02	54
K	0		0		0	
La	<0.04		0.008 ± 0.001	100	<0.2	
Mn	2.87 ± 0.25	60	2.71 ± 0.06	99	10.4 ± 0.4	56
Mo	7.2 ± 1.8	100	0.20 ± 0.05	100	22 ± 3	100
Na	15.8 ± 3.0	74	2.3 ± 0.8	96	37 ± 13	61
Ni	70.3 ± 6	100	22 ± 1	100	192 ± 5	100
Rb	1.55 ± 0.14	90	<0.003		6.5 ± 2.2	90
Sb	0.022 ± 0.002	89	<0.001		0.08 ± 0.01	87
Sc	0.16 ± 0.01	81	0.19 ± 0.001	100	0.87 ± 0.05	85
Se	0.33 ± 0.03	98	0.297 ± 0.006	100	0.94 ± 0.06	96
Sm	<0.01		0.0034 ± 0.0006	90	0.04 ± 0.01	29
Sr	2.5 ± 0.2	83	<1			
Ta	<0.004		<0.04		<0.02	
Tb	0.004 ± 0.001	73	0.004 ± 0.001	99	0.04 ± 0.01	83
Th	0.07 ± 0.01	67	0.046 ± 0.002	99	0.32 ± 0.03	67
Ti	NM <sup>d</sup>		NM <sup>d</sup>		NM <sup>d</sup>	
V	170 ± 5	100	53.8 ± 1.8	100	630 ± 49	100
Zr	<2		<0.01		<10	

<sup>a</sup> Weight percent of component relative to oil sand in parentheses. <sup>b</sup> Mean ± standard deviation. <sup>c</sup> Mean ± standard deviation. The less than sign represents the upper limit of two standard deviations. <sup>d</sup> Not measured.



$$[X]_{MF} = [X]_A - [X]_M \quad (1)$$

and

$$[X]_M = [K]_A[X]_F/[K]_F \quad (2)$$

where  $[X]_{MF}$  is the concentration of element X in mineral-free bitumen,  $[X]_A$  is the analytical concentration of element X measured in bitumen,  $[X]_F$  is the measured concentration of element X in fines,  $[K]_A$  is the measured concentration of K in the bitumen, and  $[K]_F$  is the measured concentration of K in the fines. The computed trace element concentrations in mineral-free Athabasca I and II bitumens are shown in columns 3 and 6 in Table III. Concentrations listed as less-than values are not significantly different from 0 (positive or negative) at 95% confidence limits. The less-than values were arbitrarily taken as two standard deviations for such elements.

The concentration data for the mineral-free bitumens indicate that of the 30 elements only As, Cl, Co, Cr, Fe, Ga, Hf, Mn, Na, Ni, Rb, Se, Tb, V, Mo, and Th are measurable in the mineral-free bitumen. The elements Al, Ba, Ce, Cs, Eu, La, Sm, Sr, Ta, Ti, and Zr appear to be present entirely in the inorganic particulate phase of the extracted bitumen. The trace element compositions of mineral-free Athabasca I and II bitumens are not significantly different at the 95% confidence limits (*t* test), with the exception of Co. The method therefore gives the inherent trace element data for the oil-sand bitumen that can be related to other geochemical parameters, e.g., degree of maturation, degree of microbial degradation, etc. For the determination of trace elements in oil sand bitumens, it is important that the raw oil sand not be homogenized by grinding and that other steps be taken to minimize dispersion of the fines during sample preparation.

Because the contribution of fines to the bitumen was smaller for Athabasca II than for Athabasca I, the former was selected for geochemical study (7) and the bitumen was separated into maltenes and asphaltenes. Similar calculations were made to compute the mineral-free trace element composition of the maltenes and asphaltenes and the data are also shown in Table III. The percentage,  $\%[X]_{MF}$ , of each element present in the mineral-free components relative to the measured concentration was calculated by

$$\%[X]_{MF} = \frac{[X]_{MF}}{[X]_A} \times 100 \quad (3)$$

where  $[X]_{MF}$  is the computed mineral-free concentration of X and  $[X]_A$  is the measured concentration of X in extracted component. The data in Table III show that the maltenes have much lower trace element contents than do the asphaltenes, as is the case for conventional crude oils (13, 20). The fines are a negligible contribution to all concentrations in the maltenes, which is consistent with the fact that *n*-pentane is a solvent of low polarity. Thus low-polarity maltenes components show little tendency to adsorb on or associate with finely divided mineral matter. The mineral-free trace element concentrations of asphaltenes and whole bitumen show a similar pattern, as might be expected, except that Ba, Eu, and Sm have statistically significant concentrations in the asphaltenes but not in the bitumen. It should be observed that the  $\%[X]_{MF}$  values are very similar for asphaltenes and bitumen. Elements with  $\%[X]_{MF}$  values greater than 60 can be classified as being predominantly organically

Table IV. Geochemical Classification of Elements in Athabasca II Bitumen and Asphaltenes

% [X] <sub>MF</sub>	geochemical classification	element in asphaltenes	element in bitumen
0-40	predominantly inorganic	Al, Ce, Cs, K, Mn, Sm, Sr, Ta, Zr	Al, Ba, Ce, Cs, Eu, K, Sm, Sr, Ta, Zr
60-100	predominantly organic	As, Ba, Co, Fe, Ga, Mo, Na, Ni, Rb, Sb, Sc, Se, Tb, Th, V	As, Co, Cr, Fe, Ga, Mn, Mo, Na, Ni, Rb, Sb, Sc, Se, Rb, Th, V

combined in the bitumen and asphaltenes and therefore can be used in geochemical interpretations. Elements which are associated primarily with the mineral component of the bitumen should thus not be used in geochemical studies of oil sands. The elements determined in the bitumen and asphaltenes are classified in Table IV. Nickel and vanadium are shown to be 100% organically combined in all components of the Athabasca bitumen, which is consistent with results from previous studies (1, 6, 20).

#### ACKNOWLEDGMENT

The assistance of D. Barbee, V. Craig, C. Grimm, and J. Neidiger are gratefully acknowledged. The efforts of Dean Wallace of the Alberta Research Council, Edmonton, Alberta, Canada, in obtaining oil sand samples are gratefully recognized.

#### LITERATURE CITED

- (1) Hodgson, G. G.; Baker, B. L.; Peake, E. In "Fundamental Aspects of Petroleum Geochemistry"; Colombo, U. Ed.; Elsevier: Amsterdam, 1967; pp 177-259.
- (2) Ball, J. S.; Wenger, W. J.; Hyden, H. J.; Horr, C. A.; Myers, A. T. J. *Chem. Eng. Data* 1980, 5, 553-557.
- (3) Skinner, D. A. *Ind. Eng. Chem.* 1952, 44, 1159.
- (4) Gould, K. A. *Fuel* 1980, 59, 733.
- (5) Mills, G. A. *Ind. Eng. Chem.* 1950, 42, 182.
- (6) Camp, F. W. In "The Tar Sands of Alberta, Canada", 3rd ed.; Cameron Engineers Inc.: Denver, CO, 1976.
- (7) Jacobs, F. S. Ph.D. Thesis, Washington State University, 1982.
- (8) Majid, A.; Sirianni, A. F.; Rimpester, J. A. *Fuel* 1982, 61, 477.
- (9) Bowles, K. W.; Booth, F. L. Department of Mines and Resources, Mines and Geology Branch, Bureau of Mines Fuel Research Laboratory, Ottawa, Ontario, Canada, Sept 1947.
- (10) Clark, K. A.; Pasternack, D. S. *Ind. Eng. Chem.* 1932, 24, 1410.
- (11) Shah, K. R.; Filby, R. H.; Haller, W. A. *J. Radioanal. Chem.* 1970, 6, 185-192.
- (12) Shah, K. R.; Filby, R. H.; Haller, W. A. *J. Radioanal. Chem.* 1970, 6, 413-422.
- (13) Buenafama, H. D.; Lubkowitz, J. A. *J. Radioanal. Chem.* 1977, 39, 293-300.
- (14) Jacobs, F. S.; Ekambaram, V.; Filby, R. H. *Anal. Chem.* 1982, 54, 1240.
- (15) Weeks, R. W., Jr.; McBride, W. L. *Prepr., Div. Pet. Chem., Am. Chem. Soc.* 1979, 24, 990.
- (16) Selucky, M. L.; Chu, Y.; Ruot, T.; Strausz, O. P. *Fuel* 1977, 56, 369-381.
- (17) Long, R. B. *Prepr., Div. Pet. Chem., Am. Chem. Soc.* 1979, 24, 891.
- (18) Selucky, M. L.; Ruot, T. C. S.; Strausz, O. P. In "Oil Sands and Oil Shale Chemistry"; Strausz, O. P., Low, E. M., Eds.; Verlag Chemie: New York, 1978; pp 119-144.
- (19) Filby, R. H.; Shah, K. R. *Toxicol. Environ. Chem. Rev.* 1974, 2, 1.
- (20) Filby, R. H. Ph.D. Thesis, Washington State University, 1971.
- (21) Hoffman, B. W.; Van Calker, S. B. *Anal. Chem.* 1947, 39, 1198.
- (22) Filby, R. H.; Haller, W. A.; Shah, K. R. *J. Radioanal. Chem.* 1970, 5, 277.

RECEIVED for review July 29, 1982. Accepted October 4, 1982.

# Recovery Factor for Extraction from a Solid, Extractant-Retaining Matrix

David Emlyn Hughes

Analytical Chemistry Division, Norwich Eaton Pharmaceuticals, Inc., Box 191, Norwich, New York 13815

**The theory and calculation of the recovery factor for an extraction from a solid extractant-retaining sample are presented. The recovery factor is seen to consist of two multiplicative factors, one factor for extraction efficiency and one for extract retention by the sample. Several examples are presented.**

Although liquid-liquid extraction has attracted a great deal of theoretical modeling, solvent extraction from a solid medium has drawn less attention. Liquid-solid extraction has been used for centuries for the recovery of metals, sugars, salts, and medicinals (1). Recently, much of the interest in the field has been in empirical considerations in solvent/metal-containing compounds and refinements of Soxhlet extraction. Although liquid-liquid extraction is well understood, liquid-solid extraction theory is absent from the chemical literature. The theoretical considerations presented here do not concern themselves with why a particular extract-matrix partitioning has occurred. The theoretical problem is deriving an analytical expression for the recovery factor for a liquid extraction from a solid, solvent-retaining sample. The results differ substantially from liquid-liquid systems, since liquid-solid extraction systems frequently retain extract.

When the volume of extractant is comparable to the volume of the solid matrix or when a "reverse" extraction is performed on another liquid (extraction of an organic layer with an aqueous solution), some of the extract is often physically trapped in the medium. Both solid and liquid media are therefore able to retain extract. Multiple extraction often removes sufficient analyte such that the extracts may be combined and successfully assayed.

A somewhat less defined situation exists when extraction yields insufficient extract to produce an acceptable recovery. If extract is associated with the medium in a fixed proportion, the association is reasonably constant from sample to sample. The concentration of the analyte may then be calculated.

In what at first appears to be the most analytically complex situation, some indeterminate amount of the analyte is physically trapped in the matrix. The precise volume of extract in the matrix prior to assay is dependent on the prior sample handling and may vary significantly from determination to determination. A familiar and consistent physical model is aqueous extraction from vegetable oil. Upon extraction, apparently intact droplets of extract (or extractant) appear within the vegetable oil layer. If extract is retained within vegetable oil, some unspecified amount of the analyte is still within the vegetable oil phase and is not available for assay. A mathematical model will now be presented for an extraction from a solid which retains a variable amount of extract.

After the initial extraction, the extract trapped in the sample: (1) may or may not have the same concentration as the extractant; (2) may or may not be able to be extracted further. The following discussion is consistent with IUPAC recommended nomenclature and terminology (2).

## THEORY

If the sample contains  $n_i$  mol of analyte in a volume  $V_m$  and a volume  $V_o$  of a thermodynamical ideal extractant is added, the available volume of the extract is ( $V_o + V_m - V$ ), where  $V$  is the volume occupied by the extract within the sample. If the solution is given sufficient time to equilibrate, the concentration  $\theta n_i/V$  may be such that

$$\theta n_i/V < M_{\text{ext}} \quad (1)$$

$$\theta n_i/V > M_{\text{ext}} \quad (2)$$

$$\theta n_i/V = M_{\text{ext}} \quad (3)$$

where  $M_{\text{ext}}$  is the molarity of the solution external to the matrix. The molarity of the extract concentration within the sample may therefore be less than, greater than, or equal to that of the surrounding extract.

In eq 3, the extract concentration is the same internally and externally to the sample. The internal and external extracts in this case have the same concentration and if the system is assumed to be isothermal, the expression (3) for the molal distribution constant ( $K_D$ )<sub>A</sub> of the analyte A is

$$(K_D)_A = \frac{\gamma_{\text{int}}}{\gamma_{\text{ext}}} \exp[-(\phi_{\text{ext}}^\circ - \phi_{\text{int}}^\circ)/RT] = \exp[-(\phi_{\text{ext}}^\circ - \phi_{\text{int}}^\circ)/RT] \quad (4)$$

where  $\gamma_{\text{int}}$  = molal activity coefficient within the sample extract,  $\gamma_{\text{ext}}$  = molal activity coefficient of the surrounding extract,  $\phi_{\text{ext}}^\circ$  = partial molal free energy of the extract, and  $\phi_{\text{int}}^\circ$  = partial molal free energy of the retained extract. Therefore

$$(K_D)_A = \frac{m_{\text{ext}}}{m_{\text{int}}} \exp[-(\phi_{\text{ext}}^\circ - \phi_{\text{int}}^\circ)/RT] = 1 \quad (5)$$

and

$$\phi_{\text{ext}}^\circ = \phi_{\text{int}}^\circ \quad (6)$$

where  $m_{\text{int}}$  = molality of the matrix extract and  $m_{\text{ext}}$  = molality of the extract.

Henceforth, the less cumbersome  $K_D$  will be used in place of ( $K_D$ )<sub>A</sub> since only one substance is being considered.

The conclusion is that the physically obvious  $K_D = 1$  (since  $m_{\text{ext}} = m_{\text{int}}$  and  $K_D \approx m_{\text{ext}}/m_{\text{int}}$ ) is not an approximation but is rather thermodynamically exact (4, 5).  $K_D = 1$  allows the derivation of analytical expressions for the recovery of the analyte using two extraction models. It is clear that the  $K_D = 1$  assumption is simply a mathematical convenience and not a requirement of the present model. If an apparent (nonunity) value of  $K_D$  is assumed, then the derivation is unchanged and the model may be extended to cases (1) and (2) above. The mathematical model is then completed by calculation of the recovery factor for the procedure.

In the first extraction model procedure, sufficient extractant is supplied to perform a single, simple extraction such that the liquid recovered has a volume  $V_r$ .

The molarity of the resulting solution is

$$M_1 = \frac{10^3 n_i (1 - \theta)}{V_f} \quad (7)$$

where  $n_i$  = moles of solute originally in the matrix,  $\theta$  = mole (decimal) fraction of  $n_i$  trapped in matrix after one extraction assuming  $m_{\text{int}} = m_{\text{ext}}$ , and  $V_f$  = final volume of extract, in milliliters.

In the second extraction procedure,  $V_f$  mL of extractant is added to the matrix. The molalities of the internal (sample) and external extracts are again equal by assumption

$$m_{\text{int}} = m_{\text{ext}} = 10^3 n_i / V_{fp} \quad (8)$$

where  $\rho$  = density of the extractant (g/mL). Converting to molarity

$$M_2 = \frac{10^3 \rho_{\text{sol}} m_{\text{ext}}}{10^3 + M_w m_{\text{ext}}} \quad (9)$$

and substituting in  $m_{\text{ext}}$  from (8)

$$M_2 = \frac{10^3 \rho_{\text{sol}} n_i}{V_{fp} + M_w n_i} \quad (10)$$

Note that although the total volume of the sample and extract system is indeterminate, the volume of extract is  $V_f$ .

If an aliquot of each resulting solution is now assayed by a hypothetically perfect method (since we are interested in errors inherent in the extraction, not in the subsequent assay) the recovery factor

$$R_A = \frac{M_1}{M} \frac{M_2}{M} = \frac{10^3 n_i (1 - \theta)}{V_f} \frac{10^3 \rho_{\text{sol}} n_i}{V_{fp} + M_w n_i} \quad (11)$$

where  $M = 10^3 n_i / V_f$ , that is

$$R_A = \frac{(1 - \theta) V_{fp} \rho_{\text{sol}}}{V_{fp} + M_w n_i} \quad (12)$$

for a single extraction step in the first extraction procedure.

If the retained extract is available for further extraction (7)

$$\theta = \left( \frac{V}{(K_D V_f / n) + V} \right)^n \quad (13)$$

providing the volume of extractant is divided by  $n$  and  $n$  extractions are performed. The recovery factor becomes

$$R_A = \frac{V_{fp} \rho_{\text{sol}} [1 - \{V / ((V_f / n) K_D + V)\}^n]}{V_{fp} + M_w n_i} \quad (14)$$

A slightly more general form would allow  $n$  extractions with volumes  $V_1, V_2, V_3, \dots$ , such that

$$\sum_{i=1}^n V_i = V_f \quad (15)$$

and

$$R_A = \frac{V_{fp} \rho_{\text{sol}} [1 - V^n \prod_{i=1}^n \{1 / (V_i K_D + V)\}]}{V_{fp} + M_w n_i} \quad (16)$$

Although the recovery equation is somewhat involved, further mathematical complications result if the system is not assumed to be isothermal. It is clear that although the physical model presented here lent direction to the mathematical model derivation, eq 16 could have been derived solely from conservation equations. The derivation could easily be extended to allow association and dissociation reactions (8, 9), mutual dissolution of the matrix and extracting solvent, side reactions (10), salt effects (salting-in, salting-out, common

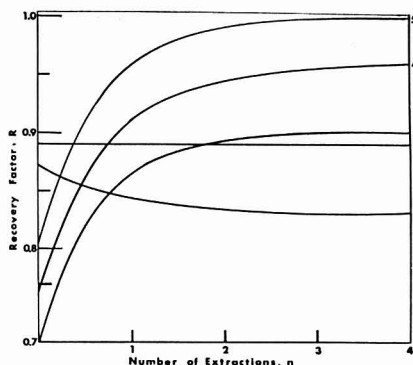


Figure 1. Extraction from an extractant-retaining sample with  $K_D = 4$ : curve 1,  $\theta n_i / V < M_{\text{ext}}$ ; curves 2–5,  $\theta n_i / V \geq M_{\text{ext}}$  and limiting  $R_A \approx 0.80, 0.90, 0.95$ , and 1.0.

ion, and Setchenow (11, 12)), and generalized distribution coefficients (13–15).

### EXAMPLES

Examination of eq 16 reveals that the recovery factor consists of two multiplicative terms

$$R_A = R_{\text{ret}} R_{\text{ext}} \quad (17)$$

where

$$R_{\text{ret}} = \left( \frac{V_{fp} \rho_{\text{sol}}}{V_{fp} + M_w n_i} \right) \quad (18)$$

and

$$R_{\text{ext}} = 1 - V^n \prod_{i=1}^n \left( \frac{1}{V_i K_D + V} \right) \quad (19)$$

$R_{\text{ret}}$  is the recovery factor due to the retention of extract by the sample and  $R_{\text{ext}}$  is the recovery factor for the extraction process.

**Example 1.** In Figure 1, curve 1, the sample extract is more dilute than the surrounding extract, as in eq 1. Further extraction allows more analyte to be retained by the sample and the recovery factor drops asymptotically until  $\theta n_i / V = M_{\text{ext}}$ . Equations 2 and 3 have similar shapes and are represented by curves 3, 4, and 5, with respective limiting  $R_{\text{ret}}$  values of 0.90, 0.95, and 1.0. Curve 2 represents that special case for eq 3 only when  $V_f K_D \gg V$  and the extract is fully retained after the first extraction with an  $R_{\text{ret}} = R \approx 0.80$ . The samples in Figure 1 would not show significantly higher recovery factor values with more elaborate (and numerous) extraction schemes.

**Example 2.** When the analyte is retained in a solid sample, at least two mechanisms may be involved. The intact extract may be trapped in the sample and the analyte may be irreversibly bound to the solid sample. The extent of these mechanisms may be determined by performing the following analyses: (a) single extraction on identical samples using  $NV_1$  mL of extractant for  $N = 1, 2, 3$ , and 6; (b) a multiple extraction ( $n = 3$ ) using  $V_1$  mL for each extraction; (c) assay of the seven samples.

For the analysis of the single extraction data, recall eq 17 and notice that  $R_{\text{ext}}$  may be rearranged to

$$1/R_{\text{ext}} = 1 + (V/K_D)(1/V_f) \quad (20)$$

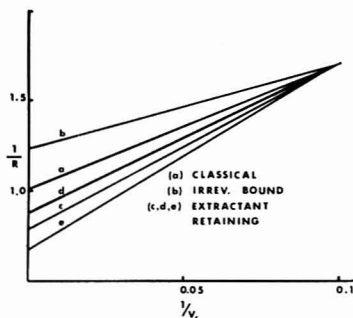


Figure 2. Dependence of the recovery factor on the extraction volume for a single extraction.

For eq 18, if the decimal fraction of analyte ( $1 - R_{irr}$ ) is irreversibly bound and if the concentration of trapped extractant is linearly dependent on  $V_1$ , then

$$R_{ret} = R_{irr} \left( 1 - \frac{1 - R_1}{2(V_f - V_1)/V_1} \right) \quad (21)$$

or

$$\frac{1}{R_{ret}} = \frac{2(V_f - V_1)/V_1}{R_{irr}(2(V_f - V_1)/V_1 + R_1 - 1)} \quad (22)$$

which approximates a straight line ( $\pm 0.4\%$ ,  $1/R \leq 1.7$ ) if  $1/R_{ret}$  is plotted vs.  $1/V_f$  and  $(V_f - V_1)/V_1 \leq 3$ .

Hence both  $R_{ret}$  and  $R_{irr}$  are linear if  $1/R$  is plotted vs.  $1/V_f$  for experimental extraction data  $V_f \leq 3V_1$ . In Figure 2,  $1/R$  data ( $R$  = assay value/accepted value) vs.  $1/V_f$  data are plotted for  $V_1 = 10$  mL. By simply relabeling the axis, any  $V_1$ ,  $2V_1$ , and  $3V_1$  scheme may be used.

If the multiple extraction scheme improved the recovery factor significantly, the data for the single extraction scheme will fall on lines similar to (a) and (b) on Figure 1. If the points fall on line a, then the solid is being extracted as if it were a classical liquid. If the  $1/R$  intercept is statistically larger than zero, some ( $1 - R$  at  $1/V_f = 0$ ) is being irreversibly retained. For line b,  $1/R = 1.2$  ( $R = 0.833$ ) or about 17% of the analyte is irreversibly retained. If an assay with a higher accuracy is required, the extractant system is to be abandoned.

If the multiple extraction scheme is ineffective in improving the recovery factor, the experimental points for the single extraction will lie on a line similar to c in Figure 2. If extractant is retained in accordance with eq 3 and eq 22, then the slope and intercept of the line may be obtained from Table I and  $R_{ret}$  = assay value ( $N = 6$ )/accepted value within  $\pm 1\%$ . In the nonequilibrated cases defined by eq 1 and eq 2, the data will be consistent with lines d and e. The line defining  $\partial n_1/V > M_{ext}$  (eq 2) may have an apparently anomalously high  $1/R$  at  $1/V_f = 1/3V_1$  due to curvature of the defining equation. Increasing  $V_f$  for lines (c-e) efficiently increases the recovery factor when compared to classical line a. When an extractant-retaining system is encountered, failure of a multiple extraction scheme implies that a single (large  $V_1$ ) extraction may significantly improve the recovery. Although lines c, d, and e in Figure 2 have intercepts corresponding to recovery factors in excess of 1, the actual function defined in eq 22 is nonlinear and converges to  $R = 1$  after  $N = 4$ .

In summary, the procedure outlined here need not be done in detail; an examination of the effect of multiple extraction and single extraction in general terms would be sufficient for

Table I. Parameters for Extractant-Retaining Systems

$1/R$ (at $V_1$ ) <sup>a</sup>	slope/ $V_1$	intercept
1	0	1.00
1.1	0.104	0.996
1.2	0.218	0.982
1.3	0.340	0.960
1.4	0.466	0.934
1.5	0.600	0.900
1.6	0.738	0.862
1.7	0.882	0.818
1.8	1.03	0.772
1.9	1.18	0.720
2.0	1.22	0.660

<sup>a</sup> Calculated from eq 22 for  $(V_f - V_1)/V_1 = 1, 2$ , and 3.

simple systems. Single extraction recovery data could be plotted as in Figure 2 and evidence for a significant intercept evaluated. If the multiple extraction appeared promising, plotting the data would indicate the presence or absence of a positive intercept and therefore irreversibly bound solute. If the multiple extraction does not greatly improve the recovery, plotting the data might reveal a statistically significant negative intercept and hence extractant retention.

It may become apparent from the above examples that solid-liquid extraction systems become increasingly similar to classical liquid-liquid systems as the extractant to matrix ratio increases. For these near-classical systems, an unsatisfactorily low recovery factor may be improved by multiple extraction, providing an extractant with a suitable  $K_D$  is chosen. For a solid-liquid extraction, multiple extraction may only slightly increase (or actually decrease) the recovery factor. These nonclassical cases are a strong indication that the solid sample is retaining some of analyte and that improved recovery may be a function of the initial extraction variables, principally, the mass of the analyte and the volume of the initial extraction. If adjustment of the initial extraction variables does not improve recovery, the analyte may be irreversibly bound to the matrix (either before or upon extraction) and a different separation system must be employed.

## GLOSSARY

$g$	number of grams of analyte
$\gamma_{int}$	molar activity coefficient of extract retained within the sample
$\gamma_{ext}$	molar activity coefficient of extract external to the sample
$(K_D)_A$ or $K_D$	molar distribution constant for species A
$m_{ext}$	molality of the extract external to the sample
$m_{int}$	molality of the extract retained within the sample
$M$	the molarity of an $R = 1$ extract, i.e., $10^3 n_1/V_f$
$M_1$	molarity of the extract in model 1
$M_2$	molarity of the extract in model 2
$M_{ext}$	general term for molarity of the extract external to the sample
$M_w$	molecular weight of the analyte
$n$	the number of extractions
$n_1$	the number of moles of analyte
$N$	multiple of $V_1$ for single extraction
$\theta$	decimal fraction of moles of analyte retained within the sample
$\phi^{\circ}_{ext}$	standard partial molal free energy of the extract external to the sample
$\phi^{\circ}_{int}$	standard partial molal free energy of the extract retained within the sample
$\rho$	density of the extractant
$\rho_{sol}$	density of the extract
$R_A$	recovery factor for species A
$R_{ext}$	extraction recovery factor
$R_{ret}$	extract retention recovery factor
$R_{irr}$	irreversibly bound analyte recovery factor

$R$	gas constant, 8.314 J/(deg mol)
$T$	Kelvin temperature
$V$	volume of extract within the sample
$V_i$	final volume of extract
$V_{i-1}$	volume of extractant of the $i$ th extraction
$V_o$	total volume of extractant

## LITERATURE CITED

- (1) Berg, Eugene W. "Physical and Chemical Methods of Separation"; McGraw-Hill: New York, 1963; p 73.
- (2) Irving, H. M. N. *Pure Appl. Chem.* 1970, 21 (1), 111-113.
- (3) Morrison, George H.; Freiser, Henry "Solvent Extraction in Analytical Chemistry"; Wiley: New York, 1963; p 9.
- (4) Berg, Eugene W. "Physical and Chemical Methods of Separation"; McGraw-Hill: New York, 1963; pp 50-52.
- (5) Castellani, Gilbert W. "Physical Chemistry"; Addison-Wesley: Reading, MA, 1964; pp 287-289.
- (6) Shoemaker, David P.; Garland, Carl W.; Steinfield, Jeffrey I. "Experiments in Physical Chemistry"; McGraw-Hill: New York, 1974; p 173.
- (7) Morrison, George H.; Freiser, Henry "Solvent Extraction in Analytical Chemistry"; Wiley: New York, 1963; pp 58-60.
- (8) Berg, Eugene W. "Physical and Chemical Methods of Separation"; McGraw-Hill: New York, 1963; pp 7-15.
- (9) Morrison, George H. *Anal. Chem.* 1950, 22, 1388-1393.
- (10) Masterson, W. L.; Lee, T. P. *J. Phys. Chem.* 1970, 74, 1776.
- (11) Ringbom, A. "Complexation in Analytical Chemistry"; Interscience: New York, 1963; pp 10-50.
- (12) Groenewald, Theo. *Anal. Chem.* 1971, 43, 1678-1683.
- (13) Lukasser, Werner; Boltz, D. F. *Anal. Chem.* 1971, 43, 1265-1272.
- (14) Lukasser, Werner; Boltz, D. F. *Anal. Chem.* 1971, 43, 1273-1277.
- (15) Atkinson, G. F. *Anal. Chem.* 1972, 44, 1098.

RECEIVED for review March 9, 1982. Accepted September 29, 1982.

## Interpretation of Sets of Pyrolysis Mass Spectra by Discriminant Analysis and Graphical Rotation

Willem Windig<sup>1</sup>

Centraalbureau voor Schimmelcultures, Oosterstraat 1, Baarn, The Netherlands, and FOM-Institute for Atomic and Molecular Physics, Kruislaan 407, 1098 SJ Amsterdam, The Netherlands

Johan Haverkamp and Piet G. Kistemaker\*

FOM-Institute for Atomic and Molecular Physics, Kruislaan 407, 1098 SJ Amsterdam, The Netherlands

Pyrolysis mass spectra of complex biological samples can be interpreted for partial chemical composition, even when exact reference spectra of the components involved are not available. The method is based on a factor analysis method: principal component analysis followed by discriminant analysis and graphical rotation. Applications of the procedure are discussed for various sets of samples, viz., fungi (taxonomy), bacteria (detection of capsular polysaccharide), and human bile (differentiation of cholelithiasis and cholecystitis patients and normals).

Pyrolysis mass spectrometry (Py-MS) is a fast method for fingerprinting complex biological materials like macromolecules, cells, and microorganisms (1). However, chemical interpretation of pyrolysis mass spectra of complex samples is hampered as: the spectra seldom exhibit single masses specific for a particular compound (so-called "pure masses" (2)), accurate reference spectra of pure components are usually not available or even not obtainable, intermolecular reactions during pyrolysis can occur so that the pyrolysis spectra are not additive. Consequently automated mixture analysis techniques like library search procedures are not easily applicable to pyrolysis mass spectra.

In Py-MS studies the main analytical goal is often to determine the nature and extent of differences within a set of related samples. Factor analysis of spectral data offers a powerful method to describe the differences efficiently. It has been shown in various applications on spectral data sets that by an adequate transformation of the factors, mixture com-

ponents can be identified and quantified (2-4). In particular target rotation methods, as developed by Malinowski, have been applied successfully (4). However such an evaluation relies on a number of assumptions with regard to the structure of the dataset, i.e., additivity of spectra, availability of accurate reference spectra, and sometimes the presence of "pure masses". As outlined before these conditions are not fulfilled in Py-MS data sets and, consequently, other—less elegant—factor transformation procedures have to be applied.

Recently we described a combination of factor analysis and graphical rotation procedures, for chemical evaluation of small sets of Py-MS spectra (5-7). The graphical rotation method consists of a systematic-stepwise-rotation of principal factors. Visual examination of a series of transformed factors can lead to recognition of mixture components. It will be clear that this method does not provide the speed and rigidity of automated procedures and that the results depend on the experience of the operator. Nevertheless, in practice the graphical rotation procedure has been proven to work out satisfactory with respect to both the time afforded and quality of the results. One advantage of this procedure over other methods is that during examination of a series of transformed factors the experienced operator can be stimulated to make reasonable guesses about the nature of a mixture component; this by the associative ability of the human mind. In this way components can be identified of which no accurate reference spectra were available at that time.

Although the factor analysis and graphical rotation method were successful for interpretation of small data sets, the technique did not work out satisfactory for larger data sets including multiple replicated spectra. The problems were 2-fold: the large number of factors obtained complicated the rotation procedure and the single factors did not discriminate well between the groups of replicated spectra. This was due to the fact that factor analysis does not describe optimally

<sup>1</sup>Present address: Biomaterials Profiling Centre, 391 South Chipeta Way, Research Park, Salt Lake City, UT 84108.

the differences between the groups with respect to the differences within the groups. An additional step in the data handling was necessary, to determine well discriminating factors. For this purpose, a transformation of the factors by discriminant analysis was applied. Graphical rotation of the discriminant functions could then be performed to interpret the differences in terms of chemical components. This method will be demonstrated on some sets of spectra of bioorganic samples, i.e., yeast strains, bacterial strains, and human bile samples. Furthermore, some criteria concerning the reliability of the discriminant functions derived for small groups will be discussed.

## MATERIAL AND METHODS

**Yeasts.** The following strains were examined (CBS numbers refer to strains deposited in the Culture Collection of the Centraalbureau voor Schimmelcultures, Baarn, The Netherlands): (a) *Rhodospiridium toruloides* (Banno), strains CBS 14, 349, 5490, 6681; (b) *Rhodospiridium infirmo-miniatum* (Fell et al.), strains CBS 323, 2427, 6352; (c) *Filobasidium capsuligenum* (Fell et al.) Rodr.Miranda, strains CBS 1906, 4736, 6122-1, 6122-2; (d) *Filobasidium unguiculatum* (Kwon Chung), strains CBS 1730, 1727, 2770; (e) *Sporobolomyces roseus* (Kluyver and Van Niel), strains CBS 486, 2646, 493, 993; (f) *Sporobolomyces albo-rubescens* (Derx), strain CBS 5331; (g) *Sporobolomyces pararoseus* (Olson and Hammer), strains CBS 484, 491, 4217. Further details on the strains are given by De Hoog (6).

Cultures were grown on YPG agar (0.5% yeast extract, 1% peptone and 1% glucose) on Petri dishes for 7 days at 22 °C. Micrograms samples of yeast were taken in duplicate directly from two replicate cultures, resulting in four samples for each strain.

**Bacteria.** *Escherichia coli* strains of different serotypes were cultured at the National Institute for Public Health (RIV), Bilthoven, The Netherlands, on blood agar dishes. All strains were cultured in duplicate under standard conditions. Bacteria were sampled with a platinum loop and directly brought on the Curie point pyrolysis sample wire.

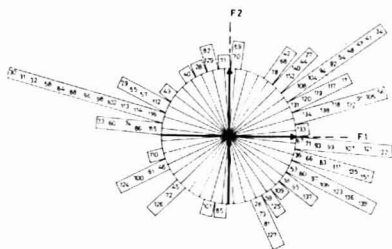
**Bile.** Samples of human bile were collected from five cholelithiasis patients (a-e), two cholecystitis patients (f and g), and two healthy individuals (h and i). Except for sample i all samples were directly taken by needle aspiration during surgical procedures. Sample i was taken by duodenal aspiration during a gastroscopy procedure. Five-microliter drops of the sample were applied directly to the Curie point wire. Every sample was analyzed in triplicate.

**Reference Materials.** The following biopolymers were used for reference purposes: bovine serum albumin (Merck AG, Darmstadt, G.F.R.); glycogen (Fluka AG, Buchs, Switzerland); chitin (B.D.H. Chemicals Ltd., Poole, U.K.); arabin (isolated from apple, Agricultural University, Wageningen, The Netherlands); fucoidin (Koch-Light Laboratories Ltd., Colnbrook Bucks England); poly( $\alpha$ 2 $\rightarrow$ 9)-N-acetylneuraminic acid (isolated from *Neisseria meningitidis*, National Institute for Public Health, Bilthoven, The Netherlands). From all reference materials 1 mg/mL suspensions in methanol were made. Aliquots of 5  $\mu$ L were applied to the Curie point wires.

**Pyrolysis Mass Spectrometry.** The pyrolysis mass spectrometric system used consists of an automatic sample changing system, a Curie point pyrolysis reactor, and a quadrupole mass spectrometer with ion counting detector. An extensive description of the system is given in ref 9-11. Pyrolysis and instrumental conditions were as follows: equilibrium temperature, 510 °C; total heating time, 0.9 s; temperature rise time, 0.1 s; inlet temperature, 150 °C; scan rate, 0.1 s/scan; total scan accumulation time, 15 s. Each spectrum is normalized for constant total intensity, in order to correct for sample size.

**Computer Programs for Data Handling.** Factor analysis, applied to standardized masses, and discriminant analysis, applied to standardized factor scores, were performed with the Statistical Package for the Social Sciences (SPSS) (12). Additional programs to display the factors and discriminant functions in the form of spectra and programs to rotate the factors and discriminant functions have been developed in our laboratory.

Because the SPSS package can handle 100 variables at most, the 100 most intense masses, out of the about 150 present, were



**Figure 1.** Representation space of the correlation matrix obtained by factor analysis of a set of mixture spectra. Bars indicate the masses within classes of 10°. This system is described by the two orthonormal axes F1 and F2.

selected for factor analysis. Those factors with eigenvalues greater than one were used for discriminant analysis. The number of discriminant functions was limited by a level of significance of 0.0005 (12). The percentage of the total variance described by the factors and discriminant functions is calculated for standardized masses. This means that every mass equally contributes to the variance calculation.

## DATA HANDLING

Both factor analysis and graphical rotation have been described previously from a geometrical point of view (5, 6). In this section these techniques will be summarized and extended to discriminant analysis. Furthermore, a brief mathematical description to document the various transformation and scaling procedures involved is given in the Appendix.

**Correlation Analysis.** Changes in concentration of chemical components in a set of mixtures analyzed by Py-MS will cause correlated intensity changes in a series of mass peaks. The identity of chemical components can in principle be deduced from these correlations and the relative intensity changes. An appropriate way to study the correlations in a set of spectra is to examine the space spanned by the oblique mass axes coordinate system, with the cosine of the angles between the axes equal to the correlation coefficients of the masses. The length of each mass axis is given by its standard deviation. As will be shown in this paper, the relevant component axes can be retrieved in this space.

**Example.** A data set, consisting of 10 "mixtures" of the biopolymers albumin, glycogen, and peptidoglycan as described in ref 5, is used to illustrate the method. The mixture spectra are exact linear combinations of the spectra of the three components and, consequently, the set of normalized spectra contains only two-dimensional information. The oblique mass axes system of this data set can thus be drawn in a plane (Figure 1). From this figure it becomes evident that various series of mass peaks are positively correlated (axis angles within 10°), noncorrelated (angles about 90°) and negatively correlated (angles 180°). Tentatively, highly correlated masses like  $m/z$  34, 41, 47, 48, 54, 92, 94, 104, and 108 might be attributed to one particular component. Negative correlations between masses result from the fact that spectra have been normalized to constant total intensity. This means that every change in a set of mass peak intensities must be accompanied by an opposite change in another set of mass peak intensities. The two-dimensional representation space can be described also by only two axes, which can be chosen arbitrarily. In the present examples the axes are determined by factor analysis. The two axes drawn in Figure 1 are the first and second factors (F1 and F2).

**Factors.** Factor analysis is generally performed on a standardized data set, i.e., the mass intensities are scaled to have a zero mean and unit standard deviation. For these data



sets the oblique mass axes have unit length and factor analysis calculates a set of orthogonal axes:

$$F_j = \alpha_{1j}m_1 + \alpha_{2j}m_2 + \dots \alpha_{nj}m_n \quad (1)$$

$j = 1, 2, \dots, p$ ;  $p \leq n$  equal to the number of masses

The loading  $\alpha_{ij}$  is the correlation coefficient of the factor  $F_j$  and mass axis  $m_i$ , and is equal to the projection of the mass axis on the factor. The variance described by factor  $F_j$  is equal to the sum of squares of the projections of  $m_i$  or  $F_j$ . Factors can be presented as factor spectra with intensities  $\alpha_{ij}$  at mass  $m_i$ . For standardized data sets the intensities  $\alpha_{ij}$  have to be multiplied with the standard deviation  $\sigma_i$  of the masses to obtain factor spectra comparable to pyrolysis mass spectra. A measure for the relative abundance of such a factor spectrum in an individual spectrum is called the factor score and can be calculated by substituting the respective mass intensities at  $m_i$  in formula 1.

**Component Axes.** The differences between the spectra in the data set and thus the structure of the representation space is determined by the variations in the concentration of chemical components. For this reason it is also possible to span the space by axes representing the chemical components involved. This becomes evident in Figure 1; in the quadrant enclosed by the positive parts of F1 and F2 (F1+ and F2+), a number of highly correlated albumin masses are present, e.g.,  $m/z$  17, 34, 48, 92, 94, 108, 117, 119, 120, and 131 (see also Figure 3e). Presumably the protein axis is located in this quadrant and, consequently, a protein subpattern is projected on F1+ and F2+.

**Graphical Rotation.** Rotation of the factor axes system can lead to an orientation where F1+ coincides with the presumed protein axis. In this orientation the factor spectrum of F1+ has to resemble a protein pyrolysis mass spectrum. Simultaneously, any protein subpattern should be absent in the orthogonal factor spectra of F2+ and F2-. The scores of the various mixture spectra on the rotated F1 describe the relative intensity of the albumin component in the mixtures. In practice the rotation is performed in steps of  $10^\circ$ . Coincidence of a factor with a component axis can be judged visually by the presence of the component pattern on the factor spectrum and the absence of this pattern on the orthogonal factor spectrum. This visually assisted process is called graphical rotation. For very complex data sets the number of factors will be large and a component axis can be projected on more than two factors. After graphical rotation to locate the optimum orientation within the subspace of the first set of two factors, further rotation is carried out in the space spanned by the rotated factor and the third factor involved, etc.

**Discriminant Analysis.** In the example discussed above only one spectrum for each mixture was involved. In pyrolysis mass spectrometric studies samples are generally analyzed in duplicate or quadruplicate in order to test the reproducibility of sample preparation and analysis conditions. A subset of spectra, in principle from identical sample material, is called a group. In many pyrolysis mass spectrometric studies one is mainly interested in the chemical components which cause the differences between the groups. For this approach the differences between the groups has to be related to the differences within the groups as is done in discriminant analysis (13, 14). In this technique a series of independent linear combinations of masses is constructed which discriminate the groups and are arranged in descending order of discriminating power. In the same way as with factors, discriminant functions can be plotted in the form of discriminant spectra. The quantitative measure of the discriminant spectrum in the individual spectra is called the discriminant score. In general nonorthogonal discriminant functions are obtained which

complicates the graphical rotation procedure. In the Appendix it will be explained that by using standardized factor scores as input for discriminant analysis, orthonormal discriminant functions can be obtained.

Besides the use of discriminant functions for the chemical interpretation of pyrolysis mass spectra, discriminant scores can be used for numerical classification of the spectra. In this classification procedure it is assumed that a statistical evaluation of the data is allowed. Because of the very limited number of spectra which constitute a group, the discriminant analysis results have to be treated with care. Therefore, we have used several criteria to test the reliability of the discriminant functions derived from data sets with small groups, in addition to the level of significance (12). The criteria used are as follows: (i) percentage of spectra classified correctly with discriminant functions determined for the total data set (complete groups); (ii) percentage of spectra classified correctly with discriminant functions determined for a partial data set (incomplete groups (15)); (iii) percentage of spectra classified identically with discriminant functions derived from a partial data set and the total set. The latter criterion is called the stability of the classification.

## RESULTS AND DISCUSSION

The applicability of this data analysis method is demonstrated from the results obtained for a series of yeast spectra as compared to chemical analysis data, a series of spectra of bacterial strains, and a series of spectra of human bile. Apart from the chemical interpretation of the results of discriminant analysis, the classification results are tested on their reliability.

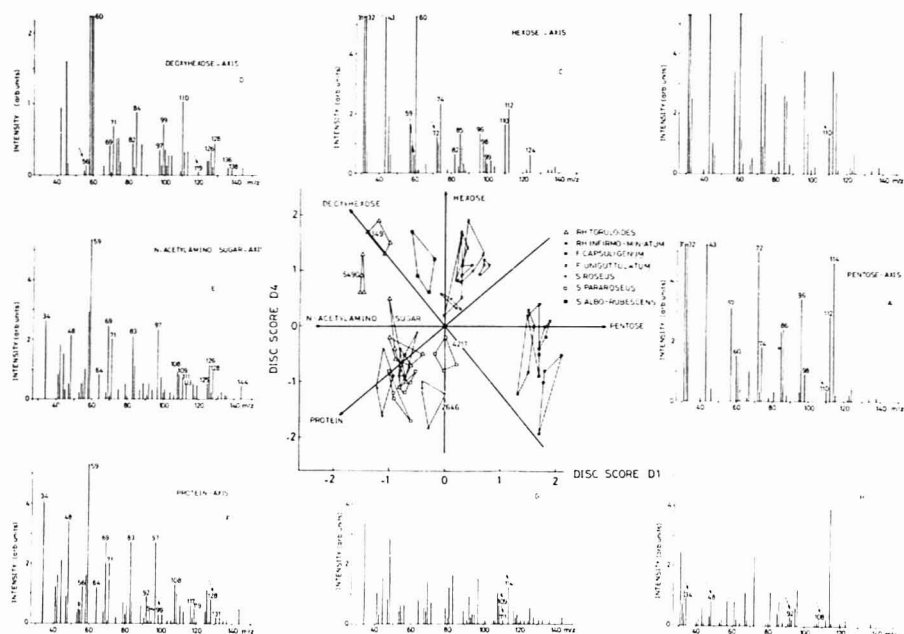
**Yeasts.** The data set consisted of the quadruplicate spectra of 22 yeast strains (22 groups). Factor analysis resulted in 15 factors with eigenvalues greater than one, describing 88% of the total variance in the data set. Discriminant analysis on the factor scores gave seven significant discriminant functions. It appeared that the first and fourth discriminant function (D1 and D4), responsible for 20 and 6% of the total variance respectively, described the main quantitative changes in five recognizable components. The spectral differences described by the other discriminant functions could not be recognized clearly in terms of other chemical components; possibly physicochemical differences between the samples (pH, salt concentration, etc.) may play a part here.

In order to find component axes in the subspace spanned by discriminant functions D1 and D4, we applied graphical rotation (Figure 2).

For the evaluation of spectra of the component axes one has to keep in mind that reference spectra cannot be identical with discriminant spectra, due to the applied normalization. Furthermore, appropriate reference spectra are generally not available and comparison can be made only with spectra of the component analyzed under other physicochemical conditions, or with spectra of structurally related materials. Thus, the reference spectra (Figure 3) should only be used to obtain a general impression of the typical fragment series for the various component groups. Another complication can occur, when the changes in several components are positively correlated; then the discriminant spectra will show superpositions of these components.

The five components found in the space described by D1 and D4 are the following:

**Pentose Axis.** This component axis (Figure 2a) is positioned along D1+ and shows a fragment pattern clearly containing a set of peaks characteristic of pentose polymers. For comparison the pyrolysis mass spectrum of an araban is given (Figure 3a). The spectrum of the component axis has many peaks in common with this typical pentose reference spectrum, e.g.,  $m/z$  31, 32, 60, 72, 74, 85, 86, 96, 98, 112, and 114. For the minimization of the pentose pattern on the orthogonal



**Figure 2.** Plot of the representation space described by D1 and D4 (central part), obtained by discriminant analysis of the pyrolysis mass spectra of the series of yeast strains. Spectral points of one group (strain) are connected. The orientation of the component axes is indicated by arrows. The positive parts of discriminant spectra of component axes are shown, together with discriminant spectra of the orthogonal axes (positive and negative parts separated and presented in the appropriate directions). Peak series characteristic for particular components are indicated by mass numbers. Mass peaks that play an important part in the component minimization procedure (see Methods) are indicated by arrows.

axis (Figure 2c,g) we focused on  $m/z$  72 and 114.

**Hexose Axis.** The discriminant spectrum of D4+ (Figure 2c) appears to represent a hexose pattern. This component axis shows a series of peaks, e.g., at  $m/z$  31, 32, 43, 60, 72, 74, 82, 85, 86, 96, 98, 102, 110, 112, and 124, which are also prominent in spectra of hexose polymers. For comparison the typical pyrolysis mass spectrum of glycogen, a glucose polymer, is shown (Figure 3b). The absence of  $m/z$  126, also characteristic of hexoses, in the discriminant spectrum, is probably due to chemical or physicochemical interference which changes the correlations within the hexose peaks. The position of this hexose axis was mainly determined on the basis of the relative intensities at  $m/z$  110 and 112. On the orthogonal axis (Figure 2a,e) the minimization of  $m/z$  102 and 110 plays an important part.

**6-Deoxyhexose Axis.** In the orientation presented in Figure 2d a subset of peaks which points to the presence of 6-deoxyhexose residues is at its optimum. For comparison the pyrolysis mass spectrum of fucoidin is given in Figure 3c, containing typical masses, e.g., at  $m/z$  58, 60, 69, 71, 82, 84, 99, 102, 110, 126, 128, 136, and 138. The position of this component axis was determined by minimization on the orthogonal axis (Figure 2b,f) of  $m/z$  99, 110, and 128. The high intensity of  $m/z$  59 is probably due to a positive correlation of the changes described by this component axis with those of the *N*-acetyl amino sugar axis.

***N*-Acetyl Amino Sugar Axis.** This component is rather difficult to recognize because of high correlation with the protein axis. The component axis (Figure 2e) was determined on the basis of minimization of the masses 59, 109, 111, and

125 on the orthogonal axis (Figure 2c,g). This peak set is, to our experience, characteristic of *N*-acetylhexosamine polymers. As a reference spectrum, that of chitin is given (Figure 3d).

**Protein Axis.** This component axis (Figure 2f) was marked on the basis of the peak set at  $m/z$  34, 48, 56, 69, 83, 92, 94, 97, 108, 117, and 131, generally present in proteins. As a typical example of a pyrolysis mass spectrum of a protein that of albumin is given in Figure 3e. For minimization on the orthogonal axis (Figure 2d,h) masses 34, 48, 56, 92, 94, 97, 108, 117, and 131 play an important part. The relatively high intensity of  $m/z$  59 in this component axis is due to a positive correlation with the *N*-acetyl amino sugar axis. The presence of the masses 126 and 144, originating from hexose, and  $m/z$  99 and 128, originating from deoxyhexoses, probably indicates an interaction of these sugars with protein.

**Comparison of the Results with Other Chemical Data.** Analysis of cell wall monosaccharides by GLC after hydrolysis and trimethylsilylation (16) revealed that strains of the genus *Filobasidium* have a relatively high xylose content. This is in accordance with the relatively high score of these strains on the pentose axis (see central part Figure 2). Also *Rh. infirmominatum* turned out to have a high xylose content (7, 16). The presence of the 6-deoxyhexose fucose in the genera *Sporobolomyces* and *Rhodospiridium* is established, in *Filobasidium capsuligenum* fucose is shown to be absent (7, 16). As yet no data are present for *F. uniguttatum*. A relatively high score on the *N*-acetyl amino sugar axis of the genera *Rhodospiridium* and *Sporobolomyces* correlates with the *N*-acetylglucosamine content as determined by GLC. This is indicative of chitin in the cell wall of these yeasts (16).

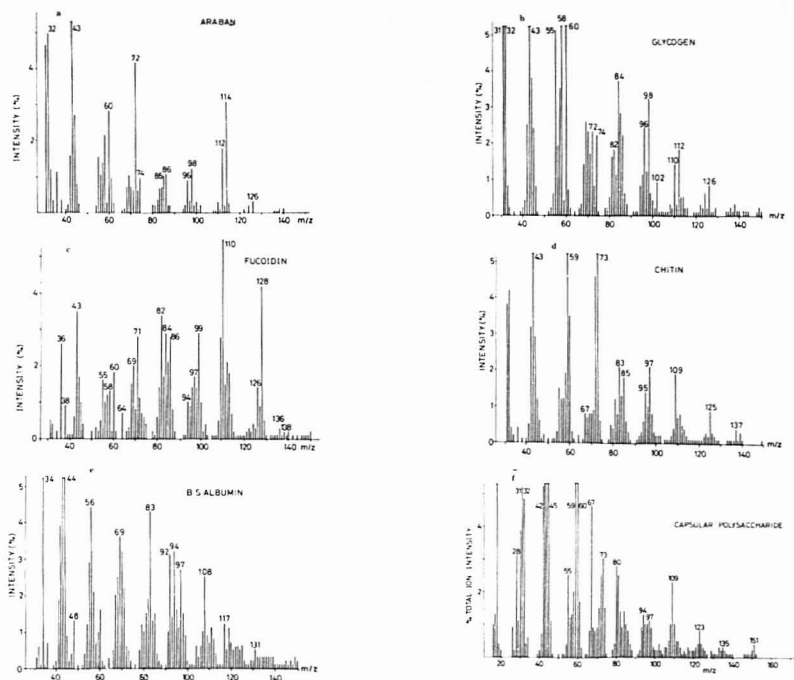


Figure 3. Reference spectra of (a) araban, (b) glycogen, (c) fucoidin, (d) chitin, (e) albumin, and (f) poly(*N*-acetylneuraminic acid).

Comparison of the *Rhodospiridium* data set with the Py-MS results of a same set of cultures analyzed before (7) showed reasonable correlations of the scores for components which are located mainly in the cell wall, i.e., pentose (correlation coefficient 0.96) 6-deoxyhexose (0.81), and *N*-acetyl amino sugar (0.85). The scores of components more uniformly present in cell wall and cell plasma (17), i.e., hexoses and proteins, were much less reproducible (correlation coefficients 0.42 and 0.45, respectively).

**Bacteria.** A set of 18 *E. coli* strains was analyzed by Py-MS, from each strain quadruplicate analyses were taken. The aim of this study was the discrimination between strains encapsulated by the so-called K1 antigen (an *N*-acetylneuraminic acid polymer) and strains lacking this antigen (18). Factor analysis applied to this data set gave 15 factors with eigenvalues greater than one. These factors described 90% of the total variance in the data set. Discriminant analysis applied to these factors gave two K1-related discriminant functions describing 9 and 8%, respectively, of the total variance. The discriminant spectra of the first and second discriminant function showed a pattern related to the Py-MS spectrum of *N*-acetylneuraminic acid polymer (19). The orientation of the *N*-acetylneuraminic acid axis (Figure 4) was determined on comparison to the pyrolysis mass spectrum of an *N*-acetylneuraminic acid polymer (Figure 3f), e.g.,  $m/z$  67, 94, 109, 117, 123, 133, 135, and 151. The absence of the prominent  $m/z$  59 in the discriminant spectrum is due to the presence of other components in this series with a dominant contribution on this mass value or to physicochemical interactions. The scores of the spectra on this component axis

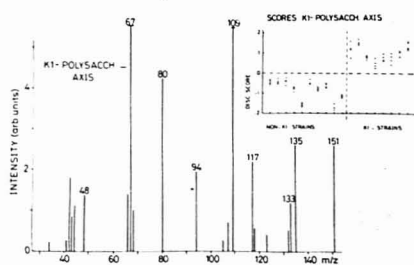


Figure 4. Component axis of the capsular polysaccharide K1 and the appropriate discriminant scores obtained from the series of *E. coli* samples.

(Figure 4) show clearly differentiation between K1 and non-K1 strains (18).

**Human Bile.** A set of nine human bile samples was analyzed by Py-MS. From each bile sample three analyses were taken. The aim of this study was to discriminate different cholelithic diseases (20). Factor analysis of this set of spectra yielded 10 factors with eigenvalues greater than one, which together described 97% of the total variance. The first two discriminant functions, describing 34% and 18% of the total variance, respectively, showed a clinically relevant discrimination between the cholelithiasis and cholecystitis samples. (The residual variance will not be evaluated here.) After

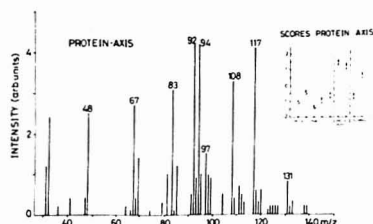


Figure 5. Component axis of protein and the appropriate discriminant scores obtained from the spectra of the bile samples.

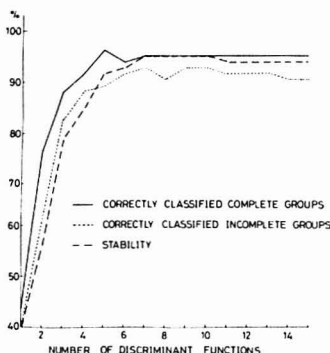


Figure 6. The classification results of discriminant analysis as a function of the number of discriminant functions, for the yeast data set.

rotation within the D1, D2 subspace a protein axis was located. The component spectrum together with the discriminant scores are presented in Figure 5. The scores show a relatively high protein content for the cholecystitis samples. One of the normal controls had a high protein content which can be explained by contamination with duodenal fluid during sampling.

**Test of Discriminant Functions on the Basis of Classification Results.** Because of the limited number of spectra per group one can question the rigidity of the discriminant function solutions. Therefore we investigated the classification results of the yeast spectra as a function of the number of spectra and variables involved. In Figure 6 the percentages of correctly classified spectra are shown for discriminant functions derived from the total data set (complete groups) and a partial data set (incomplete groups). Fifteen factor scores of the factors with an eigenvalue exceeding unity were used to characterize the spectra. From this figure it can be seen that the classification results are optimal for seven discriminant functions. The level of significance of the set of seven discriminant functions was 0.00005 (12). The stability of the classification is good indicating that the results are not seriously influenced by the small number of spectra per group. The classification results could be improved to 100% correctness by using 26 factors derived from the total data set. However simultaneously only 88% of the spectra were classified correctly with the discriminant function calculated from the partial data set. This indicates that the factors 15–26, with eigenvalues less than unity, introduced nonsignificant between-group variance into the discriminant functions. On the other hand, as can be expected, it was noticed that significant between-group variance was lost when only a few

factors with high eigenvalues were used to characterize the spectra. These results led to the general selection rule of factors with eigenvalues larger than unity and a set of discriminant functions with level of significance of 0.00005 in the analysis of pyrolysis mass spectra.

## ACKNOWLEDGMENT

The authors thank G. C. Lindeyer for development of additional computer programs, A. Tom, B. Brandt, and Y. A. Vluc for technical assistance, P. A. M. Guinée (National Institute for Public Health, Bilthoven, The Netherlands) and J. R. Cardinal and J. H. Bowers (Department of Internal Medicine, L.D.S. Hospital, Salt Lake City, UT) for providing us with samples of *E. coli* strains and bile samples, respectively, and R. Hoogerbrugge for helpful discussions.

## APPENDIX

Extensive mathematical treatment of factor analysis and discriminant analysis can be found in textbooks (4, 13, 14, 21). In this Appendix the mathematics, with the specific purpose to derive chemical component spectra from mixture spectra via factor and discriminant analysis, will be documented. Also the scaling procedures will be described.

The underlying model in the analysis is that the major part of a pyrolysis mixture spectrum can be considered as a linear combination of spectra of pure chemical components

$$S_{1(s \times m)} = C_{1(s \times n)} L_{1(n \times m)} + \Delta S_{(s \times m)}$$

where  $S_1$  is the data matrix,  $C_1$  contains the relative contributions of the components, and  $L_1$  contains the pure component spectra. In the various matrices the spectra are represented by rows.  $\Delta S$  represents noninterpretable parts in the spectra, e.g., the influence of intermolecular reactions. The number of spectra is  $s$ , the number of masses is  $m$ , and the number of components is  $n$ . The above mentioned expression can be rewritten in

$$L_{1(n \times m)} + \Delta L_{1(n \times m)} = C_1^{-1} S_{1(s \times m)} \quad (1A)$$

where

$$\Delta L_{1(n \times m)} = C_1^{-1} \Delta S_{(s \times m)}$$

It has to be noted that  $C_1^{-1}$  does not necessarily exist, however, in this case the pseudoinverse of  $C_1$  can be used.

From eq 1A it follows that in principle the chemical components involved can be approximated by linear combinations of spectra in  $S_1$ . The procedure to determine the appropriate combinations from eq 1A can be laborious; however, the number of spectra to combine can be limited by developing  $S_1$  on an orthogonal set of basis spectra, symbolically represented by the rows of  $F^T$

$$S_{1(s \times m)} = S_{F(s \times p)} F_{(p \times m)}^T \quad p \leq s \quad (2A)$$

where  $S_F$  is the score matrix containing the partial contributions of the spectra in  $F^T$  to the spectra in  $S_1$ .

Combination of eq 1A and 2A gives

$$L_{1(n \times m)} + \Delta L_{1(n \times m)} = [C_1^{-1} S_{F(s \times p)} F_{(p \times m)}^T] F_{(p \times m)}^T$$

In our applications generally only two or three basis spectra out of  $F^T$  were sufficient to reproduce the component spectra. Selection of these rows of  $F^T$  was based on the resemblance with known reference spectra.

In matrix notation the linear combination is described by

$$F_{(1 \times m)}^T = r_{(1 \times p)}^T F_{(p \times m)}^T$$

with

$$r_{(1 \times p)}^T F_{(p \times 1)} = 1$$

where the row vector  $F^T$  approximates a pure component

spectrum and is a row of  $L + \Delta L$ . The row vector  $r^T$  has only a few elements unequal to zero. The contribution of the component spectrum  $I^T$  to the spectra in  $S_i$  is given by

$$c_{(s \times 1)} = S_{F(s \times p)}^T r_{(p \times 1)}$$

Because of the contributions of  $\Delta L$  to  $L$  many times a limited resemblance of  $I^T$  and reference spectra can be expected. Therefore the appropriate linear combination is not only determined by the presence of the characteristic pattern for the component in  $I^T$  but also by the absence of this pattern on the orthogonal linear combinations. In practice this is done by investigation of a series of stepwise rotations (orthonormal combinations).

The choice of the set of orthogonal basis spectra  $F^T$  is dependent on the problems under investigation. In many cases one is interested in the overall differences in a data set or in differences between certain groups of spectra, rather than in the absolute composition. For mathematical analysis of differences in a data set, it is convenient first to standardize the data set

$$S_{(s \times m)} = (S_{1(s \times m)} - U_{1(s \times m)})\theta^{-1}_{(m \times m)} \quad (3A)$$

where  $S$  is the standardized data set,  $U_1$  the grand mean matrix, with on the rows the averaged spectra of the whole data set, and  $\theta$  a diagonal matrix with the standard deviations of the masses. For analysis of the overall differences an appropriate set of basis spectra,  $F^T$  can be derived from the eigenvectors of the variance-covariance matrix  $D$

$$D_{(m \times m)} = (1/s)S_{(m \times s)}^T S_{(s \times m)}$$

It has to be noted that for standardized data sets the variance-covariance matrix equals the correlation matrix. A property of the eigenvectors  $E$  of  $D$  is

$$E_{(m \times m)} \Lambda_{(m \times m)} E_{(m \times m)}^T = D_{(m \times m)}$$

$E$  is the orthonormal eigenvector matrix and  $\Lambda$  is the diagonal matrix with the eigenvalues of the eigenvectors. The eigenvectors are ranked according to their eigenvalue, which is a measure of the variance described by that eigenvector. The set of basis spectra is defined by

$$F_{(p \times m)}^T = \Lambda^{1/2}_{(p \times p)} E_{(p \times m)}^T \quad (4A)$$

where  $p < m$  because rows with only zero values in  $\Lambda^T$  are deleted. The rows of  $F^T$  are the factors or principal components. The row elements of  $F^T$  are the so-called loadings or correlation coefficients of the factors and the masses. As a consequence of this definition of factors the scores  $S_F$  are standardized, as can be deduced from eq 2A and 4A

$$S_{F(p \times s)}^T S_{(s \times p)} = s I_{(p \times p)}$$

where  $I$  is the identity matrix. Furthermore, the variance-covariance matrix can be reconstructed by

$$F_{(m \times p)} F_{(p \times m)}^T = D_{(m \times m)}$$

For a geometrical interpretation, the columns of  $F^T$  describe an oblique mass axes system, where the angles between mass axes, factors and component axes are determined by their correlation coefficients. This system was introduced in the paper. The rows of  $F^T$  are used as orthogonal basis spectra for the standardized data. For comparison with the original spectra, they have to be scaled by  $\theta$  (see eq 3A)

$$\tilde{S}_{(p \times m)} = F_{(p \times m)}^T \theta_{(m \times m)}$$

where  $\tilde{S}$  contains the factor spectra.

For the interpretation of differences between groups of spectra, another set of basis spectra has to be chosen. It can be shown that such a set can be derived from the eigenvectors

of the matrix  $W^{-1}B$  (13, 14), where  $B$  and  $W$  are defined by

$$B_{(m \times m)} = (G - U)_{(m \times s)}^T (G - U)_{(s \times m)}$$

where  $B$  is the between group variance matrix and  $G$  is the group mean matrix, with on every row the averaged spectrum of the particular group.

$$W_{(m \times m)} = (S - G)_{(m \times s)}^T (S - G)_{(s \times m)}$$

$W$  is the within group variance matrix. These matrices are related by

$$B_{(m \times m)} + W_{(m \times m)} = T_{(m \times m)}$$

where  $T$  is the total variance matrix

$$T_{(m \times m)} = S_{(m \times s)}^T S_{(s \times m)}$$

In our applications we performed discriminant analysis on the factor scores of the spectra instead of on the mass intensities for two reasons: (a) For our data, generally  $m > s$ , in which case  $W^{-1}$  does not exist. (b) When standardized factor scores are used, the eigenvectors of  $W^{-1}B$  are orthonormal, which is convenient for the graphical rotation procedure. This can be shown as follows: For standardized independent data  $T_{(s \times s)} = s I_{(s \times s)}$   $v$  is the number of variables. In this case  $W^{-1}_{(v \times v)} B_{(v \times v)}$  reduces to

$$s W^{-1}_{(v \times v)} - I_{(v \times v)}$$

This matrix is symmetric and, consequently, has orthogonal eigenvectors.

Discriminant analysis as performed by the SPSS package scales the discriminating eigenvectors to have a unit within-group variance. For our purposes orthonormal discriminant functions are preferred and therefore the SPSS-discriminant functions were scaled to unit length. These discriminant coefficients form an orthonormal matrix, which transforms the discriminant functions to linear combinations of masses. Graphical rotation of the discriminant spectra can be applied in order to find component axes. The advantage of the applied scaling is that the loadings again give the correlation coefficients of the masses, the discriminant functions, and the component axes.

**Registry No.** Glycogen, 9005-79-2; fucoidin, 9072-19-9; chitin, 1398-61-4; poly(N-acetylneuraminic acid), 83248-83-3.

## LITERATURE CITED

- Meuzelaar, H. L. C.; Haverkamp, J.; Hieman, F. D. "Pyrolysis Mass Spectrometry of Recent and Fossil Biomaterials; Compendium and Atlas"; Elsevier: Amsterdam, 1982.
- Knorr, F. J.; Futrell, J. H. *Anal. Chem.* **1979**, *51*, 1236-1241.
- Malinowski, E. R.; McCue, M. *Anal. Chem.* **1977**, *49*, 284-287.
- Malinowski, E. R.; Howerly, D. G. "Factor Analysis in Chemistry"; Wiley Interscience: New York, 1980.
- Windig, W.; Kistemaker, P. G.; Haverkamp, J. J. *Anal. Appl. Pyrolysis* **1981**, *3*, 199-212.
- Windig, W.; de Hoog, G. S.; Haverkamp, J. J. *Anal. Appl. Pyrolysis* **1981**, *3*, 213-220.
- Windig, W.; de Hoog, G. S.; Haverkamp, J. *Stud. Mycol.*, in press.
- de Hoog, G. S. *Stud. Mycol.*, in press.
- Meuzelaar, H. L. C.; Kistemaker, P. G.; Eshuis, W.; Engel, H. W. B. In "Rapid Methods and Automation in Microbiology"; Johnston, H. H., Newsom, S. W. B., Eds.; Learned Information: Oxford, New York, 1976; pp 225-230.
- Meuzelaar, H. L. C.; Kistemaker, P. G.; Posthumus, M. A. *Biomed. Mass Spectrom.* **1974**, *1*, 312-319.
- Meuzelaar, H. L. C.; Kistemaker, P. G. *Anal. Chem.* **1973**, *45*, 587-590.
- Nie, N. H.; Hull, C. H. G.; Jenkins, J. G.; Steinbrenner, K.; Bent, W. H. "Statistical Package for the Social Sciences", 2nd ed.; McGraw-Hill: New York, 1975.
- Cooley, W. W.; Lohnes, P. R. "Multivariate Data Analysis"; Wiley: New York, 1971; pp 243-250.
- Tatsuoka, M. M. "Multivariate Analysis"; Wiley: New York, 1971, pp 157-164.
- MacFie, H. J. H.; Gutteridge, C. S.; Norris, J. R. *J. Gen. Microbiol.* **1978**, *105*, 67-74.
- von Arx, J. A.; Weyman, A. C. M. *Antonie van Leeuwenhoek* **1979**, *45*, 547-555.
- Ainsworth, G. C.; Sussman, A. S. "The Fungi"; Academic Press: New York, 1965; Part 1.

- (18) Haverkamp, J.; Eshuis, W.; Boerboom, A. J. H.; Guinée, P. A. M. "Advances in Mass Spectrometry"; Heyden: London, 1980; Vol. 8a, pp 983-989.
- (19) Haverkamp, J.; Meuzelaar, H. L. C.; Beuvery, E. C.; Boonkamp, P. M.; Tiesjema, R. H. *Anal. Biochem.* 1980, 104, 407-418.
- (20) Meuzelaar, H. L. C.; Klismaker, P. G.; Schutgens, R. B. H.; Veder, H. A.; Cardinal, J. R.; Bowers, J. H.; Antoshchukin, A. In "Current Developments in the Clinical Applications of HPLC, GC and MS"; Lawson, A. M.; Lim, C. K.; Richmond, W., Eds.; Academic Press: London, 1980; pp 209-231.

- (21) Rummel, R. J. "Applied Factor Analysis"; Northwestern University Press: Evanston, IL, 1970.

RECEIVED for review January 18, 1982. Accepted September 20, 1982. This investigation was supported by the Royal Netherlands Academy of Arts and Sciences (KNAW) and by the Foundation for Fundamental Research on Matter (FOM).

## Ionization Spectra of Neodymium and Samarium by Resonance Ionization Mass Spectrometry

J. P. Young\* and D. L. Donohue

Analytical Chemistry Division, Oak Ridge National Laboratory, Oak Ridge, Tennessee 37830

Ionization spectra of the elements neodymium and samarium have been obtained over the wavelength range of 423-463 nm by using the technique of resonance ionization mass spectrometry (RIMS). These studies have been performed to determine the wavelengths at which ionization occurs under RIMS conditions. The observed wavelengths have been correlated where possible with allowed transitions between known electronic energy levels. RIMS has previously been applied to the measurement of isotope ratios of these rare earth elements using a single wavelength of excitation for each element. The fact that there are a number of effective wavelengths available should be of interest to other workers in the RIMS field.

Resonance ionization spectrometry (RIS) is a photoionization process in which atoms in a gas phase are ionized by the absorption of photons that energetically match transitions between quantum states of these atoms (1). General application of RIS to various analytical problems has also been discussed (2). There are several RIS schemes that have been developed (1, 2) by using two or more photons of one or several colors. Although RIS is normally used to detect atoms either by the electron or the ion generated in the photoionization process, the detection of either of these species can also be used to study the absorption spectra of amenable atoms. Worden et al. (3) have used a several-color resonant photoionization process to identify upper Rydberg states and determine ionization potentials of lanthanides and actinides. Their study made use of an atomic beam; one or two lasers were tuned to generate a particular excited state, and with a tunable laser, the autoionizing and ionizing energies of the species could be identified.

Recently, we have applied a one-color RIS scheme to the selective photoionization of either Sm or Nd for mass analysis in a mass spectrometer (4). By means of this combination technique, resonance ionization mass spectrometry (RIMS), the removal of the isobaric interference of either element on the other has been demonstrated. By observing the presence and intensity of a particular mass signal for either of these rare earth ions as the wavelength of the lasing is changed, one can obtain a spectrum of each element. Knowledge of such a spectrum is useful not only to identify analytically useful RIMS wavelengths but also to evaluate particular subsets of atomic transitions that in normal emission spectral studies

are combined with many other subsets of possible atomic transitions.

The present study was initiated in order to find suitable wavelengths for the isotopic analysis of neodymium and samarium by RIMS. In the analysis of a mixture of elements, it is necessary to know which wavelength (transition) to use to avoid overlap with interfering species. It was also found in preliminary studies that many more transitions were observed than originally expected. This complexity is a mixed blessing in that the probability of overlap with adjacent elements is increased for a particular transition but a larger choice of transitions is available for choosing a suitable RIMS wavelength.

A systematic study was therefore performed to catalog the observed wavelengths at which ionization occurs for the two elements neodymium and samarium. Due to the limitations imposed by the dye laser system, the spectra were limited to a certain range of wavelengths which is smaller than the range over which ionization occurs. However, useful transitions have been predicted to lie within the wavelength range reported here. Future work will seek to extend the wavelength range for the elements Nd and Sm, as well as to report results for other rare-earth elements.

### EXPERIMENTAL SECTION

**Laser System.** The laser system and optical components used for this investigation are the same as used in the previous RIMS study (4) except that the tuning micrometer of the NRG 0.03 dye laser module (National Research Group, Inc., Madison, WI) was equipped with a stepping motor so that the wavelength range of a particular dye could be scanned under computer control. The details of this scanning are in a later part of the Experimental Section. Three different dyes, S-420, C-440, and C-460 (available from Exciton Chemical Co., Dayton, OH), were used to cover the wavelength range of 423 to 463 nm that was used in this study. The relative intensity of these dyes as a function of wavelength is given in Figure 1. Under our experimental conditions, the dye S-420 at a wavelength of 425.8 nm yielded an energy of approximately 300  $\mu\text{J}$ . Although the relative energy correlation from dye to dye cannot be considered to be highly precise, a qualitative assessment of dye intensity vs. wavelength can be made from the data in Figure 1. The tunable laser beam was brought to a focus (4) just in front of and in the vertical center of the first slit of the ion source of the mass spectrometer, described below. The spot size of the beam at the focal plane was approximately 1 mm, but any ions generated by RIS were accepted over the entire length of the first slit, 2 cm.

It was necessary to calibrate the wavelengths of the respective dyes vs. micrometer dial reading of the dye laser module. This



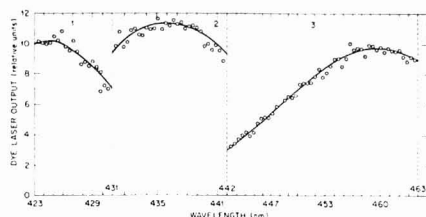


Figure 1. Dye laser output spectra for dye 1 = S-420; dye 2 = C-440; dye 3 = C-460.

was done by recording the wavelength of five or more settings of the micrometer dial of the laser by means of a  $1/2$ -m monochromator. The wavelength accuracy of the monochromator was verified by the Hg emission line at 435.8 nm. From this series of wavelength vs. laser dial readings, a calibration factor was computed which converted a given dial reading to wavelength.

**Mass Spectrometer.** The mass spectrometer has been previously described (4) and consisted of a single  $90^\circ$  magnetic sector of 30 cm radius. Ion detection was by means of a 14-stage electron multiplier (RCA Corp. type 6810A, Lancaster, PA) operated at 4000 V. Laser-generated ions, upon striking this detector, produced a signal which was processed and digitized by a 13-bit analog-to-digital converter (ADC). These digital data were accepted by a PDP-11/34 computer (Digital Equipment Corp., Maynard, MA) and stored in an array of 256 channels. Each scan of the spectrum covered 512 steps of the stepping motor driving the micrometer dial of the dye laser. The wavelength range covered was 20.8 nm. Therefore, each channel of the final data array represented a resolution element of 0.08 nm composed of the average of signals from 10 laser pulses. The estimated number of ions detected per laser pulse was 5 to 20.

Samples of Nd and Sm were prepared from the pure oxides in 1 N  $\text{HNO}_3$  solution to give a concentration of 100  $\mu\text{g}/\mu\text{L}$ . One microliter of solution was loaded onto a Re filament, and a drop of colloidal graphite suspension (Aquadag) was added to enhance the production of neutral Nd or Sm atoms in the ion source in preference to oxide species. Isotopes chosen for study ( $^{142}\text{Nd}$ ,  $^{146}\text{Nd}$ ,  $^{147}\text{Sm}$ ) were free from isobaric overlap with other elements present. A check of this fact was made by comparing spectra of two Nd isotopes; there were no significant differences due to an interfering species.

The samples were maintained at a temperature of approximately 1500  $^\circ\text{C}$  for this study. The individual scans of a given wavelength range took about 8.5 min to complete. For these studies sufficient sample was loaded on the filament that the Nd RIMS signals degraded only slowly with time, approximately 10% reduction in ion intensity per hour.

## RESULTS AND DISCUSSION

**Nd Spectrum.** Figure 2 shows the composite spectrum obtained for Nd over the wavelength range 423–463 nm. The

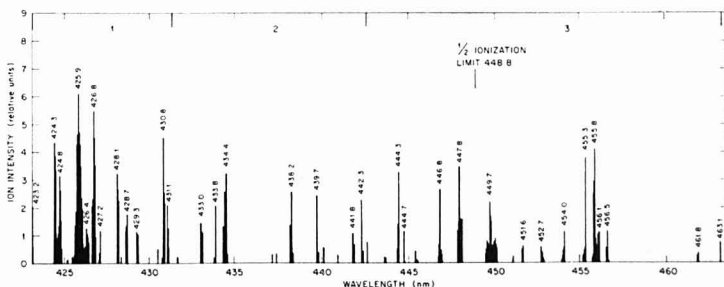


Figure 2. Resonance ionization spectrum of neodymium obtained by monitoring  $^{142}\text{Nd}$ .

Table I. RIMS Spectrum of Neodymium

obsd peak		intens	initial transition	error $\text{cm}^{-1}$
in nm (air)	in $\text{cm}^{-1}$ (vac)			
423.2	23 623	M		
424.3	23 561	S	$^1\text{I}_g - ^6\text{M}_4$	2
424.8	23 533	S		
425.9	23 473	S	$^1\text{I}_g - ^2\text{H}_3$	14
426.4	23 445	W	$^1\text{I}_g - ^4\text{H}_4$	-7
426.8	23 423	S	$^1\text{I}_g - ^2\text{H}_3$	11
427.2	23 401	M		
428.1	23 352	M		
428.7	23 320	M		
429.3	23 287	W		
430.5	23 222	W	$^1\text{I}_g - ^4\text{H}_3$	-4
430.8	23 206	S	$^1\text{I}_g - ^4\text{H}_4$	-2
431.1	23 190	M	$^1\text{I}_g - ^2\text{H}_3$	8
431.7	23 158	W		
433.0	23 088	M	$^1\text{I}_g - ^4\text{H}_4$	1
433.8	23 045	M	$^1\text{I}_g - ^2\text{H}_3$	5
434.4	23 016	S	$^1\text{I}_g - ^4\text{H}_4$	2
437.1	22 871	W		
437.4	22 856	W		
438.2	22 814	M	$^1\text{I}_g - ^4\text{H}_4$	1
439.7	22 736	M	$^1\text{I}_g - ^2\text{H}_3$	1
440.1	22 715	W		
440.9	22 674	W	$^1\text{I}_g - ^4\text{H}_4$	4
441.8	22 618	W	$^1\text{I}_g - ^4\text{H}_4$	4
442.3	22 603	M	$^1\text{I}_g - ^2\text{H}_3$	3
442.7	22 582	W		
443.6	22 536	W	$^1\text{I}_g - ^4\text{H}_3$	-6
444.3	22 501	S	$^1\text{I}_g - ^2\text{H}_3$	-10
444.7	22 481	W	$^1\text{I}_g - ^4\text{H}_4$	-10
445.3	22 450	W		
446.8	22 375	S	$^1\text{I}_g - ^2\text{H}_3$	-7
447.8	22 325	S	$^1\text{I}_g - ^6\text{M}_6$	12
449.7	22 233	M	$^1\text{I}_g - ^4\text{H}_3$	-4
451.0	22 166	W		
451.6	22 137	W		
452.7	22 083	W		
454.0	22 020	W		
455.3	21 957	S		
455.8	21 933	S	$^1\text{I}_g - ^6\text{M}_6$	6
456.1	21 919	W	$^1\text{I}_g - ^6\text{L}_7$	4
456.5	21 899	W	$^1\text{I}_g - ^6\text{M}_6$	5
461.8	21 648	W		
463.1	21 587	W		

horizontal axis consists of 430 channels each representing the sum of 10 laser pulses. Amplitude information is only approximate due to the variations in RIMS signal for each laser pulse. Reproducibility of peak heights in replicate spectra was estimated to be  $\pm 30\%$ .

A summary of the Nd RIMS spectrum shown in Figure 1 is given in Table I. As noted in the table, both the wavelength in air and the wavenumber under vacuum of the peaks are

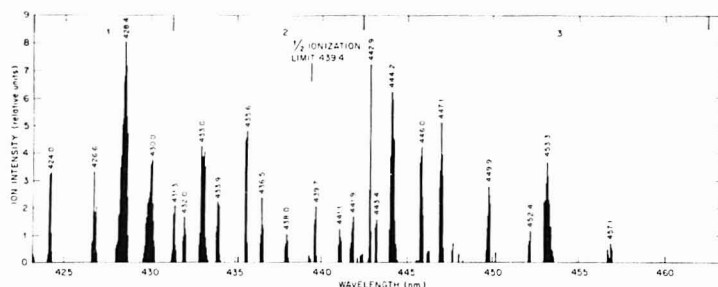


Figure 3. Resonance ionization spectrum of samarium obtained by monitoring  $^{147}\text{Sm}$ .

given. The accuracy of the wavelength assignments was based on the repeatability of five separate scans which were summed and on the accuracy of calibration of the dye laser micrometer dial. The main peaks in Figure 2 are labeled and listed in Table I with their wavelength of maximum intensity to an accuracy of  $\pm 0.1$  nm. The intensities of the various peaks are given only as strong (S), medium (M), and weak (W) because of the semiquantitative nature of the data gathering process as discussed in the Experimental Section. On the basis of assignments of energy levels for Nd (5), some of the initial transitions involved in the RIS process can be identified. It is apparent from the table that ionization is possible with photoenergies of less than half of the ionization potential,  $22280\text{ cm}^{-1}$ . An RIS scheme (1) (I, 2) requires that twice the energy of the exciting photon is equal to or greater than the ionizing potential of the atom; this, of course, assumes that the atom is in its atomic ground state. The fact that RIMS spectral peaks were observed at energies less than this limit implies that the Nd atoms generated from the thermal source were not all at the lowest lying ground state,  $^5I_4$ . As seen in the table, several of the lower energy peaks can be assigned to transitions from higher states. Of the 43 peaks given in Table I, 23 have been tentatively correlated to particular transitions; the errors in these assignments are given in the last column. The assignments were made from published spectral data (5-7). It is apparent that no assignments seem possible for almost 50% of the RIMS peaks observed. Since the sample taken for these studies was Nd and the mass detected was 142, it is probable that these peaks arise from Nd and that the photoionization proceeded by some, unidentified, allowed process. This points up a unique feature of RIMS spectral data. Such data can be useful in identifying various subsets of spectral transitions that originate from low lying levels that might be difficult to recognize in a complex emission spectrum.

**Sm Spectrum.** Figure 3 shows the ionization spectrum obtained for Sm, covering the same wavelength range as in Figure 2. Measurement conditions were kept as similar as possible so that the precision of peak heights (areas) and the accuracy of wavelength assignments are the same as those in Figure 2. The relative intensities of peaks in Figure 2 are not directly comparable to those in Figure 3, because there was no convenient means of normalizing the RIMS signals obtained for each element.

A summary of the Sm RIMS spectrum shown in Figure 3 is given in Table II. The presentation of these data is similar to that in Table I in that wavelength, wavenumber, intensity, transition, and error of tentative assignments are given. Contrary to the case of Nd in Table I, all peaks listed can be identified with known transitions in the Sm spectrum. In fact, several assignments are possible for some of the peaks, and it may well be that the peak is made up from contributions

Table II. RIMS Spectra of Samarium  
obsd peak

in nm (air)	in $\text{cm}^{-1}$ (vac)	intens	initial transition	error $\text{cm}^{-1}$
424.0	23 579	M	$^7F_2 \rightarrow ^7H_4$	-3
426.6	23 434	M	$^7F_2 \rightarrow ^7H_3$	-2
428.4	23 336	S	$^7F_2 \rightarrow ^7H_1$	1
			$^7F_2 \rightarrow ^7H_3$	3
430.0	23 249	M	$^7F_0 \rightarrow ^7G_1$	-5
			$^7F_1 \rightarrow ^7G_2$	4
431.3	23 179	M	$^7F_1 \rightarrow ^7H_2$	-5
			$^7F_4 \rightarrow ^7D_3$	1
432.0	23 142	W	$^7F_1 \rightarrow ^7D_4$	3
433.0	23 088	S	$^7F_1 \rightarrow ^7G_2$	0
433.9	23 040	M	$^7F_1 \rightarrow ^7H_2$	-5
			$^7F_2 \rightarrow ^7G_3$	0
435.6	22 950	S	$^7F_1 \rightarrow ^7G_1$	0
436.5	22 903	M	$^7F_1 \rightarrow ^7H_1$	-5
			$^7F_0 \rightarrow ^7G_1$	11
438.0	22 824	W	$^7F_2 \rightarrow ^7H_4$	-2
439.7	22 736	M	$^7F_1 \rightarrow ^7D_4$	-2
441.1	22 664	W	$^7F_2 \rightarrow ^7H_3$	-3
441.9	22 623	M	$^7F_1 \rightarrow ^7G_1$	-2
442.9	22 572	S	$^7F_2 \rightarrow ^7G_2$	-3
443.4	22 546	W	$^7F_1 \rightarrow ^7I_2$	5
444.2	22 506	S	$^7F_2 \rightarrow ^7G_3$	-1
			$^7F_2 \rightarrow ^7H_4$	1
446.0	22 415	S	$^7F_2 \rightarrow ^7I_1$	4
447.1	22 360	S	$^7F_1 \rightarrow ^7G_3$	3
			$^7F_4 \rightarrow ^7D_4$	1
449.9	22 221	M	$^7F_2 \rightarrow ^7H_3$	-1
452.4	22 098	W	$^7F_2 \rightarrow ^7G_1$	4
			$^7F_2 \rightarrow ^7D_4$	7
453.3	22 054	M	$^7F_2 \rightarrow ^7G_2$	2
			$^7F_2 \rightarrow ^7D_3$	-4
457.1	21 871	W	$^7F_4 \rightarrow ^7H_1$	7

of both. As was the case with Nd, many Sm peaks are observed at energies less than half the ionization potential of Sm,  $22760\text{ cm}^{-1}$ . In the data shown in Table II, it is obvious that transitions from the Sm ground state,  $^7F_0$ , account for few, if any, of the RIMS peaks. On the basis of the transition assignments of the Sm spectrum, it appears that the  $^7F_2$  and  $^7F_3$  levels are the most populated states. From emission spectral results (8), it has been reported that  $^7F_1$  and  $^7F_2$  states are most populated at 1270 K. The temperature of our samples was not continually monitored, but the sample temperature was the order of 1750 K. Note the assignment of the 441.1-nm and 441.9-nm peaks as arising from a  $^7F_3$  and a  $^7F_1$  level, respectively. As a check of this assignment, the relative intensities of these peaks were observed at three temperatures, 1773, 2073, and 2273 K. With increasing temperature, the population of the higher energy ground state increased relative to the lower state as expected from Maxwell-Boltzmann considerations.

It is interesting to note that there is no correlation between published data for relative oscillator strengths of Sm lines (9) and the relative intensities of the Sm RIMS peaks. Because of the power level of our laser system and the optical arrangement necessary to transmit the laser beam into the mass spectrometer, optical saturation of the ionization was not realized, and one might assume that the RIMS signals would be some function of oscillator strength of the respective transitions involved. There are certain deficiencies in our intensity monitoring procedure. With time, the concentration of the thermal sample changes. Our evaluation of laser dye intensity over the three dye ranges is only qualitative. Even within a given dye range there is, perhaps, 30% variation possible in signal strength measurement caused mainly by statistical variation in the small number of RIMS ions generated. As a result of the above reasons, or because of presently undefined reasons, there is little if any correlation of relative oscillator strength and RIMS signal. Compare, for example the strong intensity of a RIMS peak at 435.6 nm and a weak RIMS peak at 438.0 nm with reported relative oscillator strengths of 28.8 and 330, respectively (9). This observation is interesting, but until more precise control of the

experimental parameters is possible, no real conclusions can be drawn.

# LITERATURE CITED

- (1) Hurst, G. S.; Payne, M. G.; Kramer, S. D.; Young, J. P. *Rev. Mod. Phys.* **1979**, *51*, 767.
- (2) Young, J. P.; Hurst, G. S.; Kramer, S. D.; Payne, M. G. *Anal. Chem.* **1979**, *51*, 1050A.
- (3) Worden, E. F.; Conway, J. G. *ACS Symp. Ser.* **1980**, No. 131, 381-425, and references therein.
- (4) Donohue, D. L.; Young, J. P.; Smith, D. H. *Int. J. Mass Spectrom. Phys.* **1982**, *43*, 293.
- (5) Martin, W. C.; Zukauskas, R.; Hagen, L. *Natl. Stand. Ref. Data Ser. (U.S.)*, *Atti. Bur. Stand.* **1978**, NSRDS-NBS 60.
- (6) Meggers, W. F.; Corliss, C. H.; Scribner, B. F. *NBS Monogr. (U.S.)* **1975**, No. 145.
- (7) Blaise, J.; Wyard, J. F.; Hockstrad, R.; Krulver, P. J. *J. Opt. Soc. Am.* **1971**, *61*, 1335.
- (8) Parr, A. C.; Ingham, M. G. *J. Opt. Soc. Am.* **1975**, *65*, 613.
- (9) Kamasovskii, V. A.; Perkin, N. P.; Nikiforova, G. P. *Opt. Spectrosc.* **1970**, *29*, 116.

RECEIVED for review July 2, 1982. Accepted September 27, 1982. Research sponsored by the U.S. Department of Energy, Division of Chemical Sciences and the Office of Health & Environmental Research, under Contract W-7405-eng-26 with Union Carbide Corp.

## Determination of Organic-Bound Chlorine and Bromine in Human Body Fluids by Neutron Activation Analysis

James D. McKinney\*

National Institute of Environmental Health Sciences, Research Triangle Park, North Carolina 27709

Adel Abusamra and John H. Reed

Science Applications, Inc., 4030 Sorrento Valley Blvd., San Diego, California 92121

The levels of organic-bound chlorine and bromine in human milk and serum are determined by neutron activation analysis. Desalted milk and serum fractions are irradiated with neutrons in a nuclear reactor and the resulting  $\gamma$ -rays of  $^{36}\text{Cl}$  and  $^{82}\text{Br}$  are measured. The desalting procedure, achieved by using Bio-Gel molecular sieves, virtually removes all ionic chloride and bromides from milk and serum. Radioactive tracer studies with polychlorinated biphenyl- $^{14}\text{C}$  indicate a recovery of 90% through the Bio-Gel column. The total organic chlorine in 2,2-(4-chlorophenyl)-1,1-dichloroethene spiked milk and heptachlor spiked milk, determined after being desalted and irradiated according to this procedure, substantiates a good recovery of the added spike. The lower limits of detection of organic-bound chlorine and bromine in milk or serum are 50 and 5 parts per billion (ppb), respectively.

The level of organic-bound chlorine (TOCl) and bromine (TOBr) compounds has been rising in the environment due to the growing commercial use of large quantities of halogenated hydrocarbons and the previously unregulated dumping of organic waste. Halogenated hydrocarbon residues in breast milk or serum are normally measured by a combination of solvent extraction and gas chromatography with electron capture detection (GC/EC) (1). Identification and measurement of the full spectrum of halogenated organic

compounds become a difficult task. A value for TOCl and TOBr can be produced by using neutron activation analysis on desalted milk and serum fractions. This information is valuable in answering questions regarding the total amount of such compounds present in human milk or serum.

For determination of TOCl and TOBr in milk or serum, ionic species such as sodium chloride (NaCl) and sodium bromide (NaBr) must be removed completely by a desalting process before neutron activation is performed. Neal and Florini used Sephadex G-25 as a molecular sieve to remove NaCl from serum, utilizing batch extraction with a centrifuge (2). Uziel and Cohen used gel filtration for desalting certain nucleotides (3). Ludkowitz and Heurtebise determined protein-bound iodine in serum, through neutron activation, after desalting with ion exchange resins (4). Fritz and Robertson determined protein-bound trace metals in serum by using neutron activation after gel filtration with Bio-Gel P-6 (5).

The nuclear activation process does not differentiate between inorganic chlorides and chlorine bound to organic molecules. Also neutron capture can recoil organically bound chlorine into free atoms through the Szilard-Chalmers reaction (6). Preirradiation separations of ionic chlorides and bromides from organic-bound chloride and bromine species are therefore necessary.

The separation of inorganic sodium chloride and other ionic species in milk and serum from the organic-bound halogens associated with the protein and lipid fractions can be accom-

plished with Bio-Gel filtration chromatography. Bio-Gel P-2, a product of the Bio-Rad Corp., Richmond, CA, is neutral, hydrophilic, porous, poly(acrylamide) bead material with the property of retarding the movement of small ionic species relative to the movement of large globular protein macromolecules. In effect, the larger molecules are eluted first and isolated from the ionic fractions, such as  $\text{Na}^+$  and  $\text{Cl}^-$ . The separation is virtually complete as verified by tracer experiments.

### EXPERIMENTAL SECTION

**Apparatus.** The chromatography column consists of a 1.1 × 25 cm glass column with a Teflon stopcock. A glass-wool plug is placed at the bottom of the column to prevent Bio-Gel from slipping through. Bio-Gel P-2, hydrated for 4 h in a 0.1 N  $\text{NH}_4\text{NO}_3$  solution, is slurried into the glass column to fill a height of 15 cm. Columns are eluted with 100 mL of 0.1 N  $\text{NH}_4\text{NO}_3$  prior to loading the sample.

Prior to being desalted, human milk is emulsified with a  $^{45}\text{Ca}$ -in. titanium probe of an ultrasonic generator unit operated at 100 W. The Model 1510 ultrasonic unit used is produced by Braunsco Corp., San Francisco, CA. The probe of the unit is washed with acetone and distilled water after each operation.

**Nuclear Reactor.** The nuclear reactor of the University of Missouri at Columbia, with a neutron flux of  $5 \times 10^{13}$  (n/cm<sup>2</sup>)/s was used for neutron activation analysis (NAA). At the reactor, the radiochemistry laboratories are equipped with a pneumatic tube system which permits the irradiation of samples for a preset length of time and then returns them to the laboratory for further analysis. The  $\gamma$ -ray spectrometer consists of a 45-cm<sup>2</sup> Ge(Li) detector used with a 4096-channel pulse height analyzer for counting and measuring the radioactivity.

**Reagents.** Bio-Gel P-2 (size 100–200) mesh was used throughout the work. Reagent-grade ammonium nitrate was obtained from Malinkrodt Chemicals, St. Louis, MO bovine serum albumin (BSA) Cohn fraction V from Sigma Chemicals, Inc., St. Louis, MO and ultrapure water from Arrowhead Water Co., Los Angeles, CA. The water was distilled, deionized, treated by reverse osmosis, and bottled in 5-gallon clean polyethylene bottles. Polyethylene irradiation vials of 6 mL capacity were obtained from Olympic Plastics Inc., Los Angeles, CA.

**Cleaning of Glassware and Vials.** Glass beakers and columns were cleaned with 6 N  $\text{HNO}_3$ , high-purity water, reagent-grade acetone, and high-purity water and then dried under a laminar flow hood. Traces of chlorides and bromides were cleaned from the polyethylene irradiation vials by placing them on a mechanical shaker inside a polyethylene bottle and washing once with 6 N  $\text{HNO}_3$  for 6 h, three times with high-purity water for 3 h, once with reagent-grade acetone for 6 h, and three times with high-purity water for 3 h. Washed vials were placed in a clean glass tray inside a drying oven set at 70 °C for 6 h to dry. Dry vials were stored inside closed polyethylene bags until time of use and were handled with clean tongs.

**General Procedure.** One and two-tenths milliliter of human milk was transferred to a clean 10-mL glass beaker and 100  $\mu\text{L}$  of 20% bovine serum albumin (BSA) and 30  $\mu\text{L}$  of 3 N  $\text{NH}_4\text{OH}$  were added. The mixture was emulsified for 10 s with the titanium probe. One milliliter of the emulsified mixture was passed through a 1.1 × 15 cm Bio-Gel P-2 column, with 0.1 N  $\text{NH}_4\text{NO}_3$  as eluant.

The eluted milky fraction (2.5 mL) was collected and sealed in a precleaned polyvial and irradiated for 4 min at a neutron flux of  $5 \times 10^{13}$  (n/cm<sup>2</sup>)/s. After irradiation, the outside of the vial was washed with a 7 M  $\text{HNO}_3$  solution and rinsed with water. A needle syringe containing a 2 mL solution of 1% NaOH, NaCl, and KBr was injected into the vial containing the irradiated milk. The added NaCl and KBr act as carriers for any recoiled Cl and Br atoms while NaOH reacts chemically with any chlorine or bromine in the free state. The total content was transferred to a counting vial and counted for 3 min. The 1642-keV  $\gamma$ -ray of  $^{36}\text{Cl}$  and the 617-keV  $\gamma$ -ray of  $^{80}\text{Br}$  are measured and compared to a standard solution containing 5  $\mu\text{g}$  of  $\text{Cl}^-$  and 0.54  $\mu\text{g}$  of  $\text{Br}^-$ , irradiated, and counted under similar conditions.

Milk substitutes such as Similac and Enfamil were treated the same as milk. However, BSA was not added to human serum, and it was not emulsified with an ultrasonic unit before desalting.

BSA, added to milk, acts as a binder to water-soluble herbicides of chlorine-bound organic structure. The process of eluting milk or serum through Bio-Gel P-2 columns takes 15 min; three milk or serum samples can be desalted simultaneously.

**Tracer Experiments with Polychlorinated Biphenyl- $^{14}\text{C}$ , 2,4,5-Trichlorophenoxyacetic- $^{14}\text{C}$  Acid, and Sodium Chloride- $^{36}\text{Cl}$ .** Fifty milliliters of milk was placed inside a 100-mL beaker and was emulsified with the probe for 3 min. A 1.25- $\mu\text{Ci}$  portion of polychlorinated biphenyls (PCB- $^{14}\text{C}$ , 31 mCi/mmol) dissolved in 170  $\mu\text{L}$  of dimethyl sulfoxide was added. The milk was mixed and emulsified again for 3 min more. The spiked milk containing 25 nCi/mL was desalted on Bio-Gel P-2 as described in the procedure. The eluted milk fraction was collected in a liquid scintillation vial containing Rinfleur liquid scintillation cocktail and was  $\beta$  counted. By comparison of the results to reference standards, 92% of the original spike was found to be recovered. Similar tracer experiments were performed with a spike of 2,4,5-trichlorophenoxyacetic- $^{14}\text{C}$  acid (2,4,5-T- $^{14}\text{C}$ ). Carbon-14 tracer experiments, carried out in quadruplicate, were extended to serum and Enfamil. It was found in preliminary experiments that the addition of 100  $\mu\text{L}$  of 20% BSA to human milk prior to desalting is necessary to aid the binding of 2,4,5-T.

One millicurie of  $\text{Na}^{36}\text{Cl}$  in 2 mg of NaCl was mixed with 1.2 mL of human milk and desalted according to the procedure previously outlined. The desalted milk fractions were  $\gamma$ -counted for  $^{36}\text{Cl}$  content and were compared to the  $^{36}\text{Cl}$  values of the original spike.

**Recovery of 2,2-(4-Chlorophenyl)-1,1-Dichloroethene ( $p,p'$ -DDE) and Heptachlor from Spiked Milk.** Milk was also spiked with  $p,p'$ -DDE. The spiked milk was measured with NAA to contain 33  $\mu\text{g}$   $p,p'$ -DDE/mL. Aliquots of spiked milk were diluted with unspiked milk in duplicate to contain  $p,p'$ -DDE equivalent to  $1/2$ ,  $1/3$ ,  $1/6$ ,  $1/10$ ,  $1/15$ ,  $1/20$ ,  $1/30$ , and  $1/40$  of the original spike per milliliter of milk. Each of these spiked milk samples were desalted on Bio-Gel P-2 columns and analyzed with neutron activation for total organic-bound chlorine content.

For quality assurance, external (blind) heptachlor spiked milk samples containing the equivalent of nominally 0.5, 1.0, 1.5, 2, and 3  $\mu\text{g}$  of TOCl were introduced as a part of total samples supplied for analysis. Five samples of each spike level and 25 nonspiked controls were analyzed for TOCl content.

**$\gamma$ -ray Spectral Analysis.** The computer program GRPANEL was employed to process the magnetic tapes containing the  $\gamma$ -ray spectral data (7). GRPANEL is a general purpose peak-fitting program that validates the  $\gamma$ -ray energy and calculates the intensities for the  $\gamma$ -ray lines of interest. In addition, GRPANEL estimates the errors associated with the calculated intensities. An iterative least-squares procedure is used in the fitting process since the peak position and peak-shape parameters enter nonlinearly into the peak fitting algorithm.

The  $\gamma$ -ray intensities were then corrected for the various experimental parameters such as: chemical yield of the preirradiation procedure, mass of irradiated sample, duration of the neutron irradiation, delay between irradiation and sample counting, count time, analysis "dead time", and blank (vials and reagents) contributions.

The corrected intensities were then compared to intensities of  $\gamma$ -ray lines from standard solutions of chlorine and bromine irradiated along with the unknown sample.

### RESULTS AND DISCUSSION

Because of the low levels of TOCl and TOBr being analyzed, extreme care must be exercised to keep blank values low. Irradiation vials and pipet tips were handled with clean metallic tongs; clean surgical gloves were worn during laboratory operations. Table I indicates the range of chlorine and bromine in nanograms contributed from polyethylene irradiation vials, ammonium nitrate buffer solution, and (20%) BSA added to each gram of milk sample analyzed. Blank values were used to correct the results from each analysis.

Internal laboratory quality controls and external quality assurance samples were analyzed as part of laboratory procedures to check accuracy and consistency of results. With each 350 samples of milk or serum, five quality control rep-

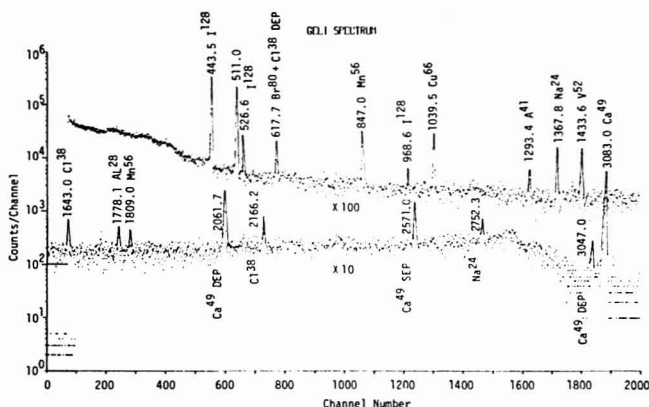
Figure 1.  $\gamma$ -ray spectrum of desalted human milk.

Table I. Chlorine and Bromine Levels in Blanks and Reagents

blanks	amt, ng	
	Cl	Br
H <sub>2</sub> O	12-15	3-5
0.1 N NH <sub>4</sub> NO <sub>3</sub>	15-30	4-7
irradiation vials	10-22	2-4
BSA (20%) solution	61	56

Table II. TOCl Level in Pooled Human Milk and Serum

pooled human milk		pooled human serum	
amt of TOCl, ppm	amt of TOBr, ppm	amt of TOCl, ppm	amt of TOBr, ppm
0.64	0.12	0.92	0.063
0.66	0.15	0.93	0.061
0.76	0.15	0.79	0.062
0.56	0.15	0.86	0.056
0.61	0.13	0.97	0.063
av	0.65 $\pm$ 0.07	0.14 $\pm$ 0.014	0.89 $\pm$ 0.07
			0.062 $\pm$ 0.03

licates of each of the following were analyzed: pooled human milk, pooled human serum, heptachlor-spiked pooled human milk, heptachlor-spiked pooled human serum, sample duplicates of human milk, sample duplicates of human serum, bovine serum albumin, 20% solution, clean, empty polyethylene irradiation vials, ammonium nitrate eluting buffer solution, and ultrapure water. Tables II and III show replication of results of some of the quality controls cited above.

Tracer experiments with PCB-<sup>14</sup>C and 2,4,5-T-<sup>14</sup>C were performed to measure the percent recovery of organic-bound chlorine compounds through the desalting process on Bio-Gel P-2. A PCB-<sup>14</sup>C mixture containing approximately 54% by weight chlorine to simulate Aroclor 1254 was used to spike pooled human milk. A recovery of greater than 90% was demonstrated for both PCB and 2,4,5-T in human milk and milk substitutes carried through the desalting procedure. The recovery data for *p,p'*-DDE shown in Table IV also demonstrates the reproducibility of the recovery over a wide concentration range.

The experiments with Na<sup>36</sup>Cl demonstrated the ability of the Bio-Gel P-2 column to separate inorganic chloride ions in milk from the TOCl fractions. The eluted milk fraction

Table III. TOCl Level in Heptachlor Spiked Milk and Serum

	pooled milk amt of TOCl, ppm	pooled serum amt of TOCl, ppm
	6.45	5.26
	6.39	4.92
	6.82	4.84
	6.53	5.52
	6.56	4.40
av	6.55 $\pm$ 0.16	5.0 $\pm$ 0.42

Table IV. Recovery of *p,p'*-DDE from Spiked Milk

	$\mu$ g of Cl due to <i>p,p'</i> -DDE		ratio of TOCl measd to calcd
	measd	calcd	
S	14.70	14.70	1.0
S/2	8.35	7.35	1.13
S/3	4.92	4.90	1.0
S/6	2.93	2.45	1.19
S/10	1.56	1.47	1.06
S/15	1.08	0.98	1.10
S/20	0.73	0.73	1.0
S/30	0.50	0.49	1.02
S/40	0.34	0.36	0.94
			1.05 $\pm$ 0.08

Table V. Separation Factors of Cl<sup>-</sup> from Desalted Fluids

sample	eluted fraction	fraction of <sup>36</sup> Cl spike
human milk	desalted milk	1 $\times$ 10 <sup>-5</sup>
	1st mL followed desalted milk	1 $\times$ 10 <sup>-5</sup>
	2nd mL followed desalted milk	1.6 $\times$ 10 <sup>-4</sup>
	3rd mL followed desalted milk	2.1 $\times$ 10 <sup>-4</sup>
cows milk	desalted milk	3.3 $\times$ 10 <sup>-4</sup>
	1st mL followed desalted milk	1 $\times$ 10 <sup>-4</sup>
Enfamil	desalted Enfamil	2 $\times$ 10 <sup>-6</sup>
	1st mL followed desalted Enfamil	3 $\times$ 10 <sup>-7</sup>
	2nd mL followed desalted Enfamil	5 $\times$ 10 <sup>-7</sup>
human serum	desalted serum	5 $\times$ 10 <sup>-4</sup>
	1st mL followed desalted serum	7 $\times$ 10 <sup>-4</sup>
	2nd mL followed desalted serum	5 $\times$ 10 <sup>-7</sup>

contained only 0.001% of the original Na<sup>36</sup>Cl spike. In addition, the first eluted milliliters that followed the desalted milk fraction also contained less than 0.001% of the original

Table VI. Chlorine Levels in Eluted Milk Fractions

fraction (mL)	amt of Cl, $\mu\text{g/mL}$	
	column 1	column 2
1	0.034	0.034
2	0.019	0.015
3	0.026	0.038
4	0.030	0.03
5 & 6 <sup>a</sup>	0.294	0.280
7	0.066	0.064
8	11.0	0.3
9	149.0	23.6
10	234.0	216.0
11	38.0	170.0
12	lost	3.52
13	0.082	0.208

<sup>a</sup> Desalted milk.

Table VII. Recovery of Heptachlor Spike from Blind Study

$\mu\text{g}$ of TOCl as heptachlor spike added	$\mu\text{g}$ of TOCl as heptachlor spike recovered
0.5	0.48 $\pm$ 0.11
1.0	0.87 $\pm$ 0.13
1.5	1.36 $\pm$ 0.14
2.0	1.78 $\pm$ 0.25
3.0	2.80 $\pm$ 0.2

$\text{Na}^{38}\text{Cl}$  spike. With NAA, human milk has been found experimentally to contain an average of 0.43 mg of Cl/g; hence, less than 5 ng of Cl<sup>-</sup> can be expected to carry over to the desalted milk fraction. This amount is considered within the blank values of the operating procedures. This experiment was run in duplicate on human milk, cows milk, Enfamil, and human serum. Results are summarized in Table V.

When human milk was desalted according to the described procedure, the results shown in Table VI are typical. The fractions of interest contained 0.294 mg/mL chlorine and were preceded by a low chlorine fraction (0.03  $\mu\text{g}$ ) and followed by another low chlorine fraction (0.066  $\mu\text{g}$ ). Eluted fractions

containing NaCl appear later in fractions 10 and 11. A second column separation does not substantially improve the desired result further supporting the efficiency of the Bio-Gel column techniques. Figure 1 exhibits a  $\gamma$ -ray spectra of neutron-irradiated human milk after desalting on Bio-Gel P-2.

The heptachlor-spiked milk samples were submitted to the analyzing laboratory in a blind study to truly test the accuracy and reproducibility of the method. The method showed good reproducibility and accuracy as shown by the results given in Table VII. TOCl from control milk ( $0.28 \pm 0.045 \mu\text{g}$ ) was used to correct the results.

## CONCLUSIONS

This work describes a method which can be automated to a large extent and applied to large numbers of human body fluids for TOCl and TOBr analysis. These levels should be useful in continuing epidemiological studies of the exposure of human populations to halogenated hydrocarbons in the environment. The method might also be useful as an ancillary method for determining fluid concentrations of halogenated hydrocarbons in toxicological studies with laboratory animals.

## ACKNOWLEDGMENT

The authors thank Phillip Albrow and his staff of the National Institute of Environmental Health Sciences for their help and assistance in this work. The experimental portion of this project was carried out by Science Applications, Inc., San Diego, CA.

Registry No.  $p,p'$ -DDE, 72-55-9; heptachlor, 76-44-8.

## LITERATURE CITED

- (1) Bjorseth, A.; Lunde, G.; Dybing, E. *Bull. Environ. Contam. Toxicol.* **1977**, *18* (5), 581-587.
- (2) Neal, M. W.; Florin, J. R. *Anal. Biochem.* **1973**, *55*, 328-330.
- (3) Uziel, M.; Cohen, W. E. *Biochem. Biophys. Acta* **1965**, *103*, 539-541.
- (4) Ludkowitz, J. A.; Heurtebise, M. *IAEA-SM-157/51*, 437-447.
- (5) Fritz, K.; Robertson, R. J. *Radioanal. Chem.* **1968**, *1*, 463-473.
- (6) Szilard, L.; Chalmers, R. A. *Nature (London)* **1934**, *132*, 462.
- (7) Gunnink, R.; Rutter, W. D. GRFANL Lawrence Livermore Laboratory; UCRL-52917; Jan 1980.

RECEIVED for review February 1, 1982. Accepted July 19, 1982.

# Mathematical Model for Concentric Nebulizer Systems

Anders Gustavsson

Department of Analytical Chemistry, The Royal Institute of Technology, Fack, S-100 44 Stockholm, Sweden

A mathematical model for concentric nebulizer systems is developed. The model is usable for the calculation of the cutoff diameter of the nebulizer system, the normal distribution parameters of the aerosol (the droplet distribution) generated by the nebulizer, the efficiency of the nebulizer system, and the aerosol concentration. The model also allows the optimization of nebulizer systems. The mathematical model is shown—by experiments—to be in agreement with practice.

There are very few articles of earlier date that describe theoretical work on nebulizers. But during the past years there has been an increased interest in nebulizers, nebulizer systems, and theory describing the way in which a nebulizer works.

This increased interest has resulted in an increased number of papers during later years. Scientists working in spectroscopy have in the last years accepted the fact that it is impossible to investigate excitation sources (e.g., plasmas, flames) without a thorough knowledge of the nebulizer system. If this knowledge is missing it is not possible to take into consideration the influence of the nebulizer system on the measured properties of the excitation source. Thus, it will not be possible to separate the properties of the nebulizer system from the properties of the excitation source.

Work on the measurement of aerosol dispersions has been published by Browner, Cresser, and Novak (1-4) and by Mohamed, Fry, and Wetzel (5). A paper on the effect of sample temperature in analytical flame spectroscopy has also been published by Browner and Cresser (6), where they have



Table I. A Comparison between Original and Recalculated  $d_0$ , Median, and Mean Values

original values from ref 7 and 8, $\mu\text{m}$	recalcd values, $\mu\text{m}$	median $\exp(\mu^*)$ , $\mu\text{m}$	mean $\exp(\mu^* + (\sigma^*)^2/2)$ , $\mu\text{m}$
15.6	15.7	13.7	15.6
17.7	17.7	13.7	15.6
19.8	19.9	13.8	15.6
19.9	19.9	13.8	15.6
22.6	22.4	13.8	15.6
25.0	25.2	13.9	15.6

applied the results of Nukiyama and Tanasawa (7, 8) to explain the small influence of the sample temperature on the signal. The investigation of the interference effects of aerosol ionic redistribution in analytical spectrometry (9) is important. A continued investigation of this phenomenon will probably explain some of the problems met when using nebulizer systems. From a theoretical point of view the cited form of the Nukiyama and Tanasawa equation (eq 8) in recent analytical literature deviates from the form used in this paper. The equation given in this paper is, however, in agreement with the form presented in the original paper (7). The deviations are related to the denominators of the equation, e.g., a missing  $\rho$  in the first term (1) and an improper square root in the second term (10-12). The main objective of this and earlier (13) work was to describe the combined process of aerosol generation, redistribution of the aerosol due to evaporation, and the separation of larger droplets in the spray chamber when nebulizing pure water. In ref 14 Smith and Browner have used another approach. They study the *analyte transport efficiency* but by doing this they have also included phenomena other than pure nebulization in their measuring object. There will be a need for more theoretical considerations to develop a model for analyte transport efficiency, which is the object of forthcoming work.

The objectives of this work were as follows: (1) to sum up the contents of the Nukiyama and Tanasawa equation and to give a short survey of the work of Nukiyama and Tanasawa that relates to nebulizers; (2) to develop a mathematical model for nebulizer systems employing concentric nebulizers; (3) to compare the model with actual measurements on the real system presented in ref 13.

## EXPERIMENTAL SECTION

The equipment used for this study is listed in ref 13, but the spray chamber listed in Table I is not from Plasma-Therm but rather from Wiklunds. The spray chamber made by Wiklunds has a larger cutoff diameter than that of Plasma-Therm.

**Measurement Procedure.** The measurement procedure for the liquid flows will be described in detail in a forthcoming paper but will be more closely described here than in ref 13 because that text has been misunderstood. Before performing any measurements—at a specified pressure drop—the system has been equilibrated. That is, the system has been running for such a long time that a stable temperature and liquid flow pattern in the spray chamber have been obtained. Then—with the system running the entire time—the uptake and waste were measured by weighing. From the weights obtained the volume uptake and volume efficiency were calculated. The volume basis is chosen to facilitate the comparison when nebulizing liquids of different density (e.g., Figures 4 and 5 in ref 13) and from the fact that the mass of analyte can be calculated directly from volumes if no analyte redistribution and/or severe evaporation occurs from the bulk of liquid in the spray chamber. The evaporation from the bulk of water will be of little consequence due to the rapid evaporation of small droplets in the aerosol saturating the gas stream.

The measurement procedure is indirect as compared to the direct method employed by Smith and Browner (14). There are—in this case—five reasons for using an indirect method: (1)

There is no analyte to be recovered due to the usage of pure water. (2) The time per measurement is small. (3) There will be no problems with water vapor in the ambient air. (4) Using a direct method would give severe problems with water evaporation. (5) The severe precision problem due to variability in the washout and in the atomic absorption measurement for indirect methods (14) is avoided because there is no analyte present.

## THEORY

A nebulizer system consists of two parts, the spray chamber and the nebulizer. The nebulizers dealt with throughout the remainder of this paper will be of the *concentric type*. The nebulizer characteristics used were defined earlier, in ref 13, but for the convenience of the reader they will be redefined here.

**Uptake:** The volume of liquid (mL) aspirated by the nebulizer per minute. The input liquid head is at -5 to -7 cm.

**Gas flow:** Flow of the nebulizing gas (L/min).

**Efficiency ( $\eta$ ):** The part of the uptake nebulized (percent by volume). The nebulized part is measured as the difference between the uptake and the quantity of liquid waste, i.e., including the water evaporated from the droplets.

**Aerosol concentration:** Concentration of the aerosol measured as the volume of nebulized liquid ( $\mu\text{L}$ ) per liter of nebulizing gas.

**Pressure drop:** Drop of pressure across the nebulizer (bar).

Before continuing with the theory it should be observed that the definition of, as well as the symbol for, the efficiency differs from that in ref 14 because of the different approaches chosen. The basic theory of nebulizer systems will be dealt with in three separate sections; namely, properties of log-normal distributions, theory of nebulizer, and theory of the nebulizer plus spray chamber. The reason for separating the last two theoretical items into two sections is to emphasize the characteristic properties of the nebulizer and the spray chamber separately.

**General Properties of log-Normal Distributions and the Validity of Using the Two-Parameter Model for Aerosols.** When treating data—which are assumed to be distributed log-normally—we can use models with a number of parameters (15). The models most commonly used have two, three, or four parameters. Here the two-parameter model will be described, because a good fit to the values presented by Nukiyama and Tanasawa was obtained by using this model.

If the distribution of a (positive) variate  $x$  is such that the distribution of the transformed variate  $y = \ln x$  is (exactly) normal (Gaussian), with mean  $\mu^*$  and standard deviation  $\sigma^*$ ,  $N(\mu^*, \sigma^*)$ , then the distribution of  $x$  is said to be log-normal. General properties of log-normal distributions are given in ref 15. In particular log-normal distributions possess moments of any order; the  $j$ th moment is denoted by  $\lambda_j$ , and

$$\lambda_j = \exp(j\mu^* + j^2(\sigma^*)^2/2) \quad (1)$$

from the properties of the moment-generating function of the normal distribution. The mean  $d_0$  and variance  $s_d^2$  for the log-normal distribution are given by

$$d_0 = \exp(\mu^* + (\sigma^*)^2/2) \quad (2)$$

$$s_d^2 = \exp(2\mu^* + (\sigma^*)^2)(\exp((\sigma^*)^2) - 1) = d_0^2\gamma^2 \quad (3)$$

$$\gamma = s_d/d_0 = \sqrt{\exp((\sigma^*)^2) - 1} \quad (4)$$

is the coefficient of variation. For small values of  $\sigma^*$  we obviously have

$$s_d/d_0 \approx \sigma^* \quad (5)$$

If two distributions have equal coefficients of variation they also have equal values of the parameter  $\sigma^*$  and conversely. A characteristic property of log-normal distributions is that

when converting them from number to mass distributions they will retain the log-normal behavior (ref 15, page 100). Hence, we can convert Nukiyama and Tanasawa's number distributions into the corresponding mass distributions without losing the log-normal properties of the distribution. Another characteristic property of log-normal distributions (15) generated under equal circumstances, i.e., aerosols generated by the same nebulizer with different flows of gas and liquid, is the nearly constant value of the coefficient of variation  $s_d/d_0$ , where  $s_d$  denotes the standard deviation of the log-normal distribution.

As pointed out in ref 15, the log-normal distribution is well established in the domain of small-particle statistics. Distributions of small particles such as are found as the result of natural and mechanical processes are often very skew. The following test has been applied to check that the intuitively reasonable assumption of a log-normal distribution is valid for droplet diameters in an aerosol produced by concentric nebulizers. In ref 8 (report no. 1) six different measures of  $d_0$  were proposed for aerosol distributions. A numerical example of these measures for a particular aerosol is given in column 1 Table 1 (taken from report no. 1, Figure 12). The values in column 2 have the same moment as the corresponding values in column 1 but they have been recalculated by using mean values of  $\mu^*$  and  $\sigma^*$  determined from the original values in column 1 using eq 1. The recalculated median and mean values of the distribution are shown in Table 1, columns 3 and 4. The  $\mu^*$  and  $\sigma^*$  values for this recalculation have been obtained from the values taken as pairs from column 1 (the last value having been paired with the first one). The similarity within the two columns three and four, respectively, and the similarity in pairs between the columns one and two shows that the two-parameter log-normal model satisfactorily describes the distribution of droplet diameters in an aerosol.

**Theory of the Nebulizer.** The theory presented in this section will be based on the work of Nukiyama and Tanasawa (7, 8). The velocities of the gas ( $v_g$ ) and the liquid ( $v_l$ ) at the nozzle face are calculated from the following expressions:

$$v_g = Q_g/A_g \quad (6)$$

$$v_l = Q_l/A_l \quad (7)$$

where  $Q_g$  and  $Q_l$  are the volume flows and  $A_g$  and  $A_l$  are the smallest areas at the nozzle face for the gas and the liquid flow, respectively. As seen from eq 6 and 7 there is no correction for stream contraction or velocity reduction. These corrections and the fluid dynamics of nebulizers will be dealt with in a future paper.

The basic idea of Nukiyama and Tanasawa was to describe the (population) mean droplet diameter ( $d_0$ ) of the droplets in the aerosol as a function of the different velocities, flows, and constants of the gas and the liquid. It should be emphasized that Nukiyama and Tanasawa treated the aerosol distributions as distributions by number and not by mass as in recent works (1-4). As can be seen from the statistical treatment in the previous section, from the theoretical treatment of small particle distributions in ref 15, from Figure 12 in report no. 1 (8), and from all of the figures in ref 16 that relate to droplet distributions, an aerosol distribution is of the logarithmic-normal (log-normal) type, i.e., by plotting the diameter on a logarithmic scale—in the distribution plot—we will get a normal distribution. Instead of treating the distributions as log-normal distributions Nukiyama and Tanasawa treated them as skew distributions only. The six different measures for  $d_0$  proposed by Nukiyama and Tanasawa gave different values of  $d_0$  due to this fact. Of the six measures Nukiyama and Tanasawa chose the area-volume measure as being the one giving large droplets a high weight in the de-

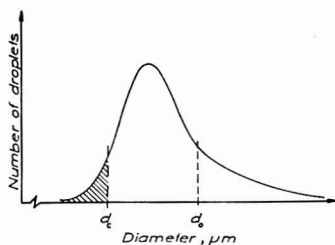


Figure 1. The typical appearance of a log-normal distribution of droplet diameters in an aerosol.

termination of  $d_0$ . For Nukiyama and Tanasawa this was a good choice since they were studying carburetor theory, but for nebulizer theory better choices can be made.

The continued work of Nukiyama and Tanasawa showed that  $d_0$  did not depend on the shape or size of the liquid and the gas nozzles or on their relative axial positions (ref 7, report no. 2). Three different types of air nozzles were tried, a convergent, a straight-bored, and a knife-edge nozzle. If  $Q_g$  was increased,  $d_0$  decreased but only to the limit where  $Q_g/Q_l = 5000$ . Nukiyama and Tanasawa concluded that  $d_0$  was a function of the velocity difference ( $v_g - v_l$ ) and  $Q_l/Q_g$ .

The final equation presented by Nukiyama and Tanasawa for  $d_0$  ( $\mu\text{m}$ ) was

$$d_0 = 585 \frac{\sqrt{\sigma}}{v \sqrt{\rho}} + 597 \left( \frac{\mu}{\sqrt{\sigma \rho}} \right)^{0.45} \left( \frac{1000 Q_l}{Q_g} \right)^{1.5} \quad (8)$$

Here,  $\rho$  is the density ( $\text{g}/\text{cm}^3$ ),  $\sigma$  is the surface tension ( $\text{dyn}/\text{cm}$ ),  $\mu$  is the coefficient of viscosity ( $\text{dyn s}/\text{cm}^2$ ), and  $v$  is the velocity difference  $v_g - v_l$  (m/s). The experimental ranges for the constants were  $0.8 < \rho < 1.2$ ,  $30 < \sigma < 73$  and  $0.01 < \mu < 0.3$ .  $\rho$ ,  $\sigma$ , and  $\mu$  are of course related to the liquid.

The Nukiyama and Tanasawa equation is strictly valid only when using air as the gas, but using another gas having nearly the same velocity of sound (e.g., argon) will give rise to a negligible error only. Equation 8 is in agreement with Nukiyama and Tanasawa's experimental findings, but it should be observed that the two members of the equation are not dimensionally equal. This does not matter when the equation is used within its limitations but it is not attractive from a scientific point of view. Before treating the nebulizer and the spray chamber as one unit, one should pay attention to the fact that the nebulizer is a device producing a log-normal droplet distribution (an aerosol) of mean diameter  $d_0$ .

**Theory of the Nebulizer Plus Spray Chamber.** The aerosol is forced to pass through a spray chamber. We can look upon this process as if the aerosol were passing through a theoretical filter having a cutoff diameter ( $d_c$ ). Droplets with a diameter  $\leq d_c$  will pass on unaffected and droplets larger than  $d_c$  will be retained (the waste). A picture of the selection process is given in Figure 1. The shaded area represents the droplets passing through the spray chamber. The selection process illustrated is of course a simplified representation of what actually occurs because the final aerosol will have droplets larger than  $d_c$ . This is due to the nontheoretical behavior of the filter (spray chamber).

The efficiency of the nebulizer system, i.e., the probability (proportion) of droplets having diameters  $\leq d_c$ , can be calculated from the expression

$$\Phi(\ln d_c - \ln d_0) / \sigma^* \quad (9)$$

where  $\Phi$  denotes the standardized normal distribution function and  $\sigma^*$  denotes the standard deviation of the normal distri-

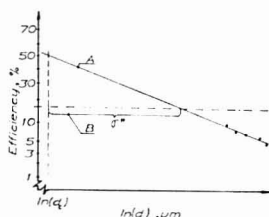


Figure 2. The estimation of  $\sigma^*$  and  $d_c$  using a normal probability paper. The horizontal line (---) denotes the 16% level.

bution corresponding to the log-normal distribution.

To sum up this section, the efficiency of a nebulizer system can be calculated if  $d_0$ ,  $d_c$ , and  $s_d$  or  $\sigma^*$  are known or if  $d_0$  is estimated with eq 8 and  $d_c$  and  $s_d/d_0$  or  $\sigma^*$  are determined in some other way (the relation between  $s_d/d_0$  and  $\sigma^*$  is given in a previous section). The theory of the spray chamber is of course also valid for aerosols produced by other types of nebulizers.

## RESULTS AND DISCUSSION

The theory presented will be used to elucidate three different problems: (1) the determination of  $d_c$  and  $\sigma^*$ ; (2) the calculation of the efficiency and the aerosol concentration for a particular nebulizer system; (3) optimization of nebulizer systems. Experimental conditions and data for this theoretical treatment are taken from ref 13.

The determination of  $d_c$  is direct and closely related to determining  $\sigma^*$  (the determination of  $d_c$  according to ref 1-4 and 17 is an alternative procedure). The nebulizer characteristics for a number of pressure drops are measured for a particular nebulizer system. The efficiencies are calculated from these nebulizer characteristics and the corresponding  $d_0$  values from the nebulizer characteristics and the Nukiyama and Tanasawa equation. The efficiencies and their corresponding  $d_0$  values are plotted on a normal probability paper, and the points should fit to a straight line, A, as exemplified in Figure 2. Next, the line A is extended until it intersects the 50% level, which occurs at  $\ln(d_c)$ .  $\sigma^*$  is obtained as the distance B at the 16% level. These percentage levels are clear from ref 15 and the properties of normal probability papers. The  $d_c$  value for this particular nebulizer system (13) is  $\approx 4.5 \mu\text{m}$ , which is in accordance with published work on aerosol measurements (ref 1, Figure 6) using a similar spray chamber. It could be somewhat surprising that the present result is in accordance with ref 1, as Nukiyama and Tanasawa used number distributions, while the other authors used mass distributions as a base for the calculations. However, Nukiyama and Tanasawa used a measure of  $d_0$  which emphasized the large droplets. Conversion of the number distributions given in ref 8 to mass distributions will yield mass distributions having a mean droplet diameter close to  $d_0$ .

The calculation of the efficiency and the aerosol concentration for a particular nebulizer system starts with the determination of the  $d_c$  value and  $\sigma^*$  as described in the previous paragraph. Next, the  $d_0$  value is calculated for a particular pressure drop by means of the nebulizer characteristics and the Nukiyama and Tanasawa equation. This  $d_0$  and the previously determined  $d_c$  and  $\sigma^*$  values give with expression 9 a value for the efficiency. The aerosol concentration is calculated with this  $\eta$  value and the nebulizer characteristics for the pressure drop in question.

In Figure 3 there is a comparison between the measured/calculated efficiency and aerosol concentration for the nebulizer system described in ref 13. The calculations were carried out as outlined in the previous paragraph. The

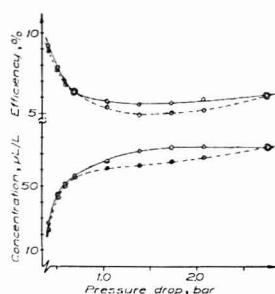


Figure 3. Comparison between the measured (—)/calculated (---) efficiency and aerosol concentration.

agreement between the measured and the calculated curves is acceptable because the difference is of the same magnitude as the experimental error. Both curves showing the variation of the efficiency with the pressure drop have minima, as reported earlier (13). These minima could not be explained at the time. But the present theoretical treatment permits the conclusion to be drawn that the minimum is an inherent property of the nebulizer system studied. It is of course possible to obtain a minima for the efficiency and not for the aerosol concentration or vice versa, depending on the flows ( $Q_1$ ,  $Q_2$ ) and the geometrical construction of the nebulizer system. The present theoretical treatment does not give an explanation for the bimodal distributions obtained by Novak and Browner (1), because this theory is intended for calculation of nebulizer characteristics and not for modification processes in aerosols.

The mathematical model is also useful for optimization of nebulizer systems. During the past years there has been a debate whether it is better to optimize a nebulizer system against the efficiency or against the uptake. It has been shown that these variables are most unsuitable for the purpose (13) and that the aerosol concentration should be used instead.

The aerosol concentration is the only variable which is directly proportional to the net intensity of the analytical signal (13). This is of course valid only if evaporation of water from the bulk of liquid in the spray chamber as well as aerosol ionic redistribution effects both are negligible and the analyte atoms are completely converted into light emitting plasma. It is clearly seen from ref 13, Figures 8 and 9, that this can be the case. When optimizing an analytical instrument that contains a nebulizer system the optimization variable should of course be the signal to noise ratio of the whole instrument.

The following variables should be included in the optimization: the flows ( $Q_1$ ,  $Q_2$ ), the areas ( $A_1$ ,  $A_2$ ), and  $d_c$ . The flows can easily be changed whereas the areas and  $d_c$  are hard to change. Apart from this, a change in the areas or  $d_c$  would probably change  $\sigma^*$ , thus complicating the optimization. The examples below showing changes in area or  $d_c$  are only included to facilitate the comparison and to indicate in what direction one should change the variables in order to improve nebulizer systems. When optimizing a particular nebulizer system, one should use the flows as variables because we then study a fixed mechanical system. In the development of a new nebulizer system the areas and  $d_c$  should also be included as variables.

When an optimization is performed, a suitable reference level must be chosen. The calculated values in Tables II and III were obtained using the 15 psi level for the concentric nebulizer (13) as reference when nebulizing pure water. The optimization starts with the determination of  $d_c$  and  $\sigma^*$ . By

Table II. Summary of the Changes for Optimization and the Resulting Gains in the Efficiency and the Aerosol Concentration

$Q_g^a$	$Q_l^a$	$A_g^a$	gain	
			$\eta$	aerosol concn
		0.5	1.18	1.18
	0.5		1.89	0.94
	0.333		2.38	0.79
	2		0.28	0.57
0.5			0.23	0.45
2			2.72	1.36
0.5	2		0.05	0.22
0.5	0.5		0.63	0.63
2	2		1.18	1.18
2	0.5		4.25	1.06
	0.5	0.5	2.72	1.36
0.5		0.5	0.28	0.57

<sup>a</sup> A value in the column indicates the factor used when changing the variable in question in relation to the reference level. Lack of value indicates no change of the variable.

Table III. The Variation of the Efficiency with the Cutoff Diameter

$d_c, \mu\text{m}$	1	3	4.5	7	10	13
$\eta, \%$	0.47	3.1	5.4	9.5	14	18

use of Nukiyama and Tanasawa equation a new  $d_0$  can be calculated from the assumed gas and liquid flows. The efficiency is calculated from  $d_0$  in the usual manner. The gain in the efficiency is obtained as a quotient between the new  $\eta$  value and the one at the reference level. To obtain the gain in aerosol concentration a correction for the change in  $Q_g$  and  $Q_l$  must be made. Table II is an epitome of the gain in efficiency and the aerosol concentration for different changes in  $Q_g$ ,  $Q_l$ , and  $A_g$ . The table shows how unfortunate it would be to choose the efficiency as response variable instead of the aerosol concentration. Table III shows the calculated variation of the efficiency with  $d_c$ , where it is assumed that the effect on  $\sigma^*$  by changing  $d_c$  (the geometrical construction of the spray chamber) is negligible.

It is seen in Table II that when making a new nebulizer system using the present system as reference level one should concentrate on making  $A_g$  smaller and  $d_c$  larger. The excitation source will of course put an upper limit to the  $d_c$  value. When optimizing this particular nebulizer system, one should increase the  $Q_g$  value and slightly alter the  $Q_l$  value. Table II shows that making the changes in the opposite direction would result in an inferior nebulizer system.  $A_l$  is not considered in Table II because it is easy to change  $Q_l$  by use of a variable pump, and  $v_l$  is so small—less than 0.5 m/s for the system studied—that the influence on  $v$  is negligible. For a thorough optimization of nebulizer systems an optimization procedure should be used (e.g., the SIMPLEX method (18))

because Table II gives only the trends.

A very interesting fact is seen in Table II, namely, the self-stabilizing property of nebulizer systems when generating the aerosol concentration. Because the flows ( $Q_l$ ,  $Q_g$ ) have a counteractive effect upon the aerosol concentration. For a high aerosol concentration a high efficiency should be used. According to eq 8 a higher  $\eta$  value is reached by using a higher  $Q_g$  and a lower  $Q_l$  value. On the other hand, increasing the  $Q_l$  and decreasing the  $Q_g$  value will make the aerosol less concentrated. Getting a low aerosol concentration, we have the opposite relations.

## CONCLUSIONS

When a nebulizer system is optimized the variable used for comparison should be the aerosol concentration and not the uptake or the efficiency. It is impossible to investigate an excitation source experimentally without including the nebulizer system in the study. The only possibility to determine the net properties of the source is by investigating the nebulizer system separately and taking its properties into consideration in the study. The theory presented above should be considered as a first attempt of getting a more unified theory for nebulizer systems.

## ACKNOWLEDGMENT

I thank Folke Ingman and Rolf Sundberg for stimulating discussions and comments relating to the manuscript.

## LITERATURE CITED

- (1) Novak, J. W.; Browner, R. F. *Anal. Chem.* **1980**, *52*, 792.
- (2) Novak, J. W.; Browner, R. F. *Appl. Spectrosc.* **1980**, *34*, 364.
- (3) Novak, J. W.; Browner, R. F. *Anal. Chem.* **1980**, *52*, 287.
- (4) Cresser, M. S.; Browner, R. F. *Spectrochim. Acta, Part B* **1980**, *35*, 73.
- (5) Mohamed, N.; Fry, R. C.; Wetzel, D. L. *Anal. Chem.* **1981**, *53*, 639.
- (6) Cresser, M. S.; Browner, R. F. *Anal. Chim. Acta* **1980**, *113*, 33.
- (7) Nukiyama, S.; Tanasawa, Y. *Trans. Soc. Mech. Eng., Tokyo* **1938-1940**, Vol. 4-6, Reports 1-6.
- (8) Nukiyama, S.; Tanasawa, Y. "Experiments on the Atomization of Liquids in an Air Stream"; Hope, E., transl.; Defense Research Board, Department of National Defense: Ottawa, Canada, 1950.
- (9) Borowiec, J. A.; Boorn, A. W.; Dillard, J. H.; Cresser, M. S.; Browner, R. F. *Anal. Chem.* **1980**, *52*, 1054.
- (10) Kirkbright, G. F.; Sargent, M. "Atomic Absorption and Fluorescence Spectroscopy"; Academic Press: London, 1977.
- (11) Cresser, M. S. "Solvent Extraction in Flame Spectroscopic Analysis"; Butterworth: London, 1978.
- (12) Stuper, J.; Dawson, J. B. *Appl. Opt.* **1968**, *7*, 1351.
- (13) Gustavsson, A. *ICP Inform. Newslett.* **1979**, *5*, 312.
- (14) Smith, D. D.; Browner, R. F. *Anal. Chem.* **1982**, *54*, 533.
- (15) Althison, J.; Brown, J. A. C. "The Lognormal Distribution"; Cambridge University Press: Cambridge, 1957.
- (16) Porstendörfer, J.; Gebhart, J.; Röbig, G. *J. Aerosol Sci.* **1977**, *8*, 371.
- (17) Skogerboe, R. K.; Olson, K. W. *Appl. Spectrosc.* **1978**, *32*, 181.
- (18) Deming, N. S.; Parker, L. R. *J. CRC Crit. Rev. Anal. Chem.* **1978**, *7*, 187.

RECEIVED for review April 22, 1981. Resubmitted October 26, 1981. Accepted September 7, 1982. I thank the Swedish Natural Science Research Council for financial support. This work was presented in part at the First Nordic Symposium on Atomic Spectroscopy 1980 in Mariehamn and the 1982 Winter Conference on Plasma Spectrochemistry in Orlando.

# Characterization of Two Modified Carbon Rod Atomizers for Atomic Absorption Spectrometry

Darryl D. Siemer\* and Leroy C. Lewis

Exxon Nuclear Idaho Co., Inc., Box 2800, Idaho Falls, Idaho 83402

A number of novel carbon rod atomizer configurations were constructed and tested with the goal of increasing the effective gas-phase temperatures experienced by volatile analyte metals. Both a "top-clamped" cup and a "tube-cup" atomizer permitted increases in the gas phase atomization temperature for lead and cadmium of more than a thousand degrees over those achievable with the two conventional CRA atomizer configurations. Additionally, from 2 to 3 orders of magnitude more concomitant transition metal chloride salt can be accommodated with the improved atomizer designs before matrix effects are observed.

The determination of lead and cadmium by graphite furnace atomic absorption spectrometry (GFAAS) is complicated by a host of "matrix effects" not usually seen in flame AAS because their volatilization temperatures overlap those of many of the compounds forming the bulk of many common sample matrices (e.g., transition or alkaline earth metal chloride salts). At the relative low gas-phase temperatures actually present within furnaces of conventional construction during the time that the analyte vapor is present, compound formation between covolatilized concomitants and the analyte is favored (1). Furnaces into which the sample is introduced after the optical path has been preheated to a relatively high temperature (e.g., the L'vov or Woodruff furnaces) are far less sensitive to matrix problems (2-4). The use of a "L'vov platform" in furnaces based on the Massmann design (e.g., the Perkin-Elmer HGA 2200, Varian Techtron GTA95, or the IL455/555/655 series) has been shown to retard evaporation of the analyte until the tube wall is several hundred degrees higher than would otherwise be the case and, consequently, significantly reduces matrix problems (5, 6).

However, owners of the Varian Techtron carbon rod atomizer (CRA) cannot use "platforms" because the atomizer's tube diameter is too small (3 mm) to accommodate them. Two approaches to increasing the effective gas-phase temperatures in these furnaces have previously been investigated. The first involves heating a longer-than-standard atomization tube from the ends, not at the center, either with a pair of "Y"-shaped rods (7) or with four separate rods (8). The second approach, recently investigated in this laboratory, involves heating the "cup" configuration CRA atomizer with rods clamped across its top, not across the bottom as is usually the case (9). Although these approaches raised the gas-phase temperatures a few hundred degrees and significantly reduced the matrix problems in lead determinations, this writer felt that better results could be achieved with the basic CRA furnace design if the system were redesigned with the achievement of high gas-phase temperatures as a primary goal. Accordingly, this paper describes some of the experimentation done and characterizes both "cup" and "tube-cup" designs featuring gas phase temperatures for lead and cadmium approximately 1000 degrees higher than are usually observed in thermally pulsed GFAAS furnaces.

## EXPERIMENTAL SECTION

The modifications made to the Varian Model AA6 spectrometer and to the Model 63 CRA furnace power supply have been dis-

cussed in previous papers (10, 11). The important differences between them and the standard equipment include considerably "faster" analog electronics in the signal processing circuitry and the addition of an optional temperature feedback controller to the furnace power supply. A Thermotest optical pyrometer interfaced with the same Hewlett-Packard computer system used to collect the atomic absorption transient signal data permitted simultaneous recording of the temperatures of a selected point on the atomizer's surface (10).

Modifications to the Model 90 CRA workhead were kept to a practical minimum in order to minimize duplication costs. First, the stack of alternating flat and corrugated stainless steel plates which are normally used to provide a laminar flow of inert gas to protect the hot graphite was replaced; instead a 4 mm thick aluminum plate pierced with 48 evenly spaced, 1.4 mm diameter (no. 54 drill) holes was used. This was done to give clearance to atomizer cups when they were lowered with respect to the center line of the rods. Second, a shield was fabricated from 2 mm thick aluminum sheet metal to loosely enclose the hot graphite working parts of the atomizer (Figure 1). This shield is very effective in retarding the back flow of air which invariably burns away the uppermost surface of both the atomizer and the rods in the standard, open-configuration workhead. Holes were drilled in the shield to accommodate the light beam and to provide access to the atomizer by the micropipet used to deposit the sample aliquots.

Finally, the HEP 312 phototransistor used to provide the temperature feedback signal to the CRA power supply was mounted in a small aluminum block; this block was in turn screwed onto the rear electrode block of the workhead. A 25-mm long piece of ceramic tubing of the type usually used to shield thermocouple wires was used as a light pipe-collimator and heat shield for the transistor. The upper end of the ceramic tubing was inserted into a short piece of opaque, black, plastic tubing and the phototransistor was glued into the other end. The rest of the temperature feedback controller was the same as described previously (11).

To conserve argon, a homemade gas control box featuring an electronic timer and a solenoid gas valve was put in series with the inert gas line from the standard Model 63 gas control system. It is triggered "ON" at the initiation of the "ASH" cycle by a signal from the CRA power supply. An argon flow rate of 8 L/min was used. A low-pressure propane line was connected to the inlet side of the automatic gas solenoid of the standard gas control system. (The solenoid valve was originally designed to permit the addition of hydrogen to the inert gas flow during the "ATOMIZE" cycle.) The occasional addition of propane (at a flow rate of 0.5 L/min) during an atomization cycle renews the surface of the hot graphite working parts of the atomizer with a layer of pyrolytic graphite and (in combination with the aluminum shield) extends their useful life to at least several weeks of continual use.

All of the data presented in this paper were obtained with atomizer components coated "in situ" with pyrolytic graphite before the experiments were performed. The standard pyrolytic graphite Varian Techtron cups were subjected to the same pre-treatment for the sake of consistency of temperature measurements made with the optical pyrometer. The appearance of the commercial graphite coating is different than that observed with the "in situ" coating process and, presumably, the emissivities of the two surfaces are different.

An inexpensive optical feedback control module compatible with Varian M 63 power supplies is commercially available (L. L. Elektronik, Department of Analytical Chemistry, University of Umeå, S-901 87, Umeå, Sweden). Its sensitive phototransducer permits accurate control of "ASHING" as well as "ATOMIZE"

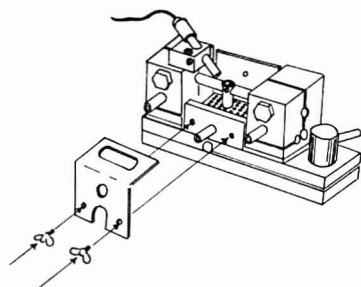


Figure 1. Drawing of the modified CRA 90 workhead depicting the aluminum gas shield and the mounting for the temperature transducer.

temperatures. The same supplier can also provide a gas control box similar to the homemade version outlined above.

In most of this work, standard 4.6 mm diameter Varian Techtron CRA rods were used. All nonstandard graphite components were machined from a dense, nonporous 6.2-mm diameter spectrographic quality graphite rod (FX9I from POCO Graphite Inc., Decatur, TX). This material is quite strong without being brittle and can be readily machined to very close tolerances.

## RESULTS AND DISCUSSION

The mean effective gas phase temperature within the atomizer while a typical volatile analyte metal is present was conveniently measured by comparing the relative integrated atomic absorbance signals observed at two prominent lead nonresonance lines. The first line, 368.3 nm ( $gf = 0.64$ ), originates from a state  $7819 \text{ cm}^{-1}$  above ground; the second at 280.2 nm ( $gf = 5.1$ ) originates from an energy level  $10650 \text{ cm}^{-1}$  above ground. The spectroscopic constants for these lines are taken from ref 12. These lines are a good choice for these measurements because the relative magnitudes of the two  $gf$  values implies that at the temperatures of interest (1200–2800 K) to this study an identical aliquot of the same lead standard solution will give measurable signal peaks at both wavelengths. However, in this study sequential signal measurements at each wavelength were used for the spectroscopic temperature calculation.

The 261.4 nm (nonresonance) and 283.3 nm (resonance) line pair that Ide et al. (13) used for a similar purpose is less satisfactory not only because the tremendous difference in sensitivity between those two lines requires two standard solutions but also because the 261.4-nm "line" is actually a doublet which renders its absorbance signal vs. mass of analyte response curve nonlinear when measurements are made with normal AAS equipment.

The optical system used measured light passing through a round 2.4-mm hole in a baffle situated as closely as possible to the optical access hole through the atomizer on the side facing the monochromator. This optical beam is only slightly smaller than the access hole itself so all of the absorbance measurements (as well as any spectroscopic temperatures derived from them) reflect mean values across the access hole's diameter. No attempt was made to spatially resolve these values either across the access hole or along the length of the atomization zone.

The following equation was used to calculate the spectroscopic temperatures in the furnace:

$$T = \frac{-4077}{(\ln 0.217)(A_{280.2}/A_{368.3})}$$

where 4077 and 0.217 are constants which combine the relative

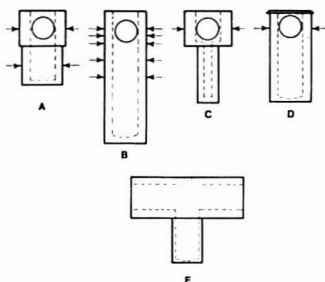


Figure 2. Some of the atomizer configurations tested. The arrows point to where the rods are clamped.

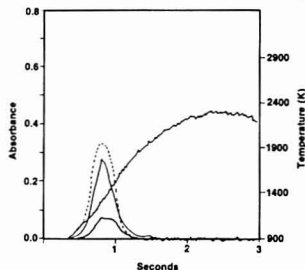


Figure 3. Absorbance signal transients seen with the standard, bottom-clamped, cup atomizer configuration.

wavelengths,  $gf$  values, and lower state energies of the two lines,  $A_{280.2}$  is the absorbance signal/g of lead at 280.2 nm, and  $A_{368.3}$  is the absorbance signal/g of lead at 368.3 nm.

Similar equations may be derived for other line pairs (e.g., the 283.3-nm resonance line and 368.3-nm nonresonance line pair) but their use is somewhat less convenient because different solutions must be pipetted for the two atomic absorption response measurements.

The approximately 5% coefficient of variation of integrated atomic absorbance signals measured at the nonresonance lead lines results in an imprecision in the calculated spectroscopic temperatures of from 30 to 100 K over the range of temperatures observed. Of course, the accuracy of the measurements is determined by the accuracy of the  $gf$  values used in the calculation. For the purpose of comparing atomizers getting exact temperatures is not as important as is consistency of approach.

In the course of this project approximately 20 different atomizer designs were built and tested. Length, diameter (inside and out), total mass, wall thickness, etc. were all varied. Figure 2 depicts a few of the various atomizers examined drawn to a common scale. In this figure the arrows point to where the center line of the rods were clamped with respect to the tube. In order to save space, only those experiments that definitely led to a clearer understanding of how these atomizers should be designed will be described in the rest of this paper.

First, a complete description of the experiments done to characterize these atomizers will be presented using the standard cup-configuration CRA atomizer as an example (Figure 3). The rods were clamped across the bottom of the cup as is recommended in the manufacturer's literature. In this figure, the atomic absorbance signals seen at the two



nonresonance lines (368.3 nm larger peak and 280.2 nm smaller peak) when 2000 ng of lead was atomized are depicted with solid lines. The dashed line is the signal seen from 2.5 ng of lead observed at the 283.3-nm resonance line. All of the figures (numbers 3-6) depicting actual instrument responses seen with the various atomizer configurations use the same format to portray the atomic absorption signals seen at the three lines. The temperature of the inner lip of the cup (recorded at the same level as the optical access hole) as measured by the optical pyrometer is also shown. A constant emissivity value of 0.7 was assumed for all measurements so recorded throughout the entire study. This value may not be accurate but since the object of the project was to compare different atomizers, the relative temperatures observed satisfy the intended purpose.

In this experiment, the power supply was used in the standard mode (i.e., no temperature feedback control) at its maximum heating rate (i.e., "10" on the front panel dial) for 1.5 s. This very short heating period was used for two reasons. First, all of the lead has left the atomizer within that time and, second, by the time that 2 s has elapsed, the bottom of the cup reaches a temperature sufficiently high to rapidly destroy the cup (by sublimation of the graphite). Also the use of the maximum possible heating rate ensures that the spectroscopic temperature measured represents the highest achievable with that atomizer and power supply combination.

Several important conclusions can be drawn from an examination of Figure 3. First, the temporal overlap of the three atomic absorption transients (i.e., the shapes of the peaks) while not identical with one another is quite similar. This means that temperature measurements based on the relative size of the two nonresonance line transients are valid to use in describing the temperatures experienced by the ground-state atoms of interest in conventional GFAAS analytical work. This is not unexpected because the shapes of these transient signals should be largely determined by the supply function ( $\tau_1$  or the rate at which the lead is volatilized) and not by the residence time ( $\tau_2$ ) of individual atoms within the cup in atomizers of this design (14). In Massmann furnaces possessing large and varying (with respect to time) thermal gradients along the optical axis, the nonresonance line signals tend to be skewed to the right (i.e., to higher temperatures) with respect to the resonance line responses (15).

Next, the apparent spectroscopic temperature calculated as explained previously is 1445 K—a couple of hundred degrees higher than is the temperature of the graphite at the same distance from the bottom of the cup at the time that the maximum signals appear. The reason for this is that the cross section of the cup is so large that the rapidly expanding gas does not achieve thermal equilibrium with the walls of the cup across the entire diameter of the cup. Since, in this case, the bottom of the cup is at a higher temperature than is the top, the gas passing upward within the cup is at a somewhat higher average temperature than are the walls of the cup at the same level. This has practical relevance in the design of the cup-type atomizers because it indicates that in order to achieve the highest possible gas-phase temperatures within a given region along a tube (i.e., at the optical access hole), the power should be applied at a point along the tube that the gas must first pass to reach the critical region.

Figure 4 gives the results of a similar experiment performed with the same cup-rod combination but with the rods now clamped across the top, not the bottom, of the cup. The ends of the rods were machined to a radius of 2.8 mm instead of the usual 2.5 mm in order to accurately fit the larger upper diameter of the cup. The homemade temperature controller was used with the light collimator of the transducer directed at the upper lip of the cup. The power supply heated the top

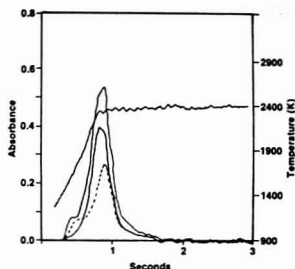


Figure 4. Absorbance signal transients observed with the rods clamped across the top of a standard CRA atomizer cup.

of the cup at the maximum possible rate until that part of the cup reached approximately 2400 K and then held that temperature constant. Only 250 ng of lead was needed in this case to get the two nonresonance lead signal transients (depicted with solid lines—the peak at 368.3 nm being the larger) but the same 2.5 ng of lead was used for the resonance line signal (dashed line).

Note that in this case, the sizes of the signals per gram of lead seen at the two nonresonance lines are much larger than they were in the last figure and also that the ratio of the size of the peak seen at the 280.2-nm line to that at the 368.3-nm line has increased. This, of course, reflects the much higher mean gas phase temperature experienced by the lead within the optical path—2145 K as compared to the 1445 K observed with the standard atomizer configuration.

However, the magnitude (area) of the resonance line signal is only about 90% as large as that observed with the standard atomizer configuration. This reflects the higher diffusion coefficients that lead atoms possess at the greater gas temperature present with the second cup-rod configuration. However, the signal is not attenuated as much as might be expected by a consideration of the difference in the atomic diffusion coefficients alone; this indicates that the convective expulsion of volatile analyte atoms by the rapidly expanding argon gas strongly affects atomic residence times ( $\tau_2$ ) in (at least) the first set of experimental conditions.

Experiments performed with cup D in Figure 2 (quite long with uniform cross sections both inside and out) involving changing of the position of the rods with respect to the optical access hole, indicated that the highest possible useful gas-phase temperatures are achieved with rods clamped so that their center line was approximately 1 mm below the center of the hole.

The position of the rods determines the temperature differential between the top and the bottom of the cup, both during the initial rapid heating which occurs when the power is first applied and after the entire cup reaches thermal equilibrium (after a few seconds). With a sufficiently long cup clamped at the top, it is possible to achieve a stable gas-phase temperature in the light path of 3000 °C before the lead at the bottom starts to volatilize. However, a practical cup atomizer must be capable of being heated at the bottom to a sufficiently high temperature to prevent the accumulation of the less volatile common matrix concomitants as the cup is used for repeated analyses of real samples. For the purpose of this project, one of the desired design criteria for the atomizer was an eventual temperature at the point upon which the sample is initially placed of 2000 K. This temperature was chosen because it is at least a couple of hundred degrees higher than the "appearance temperatures" of most of the elements (e.g., Na, K, Fe, Mg, Cu, Sn, Ca, etc.) that make up

the bulk of the common sample matrices in which lead is apt to be determined (2).

There seems to be little to be gained by designing atomizer cups with two different diameters—inside or out. At first thought, a cup featuring a small diameter, low "dead gas volume" sample well at the bottom should give better analytical sensitivity (cup C, Figure 2). The reason for this is that the convective effect of the expanding argon gas carrying the volatilized analyte out of the light path should be lessened. However, the actual sensitivity experimentally achieved was not appreciably better than with a cup of uniform cross section (e.g., cup B, Figure 2). The reason for this is probably a greater loss of analyte vapor through the walls of the cup due to a higher incidence of wall impacts. A serious disadvantage of cups featuring small sample wells is that only tiny sample aliquots can be dried without forceful ejection of the droplet by the steam generated ("bumping").

Cups of extremely small internal diameters (less than 2 mm) offer slightly greater absolute sensitivities (assuming equal wall thicknesses and lengths) than do those close to the standard (3 mm) size. However, the improvement is very slight and sample capacity drops rapidly as the diameter of the cups is reduced. The standard internal dimension is a good compromise.

An external cup diameter of 5 mm (0.20 in.) is convenient because standard CRA rods fit cups of that size without modification. Experiments performed with homemade rods with ends 6.2 mm in diameter (the size of standard spectrographic quality graphite rod stock) did not indicate that bigger rods are worth the additional trouble that it takes to machine and install them. Somewhat more current is drawn from the power supply because the cup-rod contact resistance is lower with the larger rods. However, the additional heating power is largely lost through increased thermal conduction down the rods themselves.

The optical access hole can advantageously be made somewhat larger than the 2.4 mm diameter hole used in the standard Varian Techtron CRA cups. A variation in these hole sizes from 2.0 to 2.8 mm in diameter in a single cup (cup B, Figure 2) caused no significant change either in gas-phase temperatures or in the analytical sensitivity achieved with the atomizer. The larger hole sizes, however, cause less trouble with vignetting of the light beam by the edge of the hole when the atomizer expands upon heating—a practical advantage.

The length of the cup should be sufficient to give an adequate temperature differential between the top and the bottom at the time that the analyte starts to volatilize—but not longer. Excess length reduces the final temperature achieved at the bottom of the cup (causing matrix buildup) and increases the dead volume of the atomizer causing dilution of the volatilized analyte and therefore reduced analytical sensitivity.

Typical results obtainable with a good overall compromise cup atomizer design are depicted in Figure 5. The cup used (cup D, Figure 2) has the following dimensions: 11.0 mm overall length; 5.02 mm outside diameter; 3.1 mm internal diameter (no. 31 drill); 9.91 mm depth; 2.64 mm diameter optical access hole (no. 37 drill) centered 2.34 mm below the rim of the cup. A narrow ridge 5.3 mm in diameter and 0.80 mm wide was left at the top of the cup to give a reproducible rod-cup geometry when the cup is pressed down into place.

The signal responses depicted are those from 100 ng of lead for the nonresonance lines (solid traces), 2.5 ng for the resonance line (dashed trace), and  $5 \times 10^{-11}$  g of cadmium (dotted line). Note that the signals for both lead and cadmium appear after the top of the cup has reached the temperature setpoint of the power supply (in this instance 2400 K). The spectroscopic temperature based on the relative size of the nonre-

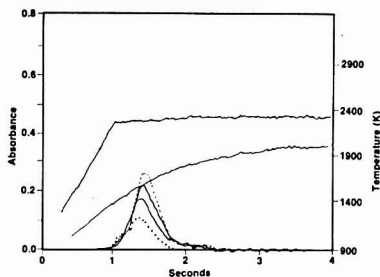


Figure 5. Absorbance signal transients observed with an optimized CRA cup atomizer.

sonance line lead signals was 2339 K. The temperature of the inside bottom of the cup as measured by the optical pyrometer (lower temperature trace) reached the desired 2000 K in approximately 4 s. In this one measurement the emissivity setting used with the pyrometer was 1.0 because the geometry approximated that of a "black body" radiator (which fact makes the nature of the graphite surface less important in determining its radiative properties).

The cup atomizer used to generate the signals depicted in Figure 5 achieved the main goals of this project, i.e., effective gas-phase temperatures for volatile metals similar to those observed in an air-acetylene flame while simultaneously preventing matrix accumulation in the cup. However, the absolute sensitivity of the atomizer (based on the relative sizes of the integrated atomic absorbance signals per gram of analyte) is approximately five times worse than can be achieved with the standard tube atomizer (using matrix-free standards). In order to combine the relatively high gas-phase temperatures achievable with the optimized cup design with the superior sensitivity of the tube-type atomizer, the "tube-cup" atomizer depicted as E in Figure 2 was constructed. Its design philosophy was such that when the analyte volatilized from the cup it would have to pass through a preheated optical path (the tube) far longer than the internal diameter of the cup itself in order to escape from the light beam. Of course, this raises the total fraction of analyte atoms within the light path at any one time and consequently increases the analytical response.

Its physical dimensions were as follows: tube length, 13.6 mm; outer tube diameter, 5.08 mm; tube inner diameter, 2.81 mm (no. 34 drill); sample access hole, 1.40 mm (no. 54 drill); hole for the cup opposite the pipet access hole, 3.66 mm (no. 27 drill); cup length, 7.4 mm; cup inner diameter, 2.81 mm (no. 34 drill); cup depth, 7.0 mm; outer diameter of cup, 3.66 mm (an interference fit into the hole drilled into the tube).

After the tube-cup atomizer was constructed, it was clamped into the workhead exactly as a standard CRA tube atomizer would be. It was heated to 2400 K in a 16:1 argon/propane sheath gas atmosphere for 6 s. This was repeated a total of five times. The resulting layer of pyrolytic graphite coated the entire surface of the atomizer and effectively sealed the cup to the tube.

Figure 6 shows the results obtained when the same series of experiments performed with the cup in Figure 5 was repeated with the tube-cup atomizer using an identical power supply setting. The tracings on this figure indicate the same experiments as in Figure 5 except that the resonance line signal for lead (dashed line) represents that seen with 1 ng (not 2.5 ng) of lead. The overall effect of the change in design is a 5-fold increase in analytical sensitivity while retaining a high effective gas-phase temperature (2436 K in this case).

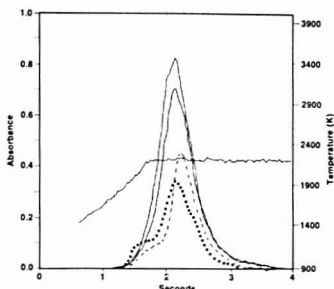


Figure 6. Absorbance signal transients observed with the tube-cup atomizer.

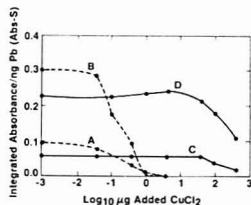


Figure 7. Integrated atomic absorbance signals per nanogram of lead as a function of the amount of copper chloride added.

In order to assess the practical value of these new atomizer designs in ameliorating gas phase related matrix problems, we prepared a series of Cu(II) chloride solutions containing, 0.1, 1, 10, and 100  $\mu\text{g}$  of the salt per 5- $\mu\text{L}$  aliquot. This salt was chosen for illustrative purposes because its severe depressive effect on lead GFAAS signals is known to be caused by gas phase reactions between the lead and the chlorine released when the readily dissociated copper salt is covalatilized with the lead (1). Figure 7 shows the integrated signals per nanogram of lead obtained with four different atomizer configurations as a function of the amount of copper(II) chloride added. No "Ashing" heating stage was used and the lead standard solution used contained no added acid (which would have acted as a "Matrix Modifier" during the drying step). Curve A is that obtained with the standard CRA cup configuration (rods across the bottom) atomizer with power supply settings of "8" for 3 s (no temperature feedback control). The second curve ("B") was generated with a standard tube configuration CRA used with a power supply setting of "7" for 4 s. Curve "C" represents the signals obtained with the top-clamped homemade cup used as described in the discussion of Figure 5. The last curve (D) shows the results seen with the "tube-cup" atomizer previously described.

Both the tube-cup atomizer and the homemade cup evince little matrix effect until the amount of copper chloride covalatilized with the lead exceeds 40  $\mu\text{g}$ —approximately 3 orders of magnitude more than can be accommodated by the popular standard tube configuration CRA atomizer (1). Even at the 100- $\mu\text{g}$  concomitant level enough of the lead signal remains (60–80%) that analyses by the standard addition technique are still possible. Similar experiments revealed that neither iron(III) nor magnesium chloride salts gave a serious signal perturbation until the amount covalatilized exceeded 40–100  $\mu\text{g}$ .

A study was performed of the effect of magnesium chloride on thallium signals; this study was similar to that done by Manning et al. (16) in their evaluation of a Massman-type

furnace modified so that samples were introduced on a tungsten wire after the tube itself had achieved thermal equilibrium. The chlorine-metal bond is considerably stronger between thallium and chlorine than between chlorine and lead. This, of course, implies that even higher effective gas-phase temperatures are needed to eliminate the matrix effect. The "tube-cup" atomizer described above gave results similar to those achieved by Manning et al., i.e., a 50% suppression of analytical response occurring at a  $\text{MgCl}_2$  concentration of approximately 0.02%.

To further increase the effective gas-phase temperature obtainable with the "tube-cup" atomizer, we shortened the tube portion of the atomizer to 9.5 mm (from 13.6 mm) and tapered the outer 2 mm of each end to a diameter just slightly larger than that of the hole itself. These modifications reduced the mass of the atomizer to 0.225 g (from 0.360 g) and consequently increased the rate of heating achieved with the power supply used. With this atomizer a stable gas-phase temperature of 2700 K is readily achieved during the entire time that thallium is in the optical path. The magnesium chloride concentration necessary to reduce thallium signals by 50% was greater than 4% with this atomizer. This concentration is much greater than that which the furnace used by Manning et al. could accommodate even when it was used at a nominal temperature of 2700  $^{\circ}\text{C}$  (16). The reason for this "tube-cup" atomizer's superior performance is probably that it does not have relatively cool tube ends through which the analyte and covalatilized matrix must pass in order to escape from the optical path.

Of course in actual analytical practice, an analyst using either of these atomizers should take advantage of the benefits to be gained by using any convenient "matrix modification" and/or "Ashing" sample pretreatment steps known to be beneficial prior to performing the actual atomization step. However, what the improved atomizer designs accomplish is to make those sample preparation steps far less critical. Therefore, these atomizers reduce the difficulty in getting reliable analytical values with samples of unknown or "difficult" composition. An additional power supply modification incorporating a second temperature sensing transducer directed at the bottom of the atomizer cup in order to permit positive control of the temperature during the "Ashing" heating stage would be very useful for practical analytical work.

Experiments with all of the atomizer configurations used indicated that use of the fastest possible heating rate is essential if the desired large temperature differential between the optical path and the sample deposition point is to be achieved. This implies that some form of feedback control of the maximum temperature should be employed to prevent over-heating of the graphite surrounding the point at which the rods are clamped. The potential heating rate achievable with the standard CRA M90 power supply is considerably greater than that of the CRA 63 used for this project (because the main power transformer has a rating of 3 kW as opposed to only 1.5 kW); however, the actual maximum heating rate (with standard CRA tubes) achieved with the M90 system is only about half as great as that gotten with the earlier model. The M90 power supply can be adjusted to permit more rapid heating ramp rates (see the CRA M90 service manual, adjust RV 104, to accomplish this). However, in any case, the "temperature" meter on the front of the power supply will give only a rough approximation of the actual graphite temperature because the resistances of the unconventional atomizers are not the same as those of the standard components.

The modified atomizers described in this paper were designed, first, to minimize the serious gas-phase matrix effects encountered in the GFAAS determination of volatile analyte

metals and, second, to be compatible with commercially available CRA workheads and power supplies with a minimum of hardware changes. The maximum volatilization temperatures achievable with them are too low for the determination of refractory analytes so the standard atomizer configurations must be used for metals less volatile than copper.

The principle followed in the design of these CRA atomizers is similar to that used by Littlejohn and Ottaway in their paper describing a Massmann tube furnace optimized for atomic emission analyses (17). Presumably then their furnace would evince lessened gas-phase matrix effects when used for absorbance measurements and, conversely, the modified CRA atomizers should be superior to the standard components for the atomic emission analysis of relatively volatile metals.

#### LITERATURE CITED

- (1) Czobik, E. J.; Matousek, J. P. *Anal. Chem.* **1977**, *50*, 2-10.
- (2) L'vov, B. V. *Spectrochim. Acta, Part B* **1978**, *33B*, 153-193.

- (3) Hageman, L.; Mubarak, A.; Woodruff, R. *Appl. Spectrosc.* **1979**, *33*, 226-230.
- (4) Hageman, L.; Nichols, H. A.; Viswandham, P.; Woodruff, R. *Anal. Chem.* **1979**, *51*, 1406.
- (5) L'vov, B. V. *Spectrochim. Acta, Part B* **1978**, *33B*, 153.
- (6) Slavin, W.; Manning, D. C. *Anal. Chem.* **1979**, *51*, 261-265.
- (7) Lawson, S. R.; Woodruff, R. *Spectrochim. Acta, Part B* **1980**, *35B*, 753.
- (8) Siemer, D. D. *Anal. Chem.* **1982**, *54*, 1659-1663.
- (9) Siemer, D. D. *Appl. Spectrosc.*, in press.
- (10) Siemer, D. D.; Baldwin, J. M. *Anal. Chem.* **1980**, *52*, 295.
- (11) Siemer, D. D. *Appl. Spectrosc.* **1979**, *33*, 613.
- (12) Cortes, C. H.; Bozman, W. R. *NBS Monogr.* (U.S.) No. 53, 289.
- (13) Ide, Y.; Yanagisawa, M.; Kitagawa, K.; Takeuchi, T. *J. Spectrosc. Soc. Jpn.* **1975**, *24*, 1435-1437.
- (14) Van der Broek, M. J. T.; de Galan, L. *Anal. Chem.* **1977**, *49*, 2186-2188.
- (15) Sturgeon, R. E.; Berman, S. S. *Anal. Chem.* **1981**, *53*, 632-639.
- (16) Manning, D. C.; Slavin, W.; Myers, S. *Anal. Chem.* **1979**, *51*, 1375-1378.
- (17) Littlejohn, D.; Ottaway, J. M. *Anal. Chim. Acta* **1979**, *107*, 139-158.

RECEIVED for review July 8, 1982. Accepted October 7, 1982.

## Synthesis of the 38 Tetrachlorodibenzofuran Isomers and Identification by Capillary Column Gas Chromatography/Mass Spectrometry

Thomas Mazer,\* Fred D. Hileman, Roy W. Noble, and Joseph J. Brooks

Monsanto Research Corporation, Dayton Laboratory, 1515 Nicholas Road, Dayton, Ohio 45418

The 38 positional isomers of tetrachlorodibenzofuran have been synthesized by pyrolysis of specific polychlorinated biphenyl congeners, ultraviolet photolysis of pentachlorodibenzofurans, and chlorination of trichlorodibenzofurans by aromatic substitution. The specificity of these reactions in combination with capillary column gas chromatography with mass spectrometric detection has allowed each of these isomers to be identified based on their relative elution order.

In recent years the polychlorinated dibenzofurans [PCDFs] have been the subject of an intense research effort owing to their structural similarity to the polychlorinated dibenzo-p-dioxins [PCDDs] (1). Particular attention has been given to the tetrachlorodibenzofurans [TCDFs] for which there are 38 positional isomers, yet no analytical scheme allowing identification of specific TCDF isomers has yet been reported. In this paper we report on the synthesis of the 38 TCDF isomers by oxidative pyrolysis, under carefully controlled reaction conditions, of specific PCB congeners (2, 3), ultraviolet [UV] photolysis of pentachlorodibenzofurans [PenCDF], and chlorination by electrophilic aromatic substitution of specific trichlorodibenzofuran [TrCDF] isomers. Characterization of the TCDF isomers was accomplished by high-resolution gas chromatography/mass spectrometry and UV photolysis (4). The final result has been the development of an analytical scheme allowing for the analysis of 2378-TCDF (notation for symbols excludes the commas necessary in full names).

#### EXPERIMENTAL SECTION

**Caution.** Persons attempting to synthesize these compounds should first familiarize themselves with their safe handling and disposal.

**PCB Congeners.** All the PCB congeners used in this study were obtained from Ultra Scientific, Inc., Hope, RI, with the exception of 2,2',3,4'- and 2,3,3',4'-tetrachlorobiphenyl, 2,2',3,3',6-pentachlorobiphenyl, and 2,2',3,3',4,6'- and 2,2',3,3',5,6'-hexachlorobiphenyl which were received from C. A. Wachtmeister, Stockholm Universitet, Wallenberglaboratoriet S-10691 Stockholm, 2,3,4,4'-tetrachlorobiphenyl and 2,3,3',4,5-pentachlorobiphenyl which were received from J. Pyle, Miami University, Oxford, OH, and 2,2',3,4',5,6-hexachlorobiphenyl which was received from M. D. Mullins, EPA, Grosse Ile, MI.

The purity of the PCB congeners was generally greater than 97% assuming an equivalent FID response for all PCBs. In those cases where a given PCB congener was contaminated with another PCB congener, pyrolysis often yielded small amounts of PCDF isomers other than those expected. In all cases these were readily discernible from the desired PCDF isomer.

**PCB Pyrolysis.** Miniglass ampoules 5-6 cm in length were prepared by sealing the large end of disposable borosilicate glass pasteur pipets (Model 13-678-20C, Fisher Scientific Co., Cincinnati, OH). Ten microliters of a solution of the PCB in hexane [10 µg/mL] was placed in the ampoule and the solvent allowed to evaporate. The tip of the ampoule was then flame sealed and the ampoule placed in a large vial along with a cold junction referenced chromel-alumel thermocouple which was connected to a digital voltmeter to allow accurate temperature measurements. The ampoule and thermocouple were placed into a muffle furnace [Type 1500, Thermolyne Corp., Dubuque, IA] operated at 600 °C. When the temperature of the ampoule reached 550 °C, pyrolysis was allowed to continue for an additional 5 s. The ampoule was removed from the furnace and allowed to cool to ambient temperature at which time it was opened and the contents thoroughly rinsed out with 1 mL of hexane.

In some cases unreacted PCBs were removed by subjecting the pyrolysate to chromatographic separation on a minicolumn of Woelm Basic Alumina (ICN Pharmaceuticals, Cleveland, OH) by eluting the PCBs with 10 mL of 2% methylene chloride in hexane, and then eluting the retained PCDFs with 15 mL of 50%

Table I. Synthesis Routes for the 38 TCDFs

TCDF	primary PCB congener	secondary PCB congener	PCDF dechlorinated	PCDF chlorinated	confirmed by photolysis
1234	23456, <sup>a</sup> 2345 <sup>a</sup>	22'346			
1236	22'346		12367		
1237	2344' <sup>a</sup>	22'344'6	12367	123	
1238			12348	238, 123, 128	yes
1239	22'346			123	
1246	22'33'6	22'356		124	
1247	22'34'56 <sup>a</sup>			124	
1248	22'355'6 <sup>a,d</sup>			124, 128	yes <sup>b</sup>
1249	22'356			124	
1267	233'4'	22'33'46'	12367		
1268	22'33'56'		12468		
1269	22'3'5 <sup>a</sup>	22'33'6, 22'33'66'			
1278	233'4'		23469	238, 128	yes <sup>b</sup>
1279	22'34' a,c	22'34' c			
1289	22'33'	22'33'6, 22'33'66'			
1346	22'346		13467		
1347	22'344'6	22'44'6	13467		
1348	22'455'	22'45'6			
1349	22'466'	22'346			
1367	23'44'	22'44'6, 23'44'6	13467, 12367		
1368	23'45'6 <sup>a</sup>	22'45'6			
1369	22'4'56	22'466', 22'45'6			
1378	22'44'5'6 <sup>a</sup>	23'44', 23'44'6			
1379	22'44' a	22'44'6			
1467	23'4'5	22'33'46'	13467, 23469		
1468	23'55' a	22'33'56'	23469		yes <sup>b</sup>
1469	22'55' a	22'33'66'			
1478	23'4'5'	22'455'	23469		
2346	22'33'45	233'45			
2347	22'344'5 <sup>a</sup>				
2348	22'3455' a	22'455', 233'45		238	
2349	22'3456' a				
2367	33'44'		12367		
2368	22'455'		23468	238	yes <sup>b</sup>
2378	22'44'55' a	33'44'			yes
2467	d		23468		yes <sup>b</sup>
2468	d		23468		yes <sup>b</sup>
3467	22'33'44' a	33'44'	13467		

<sup>a</sup> Represents those cases in which a single TCDF isomer was formed from the pyrolyses. <sup>b</sup> These TCDFs were also received from D. Firestone and checked against our own syntheses. <sup>c</sup> These are identical PCB congeners from different sources. Pyrolyses of both gave identical products. <sup>d</sup> The relative retention times of these isomers were identical with the same isomer synthesized by the palladium acetate cyclization of the appropriate diphenyl ethers (6, 7).

methylene chloride in hexane. In many instances PCDF isomers were separated from one another by using the HPLC techniques described below.

**Reversed-Phase High-Performance Liquid Chromatography (RP-HPLC).** Separation of isomers was carried out with a 25 cm × 4.6 mm μBondapak C<sub>18</sub> column (Waters Associates, Inc., Milford, MA) with 75% acetonitrile/25% water as the eluent at a flow rate of 0.75 mL/min. Altex Model 110 pumps (Beckman Instruments, Inc., Fullerton, CA) were used with a Valco Model CV-6-UHPA-N60 injector (Valco Instruments Co., Houston, TX). Fractions were collected on a Gilson FC-80 fraction collector (Gilson Medical Electronics, Middleton, WI) with sample detection being carried out with a Beckman Model 100-10 UV spectrophotometer operated at 235 nm.

**Normal-Phase (NH<sub>2</sub>) High-Performance Liquid Chromatography (NH<sub>2</sub>-HPLC).** The normal-phase HPLC system used was the same as that described for reverse-phase HPLC with the exception that a 25 cm × 4.6 mm Zorbax NH<sub>2</sub> column [Du Pont, Analytical Instrument Division, Wilmington, DE] was used with hexane as the eluent at a flow rate of 1.5 mL/min.

**Gas Chromatography/Mass Spectrometry (GC/MS) Analyses.** GC/MS analyses were performed with a Hewlett-Packard 5985B quadrupole GC/MS system operated in the electron impact ionization mode. capillary columns that were used included a 60 m × 0.25 mm i.d. glass coated with SP-2330 (Supelco, Bellefonte, PA) and a 30 m × 0.25 mm i.d. fused silica coated with SE-54 (J & W Scientific, Rancho Cordova, CA). The capillary columns were directly coupled to the ion source via a 45 cm × 0.20 mm i.d. length of fused silica coated with SE-30. Column conditions for the SP-2330 column were as follows: 200 °C, 1 min

isothermal, 8 °C/min to 250 °C, isothermal at 250 °C for the duration of the run time; hydrogen carrier gas at 15 psi yielding a linear flow velocity of 40 cm/s. For the SE-54 column the conditions were as follows: 200 °C, 1 min isothermal, 10 °C/min to 275 °C, isothermal at 275 °C for the duration of the run time; helium carrier gas at 7 psi yielding a linear flow velocity of 38.5 cm/s. All samples were introduced via splitless injection with the injector at 275 °C using tetradecane as the solvent.

Mass fragmentograms were obtained by monitoring ions characteristic of each class of PCDF possible in a synthesis experiment. This included the molecular ions for the dichloro- and trichlorodibenzofurans, the molecular ions as well as the highly characteristic COCl loss for the tetra- and pentachlorinated dibenzofurans. In addition, ions characteristic of polychlorinated diphenyl ethers were also monitored to ensure that these compounds did not interfere in the analyses. An internal standard, [<sup>12</sup>C<sub>14</sub>]2378-TCDF (KOR Isotopes, Cambridge, MA) was coinjected with each sample, requiring that *m/z* 312 also be monitored during each run.

**Spectral Sample Isolation.** In certain cases it was necessary to obtain significant amounts of PCDFs (10–50 μg) for further chlorination or photolysis studies. These PCDFs were obtained by the RP-HPLC separation of a mixture of PCDFs formed by the extensive chlorination of dibenzofuran (5). In many instances the RP-HPLC fractions were further processed by NH<sub>2</sub>-HPLC to isolate a single PCDF isomer. The identity of this isomer was then determined by its GC characteristics on the two capillary columns used in these analyses.

**Chlorination.** Chlorination of the PCDFs was accomplished by placing a solution of 200 μL of CCl<sub>4</sub> containing the PCDF to





Table III. Cross Correlation Chart of TrCDF Isomers vs. TCDF Isomers

TCDF	TrCDF																							
	123	124	126	127	128	129	134	136	137	138	139	146	147	148	149	234	236	237	238	239	246	247	248	249
1234	•	•														•								
1236	•							•									•							
1237	•			•					•									•						
1238	•				•					•									•					
1239	•					•					•									•				
1246		•	•									•									•			
1247		•		•									•									•		
1248		•			•									•									•	
1249		•				•									•									•
2346																•	•							
2347																•	•							
2348																•								
2349																•								
1346							•	•				•												
1347							•		•					•										
1348							•			•					•									
1349							•				•					•								
1267			•	•																			•	•
1268			•		•																			
1269			•			•								•	•									
1278				•	•														•	•				
1279				•		•				•	•													
1289					•	•																		
1367								•	•														•	•
1368								•		•												•		
1369								•			•		•		•								•	
1378									•	•								•	•					
1379									•		•													
1467											•	•											•	•
1468											•		•								•			
1469											•			•										
1478												•	•					•						
2367																•	•						•	•
2368																•		•				•		
2378																	•	•						
2467																			•	•			•	•
2468																				•		•		
3467																							•	•

of TCDFs. In order to identify a given TCDF, it was necessary to perform a pyrolysis of another PCB congener that would yield the desired TCDF among others. An assignment of the particular TCDF was made based on the match of the chromatographic retention characteristics of the various pyrolysates (as shown in Figure 2). As an example of this process, consider the pyrolysis of 3,3',4,4'-tetrachlorobiphenyl yielding 3467-, 2378-, and 2367-TCDF. By examination of Table I and Figure 2 it is seen that 2378-TCDF is the only TCDF formed from the pyrolysis of 2,2',4,4',5,5'-hexachlorobiphenyl and 3467-TCDF is the only TCDF formed from the pyrolysis of

2,2',3,3',4,4'-hexachlorobiphenyl. Therefore the remaining TCDF must be 2367-TCDF. This identification was subsequently confirmed by the dechlorination of 12367-PenCDF to form 2367-TCDF in a mixture with 1236-, 1237-, and 1267-TCDF.

It was found to be convenient to prepare a cross correlation chart (Table II) which lists the PCB congeners on one axis and the possible TCDF isomers formed by pyrolysis of these PCB congeners on the other axis. This chart shows the possible PCB congeners used in this study which may be pyrolyzed to yield a given TCDF or, conversely, which TCDF

Table IV. Cross Correlation Chart of PenCDF Isomers vs. TCDF Isomers

TCDF	PenCDF																												
	12346	12347	12348	12349	12467	12468	12469	12478	12479	12367	12368	12369	12378	12379	12389	12489	13467	13468	13469	13478	13479	13489	23467	23468	23469	23478	23479	12678	
1234	•	•	•	•																									
1236	•									•	•	•																	
1237		•								•			•	•															
1238			•								•		•																
1239				•								•		•	•														
1246	•				•	•	•																						
1247		•			•				•	•																			
1248			•		•			•									•												
1249				•			•		•							•													
2346	•																							•	•	•			
2347		•																					•			•	•		
2348			•																					•		•	•		
2349				•																						•	•	•	
1346	•																•	•	•										
1347		•															•			•	•								
1348			•															•		•		•							
1349				•															•		•	•							
1267					•					•																			•
1268						•					•						•												•
1269							•					•				•													
1278								•					•		•														•
1279									•					•	•							•							
1289															•	•													
1367										•							•				•								•
1368										•	•							•											•
1369										•		•							•		•								
1378													•	•						•									•
1379														•							•								
1467					•												•		•							•			
1468						•												•							•	•			
1469							•												•										
1478								•				•								•						•			
2367									•												•						•		
2368								•			•										•				•	•			
2378													•														•		
2467					•													•						•					
2468						•																			•				
3467																	•							•					

(or TCDF mixtures) would be formed from the pyrolysis of a given PCB congener.

Unless the primary PCB pyrolysis yielded a single TCDF isomer, it was necessary to prepare a confirming TCDF isomer. If the PCB congener required for a second pyrolysis was not available, either chlorination of an appropriate TrCDF or photolytic dechlorination of an appropriate PenCDF was used to give the needed TCDF. Cross correlation charts were prepared illustrating the TCDFs which may be formed from chlorinating a given TrCDF (Table III) and also a cross chart

showing the TCDFs which may be formed from dechlorinating a given PenCDF (Table IV). In Table III all the TrCDFs are listed on one axis and all the TCDFs are listed on the other axis. This chart may be used both for determining all the TCDFs that may result from the chlorination of a given TrCDF isomer and conversely for determining all the possible TrCDFs that may form by the UV photolysis of a given TCDF. The same principle is applicable for Table IV which gives TCDFs vs. PenCDFs. Obviously the tri- and pentachlorodibenzofurans used in the chlorination and dechlorination

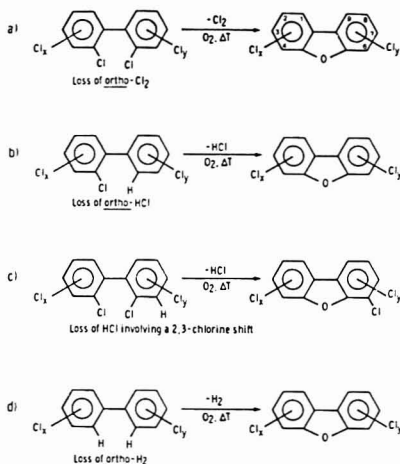


Figure 1. The four reaction routes from which PCDFs are produced from the pyrolysis of PCB congeners.

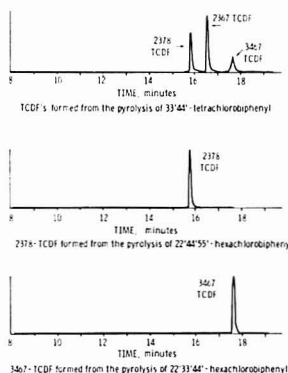


Figure 2. The GC/MS analysis of the TCDFs formed from the pyrolysis of various PCB congeners (SP-2330 capillary column).

Table V. Synthesis Routes for the TrCDF Isomers Used in This Study

TrCDF isomer	primary PCB congener	secondary PCB congener	dechlorination
123	234 <sup>a</sup>	22'346	
124	2356 <sup>a</sup>	22'356	
128	22'3'5		1278
128	22'455'	23'4'5	

<sup>a</sup> Represents those cases in which a single TrCDF isomer was formed from the pyrolysis.

reactions, respectively, also had to be of confirmed validity. Table V lists the TrCDFs which were chlorinated in this study and their routes of synthesis and confirmation. Again those PCB congeners which when pyrolyzed gave a single TrCDF isomer are footnoted. The 128-TrCDF was confirmed by the photolytic dechlorination of 1278-TCDF. Table VI gives the

Table VI. Synthesis Routes for the PenCDF Isomers Used in This Study

PenCDF isomer	primary PCB congener	secondary PCB congener
12367	22'33'44' <sup>a</sup>	22'344'6; 22'33'44'6
12348	22'3455'6 <sup>a</sup>	233'45; 22'3455'
23469	22'3455'	22'3455'
13467	22'3455'	22'344'5'
23468	22'3455'	
23467	233'44'5	22'344'5

<sup>a</sup> Represents those cases in which a single PenCDF isomer was formed from the pyrolysis.

Table VII. Relative Retention Times (RRT) for the 38 TCDFs Listed in Order of Increasing RRT on Both SP-2330 and SE-54 Capillary Columns

TCDF	RRT <sup>a</sup> (SP-2330)	TCDF	RRT <sup>a</sup> (SE-54)
1368	0.550	1368	0.846
1378	0.620	1468	0.870
1379	0.620	2468	0.882
1347	0.630	1347	0.895
1468	0.640	1247	0.897
1247	0.647	1367	0.900
1367	0.652	1378	0.900
1348	0.666	1346	0.902
1346	0.687	1246	0.903
1248	0.690	1348	0.909
1246	0.707	1379	0.909
1268	0.707	1248	0.915
1237	0.713	1268	0.925
1478	0.717	1478	0.929
1369	0.720	1467	0.935
2349	0.754	1237	0.943
1234	0.758	1369	0.944
2468	0.763	2368	0.947
1238	0.763	2467	0.961
1467	0.769	1238	0.962
1236	0.772	1469	0.963
1349	0.800	2349	0.966
1278	0.807	1234	0.968
1267	0.847	1278	0.979
1279	0.850	1267	0.991
1469	0.861	1349	0.991
1249	0.867	1249	1.000
1268	0.867	2368	1.000
2367	0.919	1279	1.002
2347	0.963	2346	1.004
1239	0.965	2347	1.004
1269	0.998	2348	1.004
2378	1.000	2367	1.026
2348	1.011	3467	1.037
2346	1.035	1269	1.038
2367	1.050	1239	1.051
3467	1.135	1236	1.051
1289	1.210	1289	1.103

<sup>a</sup> All RRT based on [<sup>21</sup>Cl]<sub>2</sub>2378-TCDF which by definition = 1.000.

same information for the PenCDFs used in the synthesis of TCDFs. It should be reemphasized that when chlorination or dechlorination was performed as a synthetic route, it was necessary to isolate the starting PCDF from any other PCDFs. Upon chlorination for example, TrCDFs and TCDFs can be formed from dichlorodibenzofurans created during the pyrolysis of the original PCB congener, thus complicating the analysis. Isolation of the PCDF in these cases was effected by HPLC fraction collection as discussed earlier with the purity of the collected fraction being confirmed by GC/MS analysis.

GC Characteristics. The GC retention characteristics are listed for both the SP-2330 and the SE-54 columns in Table

Corrected  
A-9  
201240

VII. These are relative retention times calculated relative to [ $^{37}\text{Cl}_4$ ]2378-TCDF which is assigned a value of 1.000. Of the two columns, the SP-2330 is clearly superior for the resolution of these isomers; however, both columns serve as very useful tools and, when used together, provide the primary means of performing 2378-TCDF isomer specific analyses. There are one or more TCDF isomers coeluting with 2378-TCDF on both columns; however, due to the differences in the respective liquid phases, the coeluting isomers are resolvable on the alternate column. On SE-54, 2378-TCDF coelutes with seven other isomers using a retention time window of 1.000  $\pm$  0.01. On SP-2330 only 1269-TCDF elutes with 2378-TCDF. TCDF analyses were normally conducted on the SE-54 column first due to its ease of handling and higher temperature limit allowing a broader range of PCDFs to be analyzed. If a TCDF was found within the retention time window of 2378-TCDF, then any peaks eluting at relative retention time = 1.035  $\pm$  0.01 were also quantitated since this window contains the 2367-, 3467-, and 1269-TCDFs. The analysis was repeated on SP-2330 and the peaks eluting in the 2378-TCDF window are quantitated. The now completely resolved 2367- and 3467-TCDFs were quantitated, and that sum was subtracted from the sum of 2367-, 3467-, and 1269-TCDFs on SE-54. This difference is the amount of 1269-TCDF present in the sample. This in turn is subtracted from the quantified peak in the 2378-TCDF window of SP-2330, the difference being the amount of 2378-TCDF present in the sample. As a further confirmatory step, a TCDF whose identity is in question may be isolated and subjected to UV photolysis as discussed elsewhere (4). The correct TrCDFs should then be formed as shown in Table IV and thus this technique serves as a valuable tool in TCDF isomer identification.

#### ACKNOWLEDGMENT

We wish to thank S. J. Johnson and D. E. Kirk for their diligent and careful sample preparation, S. L. Mitrosky for performing the purity analyses on the PCBs, and D. Firestone, C. A. Wachtmeister, M. D. Mullins, and J. Pyle for their kind gifts of TCDF and PCB isomer standards. We also wish to thank C. Rappe and J. Graham for the many discussions so valuable to this project.

Registry No. 1234-TCDF, 24478-72-6; 1236-TCDF, 83704-21-6; 1237-TCDF, 83704-22-7; 1238-TCDF, 62615-08-1; 1239-TCDF, 83704-23-8; 1246-TCDF, 71998-73-7; 1247-TCDF, 83719-40-8; 1248-TCDF, 64126-87-0; 1249-TCDF, 83704-24-9; 1267-TCDF, 83704-25-0; 1268-TCDF, 83710-07-0; 1269-TCDF, 70648-18-9; 1278-TCDF, 58802-20-3; 1279-TCDF, 83704-26-1; 1289-TCDF, 70648-22-5; 1346-TCDF, 83704-27-2; 1347-TCDF, 70648-16-7; 1348-TCDF, 64126-87-0; 1349-TCDF, 83704-28-3; 1367-TCDF, 57117-36-9; 1368-TCDF, 71998-72-6; 1369-TCDF, 83690-98-6; 1378-TCDF, 57117-35-8; 1379-TCDF, 64560-17-4; 1467-TCDF, 66794-59-0; 1468-TCDF, 82911-58-8; 1469-TCDF, 70648-19-0; 1478-TCDF, 83704-29-4; 2346-TCDF, 83704-30-7; 2347-TCDF, 83704-31-8; 2348-TCDF, 83704-32-9; 2349-TCDF, 83704-33-0; 2367-TCDF, 57117-39-2; 2368-TCDF, 57117-37-0; 2378-TCDF, 51207-31-9; 2467-TCDF, 57117-38-1; 2468-TCDF, 58802-19-0; 3467-TCDF, 57117-40-5; 123-TCDF, 83636-47-9; 124-TCDF, 24478-73-7; 128-TCDF, 83704-34-1; 238-TCDF, 57117-32-5; 12367-PenCDF, 57117-42-7; 12348-PenCDF, 67517-48-0; 23469-PenCDF, 83704-35-2; 13467-PenCDF, 83704-36-3; 23468-PenCDF,

67481-22-5; 23467-PenCDF, 57117-43-8; 126-TrCDF, 64560-15-2; 127-TrCDF, 83704-37-4; 129-TrCDF, 83704-38-5; 134-TrCDF, 82911-61-3; 136-TrCDF, 83704-39-6; 137-TrCDF, 64560-16-3; 138-TrCDF, 76621-12-0; 139-TrCDF, 83704-40-9; 146-TrCDF, 82911-60-2; 147-TrCDF, 83704-41-0; 148-TrCDF, 64560-14-1; 149-TrCDF, 70648-13-4; 234-TCDF, 57117-34-7; 236-TrCDF, 57117-33-6; 237-TrCDF, 58802-17-8; 239-TrCDF, 58802-18-9; 246-TrCDF, 58802-14-5; 247-TrCDF, 83704-42-1; 248-TrCDF, 54589-71-8; 249-TrCDF, 82911-59-9; 346-TrCDF, 83704-43-2; 347-TrCDF, 83704-44-3; 348-TrCDF, 83704-45-4; 349-TrCDF, 83704-46-5; 12346-PenCDF, 83704-47-6; 12347-PenCDF, 83704-48-7; 12349-PenCDF, 83704-49-8; 12467-PenCDF, 83704-50-1; 12468-PenCDF, 69698-57-3; 12469-PenCDF, 70648-24-7; 12478-PenCDF, 58802-15-6; 12479-PenCDF, 71998-74-8; 12368-PenCDF, 83704-51-2; 12369-PenCDF, 83704-52-3; 12378-PenCDF, 57117-41-6; 12379-PenCDF, 83704-53-4; 12389-PenCDF, 83704-54-5; 12489-PenCDF, 70648-23-6; 13468-PenCDF, 83704-55-6; 13469-PenCDF, 70648-15-6; 13478-PenCDF, 58802-16-7; 13479-PenCDF, 70648-20-3; 13489-PenCDF, 70872-82-1; 23478-PenCDF, 57117-31-4; 23479-PenCDF, 70648-21-4; 12678-PenCDF, 69433-00-7; 2,2',3,3'-tetrachlorobiphenyl, 38444-93-8; 2,2',3,4'-tetrachlorobiphenyl, 36559-22-5; 2,2',3,5'-tetrachlorobiphenyl, 41464-39-5; 2,2',4,4'-tetrachlorobiphenyl, 2437-79-8; 2,2',4,5'-tetrachlorobiphenyl, 41464-40-8; 2,2',5,5'-tetrachlorobiphenyl, 35693-99-3; 2,3,4,4'-tetrachlorobiphenyl, 33025-41-1; 2,3,3',4'-tetrachlorobiphenyl, 41464-43-1; 2,3,4,5'-tetrachlorobiphenyl, 33284-53-6; 2,3,4,4'-tetrachlorobiphenyl, 32598-10-0; 2,3',4,5'-tetrachlorobiphenyl, 32598-11-1; 2,3',5,5'-tetrachlorobiphenyl, 41464-42-0; 3,3',4,4'-tetrachlorobiphenyl, 32598-13-3; 2,2',3,3',6'-pentachlorobiphenyl, 52663-60-2; 2,2',3,5,6'-pentachlorobiphenyl, 73575-56-1; 2,2',3,4,6'-pentachlorobiphenyl, 55215-17-3; 2,2',4,4',6'-pentachlorobiphenyl, 39485-83-1; 2,2',4,5,6'-pentachlorobiphenyl, 37680-73-2; 2,2',4,5',6'-pentachlorobiphenyl, 60145-21-3; 2,2',4,6,6'-pentachlorobiphenyl, 56558-16-8; 2,3,4,5,6'-pentachlorobiphenyl, 18259-05-7; 2,3,3',4,5'-pentachlorobiphenyl, 70424-69-0; 2,3',4,4',6'-pentachlorobiphenyl, 56558-17-9; 2,3',4,5,6'-pentachlorobiphenyl, 56558-18-0; 2,2',3,3',4,4'-hexachlorobiphenyl, 38380-07-3; 2,2',3,3',4,5'-hexachlorobiphenyl, 55215-18-4; 2,2',3,3',4,6'-hexachlorobiphenyl, 38380-05-1; 2,2',3,3',5,6'-hexachlorobiphenyl, 52744-13-5; 2,2',3,3',6,6'-hexachlorobiphenyl, 38411-22-2; 2,2',3,4,4',5'-hexachlorobiphenyl, 35694-06-5; 2,2',3,4,4',6'-hexachlorobiphenyl, 56030-56-9; 2,2',3,4,5,5'-hexachlorobiphenyl, 52712-04-6; 2,2',3,4,5,6'-hexachlorobiphenyl, 68194-15-0; 2,2',3,4,5,6'-hexachlorobiphenyl, 68194-13-8; 2,2',3,5,5',6'-hexachlorobiphenyl, 52663-63-5; 2,2',4,4',5,5'-hexachlorobiphenyl, 35065-27-1; 2,2',4,4',5,6'-hexachlorobiphenyl, 60145-22-4; 2,2',4,4',6,6'-hexachlorobiphenyl, 33979-03-2; 2,2',3,4,5,5',6'-heptachlorobiphenyl, 52712-05-7; 2,2',3,3',4,4',6'-heptachlorodiphenyl, 52663-71-5; 2,2',3,4,4',5'-hexachlorobiphenyl, 35065-28-2; 2,3,3',4,4',5'-hexachlorobiphenyl, 38380-08-4; 2,3,4-trichlorobiphenyl, 55702-46-0; 2,3,5,6-tetrachlorobiphenyl, 33284-54-7.

#### LITERATURE CITED

- (1) Rappe, C. In "Halogenated Biphenyls, Terphenyls, Naphthalenes, Dibenzodioxins and Related Products"; Kimbrough, R. D., Ed.; Elsevier/North Holland Biomedical Press: New York, 1980; pp 48-68.
- (2) Buser, H. R.; Rappe, C. *Chemosphere* **1979**, *3*, 157-174.
- (3) Buser, H. R.; Bosshardt, H. *Chemosphere* **1978**, *1*, 109-119.
- (4) Mazer, T.; Hieman, F. D. *Chemosphere* **1982**, *7*, 651-661.
- (5) Hicks, O., Monsanto Co., St. Louis, MO, personal communication, 1981.
- (6) Gara, A.; Andersson, K.; Nilsson, C. A.; Norström, A. *Chemosphere* **1981**, *4*, 365-380.
- (7) Rappe, C. University of Umeå, S-90187 Umeå, Sweden, personal communication, 1981.

RECEIVED for review July 2, 1982. Accepted October 20, 1982.

# Selective Concentration of Aromatic Bases from Water with a Resin Adsorbent

Harold A. Stuber and Jerry A. Leenheer\*

U.S. Geological Survey, P.O. Box 25046, Mail Stop 407, Denver Federal Center, Denver, Colorado 80225

Aromatic bases are concentrated from water on columns of a resin adsorbent and recovered by aqueous-acid elution. The degree of concentration attainable depends on the ratio of the capacity factor ( $k$ ) of the neutral form of the amine to that of the ionized form. Capacity factors of ionic forms of amines on XAD-8 resin (a methacrylic ester polymer) are greater than zero, ranging from 20 to 250 times lower than those of their neutral forms; they increase with increasing hydrophobicity of the amine. Thus, desorption by acid is an elution ( $k$  during desorption  $> 0$ ) rather than a displacement ( $k$  during desorption = 0) process. The degree of concentration attainable on XAD-8 resin varies with the hydrophobicity of the amine, being limited for hydrophilic solutes (for example, pyridine) by small neutral-form  $k$ 's, reaching a maximum for amines of intermediate hydrophobicity (for example, quinoline), and decreasing for more hydrophobic solutes (for example, acridine) because of their large ionic-form  $k$ 's.

Two challenges in the analysis of organic solutes in natural waters and wastewaters are (1) the need to concentrate organic species without losses and (2) the need to separate complex mixtures into homogenous fractions. The use of column-adsorption methods to concentrate organic solutes from water has increased, because these methods are adaptable for processing large volumes of water and because they can eliminate the need for an evaporation step. To fractionate the concentrated organic solutes into homogenous groups, it usually is necessary to perform an additional chromatographic separation or an acid/base/neutral solvent extraction. New, column-based approaches that directly yield concentrated, homogenous fractions of organic-compound classes in a single operation would be valuable for both analytical and bioassay studies. This paper presents the results of a study of an approach to the "selective concentration" from water of one important class of organic compounds, the aromatic bases.

Aromatic bases, many of which are mutagens (1), occur in coal liquids (2), shale oil (3), and recent lake (4) and marine (5) sediments. Base fractions of both municipal (6) and synthetic fuels (7) wastewaters have been shown to contain the largest proportion of mutagens in these waters. We have studied the selective concentration of organic bases from water by adsorption on columns of hydrophobic adsorbents, followed by elution with aqueous acid; this concentration results in both enrichment and isolation from neutral and acidic organic solutes and salts. The technique has been used to isolate pure, aromatic-amine fractions from oil-shale wastewaters (8), while the analogous approach for organic acids (desorption with aqueous base) has been used for isolation of humic and fulvic acids from natural surface waters (9) and seawater (10) and for concentration of fatty acids (11). Leenheer (12) has developed methods, based on resin-adsorbent columns and aqueous reagents, to fractionate organic solutes in water into hydrophilic and hydrophobic acids, bases, and neutrals.

For the optimum degree of concentration with chromatographic columns, the adsorptive capacity of the sorbent needs to be maximum during the collection phase and minimum during desorption. Displacement desorption (where the capacity factor,  $k$ , of the solute in the eluting solvent is zero) produces the greatest degree of concentration (13). The concentration factor attainable for a solute by liquid chromatography (LC) will be equal to the ratio of the solute's capacity factor during adsorption ( $k_a$ ), to its capacity factor during desorption ( $k_d$ ), in the absence of band spreading (14). Therefore, to optimize the selective concentration of aromatic bases using a resin-adsorbent column, conditions need to maximize the  $k$  of the neutral species and minimize the  $k$  of the ionic form.

This study was performed to develop a compound-class fractionation sequence using aqueous eluting reagents such that organic carbon determinations can be used to monitor the fractionation. The use of organic solvents in fractionation sequences generally obviates or limits the use of organic carbon determinations. The fractionation procedures developed in this report have been applied to the analyses of organic solutes in oil shale retort water (15). The various advantages, disadvantages, and selectivities of a resin-adsorption, aqueous-elution organic-solute fractionation scheme vs. organic-solvent extraction or solvent elution fractionation schemes are discussed in a number of previous studies (8, 12, 15). The specific purposes of this study were (1) to assess the potential and limitations of the aqueous-elution, selective-concentration approach for isolating aromatic bases from water and (2) to identify the factors that control the concentration process, and, therefore, that are important in designing and optimizing selective concentrations on adsorbent resins.

## EXPERIMENTAL SECTION

**Variation of Capacity Factors of Aromatic Amines with pH.** *Preparation of Solutions:* Solutions of pyridine, 2-methylpyridine, quinoline, 2-methylquinoline, isoquinoline, 2,4,6-trimethylpyridine, and acridine were prepared by directly dissolving weighed quantities of the amines in water to obtain 10.0 mg/L of the first six amines listed and 1.0 mg/L of acridine.  $K_3PO_4$  (Baker, Reagent) was added (from a 1.0 M stock solution) so the final solution would be 0.010 M in  $K_3PO_4$ . This solution was titrated with 1.0 N HCl to attain the desired pH. The volume of HCl added was recorded and the concentration of  $Cl^-$  in the 2-L solution was calculated. Solid NaCl was then added to yield a 0.050 M solution with respect to  $Cl^-$ .

*Preparation of Resin:* Amberlite XAD-8 resin was obtained as 20-50 mesh beads from Rohm and Haas and cleaned for 24 h with four successive washes of 0.1 N NaOH, which removes a large volume of base-soluble organic carbon. The resin was sequentially Soxhlet-extracted with acetonitrile, diethyl ether, and methanol. The resin was ground in a mortar and pestle and wet-seived with distilled water and stainless-steel sieves to obtain particles in the 250-500- $\mu$ m range. The beads obtained this way were packed in a glass column and rinsed with 50 bed volumes of distilled water to remove methanol. Clean resin was stored in water.

*Columns and Conditions:* Glenco 3500 glass columns, 0.6  $\times$  15.0 cm, were packed by pouring an aqueous slurry of 250-500-

$\mu$ m XAD-8 and rinsed with 100 mL of 0.1 N NaOH, distilled water, 100 mL 0.1 N HCl, and, finally, 100 mL of distilled water.

Solutions were pumped into the columns at a flow rate of 1.0 mL/min using a Fluid Metering Inc., Model RP-SY pump and all Teflon connecting tubing, and fraction collection was done automatically. These experiments were conducted at room temperature, 20–22 °C. Void volumes were determined by measuring the breakthrough of 0.10 N NaCl using a Wescan Model 212 conductivity detector attached directly to the bottom fitting of the column.

**Analysis of Fractions:** Amines were determined by HPLC (high-performance liquid chromatography). A 25 cm  $\times$  4 mm i.d. Altex Ultrasphere Octyl (5- $\mu$ m) column was used with a mobile phase of 70% CH<sub>3</sub>OH, 30% 0.05 N sodium phosphate buffer, pH 7. A flow rate of 1.0 mL/min was used and detection was by UV absorption at 250 nm, 0.1 AUFS (absorbance units full-scale). Quantitation of the amines was by peak height comparison with standards.

**Sorption Isotherms of Aromatic Base Cations.** Stock solutions of acridine and 5,6-benzoquinoline were prepared by dissolving the solid reagent in 0.1 N HCl, followed by filtration through Gelman type AE glass-fiber filters and dilution with 0.1 N HCl to yield solutions with concentrations of 1000 mg/L. These were diluted with 0.1 N HCl to yield solutions with concentrations ranging from 1.0 to 800 mg/L. Aliquots (20.0 mL) of each of these solutions were added to pairs of 50-mL flasks, so that each flask contained the initial concentration of each amine. Approximately 3 g of suction-filtered, moist XAD-8 resin was weighed into each of the flasks; then they were stoppered and mechanically shaken for 72 h at 21 °C.

After 72 h, the solution in each flask was decanted, and the beads were transferred to Al weighing dishes. The beads were dried overnight at 80 °C and weighed. The UV absorption of acridine solutions was measured at 255.5 nm using a Cary 114 UV spectrophotometer.

The UV absorption of 5,6-benzoquinoline solutions was measured at 227 nm. Equilibrium concentration of acridine and 5,6-benzoquinoline were determined from calibration curves obtained for each solute in 0.1 N HCl. The initial concentration of the solute ( $C_i$ ), the final concentration of the solute ( $C_f$ ), and the mass of the beads were used to calculate the distribution coefficient ( $D$ ).

**Capacity Factors on Other Adsorbents.** Capacity factors at pH 10.5 and 1.7 were measured exactly as on XAD-8 resin, that is, 0.6  $\times$  15 cm columns, flow rate of 1.0 mL/min, and 10.0 mg/L concentrations (except acridine, 1.0 mg/L). Amberlite XAD-2 resin was obtained from Mallinckrodt, Inc., as 20–50-mesh macroporous beads, that were sequentially Soxhlet extracted with acetonitrile, diethyl ether, and methanol. The beads were ground and sieved to obtain particles in the 250–500- $\mu$ m bead range. Carbo-pack B is a graphitized carbon adsorbent sold for gas chromatography by Supelco, Inc., and was obtained as 250–330- $\mu$ m particles. Enzacryl K-1 gel (coarse) was obtained from Aldrich Chemical Co. Bio-Gel P-2, a copolymer of acrylamide and *N,N'*-methylenebis(acrylamide), was obtained as 50–100 mesh beads (150–300- $\mu$ m wet diameter) from Bio-Rad Laboratories. Cellulose N-1, a nonionic cellulose gel, also was obtained from Bio-Rad Laboratories. Duolite A-7 resin was obtained from Diamond Shamrock, Inc., and ground and sieved to 250–500  $\mu$ m to obtain beads in the 250–500- $\mu$ m (wet diameter) range. The resin was Soxhlet-extracted in methanol.

**Selective Concentration of Aromatic Bases on XAD-8 Resin.** One-liter samples with concentrations of 10.0 mg/L were pumped through 0.6  $\times$  15 cm columns of 100–250- $\mu$ m XAD-8 resin at a flow rate of 1.0 mL/min (except acridine and 1-aminoanthracene, 1.0 mg/L). The columns were then reverse-eluted with 0.1 N HCl at a flow rate of 0.4 mL/min. Fractions of 1.0 mL were collected (10 mL for acridine and for 1-aminoanthracene) and analyzed by HPLC. Desorption curves were constructed; the maximum concentration factor was determined as the ratio of the concentration in the most enriched fraction to the initial concentration.

## RESULTS AND DISCUSSION

Results of this study are presented in the following order: First, the effect of pH on the adsorption of aromatic bases

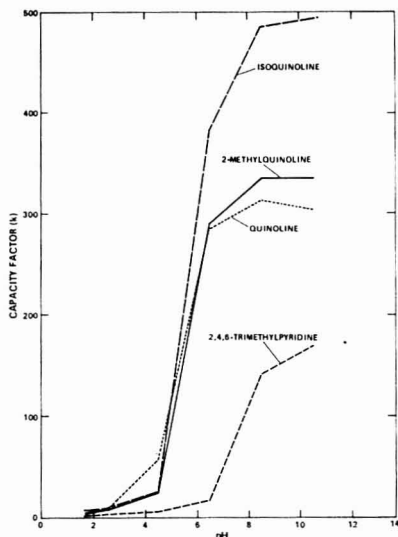


Figure 1. Capacity factors ( $k$ ) of quinolines and 2,4,6-trimethylpyridine on XAD-8 resin as function of pH.

on a resin adsorbent (XAD-8) is discussed, the variation of  $k$  with pH being fundamental to the concentration process. Second, a variety of adsorbents are evaluated for their suitability for the concentration of aromatic bases. Third, the concentrations of a series of bases are determined on XAD-8 resin using conditions chosen on the basis of the preceding results. The variation in the attainable degree of concentration with the hydrophobicity of the amine is described, as are the origins of the limitations to this approach for very hydrophilic and very hydrophobic solutes. Finally, an approach is presented that yields improved degrees of concentration for very hydrophobic solutes by using a chargeable adsorbent.

**Variation of Capacity Factors of Aromatic Bases on a Resin Adsorbent with pH.** It is known that hydrophobic effects are responsible for the adsorption of uncharged organic solutes from water onto hydrophobic adsorbents (16–18). In accordance with this known fact, the capacity factors of organic solutes on XAD-8 resin and other resin adsorbents have been closely correlated with their aqueous solubilities (18). It should be expected that the adsorptive capacity of XAD-8 resin for the uncharged forms of aromatic amines will increase with increasing hydrophobicity of the amine.

Aqueous, frontal-chromatographic-breakthrough curves of six aromatic bases on XAD-8 resin at six pH values from 1.7 to 10.5 were used to determine capacity factors, using the volume of half break-through of each base. The observed variations in  $k$  with pH are illustrated in Figure 1. For the remainder of this discussion, neutral-form capacity factors will be defined as  $k_0$  and ionic-form capacity factors as  $k_i$ .

It is apparent from the data in Figure 1 that ionization greatly decreases the capacity factors of amines on XAD-8 resin; therefore, it should be possible to concentrate these bases on XAD-8 resin by adsorption at pH 8–10 and elution at pH 1–4. The most important result is that capacity factors do not become zero at low pH but have values that increase with increasing hydrophobicity of the amine. It is notable that  $k_i$  of the amines increases in exactly the same order as  $k_0$  of the



**Table I. Capacity Factors of Acridine at Acid pH on XAD-8 Resin**

solution	pH	capacity factor ( <i>k</i> )
0.001 N HCl	3.0	166
buffer <sup>a</sup>	2.5	100
0.01 N HCl	2.0	75
buffer <sup>a</sup>	1.7	66
0.10 N HCl	1.0	21
1.0 N HCl	0	17

<sup>a</sup> Buffer described in "Experimental Section".

amines, indicating that hydrophobic effects also control adsorption of the ionic species. The finite  $k_1$ 's mean that desorption of amines from XAD-8 resin using aqueous acid will not be a displacement process ( $k_1 = 0$ ) but rather an elution process ( $k_1 > 0$ ). This is an important consideration in designing and optimizing a selective concentration procedure. The large  $k_1$  of the more hydrophobic bases (for example, acridine,  $k_1 = 17$ ; 5,6-benzoquinoline,  $k_1 = 37$ ) means that a large volume of aqueous acid may be required to effectively recover very hydrophobic solutes from a resin column, and this will limit the efficiency of the concentration.

It is advantageous to create conditions that minimize  $k_1$  during desorption in a column-concentration process to the most minimal value. Equations predicting the variation of  $k$  with pH for ionizable solutes on hydrophobic adsorbents have been presented by Horvath (19) and Pietrzyk (20). These equations predict  $k$  at any selected pH, using  $k$  values for the fully charged and uncharged forms of the molecule and the molecules'  $pK_a$ . The observed variation of  $k$  with pH for six amines on XAD-8 resin (Figure 1) agrees with the predictions of the equations of Horvath and Pietrzyk, except at pH values less than 2.6. At pH values less than 2.6,  $k_1$  values decrease much more rapidly than the equations can predict. The discrepancy is large and its cause is not certain, but one explanation might be that the resin itself becomes protonated at low pH, repelling amine cations in a type of charge exclusion. Although it was not expected, a substantial decrease in  $k_1$  for amines is observed when pH is decreased from 2.0 to 1.0. The decrease in  $k_1$  for acridine from pH 3.0 to pH 0 is shown in Table I. These results were used to select 0.1 N HCl as a suitable eluting reagent for further work on resin adsorbents in this study. HCl concentrations greater than 0.1 N did not produce large decreases in capacity factors.

A suitable pH for adsorption of most unsubstituted N-heterocycles and primary aromatic amines can be as low as 8.0, with little further gain achieved, after the pH is 2 units more than the  $pK_a$  of the base.

An important question about the validity of the selective-concentration approach concerns the nature of organic-ion adsorption on hydrophobic sorbents: If the capacity factor (and distribution coefficient) of an organic ion is significantly

concentration dependent, increasing greatly with decreasing concentration, and perhaps approaching  $k_0$  at minimal concentrations, the selective-concentration approach would not be valid for samples containing trace concentrations of constituents. If mutual charge repulsion were an important factor in the small  $k_1$  values for amine cations on XAD-8 resin at 10.0 mg/L, then  $k_1$  at 200  $\mu$ g/L might be much larger, and the degree of concentration attainable much less. Adsorption isotherms of acridine and 5,6-benzoquinoline (on XAD-8 resin in 0.1 N HCl) were found to be nearly linear at concentrations ranging from 200  $\mu$ g/L to 10 mg/L, indicating nearly constant distribution coefficients over this concentration range. These results are evidence that the selective-concentration approach will be valid for samples containing trace concentrations of constituents, with acceptance of some risk of extrapolation and the need to verify individual procedures. Previously published sorption isotherms of organic cations on resin adsorbents (21, 22) were obtained at very large equilibrium concentrations, and their nonlinearity at larger concentrations may be the result of mutual charge repulsion at the resin surfaces.

**A Survey of Adsorbents for Selective Concentration of Aromatic Amines.** Six adsorbents were evaluated for their potential for selective concentration of aromatic bases by measuring  $k_0$  and  $k_1$  of amines on these adsorbents under identical conditions. Results are shown in Table II. Of the adsorbents evaluated here, only the XAD-8 and XAD-2 resins show large enough ratios of  $k_0$  and  $k_1$  to have potential for selective concentration of lower molecular weight N-heterocycles. For the quinolines and 2,4,6-trimethylpyridine, the ratios of  $k_0$  to  $k_1$  under these conditions are in the range of 50:1 to 75:1 on both XAD-8 and XAD-2 resins. The other pyridines have larger ratios of  $k_0$  to  $k_1$  on XAD-2 resin than on XAD-8 resin, and under identical conditions, the XAD-2 resin yields greater concentration factors for pyridine than the XAD-8 resin (8). The greater  $k_1$  of acridine and more hydrophobic solutes on XAD-2 resin result in less selective concentration of very hydrophobic solutes than on the XAD-8 resin (8). A surprising result is the very small ratio of  $k_0$  to  $k_1$  on Carboxpack B, a graphitized carbon adsorbent. These small ratios are not because of anomalous  $k_0$ 's, that are similar on a per unit surface area basis to those on XAD-2 and XAD-8 resins; these ratios are small because of the anomalously large  $k_1$ 's of protonated amines. The ratios of  $k_0$  to  $k_1$  on Carboxpack B range from 2.1:1 to 5.6:1 in contrast to a typical value of 60:1 on XAD-8 and XAD-2 resins. The graphitized carbon is, therefore, not an effective adsorbent for selective concentration of aromatic amines. A possible explanation of the large  $k_1$  values of protonated aromatic amines is that a charge-transfer interaction occurs between the electron-poor heterocyclic cation and the electron-rich graphite surface. A parallel orientation of the rings would allow good  $\pi$ -orbital overlap. Although XAD-2 resin also has aromatic rings, they are isolated and do not form an extended  $\pi$  system, so XAD-2 resin

**Table II. Capacity Factors of Aromatic Amines on Six Adsorbents at pH 1.7 and 10.5**

aromatic amine	XAD-2 resin		Carboxpack-B		XAD-8		Enzacryl K-1		Biogel P-2		Cellulose N-1	
	pH 1.7	pH 10.5	pH 1.7	pH 10.5	pH 1.7	pH 10.5	pH 1.7	pH 10.5	pH 1.7	pH 10.5	pH 1.7	pH 10.5
pyridine	0.7	87	5.3	30	0.9	15	0.0	1	0	1	0	1
2-methylpyridine	1.0	103	20	103	1.2	36	0.0	1	0	1	0	1
quinoline	13.2	615	163	335	4.7	305	0.2	2.3	0	2.4	0	1.3
2-methylquinoline	13.6	645	163	345	5.1	335	0.2	2.6	0	2.5	0	1.3
isoquinoline	18.2	1390	340	810	7.2	495	0.2	3.0	0	2.5	0	1.3
2,4,6-trimethylpyridine	8.2	500	84	200	2.4	170	0.2	1	0		0	
acridine	275	>3000	340	>1000	66	>900	0.5	16	0	7.0	0	3.7

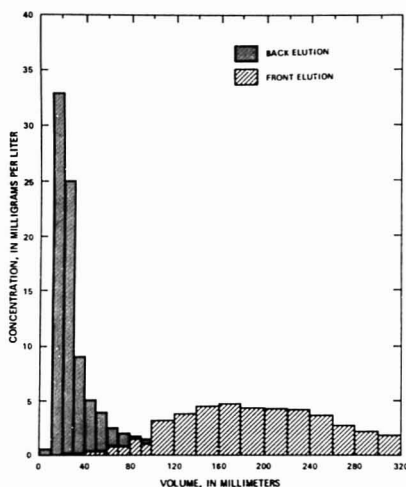


Figure 2. Comparison of front- and back-elution of acridine on 20-50 mesh XAD-8 resin ( $30 \times 0.9$  cm columns) using 0.1 N HCl. Acridine concentrated on identical columns from 1.0-L samples with acridine concentrations of 1.0 mg/L.

might have a much lesser charge-transfer forming capacity.

The more hydrophilic adsorbents (Enzacryl K-1, Biogel P-2, and Cellulose N-1) were evaluated in the anticipation that they would be useful for selective concentrations of very hydrophobic amines. Their adsorptive capacities for amines at pH 10.5 are too minimal, even for acridine, to be considered useful, although a maximum concentration factor of 28:1 was obtainable on a 1.0 mg/L acridine solution using a column of Enzacryl K-1.

Because bonded-silica HPLC packings are not very stable to alkaline and acid, and because the chromatographic response of amines on these adsorbents at acid pH shows that significant, direct interactions with underivatized silica occurs, these packings were not evaluated for selective concentration.

**Reverse Elution To Decrease Band Spreading.** The advantage of reverse elution in the selective concentration of acridine on a column that produces extensive band spreading is shown in Figure 2. Two 1.0-L samples were passed through identical columns of 20-50 mesh XAD-8 resin. One column was eluted with 0.1 N HCl in the forward direction; the other column was reverse eluted with the same reagent.

A significantly retained solute will accumulate in a narrow band at the top of the column during the collection process. If the column is then eluted in the same (forward) direction, the solute must pass through the entire column to be recovered. This can result in significant band spreading (decreasing the concentration factor), especially when  $k_d$  is large. However, if the column is eluted in the opposite (reverse) direction, the solute is recovered directly from the saturated part of the column, with little decrease in concentration because of band spreading. Reverse elution is important for solutes that saturated a large part of the column length during adsorption. In all of the following work, reverse elution was used to obtain the optimum degree of concentration.

**Concentration Factors Attainable as a Function of Amine Hydrophobicity.** To evaluate the degree of concentrations attainable on XAD-8 resin, solutions of amines (at concentrations of 10.0 mg/L) were passed through  $0.6 \times$

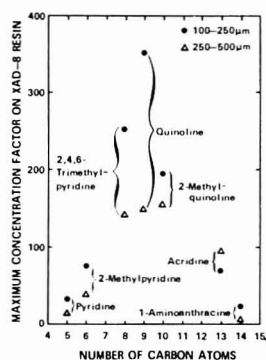


Figure 3. Maximum concentration factors obtained for aromatic bases on 250-500- $\mu$ m XAD-8 resin ( $\Delta$ ) and 100-250- $\mu$ m XAD-8 resin ( $\bullet$ ), under identical conditions. Solutions of 1.0 L with concentrations of 10.0 mg/L were concentrated at  $0.6 \times 15$  cm columns.

15 cm columns, after which the columns were reverse-eluted with 0.1 N HCl. Recovery of the amines was followed by collecting and analyzing fractions of the 0.1 N HCl effluent, yielding a desorption curve. Desorption bands were observed to be narrow for solutes with small ionic  $k'$ s and broad for solutes with large ionic  $k'$ s. Therefore, the volume of concentrate that needs to be collected varies with the hydrophobicity of the amine. This is a problem for experimental design and for choosing a standard procedure for measuring the final concentration obtained for an amine. One approach would be to pool fractions that contained, for example, 90% of the recovered solute and measure the final concentration in this volume. A more convenient measure of the degree of concentration is the concentration factor obtained at the peak of the desorption curve. This approach was used to obtain the data in Figure 3.

The data in Figure 3 show the maximum concentration factor obtained for seven amines on columns of XAD-8 resin. The concentration factors are small for the most hydrophilic solutes (pyridine and 2-methylpyridine), increase to a maximum for compounds of intermediate hydrophobicity (quinolines), and then decrease for the most hydrophilic solutes (acridine and 1-aminoanthracene). The greater concentration factors achieved using smaller resin beads are a predictable result of increased column efficiency. The attainable degree of concentration varies in a regular manner with the nature of the amine. The limitation of the method for the most hydrophilic solutes results from their limited sorptive tendency as neutral species. Only a fraction of the pyridine in the 1.0-L samples was retained on the resin; although this was recovered in a small volume, a small concentration factor results. The limitation for the most hydrophilic solutes results from their large ionic-capacity factors. Thus, 1-aminoanthracene was entirely retained on the resin but desorbed in a very broad band; only a 4-fold concentration is achieved on the 250-500- $\mu$ m particle-size resin.

The maximum concentration factor for a solute on an XAD-8 resin is correlated with the solute's ratio of  $k_0$  to  $k_1$ , measured independently. This relationship is true for pyridines and quinolines; however, the ratio of  $k_0$  to  $k_1$  could not be calculated for acridine and 1-aminoanthracene, because most of their concentrations are retained at pH 10.5 for a practical measurement of  $k_0$  by frontal chromatography. A maximum ratio of  $k_0$  to  $k_1$  at intermediate hydrophobicities probably corresponds to the maximum in the observed con-

Table III. Capacity Factors of Aromatic Amines on a Weak-Base, Anion-Exchange Resin (Duolite A-7)

aromatic amine	Duolite A-7	
	$k_0$ (pH 10.5)	$k_1$ (pH 1.7)
pyridine	3.5	>1
2-methylpyridine	8.1	>1
quinoline	63	>1
2-methylquinoline	63	>1
isoquinoline	99	>1
2,4,6-trimethylpyridine	19.5	>1
acridine	>550	~1

centration factors, but additional data are needed to verify this hypothesis.

Results of the concentration of amines on XAD-2 resin and a 10- $\mu$ m styrene-divinylbenzene adsorbent have shown that an optimum in the concentration factor occurs at solutes of lesser hydrophobicity than on XAD-8 resin. The amine hydrophobicity that yields the greatest degree of concentration is different for different adsorbents; the more hydrophilic the adsorbent, the more hydrophobic the amine will be that is optimally concentrated.

**Concentration of Very Hydrophobic Amines with a Chargeable Adsorbent.** For an effective concentration of an amine that is as hydrophobic as acridine, Duolite A-7 weak-base, anion-exchange resin was evaluated. The concept involved is that the charge the resin acquires at low pH can repel the amine cations, resulting in small  $k_1$ 's and large concentration factors for larger amines. Table III shows  $k_0$  and  $k_1$  values of amines on Duolite A-7 resin, a secondary-amine functional group, phenolformaldehyde polymer. Because  $k_0$  values are exceedingly small, this resin should be quite effective for higher molecular-weight amines. In fact, when identical 2.0-L samples of South Platte River water spiked with 10  $\mu$ g/L of acridine were concentrated on columns of XAD-8 resin and Duolite A-7 resin, the maximum concentration factor for acridine was 80 on XAD-8 resin but 540 on Duolite A-7 (8). The Duolite A-7 resin appears far more effective for acridine than XAD-8 resin, although XAD-8 resin was clearly more effective for pyridines and quinolines. Our experience with this approach has been that, whereas Duolite A-7 resin is more effective than XAD-8 resin for concentrating

hydrophobic species, it is not as selective as XAD-8 resin. For example, the concentrate obtained from the spiked river water using Duolite A-7 resin contained much colored "humic" material, while the concentrate obtained using XAD-8 resin contained only acridine by HPLC analysis. Selectivity is minimal with a weak-base, anion-exchange resin, because the capacity factors of many solutes change when the resin becomes charged by an acid, while on XAD-8 resin, only basic solutes are desorbed by acid elution. The use of a chargeable adsorbent to repel ions of like charge should be applicable to selective concentration of species too hydrophobic for concentration on neutral adsorbents.

**Registry No.** Amberlite XAD-8, 11104-40-8; pyridine, 110-86-1; 2-methylpyridine, 109-06-8; quinoline, 91-22-5; 2-methylquinoline, 91-63-4; 2,4,6-trimethylpyridine, 108-75-8; acridine, 260-94-6; isoquinoline, 119-65-3; H<sub>2</sub>O, 7732-18-5.

#### LITERATURE CITED

- (1) Yamasaki, E.; Ames, B. N. *Proc. Natl. Acad. Sci. U.S.A.* **1977**, *74*, 3555-3570.
- (2) Schiller, J. E. *Anal. Chem.* **1977**, *49*, 2292-2294.
- (3) Brown, D. G.; Earnshaw, D. G.; McDonald, F. R.; Jensen, H. B. *Anal. Chem.* **1970**, *42*, 146-151.
- (4) Wakeham, S. G. *J. Environ. Sci. Technol.* **1979**, *13*, 1118-1123.
- (5) Blumer, M.; Dorsey, T.; Sassa, J. *Science* **1977**, *195*, 283-285.
- (6) Rappaport, S. M.; Richard, M. G.; Holstein, M. C.; Talcott, R. E. *J. Environ. Sci. Technol.* **1979**, *13*, 957-961.
- (7) Rubin, I. B.; Guerin, M. R.; Hardigree, A. A.; Epler, J. L. *Environ. Res.* **1978**, *12*, 358-370.
- (8) Stuber, H. A. Ph.D. Thesis, University of Colorado, 1980.
- (9) Thurman, E. M.; Malcolm, R. L. *Environ. Sci. Technol.* **1981**, *15*, 463-466.
- (10) Steumer, D. H.; Harvey, G. R. *Deep Sea Res.* **1977**, *24*, 303-309.
- (11) Thurman, E. M.; Aiken, G. R.; Malcolm, R. L. Proceedings, Fourth Joint Conference on Sensing of Environmental Pollutants, American Chemical Society, 1978; pp 630-634.
- (12) Leenheer, J. A. *Environ. Sci. Technol.* **1981**, *15*, 578-587.
- (13) Huber, J. F. K.; Becker, R. R. *J. Chromatogr.* **1977**, *142*, 765-777.
- (14) Lankela, J.; Poppe, H. *J. Chromatogr.* **1978**, *149*, 587-598.
- (15) Leenheer, J. A.; Noyes, T. I.; Stuber, H. A. *Environ. Sci. Technol.*, in press.
- (16) Karger, B. L.; Grant, J. R.; Hartkopf, A.; Wiener, P. H. *J. Chromatogr.* **1978**, *128*, 67-78.
- (17) Locke, D. G. *J. Chromatogr. Sci.* **1974**, *12*, 433.
- (18) Thurman, E. M.; Malcolm, R. L.; Aiken, G. R. *Anal. Chem.* **1978**, *50*, 775-779.
- (19) Horvath, C.; Melander, W.; Molnar, I. *Anal. Chem.* **1977**, *49*, 142-154.
- (20) Pietrzyk, D. J.; Chu, C. H. *Anal. Chem.* **1977**, *49*, 757-764.
- (21) Cantwell, F. F.; Su Poon *Anal. Chem.* **1979**, *51*, 623-632.
- (22) Lundgren, J. L.; Schitt, A. A. *Anal. Chem.* **1977**, *49*, 974-980.

RECEIVED for review July 14, 1982. Accepted October 19, 1982.

# Comparison of Priority Pollutant Response Factors for Triple and Single Quadrupole Mass Spectrometers

A. D. Sauter\* and L. D. Betowski

U.S. Environmental Protection Agency, Environmental Monitoring Systems Laboratory, Las Vegas, Nevada 89114

J. M. Ballard

Lockheed Engineering and Management Services Company, Inc., P.O. Box 15027, Las Vegas, Nevada 89114

Seventy-four percent of the electron impact GC/MS response factors (RF) determined on a triple quadrupole mass spectrometer for 53 extractable priority pollutants were found to be within  $\pm 15\%$  of values determined in an independent interlaboratory single quadrupole GC/MS study. Furthermore, the RF values were shown to be independent of whether quadrupole Q1 or quadrupole Q3 was scanned. The precision of RF determinations for 53 extractable priority pollutants (mean relative standard deviation 11.9%) was found to be similar to that previously published for routine GC/MS multianalyte RF determinations.

Response factors are constants utilized in the internal standard quantitative analysis of organic compounds by electron impact GC/MS in environmental analysis (1). For comparable injected weights, the response factor of an analyte is simply a ratio of the ion current "area" of analyte and internal standard at their respective quantitation  $m/z$  values. A series of multianalyte, multilevel response factor precision determinations can be considered as a measure of the relative sensitivity and stability of a given instrument and, hence, its quantitative capabilities. Additionally, response factor determinations encode the entire laboratory standardization procedure from standard preparation to data transcription. Therefore, response factor monitoring is an important mechanism in establishing and maintaining control of multilaboratory programs which routinely employ GC/MS for the qualitative and quantitative analysis of organic compounds.

In an attempt to standardize the GC/MS determination of priority pollutants, the "Quality Control Protocol for the Fused Silica Capillary Column GC/MS Determination of Semivolatile Priority Pollutants" was written (2). Observance of this protocol has been shown to yield similar response factors for extractable priority pollutants on single quadrupole mass spectrometers in a recent interlaboratory study (3). An intralaboratory study which compared response factors on single quadrupole mass spectrometers of different design has shown that in many cases response factors were instrument independent (4). Response factor monitoring has been adopted as a quality control procedure in national U.S. EPA programs that utilize GC/MS for routine priority pollutant analysis (5).

A model to predict response factors has recently been proposed (5). Predicted and observed response factors were in general agreement even without consideration of ion abundance tune differences. For 41 of the extractable priority pollutants (excluding all nitrogen-containing analytes) a mean predicted/observed response factor ratio of  $1.02 \pm 0.27$  was reported (5) when tested using the interlaboratory data cited previously (3). While the discussion of the proposed model is beyond the scope of this paper, the establishment of a set of true response factors is of interest for at least two reasons.

Firstly, the ability to predict response factors would effectively establish accuracy criteria in programs that utilize GC/MS. Secondly, a scheme to predict response factors would be useful in providing a formal procedure to give quantitative results for organic compounds identified in complex mixtures by GC/MS for which standards are not readily available.

Concurrently, analytical applications of triple quadrupole mass spectrometry (TQMS) are becoming commonplace. The potential of TQMS for the direct analysis of mixtures with minimal sample preparation and without chromatographic separations has been shown (6). Others have indicated that TQMS mixture analysis can often benefit from prior chromatographic separations (7). Obviously, direct mixture analysis by TQMS affords significant logistical advantages over TQMS methods which employ chromatographic separations and is therefore preferred. Nevertheless, we anticipate that chromatographic TQMS configurations will be useful in minimizing sample matrix effects and in providing ancillary quantitative data to confirm assignments made by TQMS mixture screening schemes.

Because of our interest in standardizing and predicting GC/MS response factors, and as we are also evaluating the potential of TQMS for characterizing hazardous materials, it was of interest to compare response factors acquired on a TQMS system with response factors previously determined in an interlaboratory GC/MS study.

## EXPERIMENTAL SECTION

**Standards.** The analytical standards of extractable priority pollutants were prepared by Radian Corp. under U.S. EPA Contract No. 68-03-2765 and have been described elsewhere (8). For this work a standard was prepared consisting of acid, base/neutral, and pesticide priority pollutants in methylene chloride at a nominal concentration of  $150 \text{ ng } \mu\text{L}^{-1}$  per analyte. This standard was diluted to give two additional standards containing 100 and  $25 \text{ ng } \mu\text{L}^{-1}$  per analyte. The internal standards, phenol- $d_4$ , 6- $d_3$ , naphthalene- $d_8$ , phenanthrene- $d_{10}$ , chrysene- $d_{12}$ , and benzo[a]pyrene- $d_{12}$  were added to each standard prior to dilution to give nominal concentrations/internal standard of 20, 20, 26, 40, and  $40 \text{ ng}/\mu\text{L}$ , respectively, in each of the three composite standards. The ion abundance calibrant (decafluorotriphenyl)phosphine (DFTPP) was purchased from P.C.R. Inc., Gainesville, FL.

**Instrumentation.** The GC/TQMS data were acquired on a Finnigan triple stage quadrupole mass spectrometer (TSQ) equipped with 4500 series ion source and a continuous dynode electron multiplier with the conversion dynode maintained at  $-3.0 \text{ kV}$ . Gas chromatography was performed on a fused silica capillary column ( $30 \text{ m} \times 0.24 \text{ mm i.d.}$ ,  $0.25 \text{ } \mu\text{m}$  thick SE-54 phase; J. and W. Scientific Inc., Rancho Cordova, CA) coupled directly to the ion source. A Finnigan 9610 gas chromatograph with Grob-type split/splitless injector under data system control was used to provide splitless injections. After 30 s the split and sweep valves were opened. The carrier gas was helium at a column head pressure of 26 psig. The split and septum sweep flow rates were 35 and  $10 \text{ mL min}^{-1}$ , respectively, and carrier gas linear velocity was  $60 \text{ cm s}^{-1}$  at  $30^\circ \text{C}$ . Initial column temperature was held at

Table I. Mean Response Factor Comparison of GC/TQMS to Interlaboratory GC/MS Values

	IS <sup>a</sup>	GC/ TQMS <sup>b</sup>	GC/ MS <sup>c</sup>		IS <sup>a</sup>	GC/ TQMS <sup>b</sup>	GC/ MS <sup>c</sup>
N-nitrosodimethylamine	d3	0.43	0.42	acenaphthene	d10	0.94	0.81
bis(2-chloroethyl) ether	d3	0.87	1.01	2,4-dinitrophenol	d10	0.11	0.07
2-chlorophenol	d3	0.72	0.79	2,4-dinitrotoluene	d10	0.30	0.23
phenol	d3	1.02	1.10	4-nitrophenol	d10	0.17	0.10
1,3-dichlorobenzene	d3	0.64	0.72	fluorene	d10	1.15	0.96
1,4-dichlorobenzene	d3	0.77	0.90	4-chlorophenyl phenyl ether	d10	0.53	0.47
1,2-dichlorobenzene	d3	0.62	0.75	diethyl phthalate	d10	0.85	0.91
bis(2-chloroisopropyl) ether	d3	0.19	0.22	4,6-dinitro-o-cresol	d10	0.13	0.10
hexachloroethane	d3	0.37	0.35	N-nitrosodiphenylamine	d10	0.65	0.58
N-nitrosodi-n-propylamine	d8	0.08	0.05	4-bromophenyl phenyl ether	d10	0.25	0.24
nitrobenzene	d8	0.18	0.19	hexachlorobenzene	d10	0.27	0.24
isophorone	d8	0.76	0.84	pentachlorophenol	d10	0.14	0.13
2-nitrophenol	d8	0.21	0.22	phenanthrene	d10	1.32	1.16
2,4-dimethylphenol	d8	0.35	0.32	anthracene	d10	1.21	1.15
bis(2-chloroethoxy)methane	d8	0.44	0.51	dibutyl phthalate	d10	1.29	1.28
2,4-dichlorophenol	d8	0.29	0.30	fluoranthene	d10	1.05	1.07
1,2,4-trichlorobenzene	d8	0.30	0.32	pyrene	d10	1.13	1.08
naphthalene	d8	1.13	1.08	benzidine	d12	0.81	0.24
hexachlorobutadiene	d8	0.13	0.13	butyl benzyl phthalate	d12	0.70	0.84
4-chloro-m-cresol	d8	0.28	0.26	benz[a]anthracene	d12	1.17	1.11
hexachlorocyclopentadiene	d8	0.15	0.15	chrysene	d12	1.03	1.02
2,4,6-trichlorophenol	d8	0.19	0.19	3,3'-dichlorobenzidine	d12	0.40	0.28
2-chloronaphthalene	d8	0.65	0.63	bis(2-ethylhexyl) phthalate	d12	0.73	0.88
acenaphthylene	d8	0.42	0.72	di-n-octyl phthalate	d12	1.00	1.34
dimethyl phthalate	d8	0.59	0.62	benzo[a]pyrene	d12B	1.06	1.00
2,6-dinitrotoluene	d8	0.15	0.15	dibenz[a,h]anthracene	d12B	0.56	0.58
				benzo[g,h,i]perylene	d12B	0.59	0.64

<sup>a</sup> The internal standards employed for response factor calculation were phenol-2,4,6-*d*<sub>3</sub> (d3), naphthalene-*d*<sub>8</sub> (d8), phenanthrene-*d*<sub>10</sub> (d10), chrysene-*d*<sub>12</sub> (d12), and benzo[a]pyrene-*d*<sub>12</sub> (d12B). <sup>b</sup> RF values determined in triplicate at 25, 100, and 150 ng/μL using TQMS (Q3 scanned). <sup>c</sup> RF values determined in interlaboratory GC/MS study using single quadrupole MS device.

30 °C for 4 min and then raised at 10 °C min<sup>-1</sup> and maintained at 270 °C until all components had eluted. Total GC run time was ca. 38 min.

The conditions for electron impact ionization mass spectrometry were as follows: electron energy, 70 eV; emission current, 0.40 mA; source temperature, 90 °C. For the RF determinations, two adjacent quadrupoles (Q1 and Q2; Q2 and Q3) were operated in the all-pass (radio-frequency-only) mode while the third quadrupole (Q3 or Q1, respectively) repetitively scanned the range *m/z* 40–475 in 0.95 s. The instrument was tuned to meet DFTPP ion abundance criteria (9).

**Data System.** Data acquisition was performed under control of Finnigan MAT TSG Rev. B software with a Data General NOVA-4 minicomputer and a Control Data Corp. cartridge module disk drive. Computer generated areas were used for quantitation of analytes and internal standards. Subsequent calculations for RF, mean RF, and relative standard deviation were performed via calculators.

Qualitative identification of analytes was accomplished by reference to published relative retention times and library (EPA/NIH Mass Spectral Data Base) matches via resident software together with manual interpretation and verification.

## RESULTS AND DISCUSSION

In early work with triple quadrupole mass spectrometers, it was reported that large ion signal losses can occur in systems with aperture separated, independently driven rod systems (10). The highest ion transmission was reported for closely spaced rod systems where the radio frequency component of each rod set was synchronized in frequency and phase. It has recently been reported that theoretical and experimental data indicate that "properly designed" instruments provide high ion transmission (11). However, the same study has indicated that for instruments where ions leave and reenter the quadrupole field through restrictive apertures, ion transmission can be reduced.

Relative ion transmission is encoded in multianalyte, multilevel response factors. Response factor precision de-

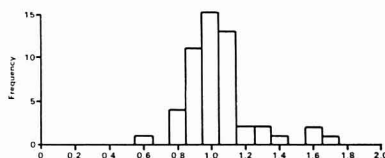


Figure 1. Distribution of response factor ratios, TQMS (Q-3 scan)/Interlaboratory GC/MS, does not include benzidine (3.38).

terminations provide information about instrument stability and performance. However, as these factors are relative measures, fundamental ion transmission characteristics are largely obscured. Nevertheless, response factor determinations acquired under rapid source introduction and scanning modes provide useful experimental insight into the quantitative properties of TQMS.

Table I shows the response factors for 53 acid and base/neutral extractable priority pollutants determined by GC/TQMS (Q3 scanned) and RF values previously determined in an interlaboratory GC/MS study (3). Figure 1 shows the distribution of TQMS/GCMS response factor ratios. Seventy-four percent of the RF values determined on the TQMS were within  $\pm 15\%$  of the mean RF values determined in the interlaboratory single quadrupole GC/MS study. The RF value for benzidine differed greatly from the interlaboratory GC/MS value. As this analyte had the second highest interlaboratory GC/MS RF RSD (47.0%), the RF value for this compound was imprecisely determined in the GC/MS work. We were not surprised at this discrepancy because we have previously encountered and discussed GC/MS analysis problems with this analyte (1, 3). Also, because other analyte, internal standard pairs had similar RF values for comparable mass ranges, the difference in GC/MS and GC/TQMS RF values for benzidine was thought to be of nonspectroscopic

Table II. Response Factor, Relative Standard Deviation Values Determined on Q3 Scanned TQMS<sup>a</sup>

	% RSD		% RSD
<i>N</i> -nitrosodimethylamine	19.5	acenaphthene	8.2
bis(2-chloroethyl) ether	9.7	2,4-dinitrophenol	44.0
2-chlorophenol	12.5	2,4-dinitrotoluene	9.8
phenol	9.2	4-nitrophenol	12.0
1,3-dichlorobenzene	6.2	fluorene	9.9
1,4-dichlorobenzene	11.4	4-chlorophenyl phenyl ether	8.9
1,2-dichlorobenzene	9.1	diethyl phthalate	8.3
bis(2-chloroisopropyl) ether	9.0	4,6-dinitro- <i>o</i> -cresol	19.9
hexachloroethane	13.0	<i>N</i> -nitrosodiphenylamine	11.6
<i>N</i> -nitrosodi- <i>n</i> -propylamine	8.5	4-bromophenyl phenyl ether	13.3
nitrobenzene	17.5	hexachlorobenzene	10.1
isophorone	11.7	pentachlorophenol	11.2
2-nitrophenol	10.6	phenanthrene	4.5
2,4-dimethyl phenol	16.1	anthracene	7.6
bis(2-chloroethoxy)methane	10.7	dibutyl phthalate	7.7
2,4-dichlorophenol	6.9	fluoranthene	15.0
1,2,4-trichlorobenzene	11.1	pyrene	9.8
naphthalene	13.2	benzidine	10.5
hexachlorobutadiene	12.6	butyl benzyl phthalate	4.7
4-chloro- <i>m</i> -cresol	5.4	benz[ <i>a</i> ]anthracene	5.3
hexachlorocyclopentadiene	11.7	chrysene	8.5
2,4,6-trichlorophenol	8.9	3,3'-dichlorobenzidine	4.0
2-chloronaphthalene	15.8	bis(2-ethylhexyl) phthalate	19.7
acenaphthylene	13.3	di- <i>n</i> -octyl phthalate	24.8
dimethyl phthalate	18.0	benzo[ <i>a</i> ]pyrene	8.9
2,6-dinitrotoluene	19.0	dibenz[ <i>a,h</i> ]anthracene	11.2
		benzo[ <i>g,h,i</i> ]perylene	10.0

<sup>a</sup> *N* = 9, triplicate determinations at 25, 100, and 150 ng over a 3-day acquisition period.

origin. Despite this anomaly these data indicate that RF values acquired within the criteria of the QC protocol are not greatly affected by the additional ion optics of the TQMS. Interlaboratory and intralaboratory comparisons of this type are complicated by the higher average variance of the former data set. For analytes of equal variance, instrumental sensitivity differences can cause RF values to be formally non-equivalent. For example, the RF values determined for bis(2-chloroethyl) ether by GC/MS and GC/TQMS were  $1.01 \pm 0.10$  and  $0.87 \pm 0.08$ , respectively. At the 95% confidence level these mean values are statistically nonequivalent, and an argument could be made that chromatographic and/or spectroscopic sensitivity differences were observed. The fact that the mean RF values for this compound are not greatly different indicates that the relative sensitivity differences were not large. The observation that the difference in mean values is often not large can be seen by inspection of Table I. It should be noted that these RF values were calculated with reference internal standards which had been selected to minimize the relative retention time and the quantitation mass difference between analyte and internal standard. Therefore, many of the compounds with small quantitation mass differences would quite likely be poor indicators of relative sensitivity differences between single and triple quadrupole mass spectrometers. However, reviewing selected analytes from Table I with relatively wide differences in quantitation mass between analyte and internal standard, e.g., the dichlorobenzenes (*m/z* 146 vs. phenol-2,4,6-*d*<sub>3</sub>, *m/z* 97), hexachlorobutadiene (*m/z* 225 vs. naphthalene-*d*<sub>8</sub>, *m/z* 136), and hexachlorobenzene (*m/z* 284 vs. phenanthrene-*d*<sub>10</sub>, *m/z* 188), it can be seen that no major relative sensitivity differences were observed which could not be accounted for by ion abundance tune differences. Also, because the TQMS-generated RF values were acquired in triplicate at 25, 100, and 150 ng  $\mu\text{L}^{-1}$  per analyte and the RF determinations for these analytes at multiple levels were precise (i.e., 6.2, 11.4, 9.1, 12.6, and 10.1 percent relative standard deviation), significant sensitivity differences were not observed over the mass and injected weight range of these experiments. In fact, the integrated ion currents for these analytes were of similar

magnitude to those obtained in routine GC/MS analysis using similar detection apparatus. This observation suggested that significantly lower quantities of these analytes could have been readily detected and quantified. Because the objective was to compare the TQMS data to data acquired in a previous interlaboratory GC/MS study, lower analyte concentrations were not examined.

The fractional ion abundance (the ratio of the quantitation *m/z* "area" to the total ion "area") of the quantitation *m/z* value is an indicator of mass dependent relative sensitivity differences. The fractional ion abundance of the quantitation mass of hexachlorobenzene (*m/z* 284) was determined for each acquisition of the GC/MS data (three acquisitions in each of four laboratories) and found to be  $14.6 \pm 1.3\%$ . For the nine RF acquisitions with the TQMS (Q3 scanned), the fractional ion abundance of *m/z* 284 of hexachlorobenzene was found to be similar, i.e.,  $13.4 \pm 1.1\%$ ; the fragmentation pattern did not show any mass dependent spectral skewing. TQMS-generated electron impact mass spectra were found to be similar to spectra acquired on a single quadrupole mass spectrometer when both were tuned to meet DFTPP ion abundance criteria.

**GC/TQMS Precision.** To examine the stability of the TQMS, we calculated the relative standard deviation of the response factors in the nine Q3-scanned acquisitions taken over a 3-day period. These data are presented in Table II for 53 extractable priority pollutants. The average relative standard deviation, 11.9%, is similar to the multiday RF determination precision (mean RSD 11.4%) previously published for similar GC/MS determinations (1). This precision level approaches the short-term consecutive injection precision, RSD 7.0%, considered acceptable in GC/MS instrument evaluation tests (12). It is noteworthy that the combination of rapid (1.0 s, 40–475 amu) scanning and sample introduction (via FSCC) and the additional ion optics of the TQMS do not appear to affect the RF values. Furthermore, as the relative standard deviation for many of the analytes studied was low, the stability of the TQMS in practice was found to be excellent. On the basis of these results, the utilization of the TQMS for routine multianalyte quantitative and qualitative



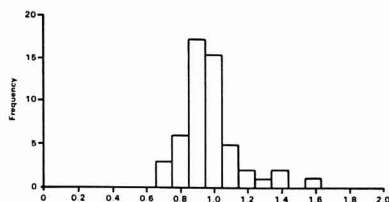


Figure 2. Distribution of response factor ratios, TQMS (Q3-scan)/TQMS (Q1-scan), does not include dibenz[*a,h*]anthracene (2.07).

FSCC GC/MS determinations of organic compounds, if required, is viable.

**Q1-Scanned GC/TQMS Response Factors.** In those instruments with interquadrupole lenses the ion beam leaves and reenters the quadrupole field and is therefore susceptible to fringe field effects (10, 11). Hunt et al. (13) have reported decreased negative ion sensitivity at  $m/z$  614 when Q1 rather than Q3 was scanned on an instrument of this type and attributed this result to fringe field effects. Dawson has also indicated that the highest absolute sensitivity of a triple quadrupole mass spectrometer is obtained when Q3 is scanned, with Q1 and Q2 in the radio-frequency-only mode (14). To determine if RF values were dependent on which quadrupole was scanned, we acquired the RF values for priority pollutants as before except that Q1 was scanned with Q2 and Q3 in the all-pass radio-frequency-only mode. Many values determined in this acquisition mode were in close agreement with Q3 values. For 48 of the extractable priority pollutants (excluding 4-nitrophenol, 2,4-dinitrophenol, 4,6-dinitro-*o*-cresol, benzinene, and 3,3'-dichlorobenzidine, analytes with high interlaboratory GC/MS RF relative standard deviations) the Q3/Q1 mean RF ratio was 1.02 with a relative standard deviation of 17.2% (Figure 2). Within the mass and injected weight ranges and ion abundance tune of this study, the relative sensitivities of analyte and internal standard are independent of which quadrupole (Q1 or Q3) is scanned. These observations are thought to arise because the multiple internal standards tend to minimize spectroscopic and chromatographic sensitivity differences between analyte and internal standard. While fundamental ion transmission characteristics are obscured by this approach, the practical observation that TQMS response factors and response factor precision are similar to routine GC/MS determinations is valuable. These data indicate that multianalyte, multilevel quantitative TQMS determinations in mixture analysis should be comparable to quantitative GC/MS data.

Since the RF values determined with the TQMS are shown to be in general agreement with values determined with single quadrupole instruments, it is apparent that the predictive response factor scheme (5) is applicable to the TQMS. Therefore, for analytes which can be introduced via FSCC, the ability to provide quantitative estimates for analytes whose structure has been determined via collision activated dissociation techniques is anticipated. Such results are of con-

siderable potential in the qualitative and quantitative deconvolution of complex mixtures by triple quadrupole mass spectrometry. We further expect that with a LC/TQMS QC protocol of similar design, the predictive scheme should be applicable to organic analytes which are not amenable to analysis by gas chromatography.

**Registry No.** *N*-Nitrosodimethylamine, 62-75-9; bis(2-chloroethyl) ether, 111-44-4; 2-chlorophenol, 95-57-8; phenol, 108-95-2; 1,3-dichlorobenzene, 641-73-1; 1,4-dichlorobenzene, 106-46-7; 1,2-dichlorobenzene, 95-50-1; bis(2-chloroisopropyl) ether, 39638-32-9; hexachloroethane, 67-72-1; *N*-nitrosodi-*n*-propylamine, 621-64-7; nitrobenzene, 98-95-3; isophorone, 78-59-1; 2-nitrophenol, 88-75-5; 2,4-dimethylphenol, 105-67-9; bis(2-chloroethoxy)methane, 111-91-1; 2,4-dichlorophenol, 120-83-2; 1,2,4-trichlorobenzene, 120-82-1; naphthalene, 91-20-3; hexachlorobutadiene, 87-68-3; 4-chloro-*m*-cresol, 59-50-7; hexachlorocyclopentadiene, 77-47-4; 2,4,6-trichlorophenol, 88-06-2; 2-chloronaphthalene, 91-58-3; acenaphthylene, 208-96-8; dimethyl phthalate, 131-11-3; 2,6-dinitrotoluene, 606-20-2; acenaphthene, 83-32-9; 2,4-dinitrophenol, 51-28-5; 2,4-dinitrotoluene, 121-14-2; 4-nitrophenol, 100-02-7; fluorene, 86-73-7; 4-chlorophenyl phenyl ether, 7005-72-3; diethyl phthalate, 84-66-2; 4,6-dinitro-*o*-cresol, 534-52-1; *N*-nitrosodiphenylamine, 86-30-6; 4-bromophenyl phenyl ether, 101-55-3; hexachlorobenzene, 118-74-1; pentachlorophenol, 87-86-5; phenanthrene, 85-01-8; anthracene, 120-12-7; dibutyl phthalate, 84-74-2; fluoranthene, 206-44-0; pyrene, 129-00-0; benzidine, 92-87-5; butyl benzyl phthalate, 85-68-7; benz[*a*]anthracene, 56-55-3; chrysene, 218-01-9; 3,3'-dichlorobenzidine, 91-94-1; bis(2-ethylhexyl) phthalate, 117-81-7; di-*n*-octyl phthalate, 117-84-0; benzo[*a*]pyrene, 50-32-8; dibenz[*a,b*]anthracene, 53-70-3; benzo[*g,h,i*]perylene, 191-24-2.

## LITERATURE CITED

- (1) Sauter, A. D.; Betowski, L. D.; Smith, T. R.; Strickler, V. A.; Belmer, R. G.; Colby, B. N.; Wilkinson, J. E. *HRC CC*, *J. High Resolut. Chromatogr. Chromatogr. Commun.* **1981**, *4*, 368-384.
- (2) Lopez-Avila, V.; Sauter, A. D. Presented at the 30th Annual Conference on Mass Spectrometry and Allied Topics, Honolulu, HI, June 6-11, 1982.
- (3) Sauter, A. D.; Mills, P. E.; Fitch, W. L.; Dyer, R. *HRC CC*, *J. High Resolut. Chromatogr. Chromatogr. Commun.* **1982**, *5*, 27-30.
- (4) Smith, T.; Moesman, N. H.; Sauter, A. D. Presented at the 1982 Pittsburgh Conference and Exposition on Analytical Chemistry and Applied Spectroscopy, Atlantic City, NJ, March 1982.
- (5) Sauter, A. D.; Fitch, W. L.; Lopez-Avila, V. Presented at the 1982 American Chemical Society Meeting, Las Vegas, NV, March 1982.
- (6) Hunt, D. F.; Shabanowitz, J.; Harvey, T. M.; Coates, M. Presented at the 30th Annual Conference on Mass Spectrometry and Allied Topics, Honolulu, HI, June 6-11, 1982.
- (7) Henion, J. D.; Skrabalak, D. S.; Thomson, B. A. Presented at the 30th Annual Conference on Mass Spectrometry and Allied Topics, Honolulu, HI, June 6-11, 1982.
- (8) "Repository Services for Priority Pollutants, Toxic Pollutants and Chromatographic Materials"; Progress Report for April-June 1981, Radcan Corp.; U.S. EPA Contract No. 68-03-2765.
- (9) Eichlerberger, J. W.; Harris, L. E.; Budde, W. L. *Anal. Chem.* **1975**, *47*, 995-1000.
- (10) Dawson, P. H. European Patent Application 80302635.0, 1980.
- (11) Dawson, P. H.; Fulford, J. E. *Int. J. Mass. Spectrom. Ion Phys.* **1982**, *42*, 195.
- (12) Budde, W. L.; Eichlerberger, J. W. EPA-600/4-80-025. U.S. EPA, Cincinnati, OH, April 1980.
- (13) Hunt, D. F.; Shabanowitz, J.; Giordani, A. B. *Anal. Chem.* **1980**, *52*, 388-390.
- (14) Dawson, P. H.; French, J. B.; Buckley, J. A.; Douglas, D. J.; Simmons, D. *Org. Mass Spectrom.* **1982**, *17*, 205-211.

RECEIVED for review August 9, 1982. Accepted October 6, 1982.

# Extension of Potentiometric Stripping Analysis to Electropositive Elements by Solvent Optimization

J. F. Coetzee\* and Abul Hussam

Department of Chemistry, University of Pittsburgh, Pittsburgh, Pennsylvania 15260

T. R. Petrick

Department of Chemistry, California State College, California, Pennsylvania 15419

The extension of potentiometric stripping analysis to the ions of such electropositive elements as the alkali and alkaline earth metals was investigated by using thin film mercury electrodes in a wide range of organic solvents and their mixtures with water. The alkali metal ions can be determined in certain organic solvents even when several mole percent of water is present. As expected, the most effective solvents are aprotic; however, an equally important factor is that the solvent should be a good hydrogen bond acceptor, thereby decreasing the reactivity of water toward the amalgam. The sum of sodium and potassium ions can be determined in such samples as blood serum and seawater after addition of dimethyl sulfoxide. Some resolution of sodium from potassium occurs in 1-methyl-2-pyrrolidinone and certain other solvents.

Potentiometric stripping analysis (PSA), which was recently introduced by Jagner (1), is similar to conventional (voltammetric) stripping analysis (VSA) in that the analyte is pre-concentrated by electrodeposition in a mercury electrode, but it differs from VSA in the method used to generate a signal by the preconcentrated analyte. Whereas in VSA the most sensitive and commonly used method is differential pulse voltammetry which produces a signal of differential current vs. potential, in PSA the plating potential is interrupted and the amalgam is allowed to react with an excess of a suitable oxidant, such as mercury(II) ion



Consequently, the redox couple  $M^{n+}/M(Hg)_x$  determines the potential of the mercury electrode until all amalgam has been oxidized, when an abrupt change in the signal of potential vs. time occurs.

Both PSA and VSA are restricted for all practical purposes to relatively noble metals when carried out in aqueous solution. However, metals forming more reactive amalgams can be determined in nonaqueous media or, more usefully, in mixtures of certain nonaqueous solvents and water. PSA offers significant advantages over VSA in media of that kind because such factors as high solution resistivity and irreversible redox couples present fewer problems. We have therefore investigated the possibility of achieving useful extensions of stripping analysis methodology by applying PSA to the determination of electropositive metals in optimized solvent mixtures. Preliminary results have been reported before (2); we now present more detailed information.

Historically, "chemical" stripping analysis (3) was a forerunner of PSA; such oxidants as  $Ce(IV)$ ,  $Fe(III)$ , and  $MnO_4^-$  were determined by allowing their solutions to react with known amounts of silver metal on a platinum electrode while monitoring potential as a function of time. Chronopotentiometric stripping analysis (CPSA) also has features (4) in

common with PSA; some of these have been compared by Buffle (5). There are nevertheless certain differences between the principles of PSA and CPSA which will be discussed elsewhere (6); we present here only our main conclusions. Under conditions of forced convection and of sufficiently long deposition time ( $t_d$ ) and a sufficiently thin mercury film (thickness  $l$ ) so that  $t_d \gg l^2/3D_a$ , where  $D_a$  is the diffusion coefficient of the metal in mercury, eq 2-4 represent the limiting stripping time or transition time ( $\tau$ ), the transient potential at time  $t$  ( $E_t$ ), and the transient potential at a time equal to half the limiting stripping time ( $E_{\tau/2}$ ).

$$\tau = \frac{n}{2} \left( \frac{D}{\delta} \right)_{M^{n+}} \left( \frac{\delta}{D} \right)_{Hg^{2+}} \left( \frac{C_{M^{n+}}}{C_{Hg^{2+}}} \right) t_d \quad (2)$$

$$E_t = E_a^\circ - \frac{RT}{nF} \ln \left( \frac{Dt_d}{\delta l} \right) \left( \frac{C_{M^{n+}}}{C_{M^{n+}} + \frac{2}{n} C_{Hg^{2+}}} \right) - \frac{RT}{nF} \ln \left( 1 - \frac{t}{\tau} \right) \quad (3)$$

$$E_{\tau/2} = E_a^\circ - \frac{RT}{nF} \ln \left( \frac{Dt_d}{\delta l} \right) \left( \frac{C_{M^{n+}}}{C_{M^{n+}} + \frac{2}{n} C_{Hg^{2+}}} \right) - \frac{RT}{nF} \ln (1/2) \quad (4)$$

Here,  $D$ ,  $\delta$ , and  $C$  are the diffusion coefficient, the diffusion layer thickness, and the bulk concentration of  $M^{n+}$  or  $Hg^{2+}$ , as indicated, and  $E_a^\circ$  is the standard (reduction) potential of the amalgam; if the convection rate is the same during deposition and stripping, then the two diffusion layer thicknesses are equal. It follows that  $E_{\tau/2}$  is more negative than the polarographic half-wave potential by the second and third terms of eq 4 and that  $\tau$  is directly proportional to the bulk concentration of  $M^{n+}$  and inversely proportional to the bulk concentration of  $Hg^{2+}$ . Equations 2-4 therefore illustrate the potential analytical utility of PSA.

## EXPERIMENTAL SECTION

**Chemicals.** Acetonitrile, propylene carbonate, dimethyl sulfoxide, ethanol, 2-propanol, and water were purified as described before (7). Other solvents tested were reagent quality and were used without further purification. Tetraethylammonium perchlorate (TEAP) and tetrabutylammonium perchlorate (TBAP) were prepared as described elsewhere (8); these salts contained 1.5 and 2.7 ppm sodium ion, respectively. Mercury(II) chloride (Baker analyzed reagent) contained 0.1 ppm sodium ion. Lyophilized human blood serum (General Diagnostics, Versatol acid-base normal) had the following composition:  $Na^+$ , 143.0;  $K^+$ , 4.7;  $Ca^{2+}$ , 2.5; and  $Mg^{2+}$ , 3.0 mM. Synthetic serum was prepared by dissolving NaCl and KCl in water at concentrations

of 143.0 mM Na<sup>+</sup> and 4.7 mM K<sup>+</sup>. Synthetic seawater was prepared to contain (in units of mM) 478.6 NaCl, 10.7 KCl, 10.7 CaCl<sub>2</sub>·2H<sub>2</sub>O, 54.7 MgCl<sub>2</sub>·6H<sub>2</sub>O,  $1.9 \times 10^{-5}$  CuSO<sub>4</sub>·5H<sub>2</sub>O,  $3.2 \times 10^{-6}$  CdCl<sub>2</sub>,  $6.3 \times 10^{-6}$  PbCl<sub>2</sub>, and  $6.3 \times 10^{-5}$  ZnCl<sub>2</sub>.

**Instrumentation.** PSA was performed with an ISS-820 ion scanning unit (Radiometer, Copenhagen) interfaced with a TTA-80 titration assembly. An electronic circuit similar to that described by Jagner (9) was built for derivative PSA. The three-electrode cell contained a planar glassy carbon electrode (Radiometer Model F 3500) with a geometric area of 0.05 cm<sup>2</sup> as working electrode, a 1-cm<sup>2</sup> platinum foil as counterelectrode, and an Ag/(0.01 M AgClO<sub>4</sub> + 0.1 M TEAP in acetonitrile) reference electrode (hereafter designated as Ag<sup>+</sup>/Ag) coupled to the analyte solution through a 0.1 M TEAP salt bridge solution in the same solvent as the analyte; the two junctions were asbestos fibers.

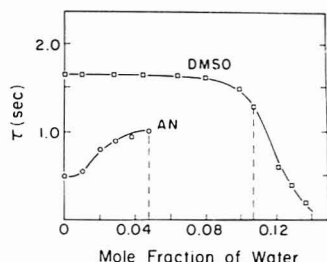
**Procedure.** The glassy carbon working electrode was cleaned before each set of experiments with a polishing grade of alumina (0.3 μm particle size) and was then washed successively with 1 M nitric acid, water, and acetone. Analyte and plating solutions were deaerated with ultrapur nitrogen presaturated with the solvent in question. Deaeration was carried out in the absence of the working electrode to avoid the deposition of gas bubbles on the electrode surface. The working electrode was then inserted and (typically) mercury was plated from  $10^{-3}$  M HgCl<sub>2</sub> +  $10^{-1}$  M TEAP for 4 min, after which the analyte solution was introduced with a microsyringe and three to five deposition-stripping cycles were carried out. Background corrections for the presence of sodium ion in the supporting and stripping electrolytes were applied.

## RESULTS AND DISCUSSION

### Potentiometric Stripping Analysis of Alkali Metal Ions

We investigated the PSA of sodium ion in a wide range of solvents, including methanol, ethanol (EtOH), 2-propanol (2-PrOH), ethylene glycol, 1,2-dimethoxyethane (DME), ethylenediamine, pyridine, acetone, acetonitrile (AN), benzonitrile, dimethyl sulfoxide (Me<sub>2</sub>SO), dimethylformamide (DMF), sulfolane, dimethyl carbonate, propylene carbonate (PC), propylene oxide, γ-butyrolactone (GBL), dioxane, 1,3-dioxolane (DL), and 1-methyl-2-pyrrolidinone (NMP). This list contains mostly aprotic solvents, several of which have found commercial application in lithium batteries, but selected protic solvents were also included for comparison. Best results were obtained in DME, Me<sub>2</sub>SO, DMF, PC, GBL, DL, NMP, and, surprisingly, EtOH and 2-PrOH. The remaining alkali metal ions as well as the alkaline earth metal ions were also tested in those solvents in which sodium ion gave good response. Several stripping agents were tested; none of these (oxygen, hydrogen peroxide, iodine, permanganate ion) had an advantage over mercury(II) ion.

The question of how much water can be tolerated in different solvents is of crucial importance. As would be expected, the reactivity of residual water toward amalgams is lowest in those solvents that are good hydrogen bond acceptors. We have reported elsewhere (10) equilibrium constants for the formation of the hydrogen bonded complexes HOH...S and S...HOH...S between solvents S and low concentrations of (monomeric) water. Typical formation constants [(mole fraction)<sup>-1</sup> at 30 °C] for the 1:1 complexes vary from 4.1 for AN to 14.2 for DME, 43.4 for DMF, and 59.4 for Me<sub>2</sub>SO. Stepwise formation constants for the 1:2 complexes vary less with the solvent and typically fall between 0.2 and 0.9 (mol fraction)<sup>-1</sup>. Distribution fractions calculated from these formation constants show that, in such solvents as DMF or Me<sub>2</sub>SO containing up to a few centimolar water (typical levels in these solvents when they are purified by other than the most rigorous procedures), little free water is present and S...HOH...S is the predominant water species. On the other hand, in such solvents as AN, HOH...S is the predominant species while considerable free water is also present. At higher water concentrations the systems become more complex owing to progressive polymerization of water, but the trends remain



**Figure 1.** Tolerance of dimethyl sulfoxide and acetonitrile to water in the potentiometric stripping of sodium amalgam. Conditions: analyte,  $10^{-4}$  M NaCl +  $10^{-3}$  M HgCl<sub>2</sub> +  $5 \times 10^{-2}$  M TEAP;  $E_d$ , -2.99 V vs. Ag<sup>+</sup>/Ag;  $t_d$ , 120 s. Dashed lines show where hydrogen evolution becomes visible to the unaided eye.

**Table I.** Features of Typical Calibration Plots for Potentiometric Stripping Analysis of Alkali Metal Ions (M<sup>+</sup>) in Various Solvents

solvent	M <sup>a</sup>	slope <sup>b</sup>	r <sup>c</sup>
Me <sub>2</sub> SO	Na	21.8	0.9999
	K	23.3	0.9997
	Rb	23.0	0.9962
	Cs	21.4	0.9998
AN	Na	11.0	0.9972
	K	12.3	0.9939
EtOH	Na	17.5	0.9983

<sup>a</sup> Conditions: ca.  $10^{-6}$  to  $10^{-4}$  M MCl +  $10^{-3}$  M HgCl<sub>2</sub> +  $10^{-1}$  M TEAP;  $E_d$ , -2.99 V vs. Ag<sup>+</sup>/Ag;  $t_d$ , 60 s.

<sup>b</sup> Units: s mM<sup>-1</sup>; represents the sensitivity of PSA.

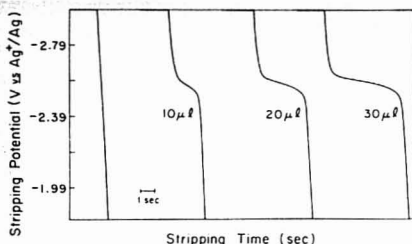
<sup>c</sup> Correlation coefficient.

the same. The marked differences in the reactivity of water in Me<sub>2</sub>SO and AN toward sodium amalgam are illustrated in Figure 1. In Me<sub>2</sub>SO, the limiting stripping time ( $\tau$ ) decreases little until ca. 8 mol % of water has been added, while in AN  $\tau$  is smaller and actually increases until ca. 5 mol % of water has been added (after which  $\tau$  decreases rapidly). This curious behavior in AN may be caused by the fact that AN itself is polymerized by sodium amalgam; such polymerization may block deposition of sodium more effectively than the formation of sodium hydroxide does. Under certain conditions, significant amounts of sodium hydroxide undoubtedly form in Me<sub>2</sub>SO as well, even at low water concentrations, because  $\tau$  does not remain directly proportional to  $t_d$  for large values of  $t_d$  and/or  $C_{Na^+}$ . We therefore recommend that  $t_d$  be optimized empirically for a given metal ion concentration and water content; reasonable values of  $t_d$  for "pure" Me<sub>2</sub>SO are 120 s for  $10^{-6}$  M Na<sup>+</sup> and 30 s for  $10^{-3}$  M Na<sup>+</sup>. Nevertheless, reproducibility of the limiting stripping time in a given Me<sub>2</sub>SO-water mixture remains satisfactory ( $\sigma \sim 0.08$  s) up to ca. 20 mol % water for Na<sup>+</sup>, and 14, 12, and 4 mol % water for K<sup>+</sup>, Rb<sup>+</sup>, and Cs<sup>+</sup>.

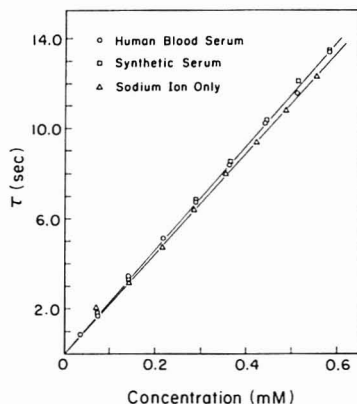
Typical results obtained for the alkali metal ions in Me<sub>2</sub>SO, AN, and EtOH are listed in Table I.

We have devoted less attention to the PSA of lithium ion. Stripping signals were obtained in a few solvents, including EtOH, 2-PrOH, and DMF, but not in Me<sub>2</sub>SO. Stripping signals were more drawn out and had poorer sensitivity than those obtained with the other alkali metal ions.

Resolution of stripping signals of mixtures of alkali metal ions is generally modest; this is in agreement with the poor resolution previously observed in polarographic half-wave potentials (11). Nevertheless, sodium and potassium ions at comparable concentrations can be resolved in GBL and NMP;



**Figure 2.** Stripping signals of human blood serum in dimethyl sulfoxide. Conditions: Successive injection of 10- $\mu$ L aliquots of serum into 20 mL of  $10^{-3}$  M  $\text{HgCl}_2$  +  $10^{-1}$  M TEAP;  $E_{\phi}$  -2.99 V vs.  $\text{Ag}^+/\text{Ag}$ ;  $t_{\phi}$  60 s.



**Figure 3.** Concentration dependence of limiting stripping time of human blood serum in dimethyl sulfoxide: (O) human blood serum,  $C_{\text{Na}^+} + C_{\text{K}^+} = 147.7$  mM; (□) synthetic serum,  $C_{\text{Na}^+} + C_{\text{K}^+} = 147.7$  mM; (Δ) sodium ion only,  $C_{\text{Na}^+} = 143.0$  mM. Conditions: samples added to  $10^{-3}$  M  $\text{HgCl}_2$  +  $10^{-1}$  M TEAP;  $E_{\phi}$  -2.99 V vs.  $\text{Ag}^+/\text{Ag}$ ;  $t_{\phi}$  60 s. Correlation coefficients for all three lines are equal to 0.9998.

we are investigating the possibility of optimizing solvent mixtures for this purpose.

**Potentiometric Stripping Analysis of Alkaline Earth Metal Ions.** The PSA of the alkaline earth metal ions is less satisfactory than that of the alkali metal ions and was studied in less detail. Nevertheless, stripping signals were obtained for  $\text{Ca}^{2+}$ ,  $\text{Sr}^{2+}$ , and  $\text{Ba}^{2+}$  ions, as well as  $\text{Mg}^{2+}$  ion, in EtOH, and for  $\text{Ca}^{2+}$  ion also in  $\text{Me}_2\text{SO}$ , DMF, GBL, and NMP.

However, signals were less sensitive, more drawn out, and less reproducible than those observed with the alkali metal ions; it is likely that these problems are caused by precipitation of the hydroxides on the electrode surface. In  $\text{Me}_2\text{SO}$ , the stripping signal of  $\text{Ca}^{2+}$  is so much less sensitive than that of  $\text{Na}^+$  or  $\text{K}^+$  that low concentrations of  $\text{Ca}^{2+}$  do not significantly interfere in the PSA of alkali metal ions in such samples as blood serum (see below); this is, of course, a blessing in disguise.

#### Potentiometric Stripping Analysis of Sodium Plus Potassium Ions in Blood Serum and Synthetic Seawater.

In Figure 2, stripping signals are shown for different concentrations of human blood serum in  $\text{Me}_2\text{SO}$  while, in Figure 3, limiting stripping times are compared for different concentrations of human blood serum, of synthetic serum containing only sodium and potassium ions, and of sodium ion only. Figure 3 shows that calcium and magnesium and other metal ions, as well as proteins, in human blood serum do not significantly interfere in the PSA of sodium and potassium ions. (It is also evident that the sensitivity for the sodium-potassium mixture is higher than that for sodium ion only at the same concentration.) Analogous results were obtained with synthetic seawater; stripping signals were essentially those produced by sodium and potassium ions, with no measurable interference from calcium and magnesium ions or from the more noble metals which are present in much lower concentrations.

In conclusion, the fact that stripping analysis, whether PSA or VSA, is a valuable complementary technique to spectroscopic methods for the determination of the more noble metals has been well established (12). We have shown in this paper that the scope of stripping analysis can be extended to some of the more electropositive metals in a simple, practical manner. We are investigating further the determination of lithium and calcium ions and the resolution of sodium ion from potassium ion.

#### LITERATURE CITED

- (1) Jagner, D.; Granell, A. *Anal. Chim. Acta* **1976**, *83*, 19-26.
- (2) Coetzee, J. F.; Hussam, A.; Petrick, T. Pittsburgh Conference on Analytical Chemistry and Applied Spectroscopy, Atlantic City, NJ, March 1981; ABC Press: Monroeville, PA, 1981; paper 77.
- (3) Bruckenstein, S.; Bixler, J. W. *Anal. Chem.* **1965**, *37*, 786-790.
- (4) Perone, S. P.; Davenport, K. K. *J. Electroanal. Chem.* **1966**, *12*, 269-276.
- (5) Buffle, J. *J. Electroanal. Chem.* **1981**, *125*, 273-294.
- (6) Coetzee, J. F.; Hussam, A., unpublished results.
- (7) Coetzee, J. F.; Istone, W. K. *Anal. Chem.* **1980**, *52*, 53-59.
- (8) Coetzee, J. F.; Martin, M. W. *Anal. Chem.* **1980**, *52*, 2412-2416.
- (9) Jagner, D.; Åren, K. *Anal. Chim. Acta* **1978**, *100*, 375-388.
- (10) Coetzee, J. F.; Hussam, A. *J. Solution Chem.* **1982**, *11*, 395-407.
- (11) Mann, C. K.; Barnes, K. K. "Electrochemical Reactions in Nonaqueous Solvents"; Marcel Dekker: New York, 1970.
- (12) Ryan, M. D.; Wilson, G. S. *Anal. Chem.* **1982**, *54*, 20R-27R.

RECEIVED for review July 12, 1982. Accepted October 18, 1982. This work was supported by the National Science Foundation under Grant Numbers CHE-7727699 and CHE-8106778.

# Determination of Petroleum Sterane Distributions by Mass Spectrometry with Selective Metastable Ion Monitoring

Geoff A. Warburton

Kratos Limited, Barton Dock Road, Urmston, Manchester M312LD, United Kingdom

John E. Zumberge\*

Cities Service Research, Box 3908, Tulsa, Oklahoma 74102

Conventional GC/MS analysis of crude oils and sedimentary rock extracts for steranes, in which the  $m/z$  217 fragment ion is monitored, often reveals a complex and incompletely resolved structural and stereoisomeric mixture of  $C_{27}$ ,  $C_{28}$ , and  $C_{29}$  steranes. Increased specificity can be achieved by monitoring the spontaneous (unimolecular) fragmentation of sterane parent ions occurring in the first field-free region of a double focusing mass spectrometer. The sterane metastable parent ion transitions, corresponding to  $372^+ \rightarrow 217^+$ ,  $386^+ \rightarrow 217^+$ , and  $400^+ \rightarrow 217^+$ , can be separately observed during a single GC/MS run by using a programmable power supply to vary the accelerating voltage while holding the magnetic and electrostatic fields at appropriate constant values.

Steroidal hydrocarbons are common constituents of crude oils and ancient sedimentary rocks. Sterane distributions can be used as indicators of petroleum source rock depositional environments because the carbon atom skeleton of steranes is a remnant of the biochemical precursor steroidal structure (1). For example, a relatively greater abundance of  $C_{29}$  steranes (e.g., stereoisomers of 24-ethylcholestanes) over  $C_{27}$  steranes could suggest that the precursor organic matter contained more land-derived biochemical compounds rather than those derived from marine organisms since sterol distributions dominated by  $C_{29}$  components are characteristic of vascular land plants (1). Steranes are also useful parameters in petroleum exploration as correlation and thermal maturity indicators (2-4). With increasing temperature, the biologically derived 20R isomer of  $5\alpha(H)$ ,  $14\alpha(H)$ ,  $17\alpha(H)$ -steranes is isomerized to the 20S configuration, which is not found in biological systems (3-5). Oils and sedimentary rocks which have experienced different degrees of thermal maturation can, therefore, have correspondingly different 20S/20R sterane ratios. In oil-oil and oil-source rock correlation studies, sterane distributions are used to identify oils which share a common source and thermal history (4).

Routine capillary gas chromatographic/mass spectrometric (GC/MS) analysis of aliphatic hydrocarbon fractions of crude oils or sedimentary rock extracts allows the monitoring of the electron impact (EI)  $m/z$  217 fragment ion which is the base peak in  $14\alpha(H)$ -sterane EI mass spectra (6). The resulting mass fragmentograms frequently reveal complex and incompletely resolved structural and stereoisomeric mixtures of  $C_{27}$ ,  $C_{28}$ , and  $C_{29}$  steranes. Most problematic is the coelution of rearranged  $C_{29}$  steranes (also known as diasteranes) with  $C_{28}$  and  $C_{27}$  normal steranes (3, 4). Thus, chromatographic coelution of sterane homologues places constraints on the accurate measurement of geochemically significant sterane components.

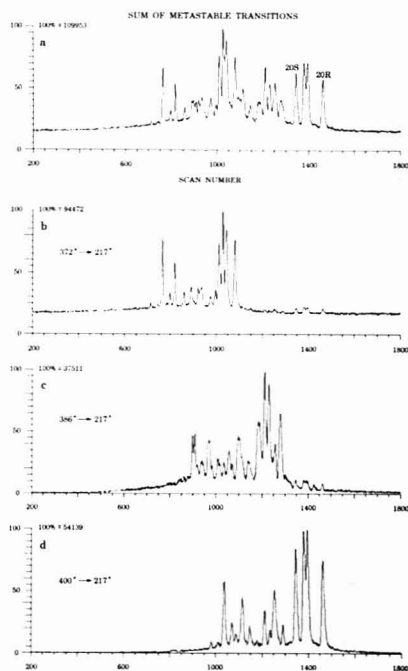


Figure 1. (a) Sterane distributions in a crude oil from the Williston Basin, Montana, using selective metastable ion monitoring (SMIM); part b represents the  $C_{27}H_{48}$  steranes while parts c and d show the  $C_{28}H_{50}$  and  $C_{29}H_{52}$  steranes, respectively.

In order to increase the specificity of petroleum sterane determinations, we used selective metastable ion monitoring (SMIM) in the GC/MS analyses of a number of crude oil aliphatic hydrocarbon fractions. Monitoring the spontaneous (unimolecular) fragmentation of sterane parent ions occurring in the first field-free region of a double focusing mass spectrometer (in which the electrostatic field precedes the magnetic sector) allows for the discrimination of steranes with disparate molecular weights. The most common steranes (both regular and rearranged) in petroleum have molecular weights of 372 amu ( $C_{27}H_{48}$ ), 386 amu ( $C_{28}H_{50}$ ), and 400 amu ( $C_{29}H_{52}$ ). The

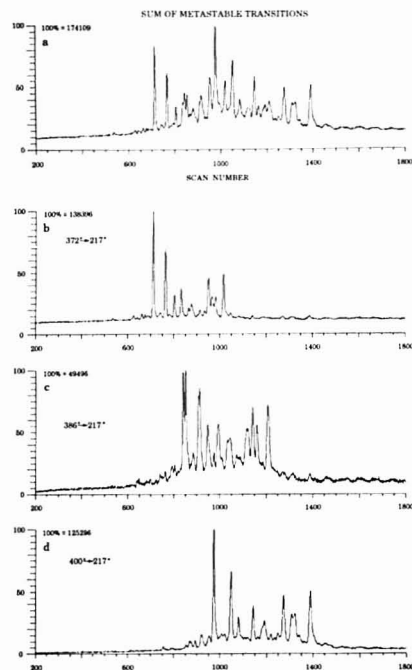


Figure 2. Steranes in a sediment sample (Coupvray) extract from the Paris Basin (3).

sterane metastable parent ion transitions ( $372^+ \rightarrow 217^+$ ,  $386^+ \rightarrow 217^+$ , and  $400^+ \rightarrow 217^+$ ) are known to occur readily in the first field-free region (7). Gallegos (7) used metastable ion methods to measure the abundances of  $C_{27}$ ,  $C_{28}$ , and  $C_{29}$  steranes in a Green River shale extract, although only direct insertion mass spectrometry (not GC/MS) was used. Separation of isomers was therefore not achieved. More recently, Gaskell and Millington (8) and Finlay and Gaskell (9) used selected metastable peak monitoring in quantitative GC/MS to detect and measure dihydrotestosterone and testosterone in human blood plasma. In the present study, we have combined the features of an abundant metastable sterane fragment ion with high-resolution capillary gas chromatography to greatly increase the specificity of petroleum sterane determinations. In addition, the three different sterane parent ion metastable transitions were monitored in a single GC/MS run by using a programmable power supply to vary the accelerating voltage, all under data system control.

### EXPERIMENTAL SECTION

Aliphatic hydrocarbon fractions were obtained from pentane-deasphalted crude oil samples (subsequent to light end evaporation) which were subjected to combined alumina/silica column liquid chromatography. Also, a cyclic/branched aliphatic hydrocarbon fraction from a sediment extract of a sample (Coupvray) from the Paris Basin (3) was examined. The aliphatic hydrocarbon fractions were then analyzed with the Kratos MS25/DS55 GC/MS system equipped with metastable ion monitoring facilities. The GC was a Carlo Erba 4160 fitted with

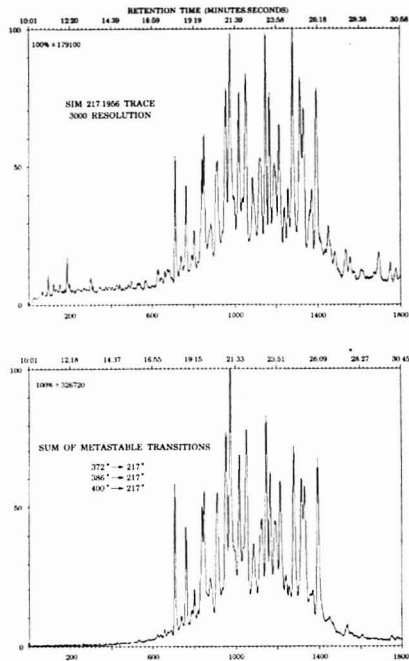


Figure 3. A comparison of sterane distributions derived from selected ion monitoring (SIM) of the  $m/z$  217 ion at 3000 resolution and SMIM from another crude oil from the Williston Basin.

a Grob type split/splitless injector (at  $270^\circ\text{C}$ ) and a 20-m fused silica capillary column coated with OV-1 (methylsilicone). Analyses were performed in the split mode (25:1). The GC column oven temperature program was the following:  $60^\circ\text{C}$  to  $100^\circ\text{C}$  at  $35^\circ\text{C}/\text{min}$  and then to  $230^\circ\text{C}$  at  $10^\circ\text{C}/\text{min}$ , subsequently ramping to  $280^\circ\text{C}$  at  $2^\circ\text{C}/\text{min}$ . The He flow rate through the GC column was about 1 mL/min made up to 30 mL/min prior to entering the GC/MS interface which consisted of a jet separator held at  $250^\circ\text{C}$ . Mass spectrometer parameters used were the following: source temperature =  $220^\circ\text{C}$ ; electron beam current =  $100\ \mu\text{A}$ ; and electron voltage =  $60\ \text{eV}$ .

The three metastable parent ion transitions monitored were  $372.3756^+ \rightarrow 217.1956^+$ ,  $386.3913^+ \rightarrow 217.1956^+$ , and  $400.4069^+ \rightarrow 217.1956^+$  which correspond to  $C_{27}\text{H}_{48}$ ,  $C_{28}\text{H}_{50}$ , and  $C_{29}\text{H}_{52}$  sterane isomers, respectively. By use of an authentic cholesterol standard in the direct insertion probe, the  $m/z$  217 ion was located by adjusting the magnet setting. The electrostatic voltage ( $E$ ) and acceleration voltage ( $V$ ) supplies were unlinked, and the  $E$  reference voltage was supplied by the internal reference of the mass spectrometer. The  $V$  reference was supplied by a binary programmable power supply driven by DS55 software. Increasing the accelerating voltage from 2 kV to 3.429 kV allowed the transition  $372^+ \rightarrow 217^+$  occurring in the first field-free region to be located at the collector (10). Similarly, increasing  $V$  to 3.558 kV and 3.687 kV allowed the transitions  $386^+ \rightarrow 217^+$  and  $400^+ \rightarrow 217^+$  to be located, respectively. The data system, DS55, was programmed to switch to each of these voltages repetitively during the GC/MS run and record the signal obtained. The dwell time on each transition was 150 ms; a sweep of  $\pm 50\ \text{ppm}$  was applied to the  $V$  reference supply to ensure collection of peak top data. Data from the MS25 were acquired through a 200-kHz preprocessor interface operating at a sampling rate of 100  $\mu\text{s}$ . The MS25



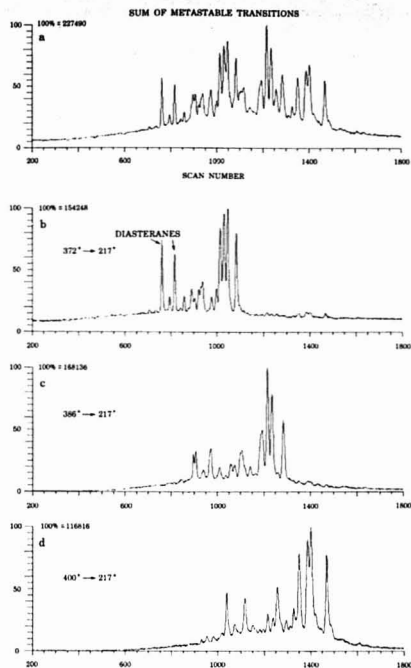


Figure 4. Steranes in a nondegraded Colombian crude oil using SMIM.

resolution was set to 600 (10% valley) for the SMIM experiments. Conventional single ion monitoring (SIM) experiments were also performed on the hydrocarbon fractions at 3000 resolution using standard DS55 SIM software in order to compare the resulting sterane distributions to those obtained during SMIM experiments. The  $m/z$  217.1956 ion was monitored along with two other masses in order to simulate the same conditions as in SMIM.

## RESULTS AND DISCUSSION

Figure 1 shows the metastable ion sterane distributions in a crude oil aliphatic hydrocarbon fraction from the Williston Basin in Montana. In this figure, b represents the  $372^+ \rightarrow 217^+$  ( $C_{27}$  steranes) transition while c and d show the  $386^+ \rightarrow 217^+$  ( $C_{28}$  steranes) and  $400^+ \rightarrow 217^+$  ( $C_{29}$  steranes) transitions, respectively. The top portion of each figure, a, is simply the computer summation of b, c, and d normalized to the most abundant component. Prior to SMIM, only the  $C_{29}$  steranes (i.e., the stereoisomers of 24-ethylcholestane) could be used for thermal maturation determinations (e.g., 20S/20R) with any degree of confidence because the  $C_{27}$  and  $C_{28}$  stereoisomers usually coelute with  $C_{29}$  diasteranes (3, 4). Also, in a number of samples an unknown component, which is not a regular  $C_{29}$  sterane, coelutes on OV-1 with the 20S isomer of 24-ethylcholestane (11). Hence, using SMIM, both  $C_{27}$  and  $C_{28}$  sterane ratios can be more precisely determined, as well as  $C_{29}$  ratios. In addition, the  $C_{27}$  isomers can be quantitatively compared to the  $C_{28}$  and  $C_{29}$  homologues by separately summing the total ion currents in b, c, and d, respectively. In this manner, the relative abundance of sterane homologues can be used for determining source rock depositional environments.

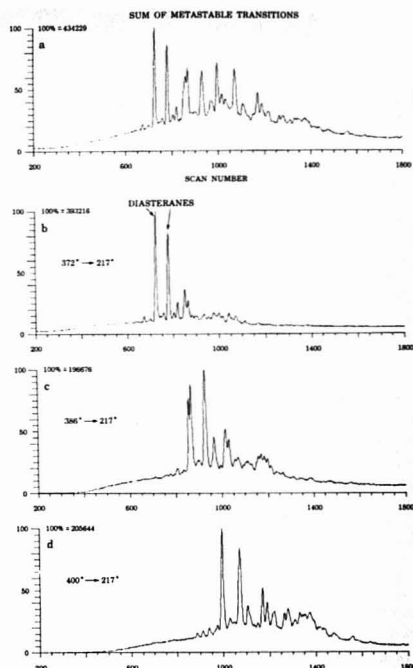


Figure 5. Sterane distributions in a biodegraded Colombian crude oil using SMIM.

Figure 2 illustrates the SMIM sterane distributions from a hydrocarbon extract of a sediment sample (Coupvray) at 2100 m from the Paris Basin. The nominal  $m/z$  217 mass fragmentogram and resulting sterane distribution of this same extract sample have been elucidated by Mackenzie et al. (3). Comparison with the sum of the metastable parent ion transitions shown in Figure 2a and the Mackenzie et al. (3) SIM distribution indicate a close correlation suggesting that SMIM is comparable to SIM in respect to relative abundances of various sterane components. However, in the SMIM technique the individual sterane homologue distributions are much more clearly defined (Figure 2b-d). Figure 3 is a comparison between medium resolution SIM of the  $m/z$  217 ion and SMIM of another crude oil from the Williston Basin. Again, the two traces are very similar.

The two oils shown in Figures 4 and 5 are from Colombia, South America. Both have the same origin (12), except that one oil (Figure 5) was subsequently severely biodegraded by bacteria in the reservoir (after generation and perhaps migration) while the other oil (Figure 4) has not been significantly altered. It has been reported (13) that the diasteranes are relatively more resistant to severe biodegradation than the regular steranes. On comparison of Figures 4 and 5, it can be seen that the Colombia oil diasteranes have survived biodegradation more effectively than the regular steranes. (Diasteranes elute prior to regular steranes of the same molecular weight as indicated in Figures 4 and 5). Also, the distributions of specific sterane homologues (i.e., either  $C_{27}$ ,  $C_{28}$ , or  $C_{29}$ ), whether regular or rearranged steranes, are ap-

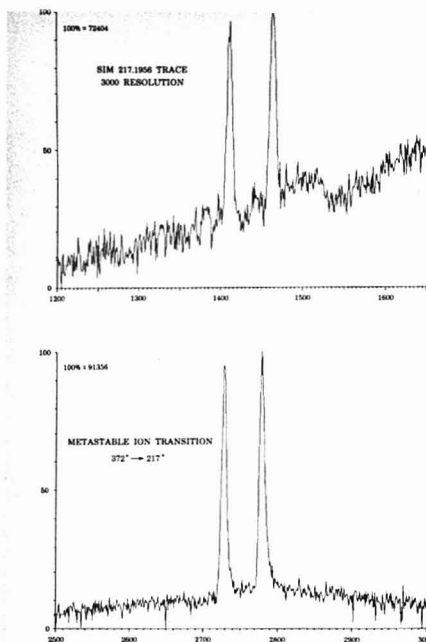


Figure 6. A sensitivity comparison between medium resolution SIM and SMIM using 100 pg of a cholestane standard (50 pg of  $5\beta(H)$ - and 50 pg of  $5\alpha(H)$ -cholestane).

parent from b, c, and d in these figures.

Figure 6 is a comparison of the conventional SIM  $m/z$  217

trace (3000 resolution) with the metastable ion transition  $372^+ \rightarrow 217^+$  trace of 100 pg of a cholestane standard (50 pg of  $5\beta(H)$ - and 50 pg of  $5\alpha(H)$ -cholestane). It is clear that SMIM is more sensitive to sterane detection than medium resolution SIM.

#### ACKNOWLEDGMENT

We thank J. M. Heard for chromatographic isolation of crude oil aliphatic hydrocarbon fractions and J. R. Maxwell for providing the Coupvray extract from the Paris Basin. We also acknowledge M. J. Leenheer, A. S. Mackenzie, J. R. Maxwell, S. E. Palmer, Z. Sofer, and R. S. Stradling for helpful comments and suggestions.

#### LITERATURE CITED

- (1) Tissot, B. P.; Welte, D. H. "Petroleum Formation and Occurrence"; Springer-Verlag: New York, 1978; Chapter 3.
- (2) Selfert, W. K.; Moldovan, J. M. *Geochim. Cosmochim. Acta* **1978**, *42*, 77-95.
- (3) Mackenzie, A. S.; Patience, R. L.; Maxwell, J. R.; Vanderbroucke, M.; Durand, B. *Geochim. Cosmochim. Acta* **1980**, *44*, 1709-1721.
- (4) Selfert, W. K.; Moldovan, J. M. *Geochim. Cosmochim. Acta* **1981**, *45*, 783-794.
- (5) Mulhern, L. J.; Ryback, G. *Nature (London)* **1975**, *256*, 301-302.
- (6) Mulhern, L. J.; Ryback, G. In "Advances in Organic Geochemistry"; Campos, R.; Goñi, J., Eds.; ENADIMSA: Madrid, Spain, 1975; pp 173-192.
- (7) Gallegos, E. J. "High Performance Mass Spectrometry"; American Chemical Society: Washington DC, 1978; Chapter 15.
- (8) Gaskell, S. J.; Millington, D. S. *Biomed. Mass Spectrom.* **1978**, *5*, 557-558.
- (9) Finlay, E. M. H.; Gaskell, S. J. *Clin. Chem. (Winston-Salem, NC)* **1981**, *27*, 1165-1170.
- (10) Jennings, K. R. "Some Aspects of Metastable Transitions, Mass Spectrometry Techniques and Application"; Milne, G. W. H., Ed.; Wiley-Interscience: New York, 1971.
- (11) Mackenzie, A. S.; Maxwell, J. R., University of Bristol, personal communication, 1982.
- (12) Zumberge, J. E. 26th International Geological Congress, Paris, 1980; Abstract, p 806.
- (13) Selfert, W. K.; Moldovan, J. M. *Geochim. Cosmochim. Acta* **1979**, *43*, 111-126.

RECEIVED for review August 16, 1982. Accepted October 6, 1982.

# Theoretical and Experimental Determination of Band Broadening in Liquid Chromatography

Jeng-Chyh Chen and Stephen G. Weber\*

Department of Chemistry, University of Pittsburgh, Pittsburgh, Pennsylvania 15260

The axial diffusion term and the mass transfer terms of the band broadening equation for liquid chromatography are derived from the random walk model. The results, while simple to derive, are very similar to the more complex mass balance model, and in certain terms give greater insight into the physical processes under consideration. The flow dispersion term is experimentally determined. Equations in the form of the van Deemter equation and the Knox equation are fitted to the experimental data after the effect of extracolumn band broadening is removed. With known theoretical terms for axial diffusion and mass transfer, the solute diffusion coefficient in the pore is obtained under the assumption of fast kinetics. It is found that an equation in the form of the van Deemter equation gives more physically meaningful results than an equation in the form of the Knox equation. For the small solutes studied, the diffusion coefficients within the porous stationary phase increase with increasing molecular weight.

When chromatographic conditions are controlled so that the solute distribution isotherm is linear, there are five processes which tend to separate a migrating solute molecule from its neighbors to cause band broadening: (1) axial molecular diffusion, (2) flow dispersion in the packed bed, (3) mass transfer between mobile zone and stationary zone, (4) mass transfer between mobile phase and stationary phase (or kinetics), (5) extracolumn band broadening.

Before one can properly discuss all the dynamic processes of chromatography, it is necessary to discuss the environment of the packing. The environment, as illustrated in Figure 1, includes stationary phase, support phase, and mobile phase. The mobile phase can be further divided into stagnant mobile phase which is in the interstices of the column packing. Flowing mobile phase is the mobile zone. The support phase, the stationary phase, and the stagnant mobile phase compose the stationary zone.

During the advances in band spreading theories, several theoretical models of band spreading have been used to derive the plate height equation (1). They are the plate model, the random walk model, nonequilibrium theory, and the mass balance model. According to Giddings the plate model has been "entirely inadequate for the current burdens of theoretical use" (2). The other three models have remained very useful in understanding the processes of band spreading in chromatography. Among these three models, the random walk model provides an approach which gives little mathematical difficulty as well as presenting an easily understood, microscopic picture of chromatographic processes.

Figure 2 illustrates the microscopic point of view of the band broadening processes in the column. Figure 2a illustrates the dispersion due to axial diffusion. Two neighboring solute molecules are separated from each other because of diffusion. The diffusion can occur outside the pores as well as inside the

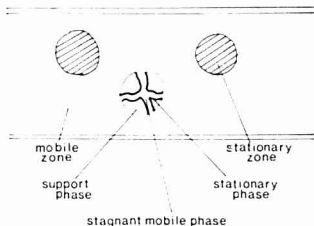
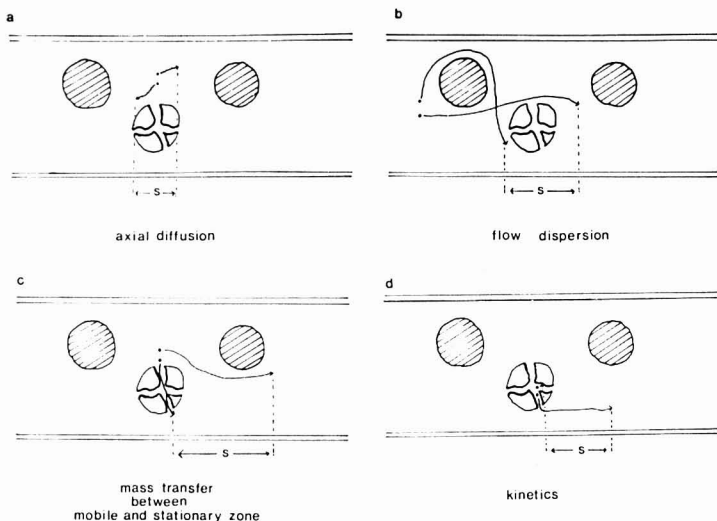


Figure 1. The environment of the packing in the column.

pores. Figure 2b illustrates the dispersion due to flow dispersion. Two neighboring solute molecules are separated by the tortuous nature of the flow coupled with diffusion. Figure 2c illustrates the dispersion due to the mass transfer between mobile and stationary zones. The neighboring solute molecules are separated because the one which transfers into the stationary zone tends to stay in the stagnant mobile phase and stationary phase while the other solute molecule in the mobile zone moves ahead. Figure 2d illustrates the dispersion due to mass transfer between mobile phase and stationary phase. Two neighboring solute molecules in the pore are separated because one transfers into the stationary phase while the other molecule diffuses out of the pore and moves ahead. Each of these processes is random in nature and independent of the others. The random walk model may be used to calculate the variance of each of these independent, random processes. In the random walk model one must compute the average length of a step in the process. For any of the processes illustrated in Figure 2 this is the average of the separation distance between the two solute molecules under scrutiny. The number of steps the molecules take is determined by knowing the time a solute molecule takes to traverse a certain distance. The specific details are left to the next section. Finally, knowing the number of steps,  $n$ , and the length of each step,  $l$ , one can immediately determine the variance of the process, since  $\sigma^2 = l^2 n$ . Since the processes are stochastically independent their variances add directly to obtain an overall peak variance, from which the height equivalent to a theoretical plate ( $H$ ) may be obtained, since  $H$  is just the variance (in units of length<sup>2</sup>) divided by the column length. In this paper, the random walk model will be used to discuss band broadening processes of diffusion and mass transfer in liquid chromatography. Due to the extremely complicated processes of flow dispersion and the resulting differences in the various theoretical derivations of band spreading due to this process, experiments were performed to clarify this term. The final plate height equation will be compared to the results of Horvath and Lin (3) and Knox (4).

## THEORY

When the solute flows through the column, it will spend



**Figure 2.** Microscopic view of band broadening processes: (a) axial diffusion, (b) flow dispersion, (c) dispersion due to mass transfer between mobile zone and stationary zone, (d) dispersion due to kinetics. In each case initially adjacent solute molecules are separated by a distance due to their taking different "steps".

some of the time in the flowing mobile phase, some of the time in the stagnant mobile phase and some of the time in or on the stationary phase. Thus, the total retention time  $t_R$  is expressed as a sum of times

$$t_R = t_s + t_{sm} + t_{fm} \quad (1)$$

where  $t_s$  is the time the solute stays in the stationary phase,  $t_{sm}$  is the time the solute stays in the stagnant mobile phase, and  $t_{fm}$  is the time the solute stays in the flowing mobile phase. For unretained solutes the retention time  $t_0$  is

$$t_0 = t_{fm} + t_{sm} \quad (2)$$

**Axial Molecular Diffusion.** The variance of the concentration distribution due to axial molecular diffusion can be obtained directly from the Einstein equation

$$\sigma_L^2 (\text{axial diffusion}) = 2D^{\text{eff}}t \quad (3)$$

where  $D^{\text{eff}}$  is the effective diffusion coefficient of the solute within the column and  $t$  is the time of solute residence in the column. The total axial diffusion has contributions from the axial diffusion in the stagnant mobile phase, and the axial diffusion in the flowing mobile phase. Therefore

$$\sigma_L^2 (\text{axial diffusion}) = 2(D_s^{\text{eff}}t_s + D_{sm}^{\text{eff}}t_{sm} + D_{fm}^{\text{eff}}t_{fm}) \quad (4)$$

where  $D_s^{\text{eff}}$  is the effective diffusion coefficient of the solute in the stationary phase,  $D_{sm}^{\text{eff}}$  is the effective diffusion coefficient of the solute in the stagnant mobile phase, and  $D_{fm}^{\text{eff}}$  is the effective diffusion coefficient of the solute in the interstitial flowing mobile phase.

Since stagnant mobile zone and flowing mobile zone are actually the same phase, the ratio  $t_{sm}/t_{fm}$  must be equal to the ratio of the volume in the pores to the volume outside the particles

$$t_{sm}/t_{fm} = \epsilon_p/\epsilon_z \quad (5)$$

where  $\epsilon_p$  is the pore porosity,  $\epsilon_z$  is the interparticular porosity, and

$$\epsilon_p = V_p/V_k \quad (6)$$

$$\epsilon_z = V_z/V_k \quad (7)$$

where  $V_p$  is the total volume in the pores,  $V_z$  is the total volume outside the particles, and  $V_k$  is the total volume of the empty column.

The reduced plate height  $h$  is defined by

$$h = \sigma_L^2/d_p L \quad (8)$$

where  $L$  is the column length and  $d_p$  is the particle diameter.

$$h_{(\text{axial diffusion})} = \frac{2 \frac{D_{sm}^{\text{eff}} \epsilon_p}{D_m \epsilon_z} + \frac{D_{fm}^{\text{eff}}}{D_m} + \frac{D_s^{\text{eff}} t_s}{D_m t_{fm}}}{\nu} \quad (9)$$

where  $\nu$  is reduced velocity which is defined as

$$\nu = \mu_e d_p / D_m \quad (10)$$

and  $\mu_e$  is the interstitial linear velocity

$$\mu_e = L/t_{fm} \quad (11)$$

where  $D_m$  is the diffusion coefficient of the solute in the bulk solvent.

**Mass Transfer between Mobile Zone and Stationary Zone.** The mass transfer term of the plate height equation has been derived by the random walk model, nonequilibrium theory, and the mass balance model (1). It will be shown that our derivation of this term by using the random walk model not only provides the simplest calculation but also gives considerable insight concerning the band broadening by this effect.

The phase capacity factor  $k'$  is the ratio of the times a solute stays in the stationary phase and the mobile phase

$$k' = \frac{t_R - t_0}{t_0} = \frac{t_s}{t_{fm} + t_{sm}} \quad (12)$$

The zone capacity factor  $k''$ , however, is the ratio of the times a solute stays in the stationary zone and the mobile zone.

$$k'' = \frac{t_R - t_{fm}}{t_{fm}} = \frac{t_s + t_{sm}}{t_{fm}} \quad (13)$$

By the random walk model, each step which transfers the solute from the mobile zone to the stationary zone must be followed by a step which transfers the solute from the stationary zone back to the mobile zone. Then the total number of adsorption steps,  $m$ , must equal the total number of desorption steps. Hence

$$k'' = \frac{(t_R - t_{fm})/m}{t_{fm}/m} = \frac{t_{sz}''}{t_{fm}''} \quad (14)$$

Where  $t_{fm}''$  is the average time which a solute stays in the mobile zone within one step of the random walk and  $t_{sz}''$  is the average time that the solute stays in the stationary zone within one random walk step. Then the total number of adsorption steps (and the total number of desorption steps) is  $L/\mu_e t_{fm}''$  so the total number of random walk steps is  $2L/\mu_e t_{fm}''$ . The distance that the zone spreads relative to its center for each step is

$$l = \mu_e t_{fm}'' - \frac{1}{1 + k''} \mu_e t_{fm}'' \quad (15)$$

where  $1/(1 + k'')$  is the fraction of solute in the mobile zone. Then the variance due to mass transfer between zones,  $\sigma_{L,miz}^2$  can be expressed by

$$\sigma_{L,miz}^2 = l^2 n = 2L \frac{k''^2}{(1 + k'')^2} \mu_e t_{fm}'' = 2L \frac{k''^2}{(1 + k'')^2} \mu_e t_{sz}'' \quad (16)$$

Thus, the reduced plate height is equal to

$$h_{miz} = \frac{2k''^2}{(1 + k'')^2} \frac{\mu_e}{D_p} t_{sz}'' \quad (17)$$

When a solute molecule stays in the stationary zone, it spends some of its time in the stationary phase and some of its time in the stagnant mobile phase. Therefore

$$t_{sz}'' = t_{sm}'' + t_s'' \quad (18)$$

where  $t_{sm}''$  is the average time a solute stays in the stagnant mobile phase within one random walk step and  $t_s''$  is the average time a solute stays in the stationary phase. Since  $t_{sm}''$  is the average time for the solute molecule to escape from the stagnant mobile phase, one can use the Einstein equation

$$t_{sm}'' = \bar{d}^2 / 2D_{sm}^{eff} \quad (19)$$

where  $\bar{d}^2$  is the mean square distance which a molecule must diffuse in order to emerge from a particle of packing. For particles of a given geometrical type,  $\bar{d}^2$  will be proportional to  $d_p^2$ , thus

$$t_{sm}'' = q' \frac{d_p^2}{2D_{sm}^{eff}} \quad (20)$$

For spherical particles (5),  $q' = 1/30$

$$t_{sm}'' = \frac{1}{30} \frac{d_p^2}{2D_{sm}^{eff}} \quad (21)$$

The time the solute stays in the stationary phase in one step is

$$t_s'' = \frac{t_s}{m} = \frac{t_s}{L/\mu_e t_{fm}''} \quad (22)$$

Equations 2, 5, 11, and 22 yield

$$t_s'' = k' \left( \frac{\epsilon_p}{\epsilon_z} + 1 \right) t_{fm}'' = k' \left( 1 + \frac{\epsilon_z}{\epsilon_p} \right) t_{sm}'' \quad (23)$$

Therefore

$$h_{miz} = \frac{2k''^2}{(1 + k'')^2} \frac{\mu_e}{D_p} \frac{1}{30} \frac{d_p^2}{2D_{sm}^{eff}} + k' \left( 1 + \frac{\epsilon_z}{\epsilon_p} \right) t_{sm}'' \quad (24)$$

From eq 21 and 24 one obtains

$$h_{miz} = \frac{2k''^2}{(1 + k'')^2} \frac{\mu_e d_p}{D_m} \frac{1}{30} \frac{D_m}{2D_{sm}^{eff}} \left( 1 + k' \left( 1 + \frac{\epsilon_z}{\epsilon_p} \right) \right) \quad (25)$$

From eq 12 and 13 one can find  $k''$  in terms of  $k'$

$$k'' = \frac{\epsilon_p}{\epsilon_z} + k' + \frac{\epsilon_p}{\epsilon_z} k' \quad (26)$$

Then eq 26 becomes

$$h_{miz} = \frac{1}{30} \frac{(\epsilon_z/\epsilon_p) k'^2}{(1 + k'')^2} \frac{D_m}{D_{sm}^{eff}} \quad (27)$$

**Mass Transfer between Mobile Phase and Stationary Phase.** The dispersion from mass transfer between mobile phase and stationary phase arises because solutes adsorbed onto the stationary phase at any instant fall behind their neighbors which diffuse out of the pore and move ahead. Since this term is determined by the adsorption and desorption rate between stationary phase and mobile phase, it is also called the kinetics term.

Let  $t_s''$  be the average residence time of a solute molecule in the mobile phase in one step of a random walk and let  $t_s''$  be the average residence time of a solute molecule in the stationary phase in one step of a random walk. The solute in the mobile phase will spend some of its time in the stagnant mobile phase and some of its time in the flowing mobile phase. As discussed before, the ratio of the residence times for a solute in flowing mobile phase to stagnant mobile phase will depend on the ratio of the volume outside the particles to the volume within the pores. Therefore, the average residence time of a solute in the flowing mobile phase will be  $t_s'' \epsilon_z/(\epsilon_p + \epsilon_z)$ . Again, the number of adsorptions should be equal to the number of desorptions. Then the total number of random walk steps,  $n$ , becomes

$$n = \frac{2L}{\mu_e^2 t_s'' \epsilon_z/(\epsilon_p + \epsilon_z)} \quad (28)$$

and the distance that the zone spreads relative to its center in each step is

$$l = \mu_e t_s'' \frac{\epsilon_z}{\epsilon_p + \epsilon_z} - \frac{1}{1 + k'} \mu_e t_s'' \frac{\epsilon_z}{\epsilon_p + \epsilon_z} \quad (29)$$

where  $1/(1 + k')$  is the fraction of the solute molecules in the mobile phase. Then the variance due to mass transfer between phases,  $\sigma_{L,mtp}^2$ , is

$$\sigma_{L,mtp}^2 = l^2 n = 2L \frac{k'^2}{(1 + k')^2} \mu_e t_s'' \frac{\epsilon_z}{\epsilon_p + \epsilon_z} \quad (30)$$

Since

Table I. Retention Time and Reduced Plate Height for Column 1

	methyl <i>p</i> -hydroxybenzoate	ethyl <i>p</i> -hydroxybenzoate	propyl <i>p</i> -hydroxybenzoate	<i>n</i> -butyl <i>p</i> -hydroxybenzoate
		Flow Rate 0.0485 mL/s		
$t_R^a$	132.77 ± 1.45	182.20 ± 2.67	277.15 ± 1.07	
$h_{tot}^a$	18.62 ± 0.14*	16.37 ± 0.17	14.59 ± 0.18	
		Flow Rate 0.0333 mL/s		
$t_R$	196.6 ± 1.1	273.8 ± 2.35	427.2 ± 5.7	733.1 ± 7.8
$h_{tot}$	14.13 ± 1.07	13.45 ± 0.74	12.04 ± 0.48	10.55 ± 0.02
		Flow Rate 0.0252 mL/s		
$t_R$	255.9 ± 1.2	352.6 ± 1.5	545.4 ± 2.2	917.3 ± 5.5
$h_{tot}$	13.72 ± 0.22*	12.66 ± 0.47	11.35 ± 0.42	9.98 ± 1.04
		Flow Rate 0.0168 mL/s		
$t_R$	392.2 ± 0.7	549.1 ± 1.6	862.9 ± 3.5	1479.7 ± 6.0
$h_{tot}$	10.22 ± 0.01	9.26 ± 0.16	8.21 ± 0.23	7.90 ± 0.73
		Flow Rate 0.0119 mL/s		
$t_R$	552.7 ± 4.0	772.7 ± 6.1	1211 ± 13.5	2075 ± 28.4
$h_{tot}$	8.91 ± 0.06*	7.68 ± 0.09*	6.89 ± 0.30	6.37 ± 0.18
		Flow Rate 0.00491 mL/s		
$t_R$	1315 ± 1	1842.6 ± 5	2905.4 ± 9	4966 ± 28.8
$h_{tot}$	6.45 ± 0.02*	5.71 ± 0.12	5.20 ± 0.08*	4.76 ± 0.67

<sup>a</sup>  $\bar{x} \pm \sigma$ .  $\bar{x}$  is the average value of three measurements, except where indicated (\*) which is the average value of two runs.  $\sigma$  is the standard deviation. The units of  $t_R$  are seconds.

Table II. Intercept of Peak Variance vs. Retention Volume for Column 1

flow rate, mL/s	$\sigma^2_{t,tot}$ intercept, s <sup>2</sup>	linear corr coeff
0.0485	3.367 ± 0.097 <sup>a</sup>	1.000
0.0333	9.95 ± 2.54	0.9995
0.0252	15.71 ± 3.91	0.9995
0.0168	16.58 ± 1.44	1.000
0.0119	35.3 ± 3.81	1.000
0.00491	152.9 ± 26.9	0.9999

<sup>a</sup>  $\bar{x} \pm \sigma$ .  $\sigma$  is the standard deviation of linear fit for intercept.

$$k' = \frac{t_s}{t_0} = \frac{t_s/(n/2)}{t_0/(n/2)} = \frac{t_d''}{t_s''} \quad (31)$$

then the reduced plate height becomes

$$h_{mip} = \frac{\sigma_L^2}{d_p L} = \frac{2k'}{(1 + k')^2 \epsilon_p + \epsilon_s} t_d'' \quad (32)$$

The average time a solute stays in the stationary phase is the mean desorption time of the absorbed molecule. Therefore

$$t_d'' = 1/k_d \quad (33)$$

where  $k_d$  is desorption rate constant. From eq 32 and 33

$$h_{mip} = \frac{2k' D_m}{(1 + k')^2 d_p^2 k_d (\epsilon_p + \epsilon_s)} \quad (34)$$

**Flow Dispersion.** Flow dispersion is an extremely complicated process. Giddings' coupling theory (5) was the first attempt to describe this process. According to that theory, flow dispersion is the result of the coupling of the flow and diffusion in packed beds. According to Klinkenberg (6) the form of the flow dispersion term depends upon many structural parameters of the column and packing. Huber et al. (7) introduced a term to consider the coupling of convective and diffusional mixing in the mobile phase. Recently, Horvath and Lin (8) modified the classical eddy diffusion concept, assuming that there is a stagnant fluid space in the interstices of the column packing, to derive the flow dispersion term. As

Groh and Halasz point out (9) all the more sophisticated attempts to describe flow dispersion resemble the coupling term of Giddings. Giddings himself has written: "The coupling expression is simply an approximation to a very complex interaction between diffusion and convection. The process has been formulated rigorously, but the boundary conditions for real granular beds are so complex, that meaningful solutions have not yet been obtained" (10). There are two commonly used equations to fit the experimental plate height data. One is the van Deemter equation (11, 12) in which the flow dispersion term is a constant  $A$ . The other is the Knox equation (13, 14) in which the flow dispersion term is  $A v^{0.33}$ . The Knox equation has been accepted by many workers, however, recently Reese and Scott (11) found that their experimental data fit the van Deemter equation extremely well when extracolumn dispersion was well controlled. They speculated that the previous work on HETP curves which required expressions which used power or exponential functions of linear velocity for some terms are due to the extracolumn dispersion effects. They point out the data they obtained were probably for the first time "under the condition where extracolumn dispersion was measured and was known to have been made insignificant". Furthermore, very recently Groh and Halasz (9) measured the band broadening in size exclusion chromatography. From measuring the band broadening in the interstitial volume, they found the exponent  $n$  of  $A v^n$  lies between 0.09 and 0.15 and is therefore more than a factor of 2 less than the value 0.33 proposed by Knox.

It was felt that the most satisfactory course would be to determine the flow dependence of the flow dispersion term experimentally.

## EXPERIMENTAL SECTION

**Apparatus.** A Waters Associates (Milford, MA) M-45 solvent delivery system was used with a Valco sample valve and a 10- $\mu$ L sample loop. The chromatograms were monitored by a Gilson (Middleton, WI) Model HM variable wavelength UV detector with an 8- $\mu$ L dead volume detector cell. The Spherisorb 10- $\mu$ m ODS column with 25 cm  $\times$  5.0 mm i.d. dimension was obtained from HPLC Technology (Lomita, CA). Two columns were employed, called column 1 and column 2. For column 1 data were obtained at six flow rates for four compounds in triplicate. For column 2, data were obtained for the same four compounds at 17 flow



Table III. Reduced Plate Height of Extracolumn Band Broadening for Column 1

flow rate, mL/s	$h_{ext}$			
	methyl <i>p</i> -hydroxybenzoate	ethyl <i>p</i> -hydroxybenzoate	propyl <i>p</i> -hydroxybenzoate	<i>n</i> -butyl <i>p</i> -hydroxybenzoate
0.0485	4.8 ± 0.1 <sup>a</sup>	2.54 ± 0.07	1.07 ± 0.03	
0.0333	5.79 ± 1.48	4.32 ± 1.10	1.37 ± 0.35	0.46 ± 0.12
0.0252	5.81 ± 1.50	3.05 ± 0.79	1.28 ± 0.33	0.45 ± 0.12
0.0168	2.70 ± 0.23	1.38 ± 0.12	0.559 ± 0.068	0.190 ± 0.017
0.0119	2.92 ± 0.32	1.49 ± 0.16	0.620 ± 0.065	0.205 ± 0.022
0.00491	2.21 ± 0.39	1.13 ± 0.20	0.453 ± 0.080	0.154 ± 0.027

<sup>a</sup> Same as Table I, footnote a.

Table IV. Reduced Plate Height of Column Band Broadening for Column 1

flow rate, mL/s	$h_{col}$			
	methyl <i>p</i> -hydroxybenzoate	ethyl <i>p</i> -hydroxybenzoate	propyl <i>p</i> -hydroxybenzoate	<i>n</i> -butyl <i>p</i> -hydroxybenzoate
0.0485	13.8 ± 0.17 <sup>a</sup>	13.83 ± 0.18	13.52 ± 0.18	
0.0333	8.34 ± 1.83	10.13 ± 1.33	10.68 ± 0.59	10.09 ± 0.12
0.0252	7.91 ± 1.52	9.61 ± 0.92	10.07 ± 0.53	9.53 ± 1.05
0.0168	7.52 ± 0.23	7.88 ± 0.20	7.65 ± 0.23	7.71 ± 0.73
0.0119	5.99 ± 0.33	6.18 ± 0.18	6.28 ± 0.31	6.17 ± 0.18
0.00491	4.24 ± 0.39	4.58 ± 0.23	4.75 ± 0.11	4.60 ± 0.67

<sup>a</sup> Same as Table I, footnote a.

rates in duplicate. The two columns had consecutive serial numbers.

**Reagents.** The methanol was supplied by MCS Manufacturing Chemists Inc. (Cincinnati, OH), tartrazine, methyl *p*-hydroxybenzoate, ethyl *p*-hydroxybenzoate, and propyl *p*-hydroxybenzoate were from Aldrich Chemical Co., Inc. (Milwaukee, WI), *n*-butyl *p*-hydroxybenzoate was from Sigma Chemical Co. (St. Louis, MO). Potassium nitrate was from J. T. Baker Chemical Co. (Pittsburgh, PA). Poly(styrenesulfonate) was from Scientific Polymer Products, Inc. (Ontario, NY).

**Data Acquisition System.** The chromatographic data were converted into digital form and stored in an LSI-11 microcomputer and then transferred to a DEC-10. The data corresponding to each peak were fit by the Cram-Chesler eight-parameter equation (15). Then this equation was numerically integrated by using Gauss-Legendre polynomials to obtain the retention time and variance of the peaks.

**Chromatographic Conditions.** The solvent was a mixture of 55% methanol and 45% water (volume ratio). The flow rate was calibrated by buret and stopwatch. The temperature was 22 °C. The solutes were detected by absorbance at 254 nm.

## RESULTS AND DISCUSSION

**The A Term.** For determination of whether the empirical flow dispersion term is near constant, A, as proposed by Scott and Halasz or is  $A\nu^{0.33}$  as proposed by Knox, the total reduced plate height,  $h_{tot}$ , was determined at different linear velocities and the plate height of extracolumn band broadening,  $h_{ext}$ , was determined by the method recently described by Kutner et al. (16). After  $h_{ext}$  was subtracted from  $h_{tot}$ , the reduced plate height of the column  $h_{col}$ , was fitted to equations of the Knox form and of the van Deemter form. In order to determine which fit was better, we compared the C (mass transfer) values of both fits with the theoretical term.

The retention time and the reduced plate height of methyl *p*-hydroxybenzoate, ethyl *p*-hydroxybenzoate, propyl *p*-hydroxybenzoate, and *n*-butyl *p*-hydroxybenzoate at different flow rates are presented in Table I. The average relative standard deviation of the retention time is less than 1% and the average relative standard deviation of the reduced plate height is about 3.3%.

The extracolumn band broadening was evaluated by using

the method described by Kutner et al. (16). The variance of the peaks  $\sigma_{L,tot}^2$  and the square of the retention volume  $V_R^2$  are input into a linear least-squares fit program. The intercept ( $\sigma_{L,tot}^2$  at  $V_R^2 = 0$ ) of  $\sigma_{L,tot}^2$  and linear correlation coefficient at different flow rates are shown in Table II. As presented in Table II, the linearity of the data at each flow rate is extremely good. The variance of the extracolumn band broadening,  $\sigma_{L,ext}^2$ , is the intercept of  $\sigma_{L,tot}^2$ . Then the reduced plate height of extracolumn band broadening can be calculated by the equation

$$h_{ext} = (\sigma_{L,ext}^2 / t_R^2) (L / d_p) \quad (35)$$

After  $h_{ext}$  was subtracted from  $h_{tot}$ , the reduced plate height of column band broadening,  $h_{col}$ , can be obtained.  $h_{ext}$  and  $h_{col}$  are presented in Table III and Table IV. Although we tried to minimize the volume of connecting tubes and used an 8-μL volume detector cell, as shown from Table III and Table IV,  $h_{ext}$  cannot be neglected compared with  $h_{col}$ . It is especially true for short retention time compounds like methyl *p*-hydroxybenzoate. We also observed that the trend of  $h_{tot}$  was decreasing with increasing retention time (Table I). However, after removing the extracolumn band broadening, there is less variation in  $h_{col}$  among the various compounds at the same flow rate (Table IV).

Before the equations are fit to  $h_{col}$ , both equations are rewritten in the form of reduced plate height as a function of linear velocity. The reason for rewriting both equations in terms of  $\mu_e$  is that one can avoid using the inaccurate estimation of the diffusion coefficient  $D_m$  in order to calculate the reduced velocity  $\nu$ .

The forms used for the equations are expressed as follows van Deemter form

$$H = \frac{B'}{\mu_e} + A' + C'\mu_e \quad (36)$$

Knox form

$$h = \frac{B}{\nu} + A\nu^{0.33} + C\nu \quad (37)$$

Table V.  $A''$  and  $C''$  for Equation 38 and Equation 39 Fit for Column 1

		$A''^a$	$C''^b$
methyl	eq 39	7.59 ± 2.70	9.83 ± 4.19
p-hydroxybenzoate	eq 38	3.20 ± 0.85	15.4 ± 2.37
ethyl	eq 39	8.96 ± 0.99	9.32 ± 1.84
p-hydroxybenzoate	eq 38	3.69 ± 0.44	16.16 ± 1.23
propyl	eq 39	9.50 ± 0.81	8.60 ± 1.50
p-hydroxybenzoate	eq 38	3.89 ± 0.44	15.92 ± 1.22
n-butyl	eq 39	9.66 ± 1.06	6.98 ± 2.37
p-hydroxybenzoate	eq 38	3.62 ± 0.58	16.04 ± 2.10

<sup>a</sup> The units of  $A''$  for eq 39 are (cm/s)<sup>-0.33</sup> and for eq 38 it is unitless. <sup>b</sup> The units of  $C''$  are (cm/s)<sup>-1</sup>.

Both equations can be rewritten in the following way:

van Deemter form

$$h = \frac{B''}{\mu_e} + A'' + C''\mu_e \quad (38)$$

Knox form

$$h = \frac{B''}{\mu_e} + A''\mu_e^{0.33} + C''\mu_e \quad (39)$$

where

$$B'' = \frac{B'}{d_p} = B \frac{D_m}{d_p} \quad (40)$$

$$C'' = \frac{C'}{d_p} = C \frac{d_p}{D_m} \quad (41)$$

$$A'' = A' \text{ for eq 38} \quad (42)$$

$$A'' = A \left( \frac{d_p}{D_m} \right)^{0.33} \text{ for eq 39} \quad (43)$$

The  $B$  value is about 1.6 to 2.0 for porous materials (17).  $D_m$  can be calculated from the Wilke-Chang equation. From the estimation of  $B$ ,  $D_m$ , and  $d_p$  we set the value of  $B''$  to be 0.01. It is noteworthy that under our chromatographic conditions the  $B''/\mu_e$  term only contributes about 4% of the reduced plate height of the column even at the slowest flow rate. We used  $B = 2.0$  as an estimate. This value may be

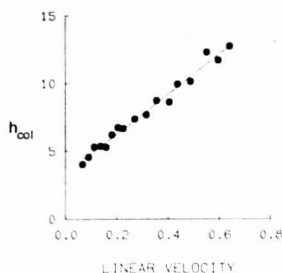


Figure 3. The fit of eq 38 for  $h_{col}$  vs.  $\mu_e$  for *n*-butyl *p*-hydroxybenzoate. We employ  $\mu_e$  rather than reduced velocity so that the potentially inaccurate estimation of  $D_m$  (from Wilke-Chang) does not enter into the calculations.

wrong by up to 50% of that value, thus the error in  $h$  due to an incorrect estimate of  $B$  may be as high as 2% of  $h$ . Therefore, any inaccuracy in the estimation of  $B$  will not have a significant effect on our results.

The  $A''$  and  $C''$  obtained from fitting  $h_{col}$  from column 1 into eq 38 and fitting  $h_{col}$  into eq 39 are presented in Table V. Figure 3 illustrates the  $h$  vs.  $\mu_e$  dependence for column 2. It is shown that both equations do not fit very well for methyl *p*-hydroxybenzoate. The reason for this is that the band broadening of methyl *p*-hydroxybenzoate is most significantly affected by extracolumn band broadening. Thus, the least accurate  $h_{col}$  were obtained for this compound. It is also shown in Table IV that the relative standard deviation of  $h_{col}$  for methyl *p*-hydroxybenzoate is up to 20% at some flow rates. For the other three compounds, both equations explain the data well. However, the values of  $C''$  obtained from the two equations are significantly different.

In order to determine which equation gives more meaningful results, one can compare the experimental  $C''$  with the theoretical prediction of that term. In the work presented here

$$C'' = \left( \frac{1}{30} \left( \frac{\epsilon_s}{\epsilon_p} \right) k'^2 \frac{D_m}{D_{sm}^{eff}} + \frac{2kD_m}{(1+k)^2 d_p^2 k_d (\epsilon_p + \epsilon_s)} \right) \frac{d_p}{D_m} \quad (44)$$

From the conclusions drawn from temperature studies in reversed-phase HPLC by Colin et al. (18), the contribution of mass transfer between mobile phase and stationary phase to the reduced plate height is probably much smaller than the contribution of mass transfer between mobile zone and sta-

Table VI.<sup>a</sup> Diffusion Coefficient Comparison for Columns 1 and 2

	$10^4 D_m$ , cm <sup>2</sup> /s (Wilke- Chang) <sup>b</sup>	$10^4 D_{sm}^{eff}$ , cm <sup>2</sup> /s				$D_m/D_{sm}^{eff}$			
		Knox form		van Deemter form		Knox form		van Deemter form	
		col 1	col 2	col 1	col 2	col 1	col 2	col 1	col 2
ethyl	5.12 ± 0.51	4.1 ± 0.9	4.3 ± 0.6	2.4 ± 0.3	2.6 ± 0.3	1.2 ± 0.3	1.2 ± 0.2	2.1 ± 0.3	2.0 ± 0.3
p-hydroxybenzoate									
propyl	4.79 ± 0.48	5.2 ± 1.0	5.4 ± 0.6	2.8 ± 0.4	3.0 ± 0.3	0.92 ± 0.20	0.89 ± 0.13	1.7 ± 0.3	1.6 ± 0.2
p-hydroxybenzoate									
n-butyl	4.50 ± 0.45	7.3 ± 2.6	6.0 ± 0.8	3.1 ± 0.5	3.6 ± 0.4	0.61 ± 0.22	0.75 ± 0.12	1.5 ± 0.3	1.3 ± 0.2
p-hydroxybenzoate									

<sup>a</sup> The standard deviation of  $d_p$  is 10%. <sup>b</sup> The standard deviation of  $D_m$  calculated by the Wilke-Chang equation is 10%. The indicated errors take into account the error from  $d_p$  and  $D_m$  (each 10%).

Table VII.<sup>a, b</sup> Equations for Band Broadening in Liquid Chromatography

	axial diffusion	flow dispersion	mass transfer between mobile zone and stationary phase	mass transfer between mobile phase and stationary phase
Chen and Weber	$2 \left( \frac{D_{sm}^{eff} \epsilon_p + D_{tm}^{eff}}{D_{sm} \epsilon_p + D_m} \right) \nu$	$A \frac{2\lambda}{1 + \omega \nu^{1/2}} + \frac{\kappa (k_o + k' + k_o k')^2}{(1 + k_o)^2 (1 + k')^2} \nu^{2/3}$	$\frac{1}{30} \frac{D_{sm} \epsilon_p k'^{1/2}}{D_{sm}^{eff} (1 + k')^2} \nu$ $\frac{1}{30} \frac{\theta (k_o + k' + k_o k')^2}{k_o (1 + k_o)^2 (1 + k')^2} \nu$	$\frac{2 \epsilon_p k' D_m}{(\epsilon_p + \epsilon_s)(1 + k')^2 d_p^2 k_d} \nu$ $\frac{2k' D_m}{(1 + k_o)(1 + k')^2 d_o^2 k_d} \nu$
Horvath and Lin	$\frac{2\gamma}{\nu}$			
Knox	$\frac{2\gamma'(1 + k')}{\nu}$	$A \nu^{0.33}$	$\frac{1}{30} \frac{D_{sm} k'}{D_d (1 + k')^2} \nu$	

<sup>a</sup>  $k_o = \epsilon_p / \epsilon_s$ ,  $b$   $k'' = k_o + k' + k_o k'$ .

tionary zone. Therefore, we first assume the second term of eq 44 is negligible. Then  $C''$  can be reduced to the form

$$C'' = \frac{1}{30} \frac{(\epsilon_s / \epsilon_p) k''^2}{(1 + k')^2} \frac{d_p}{D_{sm}^{eff}} \quad (45)$$

Thus

$$D_{sm}^{eff} = \frac{1}{30} \frac{(\epsilon_s / \epsilon_p) k''^2}{(1 + k')^2} \frac{d_p}{C''} \quad (46)$$

$k''$  can be calculated from eq 13.  $t_{fm}$  is determined by measuring the retention time of poly(styrenesulfonate) ( $M_r$   $6 \times 10^5$ ).  $\epsilon_s / \epsilon_p$  can be calculated from eq 6 where  $t_{sm} = t_o - t_{fm}$ .  $t_o$  is obtained from the retention time of potassium nitrate in the phosphate buffer (19).

The  $D_{sm}^{eff}$  values obtained from eq 46 are presented in Table VI for columns 1 and 2. The calculations for methyl *p*-benzoate were neglected because good fits for either equation were not obtained. As shown in Table VI, the  $D_{sm}^{eff}$  values are compared with  $D_m$  calculated by Wilke-Chang. The expected value for  $D_m / D_{sm}^{eff}$  is about 2.0–2.5. It is seen that the  $D_{sm}^{eff}$  values from eq 38 fall in the expected region. The  $D_{sm}^{eff}$  values from eq 39 are too large compared to  $D_m$ . It is important to check the assumption of rapid kinetics. Suppose the second term in eq 44 is not negligible. This will make  $D_{sm}^{eff}$  become a larger value than we have calculated. Then the  $D_{sm}^{eff}$  from eq 40 would be even farther away from the reasonable values. So in either case it can be concluded that the data obtained from eq 38 give more meaningful results.

Note that  $D_{sm}^{eff}$  values from both equations decrease with decreasing molecular size. This might be due to the tendency of small sized molecules to become "trapped" in small radius pores; therefore,  $D_{sm}^{eff}$  for small sized molecules is decreased. Confirming evidence comes from Table II in which the linear correlation coefficients are all above 0.999 for our solutes. This linearity indicates that the average diffusion coefficient for these solutes in the column are all the same. Thus, one might expect that in the interstitial space small molecules diffuse faster than large molecules and in the pore it is the opposite. Therefore, the average diffusion coefficients for these solutes in the column are about the same. The average diffusion coefficient is calculated by  $D_{av} = (\epsilon_s / (\epsilon_p + \epsilon_s)) D_{tm}^{eff} + (\epsilon_p / (\epsilon_p + \epsilon_s)) D_{sm}^{eff}$  from our data. The average diffusion coefficients for ethyl *p*-hydroxybenzoate, propyl *p*-hydroxybenzoate, and *n*-butyl *p*-hydroxybenzoate are all  $2.8 \times 10^{-6}$  cm<sup>2</sup>/s. This result matches with our observation. The phenomenon of the same average diffusion coefficients for a column is also shown in the data of Horvath and Lin (3). They obtained a linear relation (which depends on equal  $D$  values for their linearity) of  $\sigma$  vs.  $k'$  for their solutes in which the diffusion coefficient in the bulk ranged from  $2.62 \times 10^{-6}$  cm<sup>2</sup>/s to  $3.49 \times 10^{-6}$  cm<sup>2</sup>/s. We believe that this observation does not contradict the observation of Knox and McLennan (20) in their size exclusion chromatography experiment. For their polystyrene polymers they observed that  $D_{sm}^{eff}$  decreased with increasing molecular size for high (>4000) molecular weight polystyrene. However, for the smaller solutes, molecular weight 2000 and 4000, the trend was reversed. It is probable that, as with our small solutes, when the solute size falls into the region at the small end of the pore size distribution curve, the effect of the porous structure on the motion of solutes is enhanced.

**Comparison of Band Broadening Expressions.** During the advances of liquid chromatography, several plate height equations for liquid chromatography have been developed. The most recent developments of the plate height equation in the literature have been reported by Knox (4) and by Horvath and Lin (3). We shall discuss our equation and theirs. The three equations are expressed in Table VII.

For the axial diffusion term, our equation gives a more physically meaningful expression. In order to estimate the plate height contribution of axial diffusion from our equation, one has to estimate  $D_{tm}^{eff}/D_m$ ,  $D_{sm}^{eff}/D_m$ ,  $\epsilon_p/\epsilon_s$ , and  $D_s^{eff}/D_m$ . The ratio of the  $D_{tm}^{eff}/D_m$  is called the interparticle obstructive factor. The interparticle obstructive factor has been interpreted in terms of the tortuosity and the constriction of diffusion paths by Knox. The theoretical value and experimental value of the interparticle obstructive factor are about 0.6 (21). The ratio of  $D_{sm}^{eff}/D_m$  is called the intraparticle obstructive factor. The values of intraparticle obstructive factor for low-molecular weight solutes have been proposed from the work of Giddings and Mallik (22) and van Krefeld and van den Hoed (23) to be about  $2/3$ . Thus  $D_{sm}^{eff}/D_m \approx 0.4$ . The value of  $\epsilon_p/\epsilon_s$  can be altered by different packing materials and packing procedures. The average value for porous packing material, however, is about 0.6–1.0 (3, 9) and for pellicular packing material is near zero. The value of  $D_s^{eff}/D_m$  would depend on the nature of the stationary phase. We are unaware of data which demonstrate a strong dependence of the  $B$  term on  $k'$ , a necessary result if  $D_s^{eff}$  is significant. If we neglect the contribution from  $D_s$ , our equation predicts a  $B$  value for porous material of  $1.7 < B < 2.0$ , and for pellicular material  $B \approx 1.2$ . These estimates agree very well with experimental results (17) supporting the assumption of a minor contribution from  $D_s^{eff}$ . Preliminary results in this laboratory indicate that  $D_s^{eff}$  is at most but a few percent of  $D_m$  (24).

For the flow dispersion term, since this process is extremely complicated, we express it as an empirical term,  $A$ . The theoretical term of Horvath and Lin parallels the empirical expression of Knox. They predict that the exponent of velocity in the flow dispersion term is about 0.33. As discussed in the previous section, our experimental results parallel the observation of Reese and Scott (11) and Groh and Halasz (9); the flow dispersion term does not strongly depend on the flow rate. The fact that statistically both the Knox and van Deemter equations fit the data well should not be overlooked. There are, after all, only small differences in the format of the equations, and clearly adjustment of  $A''$ ,  $B''$ , and  $C''$  can account for changes in  $n$  in the term  $A''\mu_n^n$ . Fortunately we can rely on physical arguments to decide between the two fits.

Our mass transfer between mobile phase and stationary phase term is exactly the same as that derived by Horvath and Lin. The term for mass transfer between mobile zone and stationary zone is also similar to the derivation of Horvath and Lin. The only difference is that they use the tortuosity factor  $\theta$  and we use the ratio of  $D_m/D_{sm}^{eff}$ . The value of the tortuosity factor is believed to be about 2 (3). However,  $D_m/D_{sm}^{eff}$  may depend on size of solute, pore distribution, and pore volume (13). In fact, for  $k' = 0$ , our mass transfer term can be reduced to  $(1/30) (D_m/D_{sm}^{eff}) [k''/(1 + k'')^2] \nu$  which

is exactly the same as the mass transfer term of Knox. Furthermore, Knox has used this term to calculate  $D_m/D_{sm}^{eff}$  for size exclusion chromatography. He obtained the value of  $D_m/D_{sm}^{eff}$  for polystyrene polymers from 6.0 to 16.9 depending on the size of the solute.

From the discussion above, it will be appreciated that the agreement of the  $C$  term derivation from the mass balance model by Horvath and Lin and our derivation from the random walk model is surprisingly good. The advantage of the random walk model is that it not only provides the simplest calculation but also from its microscopic point of view it gives considerable insight concerning the band broadening by each effect.

## ACKNOWLEDGMENT

The authors wish to thank Meherun Nahar for her able assistance in acquiring data.

## LITERATURE CITED

- (1) Grushka, E.; Snyder, L. R.; Knox, J. H. *J. Chromatogr. Sci.* **1975**, *13*, 25–37.
- (2) Giddings, J. C. "Dynamics of Chromatography"; Marcel Dekker: New York, 1965; Chapter 1.
- (3) Horvath, C.; Lin, H. J. *J. Chromatogr.* **1978**, *149*, 43–70.
- (4) Knox, J. H. *J. Chromatogr. Sci.* **1977**, *15*, 352–364.
- (5) Giddings, J. C. "Dynamics of Chromatography"; Marcel Dekker: New York, 1965; Chapter 2.
- (6) Klinkenberg, A. *Anal. Chem.* **1966**, *38*, 491–492.
- (7) Huber, J. F. K.; Hulsman, J. A. R. *Anal. Chim. Acta* **1967**, *38*, 305–313.
- (8) Horvath, C.; Lin, H. J. *J. Chromatogr.* **1976**, *126*, 401–420.
- (9) Groh, R.; Halasz, I. *Anal. Chem.* **1981**, *53*, 1325–1335.
- (10) Giddings, J. C.; Bowman, L. M.; Myers, M. N. *Macromolecules* **1977**, *10*, 443.
- (11) Reese, C. Z.; Scott, R. P. W. *J. Chromatogr. Sci.* **1980**, *18*, 479–486.
- (12) Halasz, I.; Endeke, R.; Asshauer, J. *J. Chromatogr.* **1975**, *112*, 37–60.
- (13) Knox, J. H.; Vasvari, G. *J. Chromatogr.* **1973**, *83*, 181–194.
- (14) Colin, H.; Gulochon, G. *J. Chromatogr.* **1978**, *158*, 183–205.
- (15) Mott, S. D.; Grushka, E. *J. Chromatogr.* **1976**, *126*, 191–204.
- (16) Kutner, W.; Debowski, J.; Kemula, W. *J. Chromatogr.* **1981**, *218*, 45–50.
- (17) Kennedy, G. J.; Knox, J. H. *J. Chromatogr. Sci.* **1972**, *10*, 549–556.
- (18) Colin, H.; Diez-Masa, J. C.; Gulochon, G.; Czajkowska, T.; Miedziak, I. *J. Chromatogr.* **1978**, *167*, 41–65.
- (19) Wells, M. J. M.; Clark, C. R. *Anal. Chem.* **1981**, *52*, 1341–1345.
- (20) Knox, J. H.; McLennan, F. *J. Chromatogr.* **1979**, *185*, 289–304.
- (21) Knox, J. H.; McLaren, L. *Anal. Chem.* **1984**, *36*, 1477–1482.
- (22) Giddings, J. C.; Mallik, K. L. *Anal. Chem.* **1966**, *38*, 997–1000.
- (23) van Krefeld, M. E.; van den Hoed, N. *J. Chromatogr.* **1978**, *149*, 71–91.
- (24) Weber, S. G.; Chen, J.-C., unpublished observations.

RECEIVED for review May 4, 1982. Accepted October 1, 1982. This work was supported by the U.S. Public Health Service through Grant GM 28112 and Biomedical Research Support Grant 2507-RR07084 (16) through the National Institutes of Health.

## CORRESPONDENCE

### Chemiluminescent Detection of Reduced Sulfur Compounds with Ozone

*Sir:* Gaseous reduced sulfur compounds are of potential importance in the global atmospheric sulfur budget. The major source of this reduced sulfur is thought to be bacterial production, the most prevalent biogenic sulfur gas being hydrogen sulfide ( $H_2S$ ), with dimethyl sulfide (DMS), carbonyl sulfide (COS), carbon disulfide ( $CS_2$ ), mercaptans, and disulfides commonly being present in smaller amounts (1, 2). These sulfides are subsequently oxidized in the troposphere to  $SO_2$  and sulfate, thus contributing to the naturally occurring background of the latter compounds. With the recognition of acidic precipitation as a global atmospheric problem, there is a continuing need for highly sensitive and selective detection methods for these important reduced sulfur gases.

A number of analytical methods have been used to measure vapor phase organic sulfides (3-11). However, all of these methods suffer from interferences, analysis complexities, and/or lack of sufficient sensitivity to monitor reduced sulfur gases at the sub-part-per-billion levels expected in ambient air (12, 13). A method for real-time measurement of  $H_2S$ , based on the chemiluminescent reaction of  $H_2S$  with chlorine dioxide ( $ClO_2$ ) has recently been reported (14). A detection limit of 3 ppb is achieved by using photon counting techniques with a cooled photomultiplier. A major drawback to this method is that the  $ClO_2$  reagent is not easily prepared or stored. Also, formation of elemental sulfur can occur in the chemiluminescent reaction chamber, coating the cell window and reducing sensitivity during continuous operation.

With the aim of developing a simple, sensitive, selective real-time method for measurement of reduced sulfur gases, we have investigated the chemiluminescent detection of  $H_2S$ , DMS, and other reduced sulfur compounds by their oxidation with ozone. The observation of chemiluminescence in the 300 to 400 nm wavelength region resulting from the gas-phase reaction of  $O_3$  with  $H_2S$ , DMS, and methyl mercaptan ( $C_2H_5SH$ ) has been previously reported (15, 16) and the emitting species has been identified as electronically excited  $SO_2$  (16, 17). The homogeneous gas-phase reaction of ozone with hydrogen sulfide has been reported to be slow in studies at low pressures (18-21), and the oxidation mechanism is apparently complex. A reaction order for  $H_2S$  from 0.5 (18) to 2 (21) has been observed, and a heterogeneous reaction pathway has been proposed as a possible explanation of the data (22). Reported here are results of a preliminary investigation of the ozone-reduced sulfur chemiluminescence, which also imply a complex reaction mechanism (possibly both homogeneous and heterogeneous) but indicate that ozone chemiluminescence may be an extremely useful tool for the detection of  $H_2S$ , DMS, and other reduced sulfur species in the ambient atmosphere and in industrial applications (23).

#### EXPERIMENTAL SECTION

Figure 1 shows the experimental arrangement used in this investigation. A Monitor Labs Model 8410 ozone monitor was modified for use as a detector of the ozone-sulfide chemiluminescence. An electrical discharge ozone source, of the type used in Thermo-Electron oxides of nitrogen detectors, was connected to the former ethylene flow line of the 8410. A Metal Bellows Corp. Model 41 air pump was substituted for the rubber diaphragm pump in the 8410, since the rubber diaphragm would have

been destroyed by the excess ozone in the reaction mixture. A UV-transmitting, visible absorbing glass filter (Corning CS-7-60) was installed in front of the photomultiplier tube (Hamamatsu R-268) to restrict light detection to the 300-400 nm range. This filter has a peak transmittance of approximately 70% at 355 nm.

No change was made in the detector electronics or in the stainless steel reaction chamber. The reaction chamber was used at room temperature and was not thermostated. The chamber and all connecting tubing were sealed against outside light. Exhaust gases from the pump were scrubbed by a large activated charcoal trap before venting into the air to destroy excess reagent ozone and to trap any toxic reaction products.

Gas mixtures were prepared with a Dasibi Model 1005-C2 Gas Calibrator. Permeation tubes for  $H_2S$ , DMS,  $CH_3SH$ , thiophene, benzene, acetaldehyde, and propane were obtained from AID, Inc. Pressurized cylinders of ethylene and benzene in nitrogen, at approximately 1 ppm and 20 ppm, respectively, were prepared by successive dilutions starting from the pure compounds. Mixtures of 208 ppm NO in nitrogen and 99 ppm  $NO_2$  in nitrogen were used, both in aluminum cylinders from Scott Specialty Gases.

Optimization tests were run with  $H_2S$  and DMS, which showed that the maximum chemiluminescent emission from both compounds occurred at sample air and ozonizer flow rates of 100  $cm^3/min$  each and a reaction chamber pressure of just under 1 atm. These conditions were used for all sensitivity and interference tests discussed below. No separate optimization study was done for methyl mercaptan or thiophene.

#### RESULTS AND DISCUSSION

As was observed in an earlier study (16) the chemiluminescence intensity decreased in the order  $CH_3SH > CH_3SCH_3 > H_2S$ . Thiophene chemiluminescence was still less intense than that from  $H_2S$ . Initially, tank oxygen was used to supply the discharge ozonizer in order to maximize the ozone concentration in the reaction chamber. Comparative tests were conducted, however, with both dry air and tank oxygen supplied to the ozonizer. Surprisingly, when air was used in the discharge ozonizer, the signal observed from DMS increased by a factor of 3 over that found when oxygen passed through the ozone source. This large enhancement of signal when air is used in the ozonizer is reproducible for DMS, but sensitivity for thiophene shows only small improvement and that for  $H_2S$  and  $CH_3SH$  decreases slightly, relative to the sensitivity obtained by using oxygen. Sensitivities for  $CH_3SH$ , DMS,  $H_2S$ , and thiophene are in the ratio 80:30:3:1 when dry air is used in the ozonizer.

The improvement in sensitivity to DMS is not caused by trace species present in ambient air, since identical results are found with ultrapure air, ambient air that has been purified by means of charcoal scrubbers, or unpurified ambient air. Tests indicate that oxygen quenches the ozone/sulfide chemiluminescence more efficiently than nitrogen does, possibly by scavenging the radicals produced in the sulfide oxidation. However, this effect is not large enough to account for the 3-fold increase in chemiluminescence from DMS when air rather than oxygen is used in the ozonizer. The optimum sample and ozonizer gas flow rates have been found to be the same using air or oxygen for ozone generation.

Studies have disclosed that the enhancement of chemiluminescence from DMS which occurs from reactions with ozonized air is caused by the presence of oxides of nitrogen

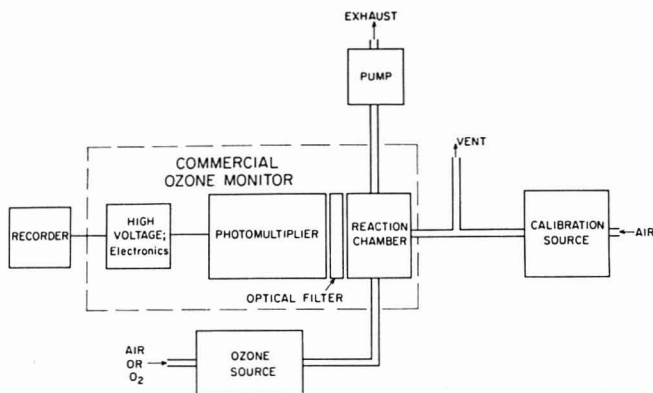


Figure 1. Block diagram of apparatus used in the investigation of ozone/sulfide chemiluminescence.

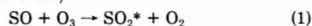
(NO<sub>x</sub>) produced from N<sub>2</sub> and O<sub>2</sub> in the electrical discharge (24). Air passed through the ozonizer discharge was analyzed with a Thermo-Electron Model 14-B NO<sub>x</sub> detector and found to contain approximately 50 ppm of NO<sub>x</sub>. When a similar NO<sub>x</sub> concentration was produced by addition of standard mixtures of NO or NO<sub>2</sub> in nitrogen to ozonized oxygen downstream of the ozonizer, the sensitivity to DMS increased by more than a factor of 2, relative to that when only nitrogen was added. Improvement of the DMS signal could be achieved by the addition of NO or NO<sub>2</sub> to the ozone flow even when air was used in the ozonizer, provided the added NO<sub>x</sub> concentration was of similar magnitude to that of the NO<sub>x</sub> produced in the ozonizer. Addition of NO or NO<sub>2</sub> in nitrogen to the ozone flow produced no improvement in sensitivity to H<sub>2</sub>S, relative to that when only nitrogen was added. No signal was observed from mixtures of sulfides and NO or NO<sub>2</sub> in the absence of ozone.

In a second study, the composition of the gas passing through the discharge ozone source was varied by premixing oxygen and nitrogen. The chemiluminescent intensity from a constant concentration (165 ppb) of H<sub>2</sub>S was found to be nearly invariant with ozonizer gas composition, from pure oxygen to 10% O<sub>2</sub>/90% N<sub>2</sub>. In contrast, the signal from 44 ppb DMS was increased over its value with ozonized oxygen with mixtures varying from 95% O<sub>2</sub> to 10% O<sub>2</sub>. The maximum signal from DMS occurred at an ozonizer gas composition of 75% O<sub>2</sub>/25% N<sub>2</sub>, being 3.5 times as great as the signal observed using pure oxygen. However, the maximum is broad and signal enhancement at an ozonizer gas composition of 20% O<sub>2</sub>/80% N<sub>2</sub> (i.e., air) was only 10% lower. In all cases the chemiluminescent emission dropped sharply to zero at ozonizer gas mixtures approaching 100% N<sub>2</sub>.

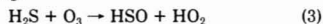
If the O<sub>3</sub> chemiluminescent method is to be useful for ambient sulfide detection, it is important to determine the effect of NO<sub>x</sub> in the sample air on the measurement of sulfide compounds in that air. Mixtures of NO and NO<sub>2</sub> with both DMS and H<sub>2</sub>S have been prepared by adding standard mixtures of NO or NO<sub>2</sub> in nitrogen to the diluent air downstream of the calibrator. No change in signal from H<sub>2</sub>S was found with the addition of NO or NO<sub>2</sub>, as expected from the discussion above. Enhancement of the signal from DMS was observed at parts per million levels of added NO<sub>x</sub>, when oxygen was used in the ozonizer, but a decrease in signal with added NO<sub>x</sub> was observed when air was used in the ozonizer. For the present report the key finding is that NO or NO<sub>2</sub> concentrations of 100 ppb or less in the sample air have

negligible effects on the intensity of DMS chemiluminescence, regardless of the composition of the ozonizer gas; hence it is clear that no interference in ambient DMS detection will result from the presence of ambient NO<sub>x</sub>.

Although the detailed mechanism of enhancement of DMS chemiluminescence by NO<sub>x</sub> is still unknown, a few comments can be made. Hales et al. (18) discuss reports of NO<sub>x</sub> interactions with H<sub>2</sub>S but support a photolytic pathway for oxidation by H<sub>2</sub>S by NO<sub>x</sub>. Photolytic reactions are ruled out in the present study by the construction of the reaction cell and plumbing system. In the study by Becker et al. (19), under reaction conditions widely different from those in the present work, NO<sub>2</sub> was found to quench the chemiluminescence from H<sub>2</sub>S, but not from CH<sub>3</sub>SH or DMS, probably by reaction with chain-propagating HS radicals formed in H<sub>2</sub>S oxidation. Such an effect was not observed in this study. The final steps in the mechanism of ozone/sulfide chemiluminescence are



Although NO<sub>2</sub> is known to react with SO more than 100 times faster than ozone does, it is clear that enhancement of DMS chemiluminescence caused by NO<sub>x</sub> does not involve an increased rate of SO oxidation, since in that case similar effects would be expected for all the sulfides studied. In the ozone stream any nitric oxide (NO) produced in the discharge would be rapidly converted to higher oxides, including NO<sub>3</sub>, which has been shown to be a strong oxidizing agent for reactive hydrocarbons (25, 26). It may be that the effects of NO<sub>x</sub> on the chemiluminescent oxidation of DMS are caused by the presence of NO<sub>3</sub>, in equilibrium with N<sub>2</sub>O<sub>5</sub>, in the ozonized air. Whereas the oxidation of H<sub>2</sub>S or CH<sub>3</sub>SH by ozone is thought to be initiated by the breaking of a hydrogen-sulfur bond (19, 20), e.g.



this cannot occur with dimethyl sulfide. We propose that the enhanced chemiluminescence from DMS in the presence of NO<sub>x</sub> is caused by some species, probably NO<sub>3</sub>, which attacks the sulfur-carbon bond more effectively than ozone does. Further studies using other organic sulfides will be performed to investigate this hypothesis.

Calibration curves have been obtained for H<sub>2</sub>S and DMS, using air in the ozone source, since this gives optimum sensitivity for DMS and nearly optimum sensitivity for H<sub>2</sub>S. These calibration curves are shown in Figure 2. As stated



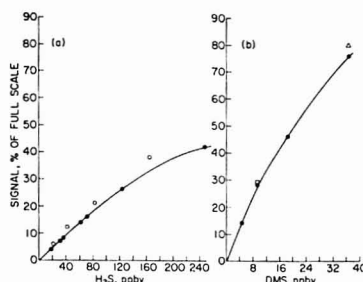


Figure 2. Calibration curves for H<sub>2</sub>S and DMS: (a) H<sub>2</sub>S, 9/1/81 (●), 12/22/81 (○); (b) DMS, 12/16/81 (●), single points on 1/14/82 (Δ), and 2/9/82 (□). In both (a) and (b), curves are drawn through the earliest calibration points only.

previously, the sensitivity for DMS is about an order of magnitude higher than that for H<sub>2</sub>S. At low sulfide concentrations (e.g., <100 ppb H<sub>2</sub>S) the emission intensity is first order with respect to sulfide, and the calibration plot is linear. At higher sulfide concentrations the reaction order decreases, e.g., an apparent reaction order for sulfide of 0.5 is observed with H<sub>2</sub>S at 500 ppb. The enhancement of DMS chemiluminescence caused by ozonation of air rather than oxygen does not change the apparent reaction order with respect to DMS. The cause of the nonlinearity in the calibration plots is not certain but may result from a heterogeneous process in the sulfide oxidation, as suggested by Cadle and Ledford (22). Although the heterogeneous formation of nitric acid from N<sub>2</sub>O<sub>3</sub> present in the ozone stream and water vapor in the sample air would be expected to occur, we find only modest dependence of signal from either H<sub>2</sub>S or DMS on the humidity of the sampled air. At 20 °C, the signal from air of 0.03% relative humidity containing 9 ppb DMS was 25% greater than from saturated air having the same DMS concentration. Similar results were found for H<sub>2</sub>S.

Figure 2 also illustrates the stability of the detector calibration; for both H<sub>2</sub>S and DMS, calibration points taken months apart are shown. Observed response variations are less than 20% for H<sub>2</sub>S over 3 months and less than 10% for DMS over 2 months. Drift in zero air signal has been less than 3% of full scale over a period of 6 months. The current system has detection limits for H<sub>2</sub>S, DMS, CH<sub>3</sub>SH, and thiophene of about 4, 0.3, 0.1, and 12 ppb, respectively, based on a signal/root mean square noise ratio of 2, and a 60 s time constant.

Table I lists several compounds which have been tested for interference in the O<sub>3</sub>/sulfide chemiluminescence, and the concentration at which the test was made. The interference values are given as the DMS concentration required to produce equivalent signal. No signal is produced by benzene and propane, as expected based on previous work on the chemiluminescent oxidation of hydrocarbons by ozone (27). Nitric oxide and nitrogen dioxide give no interference, although parts-per-million levels of NO<sub>x</sub> enhance the emission from DMS, as discussed above. Acetaldehyde gives no signal in our system; therefore, it is unlikely that other aldehydes would interfere, since only acetaldehyde was found to chemiluminesce with ozone at room temperature in the study by Finlayson et al. (28). Ethylene is the only compound tested as an interferent which gives significant signal. The selectivity for DMS with respect to ethylene is 650:1.

Recent reports have discussed the chemiluminescence resulting from the gas-phase reaction of ozone with arsine (AsH<sub>3</sub>) and other metal hydrides (29, 30). The UV portion of this

Table I. Compounds Tested for Interference in the Detection of Gaseous Sulfides by Ozone Chemiluminescence

compound	concn tested, ppmv	signal (DMS equiv), ppbv
ethylene	1.1	1.7
benzene	20	n.d. <sup>a</sup>
propane	0.24	n.d.
nitric oxide	0.14	n.d.
nitrogen dioxide	0.14	n.d.
acetaldehyde	0.32	n.d.
sulfur dioxide	0.38	n.d.

<sup>a</sup> n.d. indicates no signal detected.

chemiluminescent emission is a potential interference in the detection of gaseous reduced sulfur compounds by ozone chemiluminescence, although these metal hydride compounds are not likely to be present in ambient air.

The present detector is a relatively simple modification of an existing instrument, yet shows good sensitivity and selectivity for reduced sulfur compounds. The instrument has performed well as a sulfur-specific GC detector in laboratory tests (31). Present sensitivity is sufficient for measurements of reduced sulfur compounds in source areas or industrial environments and shows promise for use in field studies of natural sources of sulfur compounds (2), where the real-time measurement capability and ease of operation are valuable attributes. When sampling a mixture of reduced sulfur compounds, as in ambient air measurements, the differing response of the detector to different sulfur compounds might require a separation or derivatization step to assure unambiguous measurement. The ethyl iodide derivatization used by Braman and Ammons (11) is one possibility under investigation in this area. Substantial improvement in sensitivity may be possible through improved reaction cell design, increased ozone production, or the use of photon counting techniques. The intensity of ozone/sulfide chemiluminescence increases with increasing reaction chamber temperature, so that improvement in sensitivity is achievable by heating the reactor. For example, DMS chemiluminescence intensity is approximately doubled by raising the reactor temperature from 20 °C to 100 °C. Preconcentration of reduced sulfur gases prior to analysis is a possible means of further improving the detector sensitivity. Work is currently under way investigating these possibilities, studying the response of the detector to other sulfur compounds, such as COS and CS<sub>2</sub>, and further elucidating the mechanism of ozone/sulfide reaction and chemiluminescence.

#### ACKNOWLEDGMENT

The authors acknowledge helpful discussions with P. Daum, D. Stedman, and G. Senum.

Registry No. H<sub>2</sub>S, 7783-06-4; CH<sub>3</sub>SH, 74-93-1; CH<sub>3</sub>SCH<sub>3</sub>, 75-18-3; O<sub>3</sub>, 10028-15-6; thiophene, 110-02-1.

#### LITERATURE CITED

- Cullis, C. F.; Hirschler, M. M. *Atmos. Environ.* **1980**, *14*, 1263-1278.
- Adams, D. F.; Farwell, S. O.; Robinson, E.; Paack, M. R.; Bamesberger, W. L. *Environ. Sci. Technol.* **1981**, *15*, 1493-1498.
- Stevens, R. K.; Mulik, J. D.; O'Keefe, A. E.; Krost, K. J. *J. Anal. Chem.* **1979**, *43*, 827-831.
- Stevens, R. K.; O'Keefe, A. E.; Orman, G. C. *Environ. Sci. Technol.* **1980**, *14*, 652-655.
- Farwell, S. D.; Rasmussen, R. A. *J. Chromatogr. Sci.* **1978**, *14*, 224-234.
- Adams, D. F.; Jensen, G. A.; Steadman, J. P.; Koppe, R. K.; Robertson, T. J. *J. Anal. Chem.* **1980**, *38*, 1094-1096.
- Ehman, D. L. *J. Anal. Chem.* **1978**, *48*, 918-920.
- Axelrod, H. D.; Cary, J. H.; Bonelli, J. E.; Lodge, J. P., Jr. *J. Anal. Chem.* **1980**, *41*, 1856-1858.
- Natusch, D. F. S.; Klonis, H. B.; Axelrod, H. D.; Teck, R. J.; Lodge, J. P., Jr. *J. Anal. Chem.* **1972**, *44*, 2067-2070.

- (10) Black, M. S.; Herbst, R. P.; Hitchcock, D. R. *Anal. Chem.* **1978**, *50*, 848-851.
- (11) Braman, R. S.; Ammons, J. M. "Technique for Measuring Reduced Forms of Sulfur in Ambient Air"; EPA-NTIS Report No. PB 81-179 772; National Technical Information Service, 1981.
- (12) Rasmussen, R. A. *Tellus* **1974**, *26*, 254-260.
- (13) Lovelock, J. E.; Maggs, R. J.; Rasmussen, R. A. *Nature (London)* **1972**, *237*, 452-453.
- (14) Spurlin, S. R.; Yeung, E. S. *Anal. Chem.* **1982**, *54*, 318-320.
- (15) Kummer, W. A.; Pitts, J. N., Jr.; Steer, R. P. *Environ. Sci. Technol.* **1971**, *5*, 1045-1047.
- (16) Akimoto, H.; Finlayson, B. J.; Pitts, J. N., Jr. *J. Chem. Phys. Lett.* **1971**, *12*, 199-202.
- (17) Glinski, R. J.; Sedarski, J. A.; Dixon, D. A. *J. Phys. Chem.* **1981**, *85*, 2440-2443.
- (18) Hales, J. M.; Wilkes, J. O.; York, J. L. *Tellus* **1974**, *26*, 277-283.
- (19) Becker, K. H.; Innocencio, M. A.; Schurath, U. Proceedings of Symposium No. 1, *Int. J. Chem. Kinet.* **1975**, *7*, 205-220.
- (20) Glavas, S.; Toby, S. "Removal of Trace Contaminants from the Air"; Deltz, V. R., Ed.; American Chemical Society: Washington, DC, 1975; ACS Symp. Ser. No. 17, pp 122-131.
- (21) Pitts, J. N., Jr.; Finlayson, B. J.; Akimoto, H.; Kummer, W. A.; Steer, R. P. Proceedings of the International Symposium on Identification and Measurement of Environmental Pollutants, Ottawa, Canada, 1971; pp 32-37.
- (22) Cadle, R. D.; Loford, M. *Int. J. Air. Water Pollut.* **1966**, *10*, 25-30.
- (23) Kelly, T. J.; Phillips, M. F.; Tanner, R. L.; Gaffney, J. S. presented at 75th Air Pollution Control Association Annual Meeting, New Orleans, LA, June 20-25, 1982.
- (24) "Instruction Manual—Model 14B-E NO<sub>x</sub> Analyzer"; Thermo Electron Corp.: Hopkinton, MA, 1980.
- (25) Japar, S. M.; Niki, H. *J. Phys. Chem.* **1975**, *79*, 1629-1632.
- (26) Morris, E. D., Jr.; Niki, H. *J. Phys. Chem.* **1974**, *78*, 1337-1338.
- (27) Kelly, T. J.; Allar, W. J.; Premuzic, E. T.; Tanner, R. L.; Gaffney, J. S. Presented at 182nd National Meeting of the American Chemical Society, New York, Aug 23-28, 1981.
- (28) Finlayson, B. J.; Gaffney, J. S.; Pitts, J. N., Jr. *Chem. Phys. Lett.* **1972**, *17*, 22-24.
- (29) Fujiwara, K.; Watanabe, Y.; Fuwa, K.; Winefordner, J. D. *Anal. Chem.* **1982**, *54*, 125-128.
- (30) Fraser, M. E.; Stedman, D. H.; Henderson, M. J. *Anal. Chem.* **1982**, *54*, 1200-1201.
- (31) Gaffney, J. S.; Kelly, T. J.; Allar, W. J.; Orlando, T.; Matzdorf, S.; Phillips, M. F.; Tanner, R. L., unpublished work, Brookhaven National Laboratory, 1982.

Thomas J. Kelly  
Jeffrey S. Gaffney\*  
Mary F. Phillips  
Roger L. Tanner

Environmental Chemistry Division  
Department of Energy and Environment  
Brookhaven National Laboratory  
Upton, New York 11973

RECEIVED for review July 19, 1982. Accepted September 27, 1982. Support for this work by the Office of Health and Environmental Research, U.S. Department of Energy, is gratefully acknowledged. This work was performed under the auspices of the U.S. Department of Energy under Contract No. DE-AC02-76CH00016.

## Identification of Triaromatic Azaarenes in Crude Oils by High-Resolution Spectrofluorimetry in Shpol'skii Matrices

**Sir:** Many methods used in the investigation of nitrogen-containing polyaromatic compounds (azaarenes) in crude oils have benefited from continuous progress in analytical methodologies of neutral polycyclic aromatic hydrocarbons (PAH): high-performance liquid chromatography (1-3), UV spectrometry (4), and capillary column gas chromatography and combined gas chromatography/mass spectrometry (GC/MS) (5-11). Fluorescence analysis also appeared very early as a convenient and powerful method for PAH and azaarene analysis (12-14), due to both the exceptional fluorescence properties of these compounds and the great sensitivity of emission detection.

However, at room temperature, fluorescence analysis does not permit the differentiation of isomeric compounds in complex mixtures because of considerable band broadening. Of much greater potentiality in this case is certainly the application of the Shpol'skii effect which is a specific characteristic of aromatic molecules (15). When incorporated at low temperature ( $T < 77$  K) in *n*-alkane matrices, aromatic compounds exhibit well-resolved emission fluorescence spectra (bandwidths:  $1-5 \text{ cm}^{-1}$ ), which allow the detection of individual molecules in complex mixtures. Whereas several recent papers have been devoted to the identification of neutral PAH by Shpol'skii spectrometry (16-18), little analytical work to our knowledge has been reported on azaarenes using this technique (19).

We report the identification by high-resolution spectrofluorimetry of various alkylated benzo[h]quinolines extracted from crude oils. Results are in accordance with a previous work in which structure determinations were obtained by GC/MS (20). In the analysis of polyaromatic molecules, however, whether PAH's, azaarenes, or others, the GC/MS combination cannot overcome the basic weaknesses of the individual techniques: chromatography is not selective enough to separate all geometrical isomers and mass spectrometry

lacks structure indicating fragments in this case. Thus, confirmation of the identification by a complementary technique was sought. The complexity of petroleum basic fractions and the unavailability of enough sample material after suitable purification and extraction excluded the use of NMR, but high-resolution fluorimetry, which does not suffer from these drawbacks and exhibits both extreme sensitivity and tunable selectivity, was clearly the method of choice.

### EXPERIMENTAL SECTION

**Reagents and Solvents.** All solvents were of analytical grade (Merck or Carlo Erba) and glass distilled before used. For spectrofluorimetric studies, *n*-hexane (spectroscopy grade from Fluka) was dried and kept on molecular sieves (3 and 10 Å). Traces of polar molecules should be absent from Shpol'skii solvents to avoid association with azaarene molecules (19). Fluorescence transparency of the solvent was verified by room temperature spectrofluorimetry (MPF-44 Perkin-Elmer spectrofluorimeter, Norwalk, CT).

Authentic azaarenes have been prepared by synthesis (21) and their structure checked by NMR spectrometry.

**Preparation of Basic Fraction.** The general scheme of isolation of petroleum nitrogen bases was previously published (5). Results are presented here for one crude oil (Likouala, Congo), a sample in which benzoquinolines are major compounds and show a distribution typical for most crude oils (5-18, 20). Micropreparative fractionations by means of reversed-phase liquid chromatography were as previously described (20).

**Capillary Column Gas Chromatography.** Glass capillary columns coated with nonpolar (OV-73), medium polar (OV-61), and polar (SP-2340) stationary phases (10, 11) were used for identifications by means of coinjections with synthetic reference compounds. The gas chromatograph was a Perkin-Elmer Model Sigma 3 (Norwalk, CT).

**Low Temperature Fluorescence Spectrometry.** Low-temperature luminescence measurements were performed with a homemade spectrofluorimeter previously described (22). Excitation was provided by a xenon lamp (XBO Osram 450 W), the

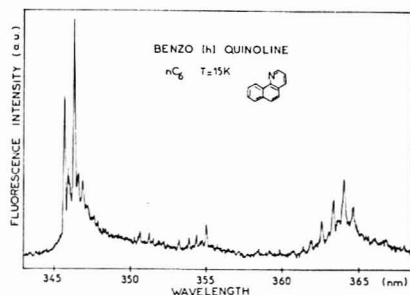


Figure 1. Fluorescence spectrum of benzo[h]quinoline in *n*-hexane frozen solution at 15 K:  $c = 10^{-6}$  M, excitation at 266 nm.

light of which was dispersed through a Jobin Yvon (H 20) monochromator (excitation bandwidth about 2.5 nm). The fluorescence emission was observed at  $90^\circ$  through a high-resolution monochromator (Jobin Yvon HR 1000, dispersion, 0.8 nm/nm). Photoelectric detection consisted of photomultiplier (EMI QB 9789).

The analyzed solutions were contained in fused silica tubes which fit into a copper block. This sample holder (maximum load of five tubes) was attached to the cold head of a closed cycle refrigerator (Model 21 SC Cryodyne CTT) operating at 15 K. The best observation of the Shpol'skii effect requires fast freezing of the solutions, otherwise aromatic aggregate formation can occur (23). This fast freezing was achieved by first immersing the sample holder into liquid nitrogen. The cool down procedure from 77 to 15 K was then completed in about half an hour.

## RESULTS AND DISCUSSION

The Shpol'skii spectrum of an aromatic molecule exhibits a characteristic multiplet structure (Figure 1) due to the existence of several different orientations of the molecule in the *n*-alkane crystalline solution (24, 25). In the case of azaphenanthrenes (i.e., benzoquinolines and alkyl derivatives), fluorescence emission in nonpolar solvents is due to  $\pi-\pi^*$  transitions whose energies are quite close to those of phenanthrene (26). Fluorescence quantum yields appear to be in the same range for alkylphenanthrenes and alkylbenzo[h]quinolines (27) but are very dependent on the nature of the solvent for nitrogen compounds (28).

Previous spectroscopic works have been made on quinolines, benzoquinolines, or phenanthrolines trapped in *n*-paraffins at 77 K (19, 29, 30), which exhibit quasi-linear luminescence spectra in nonpolar solvents. Normal hexane appears to be suitable solvent for azaphenanthrenes, just as it has been demonstrated for neutral triaromatics (28). Solutions of reference compounds and of crude oil basic fractions were adjusted to an optimum concentration of about  $10^{-6}$  M in *n*-hexane. In this concentration range, the problems which may occur in Shpol'skii matrices (nonreproducibility in the relative fluorescence intensity of peaks, intermolecular interactions, formation of aggregates) are minimized (17).

Fluorescence and phosphorescence quasi-linear spectra of the four methylated reference benzo[h]quinolines are presented in Figures 2 and 3, respectively. All the compounds exhibit simple fluorescence spectra composed of only a few quasi-lines in the emission transition where the fluorescence intensity is localized.

A bathochromic shift of the position of fluorescence bands can be observed between dimethylbenzo[h]quinolines (DM-BhQ) and trimethylbenzo[h]quinolines (TM-BhQ).

We have examined a crude oil basic fraction where  $C_2$  and  $C_3$  alkylbenzoquinolines have been shown to be the major components by LC/UV analysis. By judicious use of the

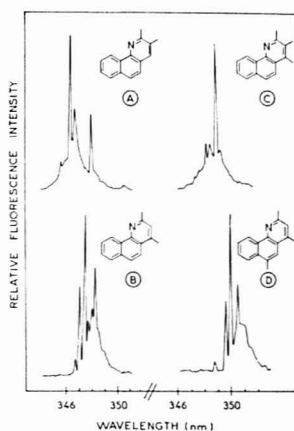


Figure 2. Fluorescence spectra of synthetic benzo[h]quinoline derivatives in *n*-hexane frozen solution at 15 K.  $c = 5 \times 10^{-6}$  M for each compound. Only the multiplet structure of the first strong emission transition is shown. (A) 2,3-dimethylbenzo[h]quinoline,  $\lambda_{exc} = 280$  nm; (B) 2,4-dimethylbenzo[h]quinoline,  $\lambda_{exc} = 279$  nm; (C) 2,3,4-trimethylbenzo[h]quinoline,  $\lambda_{exc} = 280$  nm; (D) 2,4,6-trimethylbenzo[h]quinoline,  $\lambda_{exc} = 279$  nm.

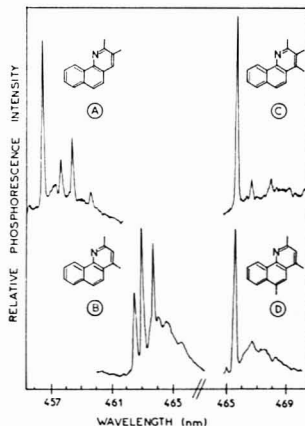
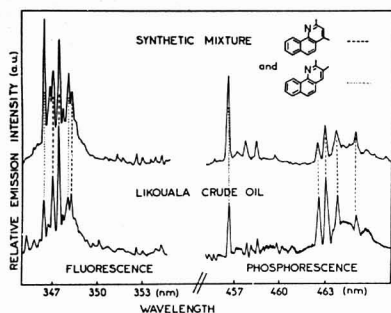


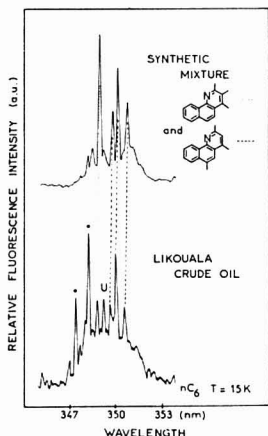
Figure 3. Phosphorescence spectra of synthetic benzo[h]quinoline derivatives in *n*-hexane frozen at 15 K. Experimental conditions and attributed spectra are as given in Figure 2.

excitation wavelength, each available isomer of DM-BhQ can be easily identified in the natural sample by comparison of its fluorescence and phosphorescence spectra with those of a synthetic mixture (Figure 4). The two TM-BhQ exhibit one strong phosphorescence quasi-line at exactly the same emission wavelength (cf. Figure 3) and cannot be differentiated in this way. The comparison of the relative fluorescence intensity of BhQ peaks in the equimolar mixture and in the crude oil fraction indicates that 2,4-DM-BhQ and 2,4,6-TM-BhQ dominate over the other respective isomer.

The four BhQ have been identified in the Likouala basic fraction by means of cojunction on three different glass ca-



**Figure 4.** Emission spectra of 2,3- and 2,4-dimethylbenzo[h]quinolines in a synthetic mixture (each isomer at  $2.5 \times 10^{-6}$  M) and in a di- and triaromatic base concentrate from Likouala crude oil, frozen in polycrystalline *n*-hexane at 15 K. Excitation was at 330 nm. Each isomer is identified by several emission peaks, by fluorescence and phosphorescence.



**Figure 5.** Fluorescence spectra of 2,3,4- and 2,4,6-trimethylbenzo[h]quinolines in a synthetic mixture (each isomer at  $2.5 \times 10^{-6}$  M) and in a di- and triaromatic base concentrate from Likouala crude oil, frozen at 15 K in polycrystalline *n*-hexane. Excitation was at 332.5 nm. Each isomer is identified by at least one characteristic emission peak. Peaks (c) in the fluorescence spectrum are attributed to 2,4-DMBHQ. Peak (u) is attributed to an unknown compound.

pillary columns. Relative distributions between isomers were found in good agreement with low-temperature fluorimetric analysis.

These analytical experiments are a good example of the application of GC, GC/MS analysis, and high-resolution spectrofluorimetry. This last technique, widely applied to the detection of neutral PAH's, demonstrates here its extensive possibilities to the characterization of N-heteroaromatic tricyclic compounds. This work will be continued by the characterization of higher molecular weight azarenes extracted from crude oils, using fluorescence analysis at two levels: determination of the ring arrangement of compounds occurring in

the basic fractions by room temperature measurements, and identification of individual compounds by high-resolution analysis at 15 K.

#### ACKNOWLEDGMENT

The crude oil sample was kindly supplied by Société Nationale Elf Aquitaine.

**Registry No.** 2,3-DM-BhQ, 37069-37-7; 2,4-DM-BhQ, 605-67-4; 2,3,4-TM-BhQ, 63042-66-0; 2,4,6-TM-BhQ, 81503-62-0.

#### LITERATURE CITED

- Ray, S.; Frei, R. W. *J. Chromatogr.* **1972**, *71*, 451-457.
- Dong, M.; Locke, D. C.; Hoffmann, D. *J. Chromatogr. Sci.* **1977**, *15*, 32-35.
- Colin, H.; Schmitter, J. M.; Guiochon, G. *Anal. Chem.* **1981**, *53*, 625-631.
- Jewell, D. M.; Hartung, G. K. *J. Chem. Eng. Data* **1964**, *9*, 297-304.
- Schmitter, J. M.; Vajta, Z.; Arpino, P. J. In "Advances in Organic Geochemistry 1979, Physical Chemistry of the Earth"; Douglas, A. G., Maxwell, J. R., Eds.; Pergamon Press: Oxford, 1980, Vol. 12, pp 67-78.
- Lee, M. L.; Bartle, K. D.; Novotny, M. V. *Anal. Chem.* **1975**, *47*, 540-542.
- Novotny, M. V.; Kump, R.; Merli, F.; Todd, L. *Anal. Chem.* **1980**, *52*, 401-406.
- Merli, F.; Novotny, M. V.; Lee, M. L. *J. Chromatogr.* **1980**, *199*, 371-378.
- Lee, M. L.; Novotny, M. V.; Bartle, K. D. In "Analytical Chemistry of Polycyclic Aromatic Compounds"; Academic Press: New York, 1981.
- Ignatiadis, I.; Schmitter, J. M.; Guiochon, G. *J. Chromatogr.* **1982**, *246*, 23-36.
- Schmitter, J. M.; Ignatiadis, I.; Guiochon, G. *J. Chromatogr.*, in press.
- Van Duuren, B. L. *Anal. Chem.* **1960**, *32*, 1436-1442.
- Durshel, H. L.; Sommers, A. L. *Anal. Chem.* **1966**, *38*, 19-28.
- MacKay, J. F.; Weber, J. M.; Latham, D. R. *Anal. Chem.* **1976**, *48*, 891-898.
- Shpol'skii, E. V. *Sov. Phys. -Usp. (Engl. Transl.)* **1962**, *5*, 522-531.
- Bikovskaya, L. A.; Personov, R. I.; Romanovskii, Y. V. *Anal. Chim. Acta* **1981**, *125*, 1-11.
- Yang, Y.; D'Silva, A. P.; Fassel, V. A. *Anal. Chem.* **1981**, *53*, 894-899.
- Rime, J.; Lamotte, M.; Jousset-Dubien, J. *Anal. Chem.* **1982**, *54*, 1059-1064.
- Nurmukhamedov, R. N. *Russ. Chem. Rev.* **1969**, *38*, 180-193.
- Schmitter, J. M.; Colin, H.; Excoffier, J. L.; Arpino, P.; Guiochon, G. *Anal. Chem.* **1982**, *54*, 769-772.
- Walls, L. P. In "Heterocyclic Compounds"; Elderfield, R. C., Ed.; Wiley-Interscience: New York, 1952; Vol. 4, pp 627-661.
- Garrigues, P.; Lamotte, M.; Ewald, M.; Jousset-Dubien, J. *C. R. Hebd. Seances Acad. Sci., Ser. II* **1981**, *293*, 567-571.
- Lim, E. C.; Yu, M. H. *J. Chem. Phys.* **1966**, *45*, 4742-4743.
- Shpol'skii, E. V.; Klimova, L. A.; Neresova, G. N.; Glyadkovskii, V. I. *Opt. Spectrosc. (Engl. Transl.)* **1968**, *24*, 25-29.
- Pfister, C. *Chem. Phys.* **1973**, *2*, 171-180.
- Perkampus, H. M.; Knop, J. V.; Knop, A.; Kassebeer, G. *Z. Naturforsch.* **1967**, *22*, 1419-1433.
- Garrigues, P.; Veyres, A., unpublished results.
- Janic, I. In "Lumin. Cryst. Mol. Solutions, Proc. Int. Conf., 1972" Williams, F., Ed.; Plenum: New York, 1973; pp 213-218.
- Janic, I.; Kawski, A. *Bull. Acad. Pol. Sci., Ser. Sci., Math., Astron. Phys.* **1972**, *20*, 235-242.
- Basara, H.; Ruziewicz, Z.; Zawadzka, H. *J. Lumin.* **1978**, *17*, 283-290.

Philippe Garrigues

Régine De Vazelles

Marc Ewald\*

Jacques Jousset-Dubien

Laboratoire de Chimie Physique A

Université de Bordeaux I

33405 Talence Cédex, France

Jean-Marie Schmitter

Georges Guiochon

Laboratoire de Chimie Analytique Physique

Ecole Polytechnique

91120 Palaiseau, France

RECEIVED for review July 19, 1982. Accepted September 20, 1982. This work was supported by grants of Délégation Générale à la Recherche Scientifique et Technique (DGRST, Paris, France; grants RAP-80-7-0256 and -79-7-1306).

# Quantitative Analysis of Coal-Derived Liquids by Thin-Layer Chromatography with Flame Ionization Detection

**Sir:** Gravity column chromatographic separation of coal-derived liquids precludes the analysis of a larger number of samples due to the cumbersome solvent removal step involved in any such procedure (1). On the other hand HPLC does not offer detectors suitable for quantitative work and procedure calibration is difficult (2). Again solvents are the main obstacle to fast analysis. In addition to that, column chromatographic procedures as applied to coal liquid or bitumen analyses are burdened by incomplete sample recoveries, characteristically between 85 and 95%, depending on sample type (3). Most of the disadvantages of column chromatography procedures can be eliminated, if thin-layer chromatography is employed, in combination with a flame ionization detector (4, 5). At least one company offers a TLC/FID instrument using sorbent coated rods. Solvent systems used in traditional column separations of fossil fuels need only little modification to be directly applicable to TLC, as shown in Figure 1. Stepwise development of the chromatogram is fast, solvent removal can be effected in a matter of minutes, and all sample components are accessible to the detector; as for the actual measurements, the rod is pulled through the detector flame at a constant rate. The rods can be placed in a frame, and their scanning is automated. Thus, up to 10 samples or sample replicas can be analyzed simultaneously. During the passage of the rod through the detector flame, the separated sample components are burned and the sorbent-coated rod is reactivated at the same time, so that a set of rods can be used for up to 50 times without appreciably changing their properties.

This contribution shows typical application of TLC/FID for the analysis of process oils from coal liquefaction and actual toluene extracts from coal liquefaction experiments.

## EXPERIMENTAL SECTION

**TLC/FID.** The samples were dissolved, typically in methylene chloride, and filtered through a narrow pore filter to remove any particulate matter and about 40  $\mu$ g of sample was applied 1 cm from the bottom of the silica gel or alumina coated rod. Several solvent systems were applied to find reasonable separation of saturates, aromatics, mobile (polar 1), and immobile (polar 2) components. Silica gel rods (15 cm long, 0.1 cm diameter, useful bed length 10 cm) were developed to 9 cm length with *n*-hexane, dried, and redeveloped with the same solvent, followed by 80% benzene in *n*-hexane over 4-5 cm of bed length. The final development was done with THF or 40% methanol in methylene chloride. Alumina rods were developed with *n*-hexane (9 cm), benzene or methylene chloride (5 cm), and methanol/methylene chloride (40:60) (2.5 cm). The rods were dried in a laboratory oven under nitrogen for 4-5 min and scanned in the FID at a rate of 0.31 cm/s. The instrument used was a combination of TLC/FID chromatograph, IATROSCAN TH-10, manufactured by Iatron Laboratories Inc., Tokyo, and a Hewlett-Packard Model 3390A integrator. Detected gases were set at flow rates of just above 2 L/min for air and 160 mL/min for hydrogen.

**SARA Analysis.** A 1-g sample was dissolved in 2 mL of methylene chloride, 80 mL of *n*-pentane was slowly added under stirring, and the precipitated asphaltenes were collected on a filter after several hours, dried under nitrogen to constant weight, and weighed. The filtrate was reduced to dryness, redissolved in a few milliliters of *n*-pentane, and applied on a 30  $\times$  1 cm column packed with Fuller's earth activated at 115  $^{\circ}$ C for 2 h. The "oils" were eluted with *n*-pentane and the "resins" with THF. The eluted fractions were evaporated to constant weight and weighed. (See ref 6 for further description of procedure.)

**Preparative TLC.** Plates (20  $\times$  20 cm) coated with alumina or silica without a binder (Merck) were activated at 150  $^{\circ}$ C and

Table I. Comparison of TLC and SARA Analyses of Anthracene Oil

	wt %		
	hydrocarbons	polar I	polar II
TLC/FID alumina	87.9	10.0	1.6
	88.0	9.6	1.9
silica	88.1	8.6	2.2
SARA	82.2	14.2	3.6
		(resins)	(asphaltenes)

200  $^{\circ}$ C, respectively. The sample solution was applied as a thin line nearly across the whole width of the plate. The same solvent systems and developing conditions were used as for rod TLC. After final drying, the respective zones were visualized with a UV lamp and scraped off the plate and the separated material was extracted with pentane and MeOH/methylene chloride in a Soxhlet min extractor.

**Infrared spectra** were obtained from methylene chloride casts, using a Perkin-Elmer Model 283 infrared spectrometer.

## RESULTS AND DISCUSSION

As pointed out above, TLC can overcome a number of problems encountered in gravity column and HPLC separations. It is fast, multiple analyses can be performed simultaneously, and all sample components are amenable to measurement. Easy solvent removal and FID detection of the "peaks" can be complemented by using an electronic integrator.

Since the separation mechanism is the same as in step elution methods of gravity column chromatography, it was important to ascertain the differences in fraction composition between the oil and resin fractions from SARA analysis, normally done on clays (6), and fractions obtained from the separation of the sample on silica gel or alumina (7, 8). Thus fractions of oils and resins from SARA separation have been individually examined through the course of development of the TL chromatogram (Figure 1) for a sample of anthracene oil. With 80/20 Bz/*n*C6 solvent only little material from the oil fraction from Fuller's earth appeared in the "resin" fraction, while "resins" supplied about 15% material to the oil fraction. Thus, the results for oils should be somewhat higher in TLC than in SARA. This is confirmed by Table I, making a comparison of SARA and TLC results.

However, either the anthracene oil contained very little asphaltenic material or the material was removed prior to analysis by TLC. A comparison of SARA and TLC results for toluene extracts of liquefaction products on the other hand showed a larger discrepancy (Table II), suggesting that part of the material precipitated as asphaltenes migrated in the "resin" and even in the "hydrocarbon" fractions. That this is the case indeed could be confirmed by dissolving the precipitated asphaltenes from the toluene extract in methylene chloride and subjecting them to TLC (Table III). The results were in accordance with our previous experience with sorbent chromatography of the resin and asphaltene fractions from oil sands bitumen (7-9). IR spectra of the same fractions obtained from preparative TLC on plates show clearly that some material, characterized by phenolic absorptions and also by an absorption at about 1740  $\text{cm}^{-1}$  was appearing together at the  $R_f$  value for the hydrocarbon peak (Figure 2). This "asphaltene" migration explains the results of Table II satisfactorily.

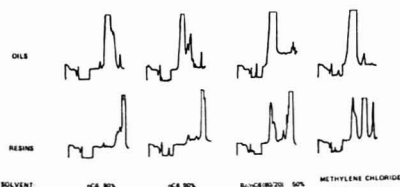


Figure 1. Progressive development of TL chromatograms of oils and resins separated by SARA method.

Table II. Comparison of TLC and SARA Analyses of Toluene Extracts from a Coal Liquefaction Experiment

	wt %		
SARA	"aromatics"	"resins"	"asphaltenes" <sup>a</sup>
R1	28.5	10.7	52.3
R14	30.4	2.4	64.8
R15	31.9	2.3	57.5
R24	64.5	9.4	22.1
R29	77.6	5.2	7.1
R18R	39.0	5.8	41.5

	wt %		
TLC <sup>b</sup>	HC	polar 1	polar 2
R1	66.3	26	7.6
R14	63.9	24.6	11.4
R15	63.6	27.4	9.0
R24	87.5	11.2	1.3
R29	90.3	9.1	0.6
R18R	70.2	21.3	8.4

<sup>a</sup> Asphaltenes separated by precipitation, resins and oils separated on Fuller's earth. <sup>b</sup> On alumina. Solvents: nC6 100%, methylene chloride 50%, MeOH/methylene chloride 25%. Asphaltenes not separated prior to analysis. Average values from five measurements.

Table III. Separation of Asphaltenes from Toluene Extract by TLC on Alumina

sample	wt %		
	HC	polar 1	polar 2
R14 (A)	27.1	62.7	10.2
(B)	22.6	60.3	17.0
	wt % recalculated for 64.8% asphaltenes obtained in SARA		
	HC	resins	asphaltenes
R14 (B)	45	41.4	
(A)	47.6	43	9.4

Another important question for quantitative analysis was the concentration/response dependence for the various separated peaks. Injecting progressively increasing quantities of a sample of anthracene oil and regression analysis of response/concentration dependence based on integrator counts furnished linear regression for each of the three peaks (Figure 3) with high correlation coefficients. Thus, the response was linear over the concentration range examined ( $5.5 \times 10^{-3}$  g/mL to  $8.8 \times 10^{-2}$  g/mL) while the actual amount of sample applied was determined to be at an optimum for 40–50  $\mu$ g sample.

It was expected that the response factors (counts/mass unit) for "oils", "polar 1", and "polar 2" would progressively depart from one due to the increasing contents of heteroelements in the respective fractions. This in fact was the case. However, once the response is linear with concentration—which was a questioned point—since unlike in GC which deals with volatile samples only, the sample must be completely burned off

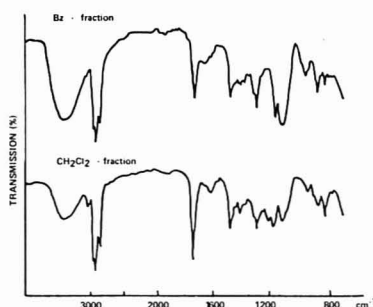


Figure 2. IR spectra of benzene and methylene chloride fractions from TLC of asphaltenes on alumina.

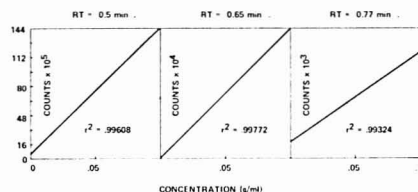


Figure 3. Regression analysis of TLC results for anthracene oil.

Table IV. Precision of TLC Separation of Anthracene Oil

	wt %		
rod	RT = 0.50 min	RT = 0.68 min	RT = 0.77 min
1	88.347	10.128	1.524
2	89.306	9.005	1.689
3	84.544	12.498	2.958
4	88.781	9.812	1.407
5	90.742	8.038	1.220
6	89.111	9.231	1.658
7	88.237	10.011	1.752
8	89.226	9.449	1.326
9	89.728	8.306	1.966
10	86.542	9.988	3.470
$\bar{x}$	88.456	9.647	1.897
std dev	1.755	1.231	0.737

during the relatively fast passage of the rod through the detector flame—calibration can be easily done by accumulating sufficient material from a TLC plate and doing the response/concentration measurement sequence. Asphaltenes-containing samples gave residual signal upon second passage of the rod through the flame. This effect could be eliminated by rotating the rods by 180 °C around their circumference, so that direct contact of the flame and the sample was accomplished. On the other hand, particulate material had to be removed from the sample prior to TLC as the hot zone temperature is not sufficient to burn it completely.

Thus, we have been able to establish that TLC/FID is suitable for quantitative analysis of coal-derived liquids after removal of particulate material and asphaltenes, with reasonably good precision (Table IV) and in short time, typically 1.5 h, while the precision of the determination can be improved considerably by running five or more (up to ten) sample replicas in parallel and averaging the results.

In addition to that, only minute sample quantities are required for the analysis (typically about 50  $\mu$ g) so that the



method is also well suited for the analysis of samples from miniautoclave experiments, minipyrrolyzers, etc. For showing distributional trends, the asphaltene does not have to be removed and comparative analyses can still be done, for example, by choosing a solvent (typically *n*-hexane with 1% methanol) in which the asphaltene is substantially insoluble, but all other components are soluble, or the system can be converted into a solvent extraction from open bed, as done previously from a column by Burke et al. (10).

#### ACKNOWLEDGMENT

Thanks are due to T. Manske for conscientious experimental work.

#### LITERATURE CITED

- (1) Haines, W. E.; Thompson, C. J. "Separating and Characterizing High-Boiling Petroleum Distillates"; The USBM-API Procedure, LERC/R1-75/5 and BERC/R1-75/2, July 1957.
- (2) Sautoni, J. C.; Swab, R. E. *J. Chromatogr. Sci.* **1975**, *13*, 361.
- (3) Farcasiu, M. *Fuel* **1977**, *56*, 9.

- (4) Yokoyama, S.; Umematsu, J.; Inoue, K.; Katoh, T.; Sanada, Y. International Conference on Coal Science; Dusseldorf, Sept 7-9, 1981.
- (5) Suzuki, Y.; Takeuchi, A. Proceedings of 21st Annual Meeting of the Japan Society for Analytical Chemistry, 1972, No. 47.
- (6) Bulmer, J. T.; Starr, J. Eds. "SYNCRUDE, Analytical Methods for Oil Sand and Bitumen Processing"; SYNCRUDE, Canada Ltd.: 1979, pp 121-123.
- (7) Selucky, M. L.; Ruot, T. C. S.; Chu, Y.; Strausz, P. In "Analytical Chemistry of Liquid Fuel Sources"; American Chemical Society: Washington, DC, 1978; Adv. Chem. Ser. No. 170, pp 117-127.
- (8) Selucky, M. L.; Ruot, T. C. S.; Chu, Y.; Strausz, O. P. *Prepr., Div. Pet. Chem., Am. Chem. Soc.* **1977**, *22* (2), 695.
- (9) Selucky, M. O.; Kim, S. S.; Skinner, F. In "Chemistry of Asphaltenes"; American Chemical Society: Washington, DC, 1981; Adv. pp 83-118.
- (10) Burke, F. P.; Winschel, R. A.; Wooton, D. L. *Fuel* **1979**, *58*, 539.

Milan L. Selucky

Coal Research Department  
Alberta Research Council  
Edmonton, Alberta T6G 2C2, Canada

RECEIVED for review July 16, 1982. Accepted September 27, 1982. Alberta Research Council, Contribution No. 1140.

## 1-Methyl-4-acetylpyridinyl Free Radical as an Electron Spin Resonance Spectral Probe of Solvent Polarity

*Sir:* Several organonitrogen free radicals have been recommended as cybotactic probes of solvent polarity because the influence of the solvent at the molecular level is observed as a systematic spectral shift in the values of the ESR hyperfine splitting constants for key basic atoms or functional groups within the indicator radicals. The most extensive and precise experimental data on such solvent effects were reported by Knauer and Napier (1), and their data base has been incorporated and reinterpreted in more recent theoretical-empirical studies on solvent polarity and hydrogen bonding by Taft, Abboud, and Kamlet (2) and by Abe, Kubota, and Ikegami (3). Because these investigations have been largely restricted to the  $A_N$ -ESR data for nitroxides, the present analytical study was undertaken in order to expand the data base for testing the reliability of the Kamlet-Taft solvent polarity scale by examining the solvent effects upon the hyperfine splitting constants for a different radical type. The specific probe selected for this purpose was 1-methyl-4-acetylpyridinyl (MAP) radical.

A detectable solvent influence upon the ESR spectrum of MAP was first identified and briefly discussed by Grossi, Minisci, and Pedulli (4). For this probe, the hyperfine splitting constant ( $A_H$ ) for the acetyl group is far more sensitive to changes in the solvent environment than is  $A_N$  for the basic nitrogen atom (5). The analysis of the observed net solvent effect upon  $A_H$ (acetyl) as summarized herein is made with the most recent form of the multiparameter model of Taft, Abboud, and Kamlet (2), using the linear free energy function in eq 1. Here, the observable is  $P$  and its reference state  $P_0$ ,

$$P = P_0 + s(\pi^* + d\delta) \quad (1)$$

$\pi^*$  is the solvent dipolarity parameter, and the  $d\delta$  term is a polarizability correction having a nonzero value for aromatic and polyhalogenated solvents (2). Equation 1 was applied to  $A_H$ (acetyl) values for MAP in nonpolar and polar aprotic solvents, and additional independent statistical tests concerned with the consistency of the data set of hyperfine splitting constants for MAP were made as well.

#### EXPERIMENTAL SECTION

The pyridinium iodide of the name compound was the initial reactant used to prepare 1-methyl-4-acetylpyridinyl radical; and the synthetic methods of Grossi, Minisci, and Pedulli (4) and

Table I. Hyperfine Splitting Constants for 1-Methyl-4-acetylpyridinyl Radical in Aprotic and Hydrogen Bonding Solvents (at 25 °C)

solvent	$\pi^*^a$	$\alpha^a$	$A_H^b$ (COCH <sub>3</sub> ) <sup>b</sup>
acetone	0.73	0	2.26
acetonitrile	0.71	0.29	2.52
acetophenone	0.90	0	2.29 <sup>c</sup>
benzene	0.59	0	1.96
bromobenzene	0.79	0	2.15 <sup>c</sup>
chlorobenzene	0.71	0	2.10 <sup>c</sup>
diethyl ether	0.27	0	1.74
dimethoxyethane	0.56	0	2.06
dimethylformamide	0.88	0	2.42
dimethyl sulfoxide	1.00	0	2.61
ethanol	0.54	0.85	3.25 <sup>c</sup>
hexamethylphosphoric triamide	0.87	0	2.44 <sup>c</sup>
<i>n</i> -hexane	-0.08	0	1.41 <sup>c</sup>
methanol	0.60	0.99	4.10
methyltetrahydrofuran	0.48 <sup>c</sup>	0	1.92
<i>i</i> -pentane	-0.03 <sup>c</sup>	0	1.44
pyridine	0.87	0	2.39 <sup>c</sup>
sulfolane	0.98	0	2.54 <sup>c</sup>
tetrahydrofuran	0.58	0	1.98
toluene	0.54	0	1.88 <sup>c</sup>
water	1.09	1.02	5.41
<i>o</i> -xylene	0.51	0	1.90 <sup>c</sup>

<sup>a</sup> Kamlet-Abboud-Taft parameters (in cm<sup>-1</sup> × 10<sup>3</sup>) from literature sources (2, 8, 11). <sup>b</sup> Values for the hyperfine splitting constants (in G) reported by Kubota and Ikegami (5). <sup>c</sup> New experimental data.

Kubota and Ikegami (5) using zinc and sodium amalgam as the reducing agents were employed without modification.

Reagent grade solvents were dried by standard methods (6) and all aprotic solvents were passed through an alumina column for final drying just prior to degassing and solution preparation. In general solute concentrations did not exceed 10<sup>-3</sup>-10<sup>-4</sup> M.

Spectral measurements were made at room conditions with a Varian E-4 EPR spectrometer having 100-kHz field modulation and a 4-min scan time. The overall uncertainty in the hyperfine splitting constants was ±0.03 G (standard deviation), based upon ten new results and five recorded scans for MAP in each solvent.

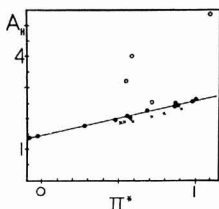


Figure 1. Comparison of the hyperfine splitting constants,  $A_H(\text{COCH}_3)$ , for the MAP radical with the Kamlet-Taft solvent dipolarity numbers,  $\pi^*$ . Points designated are (●) aprotic, (○) hydrogen bond donor, and (×) aromatic solvents as listed in Table I.

## RESULTS AND DISCUSSION

The final set of hyperfine splitting constants as  $A_H(\text{acetyl})$  for MAP are summarized in Table I, including both new data and those from published sources. In this instance the essential solute-solvent interaction appears to be localized on the carbonyl group and its polar oxygen as the principal determinant of the spin density distribution for the adjacent protons (3, 5).

Because of the seemingly high reliability of the data for the  $A_N$  values of the nitroxides in correlations with semiempirical solvent parameters (2), the initial test applied to the results for MAP was to compare graphically the various hyperfine splitting constants ( $A_H$ ) for the probe species with  $A_N$  values for di-*tert*-butyl nitroxide radical (1) in a common set of both aprotic and hydrogen bond donor solvents. The  $A_H$  values from the literature (5) for the 2-6 and 3-5 ring positions were used for this purpose as well as the data from Table I; and it should be noted that only nonlinear trends with moderate scatter were observed between  $A_N$  and  $A_H$  for the ring protons of MAP. On the other hand, an excellent linear correlation exists between  $A_N(\text{di-}t\text{-butyl nitroxide})$  and  $A_H(\text{acetyl-MAP})$  for all solvent types and including water. The corresponding linear regression in eq 2 has a correlation coefficient of 0.99 for 17 solvents and the uncertainty in the calculated  $A_H(\text{acetyl})$  is  $\pm 0.02$  G (standard deviation).

$$A_H(\text{COCH}_3) \text{ (in G)} = 1.94(A_N - 14.37) \quad (2)$$

In the Kamlet-Taft analysis of solvent influences upon an observable ( $P$ ) the net solvent effect is resolved into three independent parameters:  $\pi^*$  as noted in eq 1; the hydrogen bond acceptor basicity  $\beta$ ; and the hydrogen bond donor acidity  $\alpha$ . Because these parameters are related through a linear free energy function, any graph of  $P$  vs.  $\pi^*$  (the most fundamental variable characterizing all solvents) will be linear for nonhydrogen bonding and simple aprotic solvents; however, data points for hydrogen bond donors will be displaced from that linear function in a common direction (7). Similarly, aromatics and halogenated aliphatic solvents will exhibit a slight group displacement from the  $P$  vs.  $\pi^*$  linear trend (8). Thus, as a critical test of the conformity of the  $A_H(\text{acetyl})$  values to the expectations of the Kamlet-Taft treatment, the ESR data from Table I were used to construct Figure 1. It is clear from this plot that the  $A_H(\text{acetyl})$  data follow the general pattern anticipated from the Kamlet-Taft theory of solvent effects.

With this justification the general linear regression for the Taft-Abboud-Kamlet function (eq 1) was applied to the  $A_H(\text{acetyl})$  data for MAP in all of the aprotic solvents listed in Table I. In eq 3 the derived uncertainties are: slope and intercept,  $\pm 0.01$ ;  $A_H(\text{calcd})$ ,  $\pm 0.04$  (standard deviation); correlation coefficient, 0.99; and for the computation of  $\pi^*$  values,  $\pm 0.05$  (standard deviation). The uncertainty in the latter is

$$A_H(\text{acetyl}) \text{ (in G)} = 1.09(\pi^* - 0.14\delta) + 1.46 \quad (3)$$

Table II. Solvent Influence on Transient Electronic Absorption ( $\lambda_{\text{max}}$ ) for *p*-Aminobenzenethiyl Radical (at 23 °C)

solvent	$\lambda_{\text{max}}$ , nm <sup>a</sup>	$\pi^*$ <sup>b</sup>	$\delta$ <sup>b</sup>
anisole	575	0.73	1
benzene	570	0.59	1
benzonitrile	580	0.90	1
carbon tetrachloride	550	0.29	0
chloroform	570	0.38	0
cyclohexane	545	0.00	0
<i>o</i> -dichlorobenzene	578	0.80	1
1,2-dichloroethane	577	0.81	1
dichloromethane	577	0.80	1
dimethyl sulfoxide	610	1.00	0
<i>p</i> -dioxane	577	0.54	0
ethylacetate	578	0.55	0
fluorobenzene	570	0.62	1
mesitylene	570	0.41	1
pyridine	600	0.87	0
tetrahydrofuran	580	0.58	0
toluene	570	0.54	1

<sup>a</sup> Values for selected aprotic solvents from the data of Ito and Matsuda (10). <sup>b</sup> Kamlet-Abboud-Taft parameters from literature sources (2, 8).

comparable to the overall variation in  $\pi^*$  numbers calculated from aromatic carbon-13 NMR shifts (9). It should be noted that the value of coefficient  $d$  in eq 3 is close to the one obtained for the regression with di-*tert*-butyl nitroxide radical and, as is usually the case,  $d$  is negative in sign (2). For all aromatic solvents included in this study, the convergence in the  $d\delta$ -quantity necessitates an assumed  $\delta$  value of unity.

A final aspect of the relationship of free radical probes to the  $\pi^*$  scale was examined. Although it has been shown that the ESR data for selected free radical probes correlate well in empirical regressions like eq 1, the normalized  $\pi^*$  numbers themselves were initially derived from the solvent influence at the molecular level upon the  $p \rightarrow \pi^*$  or  $\pi \rightarrow \pi^*$  UV-visible spectral transitions of uncharged solvatochromic indicators (2, 9). Thus, it is appropriate to test whether or not solvent induced electronic spectral shifts for an uncharged free radical probe correspond to the usual solvatochromic behavior in the polarity variable ( $\pi^* + d\delta$ ). The recently published data of Ito and Matsuda (10) for the transient electronic absorption of *p*-aminobenzenethiyl radical ( $p\text{-NH}_2\text{C}_6\text{H}_4\text{S}\cdot$ ) were used for this test. For the 17 nonpolar and polar aprotic solvents in Table II, the specific linear regression function in eq 4 is valid.

$$E_T(\text{kcal/mol}) = 52.46 - 5.5(\pi^* - 0.23\delta) \quad (4)$$

Here,  $E_T$  is the transition energy corresponding to  $\lambda_{\text{max}}$  of the radical; the correlation coefficient is 0.97; and the uncertainties are as follows:  $d$  ( $\pm 0.03$ ); intercept ( $\pm 0.01$ );  $s$  ( $\pm 0.02$ );  $E_T(\text{calcd})$   $\pm 0.22$  (standard deviation). The greater uncertainties in the parameters reflect the lower precision in the  $\lambda_{\text{max}}$  values for transient spectra of the radical than for the nitroaniline indicators; however, eq 4 is sufficiently reliable to demonstrate the ( $\pi^* + d\delta$ ) response of this thiyl radical in nonhydrogen bonding media.

Therefore, at the molecular level the measured solvent influence upon both the hyperfine splitting constants and the electronic spectra for the uncharged free radical probes appears to be a composite response to the two types of interactions in aprotic media: dipolar solute-permanent dipolar solvent interactions; and dipolar solute-induced dipolar solvent interactions. In this respect the free radical probes resemble the  $\pi^*$  indicators in conforming to the Brady-Carr modification of the reaction field theory which requires both the dipolar orientation and electronic polarization interactive contributions to be resolved as separate terms (12). For the

solute, one structural parallel seems to dominate the responses of the acetyl and nitroxide radicals as the key functional groups in the two types of probe species. In both instances as the dipolar character of the solvent molecule increases there is a corresponding increase in the hyperfine splitting constant for the major functional group; and this condition accompanies the decrease in the spin density on the oxygen atom of the acetyl or nitroxide group with an increase in the net strength of the radical solute-solvent interaction.

Registry No. 1-Methyl-4-acetylpyridinyl radical, 64365-85-1.

### LITERATURE CITED

- (1) Knauer, B.; Napier, J. J. *Am. Chem. Soc.* **1976**, *98*, 4395.
- (2) Taft, R.; Abboud, J.; Kamlet, M. J. *Am. Chem. Soc.* **1981**, *103*, 1080.
- (3) Abe, T.; Kubota, S.; Ikegami, Y. J. *Phys. Chem.* **1982**, *86*, 1358.
- (4) Grossi, L.; Minisci, F.; Pedullì, G. J. *Chem. Soc., Perkin Trans. 2* **1977**, 943.

- (5) Kubota, S.; Ikegami, Y. J. *Phys. Chem.* **1978**, *82*, 2739.
- (6) Riddick, J.; Bunger, W. "Organic Solvents", 3rd ed.; Wiley-Interscience: New York, 1970; Chapter 5.
- (7) Yokoyama, T.; Taft, R.; Kamlet, M. J. *Am. Chem. Soc.* **1976**, *98*, 3233.
- (8) Kamlet, M.; Hall, T.; Boykin, J.; Taft, R. J. *Org. Chem.* **1979**, *44*, 2599.
- (9) Chawla, B.; et al. J. *Am. Chem. Soc.* **1981**, *103*, 6924.
- (10) Ito, O.; Matsuda, M. J. *Am. Chem. Soc.* **1982**, *104*, 568.
- (11) Kamlet, M.; Taft, R.; Carr, P.; Abraham, M. J. *Chem. Soc., Faraday Trans. 1* **1982**, *78*, 1689.
- (12) Brady, J.; Carr, P. J. *Phys. Chem.* **1982**, *86*, 3053.

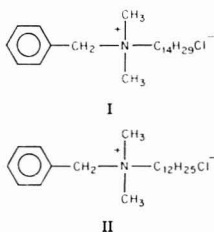
Orland W. Kolling

Chemistry Department  
Southwestern College  
Winfield, Kansas 67156

RECEIVED for review August 3, 1982. Accepted October 4, 1982.

## Quantitative Analysis of Mixed Benzalkonium Chlorides by Laser Mass Spectrometry

Sir: Laser mass spectrometry (LMS) has proved to be extremely useful for performing rapid qualitative analysis for a variety of nonvolatile and thermally labile compounds (1). Recently successful results have been obtained for qualitative analysis of a mixture of organic compounds (2). Though absolute quantification is difficult by LMS, the technique offers great potential for relative quantitative measurements. Experiments using an epoxy resin doped with organometallic complexes of metal ions indicated that LMS has high potential with regard to both reproducibility and detection limits for metal ions (3). Promising results have been obtained for quantitative LMS analysis of metals in biological specimens (4, 5). Here we report for the first time, the quantitative analysis of a mixture of organic compounds. Two quaternary ammonium salts (I, II) have been analyzed by LMS and compared with results for the same mixture from high-performed liquid chromatography (HPLC). The salts were present as chlorides.



### EXPERIMENTAL SECTION

The HPLC system consisted of a Waters 6000A pump, a Varian Varichrom detector, and a Rheodyne injection loop. The separation was carried out on a Zorbax CN column (250 × 4.6 mm, 5 μm) and a UV detector was used with 263 nm as the monitoring wavelength. The solvent system was acetonitrile-0.1 M acetate buffer solution (pH 5.0) (60/40 v/v) with a flow rate of 2.0 mL/min.

The positive ion laser mass spectra were obtained with a LAMMA-500 instrument which has been described elsewhere (3). The output of a frequency quadrupled Q-switched Nd-YAG laser (265 nm, 15 ns pulse width) is focused onto sample using one of three microscopic objectives: 10X, 32X, 100X. In this case the

32X objective was used. Changes in laser spot size and power had little effect on the mass spectra. Pulse power was varied with a set of filters and was adjusted to give the optimum power density needed to obtain a mass spectrum (~10<sup>8</sup> W/cm<sup>2</sup>).

The absolute concentration ratio of components II:I was found to be 3:0 from HPLC. For LMS analysis, the sample was dissolved in methanol and evaporated on a formvar film grid to give a uniform thin layer.

The sample was scanned by the microprobe and 12 spectra were stored and averaged using a Hewlett-Packard 1000E-series data system. The reproducibility of this experiment is ±10% relative standard deviation. Except for small intensity variations, there were no significant differences between the spectra that were averaged.

### RESULTS AND DISCUSSION

Figure 1 shows the HPLC separation of the benzalkonium chloride mixture (I, II). Because the components comprising the mixture are chemically similar and detection depends on the UV absorption of the benzyl moiety, no external standards were used for quantitation. Integration of the peak areas was done by height times width-at-half-height. This technique yielded a ratio, II:I, of 3.0. No significant amounts of the C<sub>10</sub> and C<sub>16</sub> derivatives similar to II and I could be detected by HPLC. Thus the sample was assumed to be a two-component mixture.

Figure 2 shows the positive ion laser desorption mass spectra (averaged over 12 spectra) of the benzalkonium chloride mixture. Intact cations appear at *m/z* = 304 (II) and *m/z* = 332 (I). Loss of toluene from both cations is consistent with the following fragment ions:



*m/z* = 240 derived from I



*m/z* = 212 derived from II.

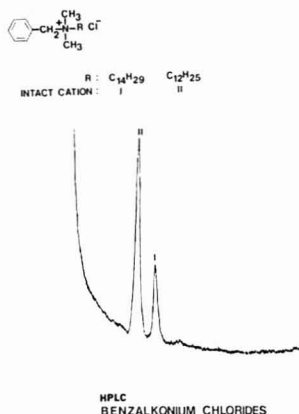


Figure 1. HPLC separation of benzalkonium chloride mixture (I, II).

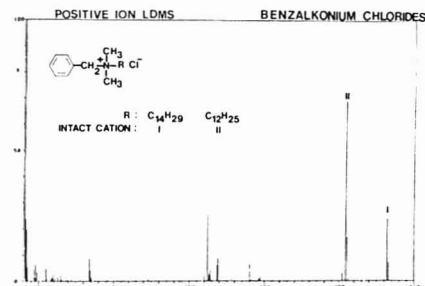


Figure 2. Laser desorption mass spectrum of benzalkonium chloride mixture (I, II).

The base peak at  $m/z = 91$  is the familiar benzyl (tropylium) ion, as would be expected.

We have used the intensities of the intact cation peaks for quantitative calculation. The ratio measured by LMS for the benzalkonium chlorides is  $II:I = 2.9 \pm 0.3$ . This is within experimental error of the value of 3.0 derived from HPLC data. This is a clear demonstration that laser desorption mass

spectrometry can be applied to analysis of mixtures of organic compounds using quasi-molecular ions. It is interesting to note that if one attempts mixture analysis from the fragment ions at  $m/z$  240 and 212 a ratio of  $II:I = 4.0$  results. This clearly differs from the HPLC ratio, indicating that one may have to exercise caution when using peaks other than those for quasi-molecular ions for quantitation.

One might argue that the intensity of the  $m/z$  304 intact cation may have a contribution from the other ( $m/z = 332$ ), as a result of a neutral loss of 28 mass units. Such a loss can be excluded, because fragmentation through a four-membered transition state, which is usually expected for quaternary ammonium salts, would not lead to loss of neutral fragment of 28 mass units. Even if it did occur, one would expect the same type of fragmentation from II which is chemically similar and of higher intensity than compound I. Such is not observed.

The analysis of the benzalkonium chloride mixture by LMS is in excellent agreement with the HPLC result, within the limit of experimental error ( $\pm 10\%$ ). This first attempt of quantitative analysis of organic compounds shows that LMS using the LAMMA 500 has potential for quantitative analysis of organic mixtures. LMS has several advantages over other techniques for quantitation. First, it requires only a small amount of sample (micrograms or less). Second, no special sample preparations are required. Third, analyses are fast. Fourth, the microprobe capabilities of the LAMMA-500 have the potential for quantitative analysis of organic inclusions in an organic matrix.

#### ACKNOWLEDGMENT

We thank N. Brake and K. Cornelius for their help with the HPLC work.

Registry No. I, 139-08-2; II, 139-07-1.

#### LITERATURE CITED

- (1) Hercules, D. M.; Day, R. J.; Balasanmugam, K.; Dang, T. A.; Li, C. P. *Anal. Chem.* **1982**, *54*, 280A.
- (2) Talmi, Y.; Dutta, K. P. *Anal. Chim. Acta* **1981**, *132*, 111-118.
- (3) Kaufmann, R.; Hillenkamp, F.; Wechsung, R. *Med. Prog. Technol.* **1979**, *6*, 109-121.
- (4) Schröder, W. H. Z. *Anal. Chem.* **1981**, *308*, 212-217.
- (5) Seydel, U.; Lindner, B. Z. *Anal. Chem.* **1981**, *308*, 253-257.

Kesagapillai Balasanmugam  
David M. Hercules\*

Department of Chemistry  
University of Pittsburgh  
Pittsburgh, Pennsylvania 15260

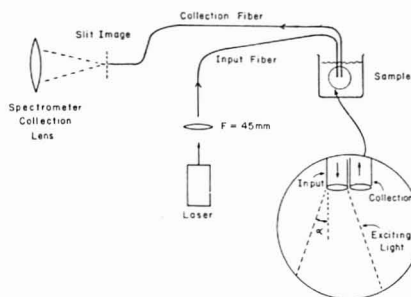
RECEIVED for review August 2, 1982. Accepted October 14, 1982. This work was supported by the National Science Foundation under Grant CHE-8108495.

## Fiber Optic Probe for Remote Raman Spectrometry

*Sir:* When combined with UV-Vis spectrophotometry, optical fibers are useful waveguides for directing radiation of the sample and returning the partially absorbed light for detection. A recent report discussed the application of fibers for remote fluorescence, where the sample may be located a great distance from the spectrometer (1). However, the poor transmission characteristics of silica fibers in the infrared region prevent their use in IR absorption spectrometry. We report here a probe for Raman spectrometry, where the advantages of fiber optics are combined with the structural

information inherent in Raman spectra. Fiber optics have been used previously for collection of Raman scattering (2) and for holding samples for Raman spectrometry (3, 4). In the present work, both the excitation beam and scattered light are carried by fibers, so the sample may be located far away from the spectrometer, in a hostile environment if necessary. In addition the probe itself is very simple and rugged and may be used for routine analysis.

The apparatus is shown in Figure 1 and is based on 200  $\mu$ m diameter multimode fibers of common use in communications.

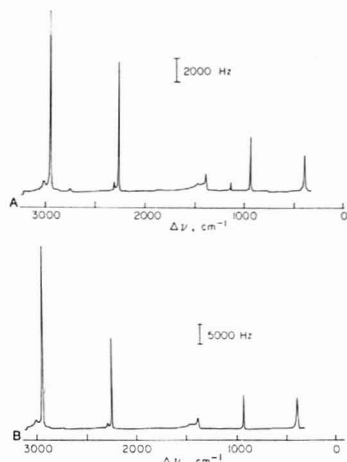


**Figure 1.** Schematic of fiber probe. Laser output is focused on input fiber and exits into solution as a cone, shown in the insert ( $\alpha = 27^\circ$ ). Adjacent to the input fiber is the collection fiber which accepts light from a similar cone. The other end of the collection fiber is positioned at the slit image of the spectrometer such that its output is focused on the input slit. Both fibers were 2 m long and the cladding was intact except for 2 cm removed at the sample end. Silica core diameter was 200  $\mu\text{m}$ .

The 200- $\mu\text{m}$  silica core is coated with a 100  $\mu\text{m}$  thick sheath of silicone rubber and then a 100- $\mu\text{m}$  protective coating of nylon. The laser beam (5145 Å) was focused into the input fiber with a 45-mm lens, with about one-third of the input light being transmitted by the fiber. Two centimeters of cladding was removed from the sample end of both input and collection fibers, and the exposed ends were placed adjacent to each other with the axes of the fibers approximately parallel. The other end of the collection fiber was positioned at the slit image of the spectrometer (5). With the monochromator tuned to a Raman line of the sample, the laser end of the input fiber and output end of the collection fiber were adjusted to maximize the signal. During the adjustments and during use of the probe, the position of the fibers in the sample was unimportant.

The laser light exits the input fiber into the sample as a cone whose size is determined by the numerical aperture of the fiber. In this case the cone had an angle at its apex of  $54^\circ$  ( $\alpha = 27^\circ$ ), so that its base was about 1 cm wide after traveling 1 cm in the sample. The collection fiber gathered scattered light from a similar cone, and the scattered light was analyzed as usual by the spectrometer. A Raman spectrum for acetonitrile using the fiber optic probe is shown in Figure 2A and is compared with a conventional spectrum obtained with the usual  $90^\circ$  sampling geometry. All parameters were identical for the two spectra except for laser power, which was 0.8 W for Figure 2B and 1.8 W (incident on the input fiber) for Figure 2A. After an adjustment was made for this power difference, the spectrum obtained with fibers is 13% as intense at that obtained conventionally. The small feature at about 1100  $\text{cm}^{-1}$  in Figure 2A was caused by a mercury line in the room lights which was collected by the fiber. Spectra were also obtained with a single fiber acting both as input and collection fiber, but a large silica background was observed in the region 200–700  $\text{cm}^{-1}$  and peaks in the C–H stretch region were observed which originated from the silicone cladding.

Several improvements in this initial design are apparent, which will augment the value of the probe. An array of six collection fibers oriented around the input fiber will increase the sensitivity over that of a conventional sampling arrangement. The six collection fibers could be oriented as a row at the spectrometer, to match the slit image. This improvement in collection optics, combined with more efficient coupling of the laser to the input fiber should allow the sensitivity to exceed that of conventional collection optics. En-



**Figure 2.** (A) Raman spectrum of neat acetonitrile using the fiber optic probe described in Figure 1. Laser power incident on the input fiber was 1.8 W (5145 Å) of which about 600 mW entered the sample. Spectral slit width was 5  $\text{cm}^{-1}$ . (B) Spectrum of neat acetonitrile obtained with conventional  $90^\circ$  collection geometry. Sample was contained in a 20-mL vial, slit image was oriented along focused beam. All other conditions were as given in A, except input laser power was 0.8 W.

capsulation of the sampling end of the fibers will permit a very rugged and corrosion resistant probe to be constructed, provided the encapsulation material has a refractive index less than that of the fiber ( $n < 1.49$ ).

Several advantages of the fiber optic probe exist for many areas of application of Raman spectrometry. First, the sample may be distant from the spectrometer, since losses in the fibers are very small (ca. 1% / m). Second, no special sample positioning is necessary once the fibers have been coupled to the laser and spectrometer. The probe is simply inserted in the sample, by an unskilled operator if necessary, with no alignment required. Third, the probe can be very small, consisting of encapsulated fibers with a total diameter of less than 1 mm. Applications to samples with limited accessibility are possible, in areas such as medicine, chemical processing, and the petroleum industry. Fourth, the probe may be positioned in hostile environments not amenable to conventional Raman, such as polymer melts, high-temperature reactors, etc. Only silica and an encapsulation material (e.g., Teflon) need be in contact with the sample and the probe could be mounted in the wall of a reactor or pipe. Fifth, the sensitivity may exceed that of conventional sampling techniques, resulting in broader applicability. Finally, it is possible to have several probes multiplexed to the same spectrometer, so several locations in a plant or research facility could make use of a single spectrometer.

While UV-Vis absorption and fluorescence spectrometry permit sensitive monitoring of known components, Raman spectrometry allows the fingerprinting of species present and is therefore structurally specific. In addition, the inherently high resolution of Raman spectra often permits the analysis of several components in a mixture simultaneously. The simplicity and versatility of the fiber optic probe described here should broaden the applicability of Raman spectrometry to a variety of analytical problems, especially as there is no need for sampling or sample preparation.

Note: Just at the time of submission of this manuscript, a commercial device was announced ("Optrode", Oriol, Stamford, CT) which is similar to that described here, but intended for fluorescence spectrometry. The advantage of using the device for Raman is that the fibers conduct well in the wavelength region used for Raman, whereas they conduct the UV light usually necessary for fluorescence much less efficiently. In addition, a review of optical waveguides applied to spectroscopy has appeared (6).

#### LITERATURE CITED

- (1) Borman, S. A. *Anal. Chem.* 1981, 53, 616A.
- (2) Eysel, A. *Spectrochim. Acta, Part A* 1971, 27A, 173.
- (3) Wairaf, G. E.; Stone, J. *Appl. Spectrosc.* 1972, 26, 585.
- (4) Stolen, R. H. In *Proceedings of the International Conference on Light Scattering in Solids*, 3rd, Balkanski, A., Ed.; 1975; p 656. *Chem. Abstr.* 1976, 85, 133491.
- (5) Reid E. S.; Cooney, R. P.; Hendra, P. J.; Fleischmann, M. J. *Electroanal. Chem.* 1977, 80, 405.

- (6) Chabay, I. *Anal. Chem.* 1982, 54, 1071A.

Richard L. McCreery\*

Department of Chemistry  
The Ohio State University  
Columbus, Ohio 43210

Martin Fleischmann  
Patrick Hendra

Department of Chemistry  
University of Southampton  
Southampton SO9 5NH, England

RECEIVED for review July 19, 1982. Accepted October 20, 1982. This work was performed while R.L.M. was on sabbatical at the University of Southampton. Partial support by the Alfred P. Sloan Foundation and the hospitality of the Chemistry Department at Southampton are acknowledged.

## AIDS FOR ANALYTICAL CHEMISTS

### Cadmium Telluride $\gamma$ -Ray Liquid Chromatography Detector for Radiopharmaceuticals

Richard E. Needham\*<sup>1</sup> and Michael F. Delaney

Winchester Engineering and Analytical Center, U.S. Food and Drug Administration, Winchester, Massachusetts 01890, and  
Department of Chemistry, Boston University, Boston, Massachusetts 02215

The separation of  $\gamma$ -emitting radiochemical species has been an important aspect of radiopharmaceutical research and quality control. Recently, high-performance liquid chromatography (HPLC) has found promising application in this area (1, 2). Typical radiopharmaceuticals contain a low-energy  $\gamma$ -emitting radioactive label (100–200 keV) which is chelated or covalently bonded to a carrier molecule of interest. Frequently encountered isotopes include technetium-99m (140 keV) and iodine-123 (159 keV). Detection of radiochemical species separated by HPLC has been accomplished by placement of a flow cell or coil in the central depression of a sodium iodide [NaI(Tl)] well-type scintillation detector, so that  $\gamma$ -rays emitted from species in the flow cell are detected by the surrounding detector. A NaI(Tl) well-type scintillation detector is not ideal for this application since (1) it is relatively large, typically a 3 in. (7.5 cm) diameter by 3 in. (7.5 cm) thick crystal with a 1 in. (2.5 cm) diameter well, (2) it requires a large and inconvenient photomultiplier tube (PMT), which restricts its placement relative to a flow cell, and (3) it is generally necessary to surround the crystal with extensive shielding to reduce background count rates.

A more satisfactory approach to the detection of  $\gamma$ -rays after HPLC separation would be to have a small volume, compact  $\gamma$  detector which could view an HPLC flow cell externally and with high detection efficiency. Cadmium telluride (CdTe) detectors are a relatively recent development which have found application as nuclear radiation dosimeters and probes (3, 4). CdTe detectors are suitable for the present application for a number of reasons: (1) the CdTe detector is a semiconductor detector, in which an electrical charge is produced directly from a  $\gamma$ -ray interaction. The need for a PMT is therefore eliminated; (2) the active volume of the detector itself is quite small (5–10 mm<sup>3</sup>) with correspondingly compact external

packaging, permitting convenient placement of the detector in confined areas; (3) the small active volume results in relatively low background count rates and maximizes detection sensitivity for small source volumes, such as HPLC flow cells; (4) the  $\gamma$  peak resolution is comparable to that of a NaI(Tl) detector; this gives energy resolution sufficient to discriminate against background and scattered radiation; (5) the detection efficiency of CdTe, because of its higher effective atomic number ( $Z_{\text{eff}} = 50$ ), is higher than that of NaI(Tl) ( $Z_{\text{eff}} = 38$ ) on an equal volume basis.

This report presents our experience with a CdTe detector which we have mounted in a commercially available refractive index (RI) HPLC detector, allowing simultaneous monitoring of the bulk properties and  $\gamma$  radiation of eluting radiochemical species.

#### EXPERIMENTAL SECTION

A 2.6 × 2.6 × 2.0 mm "cubic" CdTe detector housed in a 5 mm diameter × 12 mm cylindrical aluminum housing with a 20 cm long miniature coaxial cable lead and BNC connector (Radiation Monitoring Devices, Inc., Watertown, MA) was used. An aluminum detector holder was constructed in-house to mount the detector to the heat exchanger coil of a Micromeritics Model 771 refractive index detector (Micromeritics, Norcross, GA). The detector lead was brought outside the Dewar flask housing of the RI detector to a Radiation Monitoring Devices Model PSP-1 preamplifier/bias supply. The preamplifier signal was routed sequentially by coaxial cable to an Ortec Model 572 spectroscopy amplifier (EG+G Ortec, Oak Ridge, TN), an Ortec Model 551 single channel analyzer, and an Ortec Model 441 rate meter. The recorder output from the ratemeter was used to drive one side of a Varian Model A-25 dual channel recorder (Varian Aerograph, Walnut Creek, CA), while the second side was driven by the RI detector.

The CdTe detector was collimated by wrapping a 1.5 mm thick layer of lead foil around the cylindrical housing, in order to attenuate any extraneous radiation up to 150 keV by greater than 95%.

<sup>1</sup> Author to whom correspondence should be addressed at Winchester Engineering and Analytical Center.



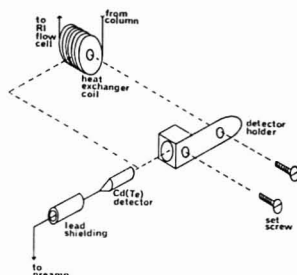


Figure 1. Exploded view of the CdTe detector, as adapted to the heat exchanger coil of the RI detector.

The detector was evaluated for background count rate, photopeak energy resolution, and photopeak counting efficiency by using spectra accumulated with a Nuclear Data 4420 multichannel analyzer system (Nuclear Data, Inc., Schaumburg, IL). Radioactive sources included point source activity standards of  $^{241}\text{Am}$ ,  $^{133}\text{Ba}$ ,  $^{57}\text{Co}$ , and  $^{203}\text{Hg}$  (Amersham International, Ltd., Amersham, U.K.) and aqueous solutions of  $^{99\text{m}}\text{Tc}$ ,  $^{67}\text{Ga}$ , and  $^{75}\text{Se}$  calibrated on a Capintec CRC-2N ionization chamber (Capintec, Inc., Mount Vernon, NY). A  $^{99\text{m}}\text{Tc}$  point source was also prepared by equilibration of a  $^{99\text{m}}\text{Tc}$  sodium pertechnetate solution with a Dowex-2X-8 anion exchange bead using the technique of Hahn and Shleien (5). The in situ response of the detector was evaluated by using  $^{99\text{m}}\text{Tc}$  sodium pertechnetate solutions injected into a pH 7.0 phosphate buffer stream, with flow maintained by an Altex Model 100 HPLC pump (Altex Scientific, Inc., Berkeley, CA). For comparison, the sensitivity and background count rate were determined for a 3 in. (7.5 cm) by 3 in. (7.5 cm) NaI(Tl) well crystal with a 1 in. (2.5 cm) diameter by 2 in. (5.0 cm) deep well (crystal housing = 0.020 in. copper) (Bicron Corp. Newbury, OH) and a 2.5 in. (6.3 cm) thick lead shield (Bicron).

## RESULTS AND DISCUSSION

The CdTe detector was positioned within the RI detector in order to achieve maximum count rate response to solutions flowing through the RI detector. Optimum response was not attained by placing the CdTe detector against the flow cell through which the RI measurement is made because of the attenuation of  $\gamma$ -rays by the steel wall (5 mm thick) of the cell. The detector was therefore positioned against a heat exchanger coil on the inlet side of the flow cell (Figure 1). The heat exchanger coil consists of 12 turns of 0.10 mm (i.d.) steel tubing wound about a 1.5 cm diameter by 1.0 cm cylindrical spool. In this configuration, the face of the detector assembly is brought to one tubing wall thickness (approximately 0.30 mm) from the radioactive solution. From consideration of the source-detector geometry, it is calculated that the detector views 15  $\mu\text{L}$  of radioactive solution.

**Linearity.** The count rate linearity of the detector and associated electronics was assessed by counts of serial dilutions of a  $^{75}\text{Se}$  liquid source placed 1 cm from the mounted detector. A linear least-squares fit of source activity vs. count rate (between 100 and 140 keV) for count rates from 18 to 4000 counts/s resulted in a correlation coefficient of 0.9998.

**$\gamma$  Resolution.**  $\gamma$  photopeak resolutions from 60 keV to 279 keV were measured as the full width at half-maximum (fwhm) and full width at tenth-maximum (fwtm), expressed as a percentage of the  $\gamma$  photopeak energy (Table I). Figure 2 shows a spectrum obtained with a  $^{99\text{m}}\text{Tc}$  solution as it was pumped through the RI detector and with the CdTe detector positioned as in Figure 1. The photopeak energy resolution is sufficient to distinguish photopeaks from scattered radiation and from fluorescence X-rays originating from the lead collimator surrounding the detector. For most measurements

Table I.  $\gamma$ -Photopeak Resolution of the CdTe Detector

energy, keV	fwhm, <sup>a</sup> %	fwtm, <sup>a</sup> %
60	32	47
81	25	37
122	23	30
140	23	31
279	14	17

<sup>a</sup> Full width at half-maximum and full width at tenth-maximum, expressed as a percentage of the photopeak energy.

Table II. Background Count Rates of the CdTe Detector<sup>a</sup>

energy range, keV	counts/min <sup>b</sup>	uncertainty <sup>b</sup>
41-60	3.03	0.08
61-80	3.64	0.07
81-100	2.70	0.07
101-120	1.61	0.08
121-140	0.95	0.08
141-160	0.60	0.02
161-180	0.39	0.01
181-200	0.26	0.02
201-220	0.16	0.01
221-240	0.12	0.02
241-260	0.07	0.01
261-280	0.04	0.01
281-300	0.02	0.01

<sup>a</sup> 1.5 mm lead shielding along side housing of detector.

<sup>b</sup> Mean  $\pm$  one standard deviation, five determinations, 60 000 s counts.

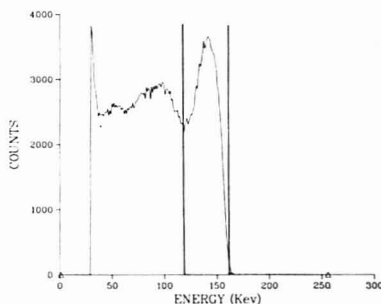


Figure 2. Energy spectrum of  $^{99\text{m}}\text{Tc}$  obtained with the CdTe detector. The photopeak is at 140 keV, while counts at 60-80 keV are from Compton scattering and lead fluorescence X-rays from the collimator. The large number of counts below 50 keV originate from preamplifier noise. Single channel analyzer settings between which counts are taken for chromatogram peak integration are shown as vertical bars.

of count rate, the single channel analyzer window was set at the fwtm energy limits of the photopeak of interest (Figure 2).

**Background.** Background count rates were determined for 10-keV energy increments (Table II). Because of the small volume of the CdTe detector, background count rates are quite low and extensive background shielding is not needed. This aids greatly in keeping the detector system compact. The small amount of shielding used (vide supra) is intended for collimation of the field of view of the detector rather than for reduction of background count rates.

**Detection Efficiency.** A point-source photopeak efficiency curve for the detector was determined by using  $^{241}\text{Am}$ ,  $^{133}\text{Ba}$ ,  $^{57}\text{Co}$ ,  $^{99\text{m}}\text{Tc}$ , and  $^{203}\text{Hg}$   $\gamma$ -rays in the 60-356 keV energy range.

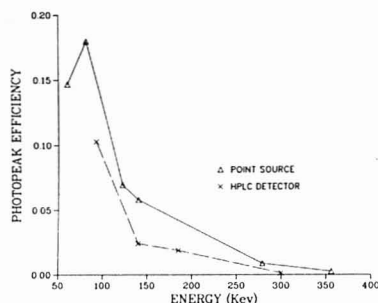


Figure 3. Point source efficiency curve (triangles) for the CdTe detector, normalized to a source-detector distance of 0.11 cm. The lower curve represents the counting efficiencies found for  $^{99m}\text{Tc}$  (140 keV) and  $^{67}\text{Ga}$  (93, 185, 300 keV) solutions passing through the heat exchanger coil with the CdTe detector positioned as in Figure 1.

Table III. Sensitivity of CdTe and NaI(Tl) Detectors for  $^{99m}\text{Tc}$ <sup>a</sup>

detector	absolute sensitivity <sup>b</sup>		rel quantitative sensitivity <sup>c</sup>	
	dpm	nCi	dpm	nCi
CdTe	$9.40 \times 10^2$	$4.30 \times 10^{-1}$	$1.60 \times 10^3$	$7.22 \times 10^1$
	$10^2$	$10^{-1}$	$10^3$	$10^1$
NaI(Tl)	$6.39 \times 10^1$	$2.88 \times 10^{-2}$	$4.83 \times 10^3$	$2.18 \times 10^0$
	$10^1$	$10^{-2}$	$10^3$	$10^0$

<sup>a</sup> Sensitivities were calculated with a calculated cell volume of 15  $\mu\text{L}$  and a measured peak width of 36 s at a flow rate of 0.51 mL/min. <sup>b</sup> Defined by Reeve and Crozier (6) as the amount of activity in the cell, over a period equal to the transit time, necessary to ensure a 95% probability of a 2:1 signal:noise ratio. <sup>c</sup> Defined by Reeve and Crozier (6) as the minimum activity which must be injected to obtain an average of 100 counts per transit period.

(Figure 3). Detection efficiency is at a maximum at 75-80 keV and becomes quite low at energies higher than about 250 keV. Detection efficiencies for calibrated solutions of  $^{99m}\text{Tc}$  and  $^{67}\text{Ga}$  citrate, pumped through the system with the CdTe detector positioned as in Figure 1, were determined and compared with the point-source efficiency. This comparison allows an assessment of the degree to which the detector efficiency in the actual case compares with the theoretical maximum represented by the point-source efficiency curve.

The steady-state flow detection efficiency for the 140-keV peak of  $^{99m}\text{Tc}$  was found to be  $2.41 \times 10^{-2}$  counts/ $\gamma$ , or 41% of the theoretical point-source efficiency. For  $^{67}\text{Ga}$   $\gamma$ -rays, flow detection efficiencies were found to be  $1.04 \times 10^{-1}$  counts/ $\gamma$  (93 keV),  $1.87 \times 10^{-2}$  counts/ $\gamma$  (185 keV), and  $1.25 \times 10^{-3}$  counts/ $\gamma$  (300 keV), all of which fall below the point-source curve (Figure 3). A closer approach to the point-source efficiency curve could certainly be achieved with an optimized flow cell design but was not attempted during the present work.

**Sensitivity.** The steady-state flow detection efficiency, background count rates, and transit times derived from replicate 20- $\mu\text{L}$  injections of  $^{99m}\text{Tc}$  sodium pertechnetate solutions into a pH 7.0 phosphate buffer stream at a flow rate of 0.50 mL/min were used to calculate absolute and quantitative detection limits for  $^{99m}\text{Tc}$  using equations derived by Reeve and Crozier (6) (Table III). A comparison was also made with a NaI(Tl) well-type scintillation detector by determining background count rates and the detection efficiency for 20- $\mu\text{L}$  volumes of  $^{99m}\text{Tc}$  at the bottom of the well (Table III). Although the NaI(Tl) detector gives a higher overall sensitivity because of an optimized source-detector geometry, the sensitivity is lower than would be predicted solely by a consideration of counting efficiencies of the two systems. This is because of the approximately 10-fold higher background count rate of the NaI(Tl) detector compared to the CdTe detector. From Table III, the quantitative sensitivity of the CdTe detector under realistic conditions is about 100 nCi ( $2.22 \times 10^5$  dpm) of  $^{99m}\text{Tc}$ ; this appears to be more than adequate for HPLC separations of radiopharmaceuticals, where radioactive concentrations of greater than 1 mCi/mL ( $2.22 \times 10^9$  dpm/mL) are routinely used. A 10- $\mu\text{L}$  injection of a 1 mCi/mL solution of  $^{99m}\text{Tc}$  would give 10  $\mu\text{Ci}$  ( $2.22 \times 10^7$  dpm) or about 100 times the quantitative limit for  $^{99m}\text{Tc}$ .

Registry No. CdTe, 1306-25-8;  $^{99m}\text{Tc}$ , 14133-76-7.

#### LITERATURE CITED

- (1) Pinkerton, T. C.; Heineman, W. R.; Deutsch, E. *Anal. Chem.* **1980**, *52*, 1106-1110.
- (2) Zodda, J. P.; Heineman, W. R.; Gilbert, T. W.; Deutsch, E. *J. Chromatogr.* **1982**, *227*, 249-255.
- (3) Siffert, P. *Nucl. Instrum. Methods* **1978**, *150*, 22-35.
- (4) Entine, G. *IEEE Trans. Nucl. Sci.* **1979**, *552*-558.
- (5) Hahn, P. B.; Schleien, B. *Anal. Chem.* **1970**, *42*, 1608-1612.
- (6) Reeve, D. R.; Crozier, A. *J. Chromatogr.* **1977**, *137*, 271-282.

RECEIVED for review August 11, 1982. Accepted October 4, 1982. The identification of equipment by name of manufacturer does not imply endorsement by the U.S. Food and Drug Administration, nor does it imply that the equipment identified is necessarily the best available for that purpose.

## Carbon as a Sample Substrate in Secondary Ion Mass Spectrometry

Mark M. Ross and Richard J. Colton\*


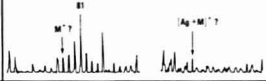
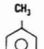
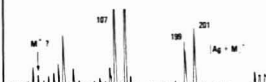
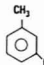

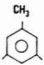

Chemistry Division, Naval Research Laboratory, Washington, D.C. 20375

Activated carbons or charcoals have long been used as adsorbents for airborne or aqueous pollutants (1, 2). In addition, carbonaceous particulate matter, or soot, produced by combustion of hydrocarbon fuels is known to contain a multitude of adsorbed compounds (3). Analysis of such adsorbed species on carbons usually involves first the extraction of the species by an appropriate solvent followed by chromatographic fractionation, and finally the separation and identification of

the components of the extract usually with a chromatographic/mass spectrometric technique. Although this analytical scheme often yields a large amount of information about the adsorbed compounds, the experimental procedure is quite tedious and time-consuming.

One objective of this research is to develop new analytical techniques for the direct and rapid identification of organic compounds adsorbed on carbon. Specifically, we plan to use

Table I. SIMS Results for the Substituted Benzenes

NAME/STRUCTURE	RELEVANT PHYSICAL CONSTANTS <sup>1</sup>	CONCENTRATION RANGE FOR DETECTION	SIMS RESULTS	
			SOLUTION/SILVER	ADSORBED ON CARBON/SILVER
 BENZENE	M.W. = 78.1 B.P. = 80.1 $\Delta H_v = 9.8$ V.P. = 104.2	—	—	
 TOLUENE	M.W. = 92.1 B.P. = 110.6 $\Delta H_v = 11.6$ V.P. = 31.5	NEAT LIQUID ONLY (SATURATED)	—	
 m XYLENE	M.W. = 106.2 B.P. = 138 $\Delta H_v = 16.2$ V.P. = 9.3	NEAT LIQUID 0.1 ml/g C	—	
 MESITYLENE	M.W. = 120.2 B.P. = 164.7 $\Delta H_v = 15$ V.P. = 2.8	NEAT LIQUID 0.1 ml/g C	—	

<sup>1</sup> M.W. = MOLECULAR WEIGHT IN GRAMS/MOLE

B.P. = BOILING POINT IN °C AT 760 Torr

 $\Delta H_v$  = HEAT OF ADSORPTION IN kcal/mole ON GRAPHITIZED CARBON BLACK

V.P. = VAPOR PRESSURE IN Torr AT 300°K AND 760 Torr

ion beam mass spectrometric methods, e.g., secondary ion mass spectrometry (SIMS) and thermal desorption gas chromatography/mass spectrometry (TD-GC/MS), to analyze the organic adsorbates. GC/MS techniques have been used previously to analyze volatile compounds on activated carbons used for water treatment (4) and to identify polycyclic aromatic compounds (PACs) found on carbon black (5). SIMS has been used recently to characterize certain organic compounds deposited onto graphite as a sample substrate (6). However, since such SIMS studies have been limited and, consequently, the fundamental mechanisms for ion emission of organics from carbon surfaces are not known, another objective of this research is to investigate the secondary ion formation and emission mechanisms of organic molecules on carbon.

Current SIMS analyses of organic compounds employ various sample preparation techniques such as depositing the organic on metal surfaces by solution deposition or burnishing (7, 8) and incorporating the organic into liquid or solid matrices, e.g., glycerol (9) and sodium or ammonium chloride (10). We report here the analysis of volatile and nonvolatile organic compounds adsorbed on an activated charcoal and the advantages of using a carbon sample matrix in SIMS as compared with organic SIMS results from metal surfaces.

### EXPERIMENTAL SECTION

The organic compounds studied are divided into two groups according to their volatility and molecular weight. The first group consists of the volatile compounds benzene, toluene, xylenes, and mesitylene. The second group consists of the PACs naphthalene, acenaphthylene, acenaphthene, fluorenone, phenanthrene, anthracene, fluoranthene, and pyrene. The carbon is an activated coconut charcoal of approximately 1000 m<sup>2</sup>/g surface area and is referred to as carbon throughout the text and as C in the tables. Before adsorbing the organic compounds the carbon is ground with a mortar and pestle.

The organic compounds are adsorbed on silver by depositing 1 or 2  $\mu$ L of a 10<sup>-3</sup> M solution of the organic in chloroform, or

of the neat organic liquid, onto a piece of acid (HNO<sub>3</sub>)-etched silver foil. The organics are adsorbed on the carbon by placing 50–200 mg of carbon into 1 mL of a solution of the organic compounds in chloroform. Once the solvent has evaporated (15–24 h), approximately 0.1 mg of the carbon is then burnished onto a piece of acid-etched silver foil. By variation of the concentration of the chloroform solution, the total quantity of the organic on carbon on silver is in the range of 10  $\mu$ g to 2 ng.

Secondary ion mass spectra are obtained with a double-focusing instrument which has been described in detail (11). The primary ion beam consisted of 4.4 keV Ar<sup>+</sup> ions with a current density in the range of (4 to 8)  $\times 10^{-8}$  A/cm<sup>2</sup>.

### RESULTS AND DISCUSSION

Results for the first group of compounds are presented in Table I. The adsorption energies reported are those measured for these compounds on graphitized carbon black (12). These compounds are normally difficult to analyze without cryogenically cooling the sample due to their volatility and the ultrahigh vacuum conditions (10<sup>-9</sup> torr) of the SIMS sample chamber. Consequently, no secondary ions characteristic of the organics are detected when silver alone served as the sample substrate. Adsorption of toluene, xylenes, and mesitylene on the carbon burnished on silver permitted detection of the [Ag + M]<sup>+</sup> ion from each of these compounds. Since toluene, but not benzene, is detected, the minimum adsorption energy necessary to permit detection is taken to be in the range of 10 to 11 kcal/mol. This energy is close to the desorption energy of 15 kcal/mol, reported by Hobson (13), below which a physically adsorbed gas is readily pumped from the wall of a high-vacuum chamber. Since the heats of adsorption of organic compounds on carbon are relatively high, the adsorbate is held in place long enough to be detected in a SIMS experiment. When the carbon matrix is saturated with toluene or mesitylene, the ion emission lasts for 1/2 to 1 h.

SIMS results obtained with the PACs are presented in Tables II and III. We found these compounds to be very difficult to analyze with SIMS (when directly deposited from

Table II. SIMS Results for PACs Naphthalene, Acenaphthylene, Acenaphthene, and 9-Fluorenone

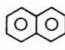
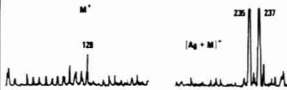

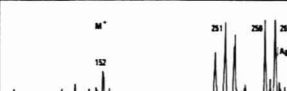

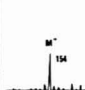
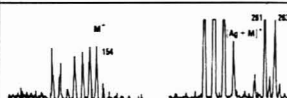
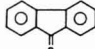
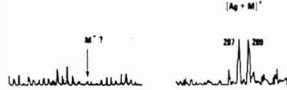
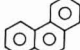
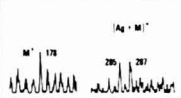
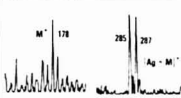
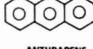
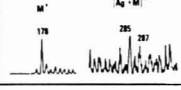
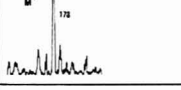
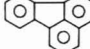
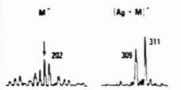


NAME/STRUCTURE	RELEVANT PHYSICAL CONSTANTS	CONCENTRATION RANGE FOR DETECTION	SIMS RESULTS	
			SOLUTION/SILVER	ADSORBED ON CARBON/SILVER
 NAPHTHALENE	M.W. = 128 B.P. = 218 V.P. = 0.29	1 mg/50 mg C (~2 µg)	—	
 ACENAPHTHYLENE	M.W. = 152 B.P. = 290	1 mg/50 mg C	—	
 ACENAPHTHENE	M.W. = 154 B.P. = 279 V.P. = $2.7 \times 10^{-2}$	SOLUTION/SILVER $M^+$ ONLY: ~1 µg ON CARBON/SILVER 1 mg/50 mg C		
 9-FLUORENONE	M.W. = 180 B.P. = 342	1 mg/50 mg C	—	

Table III. SIMS Results for PACs Phenanthrene, Anthracene, Fluoranthene, and Pyrene

NAME/STRUCTURE	RELEVANT PHYSICAL CONSTANTS	CONCENTRATION RANGE FOR DETECTION	SIMS RESULTS	
			SOLUTION/SILVER	ADSORBED ON CARBON/SILVER
 PHENANTHRENE	M.W. = 178 B.P. = 336 V.P. = $1.4 \times 10^{-3}$	SOLUTION/SILVER: $0.2 \mu\text{g} < [M] < 2 \mu\text{g}$ ON CARBON/SILVER: $M^+/[Ag+M]^+ > 10 \mu\text{g}$ $M^+$ ONLY: $< 1 \mu\text{g}$		
 ANTHRACENE	M.W. = 178 B.P. = 340 V.P. = $1.3 \times 10^{-3}$	SOLUTION/SILVER $\sim 0.2 \mu\text{g}$ ON CARBON/SILVER 1 mg/50 mg C		
 FLUORANTHENE	M.W. = 202 B.P. = 364 V.P. = $2 \times 10^{-4}$	1 mg/50 mg C	—	
 PYRENE	M.W. = 202 B.P. = 395	1 mg/50 mg C	—	

solution on silver) due to their nonpolar nature and low adsorption energies on metal surfaces. Ion emission from these compounds on silver proved to be unpredictable and irreproducible. When these organics are adsorbed on carbon, however,  $M^+$  and  $[Ag + M]^+$  molecular ions are readily and reproducibly detected for long periods of time. (For example,  $[Ag + M]^+$  ions are observed for over 1 h from a carbon charged with approximately 2 µg of an organic compound.) One possible explanation for this long-lived ion emission is that the high surface area and porosity of the carbon substrate, with sample molecules distributed throughout the three-di-

mensional structure, allow the primary ion beam to encounter fresh areas as layers of the carbon are sputtered away. Under these sputtering conditions, we have measured a detection limit of approximately 2 ng for phenanthrene on carbon.

In conclusion, the carbon matrix offers several distinct advantages for SIMS analyses of organic compounds. They are (1) the steady-state emission of molecular ions over a long period of time even while using dynamic ion beam conditions, (2) a detection limit of ~2 ng, (3) the analysis of nonvolatile nonpolar compounds such as the PACs, and (4) the analysis of some volatile compounds such as the substituted benzenes

without having to freeze the matrix. (The first three of the four advantages of carbon given above are also given by salt matrices in SIMS (7, 8, 14). A direct comparison between the carbon and salt matrices has not been made at this time.) These results show that (1) carbon can be used as a sample substrate for the SIMS analysis of organic compounds and (2) SIMS has potential as a rapid, simple, and direct analytical technique for the characterization of carbons with adsorbed compounds.

These preliminary results suggest, in addition, future SIMS analyses of real-world carbons for major adsorbed components. Already an industrial carbon has been successfully analyzed in our laboratory with the detection of the protonated molecular ion,  $[M + H]^+$ , arising from the impregnated amine. Other fundamental studies will include the analysis of different adsorbed compound types, such as PACs with heteroatoms and polar side groups.

#### ACKNOWLEDGMENT

The authors thank Jeff Wyatt and Joe Campana for many helpful discussions.

**Registry No.** C, 7440-44-0; benzene, 71-43-2; toluene, 108-88-3; *m*-xylene, 108-38-3; mesitylene, 108-67-8; naphthalene, 91-20-3; acenaphthylene, 208-96-8; acenaphthene, 83-32-9; 9-fluorenone, 486-25-9; phenanthrene, 85-01-8; anthracene, 120-12-7; fluoran-

thene, 206-44-0; pyrene, 129-00-0.

#### LITERATURE CITED

- (1) Deltz, V. R., Ed. "Removal of Trace Contaminants from the Air"; American Chemical Society: Washington, DC, 1975; ACS Symp. Ser. No. 17.
- (2) Rand, M. C.; Greenberg, A. E.; Taras, M. J., Eds. "Standard Methods for the Examination of Water and Wastewater", 14th ed.; American Public Health Association: Washington, DC, 1976.
- (3) Committee on the Biological Effects of Atmospheric Pollutants "Particulate Polycyclic Organic Matter", N.A.S.: Washington, DC 1972.
- (4) Alben, K. *Anal. Chem.* **1980**, *52*, 1821-1824.
- (5) Todd, R. G., *Diss. Abstr. Int. B* **1971**, *31*, 6671.
- (6) Unger, S. E.; Day, R. J.; Cooks, R. G., *Int. J. Mass Spectrom. Ion Phys.* **1981**, *39*, 231-255.
- (7) Day, R. J.; Unger, S. E.; Cooks, R. G. *Anal. Chem.* **1980**, *52*, 557A-572A.
- (8) Colton, R. J. *J. Vac. Sci. Technol.* **1981**, *18*, 737-747.
- (9) Barber, M.; Bordoli, R. S.; Elliott, G. J.; Sedgwick, R. D.; Tyler, A. N. *Anal. Chem.* **1982**, *54*, 645A-657A.
- (10) Lin, L. K.; Busch, K. L.; Cooks, R. G. *Anal. Chem.* **1981**, *53*, 109-113.
- (11) Colton, R. J.; Campana, J. E.; Bariak, T. M.; DeCorpo, J. J.; Wyatt, J. R., *Rev. Sci. Instrum.* **1980**, *51* (12), 1685-1689.
- (12) Kiselev, A. V.; Yashin, Y. I. "Gas-Adsorption Chromatography"; Plenum Press: New York, 1969.
- (13) Lewis, G. "Fundamentals of Vacuum Science and Technology"; McGraw-Hill: New York, 1965; p 43.
- (14) Grade, H.; Cooks, R. G. *J. Am. Chem. Soc.* **1978**, *100*, 5615-5621.

RECEIVED for review August 3, 1982. Accepted September 21, 1982.

## Statistical Evaluation of Calibration Curve Nonlinearity in Isotope Dilution Gas Chromatography/Mass Spectrometry

Jozef A. Jonckheere and Andre P. De Leenheer\*

Laboratorium voor Medische Biochemie en Klinische Analyse, Farmaceutisch Instituut, 9000 Gent, Belgium

Herman L. Steyaert

Seminarie voor Waarschijnlijkheidsrekening en Mathematische Statistiek, Rijksuniversiteit Gent, 9000 Gent, Belgium

During the past 2 decades isotope dilution mass spectrometry (IDMS) has gained a very particular place as an analytical tool. This stems mainly from the fact that an isotopically enriched analogue of the analyte is used as an internal standard. Since physicochemical properties of both analyte and internal standard are virtually identical, an optimal compensation is at work for losses of analyte in all analytical steps. As both products are simultaneously present in the mass spectrometer, specific determination of the analyte/internal standard mole ratio is possible by measuring the isotope ratio. Quantitation is performed by comparing the degree of perturbation of the isotopic composition of unknowns with the isotope ratios of mixtures with known concentrations of analyte and internal standard.

Although these principles are well documented (1), still some confusion is apparent in many IDMS calibration procedures. Specific problems arise from the presence of unlabeled material in the internal standard and the naturally occurring isotopes of the analyte. As Pickup and McPherson explained (1), the isotope ratio ( $R_m$ ) in a mixture of natural and labeled product can be expressed as

$$R_m = \frac{(x/E)p_i + (y/F)q_i}{(x/E)p_j + (y/F)q_j} \quad (1)$$

where  $x$  and  $y$  are the masses of analyte and labeled material and  $E$  and  $F$  their respective mean molecular masses. The

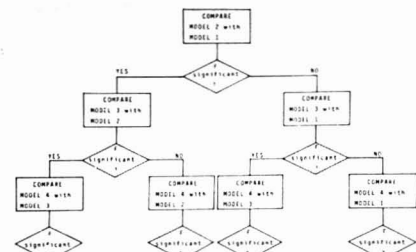
abundance of the main isotopic form of the analyte is represented by  $p_i$  whereas  $q_i$  stands for the abundance of the main isotopic form of the internal standard;  $p_j$  is then abundance of naturally occurring isotopes in the analyte and  $q_j$  the abundance of unlabeled material present in the internal standard.

Depending on the actual values of  $p_j$  and  $q_j$  in a given analytical situation, the mathematical relationship varies from linear ( $p_j$  negligible) to a nonlinear relationship (nonzero values for  $p_j$  or  $p_j$  and  $q_j$ ). The linear situation when  $p_j$  and  $q_j$  are negligible is, however, unrealistic in IDMS.

It is obvious that the use of linear least-squares procedures to describe the relationship between isotope ratios and mole ratios is only valid in the special case where  $p_j$  is negligible (i.e., highly labeled compounds). Assuming a linear relationship in all other cases will introduce gross errors. The use of inverse ratios or weighted linear regression (2) or log-log regression (3) only masks the effect of nonlinearity of calibration curves.

To circumvent these problems of nonlinearity, many authors proposed the use of the basic IDMS equation (eq 1), similar equations, or approximations of this formula, to obtain corrected isotope ratios to construct linear calibration curves (4, 5) and nonlinear curves (6) or to extrapolate the unknown concentration (7, 8).

Although these "theoretical" methods have been used widely, one should realize that the accuracy of the standard



**Figure 1.** Flow scheme for the model testing by means of an *F* test for significance.

curve is completely dependent on the validity of the proposed correction formula. Approximations by assuming the presence of only two isotopic forms (4, 7), or assuming equality of  $p_i$  and  $q_i$  (5, 6, 8) all increase the inaccuracy of the quantitation. Also the determination of the  $p_i$  and  $q_i$  values is of paramount importance to the accuracy of these standard curves. As these values are determined by measuring the isotope ratio or running a mass spectrum on pure analyte and "pure" labeled product and the  $p_i$  and  $q_i$  values are very small in comparison with  $p_1$  and  $q_1$ , the respective ratios  $p_i/p_1$  and  $q_i/q_1$  will be subjected to relatively large errors.

## EXPERIMENTAL SECTION

Instead of artificially transforming the data to a linear model, we tried to describe the relation between isotope ratios and mole ratios by means of polynomial regression, since the basic IDMS equation (eq 1), a rational function, can be seen as

$$R_m = a_0 + a_1(x/y) + a_2(x/y)^2 + \dots a_n(x/y)^n \quad (2)$$

the degree ( $n$ ) depending on the actual values of  $p_i$  and  $q_i$ .

For a given data set, we therefore calculate different polynomial functions starting from a first degree (linear equation) up to a fourth degree. The use of higher order polynomials is not advisable, to avoid oscillating of the curve through the measuring points. The residuals around the different models, i.e., the absolute differences between given mole ratios and the values calculated by the polynomial, are then used for a statistical evaluation for goodness of fit. This is done by testing the difference between the residuals of two consecutive models against the residuals of the highest degree model by means of an  $F$  test for significance ( $p = 0.95$ ). The flow scheme of the model testing is given in Figure 1. Each model is tested against a higher order model and the best one is then tested again with the following higher order model. This test indicates that, if the lower order model is true, there is only 5% chance to choose the wrong model. Also the use of weighted regression has been included to compensate for the nonconstant variance of the analytical data points.

The calculation procedure, as described, was tested by applying it to synthetic data generated with eq 1, for the analytical situation of a previous IDMS study carried out in our laboratory (9). In this assay Bromhexine, a mucolytic drug ( $C_{14}H_{20}N_2Br_2$ ) was quantitated with its trideuterated analogue of the following isotopic purity:  $d_0$ , 0.80%;  $d_1$ , 3.69%;  $d_2$ , 3.84%;  $d_3$ , 91.67%. The test has not been developed for the fragment ions used in this study since differences in fragmentation efficiency due to isotope effects make the theoretical development more difficult. By means of a computer-program based on the probability theory of Pickup and McPherson (1), the different parameters of eq 1 were calculated for the molecular ions. These values were entered in eq 1 to obtain the isotope ratios covering the range 1.67–53.6 ng of Bromhexine/53.6 ng of labeled analogue. The data points obtained were then used in the regression analysis program, to give the four polynomials and the subsequent model test. The function thus produced was further used to recalculate the mole ratios which are listed against the theoretical data points (Table I). It is seen that the model appropriately described the curvature of the calibration curve.

Table I. Calculation of Polynomial Regression Lines and Model Testing

no.	$X$	$R_m$	std dev
1	16.75	0.0631	0.0
2	33.50	0.0961	0.0
3	67.00	0.1616	0.0
4	134.00	0.2905	0.0
5	268.00	0.5404	0.0
6	536.00	1.0110	0.0

$$R_m = 3.928 \times 10^{-2} + (1.826 \times 10^{-3})x \quad r = 0.99978$$

$$S = 2.943 \times 10^{-4}$$

$$S_r = 7.357 \times 10^{-5}$$

$$R_m = 3.011 \times 10^{-2} + (1.979 \times 10^{-3})x - (2.780 \times 10^{-7})x^2$$

$$S = 5.450 \times 10^{-5}$$

$$S = 1.817 \times 10^{-8}$$

$$R_m = 2.992 \times 10^{-2} + (1.985 \times 10^{-3})x - (3.123 \times 10^{-7})x^2 + (4.332 \times 10^{-11})x^3$$

$$S_r^2 = 3.676 \times 10^{-11}$$

$$S = 1.838 \times 10^{-11}$$

$$R_m = 2.991 \times 10^{-2} + (1.986 \times 10^{-3})x - (3.181 \times 10^{-7})x^2 + (6.476 \times 10^{-11})x^3 - (2.290 \times 10^{-14})x^4$$

$$S_r^2 = 3.854 \times 10^{-12}$$

$$S = 3.854 \times 10^{-12}$$

$F$  test of 1 and 2 order  
 $p = 1.00000$  significant  
 $F$  test of 2 and 3 order  
 $p = 0.99966$  significant  
 $F$  test of 3 and 4 order  
 $p = 0.79011$  nonsignificant

$R_m$ given	Third Order $x$ calcd	std dev
0.063 08	16.748 29	0.0028
0.096 08	33.501 48	0.0025
0.161 55	67.001 41	0.0026
0.290 45	133.998 45	0.0029
0.540 40	268.000 41	0.0033
1.011 00	535.988 12	0.0036

Given the evidence on a theoretical example, the program has been applied to the experimental data of another published IDMS study (4). It should be mentioned that in this study no replicate measurements were given, so that a nonweighted regression analysis had to be performed. As is evident however from statistical literature (10), the accuracy of the calibration curve is almost invariably increased when weighting factors are incorporated, taking into account the experimentally determined variances at each measurement point. The given isotope ratios were reentered in the chosen model and, for the purpose of comparison, also in the linear equation. The difference between the calculated mole ratios and the given mole ratios is graphically represented for both the higher order equation and the linear equation (Figure 2). Clearly the higher order equation was statistically more appropriate to describe the IDMS calibration curve. Also the correlation coefficient has been calculated and indicated. As has been stressed recently (11), the use of this correlation coefficient, as a means of evaluating goodness of fit of linear regression, should clearly be discouraged. Its statistical significance indicates only that there exists "a" relationship between  $x$  and  $y$  values, without evaluating linearity. This is clearly seen in Figure 2 where despite a very high correlation coefficient the higher order model is more appropriate as proved by the  $F$  test for significance.

## RESULTS AND DISCUSSION

This study proves that the eventual curvature of IDMS calibration curves can be described very accurately by means of higher order polynomials. The ability to check different models allows one to adapt the same calculation procedure regardless the actual analytical situation, i.e., regardless the degree of labeling of the internal standard of the interference from naturally occurring isotopes of the analyte. This is especially important in those cases were, due to low efficiency of the synthesis, a large amount of unlabeled, or incompletely



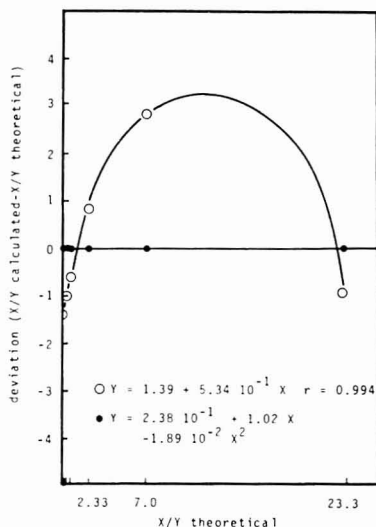


Figure 2. Difference between calculated and given mole ratios for a linear and polynomial regression line, constructed from the data in ref 4, describing an IDMS assay for  $\gamma$ -aminobutyric acid (GABA) with  $[2,2\text{-}^2\text{H}_2]\text{GABA}$  as internal standard.

labeled, product is present. Also the setup of analyses with internal standards with low mass increment is facilitated.

In contrast with the calibration methods based on expressions or approximations of the basic IDMS equation, no initial estimates of the amount of unlabeled product and/or influence of naturally occurring isotopes are necessary. Regardless the validity of the "theoretical" model used, this step greatly reduces the accuracy of such calibration procedures, because of the experimental error involved in determining these small abundances. Also, proper statistical handling of

the data is not always possible due to transformation of the experimental data.

Our proposed method is even more valuable in cases where some chromatographic separation of analyte and internal standard (using highly labeled compounds or high resolution capillary columns) occurs. This effect destroys the validity of the basic IDMS equation and subsequent calculation procedures based on this formula. Indeed the ion overlap is only partial, and no estimation of the interferences can be obtained by measuring pure product and/or internal standard separately.

It is obvious that the presented polynomial regression analysis with model-testing requires a reasonable computational facility (12). Modern mass spectrometers, however, all incorporate powerful computer systems which can handle this problem very easily.

The above summarized regression analysis by multiple polynomials is worked out in a computer program, RAMP, which is available on request in FORTRAN IV or HPL-BASIC.

## LITERATURE CITED

- (1) Pickup, J. F.; McPherson, K. *Anal. Chem.* **1976**, *48*, 1885.
- (2) Schoeller, D. A. *Biomed. Mass Spectrom.* **1976**, *3*, 265.
- (3) Van Langenhove, A.; Costello, C. E.; Biller, J. E.; Biemann, K.; Browne, T. R. *Clin. Chim. Acta* **1981**, *115*, 263.
- (4) Colby, B. N.; McCaman, M. W. *Biomed. Mass Spectrom.* **1979**, *6*, 225.
- (5) Bush, E. D.; Trager, W. F. *Biomed. Mass Spectrom.* **1981**, *8*, 211.
- (6) Min, B. H.; Garland, W. A.; Khoo, K. C.; Torres, G. S. *Biomed. Mass Spectrom.* **1978**, *5*, 692.
- (7) Gamber, P.; Lallemand, C.; Archambault, A.; Maume, B. F.; Padieu, P. *J. Chromatogr.* **1979**, *1*, 162.
- (8) Siekmann, L. "Quantitative Mass Spectrometry in Life Sciences II"; De Leenheer, A.; Roncucci, R.; Van Peteghem, C., Eds.; Elsevier: Amsterdam, 1978; p 3.
- (9) Jonckheere, J. A.; Thienpont, L. M. R.; De Leenheer, A. P. *Biomed. Mass Spectrom.* **1980**, *7*, 582.
- (10) Schwarz, L. M. *Anal. Chem.* **1979**, *51*, 6.
- (11) VanArendonk, M. D.; Skogerboe, R. K.; Grant, C. L. *Anal. Chem.* **1981**, *53*, 2349.
- (12) Mendenhall, W. "The Design and Analysis of Experiments"; Wadsworth: Belmont, 1968; Chapter 7.

RECEIVED for review April 12, 1982. Resubmitted August 16, 1982. September 24, 1982. This work was supported through a N.F.S.R. grant to J.J. and a research contract from F.G.W.O. (No. 3.0011.81).

## Desorption of Radon from Activated Carbon into a Liquid Scintillator

Howard M. Prichard\* and Koenraad Mariën

The University of Texas School of Public Health, P.O. Box 20186, Houston, Texas 77025

Activated carbon has long been noted for its ability to adsorb radon from the surrounding air and has often been exploited in measurement techniques requiring radon concentration. Radon entrained on the carbon can be measured directly by  $\gamma$  spectrometry or can be removed from heated carbon for counting in an  $\alpha$  scintillation cell. The latter approach (1) is far more sensitive than  $\gamma$  counting but does involve a considerable amount of sample manipulation. As part of an effort to develop a passive integrating radon sampler based on activated carbon adsorption, we sought a counting method that would have a level of sensitivity approaching that of the  $\alpha$  scintillation cell while involving minimal sample treatment. If radon could be reproducibly removed from activated carbon by simple desorption in a solvent such as toluene, then liquid scintillation counting would be a promising

analytical method for large-scale applications such as personal dosimetry in uranium mines. Other potential applications include the analysis of activated carbon radon flux detectors or radon entrained on low temperature activated carbon traps. From theoretical considerations, it is reasonable to expect that the general approach might be applicable to the analysis of other radioactive noble gases, such as  $^{133}\text{Xe}$  and  $^{85}\text{Kr}$ .

## EXPERIMENTAL SECTION

Initial desorption experiments were performed with sufficiently high radon concentrations to permit analysis by conventional  $\gamma$  spectrometry. Ten-gram lots of a large grained, low density activated carbon (Nuchar WVL 8X30 Mesh) were rinsed in methyl alcohol to remove fines and then dried at 110 °C for 24 h. The prepared carbon was exposed to radon gas, sealed in 22-mL glass liquid scintillation vials, and held for at least 3 h to allow for

Table I. Observed and Expected Radon Counts following Toluene Desorption

sample	obsd	expected	O/E
1	3970 ± 70 <sup>a</sup>	4040 ± 50	0.98 ± 0.02
2	3820 ± 60	4500 ± 50	0.85 ± 0.02
3	3570 ± 60	3410 ± 50	1.05 ± 0.02
4	2830 ± 60	2900 ± 40	0.98 ± 0.02
5	2980 ± 60	3190 ± 40	0.94 ± 0.02
6	2060 ± 50	1940 ± 30	1.07 ± 0.03
7	1620 ± 40	1650 ± 30	0.99 ± 0.03
8	2040 ± 50	2030 ± 30	1.00 ± 0.03

<sup>a</sup> One standard deviation.

daughter ingrowth. Each vial was then placed in a styrofoam jig and the 0.295-MeV and 0.352-MeV  $\gamma$  lines of  $^{214}\text{Pb}$  were counted with a Ge(Li) detector and a 4096 channel analyzer. The carbon was then transferred to an 80-mL separatory funnel connected to a 60-mL flask containing a known volume of reagent grade toluene. When the stopcock was opened, the toluene flowed down onto the carbon, producing an exothermic outgassing reaction. The evolved gas passed upward through the toluene, affording an opportunity for any radon in the gas to be transferred to the liquid (2). After a few seconds of gentle shaking the toluene passed entirely into the funnel and the stopcock was closed. The gas in the flask was sampled with a syringe to verify that a negligible fraction of radon had escaped to the flask. Subsequent analysis with an  $\alpha$  scintillation cell showed that this fraction was less than 0.5%. After a wait of at least 2 h for desorption, the funnel was shaken and inverted, a syringe attached below the stopcock, and the free liquid portion removed. The toluene was transferred to a 22-mL glass liquid scintillation vial for  $\gamma$  counting after a 3-h delay for the ingrowth of radon daughters. Care was taken to repeat the counting geometry used with the original carbon sample, and the resulting net counts at 0.295 and 0.352 MeV were decay corrected to the counting time of the sample before desorption. (If the toluene is to be counted by liquid scintillation, 1 or 2 mL of concentrated fluor solution must be added to the vial.)

The repeatability of the desorption procedure was tested under relaxed conditions to test the degree of care actually required for effective counting. Two gram samples of carbon were placed in glass scintillation vials sealed with thick rubber septa into which glass diffusion tubes (3) 1 cm long with an internal diameter of 0.265 cm had been placed. Sets of three or four such vials were capped and placed in an atmosphere of 50–200 pCi/L of radon-222. The vials were simultaneously uncapped, exposed for a predetermined number of hours, and then simultaneously capped. It was assumed that the sampling rate of the diffusion tubes had been selected so that after an exposure of 24 h, the "volume" of air sampled diffusively would be much less than the effective capacity of the carbon. At a convenient later time, the vials were uncapped, the stoppers removed, and 20 mL of toluene liquid scintillator was smoothly poured into the vial. The vials were quickly capped, held for 6 h or more for chemical and radiological equilibrium, and then counted with a commercial liquid scintillation counter. The observed variability within batches represents the combined effects of variations in adsorption, desorption, handling loss, and counting error.

## RESULTS AND DISCUSSION

The outcomes of eight desorptions of 10-g carbon samples are shown in Table I. The expected counts were computed on the assumption of total desorption of radon from the carbon to the toluene, followed by the establishment of full solution equilibrium between the air and toluene in the closed vessel. The expected count rate is

$$C' = \frac{CLV'}{LV + V_a} \quad (1)$$

Where  $C$  is the count rate before desorption,  $C'$  is the count rate in the recovered toluene fraction,  $V$  is the volume of the toluene injected,  $V'$  is the volume of the recovered toluene fraction, and  $V_a$  is the residual air volume in the vessel. The

Table II. Desorption of Radon from 2-g Carbon Samples

<i>n</i>	mean (cpm) <sup>a</sup>	std dev	coefficient of variation
4	444	13	2.97
3	498	4	0.72
3	217	12	5.54
3	532	18	3.33
3	515	27	5.18
3	391	6	1.64
3	281	3	1.14
4	158	8	5.32

<sup>a</sup> Standard deviations due to counting errors alone are <2 cpm.

Table III. Backgrounds, Counting Efficiencies, and Lower Limits of Detection for Several Counting Windows

window	background, cpm	efficiency, cpm/pCi	MDTA, <sup>a</sup> pCi
open	58.4	10.60	0.365
$^{32}\text{P}$ preset	19.2	8.73	0.254
$^3\text{H}/^{32}\text{P}$ preset	15.6	8.72	0.229
$^{14}\text{C}/^{32}\text{P}$ preset	12.4	7.06	0.252
optimum	12.9	8.52	0.213

<sup>a</sup> For a 60 min count with the combined probability of type I and type II errors = 0.05.

constant " $L$ " is the coefficient for the partition of radon between equal volumes of air and toluene (4). With  $L = 13$  and  $V_a = 50$  mL, the expected count rate reduces to

$$C' = CV'/(V + 3.8) \quad (2)$$

where  $V$  and  $V'$  are in milliliters. The actual  $\gamma$  counts observed in the recovered toluene fractions are consistent with this simple model. The average ratio of observed to expected counts is seen to be  $0.984 \pm 0.065$  for the eight runs in Table I. If the low value in entry 2 can be ascribed to experimental error, this becomes  $0.999 \pm 0.044$ .

Table II shows the results of the tests made under less restricted conditions. Counting was performed with 2 g of carbon residing on the bottom of the vial. It is seen that if there are losses of radon before the vial is capped and losses of pulses due to the presence of the carbon, they are at least consistent.

## SENSITIVITY

Once radon is dissolved in a liquid scintillator, the  $\alpha$  and  $\beta$  emissions of the radon series can be counted with almost complete efficiency. For every picocurie of radon-222 present, three  $\alpha$  and two hard  $\beta$  are emitted at equilibrium, providing an expected count rate of 11.1 counts  $\text{min}^{-1}$  pCi $^{-1}$ . Some counts are missed due to energy losses in the vial walls and actual count rates of 10.5 to 10.6 counts  $\text{min}^{-1}$  pCi $^{-1}$  are observed in an open counting window. As the upper and lower discriminators are varied to narrow the window, both the background count rate and the counting efficiency are reduced. An optimum setting is one that minimizes the lower limit of detection, here taken to be the minimum detectable true activity (MDTA) as defined by Altschuler and Pasternack (5). Table III shows background count rates, counting efficiencies, and MDTA's for a number of window settings on a commercial liquid scintillation counter. It is to be noted that the preset window for  $^{32}\text{P}$  in the presence of  $^3\text{H}$  produced an MDTA nearly as low as the experimentally determined optimum window. Backgrounds and counting efficiencies will vary somewhat from machine to machine, and the efficiencies of the preset windows will vary somewhat with the degree of quench in the scintillation solution.

Registry No. Carbon, 7440-44-0; radon, 10043-92-2; toluene, 108-88-3.

# LITERATURE CITED

- (1) Lucas, H. F. *Rev. Sci. Instrum.* **1957**, *28*, 60.
- (2) Pritchard, H. M. *Health Phys.*, in press.
- (3) Palmes, E. D.; Gunnison, A. F. *Am. Ind. Hyg. Assoc. J.* **1973**, *34*, 78.

- (4) Weigel, F. *Chem.-Ztg.* **1978**, *102*, 287-299.
- (5) Altshuler, B.; Pasternack, B. *Health Phys.* **1963**, *9*, 293.

RECEIVED for review July 30, 1982. Accepted September 29, 1982. This work was supported in part by Grant No. ES01742-02 from the National Institute of Environmental Health Sciences.

## Screening Method for Aroclor 1254 in Whole Blood

Shane S. Que Hee,\* Jerry A. Ward, M. Wilson Tabor, and Raymond R. Suskind

The Kettering Laboratory, University of Cincinnati Medical Center, 3223 Eden Avenue, Cincinnati, Ohio 45267

Polychlorinated biphenyls (PCBs) have been utilized as nonflammable and heat resistant oils in such articles as electrical transformers, condensers, and paint since 1930 (1). They are ubiquitous in the biosphere (2, 3). They have achieved some notoriety in the "Yusho" episode in Japan in 1968 (3) and more recently in Taiwan in 1979 (4, 5). As of November 1, 1979, use of PCBs in new heat transfer systems in U.S. factories manufacturing or processing food, drugs, and cosmetics was no longer authorized. Use in electromagnets, transformers, and heat transfer and hydraulic systems is permitted until July 1, 1984 (6). Defective fluorescent light ballasts also emit PCBs contributing to office air pollution (7). Thus, occupational and environmental exposures to PCBs will still occur into the future, and determination of PCBs in workers' blood (8, 9) will continue to be a valuable measure of PCB exposure.

The methods for separation and quantification of polychlorinated biphenyls in serum or whole blood usually involve alkaline hydrolysis, hexane extraction, and silica gel column chromatography of the concentrate of the hexane extraction (4, 9, 10). These methods are generally time-consuming and tedious: the extractions are usually multiple; the many concentrative steps may lead to losses by volatilization and adsorption; any impurities in the solvents also are concentrated, limiting sensitivity or confounding GC/MS identification. In addition, incomplete documentation of the gel type may lead to irreproducible separations from investigator to investigator.

There is a need for a semiquantitative quick-screening method to estimate PCBs in blood or serum. Such a method would be valuable to assess if further chromatography is necessary for quantification or GC/MS analysis. Aroclor 1254 was the PCB chosen for this study since it is probably the most ubiquitous PCB (9).

## EXPERIMENTAL SECTION

**Optimized Procedure.** All glassware including syringes and tubes to be utilized in collecting blood was soaked in chromic acid overnight and rinsed (five times) in order: Type I distilled water as defined by the U.S. EPA (11), acetone (Fisher Pesticide Grade A-40), Type I distilled water, hexane (Fisher Pesticide Grade H-300).

Blood was drawn through a polyethylene butterfly valve. The first 70 mL was discarded to minimize contamination in the event of later GC/MS. Blood (approximately 10 mL) was collected in prewashed 50-mL Kimax 14-930 10A tubes fitted with Teflon-lined screw caps and containing 200 USP units of heparin in 0.2 mL of aqueous isotonic saline. The heparin-containing tubes were shaken gently as the blood was collected to prevent clotting.

The samples were then placed in a polystyrene refrigerated box (4-5 °C) in which the samples were transported to the laboratory, where they were stored at 4-5 °C until analysis.

Each blood sample was allowed to equilibrate to room temperature. The total weight was then recorded. A known weight

(ca. 5.0 ± 0.1 g) of potassium hydroxide pellets (Fisher P-250) was added. Absolute ethanol (2.5 mL) was added by a premixed pipet. The caps were screwed on tightly and the tubes shaken until all the potassium hydroxide was dissolved. The solution will become hot but should not foam. The solution was digested at 90 °C for 1 h in a water bath. With the capless tubes still in the bath, the ethanol was evaporated by blowing nitrogen over the surface of the solution for 10 min using a Pasteur pipet connected by Teflon tubing to a cylinder of compressed nitrogen.

The solution was removed from the bath and allowed to cool. Pesticide Grade hexane (10 mL) was added (pipet), the caps were screwed on tightly, and the tubes were vigorously shaken for at least 15 separate shakes. The layers were allowed to separate for at least 10 min, or until no opacity was evident. An aliquot (10 µL) was then injected into the gas chromatograph to complete the screening phase.

The column used for gas chromatographic analyses was a 1.87 m × 6 mm o.d. × 2 mm i.d. Pyrex column packed with 3% OV-101 on 100/120 mesh Chromosorb W-HP. A <sup>63</sup>Ni electron capture (EC) detector was utilized in a Hewlett-Packard 5730-A gas chromatograph. The temperatures were 250 °C (injector), 203 °C (column), and 250 °C (detector). The flow of 95% argon/methane was 25.0 ± 1.5 mL/min. After 16 min the column temperature was raised to 250 °C for 30 min to allow elution of other blood compounds.

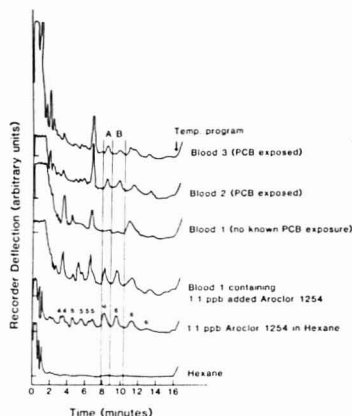
A Hewlett-Packard Reporting Integrator (HP-3390A) was utilized to visualize and quantitate the peak areas.

Preliminary examination of many blood samples revealed that the Aroclor 1254 pattern at low concentrations (<1 ppb) was not discernible (Figure 1) but was at higher concentrations. Even at the low concentration two peaks of the Aroclor 1254 formulation could be consistently utilized for quantification purposes without resorting to column chromatographic cleanup. These are depicted as peaks A and B in Figure 1. All other peaks were interfered with consistently by compounds in the blood, some more so than others.

Hexane PCB standards were utilized to obtain the injected mass of Aroclor 1254. A standard concentrate was prepared by direct weighing of the PCB and then quantitative transfer of the Aroclor 1254 with warm (35 °C) hexane to a volumetric flask to minimize adsorptive losses. Differential dilution with hexane was then utilized to obtain the desired standard concentrations. Separate calibration curves were then obtained for the peaks marked A and B in Figure 1.

The response of the EC/GC was linear up to 10 ng of injected PCB. The limit of sensitivity was approximately 2 pg of Aroclor 1254 per injection.

The PCB levels were deemed trustworthy when the parts per billion (ng of PCB/g of blood) content based on the two independent estimations from the two peaks A and B agreed closely (± 10% relative). The levels found by this procedure are maximal because it is assumed that only PCB is being quantitated. However, if the PCB level is below high levels, e.g., 5 ppb, then further analysis is unnecessary. The appearance of the chromatogram and the disagreement of PCB content as calculated separately from peaks A and B, would indicate that further



**Figure 1.** Electron capture gas chromatograms of blood samples from people exposed to Aroclor 1254 (blood samples 2 and 3) and to no known exposure (blood sample 1). The chromatogram of blood sample 1 containing 1.1 ppb Aroclor 1254 is compared with 1.1 ppb Aroclor 1254 in hexane (the numbers denote the number of chlorines) and hexane alone.

cleanup is necessary if the levels are high, e.g., 100 ppb, to obtain better precision.

It is recommended that each day of analysis begin with the following quality control procedure in this order:

Hexane alone (base line must be steady and no peaks in the areas of interest observed before proceeding), then Aroclor 1254 in hexane (10.0 ppb), then hexane extract of a hydrolyzed reference blood bank sample (10 g), and then a hexane extract of 10 g of a hydrolyzed reference blood bank sample spiked with 100 ng of Aroclor PCB. The reference blood utilized in this study contained citrate phosphate anticoagulant and was comprised of 450 mL of blood and 63 mL of USP water containing 1.66 g of trisodium citrate, 0.206 g of citric acid, 0.140 g of monobasic sodium phosphate, 2.01 g of dextrose, and 0.017 g of adenine. Its shelf life was 35 days at 4 °C.

Two separate syringes should be utilized: one for samples, another for standards. If one syringe alone was used, memory effects from concentrated PCB standards caused problems. Such effects for standards were negated by copious rinsing of the syringe until injections elicited no Aroclor 1254 pattern. Syringes should be always washed in the order, hexane, acetone, and hexane. Ten-microliter injections should always be performed.

Further cleanup may be necessary if disagreement of the levels of Aroclor 1254 calculated from the two designated peaks A and B occurs or if Aroclors of less chlorine content than Aroclor 1254 are present in low concentrations. In this case, the upper layer should be drawn off quantitatively into a measuring cylinder with a Pasteur pipet. The volumes recovered by this technique should be 9.7–9.8 mL. The volume was then noted. This hexane extract (note the volume) was then transferred to a thimble flask for rotary vacuum evaporation. The extract container was washed with hexane (1 mL  $\times$  3) after transfer of the total extract, the washings were placed also in the thimble flask, and the amalgamate was evaporated to about 1 mL.

For column chromatography, the silica gel (Davison Chemical, 100/200 mesh, Grade 923) was cleaned by Soxhlet extraction for 12 h in hexane and dried for 12 h at 200 °C. After the gel was cooled, it was kept in a screw-capped bottle. Silica gel (4.5 g) was poured slowly into 25 mL of hexane contained in a Pyrex chromatographic column (2.35 cm i.d.  $\times$  45 cm) equipped with Teflon stopcocks and a coarse glass sinter. A layer of glass wool was placed over the sinter. When packed, the silica gel was topped with a 6 mm layer of Ottawa sand, previously washed with hexane. After 140 mL of hexane was collected, the hexane layer was allowed to approach the top of the Ottawa sand layer. A collecting

beaker was placed under the spout. The 1 mL concentrate was transferred to the column by Pasteur pipet and the level of hexane dropped to allow the top of the Ottawa sand to be exposed. The container and the pipet were washed three times with small aliquots (0.5 mL) of hexane and placed on the column in the same manner as above. Hexane was then poured in gently. The first 140 mL was retained to collect all the peaks of the Aroclor. The eluate and the hexane blank were each concentrated to ca. 1 mL by rotary evaporation in a thimble round-bottom flask and the concentrates each transferred with a Pasteur pipet to individual volumetric 10-mL flasks. The thimble flask and the pipet were washed with hexane, and the washes were added to the flasks. The contents were shaken prior to analysis. Ten-microliter aliquots were then injected into the gas chromatograph.

**Method Validation.** a. *Recoveries of Aroclor 1254 for the Optimized Method.* Reference blood samples (10 g) were spiked in triplicate with 10  $\mu$ g, 1  $\mu$ g, 100 ng, 10 ng, and 0 ng of Aroclor 1254 concentrate contained in  $50 \pm 1$   $\mu$ L of hexane. A stream of nitrogen was directed to the top of the samples to evaporate the small amount of added hexane. The samples were hydrolyzed and analyzed by EC/GC in the manner given for the optimized method. The recoveries were computed based on peak areas expected for complete recovery (injected mass of PCB in same final volume of hexane), corrected for any peaks present in the blanks.

b. *Determination of Critical Collection Volume for Silica-Gel Cleanup.* Aroclor 1254 (100  $\mu$ g) in hexane was diluted to 1 mL with hexane. The procedure reported in the column chromatographic cleanup step above was then applied. EC/GC analysis of successive 10-mL amounts of eluates allowed the elution profile to be found. The procedure was also repeated with the 1 mL concentrate of 9.80 mL of hexane extract from 10 g of blood bank blood spiked with 100  $\mu$ g of Aroclor 1254, which had been hydrolyzed, extracted, and analyzed by the optimized procedure. After 140 mL of eluate had been collected, the column was eluted with dichloromethane (20 mL). The 140 mL of eluate was concentrated to 10 mL. The methylene dichloride was evaporated just to dryness by a stream of nitrogen. The residue was transferred by repetitive washings of hexane to a 10-mL volumetric flask. All concentrates were subjected to EC/GC.

c. *Determination of the Optimal Volumes of Hexane and Ethanol.* The procedure of Chen et al. (4) was taken as the starting point of the optimization. Thus, ethanol (20 mL) was utilized in the hydrolysis step, in addition to 5 g of potassium hydroxide in 10 g of blood bank blood spiked with 10  $\mu$ g of Aroclor 1254. Hexane (three 20-mL portions) was used to extract the Aroclor 1254. The extraction volumes utilized were 5, 10, and 15 mL. All extractions were done three times. Individual extracts were analyzed by EC/GC. The above procedure was repeated by using 0, 1.0, 2.0, 2.5, 3.0, 5.0, and 10 mL of ethanol. The procedures were also performed with and without the nitrogen evaporative step.

Some experiments consisted of adding the KOH first before the hydrolysis and then the ethanol.

d. *Effects of Heparin and Citrate Phosphate.* The optimized procedure was also applied to the original heparin and citrate phosphate anticoagulants at levels present in the actual blood samples.

e. *Miscellaneous:* The KOH dissolved in 10 mL of deionized distilled water was subjected to the optimized technique to assess the extent of any interferences. A representative blood sampling syringe was tested for contamination by rinsing it with 10 mL of deionized distilled water, transferring the water to the 50 mL tube, and subjecting the solution to the optimized analytical technique. The 50-mL tube was rinsed with 10 mL of hexane to assess the extent of any contamination. Deionized distilled water (10 mL) in the 50 mL tube was also analyzed. Hexane (60 and 140 mL) was concentrated to 10 mL to determine if any gas chromatographic peaks of the concentrate interfered with the analysis.

## RESULTS AND DISCUSSION

The recoveries of Aroclor 1254 from blood over the concentration range 1.09 to 1092 ppb using the optimized technique are presented in Table I. The average recovery in the range 1.09 to 109 ppb is  $(100 \pm 4)\%$ . At 1092 ppb, the average

Table 1. Recovery of Parts per Billion Quantities of Aroclor 1254 from Blood Utilizing the Two Chromatographic Peaks Designated in Figure 1<sup>a</sup>

concn in 10 g of blood <sup>b</sup> (ng of Aroclor 1254/g of blood)	extraction recovery, %
1092 ± 15	79.3 ± 1.8
109 ± 2	96.7 ± 5.5
10.9 ± 0.2	100.3 ± 5.8
1.09 ± 0.02	105 ± 14

<sup>a</sup> Data are in the form of arithmetic mean ± standard deviation. <sup>b</sup> Triplicate sample. <sup>c</sup> Number of estimates was six.

recovery is lower but is still usable since recovery is around 80% and is still precise. The reason for the lower recovery is unknown. The relative standard deviation (RSD) at 1.09 ppb is approximately 13% compared with 6% at 10.9 and 109 ppb. The larger relative error is to be expected as the detection limit is approached (ca. 0.2 ppb for a 10-g blood sample). The recoveries of PCB were also not affected by the presence of heparin and citric phosphate used at anticoagulant levels. The anticoagulants, water, KOH, syringes, and glassware were negligible sources of EC/GC interferences. All glassware must be cleaned in chromic acid to avoid contamination.

If further cleanup is necessary by column chromatography, the recovery of Aroclor 1254 is also quantitative. Mass balance was achieved and no PCB was eluted in the final worked-up methylene dichloride eluate. However, contrary to Chen et al. (4), the first 20 mL cannot be discarded since this resulted in a loss of (31 ± 2)% of Aroclor 1254. Thus, if further column chromatographic cleanup is necessary, the first 140 mL of the eluent should be retained. If an unknown Aroclor can be identified from the screening step, it is advisable to ascertain what volume will be necessary to collect it quantitatively from the column as set forth in Method Validation b.

Preliminary work revealed that the washing and drying steps for the hexane extract in Chen et al. (4) and in the NIOSH method (10) were unnecessary if the extract showed no opacity. In general, extracts were clear in 10–15 min after extraction by the optimized method.

As the starting point of the optimization, a modified Chen et al. (4) method was attempted (3 × 20 mL hexane extracts; 20 mL of ethanol in the hydrolysis; no evaporation of ethanol; no drying agent added; no washes). Three extracts were necessary to recover 20% of 1.09 ppm of spiked Aroclor 1254 in 10 g of blood. The first, second, and third extracts removed 46%, 42%, and 12% of the recovered 20%, respectively. When the extracting volume was varied, no significant differences in extraction efficiencies for 15-mL and 10-mL volumes were found for the first extraction (pooled mean was (46 ± 4)% of the 20% Aroclor recovered or for the first two extracts combined (pooled mean was (86 ± 7)%). However, at an extracting volume of 5 mL, the first extract removed only 29% of the recovered Aroclor, the second 39%, and the third 17%, for an overall recovery for the three extracts of 85% relative to the 10- to 20-mL extractions. Thus, 10 mL of hexane was as efficient a volume as 20 mL, but 5 mL was not.

When 60 mL of the amalgamated extracts was concentrated to 10 mL, recoveries appeared to be greater than expected. Solvent peaks in the Aroclor region were found when 60 mL of hexane alone was concentrated. These increased when 140 mL of hexane (the volume collected from column chromatography) was similarly concentrated. These peaks were not evident in unconcentrated solvent. Thus, either the hexane

should be cleaned up or no or few concentrative steps should be allowed in the procedure. Many different brand name hexanes were evaluated for their suitability in the course of this investigation. Distillation improved but often did not totally remove the peaks from the regions of interest after concentration. All unconcentrated varieties contained peaks at the retention times of the very light Aroclor 1254 components, limiting parts per billion quantitation of these components. The Pesticide Grade hexane utilized in the optimized procedure appeared to be the best of the hexanes evaluated in the region of the diagnostic Aroclor peaks. Its quality varied from lot to lot. The suitability of the hexane should be assessed initially before any concentrative steps or extractions are attempted with blood samples. Therefore, to circumvent difficulties, elimination of all concentrative steps in the screening step and minimization of the degree of concentration in the steps where concentration was necessary were sought. Thus, one extraction using an optimal volume of hexane after the alkaline hydrolysis was the most desirable solution to the solvent contamination problem as long as the efficiency of extraction was high and the sensitivity was adequate.

Optimization of the amount of ethanol used in the hydrolysis step was investigated as the solution to the problem of low PCB extraction efficiencies. The ethanol probably affects the partitioning behavior since Aroclor 1254 has appreciable solubility in ethanol (~100 mg/mL at 27 °C (12)). The partitioning coefficient for PCB in hexane/KOH solution should be greater than that for hexane/alcoholic KOH.

The sample foamed in the absence of ethanol, and unavoidable losses of material occurred on any attempt at partitioning. The screw caps also tended to become loose during the hydrolysis in the absence of ethanol unless they were very tight. The minimum amount of ethanol required to prevent foaming was found experimentally to be 2 mL. Hydrolyzed solutions to which 2 mL of ethanol had been added yielded only 7% recovery of Aroclor 1254 even with three hexane extractions. It appeared that the alcohol was therefore also important in the hydrolysis process.

Thus, when 0, 2.5, 3.0, 5.0, 10, and 20 mL volumes of ethanol were added at the hydrolysis step with no evaporation of the ethanol prior to extraction, the absolute extraction efficiencies for 1.08 ppm Aroclor 1254 in 10 g of blood into 10 mL of hexane were 3, 70, 73, 36, 21, and 21%, respectively. This behavior indicated that ethanol definitely affected PCB partitioning into hexane. Thus, 2.5 mL was selected as the optimum volume of ethanol. The ethanol was removed after the hydrolysis to assess if partitioning was improved. This was accomplished by a stream of nitrogen while the tube was still in the water bath. Without ethanol evaporation, 1.08 ppm Aroclor 1254 in 10 g of blood was recovered to the extent of (70 ± 2)% into 10 mL of hexane; upon evaporation of the ethanol, the efficiency was 86 ± 4%. However, 1.08 ppb of Aroclor 1254 in the same sample of blood was 90% recovered; without ethanol evaporation, the recovery was only 19%. Thus, evaporation of the ethanol before extraction was essential to attain quantitative partitioning into one 10-mL hexane extract. A careful concentration study utilizing 1.09, 10.9, 109, and 1,092 ppb of Aroclor 1254 was then initiated, yielding the results shown in Table 1.

The screening method has several advantages over existing methods; it is efficient, relatively fast for many samples since they can be processed simultaneously, and avoids the use of concentrative steps and hence the interferences of solvent contaminants. The hydrolytic and extraction processes are carried out in the same tube used for collecting and storing the blood, and the hexane extract does not need to be removed for analysis. This eliminates losses, contamination through transfer, and the need for providing volumetric glassware. The

ethanol evaporative step utilizing nitrogen also preserves the self-containment of the sample. The capping of the tube during the hydrolysis avoids external contamination. The PCB levels obtained with this method are semiquantitative but the maximum possible values of Aroclor 1254 are found in a timely manner, allowing further GC/MS analysis or cleanup depending on the sample or the concentration of PCB. This is an important consideration when many samples are to be processed in a short time.

The NIOSH procedure (10) involves many transfers, many concentrative steps, and a column chromatographic step. In addition, it advocates integrating under all the peaks of interest (or adding the heights of the peaks of interest). Three to five peaks are generally utilized. This assumes that the peaks found in blood bear the same quantitative relationship to each other as in the standard. This has been shown not to be true for PCBs found in the blood of people exposed to PCBs at some time in the past (1, 4), reflecting differential rates of metabolism of the different isomers. Since the electron capture detector does not also respond equally to all PCBs, even of those of the same molecular weight and number of chlorines (1), adding the areas or heights of EC/GC peaks representing PCBs is not valid if the peaks in the blood bear little relationship to the peaks in the original PCB source. This problem has plagued PCB analysis from the very beginning. The height ratio of peak A to peak B is 1.6, and since both peaks arise from the hexachloro isomers (Figure 1) differential rates of metabolism will affect this ratio less than for peaks with a different number of chlorines. Thus, the factors likely to cause errors in quantitation have been minimized in the screening method, although the relationship between peaks A and B in the standard is still relied upon. Other PCBs show peaks at the retention times for peaks A and B. The A/B ratio for Aroclor 1260, however, is 1:2, so permitting differentiation. Aroclor 1221 shows a ratio of 1:1, but A and B are very minor peaks. Clearly, the analyst must inspect diagnostic areas of the chromatograms to decide if other Aroclors are present. If the quantities calculated from the two peaks do not agree or if the A/B ratio is not 1.6, the liquid chromatographic cleanup step will be essential for quantitation depending on the actual maximum levels found in the screening step. Clearly, if the screening step indicates levels of 1 and 5 ppb, then proceeding further will be time wasted unless accurate levels are required.

Perchlorination (13) has been advocated as the best technique to find the total PCB content to minimize the problem of nonstandard peaks mentioned above. We did not use this technique since not all PCBs are equally toxic (3, 14), and 3,4,5,3',4',5'-hexachlorobiphenyl and the 3,4,5,3',4'- and 2,3,4,3',4'-pentachlorobiphenyls being regarded as the most toxic. The quantitation of total PCB content is therefore not necessarily a measure of toxic effect, and identification and quantitation of specific isomers may be more important to assess if health effects are likely. Isomer specific PCB analysis has been done by Ugawa et al. (15) and Chen et al. (4) utilizing capillary GC/MS. However, the capillary GC/MS technique is relatively costly, especially with regard to the standards required. The above fast-screening method will allow the analyst to decide if a more detailed investigation is warranted

in a minimum of time with minimal cleanup of commercially available solvents and with minimal glassware and its associated cleaning.

This method has been successfully applied without recourse to subsequent liquid chromatography to over 200 blood and 10 plasma samples from people known to be recently exposed to Aroclor 1254. The results of these extensive analyses will appear elsewhere. The technique is probably applicable to the analyses of other PCBs. Such PCBs as Aroclor 1016 will probably require the column chromatographic cleanup step since solvent peaks are present in the same regions as the peaks from this PCB, or alternatively the hexane solvent may have to be purified further, or both. Large quantities of PCBs (>30 ppb) are quite evident in spite of the presence of solvent or blood peaks, and Aroclors 1016, 1242, and 1248 have also been identified successfully by us without column chromatography by their characteristic EC/GC patterns (16). This initial identification is necessary for subsequent quantification purposes when the type of PCB is unknown, and so the screening technique will allow a quick decision to be made for unknown serious overexposure cases.

#### ACKNOWLEDGMENT

The authors wish to acknowledge the technical assistance of Edith Miller and the late Ms. Wolfe.

Registry No. Aroclor 1254, 11097-69-1; Aroclor 1016, 12674-11-2; Aroclor 1242, 53469-21-9; Aroclor 1248, 12672-29-6.

#### LITERATURE CITED

- (1) Cairns, T.; Siegmund, E. G. *Anal. Chem.* **1981**, *53*, 1183A-1193A.
- (2) Koeman, J. H.; Ten Noever de Braun, M. C.; de Vos, R. H. *Nature (London)* **1969**, *221*, 1126-1128.
- (3) Higuchi, K., Ed. "PCB Poisoning and Pollution"; Academic Press: New York, 1976.
- (4) Chen, P. H.; Gaw, J. M.; Wong, C. K.; Chen, C. J. *Bull. Environ. Contam. Toxicol.* **1980**, *25*, 325-329.
- (5) Kashimoto, T.; Miyata, H.; Kunita, S.; Tung, T. C.; Hsu, S. T.; Chang, K. J.; Tang, S. Y.; Ohi, G.; Nakagawa, J.; Yamamoto, S. *Arch. Environ. Health* **1981**, *36*, 321-326.
- (6) *Fed. Regist.* **1980**, *45* (May 9), 30980.
- (7) MacLeod, K. E. *Environ. Sci. Technol.* **1981**, *15*, 926-928.
- (8) Maroni, M.; Colombi, A.; Cantoni, S.; Ferioli, E.; Foa, V. *Br. J. Ind. Med.* **1981**, *38*, 49-54.
- (9) U.S. DHEW Criteria for a Recommended Standard: Occupational Exposure to Polychlorinated Biphenyls (PCBs); DHEW (NIOSH) Publ. No. 77-225, 1977.
- (10) U.S. DHEW "NIOSH Manual of Analytical Methods"; DHEW (NIOSH) Publ. No. 79-141, 1980, pp 329-1-329-7.
- (11) U.S. EPA "Handbook for Analytical Quality Control in Water and Wastewater Laboratories"; EPA 600/4-79-019, E.M.S.L., U.S. EPA, Cincinnati, OH, March 1979, p 2.2.
- (12) Hutzinger, O.; Safe, S.; Zitko, V. "The Chemistry of PCBs"; CRC Press: Boca Raton, FL, 1976; p 15.
- (13) Robbins, A. L.; Wilhite, C. R. *Bull. Environ. Contam. Toxicol.* **1979**, *21*, 428-431.
- (14) Yoshimura, H.; Yoshihara, S.; Ozawa, N.; Miki, M. *Ann. N. Y. Acad. Sci.* **1979**, *320*, 179-192.
- (15) Ugawa, M.; Nakamura, A.; Kashimoto, T. *J. Food Hyg. Soc. Jpn.* **1973**, *14*, 415-424.
- (16) Hutzinger, O.; Safe, S.; Zitko, V. "The Chemistry of PCBs"; CRC Press: Boca Raton, FL, 1974; p 21.

RECEIVED for review June 4, 1982. Accepted September 29, 1982. This work was supported by U.S. Public Health Service Grant No. ES-00159. This material was presented at the 184th American Chemical Society Meeting, Sept 13-17, 1982, at Kansas City.



## Instrument for Alternating Current Impedance Measurements

Sheng-Min Cai,<sup>1</sup> Tadeusz Malinski, Xiang-Qin Lin, Jian-Quan Ding, and Karl M. Kadish\*

Department of Chemistry, University of Houston, Houston, Texas 77004

It has long been recognized that ac impedance measurements can provide much information on electrode processes and double layer structure (1-3). Although the theory of ac impedance measurements is well developed (1), this technique has not found the popularity of other electrochemical techniques. The ac bridge method is classic and precise (4, 5), but rather inconvenient and time-consuming. Some good non-bridge instruments have been developed, but they are mostly complicated and expensive (6-10).

The general characteristics desired in an impedance measurement system are good accuracy, precision, lack of difficulty in changing frequency, the use of small ac perturbation signals, and a way to internally check for the occurrence of erroneous measurements. In this paper we report the construction of such an instrument made from common available commercial components. Most available ac impedance instrumentation uses an ac perturbation signal of about 5 mV. In these cases a 1000- $\Omega$  electrode impedance will produce a 5- $\mu$ A ac perturbation signal. In the system described here we are able to decrease the ac perturbation signal by 10 or more times from that of other instruments so that the perturbation signal is less than 0.5  $\mu$ A. A small ac perturbation is necessary for cases where a large current may cause large deviations from equilibrium during the measurement process.

## CIRCUIT

A preliminary description of this circuit has been reported (11) where currents were limited to a lower value of  $\sim 5 \mu$ A. In this paper changes have been effected such that currents as low as 0.5-0.05  $\mu$ A or less could be routinely obtained. The circuit utilized is shown in Figure 1. An EG&G Princeton Applied Research potentiostat (PAR 173) and a signal generator together with a saturated calomel reference electrode (RE) and a dc counterelectrode (DCE) were used to control the dc potential of the mercury test electrode (TE) which was either a dropping mercury electrode (DME) or hanging mercury drop electrode (HMDE).

Both ac and dc circuitry are found in Figure 1. The ac current circuit consists of a voltage controlled frequency oscillator (VCFO, Exact Electronics 502SL), four 340-k $\Omega$  resistors in series ( $R_3$ - $R_6$ ), and two 200- $\mu$ F condensers ( $C_1$  and  $C_2$ ). The resistors are used in order to keep the amplitude of the ac current constant during the measurement and the condensers ( $C_1$  and  $C_2$ ) to prevent any dc current from entering the ac current path. The resistors  $R_1$  and  $R_2$  form a voltage divider in order to decrease the voltage output of the VCFO when an ac current perturbation smaller than 0.5  $\mu$ A is desired.  $R_1$  and  $R_2$  may be changed as needed in order to obtain the desired low current signal. Typical values utilized were  $R_1 = 1000 \Omega$  and  $R_2 = 100 \Omega$  or  $R_1 = 1000 \Omega$  and  $R_2 = 10 \Omega$  for reduction of the 0.5  $\mu$ A current by a factor of 10 and 100, respectively. Disconnecting the lower terminal of  $R_2$  from ground will return the ac current to the output value of the VCFO (typically 0.5  $\mu$ A). A 12 H choke (L) and a 45-k $\Omega$  resistor ( $R_7$ ) isolate the dc circuit from the ac current circuit in Figure 1.

In order to prevent interference between the dc and ac circuits and influencing noise from the potentiostat two

counterelectrodes were used. In addition to the dc counterelectrode a 2-cm<sup>2</sup> Pt mesh served as an independent ac counterelectrode (ACE). The use of a two counterelectrode system has been discussed in ref 6 but in this case the configuration is quite different than that reported in this paper. Ordinary impedance measurement systems using constant ac voltage perturbation prevent the use of two counterelectrodes because the currents from dc circuit and from the ac circuit are mixed together in the potentiostat. In the presented system the dc current and ac current are well separated by the condensers  $C_1$  and  $C_2$  so we can utilize two counterelectrodes.

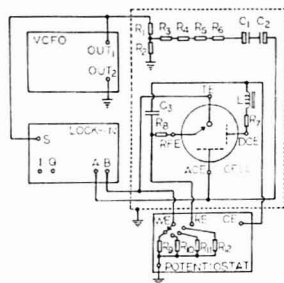
A PAR Model 5204 lock-in analyzer was used to measure the impedance of the TE. This instrument contains in-phase and quadrature meter reading (12). Since the output voltage of the VCFO is used as the reference signal of the lock-in amplifier, the ac current is in phase with the lock-in amplifier output voltage (because the circuit is resistive in character). The in-phase meter reading of the lock-in analyzer shows the resistive component,  $Z_R$ , of the impedance value, while the quadrature meter reading shows the negative value of the capacitive component,  $Z_C$ . In the electrochemical cell equivalent circuit (Figure 2a), the  $Z_R$  and  $Z_C$  components are connected in series (12, 13) and can be recorded simultaneously as output from the lock-in amplifier using a storage oscilloscope, an X-Y recorder, or a digital voltmeter as a recording instrument. Alternatively, they may be read directly from the meter.

The two floating inputs of the lock-in analyzer are connected to both the ACE (input A) and the TE (input B), and the TE is not grounded. The ac signal flows from the "live" terminal of the VCFO output (labeled OUT 1) via resistors  $R_3$  to  $R_6$  and the condensers  $C_1$  and  $C_2$  to the ACE. An ac path to ground from the test electrode must be provided because one terminal of the VCFO output is grounded (labeled OUT 2 in Figure 1). The test electrode cannot be directly grounded because the design of most potentiostats prevent this. However, the working electrode terminal of the PAR Model 173 potentiostat is connected to ground via internal resistors in the potentiostat and this provides the path to ground for the ac current. These internal resistors vary between 1  $\Omega$  and 10 k $\Omega$  depending on the current sensitivity of the potentiostat. For the specific currents utilized the range is between 1  $\Omega$  and 1000  $\Omega$ . Since these resistors are small compared to the sum of  $R_3$ ,  $R_4$ ,  $R_5$ , and  $R_6$  (1360 k $\Omega$ ) they do not influence the amplitude of the ac current.

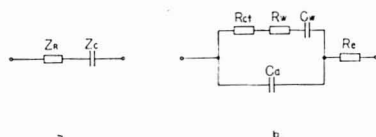
A 20-k $\Omega$  resistor ( $R_8$ ) and a 1- $\mu$ F capacitor ( $C_3$ ) form a filter preventing the ac signal from entering the potentiostat which would cause self-oscillation. The time constant of  $R_8C_3$  is large enough to reject the ac signal but not so large as to influence the dc voltage which is scanned linearly. For this voltage scan an external signal generator must be used in conjunction with the Model 173 potentiostat. Other potentiostats such as the IBM Model EC 225 have a built-in signal generator and an external triangular function is not needed.

The main problem of making the system an automatic frequency scanning one is the necessity to adjust the phase shift of the lock-in amplifier to make the resistive component measurement exactly in phase with the ac current flowing in the circuit. One solution to this problem is to keep the stray capacitance of resistors  $R_3$  to  $R_6$  in the ac current circuit as

<sup>1</sup> On leave from Chemistry Department, Peking University, Beijing, People's Republic of China.



**Figure 1.** Alternating current impedance circuit diagram: voltage control frequency oscillator (VCFO); lock-in analyzer (LOCK-IN); test electrode (TE); reference electrode (RE); alternating current counter-electrode (ACE); direct current counter-electrode (DCE); reference electrode, working electrode, and counter-electrode inputs of the potentiostat (RE, WE, CE); floating inputs of lock-in (A, B); reference signal input of lock-in (S); in-phase output of lock-in (I); quadrature phase output of lock-in (Q); output terminals of VCFO (OUT<sub>1</sub>, OUT<sub>2</sub>); resistors ( $R_1$ – $R_{12}$ ); capacitors ( $C_1$ – $C_3$ ); resistors of 1  $\Omega$ , 10  $\Omega$ , 100  $\Omega$ , and 1000  $\Omega$  for current range 1 A, 0.1 A, 0.01 A, and 0.001 A which are built into the potentiostat ( $R_9$ ,  $R_{10}$ ,  $R_{11}$ , and  $R_{12}$ ).



**Figure 2.** Interconversion of (a) series and (b) parallel equivalent circuits:  $Z_R$ , resistive component of the impedance;  $Z_C$ , capacitive component of the impedance;  $R_e$ , electrolyte resistance;  $R_{ct}$ , charge transfer resistance;  $C_d$ , double layer capacitance;  $R_W$ , diffusion resistance (Warburg resistance);  $C_W$ , diffusion capacitance (Warburg capacitance).

low as possible. This is best accomplished by connecting several smaller resistors in series rather than utilizing one large resistor. In Figure 1 four 340-k $\Omega$  resistors are utilized to produce a total 1360-k $\Omega$  resistance. These small resistors are separated 5 cm from each other and aligned in a straight line and the whole chain of resistors is at least 10 cm from any circuit.

Finally, in order to shield the electronics from external electrical interference in the laboratory, all resistors, condensers, and filters and the electrolytic cell were put into a grounded 40  $\times$  40  $\times$  60 cm metallic box constructed from 0.5 mm sheet metal. This is shown by the dashed line in Figure 1.

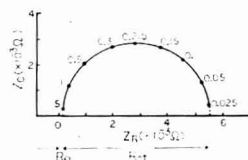
A square wave is usually utilized as the reference signal of lock-in amplifiers (13). In this case manual adjustment of the phase is required because a 5° or more shift of the phase with frequency is observed, making an automatically obtained complex plane spectrum (impedance diagram) almost impossible. On the other hand, when a sine wave of approximately 3  $V_{pp}$  is used as the reference signal, one can obtain a complex plane spectrum between 5 and 50 kHz automatically with less than a 2° phase shift over the total range of frequency. Better precision may be obtained by manual adjustment.

**Calibration, Operation, and Performance.** For high precision measurements manual adjustment of the lock-in amplifier phase shift may be made prior to each experiment at a specified frequency in order to offset the phase change in the exterior circuit. For calibration, a standard resistor

**Table I.** Frequency Dependence of Current, Resistance, and Capacitance at Fixed Phase Shift with a Dummy Cell<sup>a</sup>

frequency, Hz	C, $\mu$ F	R, $\Omega$	dc current, $\mu$ A	
			without ac perturbation	with ac perturbation
5	1.00	103	10.0	10.0
50	1.00	100	10.0	10.0
500	1.00	101	10.0	10.0
5000	1.00	100	10.0	10.0
50000	0.95	99	10.0	10.0

<sup>a</sup> The following conditions were set for the experiment:  $R = 100 \Omega$  and  $C = 1.00 \mu$ F in series connection; phase shift = +0.3°; ac current = 0.5  $\mu$ A.



**Figure 3.** Complex plane spectrum (impedance diagram) of Zn(Hg) ( $10^{-3}$  M)/Zn<sup>2+</sup> ( $10^{-3}$  M), 1 M KCl system at -1.00 V (vs. SCE); ac current 0.5  $\mu$ A. Numbers by points are frequencies in kilohertz.

( $R_{std}$ ) is used in place of the test electrode and connected to the ACE. The phase shift of the lock-in amplifier is set so that the quadrature meter reading ( $V_q$ ) is zero and at the same time the reading of the in-phase meter ( $V_i$ ) reaches a maximum. Manual phase shift adjustment also serves as a useful criterion to prove the instrument is functioning correctly. The frequency dependence of current, resistance, and capacitance at fixed phase shift is shown in Table I. Since the reading of in-phase meter  $V_i$  is known, one can calibrate the ac current by using eq 1.

$$V_i = i_0 R_{std} \quad (1)$$

The output voltage of the VCFO should be slightly adjusted in order to make  $i_0$  exactly equal to the ac current expected (such as 0.05  $\mu$ A, 0.005  $\mu$ A, etc.). This calibration is standard procedure before measurements of impedance vs. potential, and phase shifts of less than  $\pm 2^\circ$  are satisfactory. Calculation of resistance and capacitance can be done by using the following equations:

$$Z_R = V_i / i_0 \quad (2)$$

$$Z_C = V_q / i_0 \quad (3)$$

$$Z_C = 1/2 \pi f C \quad (4)$$

where  $f$  is the frequency. An equivalent circuit of the electrochemical cell is shown in Figure 2b.

The electrolyte resistance,  $R_e$ , charge transfer resistance,  $R_{ct}$ , double layer capacitance,  $C_d$ , Warburg resistance,  $R_W$ , and Warburg capacitance,  $C_W$ , can be calculated from the impedance measurements under different experimental conditions (1). For automatic measuring  $Z_R$  and  $Z_C$  are simultaneously recorded on an X-Y recorder.

In order to test the performance of the instrumentation, we made impedance measurements of an organic and an inorganic system. In addition the response of the instrumentation was examined under conditions of both changing fre-

Table II. Kinetic Parameters of the (Hg)/Zn ( $10^{-3}$  M)/Zn $^{2+}$  ( $10^{-3}$  M) Couple at an HMDE in 1.0 Molar Supporting Electrolyte<sup>a</sup>

supporting electrolyte	$k^0$ , cm/s		$i_0^*$ , A/cm $^2$	
	this work	lit.	this work	lit.
KNO $_3$	$2.3 \times 10^{-3}$	$3.5 \times 10^{-3}$ <sup>b</sup>	$4.5 \times 10^{-4}$	$6.3 \times 10^{-4}$ <sup>c</sup>
KCl	$2.6 \times 10^{-3}$	$4.0 \times 10^{-3}$ <sup>b</sup>	$5.0 \times 10^{-4}$	

<sup>a</sup> Measured at 50 Hz and at -1.00 V (vs. SCE). <sup>b</sup> Reference 14. <sup>c</sup> Reference 16.

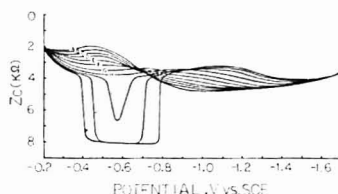


Figure 4. Potential dependence of the capacity component of adenine in a borate buffer pH 9 at a DME. Adenine concentration was as (A) 0.0; (B) 0.031 mM; (C) 0.063 mM; (D) 0.125 mM; (E) 0.25 mM; (F) 0.5 mM; (G) 1.0 mM; (H) 2.0 mM; (I) 4.0 mM; (J) 5.0 mM; (K) 8.0 mM. Curves were taken at 100 Hz; ac current was 0.5  $\mu$ A and scan rate was 5 mV/s.

quency and changing potential.

The first system selected was that of the Zn(II)/Zn(Hg) reaction in aqueous KNO $_3$  or KCl media (Figure 3). This reaction has been investigated by using ac impedance methods. Results from the literature and our experimental data under the same solution condition are listed in Table II. Both  $i_0^*$  and  $k^0$  were calculated according to literature procedures (1, 14). Given the uncertainties in solution purification and the usual systematic errors from laboratory to laboratory, the values obtained by our instrumentation appear to be acceptable. More importantly, however, is the fact that a typical impedance diagram used for the calculation of  $i_0^*$  (or  $k^0$ ) can be made in 5 min as compared to 1 h or more needed for manual determination.

In Figure 4 a plot of the impedance of double layer capacity  $c$  vs. potential is shown for adenine at different concentrations. Measurements were done at a DME in borate buffer solution (ionic strength 0.5 M) using sampled measurements. The adsorption of adenine on Hg has been studied before using a quadrature component of ac sinusoidal polarography (15).

The data obtained in the present work suggest that using impedance measurements one can obtain a  $Z_C$ -V curve in approximately the same period of time as in ac polarography but with better accuracy. The accuracy of measurement of  $Z_C$  by the described ac impedance method is about 0.5% in comparison to the 1-2% accuracy in quadrature ac polarography.

In conclusion the instrument described in this paper offers advantages not only in cost but in a substantial savings of time. If the frequency is changed automatically, numerous complex plane spectra may be rapidly obtained in the time that is usually needed for the obtaining of a single measurement set using the classical ac bridge technique. In addition, through the use of small amplitude ac currents one is not faced with the problem of deviations from equilibria which may occur with large currents. Finally, this method, using the described instrumentation, leads to higher accuracy than that obtained by sinusoidal ac polarography.

#### ACKNOWLEDGMENT

We acknowledge the loan of a lock-in analyzer from EG&G Princeton Applied Research.

Registry No. Zn, 7440-66-6; KNO $_3$ , 7757-79-1; KCl, 7447-40-7; Zn(Hg), 11146-96-6; Hg, 7439-97-6; adenine, 73-24-5.

#### LITERATURE CITED

- (1) Sluyter-Rehbach, M.; Sluyters, J. H. "Electrochemical Chemistry"; Marcel Dekker: New York, 1970; Vol. 4, pp 1-121.
- (2) Archer, W. I.; Armstrong, R. D. "Electrochemistry"; Burlington House: London, 1978; Vol. 7, pp 157-201.
- (3) Armstrong, R. D.; Bell, M. F.; Metcalfe, A. A. "Electrochemistry"; Burlington House: London, 1978; Vol. 6, pp 98-121.
- (4) Grahame, D. C. *Chem. Rev.* **1947**, *41*, 441-501.
- (5) Grahame, D. C. *J. Am. Chem. Soc.* **1941**, *63*, 1207-1215.
- (6) Gabrielli, C. "Identification of Electrochemical Processes by Frequency Response Analysis"; Solartion: Paris, 1980.
- (7) Brieler, M. W. *J. Electrochem. Soc.* **1985**, *112*, 845-849.
- (8) Tshernikovskii, N.; Gileadi, E. *Electrochim. Acta* **1971**, *16*, 579-584.
- (9) Bower, G. P.; Caldwell, I. *Electrochim. Acta* **1981**, *26*, 625-629.
- (10) Feller, H. G.; Ratzel-Scheibe, H. J.; Wendt, W. *Electrochim. Acta* **1972**, *17*, 187-195.
- (11) Cal, S. M.; Liu, C. Y.; Wilhelm, S. M.; Hackerman, N. Extended Abstract of Electrochemical Society 161st Meeting, No. 697, Montreal, 1982.
- (12) Operating and Service Manual for EG&G Princeton Applied Research Model 5204 Lock-In Analyzer, Princeton, NJ.
- (13) O'Haver, T. C. *J. Chem. Educ.* **1972**, *49*, A131-134 and A211-222.
- (14) Vetter, K. "Electrochemische Kinetik"; Springer-Verlag: Germany, 1961.
- (15) Knoshka, H.; Christian, S. D.; Dryhurst, G. J. *Electroanal. Chem.* **1977**, *83*, 151-166.
- (16) Parsons, R. "Handbook of Electrochemical Constants"; Butterworths: London, 1959.

RECEIVED for review August 19, 1982. Accepted October 7, 1982. The support of the National Science Foundation (Grant CHE 7921536) and the National Institutes of Health (Grant GM 25172) is gratefully acknowledged.

## Impedance Measurements for Evaluating the Stability of Aqueous Saturated Calomel Reference Electrodes in Nonaqueous Solvents

Karl M. Kadish,\* Sheng-Min Cal,<sup>1</sup> Tadeusz Malinski, Jian-Quan Ding, and Xiang-Qin Lin

Department of Chemistry, University of Houston, Houston, Texas 77004

The increased use of nonaqueous solvents for electrochemical studies has led to the utilization of numerous novel reference electrodes suitable for these solvents. These electrodes

and their specific advantages and disadvantages are discussed in several comprehensive monographs (1-4). In almost all cases the authors recommend against the use of an aqueous saturated calomel electrode (SCE) in nonaqueous media. However, despite these warnings, the most often utilized electrode in nonaqueous media remains as the saturated

<sup>1</sup> On leave from the Chemistry Department, Peking University, Beijing, People's Republic of China.

Table I. Types of Saturated Calomel Electrodes Investigated

electrode no.	model	type frit
1	IBM Model 43	porous vycor
2	IBM Model 43	porous vycor
3	"home made"	porous vycor
4	Metrohm EA402	asbestos fiber
5	Metrohm EA402	asbestos fiber
6	Metrohm EA404	asbestos fiber
7	Fisher Dri-Pak	asbestos fiber
8	Fisher Dri-Pak	asbestos fiber
9	Radiometer K	cellulose pulp

calomel electrode. A survey of the literature in *Inorganic Chemistry* from 1979 to 1982 showed that over 75% of the 50 plus studies concerning some aspect of nonaqueous electrochemistry were carried out with an aqueous SCE.

For measurements in nonaqueous media the SCE is usually connected by means of a nonaqueous salt bridge (e.g., nonaqueous solution of tetraalkylammonium salt) to the electrolyte under study. This kind of double junction bridge separates the investigated nonaqueous solution from contact with the aqueous KCl solution in the SCE. However, the choice of this particular bridge arrangement in conjunction with an SCE is not perfect because potassium chloride has a limited solubility in many nonaqueous solvents (4). In addition the junction can be readily clogged, which leads to erratic junction potentials due to nonaqueous contamination in the frit. In these cases there is also the possibility that traces of nonaqueous solvent cannot be easily removed because of adsorption, even if the SCE is stored in aqueous saturated KCl for a long time after use. Special problems are also encountered in dichloromethane. This low dielectric constant solvent is not miscible with water and tends to promote clogging at the capillary tip. This leads to both erroneous potentials and high cell resistances which will produce distorted current voltage curves (due to  $iR$  loss).

Because of these above problems the stability of an SCE after use in nonaqueous solvents must be checked frequently by comparison with standard reference electrodes which have not been subjected to use in nonaqueous media. This most often involves a check of the potential difference between the two electrodes which should not exceed 1–2 mV.

For a number of years our laboratory has used the saturated calomel electrode as a reference electrode in nonaqueous media (5–7). For these studies we have utilized a bridge to separate the aqueous and the nonaqueous solvent systems. This bridge was filled with the nonaqueous solvent containing 0.1 M tetrabutylammonium perchlorate. As required, we have periodically checked the potential against a fresh electrode and, in addition, have reported potentials vs. a  $\text{Fc}^+/\text{Fc}$  (ferrocene/ferrocenium) internal standard. While this method seemed to work well and helped us to identify faulty reference electrodes in most cases, it was evident that the measurement of potential alone was not sufficient to identify an electrode which was not operating "correctly". For this reason we have devised a technique utilizing the ac impedance method which will give us the value of resistance and capacitance of an electrode after use in a nonaqueous solvent.

In this paper we report the results of a typical measurement of reference electrode potential and resistance before and after use in nonaqueous solvents. Measurements were made in dimethyl sulfoxide ( $\text{Me}_2\text{SO}$ ), acetonitrile ( $\text{CH}_3\text{CN}$ ), and methylene chloride ( $\text{CH}_2\text{Cl}_2$ ), although results are only reported in this latter solvent, which is the worst case. The eight commercially available electrodes and one homemade electrode listed in Table I were investigated. All of the electrodes were used extensively in  $\text{CH}_2\text{Cl}_2$  although three of these had

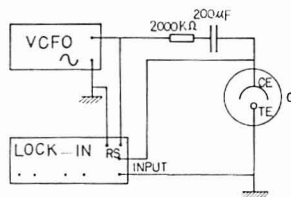


Figure 1. Schematic diagram of instrument for ac impedance measurements: VCFO, voltage controlled frequency oscillator; lock-in, lock-in analyzer; C, cell; RS, reference signal input; TE, test electrode; CE, ac counterelectrode.

been discarded due to some previously undefined malfunction. Of the nine electrodes, three contained porous vycor frits, five contained asbestos fiber frits, and one contained a cellulose pulp frit.

Our aim in the study was to report the potential, resistance, and capacitance (the last two were calculated from impedance measurements) of these electrodes at a given point in time and to then select three of these electrodes for measurements after long-term storage in  $\text{CH}_2\text{Cl}_2$  (which might simulate an experiment). At the end of this time the electrodes would be placed in saturated KCl and the time to reach reequilibrium measured.

## EXPERIMENTAL SECTION

**Reagents and Solutions.** Three different nonaqueous, aprotic solvents were used throughout this study.  $\text{CH}_2\text{Cl}_2$  was obtained from Fisher Scientific as technical grade and was distilled from  $\text{P}_2\text{O}_5$  and stored in the dark over activated 4-Å molecular sieves prior to use.  $\text{Me}_2\text{SO}$  (Eastman Chemicals) and  $\text{CH}_3\text{CN}$  (Coleman) were received as reagent grade from the manufacturer and were dried over 4-Å molecular sieves prior to use. KCl (Fisher Scientific) analytical grade was used as received.

**Instrumentation and Measurements.** Impedance measurements were made with a home built instrument whose design has been described in the literature (8, 9). The block diagram of this instrument is shown in Figure 1. A large (2 cm<sup>2</sup>) platinum mesh electrode was used as an alternating current counterelectrode (CE). A Hewlett-Packard Model 3310 generator (VCFO) which generated a sinusoidal wave with a frequency of 1000 Hz was connected to the CE via a 200-kΩ resistor and a 200-μF capacitor. The amplitude and phase of the signal voltage between the test electrode (TE), which in this case was the SCE, and the counterelectrode were measured with a PAR Model 5204 lock-in analyzer. For measurements of potential a digital voltmeter (Ballantine-STD) with high input resistance was used. All reported potentials are referred to an IBM Model 43 standard reference electrode which is listed as electrode number 1 in Table I.

## RESULTS AND DISCUSSION

Using a lock-in analyzer one can simultaneously measure the resistive component (ac voltage component  $V_R$ ) and capacitive component (ac voltage component  $V_C$ ) of an electrochemical cell. The resistive component is in-phase with the ac current,  $i$ , and the capacitive component is  $\pi/2$  out-of-phase with the current. A total resistance,  $R$ , can be calculated from eq 1 and the total capacitance,  $C$ , from eq 2 where  $f$  is the frequency of the alternating current.

$$R = V_R/i \quad (1)$$

$$C = i/2\pi fV_C \quad (2)$$

Because a resistance of 2000 kΩ was inserted into the circuit (see Figure 1) the ac current passing through the SCE is very small (less than 0.05 μA). Use of a small current is necessary in order to prevent polarization of the electrode during the

Table II. Properties of Saturated Calomel Electrodes

electrode	frit	potential difference, <sup>a</sup> mV	capacitance, $\mu$ F	resistance, $\Omega$
1	porous vycor		40.0	400
2	porous vycor <sup>b</sup>	-0.1	40.0	250
3	porous vycor	0.0	9.6	380
4	asbestos fiber	-0.3	11.0	850
5	asbestos fiber	-0.3	14.0	1000
6	asbestos fiber <sup>b</sup>	-1.2	9.2	760
7	asbestos fiber	-0.4	4.0	1500
8	asbestos fiber <sup>b</sup>	0.1	3.0	1660
9	cellulose pulp	-0.9	1.9	280

<sup>a</sup> Defined as potential difference between given reference electrode and electrode number 1. <sup>b</sup> Due to some undefined problems these electrodes had not been used in experiments for periods of 6 months or longer. The values presented are after treatment of the electrode as defined in the text. The original values are given in Table III.

measurement process. In this study potentials were found to vary by less than 0.1 mV when 0.05  $\mu$ A current was passed through the SCE for a period of up to 24 h.

For purposes of our measurements the calomel reference electrode can be represented by the equivalent circuit shown in Figure 2. Because of the small current passing through the circuit, and the small solubility of  $Hg_2Cl_2$ , the reaction  $Hg \rightleftharpoons Hg_2^{2+}$  can be considered as negligible. Under these conditions the Warburg impedance ( $R_w + C_w$ ) reaches a high value. Thus, the faradaic impedance contributions from  $R_{ct}$ ,  $R_w$ , and  $C_w$  are negligible as a first approximation. In this case the calculated impedance values of  $R$  and  $C$  are approximately equal to  $R_e$  and  $C_d$ , where  $R_e$  represents the sum of solution resistance in the bridge and the SCE. (There is also a small

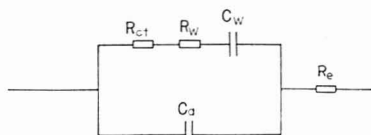


Figure 2. Equivalent circuit of the electrochemical impedance for reference electrode:  $R_{ct}$ , electrolyte resistance;  $R_w$ , charge transfer resistance;  $C_d$ , double layer capacity;  $R_e$ , diffusion resistance (Warburg resistance);  $C_w$ , diffusion capacity (Warburg capacity).

resistance of the connecting wires which is considered negligible.) The measured capacitance,  $C_d$ , is dependent on the capacitance of the double layer between the calomel, KCl, and mercury of the SCE, and gives important information about the contact area between the calomel paste and the mercury.

Table I lists the nine electrodes which were investigated in this study. These electrodes were from five different sources (four were commercially available and one was home made) and contained three different types of frits (porous vycor, asbestos fiber, and cellulose pulp). All of the electrodes had been used extensively in a variety of nonaqueous solvents.

Table II lists the potential differences, capacitances, and resistances of the nine different electrodes listed in Table I. Six of these electrodes were in regular use before the measurement had been carried out and had been properly stored in saturated KCl. Three of the electrodes (no. 2, 6, and 8) had been neglected due to some undefined problem which involved either unstable potential or abnormally high resistance. As might be expected, the three electrodes that had been discarded showed large deviations in potential, capacitance, or resistance. In these cases the values presented in Table II are after appropriate treatment of the electrode. Electrode 2 had a dirty frit and was not saturated with KCl; electrode 6 had a poor connection between the mercury and

Table III. Properties of "Bad" Calomel Electrodes Before and After Treatment

electrode	problem	frit	treatment <sup>a</sup>	potential difference, <sup>b</sup> mV	capacitance, $\mu$ F	resistance, $\Omega$
2	c	porous vycor	before	-14.4	13.0	400
			after	-0.1	40.0 <sup>f</sup>	250
6	d	asbestos fiber	before	-36.6	0.3	8600
			after	-1.2	9.2 <sup>f</sup>	760
8	e	asbestos fiber	before	-1.5	2.5	3000
			after	0.1	3.0 <sup>f</sup>	1660

<sup>a</sup> According to the procedure described in the text. <sup>b</sup> Potential differences measured vs. SCE labeled as number 1 (see Table I). <sup>c</sup> Dirty frit; KCl solution was not saturated. <sup>d</sup> Poor connection between mercury and calomel paste. <sup>e</sup> Frit was dirty and clogged. <sup>f</sup> After improving the contact between mercury and calomel.

Table IV. Change of Potential and Resistance of Electrodes After Storage in  $CH_2Cl_2$  and Reequilibrium After Saturated KCl Storage

solvent	time, min	electrode 2			electrode 4			electrode 9		
		$\Delta E$ , <sup>b</sup> mV	$R$ , $\Omega$	$\Delta R$ , <sup>c</sup> $\Omega$	$\Delta E$ , mV	$R$ , $\Omega$	$\Delta R$ , $\Omega$	$\Delta E$ , mV	$R$ , $\Omega$	$\Delta R$ , $\Omega$
$CH_2Cl_2$	0	0.0	380	0	0.0	850	0	0.0	280	0
	120	0.0			0.0			0.0		
	480	0.0			-0.2			0.2		
	720	0.1			-0.2			0.3		
	1440	0.3	400	20	-0.4	900	50	0.5	320	40
saturated KCl <sup>d</sup>	1	0.3	400	20	-0.4	900	50	0.5	320	40
	2	0.2			-0.3			0.4		
	3	0.1			-0.3			0.3		
	4	0.0			-0.2			0.2		
	10	0.0			-0.1			0.1		
	30	0.0	380	0	0.0	850	0	0.0	280	0

<sup>a</sup> Time measured after 24 h of storage in  $CH_2Cl_2$ . <sup>b</sup> Change in potential as a function of time. <sup>c</sup> Change of resistance as a function of time.

the calomel paste; and electrode 8 had a frit which was clogged and dirty.

The properties of these three electrodes before and after treatment are listed in Table III. As part of the treatment every frit was washed and cleaned, the connection between the mercury and the calomel paste was fixed, and the electrodes were filled with freshly prepared saturated KCl. These electrodes were then stored for 48 h in saturated KCl and measurements repeated. In every case the resistance was lower and the capacitance was higher. In addition, the potential of all three electrodes was much closer to the potential of our standard reference SCE labeled as number 1.

The data in Table II show that all of the electrodes have similar correct potentials. Thus, this might be one criterion for stating all of the electrodes are good for use as standard reference electrodes. On the other hand, the electrodes differ substantially in terms of their capacitance and resistance and can be grouped according to both the model of the electrode and the type of frit. The lowest resistances are found for electrodes with porous vycor and the cellulose pulp frits (250-400  $\Omega$ ) while the highest are for the electrodes with asbestos fiber frits (760-1660  $\Omega$ ). In this grouping the lower values are found for the three Metrohm electrodes while the highest are for the two Fisher electrodes.

As seen in Table II the values of capacitance vary between a low of 1.9 and 40  $\mu\text{F}$ . These values reflect the contact between the mercury and the calomel which is an important factor in the stability of the electrode potential. The higher the value of capacitance, the larger the contact area, and the more stable will be the electrode potential. All of the electrodes from a given manufacturer had similar values of capacitance as might be expected. The IBM electrodes (1 and 2) had identical values of 40  $\mu\text{F}$  and were larger than the three Metrohm electrodes (4, 5, and 6) which ranged from 9.2 to 14.0  $\mu\text{F}$ . The home made electrode (electrode 3) had a capacity of 9.6  $\mu\text{F}$ . This electrode had a relatively small dispersion of mercury in the calomel paste and also had a shorter KCl bridge than did electrode 1 and 2. Finally, both the Fisher and the Radiometer electrodes had a low capacity of 1.9-4.0  $\mu\text{F}$ .

Data collected in Table IV represent the influence of  $\text{CH}_2\text{Cl}_2$  on the potential and resistance of three representative electrodes. Electrode 2 contains a porous vycor frit, electrode 4 an asbestos fiber frit, and electrode 9 a cellulose pulp frit. Table IV also includes data on reequilibrium of the electrodes in KCl after storage in  $\text{CH}_2\text{Cl}_2$  for periods of 2-24 h.

After each interval of time the electrodes were transferred to an aqueous saturated KCl solution and impedance measurements were made. Although only 30 min was required for reequilibrium in KCl (see following sections) the electrodes were stored in KCl for a minimum of 3 h between measurements in  $\text{CH}_2\text{Cl}_2$ .

After 2 h of storage in  $\text{CH}_2\text{Cl}_2$ , no change in potential was observed, as seen in Table IV. In fact, very little change was observed even after 24 h. In the very worst case only a 0.5 mV difference in potential and a 50  $\Omega$  increase in resistance were obtained. Similar small changes were observed in  $\text{Me}_2\text{SO}$  and  $\text{CH}_3\text{CN}$ . More surprisingly immersion of the electrodes in saturated KCl for 4-30 min after being in  $\text{CH}_2\text{Cl}_2$  for 24 h produces identical potentials and resistances as in the original measurement.

In conclusion, one can see that potentials alone are not sufficient to characterize a properly operating reference electrode. Furthermore, the influence of nonaqueous solvents on an aqueous calomel reference electrode seems to be far less than had been expected, as any observed differences in potential and resistance caused by storing the electrodes in nonaqueous solvent for up to 24 h appear to be transient. This should not be construed as a recommendation for use of an aqueous SCE in nonaqueous solvents but should only be used as a guide in determining when an electrode might be faulty.

#### LITERATURE CITED

- Hills, G. J.; Ives, D. J. G. "Reference Electrodes"; Ives, D. J. G., Jane, G. J., Eds.; Academic Press: New York, 1961; Chapter 10.
- Strehlow, H. In "The Chemistry of Nonaqueous Solvents"; Lagowski, J. J. Ed., Academic Press: New York, 1967; Vol. II, Chapter 4.
- Butler, J. N. In "Advances in Electrochemistry and Electrochemical Engineering"; Delahay, P., Ed.; Interscience: New York, 1970; Vol. 7, pp 106-114.
- Sawyer, D. T.; Roberts, J. L., Jr. "Experimental Electrochemistry for Chemists"; Wiley: New York, 1974.
- Kadish, K. M.; Morrison, M. M. J. *Am. Chem. Soc.* **1976**, *98*, 3326.
- Kadish, K. M.; Bottomley, L. A.; Brace, J.; Winograd, N. J. *Am. Chem. Soc.* **1980**, *102*, 4341.
- Bottomley, L. A.; Kadish, K. M. *Inorg. Chem.* **1981**, *20*, 1348.
- Cai, S. M.; Liu, C. Y.; Wilheim, W. M.; Hackerman, N. Extended Abstract of Electrochemical Society of 161st Meeting, No. 697, Montreal, 1982.
- Cai, S. M.; Malinski, T.; Lin, X.-G.; Ding, J. Q.; Kadish, K. M. *Anal. Chem.* **1983**, *55*, 161-163.

RECEIVED for review July 23, 1982. Accepted September 24, 1982. This work was supported by the National Science Foundation (Grant CHE 7921536) and the National Institutes of Health (Grant GM 25172).

## Back-Extraction with Three Aqueous Stripping Systems for 16 Elements from Organometallic-Halide Extracts

J. Robert Clark\* and John G. Viets

U.S. Geological Survey, Denver, Colorado 80225

Detailed stripping curves have been determined for Cu, Ag, Au, Zn, Cd, Hg, Ga, In, Tl, Sn, Pb, As, Sb, Bi, Se, and Te, which are extracted by the Methyl isobutyl ketone-Amine synergetic Iodine Complex (MAGIC) extraction system (1). Stripping was accomplished with a  $\text{HNO}_3\text{-H}_2\text{O}_2$  system, a  $\text{CH}_3\text{COOH-H}_2\text{O}_2$  system, and a  $\text{H}_2\text{SO}_4\text{-H}_2\text{O}_2$  system (2). The mechanisms by which stripping is accomplished include poisoning of amine ion exchange agents with anions that are

incompatible with the extraction system, and oxidation of halide (mostly iodide) complexing ions. Most of these 16 elements can be separated from many other elements in the organic extracts by sequentially stripping the organic phase with various combinations of these three systems.

The MAGIC extraction system (1) makes it possible to concentrate and separate 18 trace elements (Pt and Pd, in addition to the list above) from analytically interfering rock



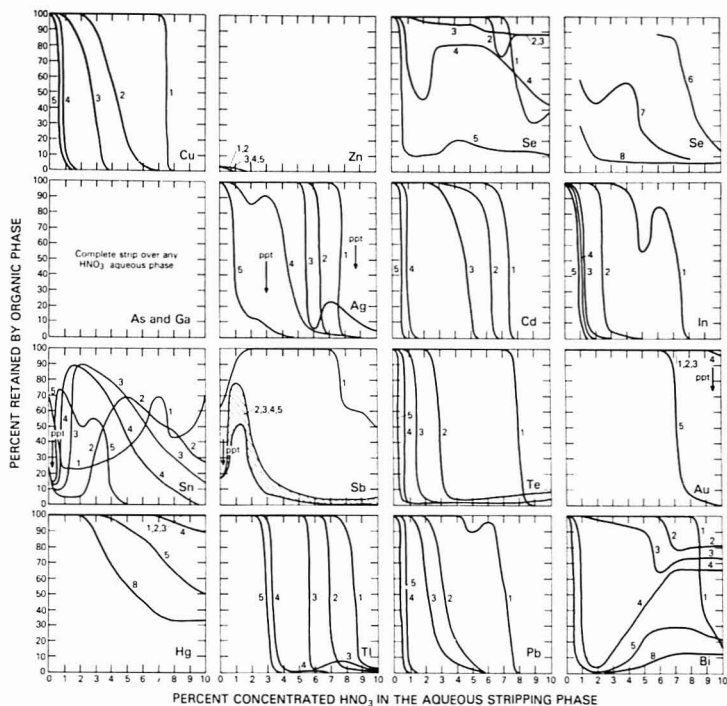


Figure 1. Nitric acid stripping curves: (1)  $\text{HNO}_3$  only; (2) concentrated  $\text{HNO}_3\text{:H}_2\text{O}_2 = 10:1$ ; (3) concentrated  $\text{HNO}_3\text{:H}_2\text{O}_2 = 5:1$ ; (4) concentrated  $\text{HNO}_3\text{:H}_2\text{O}_2 = 2:1$ ; (5) concentrated  $\text{HNO}_3\text{:H}_2\text{O}_2 = 1:2$ ; (6) concentrated  $\text{HNO}_3\text{:H}_2\text{O}_2 = 5:1$ , and percent concentrated  $\text{CH}_3\text{COOH} =$  percent concentrated  $\text{HNO}_3$ ; (7) concentrated  $\text{HNO}_3\text{:H}_2\text{O}_2 = 2:1$ , and percent concentrated  $\text{CH}_3\text{COOH} =$  percent concentrated  $\text{HNO}_3$ ; (8) concentrated  $\text{HNO}_3\text{:H}_2\text{O}_2 = 1:2$ , and percent concentrated  $\text{CH}_3\text{COOH} =$  percent concentrated  $\text{HNO}_3$ .

matrices in one operation. Aliquat-336, alamine-336, methyl isobutyl ketone, and hexane, combined in an organic phase, are used to extract these 18 elements, predominantly as iodide complexes, from an aqueous phase. An analytical geochemist can then treat the organic extract with these stripping systems (2) prior to performing flameless atomic absorption determinations, thereby eliminating organic and interelement interferences. Metallurgists and chemical engineers have expressed interest in utilizing both the extraction and stripping systems for concentrating and then separating various by-product metals in mineral processing and in recovering metals from spent catalysts or recycled wastes.

Details of the MAGIC extraction system and these stripping procedures have been published (1, 2). The previous description of the stripping systems contained only distribution diagrams. All of the stripping curves are being presented in this paper.

It was observed earlier that small amounts of the nitrate ion had a poisoning effect on the extraction of some of the elements in the MAGIC system (3). Dilute nitric acid solutions have been used previously for stripping zinc (4), cadmium (5), and uranium (6), from Aliquat-336. The acetate ion has also been found to produce adverse effects on the extraction of some elements. Hydrogen peroxide in an acid solution will oxidize the iodide ion to iodate and, thereby, destroy the organometallic iodide complexes in the extract. In the

$\text{HNO}_3\text{-H}_2\text{O}_2$  system, the poisoning effect of the nitrate ion is combined with the oxidizing effects of  $\text{H}_2\text{O}_2$  and  $\text{HNO}_3$ . The  $\text{CH}_3\text{COOH-H}_2\text{O}_2$  system combines the poisoning effect of the acetate ion and the oxidizing effect of  $\text{H}_2\text{O}_2$ . Sulfuric acid has no effect on any of the extraction mechanisms in the MAGIC system. When  $\text{H}_2\text{SO}_4$  is combined with  $\text{H}_2\text{O}_2$ , the only effect is the progressive decrease of the activity of iodide with increasing  $\text{H}_2\text{O}_2$  and acid concentrations.

## EXPERIMENTAL SECTION

All stripping determinations were made by atomic absorption spectrometry, as described previously (2). Reagent grade chemicals were used, except as detailed earlier, and a stock organic extract was prepared, as outlined previously. Stock stripping solutions were prepared at specific ratios of concentrated acid to total  $\text{H}_2\text{O}_2$  content. Table I outlines the mixtures in the stock stripping solutions. Most of these stripping solutions were diluted in test tubes to provided acid strengths from 0 to 10% concentrated acid in 1% increments. A few of the solutions were tested only over a narrow range of acidities and for only a few elements. An equal volume of stock organic extract was added to each test tube, and the contents were periodically shaken over a 48-h period of time. Aqueous to organic ratios were always 1:1, since different ratios produce different stripping curves.

## RESULTS AND DISCUSSION

Platinum and palladium were dropped from this study for

Table I. Stock Stripping Solutions

acid	vol % of concd acid	[acid], M	vol % of concd (30 wt %) $\text{H}_2\text{O}_2$	approx. overall wt/vol % $\text{H}_2\text{O}_2$	vol % concd acid: overall wt/vol % $\text{H}_2\text{O}_2$	figure no.	curve no.
nitric acid, $\text{HNO}_3$	20	3.2	0	0		1	1
nitric acid, $\text{HNO}_3$	20	3.2	6.7	2	10:1	1	2
nitric acid, $\text{HNO}_3$	20	3.2	13.3	4	5:1	1	3
nitric acid, $\text{HNO}_3$	20	3.2	33.3	10	2:1	1	4
nitric acid, $\text{HNO}_3$	10	1.6	66.7	20	1:2	1	5
nitric acid, $\text{HNO}_3$ , plus acetic acid, $\text{CH}_3\text{COOH}$	20/20	3.2/3.5	13.3	4	5:1	1	6
nitric acid, $\text{HNO}_3$ , plus acetic acid, $\text{CH}_3\text{COOH}$	20/20	3.2/3.5	33.3	10	2:1	1	7
nitric acid, $\text{HNO}_3$ , plus acetic acid, $\text{CH}_3\text{COOH}$	10/10	1.6/1.75	66.7	20	1:2	1	8
acetic acid, $\text{CH}_3\text{COOH}$	20	3.5	0	0		2	1
acetic acid, $\text{CH}_3\text{COOH}$	20	3.5	6.7	2	10:1	2	2
acetic acid, $\text{CH}_3\text{COOH}$	20	3.5	13.3	4	5:1	2	3
acetic acid, $\text{CH}_3\text{COOH}$	20	3.5	33.3	10	2:1	2	4
acetic acid, $\text{CH}_3\text{COOH}$	20	3.5	66.7	20	1:1	2	5
acetic acid, $\text{CH}_3\text{COOH}$	10	1.75	66.7	20	1:2	2	6
sulfuric acid, $\text{H}_2\text{SO}_4$	20	3.6	0	0		3	1
sulfuric acid, $\text{H}_2\text{SO}_4$	20	3.6	6.7	2	10:1	3	2
sulfuric acid, $\text{H}_2\text{SO}_4$ , plus acetic acid, $\text{CH}_3\text{COOH}$	20/10	3.6/1.75	13.3	4	5:1	3	3
			0	0		3	4

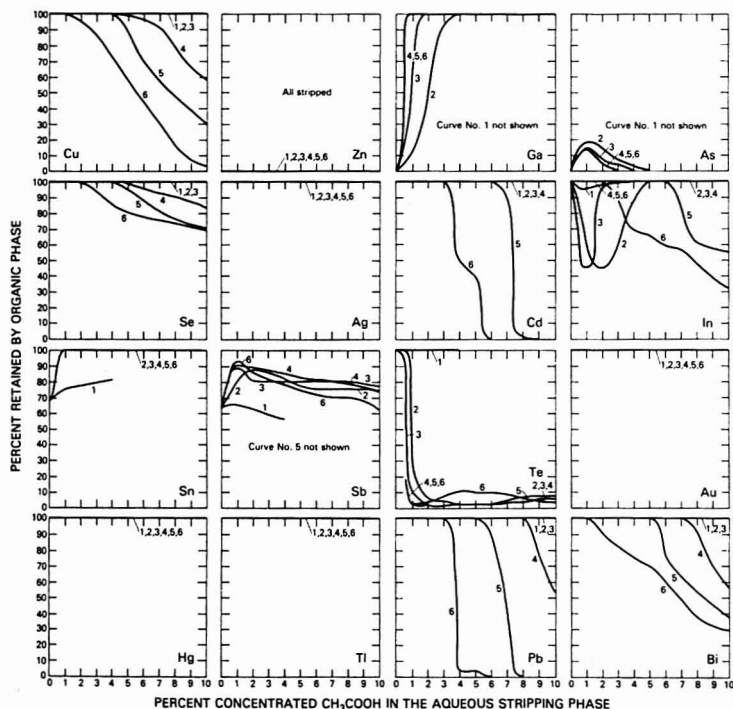


Figure 2. Acetic acid stripping curves: (1)  $\text{CH}_3\text{COOH}$  only; (2) concentrated  $\text{CH}_3\text{COOH}:\text{H}_2\text{O}_2 = 10:1$ ; (3) concentrated  $\text{CH}_3\text{COOH}:\text{H}_2\text{O}_2 = 5:1$ ; (4) concentrated  $\text{CH}_3\text{COOH}:\text{H}_2\text{O}_2 = 2:1$ ; (5) concentrated  $\text{CH}_3\text{COOH}:\text{H}_2\text{O}_2 = 1:1$ ; (6) concentrated  $\text{CH}_3\text{COOH}:\text{H}_2\text{O}_2 = 1:2$ .

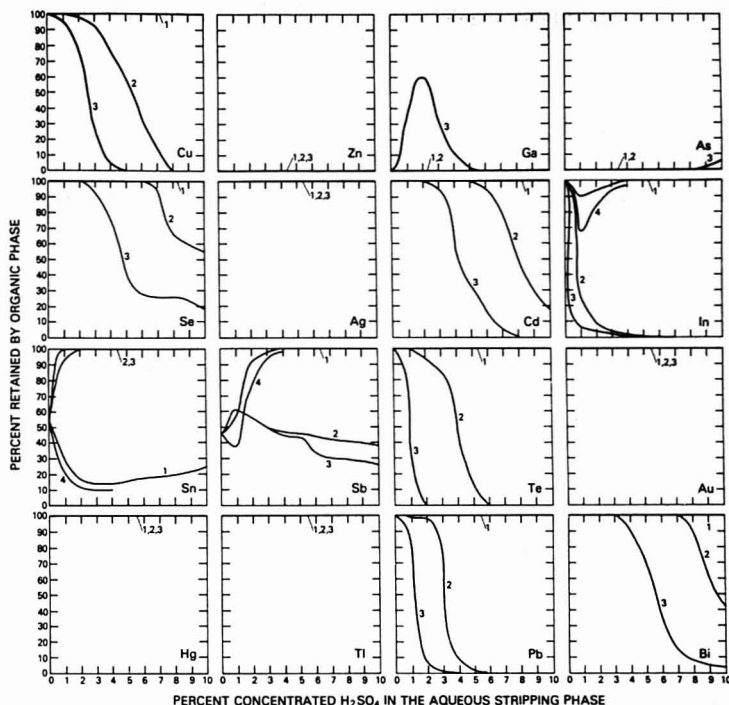


Figure 3. Sulfuric acid stripping curves: (1)  $\text{H}_2\text{SO}_4$  only; (2) concentrated  $\text{H}_2\text{SO}_4\text{:H}_2\text{O}_2 = 10:1$ ; (3) concentrated  $\text{H}_2\text{SO}_4\text{:H}_2\text{O}_2 = 5:1$ ; (4) concentrated  $\text{CH}_3\text{COOH} = 1/2$  concentrated  $\text{H}_2\text{SO}_4$ , and no  $\text{H}_2\text{O}_2$  present.

reasons previously described (2). All detailed stripping curves are presented in Figures 1-3. Those elements which are extracted by only one mechanism (Zn), or the extraction of which are, in part, dependent upon a high acid concentration (As) can be removed from the extract by simply backwashing the extract with a dilute acid solution. Most of the 16 elements are strongly bound in the extract as iodides, and they are stripped as the iodide activity is progressively reduced to zero. The oxidation-stripping reaction then attacks the lesser amounts of bromide and chloride in the extract, in that sequence. Elements, such as Au, Hg, and Bi, tend to remain in the extract until the total halide ion activity is reduced to a point that they begin to partition into the aqueous phase or form a precipitate (Au). There are valence changes and periodic trends, which have been described earlier (2), that also bear upon the resulting stripping sequences.

#### ACKNOWLEDGMENT

The authors are grateful for the critical reviews provided

by Richard O'Leary and Delmont Hopkins of the U.S. Geological Survey.

#### LITERATURE CITED

- (1) Clark, J. R.; Viets, J. G. *Anal. Chem.* **1981**, *53*, 61.
- (2) Clark, J. R.; Viets, J. G. *Anal. Chem.* **1981**, *53*, 65.
- (3) Viets, J. G. *Anal. Chem.* **1978**, *50*, 1097.
- (4) McDonald, C. W.; Rhodes, T. *Anal. Chem.* **1974**, *46*, 300.
- (5) McDonald, C. W.; Moore, F. L. *Anal. Chem.* **1973**, *45*, 963.
- (6) Barbano, P. G.; Rigali, L. *Anal. Chim. Acta* **1978**, *96*, 199.

RECEIVED for review March 23, 1982. Resubmitted and Accepted August 31, 1982. This study was conducted in the exploration geochemistry laboratories of the Geology Department of the Colorado School of Mines and in the laboratories of the U.S. Geological Survey. Use of brand names in this paper is for descriptive purposes only and does not constitute endorsement by the U.S. Geological Survey.

There were unfortunate errors in placement in the 1982 "A"-Page Index which appeared on page 2683 of the December issue. The correct index is given below.

## "A"-PAGE INDEX

### A/C Interface

- Local area networks: part I. Raymond E. Dessy. 1167 A  
Local area networks: part II. Ray Miller, N. Bruce Angelo, Richard T. Sloan, Wayne G. Nunn, J. P. Koontz, W. S. Woodward, J. Hinderliter-Smith, D. F. Smith, Raymond Dessy, Ian Chapple, James Currie, Stephen Dueball, Mark Thompson, David Duchamp, and Edward C. Olson. 1295 A

### Analytical Approach

- Analysis of rubber and plastic chemicals by LC/spectroscopy. Jerry B. Pausch. 89 A  
Arson analysis by mass chromatography. R. Martin Smith. 1399 A  
Sampling and analysis of radioactive solutions. David H. Smith, R. L. Walker, and J. A. Carter. 827 A  
The bust of Nefertiti. H. G. Wiedemann and G. Bayer. 619 A  
What is causing failures of aluminum wire connections in residential circuits? Dale E. Newbury. 1059 A

### Editors' Column

- A/C interface. 1002 A  
Charles Norwood Reilly, March 2, 1925–December 31, 1981. 426 A  
Developments in analytical education. 1109 A  
How to attract students to analytical chemistry. 548 A  
I. M. Kolthoff to be honored for excellence in teaching. 1463 A  
IUPAC nomenclature. 778 A  
Japan Society for Analytical Chemistry celebrates its 30th anniversary. 136 A  
Liquid chromatography of proteins and peptides. 21 A  
New clinical applications for familiar analytical concepts. 890 A  
Pittsburgh Conference, Atlantic City, N. J., March 8–12, 1982. 682 A  
Symposium on the future of analytical chemistry at FACSS. 1354 A  
University instrument funding. 1225 A

### Focus

- Analytical applications of NMR: summer symposium on analytical chemistry. 1129 A  
Careers in forensic science. 449 A  
Computers and automation for analytical

- chemistry: what is on the horizon? 567 A  
Field flow fractionation: steric transition. 787 A  
Fusion energy research. 1474 A  
GC/IR, LC/IR, GC/IR/MS. 901 A  
HPTLC: taking off. 790 A  
LC detectors: the search is on for the ultimate detector. 327 A  
Math is cheaper than physics. 1379 A  
Napoleonic analysis. 1477 A  
New electroanalytical pulse techniques. 698 A  
NIR litigation. 1250 A  
Nonlinear Raman spectroscopy. 1021 A  
RIMS: nuclear analysis. 1476 A  
Supercritical fluids can be nice. 1249 A  
Symposium on fast atom and ion induced mass spectrometry of nonvolatile organic solids. Catherine J. McNeal. 43 A  
Tylenol analysis. 1474 A

### Instrumentation

- A look at the electronic analytical balance. Randall M. Schoonover. 973 A  
Bioanalysis with potentiometric membrane electrodes. G. A. Rechnitz. 1194 A  
Cybernetic control of an electrochemical repertoire. Peixin He, James P. Avery, and Larry R. Faulkner. 1313 A  
Electronics, instrumentation, and microcomputers: principles and practice for the microcircuit age. J. P. Avery, S. R. Crouch, C. G. Enke, F. J. Holler, and H. V. Malmstadt. 367 A  
Fast atom bombardment mass spectrometry. Michael Barber, Robert S. Bordoli, Gerard J. Elliott, R. Donald Sedgwick, and Andrew N. Tyler. 645 A  
Flow cytometry and sorting. Dan Pinkel. 503 A  
Furnace atomic absorption—a method approaching maturity. S. R. Koortyohann and M. L. Kaiser. 1515 A  
High-sensitivity spectrophotometry. T. D. Harris. 741 A  
Liquid chromatography/electrochemistry: thin-layer multiple electrode detection. Daryl A. Roston, Ronald E. Shoup, and Peter T. Kissinger. 1417 A  
Mass spectrometry of middle molecules. Catherine Fenselau. 105 A  
Optical waveguides: photon plumbing for the chemistry lab: fiber optics, waveguides, and evanescent waves as tools for chemical analysis. Ilan Chabay. 1071 A  
Selecting instrument interfaces for real-time data acquisition. Joseph G. Lisowski. 849 A  
X-ray fluorescence spectrometry on the

- surface of Venus. Yu. A. Surkov, O. P. Shcheglov, L. P. Moskaliyeva, V. S. Kirichenko, A. D. Dudin, V. L. Gimadov, S. S. Kurochkin, and V. N. Rasputny. 957 A

### Regulations

- Evaluation of analytical methods used for regulation of foods and drugs. William Horwitz. 67 A  
Symposium on improving the analytical chemistry/regulatory interface, October 19–21, 1982. Preliminary announcement. Thomas Cairns, Michael Hoffman, and Curt Reimann. 349 A  
Symposium on improving the analytical chemistry/regulatory interface, October 19–21, 1982. Final announcement. Thomas Cairns, Michael Hoffman, and Curt Reimann. 933 A

### Reports

- Allerton analytical conferences. T. J. Logan. 1467 A  
Analytical chemists on postage stamps. Alan H. Ullman. 780 A  
Atomic absorption spectroscopy: the present and future. Walter Slavin. 685 A  
Forensic toxicology in the 1980s: the role of the analytical chemist. Bryan S. Finkle. 433 A  
Hydrodynamic chromatography. Hamish Small and Martin A. Langhorst. 892 A  
Information theory in analytical chemistry. Karel Eckschlager and Vladimir Stěpánek. 1115 A  
Laser-enhanced ionization spectrometry. J. C. Travis, G. C. Turk, and R. B. Green. 1006 A  
Laser microprobe mass spectrometry 1: basic principles and performance characteristics. Eric Denoyer, René Van Grieken, Fred Adams, and David F. S. Natusch. 26 A  
Laser microprobe mass spectrometry 2: applications to structural analysis. David M. Hercules, R. J. Day, K. Balasubramanian, Tuan A. Dang, and C. P. Li. 280 A  
NBS clean laboratories for trace element analysis. John R. Moody. 1358 A  
NBS standard reference materials: update 1982. Robert Alvarez, Stanley D. Rasberry, and George A. Urano. 1226 A  
Presampling factors in the elemental composition of biological systems. Venkatesh Iyengar. 554 A  
Trace analysis of the dioxins. F. W. Karsick and F. I. Onuska. 309 A

# MANUSCRIPT REQUIREMENTS

The following guide is published by the Editors of ANALYTICAL CHEMISTRY to aid authors in writing, and editors and reviewers in expediting review and publication of manuscripts.

**SCOPE.** The journal is devoted to the dissemination of knowledge concerning all branches of analytical chemistry. Articles either are entirely theoretical with regard to analysis or are reports of laboratory experiments that support, argue, refute, or extend established theory. Articles may contribute to any of the phases of analytical operations, such as sampling, preliminary chemical reactions, separations, instrumentation, measurements, and data processing. They need not refer to existing or even potential analytical methods in themselves, but may be confined to the principles and methodology underlying such methods.

In addition to regular research papers, *Correspondence* and *Aids* are published. *Correspondence* may be brief disclosures of new analytical concepts of unusual significance. They may also represent important comments on the work of others, in which case the authors of the work being discussed will, ordinarily, be allowed to reply. *Aids for Analytical Chemists* should be brief descriptions of novel apparatus or techniques, requiring real ingenuity on the author's part, which offer definite advantages over similar ones already available.

Papers involving extensive use of computers will be judged by the usual criteria of originality, technical content, and value to the field. They should include a statement of the objectives and the procedural steps to the objective, and the results. However, details of procedural steps, including programs, should be omitted. Availability of the latter through commercial collections or by writing to the author should be clearly indicated in the text. Computational techniques for calculations of well-known analytical methods cannot be considered.

Papers involving experimental data should offer a new or modified approach to analysis in a particular field, not just extend the existing library of data.

**SUBMISSION OF MANUSCRIPTS.** Four complete copies of the manuscript are required. All copy must be typed double- or triple-spaced on 22 × 28 cm (8½ × 11 in.) or A4 paper, with text, tables, and illustrations of a size that can be mailed to reviewers under one cover.

Reviewers suggested by authors may be used at the discretion of the editors.

Send all copies of the manuscript with covering letter to ANALYTICAL CHEMISTRY, 1155 Sixteenth St., N.W., Washington, DC 20036.

**TITLE.** Use specific and informative titles with a high keyword content. Avoid unnecessary phrases ("on the," "a study of") and articles (a, an, the), as well as words that are either obvious (new, novel, useful, improved) or relative (versatile, rapid, simple, inexpensive). Indicate, where applicable, compound or element determined, method, and special reagents—e.g., "Spectrophotometric Determination of Thallium in Zinc Cadmium with Rhodamine B". Do not use symbols, abbreviations, or series designations. Use one complete title rather than a title and subtitle. Be informative but brief. Careful attention should be paid to the choice of words—e.g., *trace* or *micro*, *determination* or *analysis*, etc.—to reflect correct usage.

**AUTHORSHIP.** Give authors' names in as complete a form as possible. First names, initials, and surnames should be included. Omit professional and official titles. Give complete mailing address for place where work was done and include telephone number of the corresponding author. Add current

address of each author, if different, on the title page of the manuscript with a numerical superscript and footnote. Corresponding author is indicated by an asterisk.

**ABSTRACT.** Abstracts are required for all manuscripts, but will not be published with *Correspondence* and *Aids*. (Put on separate page for these categories.) The abstract is to be self-explanatory and suitable for reproduction by abstracting services without rewriting. It indicates what is new, different, and significant. State the objectives of the study, the limits of detection, the degree of accuracy and precision, and the major unique reagents, times, and temperatures, but avoid the lengthy stepwise recipe. The length of the abstract should reflect the content and length of the manuscript, but should not exceed 150 words.

**TEXT.** Consult the publication for general style. Write for the specialist. Do not include information and details or techniques that should be common knowledge to the specialist.

**General Organization.** Indicate the breakdown among and within sections with center heads and side heads. Results and Discussion follow Experimental Section. Keep all information pertinent to a particular section within that section—e.g., do not present results in the Experimental Section. Avoid repetition. Do not use footnotes for descriptive or explanatory information; include the information at an appropriate place in the text.

## INTRODUCTION

Discuss the relationship of your work to previously published work, but do not repeat published information. If a recent article has summarized work on the subject, cite this article rather than repeating individual citations.

## EXPERIMENTAL SECTION

Use complete sentences—i.e., do not use outline form. Be consistent in voice and tense.

**APPARATUS.** List only devices of specialized nature. Do not include equipment that is standard in an analytical laboratory and used in the normal way.

**REAGENTS.** List and describe preparation of special reagents only. Do not list reagents normally found in the laboratory and preparations described in standard handbooks and texts.

**PROCEDURE.** Omit details of procedures that are common knowledge to those in the field. Describe pertinent and critical factors involved in reactions so that the method can be reproduced, but avoid excessive description. Brief highlights of published procedures may be included; details should be left to references.

**Caution:** Describe any procedures that are hazardous and list any reagents that are toxic.

## RESULTS AND DISCUSSION

Be complete and relevant but concise. Omit calculations that are well-known to the specialist.

## CONCLUSIONS

Use Conclusions only when necessary for interpretation and not to summarize information already given in the text or abstract.

## ACKNOWLEDGMENT

Acknowledge professional technical assistance and source of special materials only. Do not use professional titles.

**LITERATURE CITED.** References that are considered part of the permanent literature are to be numbered in one consecutive series by order of mention in the text. However, the

complete list of literature citations is placed on a separate page at the end of the manuscript. Reference numbers in the text are in parentheses and on line. Repetition is avoided by using the number corresponding to the original reference. Descriptive or explanatory (footnote) material is not given a reference number or included in the literature cited. This material must be included in the body of the text.

Use *Chemical Abstracts Service Source Index* abbreviations for journal names and include publication year, volume, and page number (inclusive pagination is recommended). Include *Chemical Abstracts* reference for foreign publications that are not readily available. List submitted articles as "in press" only if formally accepted for publication, and give the volume number and year if known. Otherwise use "unpublished work" with place where work was done and date. Include name, affiliation, and date for "personal communications".

Please use the format given in the following examples.

(1) Koile, Ross C.; Johnson, Dennis C. *Anal. Chem.* 1979, 51, 741-744.

(2) Willard, Hobart H.; Merritt, Lynne L., Jr.; Dean, John A.; Settle, Frank A., Jr. "Instrumental Methods of Analysis", 6th ed.; Van Nostrand: New York, 1981; Chapter 2.

**CREDIT.** On a separate page, give credit for financial support, meeting presentation information, and auspices under which work was done, including permission to publish. In the JOURNAL this information will immediately follow the received and accepted dates, and is not a part of the Acknowledgment.

**FIGURES AND TABLES.** Do not use figures or tables that duplicate each other or material already in the text. *Omit straight line graphs*; give information in a table, or in a sentence or two in the text. Do not include tables or figures found elsewhere in the literature.

**Tables.** Prepare tables in a consistent form, furnish each with an appropriate title, and number consecutively with Roman numerals in the order of reference in the text. Type each table on a separate page, and collate at end of manuscript.

**Figures.** Submit original drawings (or sharp glossy prints) of graphs and diagrams prepared on tracing cloth or plain white paper. If structures are given in the text, original drawings are to be provided. All lines, lettering, and numbering should be sharp and unbroken. If coordinate paper is used, use nonphotographic blue cross-hatch lines. Use black India ink and a lettering set for all letters, numbers, and symbols. Do not use a typewriter to letter illustrations.

Design illustrations to fit the width of one journal column (8.3 cm). The width of original drawings should be twice the publication size. Letters and symbols should be about 4 mm high on the original (2 mm in reduced journal version). Lines should be drawn with a light (#1 Leroy for graph grids), medium (#2 Leroy for graph borders or reference lines), or heavy (#5 Leroy for graph curves or emphasis) thickness on the original. Lettering on copy should be in proportion. Label ordinates and abscissas of graphs along the axes and outside the graph proper.

Supply glossy prints of photographs. Sharp contrasts are essential. Label each figure on the back with the name of the corresponding author and the figure number.

Number all figures consecutively with Arabic numerals in the order of reference in the text.

If drawings are mailed under separate cover, identify by name of author and title of manuscript.

**Figure Captions.** Include, on one page, a list of all captions and legends for illustrations. Make the legend a part of the caption rather than inserting it within the figure. Keep captions as brief as possible and include detailed information in the text.

**BRIEF.** On a separate page, state in 30 words or less the significant results obtained, emphasizing precision and accuracy data when possible. Do not repeat the title. No Briefs are necessary for *Correspondence* or *Aids*.

**NOMENCLATURE.** Nomenclature conforms with rules established by the International Union of Pure and Applied Chemistry, the Nomenclature Committee of the American Chemical Society, and the Chemical Abstracts Service. Consult Kurt Loening, P.O. Box 3012, Chemical Abstracts Service, Columbus, OH 43210, for advice.

Avoid trivial names. Well-known symbols and formulas may be used (write out in title and abstract) if no ambiguity is likely. Define trade names and abbreviations at point of first use. First letter of trade names is capitalized.

Use SI units of measurement (with acceptable exceptions) and give dimensions for all terms. If nomenclature is specialized, as in mathematical and engineering reports, include a Nomenclature section at end of paper, giving definitions and dimensions for all terms. Write out names of Greek letters and other special symbols in margin of manuscript at point of first use.

Type all equations and formulas clearly and number all equations in consecutive order. Place superscripts and subscripts accurately, indicate capital letters, and distinguish between characters which are alike on the keyboard—e.g., one and the letter "el", zero and the letter "oh". Avoid superscripts that may be confused with exponents.

For numbers less than one, a zero precedes the decimal point.

For specialized nomenclature used by this JOURNAL, see "Guide for Use of Terms in Reporting Data in ANALYTICAL CHEMISTRY", "Spectrometry Nomenclature", and "SI Units", which appear annually, with the "Manuscript Requirements", at the end of the technical section in the January issue. From time to time, ANALYTICAL CHEMISTRY publishes special nomenclature guides promulgated by various organizations.

General information about American Chemical Society publications, including preparation of manuscripts, is given in the "Handbook for Authors of Papers in American Chemical Society Publications", available from Distribution Office, American Chemical Society, 1155 16th St., N.W., Washington, DC 20036.

## Analysis, Identification, Determination, and Assay

While most chemists probably realize the difference between the terms *analyze*, *identify*, and *determine*, they are frequently careless when using them. Most frequently the term *analysis* is used when *determination* is meant.

A study of the nomenclature problem indicates that only samples are *analyzed*; elements, ions, and compounds are *identified* or *determined*. The difficulty occurs when the sample is nominally an element or compound (of unknown purity). "Analysis of —" (an element or compound) must be understood to mean the identification or determination of impurities. When the intent is to determine how much of such a sample is the material indicated by the name, *assay* is the proper word.



# Guide for Use of Terms in Reporting Data in

## ANALYTICAL CHEMISTRY

*It is important to know the meaning of the terms an author uses. For publications in ANALYTICAL CHEMISTRY, the following definitions are applicable and it is understood that they are used with a series of normally distributed replicate results with no prior information on bias of the method. They are endorsed by members of the Advisory Board. The Guide is necessarily incomplete, and it should be used only with an understanding of its limitations; one is that a value obtained for a term is usually based on a relatively small number of observations, and it is therefore to be regarded as an estimate of the parameter. For appropriate background, the reader should consult a reputable text on the subject of data evaluation.*

**Set** refers to a number  $n$  of independent replicate measurements of some property. Authors are encouraged to report this number  $n$ .

**Precision** relates to the reproducibility of measurements within a set, that is, to the scatter or dispersion of a set about its central value.

**Accuracy** normally refers to the difference (error or bias) between the mean,  $\bar{X}$ , of the set of results and the value  $X$ , which is accepted as the true or correct value for the quantity measured. It is also used as the difference between an individual value  $X_i$  and  $\bar{X}$ . The *absolute accuracy* of the mean is given by  $\bar{X} - X$  and of an individual value by  $X_i - \bar{X}$ . The *relative accuracy* of the mean is given by  $(\bar{X} - X)/\bar{X}$ , and the percentage accuracy  $100(\bar{X} - X)/\bar{X}$ .

**Measures of the Central Value of a Set.** MEAN (or Average or Arithmetic Mean) is the sum  $\sum_{i=1}^n X_i$  of the values of individual results divided by the number,  $n$ , of results in the set. The mean is given by

$$\bar{X} = (X_1 + X_2 + \dots + X_i + \dots + X_n)/n = \sum_{i=1}^n X_i/n$$

MEDIAN is the middle result of an odd number of results, or the average of the central pair for an even number, when they are arranged in order of magnitude. The median is less affected by extreme values than is the mean.

**Measures of Precision within a Set.** STANDARD DEVIATION is the square root of the quantity (sum of squares of deviations of individual results from the mean, divided by one less than the number of results in the set). The standard deviation,  $s$ , is given by

$$s = \sqrt{\frac{\sum_{i=1}^n (X_i - \bar{X})^2}{(n-1)}}$$

Standard deviation has the same units as the measurement. It becomes a more reliable expression of precision as  $n$  becomes large. When the measurements are independent and normally distributed, the most useful statistics are the mean for the central value and the standard deviation for the dispersion.

VARIANCE,  $s^2$ , is the square of the standard deviation.

RELATIVE STANDARD DEVIATION is the standard deviation expressed as a fraction of the mean,  $s/\bar{X}$ . It is sometimes multiplied by 100 and expressed as a percentage. Relative standard deviation is preferred over "coefficient of variation".

MEAN (or AVERAGE) DEVIATION is the mean of the deviations of the individual measurements from the mean of the set without regard to sign. It is given by  $\sum_{i=1}^n |X_i - \bar{X}|/n$ . The mean deviation is not recommended as a measure of precision except when the set consists of only a few measurements.

RANGE is the difference in magnitude between the largest and smallest results in a set. The range is not recommended as a measure of precision except when the set consists of only a few measurements. If range is used, the number of measurements in the set must be indicated.

**Measure of Precision of a Mean.** CONFIDENCE LIMITS (or Interval) are the limits around the measured mean within which the mean value for an infinite number of measurements can be expected to be found with the stated level of probability. Confidence limits for independent normally distributed measurements are given by

$$\text{confidence limits} = \bar{X} \pm ts/\sqrt{n}$$

where  $s$  is the standard deviation and  $t$  is the  $t$ -table value at the stated confidence level. The use of standard error,  $s/n^{1/2}$ , to express precision of a mean is acceptable only if the authors clearly make the distinction from standard deviation.

## Spectrometry Nomenclature

*We have compiled the following list of terms, their definitions, and abbreviations, which occur most frequently in papers on spectrometry. The list indicates our preferred usages in an attempt to obtain some consistency in a field where much discrepancy exists.*

**Absorbance,  $A$**  (not optical density, absorptancy, or extinction). Logarithm to the base 10 of the reciprocal of the transmittance  $A = \log_{10} (1/T)$ .

**Absorptivity,  $a$**  (not  $k$ ). (Not absorptancy index, specific extinction, or extinction coefficient.) Absorbance divided by the product of the concentration of the substance and the sample path length,

$$a = \frac{A}{bc}$$

**Absorptivity, Molar,  $\epsilon$**  (not molar absorptance index, molar extinction coefficient, or molar absorption coefficient). Product of the absorptivity,  $a$ , and the molecular weight of the substance.

**Angstrom, Å.** Unit of length equal to  $1/6438.4696$  of wavelength of red line of Cd. For practical purposes, it is considered equal to  $10^{-8}$  cm.

**Beer's Law** (representing Beer-Lambert law). Absorptivity of a substance is a constant with respect to changes in concentration.

**Concentration,  $c$ .** Quantity of the substance contained in a unit quantity of sample. (In absorption spectrometry it is usually expressed in grams per liter.)

**Frequency.** Number of cycles per unit time.

**Infrared.** The region of the electromagnetic spectrum extending from approximately 0.78 to 300  $\mu\text{m}$ .

**Micrometer,  $\mu\text{m}$ .** Unit of length equal to  $10^{-6}$  m. (Do not use micron.)

**Nanometer, nm.** Unit of length equal to  $10^{-9}$  m. (Do not use millimicron.)

**Sample Path Length,  $b$**  (not  $l$  or  $d$ ). Internal cell or sample length, usually given in centimeters.

**Spectrograph.** Instrument with an entrance slit and dis-

persing device that uses photography to obtain a record of spectral range. The radiant power passing through the optical system is integrated over time, and the quantity recorded is a function of radiant energy.

**Spectrometer, Optical.** Instrument with an entrance slit, a dispersing device, and with one or more exit slits, with which measurements are made at selected wavelengths within the spectral range, or by scanning over the range. The quantity detected is a function of radiant power.

**Spectrometry.** Branch of physical science treating the measurement of spectra.

**Spectrophotometer.** Spectrometer with associated equipment, so that it furnishes the ratio, or a function of the ratio, of the radiant power of two beams as a function of spectral wavelength. These two beams may be separated in time, space, or both.

**Transmittance,  $T$**  (not transmittancy or transmission). The ratio of the radiant power transmitted by a sample to the radiant power incident on the sample.

**Ultraviolet.** The region of the electromagnetic spectrum from approximately 10 to 380 nm. The term without further qualification usually refers to the region from 200 to 380 nm.

**Visible.** Pertaining to radiant energy in the electromagnetic spectral range visible to the human eye (approximately 380 to 780 nm).

**Wavelength** (one word). The distance, measured along the line of propagation, between two points that are in phase on adjacent waves—units Å, µm, and nm.

**Wavenumber** (one word). Number of waves per unit length. The usual unit of wavenumber is the reciprocal centimeter,  $\text{cm}^{-1}$ . In terms of this unit, the wavenumber is the reciprocal of the wavelength when the latter is in centimeters in vacuo.

## SI Units

The move toward the usage of the International System of Units (SI) has been agreed to by ACS editors as general ACS policy. Although, in principle, the change to strict SI usage is desirable, necessary adjustments dictated by practical reality must be considered. This guide gives authors an idea of what exceptions are acceptable in articles published in ANALYTICAL CHEMISTRY. Also included are the SI base units, derived units, and prefixes. Units that are not compatible with SI or the acceptable exceptions, but which must be used in a manuscript, should be followed by the SI equivalent in parentheses, e.g., 1-in. (2.54 cm) tubing or 1-in. (2.54 cm) tubing. The number in the SI equivalent should include only as many digits as are pertinent for any particular use.

### SI Base Units

Length	meter	m
Mass	kilogram	kg
Time	second	s
Electric current	ampere	A
Thermodynamic temperature	kelvin	K
Amount of substance	mole	mol
Luminous intensity	candela	cd

(supplementary units)

Plane angle	radian	rad
Solid angle	steradian	sr

### SI Derived Units

Area	square meter	$\text{m}^2$
Concentration	mole per cubic meter	$\text{mol}/\text{m}^3$
Density	kilogram per cubic meter	$\text{kg}/\text{m}^3$
Velocity	meter per second	$\text{m}/\text{s}$
Volume	cubic meter	$\text{m}^3$
Wavenumber	1 per meter	$\text{m}^{-1}$

(with special names)

Capacitance	farad	F
Conductance	siemens	S
Electric charge, quantity of electricity	coulomb	C
Electric potential, potential difference, electromotive force	volt	V
Energy, work, quantity of heat	joule	J
Force	newton	N
Frequency	hertz	Hz
Illuminance	lux	lx
Inductance	henry	H
Luminous flux	lumen	lm
Magnetic flux	weber	Wb
Magnetic flux density	tesla	T
Power	watt	W
Pressure	pascal	Pa
Radioactive activity	becquerel	Bq
Resistance	ohm	$\Omega$

### SI Prefixes

$10^{15}$	exa	E
$10^{12}$	peta	P
$10^{12}$	tera	T
$10^9$	giga	G
$10^6$	mega	M
$10^3$	kilo	k
$10^2$	hecto	h
$10^1$	deka	da
$10^{-1}$	deci	d
$10^{-2}$	centi	c
$10^{-3}$	milli	m
$10^{-6}$	micro	$\mu$
$10^{-9}$	nano	n
$10^{-12}$	pico	p
$10^{-15}$	femto	f
$10^{-18}$	atto	a

### Acceptable Exceptions

Area	barn
Concentration	molal = mole per kilogram ( $m = \text{mol kg}^{-1}$ ) molar = mole per liter ( $M = \text{mol L}^{-1}$ ); not formal or normal
Conductance	mho ( $\Omega^{-1}$ )
Density	gram per cubic centimeter ( $\text{g}/\text{cm}^3$ )
Energy	electronvolt (eV); also keV, MeV
Length	angstrom (Å)
Plane angle	degree ( $^\circ$ ), minute ( $'$ ), second ( $''$ )
Pressure	atmosphere (atm), bar, torr
Radioactivity of radionuclides	disintegrations per second (dps)
Second-order rate constants	1 per (mole per liter) per second ( $\text{M}^{-1} \text{s}^{-1}$ )
Temperature	degree Celsius ( $^\circ\text{C}$ )
Time	minute (min), hour (h), day (d), etc.
Volume	liter (L), milliliter (mL), microliter ( $\mu\text{L}$ )
Wavenumber	1 per centimeter ( $\text{cm}^{-1}$ )



## Name of American Chemical Society Publication

Author(s)

Ms No.

Ms Title

Received

This manuscript will be considered with the understanding you have submitted it on an exclusive basis. You will be notified of a decision as soon as possible.

[THIS FORM MAY  
BE REPRODUCED]

Print or  
Type  
Author's  
Name and  
Address

## COPYRIGHT TRANSFER

The undersigned, with the consent of all authors, hereby transfers, to the extent that there is copyright to be transferred, the exclusive copyright interest in the above cited manuscript (subsequently referred to as the "work") to the American Chemical Society subject to the following (Note: if the manuscript is not accepted by ACS or if it is withdrawn prior to acceptance by ACS, this transfer will be null and void and the form will be returned.):

- A. The undersigned author and all coauthors retain the right to revise, adapt, prepare derivative works, present orally, or distribute the work provided that all such use is for the personal noncommercial benefit of the author(s) and is consistent with any prior contractual agreement between the undersigned and/or coauthors and their employer(s).
- B. In all instances where the work is prepared as a "work made for hire" for an employer, the employer(s) of the author(s) retain(s) the right to revise, adapt, prepare derivative works, publish, reprint, reproduce, and distribute the work provided that all such use is for the promotion of its business enterprise and does not imply the endorsement of the American Chemical Society.
- C. Whenever the American Chemical Society is approached by third parties for individual permission to use, reprint, or republish specified articles (except for classroom use, library reserve, or to reprint in a collective work) the undersigned author's or employer's permission will also be required.
- D. No proprietary right other than copyright is claimed by the American Chemical Society.
- E. For works prepared under U.S. Government contract or by employees of a foreign government or its instrumentalities, the American Chemical Society recognizes that government's prior nonexclusive, royalty-free license to publish, translate, reproduce, use, or dispose of the published form of the work, or allow others to do so for noncommercial government purposes. State contract number: \_\_\_\_\_

SIGN HERE FOR COPYRIGHT TRANSFER [Individual Author or Employer's Authorized Agent (work made for hire)]

Print Author's Name

Print Agent's Name and Title

Original Signature of Author on Behalf of All Authors (in Ink)

Date

Original Signature of Agent (in Ink)

## CERTIFICATION AS A WORK OF THE U.S. GOVERNMENT

This is to certify that **ALL** authors are or were bona fide officers or employees of the U.S. Government at the time the paper was prepared, and that the work is a "work of the U.S. Government" (prepared by an officer or employee of the U.S. Government as a part of official duties), and, therefore, it is not subject to U.S. copyright. (This section should NOT be signed if the work was prepared under a government contract or coauthored by a non-U.S. Government employee.)

## INDIVIDUAL AUTHOR OR AGENCY REPRESENTATIVE

Print Author's Name

Print Agency Representative's Name and Title

Original Signature of Author (in Ink)

Date

Original Signature of Agency Representative (in Ink)

**FOREIGN COPYRIGHT RESERVED** (NOTE: If your government permits copyright to be transferred, refer to section E and sign this form in the top section.)



If **ALL** authors are employees of a foreign government that reserves its own copyright as mandated by national law, **DO NOT SIGN THIS FORM**. Please check this box as your request for the FOREIGN GOVERNMENT COPYRIGHT FORM (Blue Form) which you will be required to sign. If you check this box, mail this form to: Copyright Administrator, Books and Journals Division, American Chemical Society, 1155 Sixteenth Street, N.W. Washington, D.C. 20036, U.S.A.

กำหนดส่ง

21. ต.ค. 2526

# AUTHOR INDEX

- Abusamra, A., 91  
 Allison, L. A., 8
- Balasanmugam, K., 145  
 Ballard, J. M., 116  
 Betowski, L. D., 116  
 Bowen, J. M., 32  
 Brooks, J. J., 104
- Cal, S.-M., 161, 163  
 Cedergren, A., 2  
 Chen, J.-C., 127  
 Chewter, L. A., 68  
 Clark, J. R., 166  
 Coetzee, J. F., 120  
 Colton, R. J., 150
- Danielson, N. D., 17  
 Davis, D. M., 32  
 Delaney, M. F., 148  
 De Leenheer, A. P., 153  
 De Vazelles, R., 138  
 Ding, J.-Q., 161, 163  
 Donohue, D. L., 88  
 Dorn, H. C., 22
- Eaton, W. S., 57  
 Ewald, M., 138
- Farmanian, P. A., 42  
 Filby, R. H., 74  
 Fleischmann, M., 146  
 Fritz, J. S., 12
- Gaffney, J. S., 135  
 Garrigues, P., 138  
 Glass, T. E., 22  
 Goff, E. U., 29  
 Gold, H. S., 49  
 Gulochon, G., 138  
 Gustavsson, A., 94
- Hart, E. J., 46  
 Haverkamp, J., 81  
 Haw, J. F., 22  
 Hendra, P., 146  
 Hercules, D. M., 145  
 Hilleman, F. D., 104  
 Holzman, J., 46  
 Hughes, D. E., 78  
 Hussam, A., 120
- Jacobs, F. S., 74  
 Johnson, E. L., 4  
 Jonckheere, J. A., 153  
 Jousot-Dubien, J., 138
- Kadish, K. M., 161, 163  
 Kelly, T. J., 135  
 Kistemaker, P. G., 81  
 Kitamura, K., 54  
 Kolling, O. W., 143  
 Kwan, J. T., 42
- Lampert, R. A., 68  
 Leenheer, J. A., 111  
 Lewis, L. C., 99  
 Lin, X.-Q., 161, 163
- Lindgren, M., 2
- Majima, R., 54  
 Malinski, T., 161, 163  
 Mariën, K., 155  
 Mazer, T., 104  
 McCreery, R. L., 146  
 McKinney, J. D., 91  
 Meech, S. R., 68  
 Mizutani, F., 35
- Needham, R. E., 148  
 Noble, R. W., 104
- O'Connor, D. V., 68
- Petrick, T. R., 120  
 Phillips, D., 68  
 Phillips, M. F., 135  
 Prichard, H. M., 155  
 Purdie, N., 32
- Que Hee, S. S., 157
- Reed, J. H., 91  
 Richardson, H. H., 32  
 Roberts, A. J., 68  
 Rockley, M. G., 32  
 Rocklin, R. D., 4  
 Ross, M. M., 150
- Sasaki, K., 35  
 Sauter, A. D., 116  
 Schmitter, J.-M., 138  
 Schwager, I., 42
- Sehested, K., 46  
 Selucky, M. L., 141  
 Sevenich, G. J., 12  
 Shimura, Y., 35  
 Shoup, R. E., 8  
 Sieck, L. W., 38  
 Siemer, D. D., 2, 99  
 Siergiej, R. W., 17  
 Stadalius, M. A., 49  
 Staiger, D. B., 64  
 Steyaert, H. L., 153  
 Stuber, H. A., 111  
 Sundén, T., 2  
 Suskind, R. R., 157
- Tabor, M. W., 157  
 Tanner, R. L., 135
- Viets, J. G., 166
- Walters, J. P., 57  
 Warburton, G. A., 123  
 Ward, J. A., 157  
 Warren, R. J., 64  
 Weber, S. G., 127  
 Weinberg, V. A., 42  
 Windig, W., 81  
 Woodard, M., 32
- Yen, T. F., 42  
 Young, J. P., 88  
 Yu, W. C., 29
- Zuber, G. E., 64  
 Zumberge, J. E., 123

## Future Articles

### Reduction of Matrix Interferences in Furnace Atomic Absorption Spectrometry

J. J. Sotera, L. C. Cristiano, M. K. Conley, and H. L. Kahn

### Preparation of Gas Cylinder Standards for the Measurement of Trace Levels of Benzene and Tetrachloroethylene

William P. Schmidt and Harry L. Rook

### Dynamic Coupled-Column Liquid Chromatographic Determination of Ambient Temperature Vapor Pressures of Polynuclear Aromatic Hydrocarbons

W. J. Sonnefeld, W. H. Zoller, and W. E. May

### Isocratic Nonaqueous Reversed-Phase Liquid Chromatography of Carotenoids

H. J. C. F. Nelis and A. P. De Leenheer

### Statistical Theory of Component Overlap in Multicomponent Chromatograms

Joe M. Davis and J. Calvin Giddings

### Transmission of Organic Molecules by a Silicone Membrane Gas Chromatograph/Mass Spectrometer Interface

Casper C. Greenwalt, Kent J. Voorhees, and Jean H. Futrell

### Laser Modulated Electron Capture Detection for Gas Chromatography

Norman J. Dovichi and Richard A. Keller

### Computer-Assisted Prediction of Liquid Chromatographic Retention Indexes of Polycyclic Aromatic Hydrocarbons

Mohamed Noor Hasan and Peter C. Jurs

### Photoacoustic Cell for Fourier Transform Infrared Spectrometry of Surface Species

John B. Kinney and Ralph H. Staley

### Determination of the Molar Substitution Ratio for Hydroxyethyl Starches by Gas Chromatography

Ying-Chi Lee, David M. Baaske, and James E. Carter



# DIP IN, READOUT.

## **That's all there is to colorimetric determinations with Brinkmann Dipping Probe Colorimeters.**

Simple, accurate and versatile, that's the Brinkmann Dipping Probe Colorimeter. Widely used in industry, educational institutions and clinical/medical facilities, it eliminates cuvette breakage and cleaning because no sample transfer to a cuvette is required. The fiber optic probe tip can be directly dipped into any size container—test tube, vat or permanently installed into a pipeline for process monitoring. The readout is instantaneous (either digital or analog). And since the interchangeable probe tips are the only parts of the colorimeter that come in contact with the test solution, there is no measurable carryover between tests and no sample contamination.

Brinkmann Colorimeters are available with built-in filter wheels for applications at six specific wavelengths or with interchangeable filters for single or multi wavelength applications. Accessories to help customize colorimeters for your specific applications are also available.

For literature on the dip in colorimeter write: Brinkmann Instruments Co., Division of Sybron Corporation, Cantiague Road, Westbury, NY 11590; or call 516/334-7500. In Canada: Brinkmann Instruments (Canada), Ltd.

## **SYBRON | Brinkmann**

CIRCLE 24 ON READER SERVICE CARD